NASA SP-160

VIBRATION OF PLATES

LEISSA

DISTRIBUTION STATEMENT A
Approved for public release;
Distribution Unlimited

19960503 099

DEPARTMENT OF DEFENSE
PLASTICS TECHNICAL EVALUATION CENTER
PICATINNY ARSENAL, DOVER, N. J.

PLASTICS TECH EVAL CEN

NATIONAL AERONAUTICS AND SPACE ADMINISTRATION

NASA SP-160

VIBRATION OF PLATES

Arthur W. Leissa

Ohio State University
Columbus, Ohio

DISTRIBUTION STATEMENT A
Approved for public release;
Distribution Unlimited



Scientific and Technical Information Division
OFFICE OF TECHNOLOGY UTILIZATION
1969
NATIONAL AERONAUTICS AND SPACE ADMINISTRATION
Washington, D.C.

DTIC QUALITY INSPECTED 1

For sale by the Superintendent of Documents
U.S. Government Printing Office, Washington, D.C. 20402
Price $3.50 (paper cover)
Library of Congress Catalog Card Number 67–62660

Preface

The ever-increasing rate of scientific research throughout the world, and particularly in the United States, is a well-known fact. This increase is partly evidenced by the growing number of books, papers, and reports published every year. Indeed, we are faced with an information retrieval problem. If the results of a piece of scientific work are to provide useful knowledge, the expository technical papers or reports must be generally known and available, and they must be capable of being understood and evaluated by the reader (the problem of language is included here). The present monograph attempts to bridge these gaps in one field—the vibration of plates.

From the beginning, two objectives were intrinsic in this work:

(1) A comprehensive set of available results for the frequencies and mode shapes of free vibration of plates would be provided for the design or development engineer.

(2) A summary of all known results would be provided for the researcher in the field of plate vibrations.

These objectives will be elaborated upon below.

Several years ago I observed the following incident at a major aerospace company. An engineer needed to know the first three frequencies and mode shapes of a rectangular plate of a certain aspect ratio and with certain simple restraint conditions along its edges. A literature search was conducted by the engineer for 2 weeks, during which only the first two frequencies and no accurate mode shapes were found. Since he had neither the analytical capability of solving the problem nor the money and time needed for an experimental program, the engineer was forced to drop the problem at this point.

In the present study all direct results which are known for the aforementioned problem are presented. Furthermore, from a brief comparison among the known results for other boundary conditions, estimates of additional frequencies and mode shapes can be made. This is one way in which the engineer can develop a qualitative understanding of plate vibrational behavior. For the aforementioned problem, at least two approximate formulas are given for estimates of frequencies. Finally, the mathematical techniques used in the literature to solve the problem or related ones are pointed out in case more accurate results are needed.

It is my hope that this monograph will reduce duplication of research effort in plate vibrations in the future (a very pointed example is that of the square plate clamped all around). In addition, the researcher is provided accurate numerical results for the testing of new methods (this is the reason that results are given to eight significant figures in some cases). Finally, it is hoped that this work will give added perspective to the merits and complexities of applying analytical techniques to eigenvalue problems.

Gaps in knowledge are made implicitly obvious by examining this work. For example, analytical results have been found for a clamped elliptical plate, and experimental results for the free case, but no results whatsoever have been found for the simply supported case.

The scope of this study was limited by several considerations. Only the analytical results from plate theories were considered; that is, the governing equations are two-dimensional, not three-dimensional. Materials were restricted to those which are linearly elastic. Structures were not included in the study; for example, a rectangular plate supported by one or more edge beams was considered to be a structure.

The primary logical division of this work is by the complexity of the governing differential equations. Thus, the first eight chapters deal with the simplest "classical theory" of plates. The next three chapters introduce the complications of anisotropy, in-plane force, and variable thickness. Other complications are discussed in the twelfth chapter. The first subdivision is by geometrical shape; that is, circles, ellipses, rectangles, parallelograms, and so forth. Further subdivision accounts for holes, boundary conditions, added masses or springs, and so forth.

It is presupposed that the user of this monograph will have at least an elementary understanding of plate theory. In order to increase understanding and to define notation and assumptions more clearly, a reasonably rigorous derivation of the plate equations is made in the appendix.

Some statements about the format of presentation will be useful in understanding this work. It will be seen that the majority of results available are for the natural frequencies of free vibration and quite often only the fundamental (lowest) frequency. Patterns showing node lines are frequently available for the higher modes. Mode shapes (deflection surfaces in two dimensions) are usually not completely specified in the literature. It should be remarked here that the mode shapes (eigenfunctions) cannot be completely determined until the frequencies (eigenvalues) are found. The mode shapes are generally known less accurately than the frequencies.

Virtually no one in the literature evaluates the bending stresses due to a unit amplitude of motion. This information is obviously important, particularly for fatigue studies. The lack of results is undoubtedly due to the fact that the stresses must be obtained from second derivatives of the mode shapes. Not only does this require additional computational work, but also the mode shapes usually are not known with sufficient accuracy to give meaningful results for stresses.

Frequency data were converted to the angular frequency ω (radians/unit time) or to a corresponding nondimensional frequency parameter, where possible. Almost always the number of significant figures was kept the same as that in the original publication. In no case were significant figures added. In some few cases the number of significant figures was reduced because the accuracy of the calculations in the publication did not justify the numbers given. Curves were not replotted but were photographically enlarged and traced to maximize accuracy. Quite often, when they are available, both tabular and graphical results are given for a problem. Tabular results are particularly important for measuring the accuracy of an analytical method, whereas curves are valuable for interpolation, extrapolation, and qualitative studies. In some cases many sets of results are given for the same problem.

In these cases each set was derived by a different theoretical or experimental technique; this permits a comparison of techniques.

Two of the major goals of the project were accuracy and completeness. Some of the efforts made to maintain accuracy have been described in the foregoing paragraphs. Reasonable completeness of results published through the end of the year 1965 is claimed. Writing of the manuscript began in the summer of that year. In addition to the well-known abstracting journals, several special-purpose bibliographies were used in order to procure pertinent technical papers and reports. Further references were obtained from the discussion and reference lists within those already procured. Approximately 150 letters were sent to people throughout the world who were known to be active in the field of continuum vibrations. These letters listed their publications already in hand and asked for copies of any others which they deemed applicable. Through these efforts I have come to possess a reasonably complete set of literature in the field of plate vibrations. However, in spite of this, I am convinced that some significant publications are not included, particularly some which are known to exist but have been thus far unobtainable, especially books by Soviet researchers.

In light of the preceding paragraph, I expect—indeed, hope—to receive considerable valuable criticism pointing out errors or omissions. In addition, I would appreciate receiving copies of recent or forthcoming publications and reports which are pertinent. It is my intention to write a supplement to this volume after a few years have elapsed; such a document will correct any major mistakes or omissions in this work and will report on further advances in the field.

For historical record and recognition it should be pointed out that, approximately 6 months after this project began, I discovered a notable work entitled "Free Vibrations of Plates and Shells," by V. S. Gontkevich, published (in Russian) in 1964. A subsequent complete translation into English was made under the sponsorship of the Lockheed Missiles & Space Co. This book purports to do what the present monograph does and, in addition to plates and shells, covers the fields of membranes and stiffened plates. I do not wish to criticize the work of Mr. Gontkevich. Indeed, if used with great care, his work can be used to supplement this monograph. Nevertheless, two objective comments concerning Gontkevich's work must be made for the record:

(1) The number of references on plate vibrations included is less than half of those in the present monograph.

(2) The large number of typographical mistakes made and the difficulty in interpreting the work (in either the original Russian or in the English translation) decrease its usefulness enormously.

The present monograph, sponsored by the National Aeronautics and Space Administration, is my first major undertaking in the area of continuum vibrations. It is to be continued by a 2-year project which is currently in progress and summarizes the field of vibrations of shells. I would appreciate receiving technical papers and reports related to that field from the readers of this work.

The support of the National Aeronautics and Space Administration is gratefully acknowledged. In particular, I am indebted to Mr. Douglas Michel of NASA, who not only recognized the potential value of this work, but was thinking of it before my proposal ever reached him. His technical com-

ments and advice during the course of the work were also greatly appreciated. I particularly wish to thank Messrs. Milton Vagins and S. G. Sampath, who did all the necessary work so that I could be free for the actual summarization and writing. Without their efforts in supervising the procurement of papers, in manuscript editing, and in providing technical criticism, this work would not have been possible. I wish to recognize the contributions of the project advisory panel, which consisted of Mr. Michel, Drs. Robert Fulton, W. H. Hoppmann, T. C. Huang, Eric Reissner, and Howard Wolko, who generously met with me twice during the course of the project and offered their comments. I also thank my colleagues, Drs. C. T. West and F. W. Niedenfuhr, for their technical advice. Finally, the enormous editorial assistance of Mr. Chester Ball, Mrs. Ada Simon, and Miss Doris Byrd of The Ohio State University is gratefully acknowledged.

ARTHUR W. LEISSA
The Ohio State University

Contents

CHAPTER		PAGE
1	Fundamental Equations of Classical Plate Theory	1
2	Circular Plates	7
3	Elliptical Plates	37
4	Rectangular Plates	41
5	Parallelogram Plates	161
6	Other Quadrilateral Plates	193
7	Triangular Plates	205
8	Plates of Other Shapes	237
9	Anisotropic Plates	245
10	Plates With Inplane Forces	267
11	Plates With Variable Thickness	285
12	Other Considerations	299
	Appendix—Plate Equations	331
	Author Index	341
	Subject Index	345

Chapter 1

Fundamental Equations of Classical Plate Theory

The classical differential equation of motion for the transverse displacement w of a plate is given by (see app. A):

$$D\nabla^4 w+\rho\frac{\partial^2 w}{\partial t^2}=0 \tag{1.1}$$

where D is the flexural rigidity and is defined by

$$D=\frac{Eh^3}{12(1-\nu^2)} \tag{1.2}$$

E is Young's modulus, h is the plate thickness, ν is Poisson's ratio, ρ is mass density per unit area of the plate, t is time, and $\nabla^4=\nabla^2\nabla^2$, where ∇^2 is the Laplacian operator.

When free vibrations are assumed, the motion is expressed as

$$w=W\cos\omega t \tag{1.3}$$

where ω is the circular frequency (expressed in radians/unit time) and W is a function only of the position coordinates. Substituting equation (1.3) into equation (1.1) yields

$$(\nabla^4-k^4)W=0 \tag{1.4}$$

where k is a parameter of convenience defined as

$$k^4=\frac{\rho\omega^2}{D} \tag{1.5}$$

It is usually convenient to factor equation (1.4) into

$$(\nabla^2+k^2)(\nabla^2-k^2)W=0 \tag{1.6}$$

whence, by the theory of linear differential equations, the complete solution to equation (1.6) can be obtained by superimposing the solutions to the equations

$$\left.\begin{aligned}\nabla^2W_1+k^2W_1=0\\ \nabla^2W_2-k^2W_2=0\end{aligned}\right\} \tag{1.7}$$

In the case of a plate supported by (or embedded in) a massless elastic medium (or foundation), equation (1.1) becomes

$$D\nabla^4 w+Kw+\rho\frac{\partial^2 w}{\partial t^2}=0 \tag{1.8}$$

where K is the stiffness of the foundation measured in units of force per unit length of deflection per unit area of contact. If the foundation has significant mass, then its differential equation must also be written and a coupled system of differential equations solved, which is beyond the scope of the present work.

Assuming the deflection form (eq. (1.3)) and substituting into equation (1.8) again results in equation (1.4), where now

$$k^4=\frac{\rho\omega^2-K}{D} \tag{1.9}$$

Thus, all results presented in this section as pertaining to the classical plate equation (eq. (1.1)) can also apply to the case of elastic foundations by the simple use of equation (1.9) in place of equation (1.5).

1.1 POLAR COORDINATES

The location of a point P in polar coordinates is shown in figure 1.1.

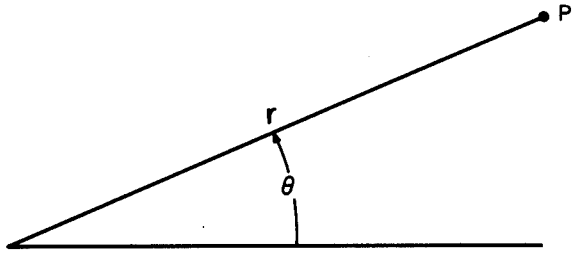


FIGURE 1.1.—Polar coordinate system.

1.1.1 Classical Equations

The Laplacian operator expressed in polar coordinates is

$$\nabla^2=\frac{\partial^2}{\partial r^2}+\frac{1}{r}\frac{\partial}{\partial r}+\frac{1}{r^2}\frac{\partial^2}{\partial\theta^2} \tag{1.10}$$

Bending and twisting moments are related to the displacements by

$$\left.\begin{aligned} M_r&=-D\left[\frac{\partial^2 w}{\partial r^2}+\nu\left(\frac{1}{r}\frac{\partial w}{\partial r}+\frac{1}{r^2}\frac{\partial^2 w}{\partial\theta^2}\right)\right]\\ M_\theta&=-D\left[\frac{1}{r}\frac{\partial w}{\partial r}+\frac{1}{r^2}\frac{\partial^2 w}{\partial\theta^2}+\nu\frac{\partial^2 w}{\partial r^2}\right]\\ M_{r\theta}&=-D(1-\nu)\frac{\partial}{\partial r}\left(\frac{1}{r}\frac{\partial w}{\partial\theta}\right)\end{aligned}\right\} \tag{1.11}$$

Transverse shearing forces are given by

$$\left.\begin{aligned} Q_r&=-D\frac{\partial}{\partial r}(\nabla^2 w)\\ Q_\theta&=-D\frac{1}{r}\frac{\partial}{\partial\theta}(\nabla^2 w)\end{aligned}\right\} \tag{1.12}$$

and the Kelvin-Kirchhoff edge reactions are

$$\left.\begin{aligned} V_r&=Q_r+\frac{1}{r}\frac{\partial M_{r\theta}}{\partial\theta}\\ V_\theta&=Q_\theta+\frac{\partial M_{r\theta}}{\partial r}\end{aligned}\right\} \tag{1.13}$$

The strain energy of bending and twisting of a plate expressed in polar coordinates is

$$U=\frac{D}{2}\int_A\left(\left(\frac{\partial^2 w}{\partial r^2}+\frac{1}{r}\frac{\partial w}{\partial r}+\frac{1}{r^2}\frac{\partial^2 w}{\partial\theta^2}\right)^2 -2(1-\nu)\left\{\frac{\partial^2 w}{\partial r^2}\left(\frac{1}{r}\frac{\partial w}{\partial r}+\frac{1}{r^2}\frac{\partial^2 w}{\partial\theta^2}\right) -\left[\frac{\partial}{\partial r}\left(\frac{1}{r}\frac{\partial w}{\partial\theta}\right)\right]^2\right\}\right)dA \tag{1.14}$$

where $dA=r\,dr\,d\theta$.

1.1.2 Solutions

When Fourier components in θ are assumed,

$$W(r,\theta)=\sum_{n=0}^{\infty}W_n(r)\cos n\theta+\sum_{n=1}^{\infty}W_n^*(r)\sin n\theta \tag{1.15}$$

substituting equation (1.15) into equation (1.7) yields

$$\left.\begin{aligned} \frac{d^2W_{n_1}}{dr^2}+\frac{1}{r}\frac{dW_{n_1}}{dr}-\left(\frac{n^2}{r^2}-k^2\right)W_{n_1}&=0\\ \frac{d^2W_{n_2}}{dr^2}+\frac{1}{r}\frac{dW_{n_2}}{dr}-\left(\frac{n^2}{r^2}+k^2\right)W_{n_2}&=0\end{aligned}\right\} \tag{1.16}$$

and two identical equations for W_n^*. Equations (1.16) are recognized as forms of Bessel's equation having solutions (cf. work of McLachlan, ref. 1.1)

$$\left.\begin{aligned} W_{n_1}&=A_nJ_n(kr)+B_nY_n(kr)\\ W_{n_2}&=C_nI_n(kr)+D_nK_n(kr)\end{aligned}\right\} \tag{1.17}$$

respectively, where J_n and Y_n are the Bessel functions of the first and second kinds, respectively, and I_n and K_n are modified Bessel functions of the first and second kinds, respectively. The coefficients $A_n, \ldots, D_n$ determine the mode shape and are solved for from the boundary conditions. Thus, the general solution to equation (1.4) in polar coordinates is

$$\begin{aligned} W(r,\theta)=&\sum_{n=0}^{\infty}[A_nJ_n(kr)+B_nY_n(kr)\\ &+C_nI_n(kr)+D_nK_n(kr)]\cos n\theta\\ &+\sum_{n=1}^{\infty}[A_n^*J_n(kr)+B_n^*Y_n(kr)\\ &+C_n^*I_n(kr)+D_n^*K_n(kr)]\sin n\theta\end{aligned} \tag{1.18}$$

1.2 ELLIPTICAL COORDINATES

Elliptical coordinates ξ, η are shown in figure 1.2 and are related to rectangular coordinates x, y by the relation

$$x+iy=c\cosh(\xi+i\eta)\qquad(i=\sqrt{-1}) \tag{1.19}$$

where $2c$ is the interfocal distance. Separating real and imaginary parts of equation (1.19) yields

$$\left.\begin{aligned} x&=c\cosh\xi\cos\eta\\ y&=c\sinh\xi\sin\eta\end{aligned}\right\} \tag{1.20}$$

1.2.1 Classical Equations

The Laplacian operator in elliptical coordinates is (refs. 1.2 to 1.4)

$$\nabla^2=\frac{2}{c^2(\cosh 2\xi-\cos 2\eta)}\left(\frac{\partial^2}{\partial\xi^2}+\frac{\partial^2}{\partial\eta^2}\right) \tag{1.21}$$

Bending and twisting moments are related to the displacements by

$$\left.\begin{aligned}
M_\xi &= -\frac{2D}{c^2(\cosh 2\xi-\cos 2\eta)}\left[\frac{\partial^2 w}{\partial \xi^2}+\nu\frac{\partial^2 w}{\partial \eta^2}-\frac{(1-\nu)\sinh 2\xi}{(\cosh 2\xi-\cos 2\eta)}\frac{\partial w}{\partial \xi}+\frac{(1-\nu)\sin 2\eta}{(\cosh 2\xi-\cos 2\eta)}\frac{\partial w}{\partial \eta}\right]\\
M_\eta &= -\frac{2D}{c^2(\cosh 2\xi-\cos 2\eta)}\left[\nu\frac{\partial^2 w}{\partial \xi^2}+\frac{\partial^2 w}{\partial \eta^2}+\frac{(1-\nu)\sinh 2\xi}{(\cosh 2\xi-\cos 2\eta)}\frac{\partial w}{\partial \xi}-\frac{(1-\nu)\sin 2\eta}{(\cosh 2\xi-\cos 2\eta)}\frac{\partial w}{\partial \eta}\right]\\
M_{\xi\eta} &= -\frac{2D(1-\nu)}{c^2(\cosh 2\xi-\cos 2\eta)^2}\left[\frac{\partial w}{\partial \xi}\sin 2\eta+\frac{\partial w}{\partial \eta}\sinh 2\xi-\frac{\partial^2 w}{\partial \xi\partial \eta}(\cosh 2\xi-\cos 2\eta)\right]
\end{aligned}\right\} \quad (1.22)$$

and the transverse shearing forces are given by (ref. 1.4)

$$\left.\begin{aligned}
Q_\xi &= \frac{2\sqrt{2}D}{c^3(\cosh 2\xi-\cos 2\eta)^{5/2}}\left[2\sinh 2\xi\left(\frac{\partial^2 w}{\partial \xi^2}+\frac{\partial^2 w}{\partial \eta^2}\right)-(\cosh 2\xi-\cos 2\eta)\frac{\partial}{\partial \xi}\left(\frac{\partial^2 w}{\partial \xi^2}+\frac{\partial^2 w}{\partial \eta^2}\right)\right]\\
Q_\eta &= \frac{2\sqrt{2}D}{c^3(\cosh 2\xi-\cos 2\eta)^{5/2}}\left[2\sin 2\eta\left(\frac{\partial^2 w}{\partial \xi^2}+\frac{\partial^2 w}{\partial \eta^2}\right)-(\cosh 2\xi-\cos 2\eta)\frac{\partial}{\partial \eta}\left(\frac{\partial^2 w}{\partial \xi^2}+\frac{\partial^2 w}{\partial \eta^2}\right)\right]
\end{aligned}\right\} \quad (1.23)$$

1.2.2 Solutions

It has been shown (ref. 1.5) that equations (1.7) have solutions composed of two parts:

$$\left.\begin{aligned}
W_1 &= \sum_{m=0}^{\infty}[C_m Ce_m(\xi,q)+F_m Fey_m(\xi,q)]ce_m(\eta,q)\\
&\quad+\sum_{m=1}^{\infty}[S_m Se_m(\xi,q)+G_m Gey_m(\xi,q)]se_m(\eta,q)\\
W_2 &= \sum_{m=0}^{\infty}[C_m^* Ce_m(\xi,-q)\\
&\quad+F_m^* Fek_m(\xi,-q)]ce_m(\eta,-q)\\
&\quad+\sum_{m=1}^{\infty}[S_m^* Se_m(\xi,-q)\\
&\quad+G_m^* Gek_m(\xi,-q)]se_m(\eta,-q)
\end{aligned}\right\} \quad (1.24)$$

where Ce_m, ce_m, Se_m, se_m, Fey_m, Fek_m, Gey_m, and Gek_m are ordinary and modified Mathieu functions of order m; C_m, C_m^*, S_m, S_m^*, F_m, F_m^*, G_m, and G_m^* are constants of integration; and

$$q=k^2=\omega\sqrt{\rho/D} \quad (1.25)$$

The complete solution to equation (1.4) is then

$$W=W_1+W_2 \quad (1.26)$$

For a solid region containing the origin, regularity conditions require that half of the terms in equations (1.24) be discarded, and the complete solution becomes:

$$\begin{aligned}
W &= \sum_{m=0}^{\infty}[C_m Ce_m(\xi,q)ce_m(\eta,q)\\
&\quad+C_m^* Ce_m(\xi,q)ce_m(\eta,-q)]\\
&\quad+\sum_{m=1}^{\infty}[S_m Se_m(\xi,q)se_m(\eta,q)\\
&\quad+S_m^* Se_m(\xi,-q)se_m(\eta,-q)]
\end{aligned} \quad (1.27)$$

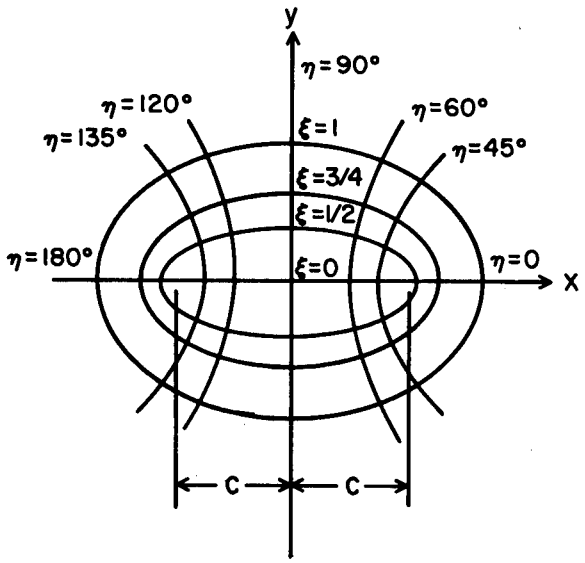


FIGURE 1.2.—Elliptical coordinate system.

1.3 RECTANGULAR COORDINATES

The rectangular coordinates of a point P are shown in figure 1.3.

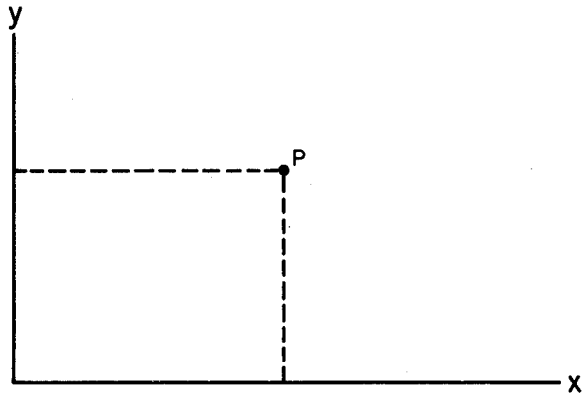


FIGURE 1.3.—Rectangular coordinate system.

1.3.1 Classical Equations

The Laplacian operator in rectangular coordinates is

$$\nabla^2=\frac{\partial^2}{\partial x^2}+\frac{\partial^2}{\partial y^2} \tag{1.28}$$

Bending and twisting moments are related to the displacements by

$$\left.\begin{aligned} M_x &= -D\left(\frac{\partial^2 w}{\partial x^2}+\nu\frac{\partial^2 w}{\partial y^2}\right)\\ M_y &= -D\left(\frac{\partial^2 w}{\partial y^2}+\nu\frac{\partial^2 w}{\partial x^2}\right)\\ M_{xy} &= -D(1-\nu)\frac{\partial^2 w}{\partial x\,\partial y}\end{aligned}\right\} \tag{1.29}$$

Transverse shearing forces are given by

$$\left.\begin{aligned} Q_x &= -D\frac{\partial}{\partial x}(\nabla^2 w)\\ Q_y &= -D\frac{\partial}{\partial y}(\nabla^2 w)\end{aligned}\right\} \tag{1.30}$$

and the Kelvin-Kirchhoff edge reactions are

$$\left.\begin{aligned} V_x &= Q_x+\frac{\partial M_{xy}}{\partial y}\\ V_y &= Q_y+\frac{\partial M_{xy}}{\partial x}\end{aligned}\right\} \tag{1.31}$$

The strain energy of bending and twisting of a plate expressed in rectangular coordinates is

$$U=\frac{D}{2}\int_A\left\{\left(\frac{\partial^2 w}{\partial x^2}+\frac{\partial^2 w}{\partial y^2}\right)^2 -2(1-\nu)\left[\frac{\partial^2 w}{\partial x^2}\frac{\partial^2 w}{\partial y^2}-\left(\frac{\partial^2 w}{\partial x\,\partial y}\right)^2\right]\right\}dA \tag{1.32}$$

where $dA=dx\,dy$.

1.3.2 Solutions

General solutions to equation (1.4) in rectangular coordinates may be obtained by assuming Fourier series in one of the variables, say x; that is,

$$W(x,y)=\sum_{m=1}^{\infty}Y_m(y)\sin\alpha x+\sum_{m=0}^{\infty}Y_m^*(y)\cos\alpha x \tag{1.33}$$

Substituting equation (1.33) into equation (1.7) yields

$$\left.\begin{aligned} \frac{d^2Y_{m_1}}{dy^2}+(k^2-\alpha^2)Y_{m_1}&=0\\ \frac{d^2Y_{m_2}}{dy^2}-(k^2+\alpha^2)Y_{m_2}&=0\end{aligned}\right\} \tag{1.34}$$

and two similar equations for Y_m^*. With the assumption that $k^2>\alpha^2$, solutions to equations (1.34) are well known as

$$\left.\begin{aligned} Y_{m_1}&=A_m\sin\sqrt{k^2-\alpha^2}y+B_m\cos\sqrt{k^2-\alpha^2}y\\ Y_{m_2}&=C_m\sinh\sqrt{k^2+\alpha^2}y+D_m\cosh\sqrt{k^2+\alpha^2}y\end{aligned}\right\} \tag{1.35}$$

where $A_m, \ldots, D_m$ are arbitrary coefficients determining the mode shape and are obtained from the boundary conditions. If $k^2<\alpha^2$, it is necessary to rewrite Y_{m_1} as

$$Y_{m_1}=A_m\sinh\sqrt{\alpha^2-k^2}y+B_m\cosh\sqrt{\alpha^2-k^2}y \tag{1.36}$$

Thus the complete solution to equation (1.4) may be written as

$$\begin{aligned} W(x,y)=\sum_{m=1}^{\infty}&(A_m\sin\sqrt{k^2-\alpha^2}y+B_m\cos\sqrt{k^2-\alpha^2}y\\ &+C_m\sinh\sqrt{k^2+\alpha^2}y\\ &+D_m\cosh\sqrt{k^2+\alpha^2}y)\sin\alpha x\\ &+\sum_{m=0}^{\infty}(A_m^*\sin\sqrt{k^2-\alpha^2}y+B_m^*\cos\sqrt{k^2-\alpha^2}y\\ &+C_m^*\sinh\sqrt{k^2+\alpha^2}y\\ &+D_m^*\cosh\sqrt{k^2+\alpha^2}y)\cos\alpha x\end{aligned} \tag{1.37}$$

1.4 SKEW COORDINATES

The skew coordinates ξ, η of a point P are shown in figure 1.4. The skew coordinates are related to rectangular coordinates by

$$\left.\begin{aligned}\xi&=x-y\tan\alpha\\ \eta&=\frac{y}{\cos\alpha}\end{aligned}\right\} \tag{1.38}$$

1.4.1 Classical Equations

The Laplacian operator in skew coordinates is (ref. 1.6)

$$\nabla^2=\frac{1}{\cos^2\alpha}\left(\frac{\partial^2}{\partial\xi^2}-2\sin\alpha\frac{\partial^2}{\partial\xi\partial\eta}+\frac{\partial^2}{\partial\eta^2}\right) \tag{1.39}$$

Bending and twisting moments are related to the displacements by

$$\left.\begin{aligned}M_\xi&=-D\left[\frac{\partial^2w}{\partial\xi^2}+\frac{\nu}{\cos^2\alpha}\left(\sin^2\alpha\frac{\partial^2w}{\partial\xi^2}-2\sin\alpha\frac{\partial^2w}{\partial\xi\partial\eta}+\frac{\partial^2w}{\partial\eta^2}\right)\right]\\ M_\eta&=-D\left[\frac{1}{\cos^2\alpha}\left(\sin^2\alpha\frac{\partial^2w}{\partial\xi^2}-2\sin\alpha\frac{\partial^2w}{\partial\xi\partial\eta}+\frac{\partial^2w}{\partial\eta^2}\right)+\nu\frac{\partial^2w}{\partial\xi^2}\right]\\ M_{\xi\eta}&=-D\frac{(1-\nu)}{\cos\alpha}\left(\frac{\partial^2w}{\partial\xi\partial\eta}-\sin\alpha\frac{\partial^2w}{\partial\xi^2}\right)\end{aligned}\right\} \tag{1.40}$$

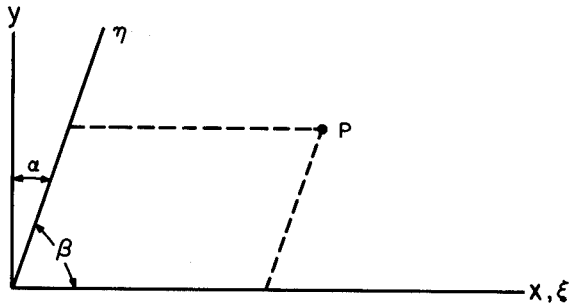


FIGURE 1.4.—Skew coordinate system.

Transverse shearing forces are (ref. 1.7):

$$\left.\begin{aligned}Q_\xi&=-\frac{D}{\sin^3\beta}\left[\frac{\partial^3w}{\partial\xi^3}-3\cos\beta\frac{\partial^3w}{\partial\xi^2\partial\eta}+(1+2\cos^2\beta)\frac{\partial^3w}{\partial\xi\partial\eta^2}-\cos\beta\frac{\partial^3w}{\partial\eta^3}\right]\\ Q_\eta&=-\frac{D}{\sin^3\beta}\left[\frac{\partial^3w}{\partial\eta^2}-3\cos\beta\frac{\partial^3w}{\partial\xi\partial\eta^2}+(1+2\cos^2\beta)\frac{\partial^3w}{\partial\xi^2\partial\eta}-\cos\beta\frac{\partial^3w}{\partial\xi^3}\right]\end{aligned}\right\} \tag{1.41}$$

where $\beta=(\pi/2)-\alpha$. The edge reactions are (ref. 1.7):

$$\left.\begin{aligned}V_\xi&=-\frac{D}{\sin^3\beta}\left[\frac{\partial^3w}{\partial\xi^3}-4\cos\beta\frac{\partial^3w}{\partial\xi^2\partial\eta}-(2+3\cos^2\beta-\nu\sin^2\beta)\frac{\partial^3w}{\partial\xi\partial\eta^2}-2\cos\beta\frac{\partial^3w}{\partial\eta^3}\right]\\ V_\eta&=-\frac{D}{\sin^3\beta}\left[\frac{\partial^3w}{\partial\eta^3}-4\cos\beta\frac{\partial^3w}{\partial\xi\partial\eta^2}-(2+3\cos^2\beta-\nu\sin^2\beta)\frac{\partial^3w}{\partial\xi^2\partial\eta}-2\cos\beta\frac{\partial^3w}{\partial\xi^3}\right]\end{aligned}\right\} \tag{1.42}$$

The strain energy of bending and twisting of a plate expressed in skew coordinates is

$$U=\frac{D}{2}\int_A\left\{\frac{1}{\cos^4\alpha}\left(\frac{\partial^2w}{\partial\xi^2}-2\frac{\partial^2w}{\partial\xi\partial\eta}+\frac{\partial^2w}{\partial\eta^2}\right)-\frac{2(1-\nu)}{\cos^2\alpha}\left[\frac{\partial^2w}{\partial\xi^2}\frac{\partial^2w}{\partial\eta^2}-\left(\frac{\partial^2w}{\partial\xi\partial\eta}\right)^2\right]\right\}dA \tag{1.43}$$

where $dA=\cos\alpha\, d\xi\, d\eta$.

1.4.2 Solutions

There are no known general solutions to equation (1.4) in skew coordinates which allow a separation of variables.

REFERENCES

1.1. McLACHLAN, N.: Bessel Functions for Engineers. Oxford Eng. Sci. Ser., Oxford Univ. Press (London), 1948.

1.2. NASH, W. A.: Bending of an Elliptical Plate by Edge Loading. J. Appl. Mech., vol. 17, no. 3, Sept. 1950, pp. 269–274.

1.3. GALERKIN, B. G.: Berechnung der frei gelagerten elliptischen Platte auf Biegung. ZAMM, Bd. 3, 1923, pp. 113–117.

1.4. CHENG, SHUN: Bending of an Elliptic Plate Under a Moment at the Center. Tech. Sum. Rept. No. 444, Math. Res. Center, Univ. Wisconsin, Dec. 1963.

1.5. MCLACHLAN, N.: Theory and Application of Mathieu Functions. Oxford Univ. Press (London), 1947.

1.6. MORLEY, L. S. D.: Skew Plates and Structures. Macmillan Co., Inc., 1963.

1.7. ÖDMAN, S. T. A.: Studies of Boundary Value Problems. Part II, Characteristic Functions of Rectangular Plates. Proc. NR 24, Swedish Cement and Concrete Res. Inst., Roy. Inst. Tech. (Stockholm), 1955, pp. 7–62.

Chapter 2

Circular Plates

2.1 SOLID CIRCULAR PLATES

When the origin of a polar coordinate system is taken to coincide with the center of the circular plate and plates having no internal holes are considered, the terms of equation (1.18) involving $Y_n(kr)$ and $K_n(kr)$ must be discarded in order to avoid infinite deflections and stresses at $r=0$. If the boundary conditions possess symmetry with respect to one or more diameters of the circle, then the terms involving sin $n\theta$ are not needed. When these simplifications are employed, equation (1.18) becomes for a typical mode:

$$W_n=[A_nJ_n(kr)+C_nI_n(kr)]\cos n\theta \quad (2.1)$$

where it will be understood in what follows that n can take on all values from 0 to ∞. The subscript n will also correspond to the number of nodal diameters.

2.1.1 Plates Clamped All Around

Let the outside radius of the plate clamped all around be a (see fig. 2.1). The boundary conditions are:

$$\left.\begin{aligned} W(a)&=0\\ \frac{\partial W(a)}{\partial r}&=0\end{aligned}\right\} \quad (2.2)$$

When equation (2.1) is substituted into equations (2.2), the existence of a nontrivial solution yields the characteristic determinant

$$\begin{vmatrix} J_n(\lambda) & I_n(\lambda)\\ J_n'(\lambda) & I_n'(\lambda)\end{vmatrix}=0 \quad (2.3)$$

where $\lambda\equiv ka$ and the primes are used to indicate differentiation with respect to the argument, in this case kr. Using the recursion relationships (ref. 2.1)

$$\left.\begin{aligned} \lambda J_n'(\lambda)&=nJ_n(\lambda)-\lambda J_{n+1}(\lambda)\\ \lambda I_n'(\lambda)&=nI_n(\lambda)+\lambda I_{n+1}(\lambda)\end{aligned}\right\} \quad (2.4)$$

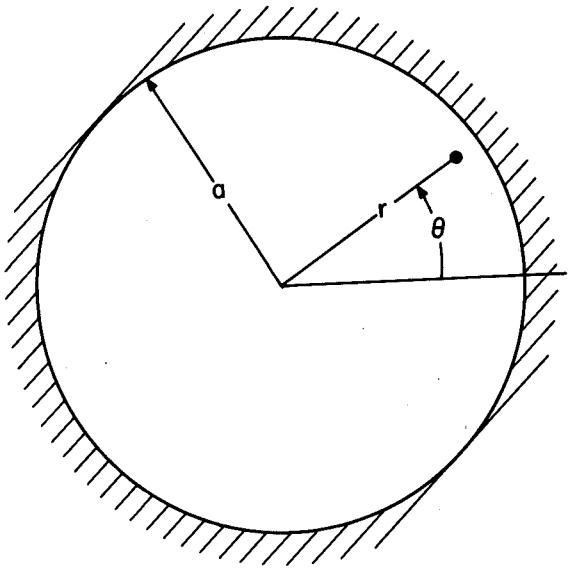


FIGURE 2.1.—Clamped circular plate.

and expanding equation (2.3) gives

$$J_n(\lambda)I_{n+1}(\lambda)+I_n(\lambda)J_{n+1}(\lambda)=0 \quad (2.5)$$

The eigenvalues λ determining the frequencies ω are the roots of equation (2.5).

The Bessel functions are widely tabulated for small values of n. The Harvard tables (ref. 2.2) are available for $n\leqq 120$. Otherwise, the recursion relationships

$$\left.\begin{aligned} J_{n+2}&=\frac{2}{\lambda}(n+1)J_{n+1}-J_n\\ I_{n+2}&=-\frac{2}{\lambda}(n+1)I_{n+1}+I_n\end{aligned}\right\} \quad (2.6)$$

or various forms of series expansions for the Bessel functions may be used.

Values of λ^2 taken from references 2.3 to 2.5 are tabulated in table 2.1, where n refers to the number of nodal diameters and s is the number of nodal circles, not including the boundary

TABLE 2.1.—*Values of* $\lambda^2=\omega a^2\sqrt{\rho/D}$ *for a Clamped Circular Plate*

s	λ^2 for values of n of—														
	0	1	2	3	4	5	6	7	8	9	10	11	12	13	14
0	10.2158	21.26	34.88	51.04	69.6659	90.7390	114.2126	140.0561	168.2445	198.7561	231.5732	266.6790	304.0601	343.7038	385.5996
1	39.771	60.82	84.58	111.01	140.1079	171.8029	206.0706	242.8782	282.1977	324.0036	368.2734				
2	89.104	120.08	153.81	190.30	229.5186	271.4283	316.0015	363.2097							
3	158.183	199.06	242.71	289.17	338.4113	390.3896									
4	247.005	297.77	351.38	407.72											
5	355.568	416.20	479.65	545.97											
6	483.872	554.37	627.75	703.95											
7	631.914	712.30	795.52	881.67											
8	799.702	889.95	983.07	1079.0											
9	987.216	1087.4	1190.4	1296.2											

circle. It is seen from equations (2.2) that the frequency does not depend upon Poisson's ratio in the clamped case. An accurate transcendental approximating equation for additional roots of equation (2.5) is given in reference 2.5.

The mode shapes of equation (2.1) are determined from either of equations (2.2). Using the first of equations (2.2)

$$\frac{A_n}{C_n}=-\frac{I_n(\lambda)}{J_n(\lambda)} \tag{2.7}$$

where the λ values are taken from table 2.1. The radii of nodal circles $\rho=r/a$ are determined from the equation

$$\frac{J_n(\lambda\rho)}{J_n(\lambda)}=\frac{I_n(\lambda\rho)}{I_n(\lambda)} \tag{2.8}$$

and are presented in table 2.2 as taken from reference 2.6.

The procedure for determining the motion of a plate subjected to arbitrary initial displacement and velocity conditions is given in reference 2.7.

The problem of finding stresses in a vibrating clamped circular plate was discussed by Ungar (ref. 2.8). The problem was also discussed in references 2.9 to 2.18.

For more information concerning this problem, see the section in the present work on in-plane forces in clamped circular plates (10.1.1).

2.1.2 Plates Simply Supported All Around

Let the outside radius of the simply supported plate be a (see fig. 2.2). The boundary conditions are

$$\left.\begin{aligned} W(a)&=0\\ M_r(a)&=0 \end{aligned}\right\} \tag{2.9}$$

Substituting equation (2.1) and equation (1.11) into equations (2.9) and noting that $\partial^2 w/\partial\theta^2=0$ on the boundary give the equations

$$\left.\begin{aligned} &A_nJ_n(\lambda)+C_nI_n(\lambda)=0\\ &A_n\left[J_n''(\lambda)+\frac{\nu}{\lambda}J_n'(\lambda)\right]+C_n\left[I_n''(\lambda)+\frac{\nu}{\lambda}I_n'(\lambda)\right]=0 \end{aligned}\right\} \tag{2.10}$$

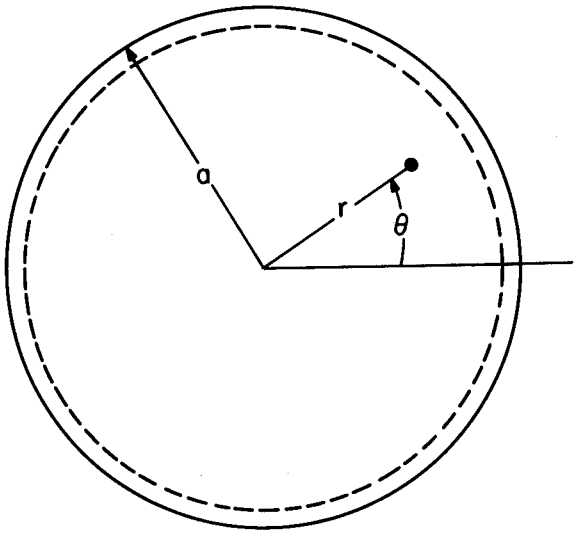


FIGURE 2.2.—Simply supported circular plate.

TABLE 2.2.—*Radii of Nodal Circles* $\rho=r/a$ *for Clamped Circular Plate*

s	ρ for values of n of—					
	0	1	2	3	4	5
1	1.0	1.0	1.0	1.0	1.0	1.0
	.379	.4899	.559	.606	.641	.669
2	1.0	1.0	1.0	1.0	1.0	1.0
	.583	.640	.679	.708	.730	.749
	.255	.350	.414	.462	.501	.532
3	1.0	1.0	1.0	1.0	1.0	1.0
	.688	.721	.746	.765	.781	.787
	.439	.497	.540	.574	.601	.618
	.191	.272	.330	.375	.412	.439
4	1.0	1.0	1.0	1.0	----	----
	.749	.767	.789	.803	----	----
	.550	.589	.620	.645	----	----
	.351	.407	.449	.488	----	----
	.153	.222	.274	.316	----	----
5	1.0	1.0	----	----	----	----
	.791	.807	----	----	----	----
	.625	.653	----	----	----	----
	.459	.499	----	----	----	----
	.293	.344	----	----	----	----
	.127	.188	----	----	----	----
6	1.0	1.0	----	----	----	----
	.822	.833	----	----	----	----
	.678	.699	----	----	----	----
	.535	.566	----	----	----	----
	.393	.432	----	----	----	----
	.251	.298	----	----	----	----
	.109	.163	----	----	----	----
7	1.0	1.0	----	----	----	----
	.844	.853	----	----	----	----
	.720	.735	----	----	----	----
	.593	.617	----	----	----	----
	.469	.499	----	----	----	----
	.344	.381	----	----	----	----
	.220	.263	----	----	----	----
	.096	.144	----	----	----	----

where the notation of the previous section is used. It has been shown (ref. 2.11) that equations (2.10) lead to the frequency equation

$$\frac{J_{n+1}(\lambda)}{J_n(\lambda)}+\frac{I_{n+1}(\lambda)}{I_n(\lambda)}=\frac{2\lambda}{1-\nu} \qquad (2.11)$$

Roots of equation (2.11) and radii of nodal circles for $\nu=0.3$ are taken from reference 2.6 and presented in tables 2.3 and 2.4, respectively. Poisson, in an early paper (ref. 2.12), and Prescott (ref. 2.11) give $\lambda=2.204$ for $\nu=0.25$. Bodine (ref. 2.19) (see section entitled "Plates

TABLE 2.3.—*Values of* $\lambda^2=\omega a^2\sqrt{\rho/D}$ *for a Simply Supported Circular Plate;* $\nu=0.3$

s	λ² for values of n of—		
	0	1	2
0	4.977	13.94	25.65
1	29.76	48.51	70.14
2	74.20	102.80	134.33
3	138.34	176.84	218.24

TABLE 2.4.—*Radii of Nodal Circles* $\rho=r/a$ *for a Simply Supported Circular Plate;* $\nu=0.3$

s	ρ for values of n of—		
	0	1	2
0	1	1	1
1	1	1	1
	.441	.550	.613
2	1	1	1
	.644	.692	.726
	.279	.378	.443
3	1	1	1
	.736	.765	.787
	.469	.528	.570
	.204	.288	.348

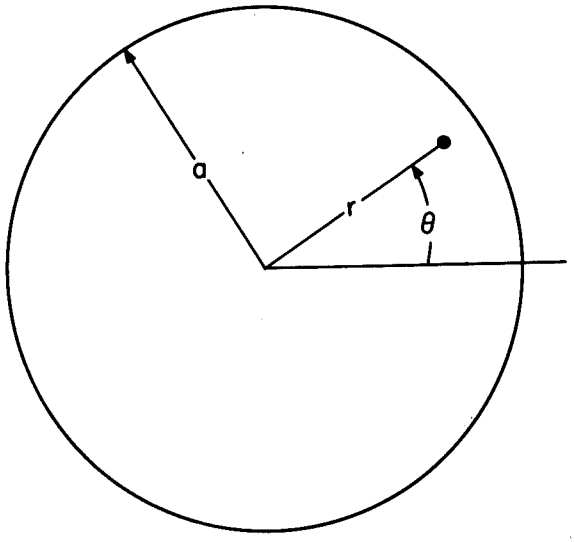


FIGURE 2.3.—Free circular plate.

Supported on Circle of Arbitrary Radius" (2.1.7)) gives $\lambda=2.228$ for $\nu=0.333$.

The mode shapes are most conveniently determined from the first of equations (2.10) by use of the roots of table 2.3; that is,

$$\frac{A_n}{C_n}=-\frac{I_n(\lambda)}{J_n(\lambda)} \tag{2.12}$$

The procedure for determining the motion of a plate subjected to arbitrary initial displacement and velocity conditions is given in reference 2.7.

The simply supported case is also solved in reference 2.20.

For more information concerning this problem, see section entitled "Simply Supported Circular Plates" (10.1.2).

2.1.3 Completely Free Plates

Let the outside radius of the completely free plate be a (see fig. 2.3). The boundary conditions are

$$\left.\begin{aligned} M_r(a)&=0\\ V_r(a)&=0 \end{aligned}\right\} \tag{2.13}$$

Using equations (1.11), (1.12), (1.13), it has been shown (ref. 2.3) that equations (2.13) yield the frequency equation

$$\frac{\lambda^2 J_n(\lambda)+(1-\nu)[\lambda J_n'(\lambda)-n^2 J_n(\lambda)]}{\lambda^2 I_n(\lambda)-(1-\nu)[\lambda I_n'(\lambda)-n^2 I_n(\lambda)]}=\frac{\lambda^3 I_n'(\lambda)+(1-\nu)n^2[\lambda J_n'(\lambda)-J_n(\lambda)]}{\lambda^3 I_n'(\lambda)-(1-\nu)n^2[\lambda I_n'(\lambda)-I_n(\lambda)]} \tag{2.14}$$

It has also been shown (ref. 2.20) that, when $\lambda>>n$, one can replace equation (2.14) by the approximate formula

$$\frac{J_n(\lambda)}{J_n'(\lambda)}\cong\frac{[\lambda^2+2(1-\nu)n^2][I_n(\lambda)/I_n'(\lambda)]-2\lambda(1-\nu)}{\lambda^2-2(1-\nu)n^2} \tag{2.15}$$

According to reference 2.20, the roots of equation (2.14) are located between the zeroes of the functions $J_n'(\lambda)$ and $J_n(\lambda)$ and the larger roots may be calculated from the series expansion

$$\lambda=\alpha-\frac{m+1}{8\alpha}-\frac{4(7m^2+22m+11)}{3(8\alpha)^3}-\cdots \tag{2.16}$$

where $m=4n^2$ and $\alpha=(\pi/2)(n+2s)$. The asymptotic value is

$$\lambda\cong\frac{\pi}{2}(n+2s) \tag{2.17}$$

Using equations (2.15) and (2.16), values of λ^2 are computed in reference 2.20 for $\nu=0.33$, and in reference 2.3, for $\nu=0.25$. These are presented in tables 2.5 and 2.6, respectively.

TABLE 2.5.—*Values of* $\lambda^2=\omega a^2\sqrt{\rho/D}$ *for a Completely Free Circular Plate;* $\nu=0.33$

s	λ^2 for values of n of—						
	0	1	2	3	4	5	6
0			5. 253	12. 23	[a] 21. 6	[a] 33. 1	[a] 46. 2
1	9. 084	20. 52	35. 25	52. 91	[a] 73. 1	[a] 95. 8	[a] 121. 0
2	38. 55	59. 86	83. 9	111. 3	142. 8	175. 0	210. 3
3	87. 80	119. 0	154. 0	192. 1	232. 3	274. 6	319. 7
4	157. 0	198. 2	242. 7	290. 7	340. 4	392. 4	447. 3
5	245. 9	296. 9	350. 8	408. 4	467. 9	529. 5	593. 9
6	354. 6	415. 3	479. 2	546. 2	615. 0	686. 4	760. 1
7	483. 1	651. 8	627. 0	703. 3	781. 8	864. 4	952. 3
8	631. 0	711. 3	794. 7	880. 3	968. 5	1061	1158. 7
9	798. 6	888. 6	981. 6	1076	1175	1277	1384
10	986. 0	1086	1188	1292	1401	1513	1631

[a] Values true within 2 percent (ref. 2.20).

TABLE 2.6.—*Values of* $\lambda^2=\omega a^2\sqrt{\rho/D}$ *for a Completely Free Circular Plate;* $\nu=0.25$

s	λ^2 for values of n of—			
	0	1	2	3
0			5. 513	12. 75
1	8. 892	20. 41	35. 28	53. 16
2	38. 34	59. 74	84. 38	112. 36
3	87. 65	118. 88	153. 29	191. 02
4	156. 73	196. 67	241. 99	289. 51
5	245. 52	296. 46	350. 48	408. 16
6	354. 08	414. 86	478. 73	545. 83
7	482. 37	553. 00	626. 75	703. 63
8	630. 41	710. 92	794. 51	881. 20
9	798. 23	888. 58	982. 01	1078. 5

The radii $\rho=r/a$ of the nodal circles may be found from reference 2.20:

$$J_n(\lambda\rho)=\frac{(1-\nu)[\lambda J_n'(\lambda)-n^2J_n(\lambda)]+\lambda^2J_n(\lambda)}{(1-\nu)\left[\lambda\dfrac{I_n'(\lambda)}{I_n(\lambda\rho)}-n^2\dfrac{I_n(\lambda)}{I_n(\lambda\rho)}\right]-\lambda^2\dfrac{I_n(\lambda)}{I_n(\lambda\rho)}} \tag{2.18}$$

Table 2.7 gives values of $\rho=r/a$ for $\nu=0.33$ computed from equation (2.18).

For large values of n and s it has been shown (ref. 2.20) that the radii of nodal circles can be computed from the approximate formula

TABLE 2.7.—*Radii of Nodal Circles* $\rho=r/a$ *for a Completely Free Circular Plate;* $\nu=0.33$

s	ρ for values of n of—					
	0	1	2	3	4	5
1	0. 680	0. 781	0. 822	0. 847	0. 863	0. 881
2	. 841	. 871	. 8897	. 925	. 926	. 993
	. 391	. 4972	. 562	. 605	. 635	. 663
3	. 893	. 932	. 936	. 939	. 943	. 947
	. 591	. 643	. 678	. 704	. 726	. 745
	. 257	. 351	. 414	. 460	. 498	. 529
4	. 941	. 946	. 950	. 951	. 955	. 958
	. 691	. 723	. 746	. 763	. 779	. 793
	. 441	. 498	. 540	. 572	. 600	. 623
	. 192	. 272	. 330	. 374	. 411	. 443
5	. 952	. 956	. 959	. 960	. 963	. 966
	. 752	. 773	. 790	. 803	. 814	. 825
	. 52	. 590	. 620	. 644	. 644	. 682
	. 352	. 407	. 449	. 483	. 512	. 536
	. 154	. 222	. 274	. 316	. 351	. 381

$$(\rho)_n^s=\frac{\lambda_n^p}{\lambda_n^s} \tag{2.19}$$

where λ_n^p is the pth root of the equation $J_n(\lambda)=0$.

Experimental results were obtained for a free circular brass plate (ref. 2.21). The ratios of frequencies of free vibration ω to the fundamental frequency ω_0 are presented in table 2.8

TABLE 2.8.—*Experimental Values of Frequency Ratios ω/ω_0 for a Completely Free Circular Brass Plate*

[Figures in parentheses have been estimated by extrapolation only or by rough measurements on a large plate 18.36 in. in diam]

Circles s	ω/ω_0 for values of n of—																								
	0	1	2	3	4	5	6	7	8	9	10	11	12	13	14	15	16	17	18	19	20	21	22	23	24
0	------	------	[a]1	2.29	4.10	6.19	8.80	11.7	15.1	18.8	23.0	27.6	33.0	38.0	44.5	51.0	58.0	65.5	74.3	83.5	90.9	100	109	118	127
1	1.70	3.99	6.79	10.3	13.8	18.1	23.1	28.6	34.7	40.8	47.5	54.7	63.0	72.5	(81)	(90)	(97)	(108)	(120)	(135)	------	------	------	------	------
2	7.51	11.7	16.1	21.2	27.1	33.4	40.5	47.7	56.0	65	75	86	100	(115)	------	------	------	------	------	------	------	------	------	------	------
3	16.4	22.7	29.4	36.3	43.0	50.5	59	69	80	90	(104)	(118)	(135)		------	------	------	------	------	------	------	------	------	------	------
4	29.1	37.0	43.2	53.1	63.0	74	86	99	(120)	(145)	------	------	------	------	------	------	------	------	------	------	------	------	------	------	------
5	47.0	56.0	66	77	92	(110)	(135)	------	------	------	------	------	------	------	------	------	------	------	------	------	------	------	------	------	------
6	72.7	83	100	(127)	(147)	------	------	------	------	------	------	------	------	------	------	------	------	------	------	------	------	------	------	------	------
7	(110)	(132)	(160)	------	------	------	------	------	------	------	------	------	------	------	------	------	------	------	------	------	------	------	------	------	------

[a] Actual frequencies of the plates 12.0 and 10.1 in. in diameter were 80.9 and 113.3 cps, respectively; t=0.0788 in.

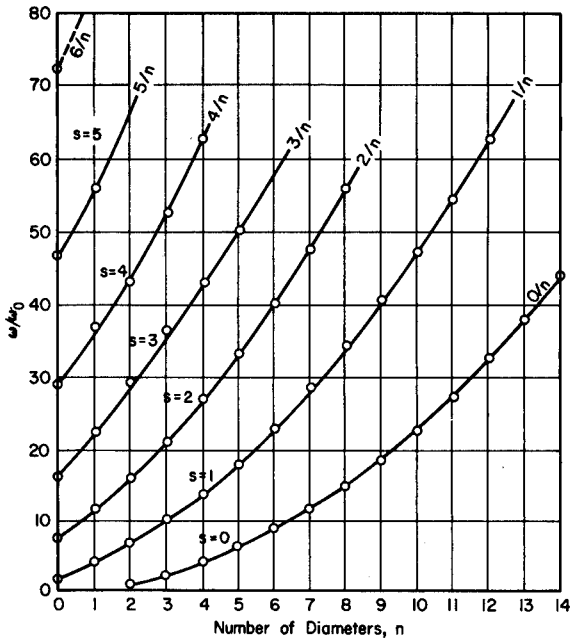


FIGURE 2.4.—Experimental values of frequency ratios ω/ω_0 for a completely free circular brass plate. (After ref. 2.21)

and figure 2.4 taken from reference 2.21. Radii of nodal circles $\rho=r/a$ are given in table 2.9. Other experimental data are presented in references 2.20 and 2.22 to 2.28. Further discussion of this problem is given in references 2.10, 2.11, 2.12, 2.15, 2.17, 2.29, 2.30, and 2.31.

2.1.4 Plates With Elastic Edge Supports

Consider a circular plate of radius a supported elastically by springs uniformly distributed about its contour as shown in figure 2.5. Translation in the direction of w is opposed by springs having distributed stiffness K_w (force/(unit length)^2). Edge rotation ψ is opposed by spiral springs having distributed stiffness K_ψ (moment/unit length).

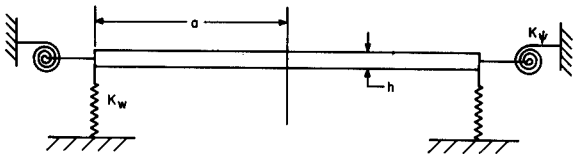


FIGURE 2.5.—Elastically supported circular plate.

TABLE 2.9.—*Experimentally Determined Radii of Nodal Circles* ρ=r/a *for a Completely Free Circular Brass Plate*

Circles s	ρ for values of n of—											
	0	1	2	3	4	5	6	7	8	9	10	11
1	0. 680	0. 781	0. 823	0. 843	0. 859	0. 871	0. 880	0. 889	0. 897	0. 903	0. 909	0. 912
2	. 391	. 497	. 562	. 604	. 635	. 662	. 681	. 702	. 715	-------	-------	------
	. 843	. 867	. 887	. 898	. 906	. 915	. 922	. 927	. 932	-------	-------	------
3	. 257	. 349	. 415	. 461	. 505	. 531	-------	-------	-------	-------	-------	------
	. 591	. 643	. 681	. 706	. 728	. 745	-------	-------	-------	-------	-------	------
	. 895	. 902	. 913	. 919	. 925	. 933	-------	-------	-------	-------	-------	------
4	. 190	. 269	. 328	. 374	. 411	. 443	-------	-------	-------	-------	-------	------
	. 441	. 495	. 540	. 571	. 596	. 623	-------	-------	-------	-------	-------	------
	. 692	. 726	. 748	. 764	. 779	. 794	-------	-------	-------	-------	-------	------
	. 918	. 928	. 934	. 938	. 941	. 944	-------	-------	-------	-------	-------	------
5	. 154	-------	-------	-------	-------	-------	-------	-------	-------	-------	-------	------
	. 351	-------	-------	-------	-------	-------	-------	-------	-------	-------	-------	------
	. 548	-------	-------	-------	-------	-------	-------	-------	-------	-------	-------	------
	. 753	-------	-------	-------	-------	-------	-------	-------	-------	-------	-------	------
	. 956	-------	-------	-------	-------	-------	-------	-------	-------	-------	-------	------
6	. 131	-------	-------	-------	-------	-------	-------	-------	-------	-------	-------	------
	. 292	-------	-------	-------	-------	-------	-------	-------	-------	-------	-------	------
	. 456	-------	-------	-------	-------	-------	-------	-------	-------	-------	-------	------
	. 624	-------	-------	-------	-------	-------	-------	-------	-------	-------	-------	------
	. 794	-------	-------	-------	-------	-------	-------	-------	-------	-------	-------	------
	. 958	-------	-------	-------	-------	-------	-------	-------	-------	-------	-------	------

The boundary conditions are

$$\left.\begin{aligned} M_r(a,\theta)&=K_\psi \frac{\partial w}{\partial r}(a,\theta) \\ V_r(a,\theta)&=-K_w W(a,\theta) \end{aligned}\right\} \qquad (2.20)$$

Substituting equation (2.1) into equations (2.20) and using recursion formulas of the type of equations (2.4) and (2.6), it can be shown that equations (2.20) become

$$\begin{aligned} A_n\Big\{ &[J_{n+2}(\lambda)+J_{n-2}(\lambda)] \\ &-\frac{2}{\lambda}\left(\nu+\frac{K_\psi a}{D}\right)[J_{n+1}(\lambda)-J_{n-1}(\lambda)] \\ &-\left(2+\frac{4\nu n^2}{\lambda^2}\right)J_n(\lambda)\Big\} \\ &+B_n\Big\{[I_{n+2}(\lambda)+I_{n-2}(\lambda)] \\ &+\frac{2}{\lambda}\left(\nu+\frac{K_\psi a}{D}\right)[I_{n+1}(\lambda)+I_{n-1}(\lambda)] \\ &+\left(2-\frac{4\nu n^2}{\lambda^2}\right)I_n(\lambda)\Big\}=0 \end{aligned} \qquad (2.21)$$

and

$$\begin{aligned} A_n\Big\{ &-[J_{n+3}(\lambda)-J_{n-3}(\lambda)]+\frac{2}{\lambda}[J_{n+2}(\lambda)+J_{n+1}(\lambda)] \\ &+\left[3+\frac{4}{\lambda^2}+\frac{4(2-\nu)n^2}{\lambda^2}\right][J_{n+1}(\lambda)-J_{n-1}(\lambda)] \\ &+\frac{4}{\lambda^3}\left[2(3-\nu)n^2-\lambda^2-\frac{2K_w a^2}{D}\right]J_n(\lambda)\Big\} \\ &+B_n\Big\{[I_{n+3}(\lambda)+I_{n-3}(\lambda)] \\ &+\frac{2}{\lambda}[I_{n+2}(\lambda)+I_{n-2}(\lambda)] \\ &+\left[3-\frac{4}{\lambda^2}-\frac{4(2-\nu)n^2}{\lambda^2}\right][I_{n+1}(\lambda)+I_{n-1}(\lambda)] \\ &+\frac{4}{\lambda^3}2(2-3\nu)n^2+\lambda^2-\frac{2K_w a^2}{D}\Big\}I_n(\lambda)=0 \end{aligned} \qquad (2.22)$$

Formulation of the second-order characteristic determinant for the frequencies from equations (2.21) and (2.22) is a trivial operation. In the case $n=0$, the frequency equation simplifies to

$$\frac{J_0(\lambda)+p\,J_1(\lambda)}{J_1(\lambda)-q\,J_0(\lambda)}=-\frac{I_0+pI_1(\lambda)}{I_1-qI_0(\lambda)} \qquad (2.23)$$

where

$$\lambda p\equiv\frac{K_\psi a}{D}-(1-\nu)$$

and

$$\lambda^3 q=\frac{K_w a^3}{D}$$

The problem was formulated in a similar manner in reference 2.32 for the special case when only an elastic moment edge constraint is allowed; that is, the boundary conditions are

$$\left.\begin{aligned} M_r(a,\theta)&=K_\psi \frac{\partial W}{\partial r}(a,\theta) \\ W(a,\theta)&=0 \end{aligned}\right\} \qquad (2.24)$$

This case is obtained by setting $K_w=\infty$ in equation (2.22). Numerical results for the first four frequencies for equations (2.24) for varying amounts of rotational constraint are given in table 2.10. Poisson's ratio is not given in reference 2.32, but it appears to be 0.3 for table 2.10.

TABLE 2.10.—*Values of* $\lambda^2=\omega a^2\sqrt{\rho/D}$ *for a Circular Plate With No Edge Deflections and Elastic Moment Constraint;* $\nu=0.3$

$\frac{K_\psi D}{a}$	λ^2 for values of n of—			
	0		1	2
	$s=0$	$s=1$		
$\to\infty$	10.2	39.7	21.2	34.8
10^0	10.2	39.7	21.2	34.8
10^{-1}	10.0	39.1	20.9	34.2
10^{-2}	8.76	35.2	18.6	30.8
10^{-3}	6.05	30.8	15.0	26.7
$\to 0$	4.93	29.7	13.9	25.6

2.1.5 Plates Clamped Along Part of Boundary and Simply Supported Along Remainder

Figure 2.6 shows a circular plate which is clamped along its edge for the interval $-\gamma<\theta<\gamma$ and simply supported on $\gamma<\theta<2\pi-\gamma$. This problem was solved by Bartlett (ref. 2.33) by an interesting variational approach to give

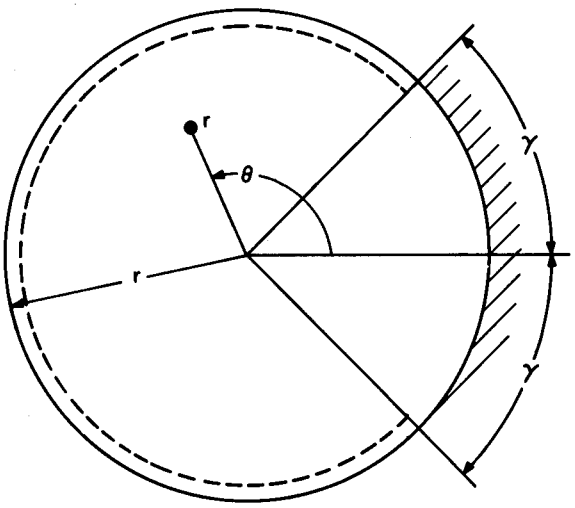


FIGURE 2.6.—Circular plate partially clamped and partially simply supported.

upper and lower bounds for the eigenvalues. The method is based upon two perturbations. One is a perturbation of the problem when the plate is clamped all around ($\gamma=\pi$) and yields upper bounds for λ; the other is a perturbation of the simply supported case ($\gamma=0$) and yields lower bounds. Upper and lower bounds for λ^2 for the case $\nu=1/4$ are presented in table 2.11 as taken from reference 2.33.

An approximate solution to this problem was given by Noble (ref. 2.34), who showed that a good approximation of the frequency parameter λ is given by the roots of the equation

$$2\lambda\left[\frac{J_1(\lambda)}{J_0(\lambda)}+\frac{I_1(\lambda)}{I_0(\lambda)}\right]^{-1}=(1-\nu)+\frac{1}{\ln(\sin\gamma/2)} \tag{2.25}$$

A comparison of the values of λ obtained from equation (2.25) and the more accurate results of reference 2.33 is given in figure 2.7.

This problem was also discussed in references

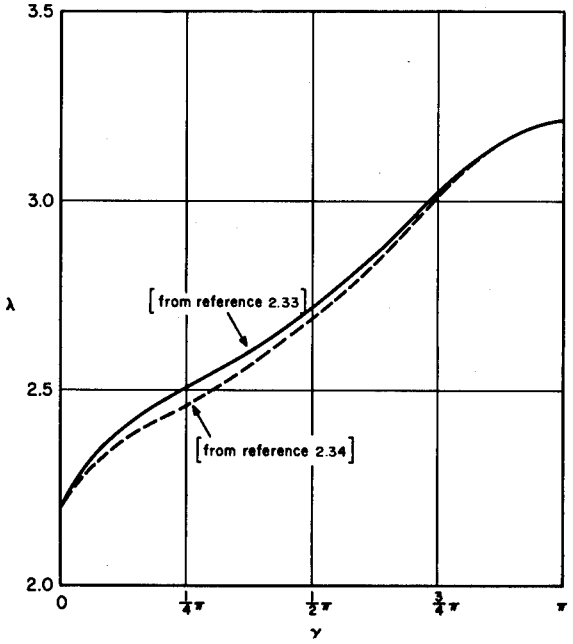


FIGURE 2.7.—Comparison of frequency parameters obtained by two methods for a circular plate with mixed boundary conditions; $\nu=1/4$. (After ref. 2.34)

2.35 and 2.36 wherein a method superimposing concentrated moments along parts of the boundary to be clamped was proposed. A numerical solution $\lambda=(\rho\omega^2/D)^{1/4}a=3.98$ is given for the case when one-fourth of the boundary is clamped, but this is clearly erroneous because it is greater than the value for a completely clamped plate.

2.1.6 Plates Clamped at Center With Various Conditions on Contour

In the case of plates clamped at the center that have various conditions on contour, it is obvious that for two or more nodal diameters ($n\geqq 2$) the resultant frequencies and mode

TABLE 2.11.—*Values of* $\lambda^2=\omega a^2\sqrt{\rho/D}$ *for a Circular Plate Clamped Along the Boundary Through an Angle* 2γ *and Simply Supported Along the Rest of the Boundary;* $\nu=1/4$

Bound	λ^2 for values of γ of—								
	0	$\pi/8$	$2\pi/8$	$3\pi/8$	$4\pi/8$	$5\pi/8$	$6\pi/8$	$7\pi/8$	π
Upper	-------	5. 871	6. 350	6. 880	7. 508	8. 231	9. 120	9. 885	10. 21
Lower	4. 862	5. 842	6. 335	6. 864	7. 480	8. 162	8. 880	9. 126	-------

shapes are identical to those obtained in the previous sections when no constraint was applied at the center. This can be seen because at the intersection of two node lines the slopes in all directions, as well as the deflection, are zero.

Southwell (ref. 2.37) discussed the problem of a free disk clamped at the center as a special case of an annulus free on the outside and clamped on the inner edge (see section entitled "Annular Plates Free on Outside and Clamped on Inside" (2.2.7)). It is necessary to evaluate the fourth-order characteristic determinant by a careful limit process as the inner radius approaches zero. He showed that in the case of one nodal diameter ($n=1$) the set of frequencies is identical to those for the completely free plate. For the axisymmetric case ($n=0$), the first four roots for $\nu=0.3$ are given as:

$$\lambda^2=\omega a^2\sqrt{\rho/D}=3.752$$
$$=20.91$$
$$=60.68$$
$$=119.7$$

Colwell and Hardy (ref. 2.20) showed that the frequency equation for the axisymmetric case can be approximated accurately by

$$\frac{EJ_0(\lambda)-Y_0(\lambda)}{EJ_1(\lambda)-Y_1(\lambda)}=\frac{2(1-\nu)}{\lambda}-\frac{I_0(\lambda)}{I_1(\lambda)} \quad (2.26)$$

where $E=(\ln 2)-$Euler's constant$=0.11593$. The first 11 roots of equation (2.26) for $\nu=1/3$ are given in table 2.12. It is seen that higher roots of λ are separated by π.

The equation determining nodal radii $\rho=r/a$ is (ref. 2.20)

$$EJ_0(\lambda\rho)=Y_0(\lambda\rho) \quad (2.27)$$

and has roots given in table 2.13 for $\nu=1/3$.

Reference 2.11 gives $\omega a^2\sqrt{\rho/D}=3.717$ for $\nu=0.25$.

The axisymmetric cases for the plates having simply supported or clamped edges in addition to a point support at the center are discussed in reference 2.38. The frequency equation for the simply supported plate becomes

$$(1-\nu)\left\{[I_0(\lambda)-J_0(\lambda)]\left[Y_1(\lambda)+\frac{2}{\pi}K_1(\lambda)\right]+[J_1(\lambda)+I_1(\lambda)]\left[Y_0(\lambda)+\frac{2}{\pi}K_0(\lambda)\right]\right\}$$
$$-2\lambda\left[I_0(\lambda)Y_0(\lambda)+\frac{2}{\pi}J_0(\lambda)K_0(\lambda)\right]=0 \quad (2.28)$$

which has as its first two roots (ν is not given, but apparently is 0.3):

$$\lambda^2=14.8$$
$$=49.4$$

TABLE 2.12.—*Values of* $\lambda^2=\omega a^2\sqrt{\rho/D}$ *for Axisymmetric Vibrations of a Free Circular Plate Fixed at the Center;* $\nu=1/3$

s	0	1	2	3	4	5	6	7	8	9	10
λ^2_____	3. 752	20. 91	61. 2	120. 6	199. 9	298. 2	416. 6	555. 1	712. 9	890. 4	1088

TABLE 2.13.—*Roots for Determining Relative Radii* $\rho=r/a$ *for a Free Circular Plate Fixed at the Center;* $\nu=1/3$

[Values of ρ are determined by dividing each of successive roots by value of λ of desired mode]

s	1	2	3	4	5	6	7	8	9	10
$\lambda\rho$_____	3. 97	7. 08	10. 20	13. 33	16. 49	19. 61	22. 75	25. 90	29. 04	32. 18

The frequency equation for the clamped plate is

$$[J_0(\lambda)-I_0(\lambda)]\left[Y_1(\lambda)+\frac{2}{\pi}K_1(\lambda)\right] -[J_1(\lambda)+I_1(\lambda)]\left[Y_0(\lambda)+\frac{2}{\pi}K_0(\lambda)\right]=0 \quad (2.29)$$

which has as its first two roots:

$$\lambda^2=22.7$$
$$=61.9$$

2.1.7 Plates Supported on Circle of Arbitrary Radius

A circular plate having a free outside edge of radius a is supported on a concentric ring having a radius b as shown in figure 2.8. The solution of this problem is very straightforward. One can recognize symmetry and take

$$W_{n_i}=A_{n_i}J_n(kr)+B_{n_i}Y_n(kr)+C_{n_i}I_n(kr) +D_{n_i}K_n(kr) \qquad (i=1,2) \quad (2.30)$$

from equation (1.18), where the subscript 1 refers to the region $0<r<b$ and the subscript 2 refers to $b<r<a$; B_{n_1} and D_{n_1} are discarded to satisfy regularity conditions at $r=0$. The remaining six boundary and continuity conditions

$$\left.\begin{aligned} &w_1(b)=w_2(b)=0\\ &\frac{\partial w_1(b)}{\partial r}=\frac{\partial w_2(b)}{\partial r}\\ &\frac{\partial^2 w_1(b)}{\partial r^2}=\frac{\partial^2 w_2(b)}{\partial r^2}\\ &M_{r_2}(a)=V_{r_2}(a)=0 \end{aligned}\right\} \quad (2.31)$$

are satisfied by substituting equation (2.30) into equations (2.31) and forming a sixth-order characteristic determinant equation. The roots of the determinant are found by evaluating it by computer for many values of λ for a given b/a ratio.

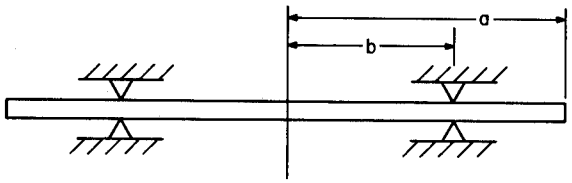


FIGURE 2.8.—Circular plate supported on a concentric circle.

The numerical solution of this problem is reported in reference 2.19 for the fundamental mode. The frequency parameter λ^2 is plotted in figure 2.9 and mode shapes for three representative b/a ratios are shown in figure 2.10, both for $\nu=1/3$.

2.1.8 Plates With Concentrated Mass at Center

The problems of free and clamped circular plates having a concentrated mass m at the center were solved by Roberson (refs. 2.39 and 2.40) for the case of axisymmetric modes. The concentrated mass was treated as an impulse in the mass density function. The impulsive change in density makes it convenient to solve the problem by Laplace transform methods.

In the case of the plate having free edges, it is shown (ref. 2.39) that the frequency equation takes the form

$$\frac{\phi_3}{\lambda^2(\phi_1+\phi_2)}=\frac{\mu}{4} \quad (2.32)$$

where

$$\left.\begin{aligned} \phi_1(\lambda)&=\frac{\pi}{2}\left[Y_1(\lambda)I_0(\lambda)+Y_0(\lambda)I_1(\lambda) -\frac{2}{\lambda}(1-\nu)Y_1(\lambda)I_1(\lambda)\right]-\frac{1}{\lambda}\\ \phi_2(\lambda)&=\left[J_1(\lambda)K_0(\lambda)-J_0(\lambda)K_1(\lambda) +\frac{2}{\lambda}(1-\nu)J_1(\lambda)I_1(\lambda)\right]-\frac{1}{\lambda}\\ \phi_3(\lambda)&=\left[J_0(\lambda)I_1(\lambda)+J_1(\lambda)I_0(\lambda) -\frac{2}{\lambda}(1-\nu)J_1(\lambda)I_1(\lambda)\right] \end{aligned}\right\} \quad (2.33)$$

and μ is the ratio of the concentrated mass at the center to the mass of the plate; that is,

$$\mu=\frac{m}{\pi\rho a^2} \quad (2.34)$$

The first four roots of equation (2.32) are shown graphically in figure 2.11 (for $\nu=0.3$) as functions of the mass ratio μ. An asymptotic-

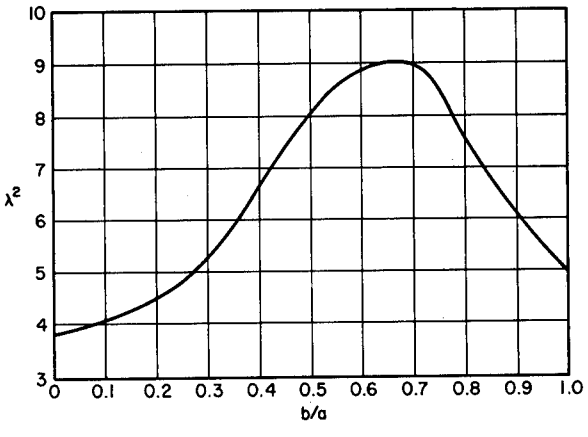


FIGURE 2.9.—Values of $\lambda^2=\omega a^2\sqrt{\rho/D}$ for a circular plate of radius a supported on a concentric circle of radius b (for fundamental mode); $\nu=1/3$. (After ref. 2.19)

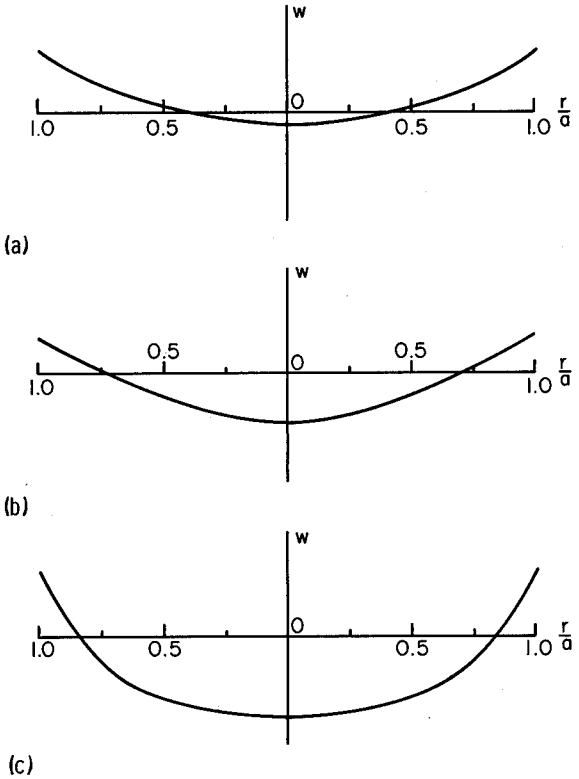


FIGURE 2.10.—Fundamental mode shapes for a circular plate supported on a concentric circle; $\nu=1/3$. (a) $b/a=0.392$; $\lambda^2=6.502$. (b) $b/a=0.699$; $\lambda^2=9.024$. (c) $b/a=0.814$; $\lambda^2=7.301$. (After ref. 2.19)

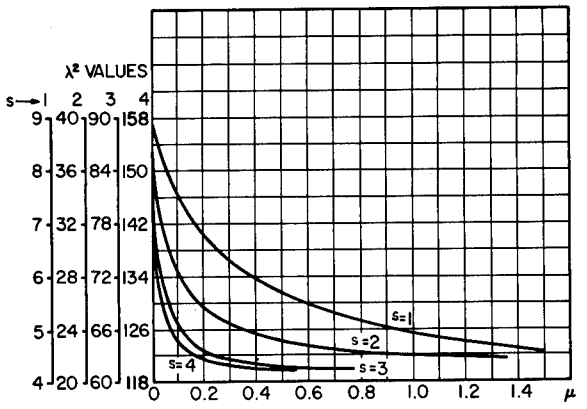


FIGURE 2.11.—Values of $\lambda^2=\omega a^2\sqrt{\rho/D}$ for various mass ratios for a free circular plate having a concentrated mass at the center; $\nu=0.3$. (After ref. 2.39)

expansion estimate of the higher roots for the above problem can be obtained from the frequency equation

$$\tan\lambda=-\left(\frac{\pi\mu}{8}\right)\lambda^2 \tag{2.35}$$

The accuracy of equation (2.35) is shown by table 2.14 for the extreme mass ratios of $\mu=\infty$ and $\mu=0$. The first mode shape is shown in figure 2.12 for three values of mass ratio.

For the clamped plate (ref. 2.40) the frequency equation is also given by equation (2.32) where, in this case,

$$\left.\begin{aligned}\phi_1(\lambda)&=\frac{\pi}{2}[I_1(\lambda)Y_0(\lambda)+I_0(\lambda)Y_1(\lambda)]+\frac{1}{\lambda}\\ \phi_2(\lambda)&=J_1(\lambda)K_0(\lambda)-J_0(\lambda)K_1(\lambda)+\frac{1}{\lambda}\\ \phi_3(\lambda)&=I_0(\lambda)J_1(\lambda)+I_1(\lambda)J_0(\lambda)\end{aligned}\right\} \tag{2.36}$$

The first four roots of equation (2.32) are shown graphically in figure 2.13 as functions of the mass ratio μ. It is noted that in the case of clamped edges the frequencies are independent of Poisson's ratio. More precise values of λ^2 for $\mu=0$, 0.05, and 0.10 are given in table 2.15.

It should be noted that for both types of edge conditions (free or clamped) the frequency changes rapidly with the addition of a small amount of mass at the center, particularly for the higher modes.

TABLE 2.14.—*Comparison of Roots λ^2 From Asymptotic-Expansion Estimate With Exact Values; $\nu=0.3$*

s	λ^2 for values of μ of—					
	∞			0		
	Value from eq. (2.32)	Estimate from eq. (2.35) $[(2s-1)(\pi/2)]^2$	Error of estimate, percent	Value from eq. (2.32)	Estimate from eq. (2.35) $(s\pi)^2$	Error of estimate, percent
1	3.73	2.47	−33.8	9.006	9.87	9.6
2	20.9	22.20	6.2	38.44	39.48	2.7
3	60.5	61.69	1.9	87.76	88.83	1.2
4	119.7	120.91	1.0	156.75	157.90	.7
5		199.85			246.74	
6		298.56			355.32	
7		416.98			483.60	

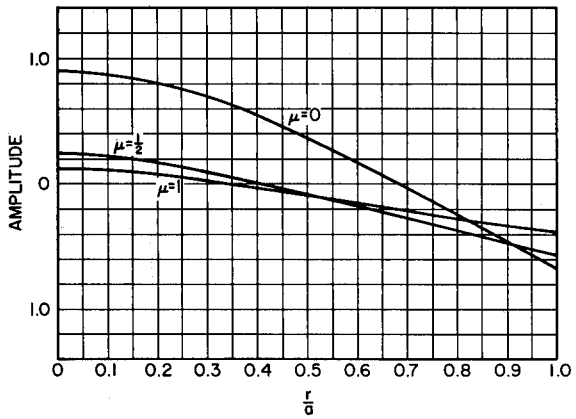


FIGURE 2.12.—First mode shape for a free plate having a concentrated mass at its center; $\nu=0.3$. (After ref. 2.39)

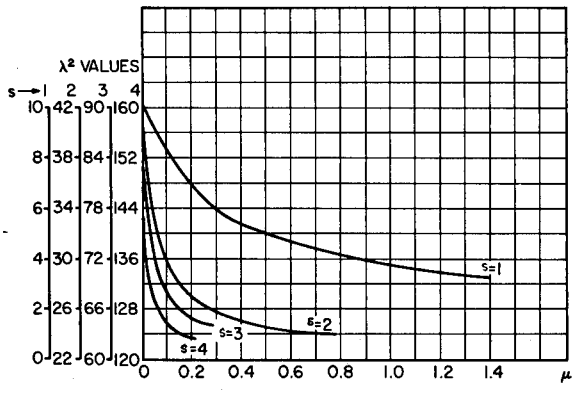


FIGURE 2.13.—Values of $\lambda^2=\omega a^2\sqrt{\rho/D}$ for various mass ratios for a clamped circular plate having a concentrated mass at the center. (After ref. 2.40)

TABLE 2.15.—*Precise Values of $\lambda^2=\omega a^2\sqrt{\rho/D}$ for a Clamped Circular Plate Having a Concentrated Mass at the Center*

s	λ^2 for values of μ of—		
	0	0.05	0.10
1	10.214	9.0120	8.1111
2	39.766	32.833	29.681
3	89.114	72.012	67.733
4	158.18	129.39	125.69

The clamped case having a general concentrated impedance at the center was discussed in reference 2.41, though no numerical results were presented therein.

2.2 ANNULAR PLATES

An annular plate consists of a circular outer boundary and a concentric circular inner boundary. Throughout this work the radii a and b will define the outer and inner boundaries, respectively.

There exist nine possible combinations of simple boundary conditions (i.e., clamped, simply supported, or free) for the two boundaries. An outstanding set of results was given by Raju (ref. 2.42) for all nine combinations of boundary conditions for a Poisson's ratio of 1/3, and the results which follow draw heavily from his work.

Joga-Rao and Pickett (ref. 2.43) also evaluated the exact characteristic determinants in the axisymmetric case when the outside boundary is clamped, simply supported, or free and the inside boundary is free. Their results closely match those of Raju and will not be repeated here. They also analyzed these cases for $a/b=0.5$ by the Rayleigh-Ritz method and obtained confirming results.

Two-term Rayleigh-Ritz solutions were used in reference 2.44 to obtain approximate axisymmetric frequency parameters for all but the free-free cases. These results are summarized in table 2.16 for $\nu=1/3$ and are compared with exact solutions. The b/a ratio is 0.5 throughout the table.

Sakharov (ref. 2.45) solved the cases for plates with the outside clamped or simply supported and the inside free, and Gontkevich (ref. 2.6) presented results for four additional cases but omitted those for the simply supported inside boundary. Vogel and Skinner (ref. 2.46) in a recent paper also obtained exact solutions for all nine cases.

In addition, Southwell (ref. 2.37) presented results for the outside-free, inside-clamped case; Hort and Koenig (ref. 2.47) and Kumai (ref. 2.48) gave theoretical and experimental results for annular plates of given dimensions; reference 2.47 deals with the free-free case and reference 2.48, with the case for both edges either clamped or simply supported.

2.2.1 Annular Plates Clamped on Outside and Inside

Substituting the complete solution (eq. (1.18)) for the cos $n\theta$ terms into the boundary conditions $W=\mathrm{d}W/\mathrm{d}r=0$ at $r=a$ and $r=b$ yields four homogeneous equations in A_n, B_n, C_n, and D_n for which a nontrivial solution can exist only if the determinant of coefficients is zero. Using recursion relationships of the types in equations (2.4) and equations (2.6), derivatives of the Bessel functions can be expressed in terms of functions of the zeroth and first orders. The frequency determinants for $n=0$ (axisymmetric), $n=1$ (one diametral node), and $n=2$ (two diametral nodes) are given below (ref. 2.6).

TABLE 2.16.—*Axisymmetric Frequency Parameters for Annular Plates;* $\nu=1/3$; b/a=0.5

Boundary conditions [a]		Deflection function $W(r)$	$\omega a^2\sqrt{\rho/D}$	
$r=a$	$r=b$		Exact solution	Rayleigh-Ritz solution
C	C	$A[1-(r/b)^2]^2[1-(r/a)^2]\ln(r/a)+B[1-(r/b)^2]^2[1-(r/a)^2]^2$	89.30	89.42
C	SS	$A[1-(r/b)^2][1-(r/a)^2]\ln(r/a)+B[1-(r/b)^2][1-(r/a)^2]^2$	64.06	65.17
C	F	$A[1-(r/a)^2]\ln(r/a)+B[1-(r/a)^2]^2$	17.51	17.56
SS	C	$A[1-(r/b)^2]^2\ln(r/a)+B[1-(r/b)^2]^2[1-(r/a)^2]$	59.91	61.81
SS	SS	$A[1-(r/b)^2]\ln(r/a)+B[1-(r/b)^2][1-(r/a)^2]$	40.01	43.19
SS	F	$A\ln(r/a)+B[1-(r/a)^2]+C(r/a)^2[1-(r/a)^2]$	5.040	5.062
F	C	$A[1-(r/b)^2]\ln(r/b)+B[1-(r/b)^2]^2$	13.05	13.59
F	SS	$A\ln(r/b)+B[1-(r/b)^2]+C(r/a)^2[1-(r/b)^2]$	4.060	4.084

[a] C, clamped; SS, simply supported; F, free.

For $n=0$,

$$\begin{vmatrix} J_0(\lambda) & Y_0(\lambda) & I_0(\lambda) & K_0(\lambda) \\ J_1(\lambda) & Y_1(\lambda) & -I_1(\lambda) & K_1(\lambda) \\ J_0(\alpha\lambda) & Y_0(\alpha\lambda) & I_0(\alpha\lambda) & K_0(\alpha\lambda) \\ J_1(\alpha\lambda) & Y_1(\alpha\lambda) & -I_1(\alpha\lambda) & K_1(\alpha\lambda) \end{vmatrix} = 0$$

where $\alpha=b/a$.

For $n=1$,

$$\begin{vmatrix} J_1(\lambda) & Y_1(\lambda) & I_1(\lambda) & K_1(\lambda) \\ J_0(\lambda) & Y_0(\lambda) & I_0(\lambda) & -K_0(\lambda) \\ J_1(\alpha\lambda) & Y_1(\alpha\lambda) & I_1(\alpha\lambda) & K_1(\alpha\lambda) \\ J_0(\alpha\lambda) & Y_0(\alpha\lambda) & I_0(\alpha\lambda) & -K_0(\alpha\lambda) \end{vmatrix} = 0$$

For $n=2$,

$$\begin{vmatrix} J_0(\lambda) & Y_0(\lambda) & -I_0(\lambda)+\frac{4}{\lambda}I_1(\lambda) & -K_0(\lambda)-\frac{4}{\lambda}K_1(\lambda) \\ J_1(\lambda) & Y_1(\lambda) & I_1(\lambda) & -K_1(\lambda) \\ J_0(\alpha\lambda) & Y_0(\alpha\lambda) & -I_0(\alpha\lambda)+\frac{4}{\alpha\lambda}I_1(\alpha\lambda) & -K_0(\alpha\lambda)-\frac{4}{\alpha\lambda}K_1(\alpha\lambda) \\ J_1(\alpha\lambda) & Y_1(\alpha\lambda) & I_1(\alpha\lambda) & -K_1(\alpha\lambda) \end{vmatrix} = 0$$

Fundamental roots for these three frequency equations are given in table 2.17.

TABLE 2.17.—*Values of* $\lambda^2=\omega a^2\sqrt{\rho/D}$ *for a Clamped, Clamped Annulus*

n	λ^2 for values of b/a of—					
	0.1	0.2	0.3	0.4	0.5	0.6
0	27.25	----------	45.36	62.33	89.30	----------
1	28.84	36.23	----------	62.92	----------	108.16
2	36.609	41.796	----------	66.406	----------	123.766

These results are plotted in figure 2.14, along with the eigenvalues for the second mode of $n=0$ taken from reference 2.6. Extrapolations are shown as dashed lines as they were proposed in reference 2.42. Note that for $b/a=0$ accurate values are given in the section entitled "Plates Clamped at Center With Various Conditions on Contour" (2.1.6).

A more comprehensive set of results is given in table 2.18 (see ref. 2.46).

Theoretical and experimental results for $0 \leqq b/a \leqq 0.5$ are given for the first three mode shapes in reference 2.48. Additional information is given in table 2.16.

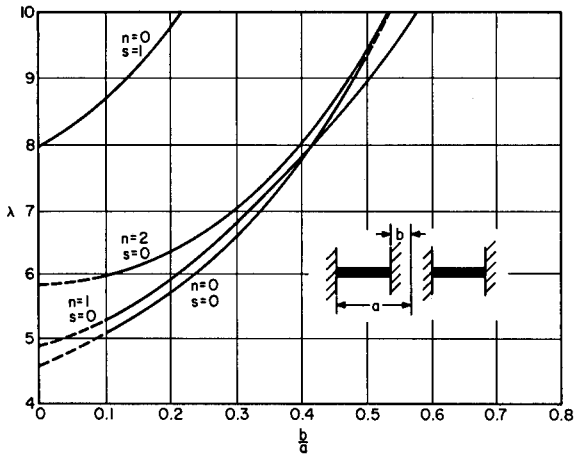


FIGURE 2.14.—Values of $\lambda=(\rho\omega^2/D)^{1/4}a$ for a clamped, clamped annulus. (After refs. 2.6 and 2.42)

2.2.2 Annular Plates Clamped on Outside and Simply Supported on Inside

The case of plates clamped on the outside and simply supported on the inside is not discussed in reference 2.6. Fundamental eigenvalues from reference 2.42 are given in table 2.19 and are plotted in figure 2.15. Accurate values for $b/a=0$ are given in the section entitled "Plates Clamped at Center With Various Conditions on Contour" (2.1.6). Additional information is given in table 2.16.

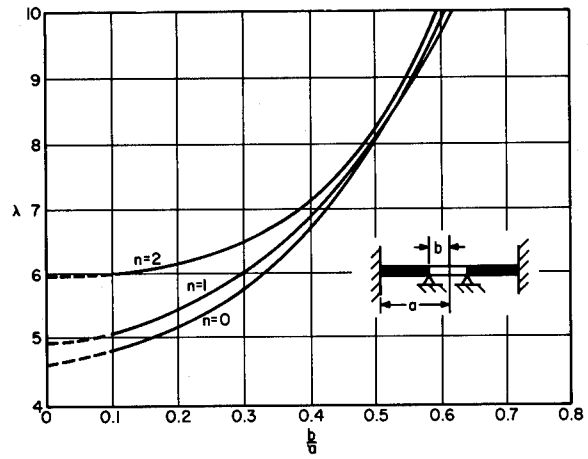


FIGURE 2.15.—Values of $\lambda=(\rho\omega^2/D)^{1/4}a$ for a clamped, simply supported annulus; $\nu=1/3$. (After ref. 2.42)

TABLE 2.19.—*Values of* $\lambda^2=\omega a^2\sqrt{\rho/D}$ *for a Clamped, Simply Supported Annulus;* $\nu=1/3$

n	λ^2 for values of b/a of—					
	0.1	0.2	0.3	0.4	0.5	0.6
0	22.61	26.57	33.66	44.89	64.06	99.16
1	25.20	29.11	-------	47.09	-------	98.01
2	35.39	37.54	-------	51.81	-------	104.45

A more comprehensive set of results is given in table 2.20 (see ref. 2.46).

TABLE 2.18.—*Frequency Parameters* $\omega a^2\sqrt{\rho/D}$ *for a Clamped, Clamped Annular Plate*

n	s	$\omega a^2\sqrt{\rho/D}$ for values of b/a of—				
		0.1	0.3	0.5	0.7	0.9
0	0	27.3	45.2	89.2	248	2237
1	0	28.4	46.6	90.2	249	2238
2	0	36.7	51.0	93.3	251	------
3	0	51.2	60.0	99.0	256	2243
0	1	75.3	125	246	686	6167
1	1	78.6	127	248	686	6167
2	1	90.5	134	253	689	------
3	1	112	145	259	694	6174

TABLE 2.20.—*Frequency Parameters* $\omega a^2\sqrt{\rho/D}$ *for a Clamped, Simply Supported Annular Plate*

n	s	$\omega a^2\sqrt{\rho/D}$ for values of b/a of—				
		0.1	0.3	0.5	0.7	0.9
0	0	22.6	33.7	63.9	175	1550
1	0	25.1	35.8	65.4	175	1551
2	0	35.4	42.8	70.0	178	1553
3	0	51.0	54.7	78.1	185	1558
0	1	65.6	104	202	558	5004
1	1	70.5	107	203	560	5004
2	1	86.7	116	210	563	5007
3	1	111.0	130	218	570	5012

2.2.3 Annular Plates Clamped on Outside and Free on Inside

The frequency determinants for $n=0$, 1, and 2 taken from reference 2.45 for plates clamped on the outside and free on the inside are as follows:

For $n=0$,

$$\begin{vmatrix} J_0(\lambda) & Y_0(\lambda) & I_0(\lambda) & K_0(\lambda) \\ J_1(\lambda) & -Y_1(\lambda) & I_1(\lambda) & -K_1(\lambda) \\ J_1(\alpha\lambda) & Y_1(\alpha\lambda) & I_1(\alpha\lambda) & -K_1(\alpha\lambda) \\ J_0(\alpha\lambda) & -Y_0(\alpha\lambda) & I_0(\alpha\lambda)+AI_1(\alpha\lambda) & K_0(\alpha\lambda)+BK_1(\alpha\lambda) \end{vmatrix}=0$$

where

$$A=-\frac{2(1-\nu)}{\alpha\lambda} \qquad B=\frac{2(1-\nu)}{\alpha\lambda}$$

For $n=1$,

$$\begin{vmatrix} J_0(\lambda) & Y_0(\lambda) & I_0(\lambda) & K_0(\lambda) \\ J_1(\lambda) & Y_1(\lambda) & I_1(\lambda) & -K_1(\lambda) \\ -J_1(\alpha\lambda) & -Y_1(\alpha\lambda) & CJ_0(\alpha\lambda)+DI_1(\alpha\lambda) & -K_1(\alpha\lambda) \\ J_0(\alpha\lambda) & Y_0(\alpha\lambda) & BJ_0(\alpha\lambda)+AI_1(\alpha\lambda) & K_0(\alpha\lambda)+BK_1(\alpha\lambda) \end{vmatrix}=0$$

where

$$A=\frac{8(1-\nu)}{(\alpha\lambda)^3} \qquad B=-1+\frac{4(1-\nu)}{(\alpha\lambda)^3} \qquad C=-\frac{2(1-\nu)}{\alpha\lambda} \qquad D=1+\frac{4(1-\nu)}{(\alpha\lambda)^2}$$

For $n=2$,

$$\begin{vmatrix} J_1(\lambda) & Y_1(\lambda) & I_1(\lambda) & -K_1(\lambda) \\ J_0(\lambda) & Y_0(\lambda) & \frac{4}{\lambda}I_1(\lambda)-I_0(\lambda) & -\frac{4}{\lambda}K_1(\lambda)-K_0(\lambda) \\ J_0(\alpha\lambda) & Y_0(\alpha\lambda) & A^*I_0(\alpha\lambda)-B^*I_1(\alpha\lambda) & A^*K_0(\alpha\lambda)+B^*K_1(\alpha\lambda) \\ J_1(\alpha\lambda) & Y_1(\alpha\lambda) & CI_0(\alpha\lambda)-DI_1(\alpha\lambda) & CK_0(\alpha\lambda)+DK_1(\alpha\lambda) \end{vmatrix}=0$$

where

$$A^*=1-AC, \qquad A=\frac{\alpha\lambda}{4}-\frac{3+\nu}{2\alpha\lambda}, \qquad B^*=B-AD, \qquad B=\frac{\alpha\lambda}{4}+\frac{3+\nu}{2\alpha\lambda},$$

$$C=\frac{48(1-\nu)\alpha\lambda}{12(1-\nu)^2-(\alpha\lambda)^4}, \qquad D=\frac{12(1-\nu)[(7+\nu)+(\alpha\lambda)^2]-(\alpha\lambda)^4}{12(1-\nu)^2-(\alpha\lambda)^4}$$

Eigenvalues from reference 2.42 are given in table 2.21 and figure 2.16. Results for $b/a=0$ are also given in the section entitled "Completely Free Plates" (2.1.3).

TABLE 2.21.—*Values of* $\lambda^2=\omega a^2\sqrt{\rho/D}$ *for a Clamped, Free Annulus;* $\nu=1/3$

n	λ^2 for values of b/a of—								
	0	0.1	0.2	0.3	0.4	0.5	0.6	0.7	0.8
0	10.24	10.18	10.34	11.37	13.54	17.51	25.60	42.38	85.32
1	21.25	21.17	20.48	--------	19.80	21.76	28.52	51.12	--------
2	34.88	34.52	33.86	--------	31.34	--------	36.60	--------	72.17

Numerical problems make it difficult to evaluate the frequency determinant as $b/a\to1$. Reference 2.43 gives an approximate value of $\lambda=15$ for $b/a=0.9$. Additional information appears in table 2.16.

A more comprehensive set of results is given in table 2.22 (see ref. 2.46).

TABLE 2.22.—*Frequency Parameters* $\omega a^2\sqrt{\rho/D}$ *for a Clamped, Free Annular Plate*

n	s	$\omega a^2\sqrt{\rho/D}$ for values of b/a of—				
		0.1	0.3	0.5	0.7	0.9
0	0	10.2	11.4	17.7	43.1	360
1	0	21.1	19.5	22.0	45.3	362
2	0	34.5	32.5	32.0	51.5	365
3	0	51.0	49.1	45.8	61.3	370
0	1	39.5	51.7	93.8	253	2219
1	1	60.0	59.8	97.3	254	2220
2	1	83.4	79.0	108.0	259	2225
0	2	90.4	132.0	253.0	692	6183

TABLE 2.23.—*Values of* $\lambda^2=\omega a^2\sqrt{\rho/D}$ *for a Simply Supported, Clamped Annulus;* $\nu=1/3$

n	λ^2 for values of b/a of—					
	0.1	0.2	0.3	0.4	0.5	0.6
0	17. 85	22. 79	30. 05	41. 23	59. 91	95. 16
1	19. 44	24. 32	----------	42. 56	----------	96. 67
2	28. 25	31. 08	----------	46. 81	----------	98. 84

2.2.4 Annular Plates Simply Supported on Outside and Clamped on Inside

The frequency determinants for $n=0$, 1, and 2 taken from reference 2.6 for plates simply supported on the outside and clamped on the inside are as follows:

For $n=0$,

$$\begin{vmatrix} J_0(\lambda) & Y_0(\lambda) & I_0(\lambda) & K_0(\lambda) \\ J_1(\lambda) & Y_1(\lambda) & \frac{2\lambda}{1-\nu}I_0(\lambda)-I_1(\lambda) & -\frac{2\lambda}{1-\nu}K_0(\lambda)-K_1(\lambda) \\ J_0(\alpha\lambda) & Y_0(\alpha\lambda) & I_0(\alpha\lambda) & K_0(\alpha\lambda) \\ J_1(\alpha\lambda) & Y_1(\alpha\lambda) & -I_1(\alpha\lambda) & K_1(\alpha\lambda) \end{vmatrix}=0$$

For $n=1$,

$$\begin{vmatrix} J_1(\lambda) & Y_1(\lambda) & I_1(\lambda) & K_1(\lambda) \\ J_0(\lambda) & Y_0(\lambda) & I_0(\lambda)-\frac{2\lambda}{1-\nu}I_1(\lambda) & -K_0(\lambda)-\frac{2\lambda}{1-\nu}K_1(\lambda) \\ J_0(\alpha\lambda) & Y_0(\alpha\lambda) & I_0(\alpha\lambda) & -K_0(\alpha\lambda) \\ J_1(\alpha\lambda) & Y_1(\alpha\lambda) & I_1(\alpha\lambda) & K_1(\alpha\lambda) \end{vmatrix}=0$$

For $n=2$,

$$\begin{vmatrix} J_1(\lambda) & Y_1(\lambda) & AI_1(\lambda)-\frac{2\lambda}{1-\nu}I_0(\lambda) & -AK_1(\lambda)-\frac{2\lambda}{1-\nu}K_0(\lambda) \\ J_0(\lambda) & Y_0(\lambda) & \frac{4}{\lambda}BI_1(\lambda)-AI_0(\lambda) & -\frac{4}{\lambda}BK_1(\lambda)-AK_0(\lambda) \\ J_1(\alpha\lambda) & Y_1(\alpha\lambda) & I_1(\alpha\lambda) & -K_1(\alpha\lambda) \\ J_0(\alpha\lambda) & Y_0(\alpha\lambda) & -I_0(\alpha\lambda)+\frac{4}{\alpha\lambda}I_1(\alpha\lambda) & -K_0(\alpha\lambda)-\frac{4}{\alpha\lambda}K_1(\alpha\lambda) \end{vmatrix}=0$$

where

$$A=\frac{5-\nu}{1-\nu} \qquad B=\frac{3-\nu}{1-\nu}$$

Eigenvalues from reference 2.42 are given in table 2.23 and figure 2.17. Eigenvalues for the second mode of $n=0$, taken from reference 2.6, are also given in figure 2.17. Additional information appears in table 2.16.

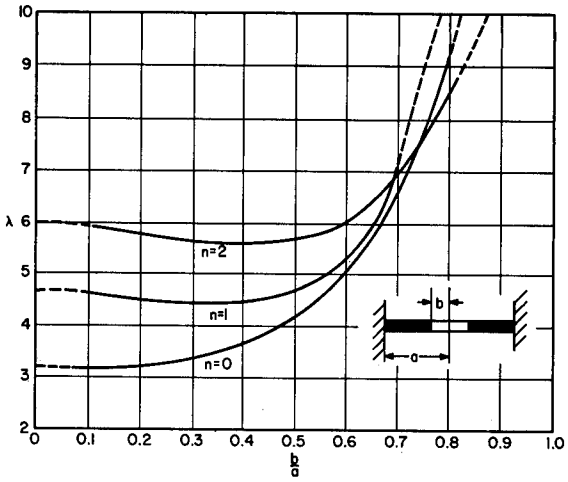


FIGURE 2.16.—Values of $\lambda=(\rho\omega^2/D)^{1/4}a$ for a clamped, free annulus; $\nu=1/3$. (After ref. 2.42)

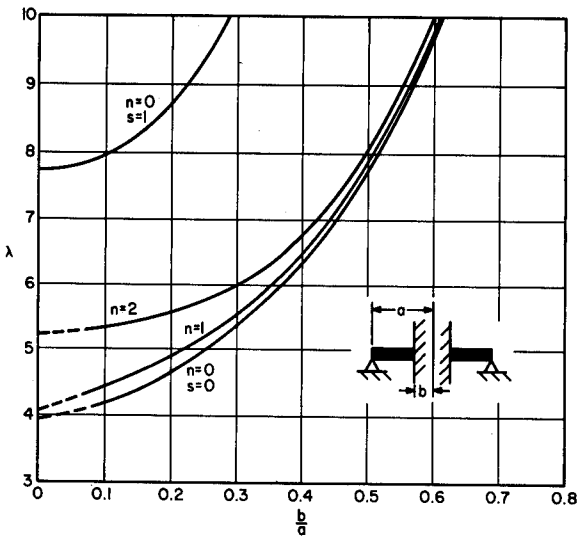


FIGURE 2.17.—Values of $\lambda=(\rho\omega^2/D)^{1/4}a$ for a simply supported, clamped annulus; $\nu=1/3$. (After ref. 2.42)

A more comprehensive set of results is given in table 2.24 (see ref. 2.46).

TABLE 2.24.—*Frequency Parameters* $\omega a^2\sqrt{\rho/D}$ *for a Simply Supported, Clamped Annular Plate*

n	s	$\omega a^2\sqrt{\rho/D}$ for values of b/a of—				
		0.1	0.3	0.5	0.7	0.9
0	0	17. 8	29. 9	59. 8	168	1535
1	0	19. 0	31. 4	61. 0	170	1536
2	0	26. 8	36. 2	64. 6	172	1538
3	0	40. 0	45. 4	71. 0	177	1541
0	1	60. 1	100	198	552	4989
1	1	62. 8	102	200	553	4989
2	1	74. 7	109	205	557	4992
3	1	95. 3	120	211	563	4997

2.2.5 Annular Plates Simply Supported on Both Edges

The case of annular plates simply supported on both edges is not discussed in reference 2.6. Eigenvalues from reference 2.42 are given in table 2.25 and figure 2.18.

TABLE 2.25.—*Values of* $\lambda^2=\omega a^2\sqrt{\rho/D}$ *for an Annular Plate Simply Supported on Both Edges;* $\nu=1/3$

n	λ^2 for values of b/a of—						
	0.1	0.2	0.3	0.4	0.5	0.6	0.7
0	14. 44	17. 39	21. 31	28. 25	40. 01	62. 09	110. 67
1	16. 77	19. 19	----------	30. 00	----------	62. 41	----------
2	25. 97	27. 55	----------	36. 14	----------	68. 41	----------

A more comprehensive set of results is given in table 2.26 (see ref. 2.46).

TABLE 2.26.—*Frequency Parameters* $\omega a^2\sqrt{\rho/D}$ *for a Simply Supported, Simply Supported Annular Plate*

n	s	$\omega a^2\sqrt{\rho/D}$ for values of b/a of—				
		0.1	0.3	0.5	0.7	0.9
0	0	14. 5	21. 1	40. 0	110	988
1	0	16. 7	23. 3	41. 8	112	988
2	0	25. 9	30. 2	47. 1	116	993
3	0	40. 0	42. 0	56. 0	122	998
0	1	51. 7	81. 8	159	439	3948
1	1	56. 5	84. 6	161	441	3948
2	1	71. 7	933	167	444	3952
3	1	94. 7	108	177	453	3958

Theoretical and experimental results for $0 \leqq b/a \leqq 0.5$ are given for the first three mode shapes in reference 2.48. Additional information appears in table 2.16.

2.2.6 Annular Plates Simply Supported on Outside and Free on Inside

The frequency determinants for $n=0$, 1, and 2 taken from reference 2.45 are as follows:

For $n=0$,

$$\begin{vmatrix} J_0(\lambda) & Y_0(\lambda) & I_0(\lambda) & K_0(\lambda) \\ -J_1(\lambda) & -Y_1(\lambda) & I_1(\lambda)+AI_0(\lambda) & -K_1(\lambda)+AK_0(\lambda) \\ J_1(\alpha\lambda) & Y_1(\alpha\lambda) & I_1(\alpha\lambda) & -K_1(\alpha\lambda) \\ -J_0(\alpha\lambda) & -Y_0(\alpha\lambda) & I_0(\alpha\lambda)-BI_1(\alpha\lambda) & K_0(\alpha\lambda)+BK_1(\alpha\lambda) \end{vmatrix} = 0$$

where

$$A=-\frac{2\lambda}{1-\nu} \qquad B=\frac{2(1-\nu)}{\alpha\lambda}$$

For $n=1$,

$$\begin{vmatrix} J_0(\lambda) & Y_0(\lambda) & I_0(\lambda)-EI_1(\lambda) & -K_0(\lambda)-EK_1(\lambda) \\ J_1(\lambda) & Y_1(\lambda) & I_1(\lambda) & K_1(\lambda) \\ -J_1(\alpha\lambda) & -Y_1(\alpha\lambda) & CI_0(\alpha\lambda)+DI_1(\alpha\lambda) & -CK_0(\alpha\lambda)+DK_1(\alpha\lambda) \\ J_0(\alpha\lambda) & Y_0(\alpha\lambda) & BI_0(\alpha\lambda)+AI_1(\alpha\lambda) & -BK_0(\alpha\lambda)+AK_1(\alpha\lambda) \end{vmatrix} = 0$$

where

$$A=-\frac{8(1-\nu)}{(\alpha\lambda)^3} \qquad B=-1+\frac{4(1-\nu)}{(\alpha\lambda)^2} \qquad C=-\frac{2(1-\nu)}{\alpha\lambda} \qquad D=1+\frac{4(1-\nu)}{(\alpha\lambda)^2} \qquad E=\frac{2\lambda}{1-\nu}$$

For $n=2$,

$$\begin{vmatrix} J_1(\lambda) & Y_1(\lambda) & EI_1(\lambda)-FI_0(\lambda) & -EK_1(\lambda)-FK_0(\lambda) \\ J_0(\lambda) & Y_0(\lambda) & GI_1(\lambda)-EI_0(\lambda) & -GK_1(\lambda)-EK_0(\lambda) \\ J_0(\alpha\lambda) & Y_0(\alpha\lambda) & A^*I_0(\alpha\lambda)-B^*I_1(\alpha\lambda) & A^*K_0(\alpha\lambda)+B^*K_1(\alpha\lambda) \\ J_1(\alpha\lambda) & Y_1(\alpha\lambda) & CI_0(\alpha\lambda)-DI_1(\alpha\lambda) & CK_0(\alpha\lambda)+DK_1(\alpha\lambda) \end{vmatrix} = 0$$

where

$$A^*=1-AC \qquad B^*=B-AD \qquad A=-\frac{3+\nu}{2\alpha}+\frac{\alpha\lambda}{4} \qquad B=\frac{3+\nu}{2\alpha}+\frac{\alpha\lambda}{4} \qquad C=\frac{48(1-\nu)\alpha\lambda}{12(1-\nu)^2-(\alpha\lambda)^4}$$

$$D=\frac{12(1-\nu)[(7+\nu)+(\alpha\lambda)^2]-(\alpha\lambda)^4}{12(1-\nu)^2-(\alpha\lambda)^4} \qquad E=\frac{5-\nu}{1-\nu} \qquad F=\frac{2\lambda}{1-\nu} \qquad G=\frac{4}{\lambda}\frac{3-\nu}{1-\nu}$$

Eigenvalues from reference 2.42 are given in table 2.27 and figure 2.19. Values for $b/a=0$ are also given in section 2.1.3. Additional information appears in table 2.16. A more comprehensive set of results is given in table 2.28 (from ref. 2.46).

TABLE 2.27.—*Values of* $\lambda^2=\omega a^2\sqrt{\rho/D}$ *for a Simply Supported, Free Annulus;* $\nu=1/3$

n	λ^2 for values of b/a of—									
	0	0.1	0.2	0.3	0.4	0.5	0.6	0.7	0.8	0.9
0	--------	4. 933	4. 726	4. 654	4. 752	5. 040	5. 664	6. 864	9. 431	17. 81
1	13. 93	13. 91	12. 60	--------	11. 66	--------	12. 27	--------	17. 05	--------
2	25. 65	25. 43	24. 97	--------	23. 09	--------	22. 20	--------	29. 92	--------

TABLE 2.28.—*Frequency Parameters* $\omega a^2\sqrt{\rho/D}$ *for a Simply Supported, Free Annular Plate*

n	s	$\omega a^2\sqrt{\rho/D}$ for values of b/a of—				
		0.1	0.3	0.5	0.7	0.9
0	0	4. 86	4. 66	5. 07	6. 93	17. 7
1	0	13. 9	12. 8	11. 6	13. 3	29. 7
2	0	25. 4	24. 1	22. 3	24. 3	51. 2
3	0	40. 0	38. 8	35. 7	37. 2	74. 5
0	1	29. 4	37. 0	65. 8	175	1550
1	1	48. 0	45. 8	69. 9	178	1553
2	1	69. 2	65. 1	81. 1	185	1558
0	2	74. 8	107	203	558	5004

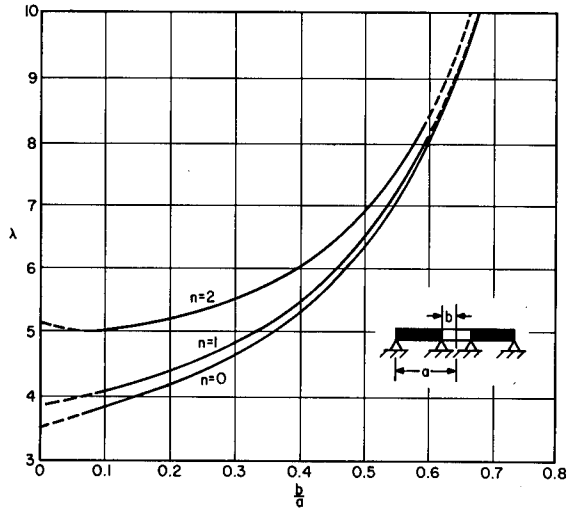


FIGURE 2.18.—Values of $\lambda=(\rho\omega^2/D)^{1/4}a$ for a simply supported, simply supported annulus; $\nu=1/3$. (After ref. 2.42)

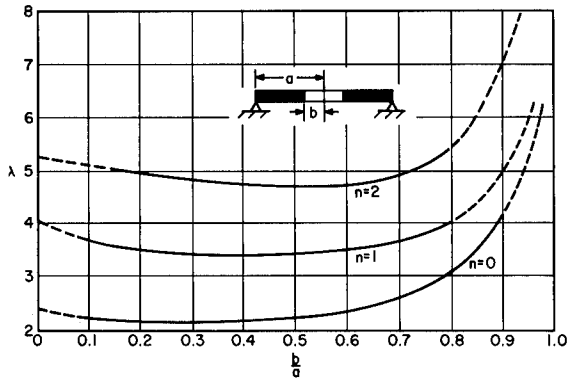


FIGURE 2.19.—Values of $\lambda=(\rho\omega^2/D)^{1/4}a$ for a simply supported, free annulus; $\nu=1/3$. (After ref. 2.42)

2.2.7 Annular Plates Free on Outside and Clamped on Inside

The frequency determinants for $n=0, 1, 2$ taken from reference 2.6 are as follows:

For $n=0$,

$$\begin{vmatrix} J_0(\lambda) & Y_0(\lambda) & -I_0(\lambda)+\frac{2(1-\nu)}{\lambda}I_1(\lambda) & -K_0(\lambda)-\frac{2(1-\nu)}{\lambda}K_1(\lambda) \\ J_1(\lambda) & Y_1(\lambda) & I_1(\lambda) & -K_1(\lambda) \\ J_0(\alpha\lambda) & Y_0(\alpha\lambda) & I_0(\alpha\lambda) & K_0(\alpha\lambda) \\ J_1(\alpha\lambda) & Y_1(\alpha\lambda) & -I_1(\alpha\lambda) & K_1(\alpha\lambda) \end{vmatrix}=0$$

For $n=1$,

$$\begin{vmatrix} J_0(\lambda) & Y_0(\lambda) & AI_0(\lambda)-BI_1(\lambda) & -K_0(\lambda)-\frac{2(1-\nu)}{\lambda}K_1(\lambda) \\ J_1(\lambda) & Y_1(\lambda) & I_1(\lambda) & -K_1(\lambda) \\ J_0(\alpha\lambda) & Y_0(\alpha\lambda) & I_0(\alpha\lambda) & K_0(\alpha\lambda) \\ J_1(\alpha\lambda) & Y_1(\alpha\lambda) & I_1(\alpha\lambda) & K_1(\alpha\lambda) \end{vmatrix}=0$$

where

$$A=-1+\frac{4(1-\nu)}{\lambda^2} \qquad B=\frac{8(1-\nu)}{\lambda^3}$$

For $n=2$,

$$\begin{vmatrix} J_0(\lambda) & Y_0(\lambda) & (1-4AB\lambda)I_0(\lambda)-DI_1(\lambda) & (1-4AB\lambda)K_0(\lambda)+DK_1(\lambda) \\ J_1(\lambda) & Y_1(\lambda) & 4B\lambda I_0(\lambda)-CI_1(\lambda) & 4B\lambda K_0(\lambda)+CK_1(\lambda) \\ J_0(\alpha\lambda) & Y_0(\alpha\lambda) & -I_0(\alpha\lambda)+\frac{4}{\alpha\lambda}I_1(\alpha\lambda) & -K_0(\alpha\lambda)-\frac{4}{\alpha\lambda}K_1(\alpha\lambda) \\ J_1(\alpha\lambda) & Y_1(\alpha\lambda) & I_1(\alpha\lambda) & -K_1(\alpha\lambda) \end{vmatrix}$$

where

$$A=\frac{\lambda}{4}-\frac{3+\nu}{2\lambda} \qquad B=\frac{12(1-\nu)}{12(1-\nu^2)-\lambda^4} \qquad C=\frac{12(1-\nu)(7+\nu+\lambda^2)-\lambda^4}{12(1-\nu^2)-\lambda^4} \qquad D=\frac{\lambda}{4}+\frac{3+\nu}{2\lambda}-AC$$

Eigenvalues from reference 2.42 are given in table 2.29 and figure 2.20. Accurate values for $b/a=0$ are given in the section entitled "Plates Clamped at Center With Various Conditions on Contour" (2.1.6).

TABLE 2.29.—*Values of* $\lambda^2=\omega a^2\sqrt{\rho/D}$ *for a Free, Clamped Annulus;* $\nu=1/3$

n	λ^2 for values of b/a of—							
	0.1	0.2	0.3	0.4	0.5	0.6	0.7	0.8
0	4. 235	5. 244	6. 739	7. 036	13. 05	20. 63	36. 60	81. 45
1	3. 482	4. 814	----------	9. 096	----------	20. 93	----------	45. 09
2	5. 499	6. 345	----------	10. 37	----------	21. 63	----------	67. 65

A more comprehensive set of results is given in table 2.30 (see ref. 2.46).

TABLE 2.30.—*Frequency Parameters* $\omega a^2\sqrt{\rho/D}$ *for a Free, Clamped Annular Plate*

n	s	$\omega a^2\sqrt{\rho/D}$ for values of b/a of—				
		0.1	0.3	0.5	0.7	0.9
1	0	3. 14	6. 33	13. 3	37. 5	345
0	0	4. 23	6. 66	13. 0	37. 0	51. 5
2	0	5. 62	7. 96	14. 7	39. 3	347
3	0	12. 4	13. 27	18. 5	42. 6	352
0	1	25. 3	42. 6	85. 1	239	970
1	1	27. 3	44. 6	86. 7	241	2189
2	1	37. 0	50. 9	91. 7	246	2194
3	1	53. 2	62. 1	100	253	2200

Additional data for this case are available from the work of Southwell (ref. 2.37), who saved considerable effort in computation of the Bessel functions by assuming arguments of λ and then finding the b/a ratios to which these correspond. These additional data are presented in table 2.31 for $\nu=0.3$. Results appear also in table 2.16. This problem was also discussed in reference 2.15.

TABLE 2.31.—*Additional Values of* $\lambda^2=\omega a^2\sqrt{\rho/D}$ *for a Free, Clamped Annulus;* $\nu=0.3$

$n=0$		$n=1$		$n=2$		$n=3$	
b/a	λ^2	b/a	λ^2	b/a	λ^2	b/a	λ^2
0. 276	6. 25	0. 060	2. 82	0. 186	6. 25	0. 43	16. 0
. 642	25. 0	. 397	9. 00	. 349	9. 00	. 59	25
. 840	81. 0	. 603	21. 2	. 522	16. 0	. 71	49
		. 634	25. 0	. 769	64. 0	. 82	100
		. 771	64. 0	. 81	100		
		. 827	121. 0				

2.2.8 Annular Plates Free on Outside and Simply Supported on Inside

The case of annular plates free on the outside and simply supported on the inside is not discussed in reference 2.6. Eigenvalues from reference 2.42 are given in table 2.32 and figure 2.21. Additional information appears in table 2.16.

TABLE 2.32.—*Values of* $\lambda^2=\omega a^2\sqrt{\rho/D}$ *for a Free, Simply Supported Annulus;* $\nu=1/3$

n	λ^2 for values of b/a of—								
	0.1	0.2	0.3	0.4	0.5	0.6	0.7	0.8	0.9
0	3. 516	3. 312	3. 378	3. 610	4. 060	4. 951	6. 101	8. 779	18. 92
1	2. 403	2. 816		3. 940		6. 027		12. 55	
2	5. 313	5. 513		6. 620		9. 653		19. 95	

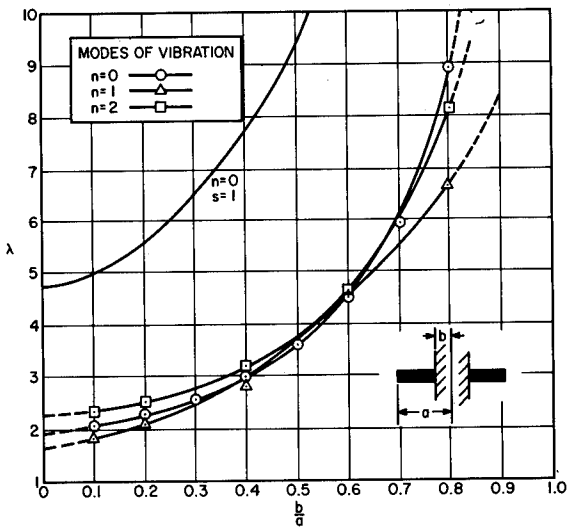


FIGURE 2.20.—Values of $\lambda=(\rho\omega^2/D)^{1/4}a$ for a free, clamped annulus; $\nu=1/3$. (After ref. 2.42)

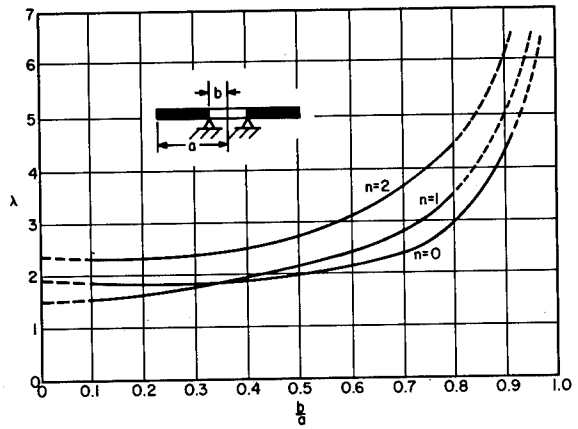


FIGURE 2.21.—Values of $\lambda=(\rho\omega^2/D)^{1/4}a$ for a free, simply supported annulus; $\nu=1/3$. (After ref. 2.42)

A more comprehensive set of results is given in table 2.33 (see ref. 2.46).

TABLE 2.33.—*Frequency Parameters* $\omega a^2\sqrt{\rho/D}$ *for a Free, Simply Supported Annular Plate*

n	s	$\omega a^2\sqrt{\rho/D}$ for values of b/a of—				
		0.1	0.3	0.5	0.7	0.9
1	0	2.30	3.32	4.86	8.34	25.9
0	0	3.45	3.42	4.11	6.18	17.2
2	0	5.42	6.08	7.98	13.4	42.6
3	0	12.4	12.6	14.0	20.5	61.4
0	1	20.8	31.6	61.0	170	1535
1	1	24.1	34.5	63.3	172	1536
2	1	35.8	43.0	69.7	177	1541
3	1	53.0	56.7	80.3	185	1548

2.2.9 Annular Plates Free on Both Edges

The frequency determinants for $n=0$, 1, and 2 taken from reference 2.6 for annular plates free on both edges are as follows:

For $n=0$,

$$\begin{vmatrix} J_0(\lambda) & Y_0(\lambda) & -I_0(\lambda)+AI_1(\lambda) & -K_0(\lambda)-AK_1(\lambda) \\ J_1(\lambda) & Y_1(\lambda) & I_1(\lambda) & -K_1(\lambda) \\ J_0(\alpha\lambda) & Y_0(\alpha\lambda) & -I_0(\alpha\lambda)+BI_1(\alpha\lambda) & -K_0(\alpha\lambda)-BK_1(\alpha\lambda) \\ J_1(\alpha\lambda) & Y_1(\alpha\lambda) & I_1(\alpha\lambda) & -K_1(\alpha\lambda) \end{vmatrix} = 0$$

where

$$A=\frac{2(1-\nu)}{\lambda} \qquad B=\frac{2(1-\nu)}{\alpha\lambda}$$

For $n=1$,

$$\begin{vmatrix} J_0(\lambda) & Y_0(\lambda) & \left(-1+\frac{\lambda}{2}A\right)I_0(\lambda)-AI(\lambda) & -\left(-1+\frac{\lambda}{2}A\right)K_0(\lambda)-AK(\lambda) \\ J_1(\lambda) & Y_1(\lambda) & \frac{\lambda^2}{4}AI_0(\lambda)-\left(1+\frac{\lambda}{2}A\right)I_1(\lambda) & -\frac{\lambda^2}{4}AK_0(\lambda)-\left(1+\frac{\lambda}{2}A\right)K_1(\lambda) \\ J_0(\alpha\lambda) & Y_0(\alpha\lambda) & \left(-1+\frac{\alpha\lambda}{2}B\right)I_0(\alpha\lambda)-BI_1(\alpha\lambda) & -\left(-1+\frac{\alpha\lambda}{2}B\right)K_0(\alpha\lambda)-BK_1(\alpha\lambda) \\ J_1(\alpha\lambda) & Y_1(\alpha\lambda) & \frac{(\alpha\lambda)^2}{4}BI_0(\alpha\lambda)-\left(1+\frac{\alpha\lambda}{2}B\right)I_1(\alpha\lambda) & \left[-\frac{(\alpha\lambda)^2}{4}BK_0(\alpha\lambda)-\left(1+\frac{\alpha\lambda}{2}B\right)K_1(\alpha\lambda)\right] \end{vmatrix}=0$$

where

$$A=\frac{8(1-\nu)}{\lambda^3} \qquad B=\frac{8(1-\nu)}{(\alpha\lambda)^3}$$

For $n=2$,

$$\begin{vmatrix} J_0(\lambda) & Y_0(\lambda) & AI_0(\lambda)-BI_1(\lambda) & AK_0(\lambda)+BK_1(\lambda) \\ J_1(\lambda) & Y_1(\lambda) & CI_0(\lambda)-DI_1(\lambda) & CK_0(\lambda)+DK_1(\lambda) \\ J_0(\alpha\lambda) & Y_0(\alpha\lambda) & A^*I_0(\alpha\lambda)-B^*I_1(\alpha\lambda) & A^*K_0(\alpha\lambda)+B^*K_1(\alpha\lambda) \\ J_1(\alpha\lambda) & Y_1(\alpha\lambda) & C^*I_0(\alpha\lambda)-D^*I_1(\alpha\lambda) & C^*K_0(\alpha\lambda)+D^*K_1(\alpha\lambda) \end{vmatrix}=0$$

where

$$A=1-\left(\frac{\lambda}{4}-\frac{3+\nu}{2\lambda}\right)C \qquad B=\frac{\lambda}{4}+\frac{3+\nu}{2\lambda}-\left(\frac{\lambda}{4}-\frac{3+\nu}{2\alpha\lambda}\right)D \qquad C=\frac{48(1-\nu)\lambda}{12(1-\nu^2)-\lambda}$$

$$D=\frac{12(1-\nu)(7+\nu+\lambda^2)-\lambda^4}{12(1-\nu^2)-\lambda^4} \qquad A^*=1-\left(\frac{\alpha\lambda}{4}-\frac{3+\nu}{2\lambda}\right) \qquad B^*=\frac{\alpha\lambda}{4}+\frac{3+\nu}{2\alpha\lambda}-\left(\frac{\alpha\lambda}{4}-\frac{3+\nu}{2\alpha\lambda}\right)D^*$$

$$C^*=\frac{48(1-\nu)(\alpha\lambda)}{12(1-\nu^2)-(\alpha\lambda)^4} \qquad D^*=\frac{12(1-\nu)[7+\nu+(\alpha\lambda)^2]-(\alpha\lambda)^4}{12(1-\nu^2)-(\lambda)^4}$$

Eigenvalues from reference 2.42 are given in table 2.34 for the lowest root of $n=2$. The lowest roots of $n=0$ and $n=1$ are rigid body translation and rotation modes, respectively. Other eigenvalues are plotted in figure 2.22 as taken from reference 2.6. Labels near the ordinate identify roots for $b/a=0$ given in the section entitled "Completely Free Plates" (2.1.3).

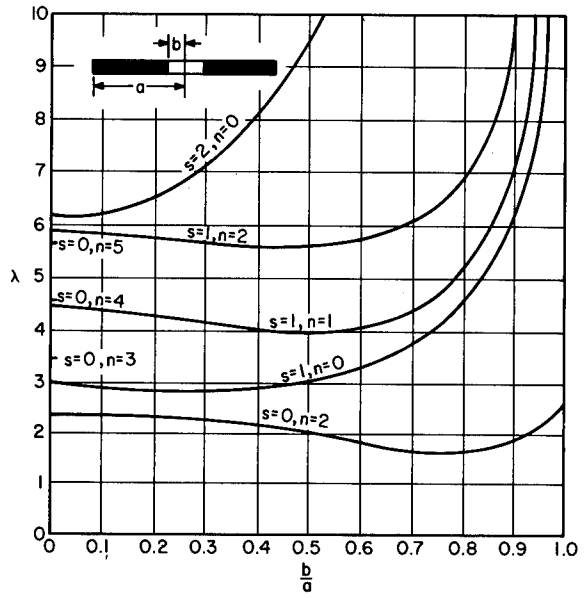


FIGURE 2.22.—Values of $\lambda=(\rho\omega^2/D)^{1/4}a$ for a free, free annulus; $\nu=1/3$. (After ref. 2.6)

TABLE 2.34.—*Values of* $\lambda^2=\omega a^2\sqrt{\rho/D}$ *for an Annular Plate Free on Both Edges;* $\nu=1/3$

n	λ^2 for values of b/a of—								
	0.1	0.2	0.3	0.4	0.5	0.6	0.7	0.8	0.9
2	5. 203	5. 053	4. 822	4. 567	4. 203	3. 865	3. 519	3. 200	2. 890

TABLE 2.35.—*Frequency Parameters* $\omega a^2\sqrt{\rho/D}$ *for a Free, Free Annular Plate*

n	s	$\omega a^2\sqrt{\rho/D}$ for values of b/a of—				
		0.1	0.3	0.5	0.7	0.9
2	0	5. 30	4. 91	4. 28	3. 57	2. 94
3	0	12. 4	12. 26	11. 4	9. 86	8. 14
0	1	8. 77	8. 36	9. 32	13. 2	34. 9
1	1	20. 5	18. 3	17. 2	22. 0	55. 7
2	1	34. 9	33. 0	31. 1	37. 8	93. 8
3	1	53. 0	51. 0	47. 4	55. 7	135
0	2	38. 2	50. 4	92. 3	251	2238
1	2	59. 0	58. 8	96. 3	253	2240

A more comprehensive set of results is given in table 2.35 (see ref. 2.46).

2.2.10 Annular Plates Clamped on Outside With Rigid Mass on Inside

Considering only axisymmetric vibrations the boundary conditions for annular plates clamped on the outside with a rigid mass on the inside (fig. 2.23) are

$$\left.\begin{aligned} &w(a,\theta,t)=\frac{\partial w}{\partial r}(a,\theta,t)=\frac{\partial w}{\partial r}(b,\theta,t)=0\\ &2\pi bV_r(b,\theta,t)=M\frac{\partial^2 w}{\partial t^2}(b,\theta,t)\end{aligned}\right\} \quad (2.37)$$

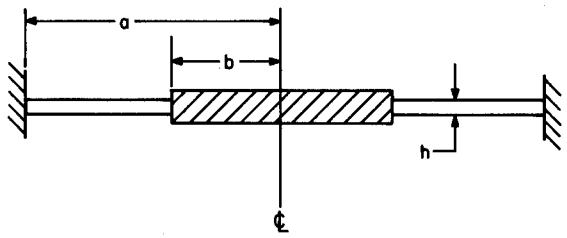


FIGURE 2.23.—Annular plate clamped on outside, rigid mass on inside.

where M is the total mass of the rigid insert. In the general case the condition of zero slope at the junction with the rigid mass would be replaced by an equation of motion relating the integral of the components of torque along the edge $r=b$ about a diametral axis to the product of the mass moment of inertia and the rotational acceleration about the axis.

Letting $n=0$ in equation (1.18) and substituting into equation (2.37) result in a fourth-order frequency determinant. Expanding this by making use of the recursion formulas for derivatives of Bessel functions yields a characteristic equation which was given by Handelman and Cohen (ref. 2.49):

$$\begin{aligned}&([J_0(\lambda)I_1(\lambda)+J_1(\lambda)I_0(\lambda)]\{4\lambda Y_1(\lambda\alpha)\\&+\alpha\lambda^2\gamma[Y_1(\lambda\alpha)K_0(\lambda\alpha)-K_1(\lambda\alpha)Y_0(\lambda\alpha)]\})\\&+([J_0(\lambda)K_1(\lambda)-K_0(\lambda)J_1(\lambda)]\{4\lambda I_1(\lambda\alpha)Y_1(\lambda\alpha)\\&-\alpha\lambda^2\gamma[I_1(\lambda\alpha)Y_0(\lambda\alpha)+I_0(\lambda\alpha)Y_1(\lambda\alpha)]\})\\&+([Y_0(\lambda)I_1(\lambda)+I_0(\lambda)Y_1(\lambda)]\{4\lambda J_1(\lambda)K_1(\lambda)\\&+\alpha\lambda^2\gamma[J_1(\lambda\alpha)K_0(\lambda\alpha)-K_1(\lambda\alpha)J_0(\lambda\alpha)]\})\\&+([Y_0(\lambda)K_1(\lambda)-K_0(\lambda)Y_1(\lambda)]\\&\{-4\lambda J_1(\lambda\alpha)I_1(\lambda\alpha)+\alpha\lambda^2\gamma[J_1(\lambda\alpha)I_0(\lambda\alpha)\\&+I_1(\lambda\alpha)J_0(\lambda\alpha)]\})=\frac{4\gamma}{\pi}\end{aligned} \quad (2.38)$$

where

$$\lambda=(\omega^2\rho/D)^{1/4}a \quad (2.39)$$

and

$$\alpha=b/a \qquad \gamma=\rho'/\rho$$

where ρ' is the mass per unit area of the rigid, inner mass.

Equation (2.38) was solved for the fundamental root λ for two values of α and $\gamma=2$ and

10. These results are shown as small circles in figure 2.24. Because of the complexity of equation (2.38) its numerical evaluation was limited in reference 2.49 and, in its place, a minimal principle was used to obtain approximate eigenvalues which are upper bounds. These results appear as curves in figure 2.24.

In figure 2.24 it is seen that for high mass-density ratio γ there exists a ratio of radii α for which the frequency is identical to that for the clamped solid circular plate without central mass. The critical values of γ for which this occurs are shown in figure 2.25 as a function of α (see ref. 2.49).

REFERENCES

2.1. McLachlan, N.: Bessel Functions for Engineers. Oxford Eng. Sci. Ser., Oxford Univ. Press (London), 1948.

2.2. Anon.: Tables of the Bessel Functions of the First Kind (Orders 0 to 135). Harvard Univ. Press (Cambridge, Mass.), 1947.

2.3. Airey, J.: The Vibration of Circular Plates and Their Relation to Bessel Functions. Proc. Phys. Soc. (London), vol. 23, 1911, pp. 225–232.

2.4. Blanch, G.: Notes on Zeros of $I_{n+1}(x)\ J_n(x) + J_{n+1}(x) I_n(x) = 0$. Math. Tables and Other Aids to Comput., vol. 6, no. 37, 1952, p. 58.

2.5. Carrington, H.: The Frequencies of Vibration of Flat Circular Plates Fixed at the Circumference. Phil. Mag., vol. 50, no. 6, 1925, pp. 1261–1264.

2.6. Gontkevich, V. S.: Natural Vibrations of Plates and Shells. A. P. Filippov, ed., Nauk. Dumka (Kiev), 1964. (Transl. by Lockheed Missiles & Space Co. (Sunnyvale, Calif.).)

2.7. Reid, W. P.: Free Vibrations of a Circular Plate. J. Soc. Ind. Appl. Math., vol. 10, no. 4, Dec. 1962, pp. 668–674.

2.8. Ungar, E. E.: Maximum Stresses in Beams and Plates Vibrating at Resonance. Trans. ASME, J. Eng. Ind., vol. 84B, Feb. 1962, pp. 149–155.

2.9. Nowacki, W.: Dynamics of Elastic Systems. John Wiley & Sons, Inc., 1963.

2.10. Filippov, A. P.: Vibrations of Elastic Systems. AN UkrSSR Press, 1956. (In Russian.)

2.11. Prescott, T.: Applied Elasticity. Dover Pub., Inc., 1961. (Originally published by Longmans, Green & Co., 1924.)

2.12. Poisson, S. D.: L'Équilibre et le Mouvement des Corps Élastiques. Mem. Acad. Roy. des Sci. de L'Inst. France, ser. 2, vol. 8, 1829, p. 357.

2.13. Schulze, F. A.: Einige neue Methoden zür Bestimmung der Schwingungszahlen höchster hörbarer und unhörbarer Töne—Anwendung auf die Töne der Galtonpfeife und die Bestimmung der oberen Hörgrenze. Ann. Physik, Bd. 24, Heft 15, 1907.

2.14. Lauricella, G.: Sulle Vibrazioni delle Piastre Elastiche Incastrate. Atti. Accad. Naz. Lincei, Rend., Classe Sci. Fis., Mat. Nat., vol. 17, ser. 5, pt. 2, 1908, pp. 193–204.

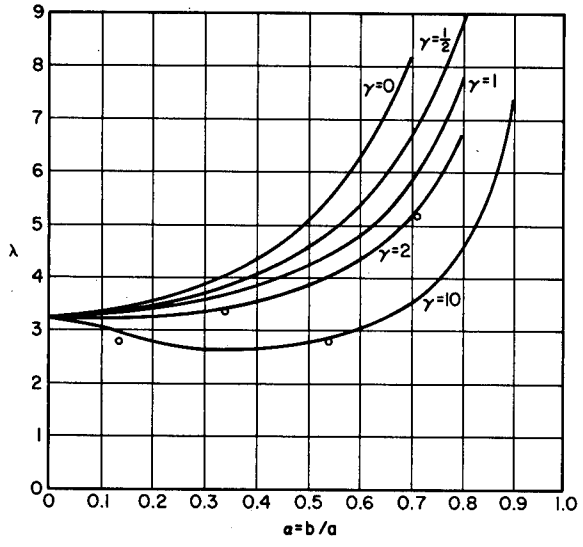


FIGURE 2.24.—Frequency parameter $\lambda = (\rho\omega^2/D)^{1/4}a$ for an annular plate clamped on the outside and having a rigid mass on the inside.

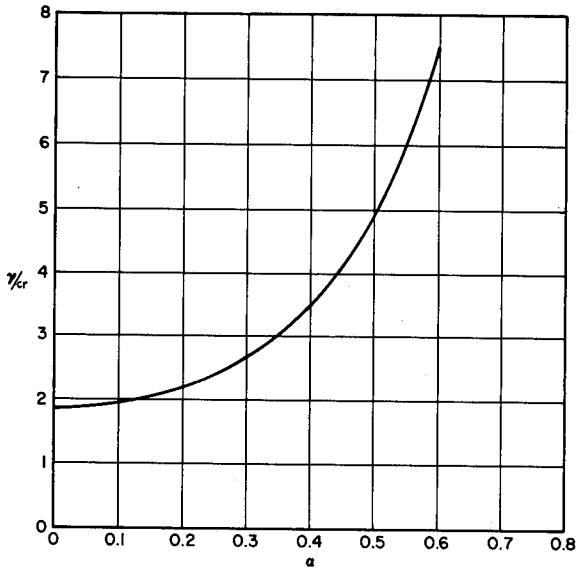


FIGURE 2.25.—Critical mass density ratios γ_c.

2.15. PFEIFFER, F.: Übergang zu Systemen mit unendlich vielen Freiheitsgraden. Ch. 4, Handbuch der Phys., Julius Springer (Berlin), 1928, pp. 337–402.

2.16. COURANT, F.; AND HILBERT, D.: Methods of Mathematical Physics. Vol. I. Julius Springer (Berlin), 1924. Interscience Publ., Inc. (New York, N.Y.), 1953.

2.17. RAYLEIGH, LORD: Theory of Sound. Vol. I and vol. II. Dover Pub., 1945. (Originally published in 1877.)

2.18. POLYA, G.; AND SZEGÖ, G.: Isoperimetric Inequalities in Mathematical Physics. Princeton Univ. Press (Princeton, N.J.), 1951.

2.19. BODINE, R. Y.: The Fundamental Frequencies of a Thin Flat Circular Plate Simply Supported Along a Circle of Arbitrary Radius. ASME Paper no. APMW–10, J. Appl. Mech., vol. 26, Dec. 1959, pp. 666–668.

2.20. COLWELL, R. C.; AND HARDY, H. C.: The Frequencies and Nodal Systems of Circular Plates. Phil. Mag., ser. 7, vol. 24, no. 165, Dec. 1937, pp. 1041–1055.

2.21. WALLER, MARY D.: Vibrations of Free Circular Plates. Proc. Phys. Soc. (London), vol. 50, 1938, pp. 70–76.

2.22. GRINSTED, B.: Nodal Pattern Analysis. Proc. Inst. Mech. Eng., ser. A, vol. 166, 1952, pp. 309–326.

2.23. KIRCHHOFF, G.: Über das Gleichgewicht und die Bewegung einer elastischen Scheibe. Math. J. (Crelle), Bd. 40, no. 5, 1850, pp. 51–58.

2.24. WOOD, A. B.: An Experimental Determination of the Frequencies of Free Circular Plates. Proc. Phys. Soc. (London), vol. 47, no. 5, 1935, pp. 794–799.

2.25. COLWELL, R. C.; STEWART, J. K.; AND ARNETT, H. D.: Symmetrical Sand Figures on Circular Plates. J. Acoust. Soc. Am., vol. 12, Oct. 1940, pp. 260–265.

2.26. COLWELL, R. C.: The Vibrations of a Circular Plate. J. Franklin Inst., vol. 213, no. 1276–1277, 1932, pp. 373–380.

2.27. STEWART, J. K.; AND COLWELL, R. C.: The Calculation of Chladni Patterns. J. Acoust. Soc. Am., vol. 11, July 1939, pp. 147–151.

2.28. CHLADNI, E. F. F.: Die Akustik. Leipzig, 1802.

2.29. COLWELL, R. C.; STEWART, J. K.; AND FRIEND, A. W.: Symmetrical Figures on Circular Plates and Membranes. Phil. Mag., ser. 7, vol. 27, 1939, pp. 123–128.

2.30. TIMOSHENKO, S.; AND WOINOWSKY-KRIEGER, S.: Theory of Plates and Shells. Second ed., McGraw-Hill Book Co., Inc., 1959.

2.31. KIRCHHOFF, G.: Ges. Abhandl. (Leipzig), 1882, p. 259.

2.32. KANTHAM, C. L.: Bending and Vibration of Elastically Restrained Circular Plates. J. Franklin Inst., vol. 265, no. 6, June 1958, pp. 483–491.

2.33. BARTLETT, C. C.: The Vibration and Buckling of a Circular Plate Clamped on Part of Its Boundary and Simply Supported on the Remainder. Quart. J. Mech. Appl. Math., vol. 16, pt. 4, 1963, pp. 431–440.

2.34. NOBLE, BEN: The Vibration and Buckling of a Circular Plate Clamped on Part of Its Boundary and Simply Supported on the Remainder. Proc. 9th Midwest. Conf. Solid and Fluid Mech., Aug. 1965.

2.35. NOWACKI, W.; AND OLESIAK, Z.: Vibration, Buckling, and Bending of a Circular Plate Clamped Along Part of Its Periphery and Simply Supported on the Remaining Part. Bull. Acad. Pol. Sci., cl. IV, vol. 4, no. 4, 1956, pp. 247–258.

2.36. NOWACKI, W.; AND OLESIAK, Z.: The Problem of a Circular Plate Partially Clamped and Partially Simply Supported Along the Periphery. Arch. Mech. Stos., vol. 8, 1956, pp. 233–255. (In Polish.)

2.37. SOUTHWELL, R. V.: On the Free Transverse Vibrations of a Uniform Circular Disc Clamped at Its Centre and on the Effect of Rotation. Proc. Roy. Soc. (London), ser. A, vol. 101, 1922, pp. 133–153.

2.38. SAKHAROV, I. E.: Dynamic Stiffness in the Theory of Axisymmetric Vibrations of Circular and Annular Plates. Izv. An SSSR, OTN, Mekh. i Mashin., no. 5, 1959, pp. 90–98. (In Russian.)

2.39. ROBERSON, R. E.: Transverse Vibrations of a Free Circular Plate Carrying Concentrated Mass. J. Appl. Mech., vol. 18, no. 3, Sept. 1951, pp. 280–282.

2.40. ROBERSON, R. E.: Vibrations of a Clamped Circular Plate Carrying Concentrated Mass. J. Appl. Mech., vol. 18, no. 4, Dec. 1951, pp. 349–352.

2.41. TYUTEKIN, V. V.: Flexural Oscillations of a Circular Elastic Plate Loaded at the Center. Akusticheskii Zhurnal, vol. 6, no. 3, July 1960, pp. 388–391. (In Russian.)

2.42. RAJU, P. N.: Vibrations of Annular Plates. J. Aeron. Soc. India, vol. 14, no. 2, May 1962, pp. 37–52.

2.43. JOGA-RAO, C. V.; AND PICKETT, GERALD: Vibrations of Plates of Irregular Shapes and Plates With Holes. J. Aeron. Soc. India, vol. 13, no. 3, 1961, pp. 83–88.

2.44. JOGA-RAO, C. V.; AND VIJAYAKUMAR, K.: On Admissible Functions for Flexural Vibration and Buckling of Annular Plates. J. Aeron. Soc. India, vol. 15, no. 1, Feb. 1963, pp. 1–5.

2.45. SAKHAROV, I. E.: Natural Vibrations Frequencies of Annular Plates. Izv. An SSSR, OTN, no. 5, 1957, pp. 107–110. (In Russian.)

2.46. VOGEL, S. M.; AND SKINNER, D. W.: Natural Frequencies of Transversely Vibrating Uniform Annular Plates. J. Appl. Mech., vol. 32, Dec. 1965, pp. 926–931.

2.47. HORT, W.; AND KOENIG, M.: Studien über Schwingungen von Kreisplatten und Ringen I. Z. Tech. Phys., ser. 373, Bd. 9, Heft 10, 1928, pp. 373–382.

2.48. KUMAI, T.: The Flexural Vibrations of a Square Plate With a Central Circular Hole. Proc. 2d Jap. Nat. Congr. Appl. Mech., 1952, pp. 339–342.

2.49. HANDELMAN, G.; AND COHEN, H.: On the Effects of the Addition of Mass to Vibrating Systems. AFOSR TN 56-387 (ASTIA Doc. No. 96045), Sept. 1956. Also Proc. 9th Int. Congr. Appl. Mech., vol. VII, 1957, pp. 509–518.

Chapter 3

Elliptical Plates

The elliptical boundary will be taken to be one of the confocal ellipses of an elliptical coordinate system. The semimajor and semiminor axes of the ellipse will be taken as a and b, respectively (see fig. 3.1). The eccentricity ϵ of the ellipse is related to a and b by

$$\epsilon=\sqrt{1-(b/a)^2} \tag{3.1}$$

For a mode shape having symmetry with respect to both axes of the ellipse (m even) or with respect to the minor axis (m odd), equation (1.27) reduces to

$$W=\sum_{m=0}^{\infty}[C_m Ce_m(\xi, q)ce_m(\eta, q) + C_m^* Ce_m(\xi,-q)ce_m(\eta,-q)] \tag{3.2}$$

For mode shapes which are antisymmetric about both axes (m even) or with respect to the major axis of the ellipse (m odd), equation (1.27) reduces to

$$W=\sum_{m=1}^{\infty}[S_m Se_m(\xi, q)se_m(\eta, q) + S_m^* Se_m(\xi,-q)se_m(\eta,-q)] \tag{3.3}$$

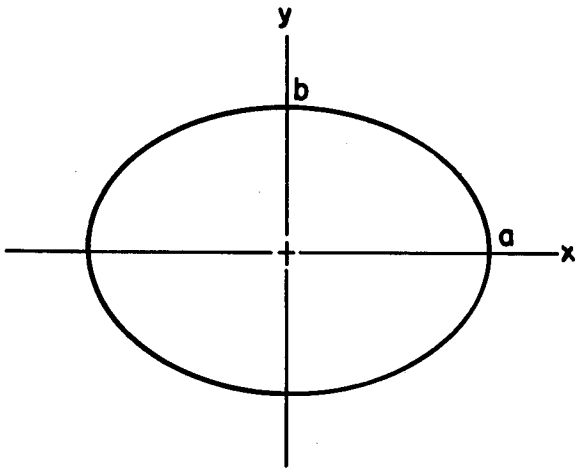


FIGURE 3.1.—Elliptical plate.

3.1 CLAMPED PLATES

When equation (3.2) is used and the conditions of zero deflection and slope around the boundary are applied, a characteristic determinant of unbounded order is obtained. Shibaoka (ref. 3.1) solved the problem of clamped elliptical plates by beginning with the element in the upper left-hand corner and taking a series of finite determinants containing that element. As successive determinants were taken, convergence to a lowest root was established. Table 3.1 shows the fundamental roots obtained for three values of a/b and corresponding eccentricities. The convergence is slower for large values of a/b. Only third-order determinants were required to establish the convergence to the number of figures given for $a/b=1.25$ and 2.00, but a fourth-order determinant was required for $a/b=3.00$.

TABLE 3.1.—*Values of* $\lambda^2=\omega a^2\sqrt{\rho/D}$ *for a Clamped Elliptical Plate*

a/b	ϵ	$\lambda^2=\omega a^2\sqrt{\rho/D}$
1.25	0.600	13.1
2.00	.866	27.5
3.00	.943	56.9

In reference 3.1 an expansion formula is also derived for elliptical plates of small eccentricity. It is

$$\lambda=(\rho\omega^2/D)^{1/4}a=3.1961+0.7991\epsilon^2+0.7892\epsilon^4 \tag{3.4}$$

where 3.1961 is the fundamental eigenvalue for a clamped circular plate of radius a.

The problem was also solved by using the Rayleigh technique (ref. 3.1). A function

$$W=W_0\left(1-\frac{x^2}{a^2}-\frac{y^2}{b^2}\right)^2 \tag{3.5}$$

was chosen to satisfy the boundary conditions exactly. The Rayleigh quotient gives the approximate frequency formula

$$\omega=\frac{1}{a^2}\sqrt{40\left[1+\frac{2}{3}\left(\frac{a}{b}\right)^2+\left(\frac{a}{b}\right)^4\right](D/\rho)} \tag{3.6}$$

The Galerkin method and a two-term deflection function

$$W=A_1\left(\frac{x^2}{a^2}+\frac{y^2}{b^2}-1\right)^2+A_2\left(\frac{x^2}{a^2}+\frac{y^2}{b^2}-1\right)^3 \tag{3.7}$$

were also used to solve the problem (ref. 3.2). By use of equation (3.7), the eigenvalues are found to be

$$\lambda_1^4=\rho\omega_1^2a^4/D=39.218\left[1+\frac{2}{3}\left(\frac{a}{b}\right)^2+\left(\frac{a}{b}\right)^4\right] \tag{3.8}$$

and

$$\lambda_2^4=\rho\omega_2^2a^4/D=129.18\left[1+\frac{2}{3}\left(\frac{a}{b}\right)^2+\left(\frac{a}{b}\right)^4\right] \tag{3.9}$$

Values of λ^2 from equation (3.8) for various ratios of a/b are given in table 3.2.

TABLE 3.2.—*Approximate Values of* $\lambda^2=\omega a^2\sqrt{\rho/D}$ *for a Clamped Elliptical Plate*

a/b	λ^2
1.0	10. 217
1.1	11. 314
1.2	12. 566
1.5	17. 025
2.0	27. 746
3.0	58. 693
5.0	158. 85

Comparing equations (3.8) and (3.6) with table 3.1, it is seen that equation (3.8) gives results only slightly more accurate than those of equation (3.6) and the ratio of frequencies obtained from equations (3.6) and (3.8) does not vary with a/b.

In reference 3.3 the differential equation (eq. (1.4)) expressed in terms of elliptical coordinates (eq. (1.20)) is transformed into a form yielding a solution in "epicycloidal transcendental functions." The characteristic determinant for the clamped case is presented, but not evaluated.

In reference 3.4 a minimal energy method is used with a deflection function of the form

$$W(r,\theta)=(1-\rho^2)^2[A_1+A_1\rho^2+A_2\rho^4+(A_3\rho^2+A_4\rho^4)\cos 2\theta+A_5\rho^4\cos 4\theta] \tag{3.10}$$

where ρ and θ are related to rectangular coordinates by the parametric equations

$$\left.\begin{aligned}x&=\rho\cos\theta\\ y&=\frac{b}{a}\rho\sin\theta\end{aligned}\right\} \tag{3.11}$$

to obtain fundamental frequency parameters. Results are given in table 3.3.

The problem was also formulated in terms of Mathieu functions and discussed in reference 3.5. It is also discussed in reference 3.6.

3.2 FREE PLATES

Experimental results for free elliptical brass plates having a/b ratios of 2 and 1.25 were obtained by Waller (ref. 3.7). Table 3.4 gives ratios of frequencies for $a/b=1.98$ relative to the fundamental frequency. The fundamental frequency upon which the table is based is given in reference 3.7 as 438 cycles per second

TABLE 3.3.—*Approximate Frequency Parameters* $\lambda^2=\omega a^2\sqrt{\rho/D}$ *for a Clamped Elliptical Plate*

b/a	1.0	0.9	0.8	0.7	0.6	0.5	0.4	0.3	0.2	0.1
λ^2	10. 216	11. 443	13. 229	15. 928	20. 195	27. 378	40. 649	69. 163	149. 89	583. 10

TABLE 3.4.—*Experimentally Determined Relative Frequencies for a Free Elliptical Brass Plate;* a/b=*1.98*

s	Frequency for value of n of—						
	0	1	2	3	4	5	6
0	------	------	1	2. 58	4. 7	7. 3	10
1	------	1. 77	3. 27	5. 68	8. 29	11	----
2	4. 25	6. 57	9. 43	12. 6	------	------	----
3	10. 6	14	------	------	------	------	----
4	17	22	------	------	------	------	----

for a brass plate with a major axis of 4.99 inches, a minor axis of 2.52 inches, and a thickness of 0.0638 inch. The mode indicators s and n indicate the number of nodal lines running approximately in the directions of the major and minor axes, respectively. This is illustrated in figure 3.2, where node patterns corresponding to some of the frequencies in table 3.4 are shown.

Frequency ratios for $a/b=1.24$ are given in table 3.5. The fundamental frequency for a brass plate having a major axis of 4.96 inches, a minor axis of 4.00 inches, and a thickness of 0.0638 inch was found (ref. 3.7) to be 414 cps.

This problem is also discussed in reference 3.8.

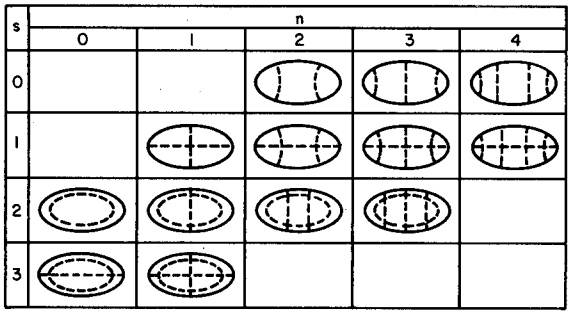


FIGURE 3.2.—Nodal lines for a free elliptical brass plate with $a/b=1.98$. (After ref. 3.7)

TABLE 3.5.—*Experimentally Determined Relative Frequencies for a Free Elliptical Brass Plate;* a/b=*1.24*

s	Frequency for value of n of—							
	0	1	2	3	4	5	6	7
0	------	------	1	2. 45	4. 28	6. 66	9. 39	13
1	------	1. 07	2. 59	4. 34	6. 8	9. 6	-----	---
2	2. 03	3. 99	6. 71	10	-----	-----	-----	---
3	4. 42	7. 41	10. 7	14	-----	-----	-----	---
4	9. 01	12	------	------	-----	-----	-----	---
5	14	------	------	------	-----	-----	-----	---

REFERENCES

3.1. SHIBAOKA, Y.: On the Transverse Vibration of an Elliptic Plate With Clamped Edge. J. Phys. Soc. Japan, vol. 11, no. 7, 1956, pp. 797–803.

3.2. MCNITT, R. P.: Free Vibration of a Clamped Elliptical Plate. J. Aerospace Sci., vol. 29, no. 9, Sept. 1962, pp. 1124–1125.

3.3. PIGNEDOLI, A.: On the Vibrations of an Elastic Plate With an Elliptic Embedded Edge. Actes IX Cong. Int. Mec. Appl., vol. 7, 1957, pp. 300–306.

3.4. COTUGNO, N.; AND MENGOTTI-MARZOLLA, C.: Approssimazione per Eccesso della Piu Bassa Frequenza di una Piastra Ellittica Omogenea Incastrata. Atti. Accad. Naz. Lincei, Rend., Classe Sci. Fis., Mat. Nat., vol. 5, ser. 8, sem. 2, Jan. 1943, pp. 324–327.

3.5. MCLACHLAN, N. W.: Vibrational Problems in Elliptical Coordinates. Quart. Appl. Math., vol. 5, no. 3, 1947, pp. 289–297.

3.6. ASTOLFO, E.: Valutazione per Eccesso della Piu Bassa Frequenza delle Oscillazioni Proprie di una Piastra Ellittica Omogenea Incastrata. Ric. Sci. e Ricostruz. (C.N.R. Roma), vol. 17, no. 12, Dec. 1947.

3.7. WALLER, MARY D.: Vibrations of Free Elliptical Plates. Proc. Phys. Soc. (London), ser. B, vol. 63, 1950, pp. 451–455.

3.8. WALLER, M. D.: Concerning Combined and Degenerate Vibrations of Plates. Acustica, vol. 3, 1953, pp. 370–374.

Chapter 4

Rectangular Plates

Altogether there are 21 combinations of simple boundary conditions (i.e., either clamped (C), simply supported (SS), or free (F)) for rectangular plates. Frequency parameters are expressed in terms of $\omega a^2\sqrt{\rho/D}$, where a is a length dimension, and do not depend upon Poisson's ratio unless at least one of the edges of the plate is free. However, because D contains ν, the frequencies themselves depend upon ν for all cases.

Warburton (ref. 4.1) presented the first comprehensive collection of solutions for rectangular plates. He used the Rayleigh method with deflection functions as the product of beam functions; that is,

$$W(x,y)=X(x)Y(y) \tag{4.1}$$

where $X(x)$ and $Y(y)$ are chosen as the fundamental mode shapes of beams having the boundary conditions of the plate. This choice of functions then exactly satisfies all boundary conditions for the plate, except in the case of the free edge, where the shear condition is approximately satisfied. The six possible distinct sets of boundary conditions along the edges $x=0$ and $x=a$ are satisfied by the following mode shapes:

(*a*) Simply Supported at $x=0$ and $x=a$:

$$X(x)=\sin\frac{(m-1)\pi x}{a} \qquad (m=2,3,4,\ldots) \tag{4.2}$$

(*b*) Clamped at $x=0$ and $x=a$:

$$X(x)=\cos\gamma_1\left(\frac{x}{a}-\frac{1}{2}\right)+\frac{\sin(\gamma_1/2)}{\sinh(\gamma_1/2)}\cosh\gamma_1\left(\frac{x}{a}-\frac{1}{2}\right) \qquad (m=2,4,6,\ldots) \tag{4.3}$$

where the values of γ_1 are obtained as roots of

$$\tan(\gamma_1/2)+\tanh(\gamma_1/2)=0 \tag{4.4}$$

and

$$X(x)=\sin\gamma_2\left(\frac{x}{a}-\frac{1}{2}\right)-\frac{\sin(\gamma_2/2)}{\sinh(\gamma_2/2)}\sinh\gamma_2\left(\frac{x}{a}-\frac{1}{2}\right) \qquad (m=3,5,7,\ldots) \tag{4.5}$$

where the values of γ_2 are obtained as roots of

$$\tan(\gamma_2/2)-\tanh(\gamma_2/2)=0 \tag{4.6}$$

(*c*) Free at $x=0$ and $x=a$:

$$X(x)=1 \qquad (m=0) \tag{4.7}$$

$$X(x)=1-\frac{2x}{a} \qquad (m=1) \tag{4.8}$$

$$X(x)=\cos\gamma_1\left(\frac{x}{a}-\frac{1}{2}\right)-\frac{\sin(\gamma_1/2)}{\sinh(\gamma_1/2)}\cosh\gamma_1\left(\frac{x}{a}-\frac{1}{2}\right) \qquad (m=2,4,6,\ldots) \tag{4.9}$$

and

$$X(x)=\sin\gamma_2\left(\frac{x}{a}-\frac{1}{2}\right)+\frac{\sin(\gamma_2/2)}{\sinh(\gamma_2/2)}\sinh\gamma_2\left(\frac{x}{a}-\frac{1}{2}\right) \qquad (m=3,5,7,\ldots) \tag{4.10}$$

with γ_1 and γ_2 as defined in equations (4.4) and (4.6).

(*d*) Clamped at $x=0$ and Free at $x=a$:

$$X(x)=\cos\frac{\gamma_3 x}{a}-\cosh\frac{\gamma_3 x}{a}+\left(\frac{\sin\gamma_3-\sinh\gamma_3}{\cos\gamma_3-\cosh\gamma_3}\right)\left(\sin\frac{\gamma_3 x}{a}-\sinh\frac{\gamma_3 x}{a}\right) \qquad (m=1,2,3,\ldots) \tag{4.11}$$

where

$$\cos\gamma_3\cosh\gamma_3=-1 \tag{4.12}$$

(*e*) Clamped at $x=0$ and Simply Supported at $x=a$:

$$X(x)=\sin\gamma_2\left(\frac{x}{2a}-\frac{1}{2}\right)-\frac{\sin(\gamma_2/2)}{\sinh(\gamma_2/2)}\sinh\gamma_2\left(\frac{x}{2a}-\frac{1}{2}\right) \qquad (m=2,3,4,\cdots) \tag{4.13}$$

308-337 O—70——4

with γ_2 as defined in equation (4.6).

(*f*) Free at $x=0$ and Simply Supported at $x=a$:

$$X(x)=1-\frac{x}{a} \qquad (m=1) \tag{4.14}$$

$$X(x)=\sin\gamma_2\left(\frac{x}{2a}-\frac{1}{2}\right)+\frac{\sin(\gamma_2/2)}{\sinh(\gamma_2/2)}\sinh\gamma_2\left(\frac{x}{2a}-\frac{1}{2}\right) \qquad (m=2,3,4,\cdots) \tag{4.15}$$

with γ_2 as defined in equation (4.6).

The functions $Y(y)$ are similarly chosen by the conditions at $y=0$ and $y=a$ by replacing x by y, a by b, and m by n in equations (4.2) to (4.15). The indicators n and m are seen to be the number of nodal lines lying in the x- and y-directions, respectively, including the boundaries as nodal lines, except when the boundary is free.

The frequency ω is given by reference 4.1 as

$$\omega^2=\frac{\pi^4 D}{a^4\rho}\left\{G_x^4+G_y^4\left(\frac{a}{b}\right)^4+2\left(\frac{a}{b}\right)^2[\nu H_x H_y+(1-\nu)J_x J_y]\right\} \tag{4.16}$$

where G_x, H_x, and J_x are functions determined from table 4.1 according to the conditions at $x=0$ and $x=a$.

The quantities G_y, H_y, and J_y are obtained from table 4.1 by replacing x by y and m by n.

Another comprehensive set of solutions was later given by Janich (ref. 4.2). Fundamental frequencies were obtained for 18 combinations of boundary conditions. He, too, used the

TABLE 4.1.—*Frequency Coefficients in Equation (4.16)*

Boundary conditions at—	m	G_x	H_x	J_x
SS[a]	2, 3, 4, . . .	$m-1$	$(m-1)^2$	$(m-1)^2$
SS[b]	2, 3, 4, . . .	$m-1$	$(m-1)^2$	$(m-1)^2$
C[a]	2	1. 506	1. 248	1. 248
C[b]	3, 4, 5, . . .	$m-\frac{1}{2}$	$\left(m-\frac{1}{2}\right)^2\left[1-\frac{2}{\left(m-\frac{1}{2}\right)\pi}\right]$	$\left(m-\frac{1}{2}\right)^2\left[1-\frac{2}{\left(m-\frac{1}{2}\right)\pi}\right]$
F[a]	0	0	0	0
	1	0	0	$12/\pi^2$
	2	1. 506	1. 248	5. 017
F[b]	3, 4, 5, . . .	$m-\frac{1}{2}$	$\left(m-\frac{1}{2}\right)^2\left[1-\frac{2}{\left(m-\frac{1}{2}\right)\pi}\right]$	$\left(m-\frac{1}{2}\right)^2\left[1+\frac{6}{\left(m-\frac{1}{2}\right)\pi}\right]$
C[a]	2, 3, 4, . . .	$m-\frac{3}{4}$	$\left(m-\frac{3}{4}\right)^2\left[1-\frac{1}{\left(m-\frac{3}{4}\right)\pi}\right]$	$\left(m-\frac{3}{4}\right)^2\left[1-\frac{1}{\left(m-\frac{3}{4}\right)\pi}\right]$
SS[b]	2, 3, 4, . . .	$m-\frac{3}{4}$	$\left(m-\frac{3}{4}\right)^2\left[1-\frac{1}{\left(m-\frac{3}{4}\right)\pi}\right]$	$\left(m-\frac{3}{4}\right)^2\left[1-\frac{1}{\left(m-\frac{3}{4}\right)\pi}\right]$
F[a]	1	0	0	$3/\pi^2$
SS[b]	2, 3, 4, . . .	$m-\frac{3}{4}$	$\left(m-\frac{3}{4}\right)^2\left[1-\frac{1}{\left(m-\frac{3}{4}\right)\pi}\right]$	$\left(m-\frac{3}{4}\right)^2\left[1+\frac{3}{\left(m-\frac{3}{4}\right)\pi}\right]$
C[a]	1	0. 597	−0. 0870	0. 471
	2	1. 494	1. 347	3. 284
F[b]	3, 4, 5, . . .	$m-\frac{1}{2}$	$\left(m-\frac{1}{2}\right)^2\left[1-\frac{2}{\left(m-\frac{1}{2}\right)\pi}\right]$	$\left(m-\frac{1}{2}\right)^2\left[1+\frac{2}{\left(m-\frac{1}{2}\right)\pi}\right]$

[a] $x=0$.
[b] $x=a$.

Rayleigh method, but used simple trigonometric functions which satisfied only the geometric boundary conditions. The mode shapes used in reference 4.2 are given in table 4.2.

The frequency ω is given in reference 4.2 for $\nu=0.25$ by

$$\omega^2=\frac{\pi^4 D}{a^4\rho}\frac{K}{N} \tag{4.17}$$

with K and N given in table 4.2.

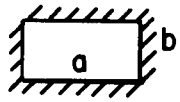
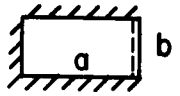
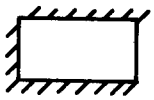
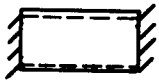
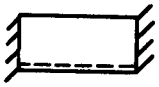
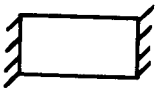
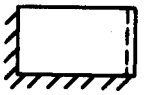
The results of references 4.1 and 4.2 are both obtained by the Rayleigh method and, hence, yield upper bounds on the frequency values. However, it must be pointed out that both sets of results have limitations in accuracy. The three cases not included in table 4.2 (F–F–F–F, SS–F–F–F, and SS–SS–F–F) yield such poor results with mode shapes of the same type that they were not included in reference 4.2. The force-type boundary conditions as well as the geometric are satisfied in reference 4.1; this usually improves the accuracy of the solution, but *occasionally makes it worse*. The results determined from table 4.1 will decrease in accuracy for higher mode shapes (increasing values of m and n).

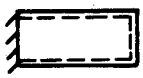
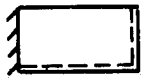
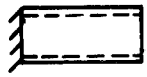
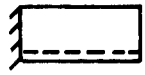
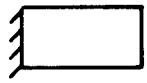
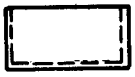
A partial summary of vibration frequencies for rectangular plates was given in reference 4.3.

4.1 SS–SS–SS–SS

The problem of plates with all sides SS is the most simple to solve for the rectangular plate.

TABLE 4.2.—*Frequency Coefficients for Equation (4.17) and Different Mode Shapes; $\nu=0.25$*

Boundary conditions	Deflection function or mode shape	N	K
	$\left(\cos\frac{2\pi x}{a}-1\right)\left(\cos\frac{2\pi y}{b}-1\right)$	2.25	$12+8\left(\frac{a}{b}\right)^2+12\left(\frac{a}{b}\right)^4$
	$\left(\cos\frac{3\pi x}{2a}-\cos\frac{\pi x}{2a}\right)\left(\cos\frac{2\pi y}{b}-1\right)$	1.50	$3.85+5\left(\frac{a}{b}\right)^2+8\left(\frac{a}{b}\right)^4$
	$\left(1-\cos\frac{\pi x}{2a}\right)\left(\cos\frac{2\pi y}{b}-1\right)$	.340	$0.0468+0.340\left(\frac{a}{b}\right)^2+1.814\left(\frac{a}{b}\right)^4$
	$\left(\cos\frac{2\pi x}{a}-1\right)\sin\frac{\pi y}{b}$	.75	$4+2\left(\frac{a}{b}\right)^2+0.75\left(\frac{a}{b}\right)^4$
	$\left(\cos\frac{2\pi x}{a}-1\right)\frac{y}{b}$	.50	$2.67+0.304\left(\frac{a}{b}\right)^2$
	$\cos\frac{2\pi x}{a}-1$	1.50	8
	$\left(\cos\frac{3\pi x}{2a}-\cos\frac{\pi x}{2a}\right)\left(\cos\frac{3\pi y}{2b}-\cos\frac{\pi y}{2b}\right)$	1.00	$2.56+3.12\left(\frac{a}{b}\right)^2+2.56\left(\frac{a}{b}\right)^4$
	$\left(\cos\frac{3\pi x}{2a}-\cos\frac{\pi x}{2a}\right)\left(1-\cos\frac{\pi y}{2b}\right)$	.227	$0.581+0.213\left(\frac{a}{b}\right)^2+0.031\left(\frac{a}{b}\right)^4$

Boundary conditions	Deflection function or mode shape	N	K
	$\left(1-\cos\frac{\pi x}{2a}\right)\left(1-\cos\frac{\pi y}{2b}\right)$	0.0514	$0.0071+0.024\left(\frac{a}{b}\right)^2+0.0071\left(\frac{a}{b}\right)^4$
	$\left(\cos\frac{3\pi x}{2a}-\cos\frac{\pi x}{2a}\right)\sin\frac{\pi y}{b}$	.50	$1.28+1.25\left(\frac{a}{b}\right)^2+0.50\left(\frac{a}{b}\right)^4$
	$\left(\cos\frac{3\pi x}{2a}-\cos\frac{\pi x}{2a}\right)\frac{y}{b}$	.333	$0.853+0.190\left(\frac{a}{b}\right)^2$
	$\cos\frac{3\pi x}{2a}-\cos\frac{\pi x}{2a}$	1.00	2.56
	$\left(1-\cos\frac{\pi x}{2a}\right)\frac{\pi^2}{b^2}\sin\frac{\pi y}{b}$	.1134	$0.0156+0.0852\left(\frac{a}{b}\right)^2+0.1134\left(\frac{a}{b}\right)^4$
	$\left(1-\cos\frac{\pi x}{2a}\right)\frac{y}{b}$	.0756	$0.0104+0.0190\left(\frac{a}{b}\right)^2$
	$1-\cos\frac{\pi x}{2a}$	.2268	0.0313
	$\sin\frac{\pi x}{a}\sin\frac{\pi y}{b}$	.25	$0.25+0.50\left(\frac{a}{b}\right)^2+0.25\left(\frac{a}{b}\right)^4$
	$\left(\sin\frac{\pi x}{a}\right)\frac{y}{b}$	.1667	$0.1667+0.0760\left(\frac{a}{b}\right)^2$
	$\sin\frac{\pi x}{a}$	.50	0.50

The boundary conditions are

$$\left.\begin{aligned} w=0, M_x=0 \quad & (\text{for } x=0, a) \\ w=0, M_y=0 \quad & (\text{for } y=0, b) \end{aligned}\right\} \tag{4.18}$$

When equations (1.29) are used it is seen that

$$W_{mn}=A_{mn}\sin\frac{m\pi x}{a}\sin\frac{n\pi y}{b} \tag{4.19}$$

satisfies the boundary conditions, where A_{mn} is an amplitude coefficient determined from the initial conditions of the problem and m and n are integers. Substituting equation (4.19) into equation (1.4) gives the frequency

$$\omega=\sqrt{\frac{D}{\rho}}\left[\left(\frac{m\pi}{a}\right)^2+\left(\frac{n\pi}{b}\right)^2\right] \tag{4.20}$$

A plot of four frequency parameters as a function of the b/a ratio was made by Vet (ref. 4.4) and is shown in figure 4.1.

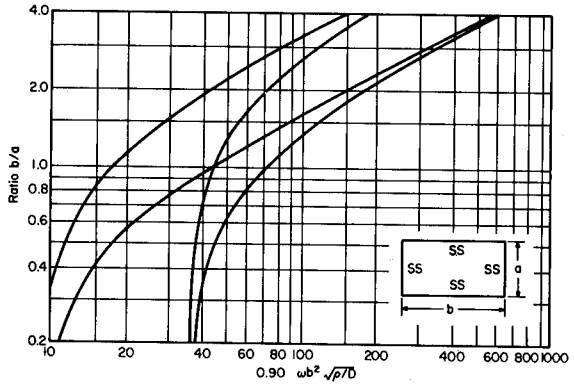


FIGURE 4.1.—Frequency parameter $0.90\omega b^2\sqrt{\rho/D}$ for SS–SS–SS–SS rectangular plate. (After ref. 4.4)

The node lines for a general rectangle are simply straight lines parallel to the edges as shown in figure 4.2. For square plates, however, two mode shapes may have the same frequency and exist simultaneously, their relative amplitudes depending upon the initial conditions. Sequences of nodal patterns obtainable for a given frequency are shown for three cases from reference 4.5 in figure 4.3. The problem was also solved in reference 4.6 by replacing the plate by an assemblage of beams and concentrated masses.

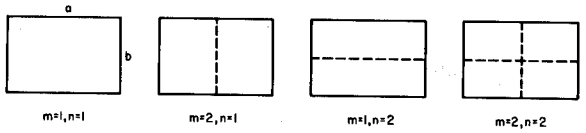


FIGURE 4.2.—Nodal patterns for SS rectangular plate with $a>b$.

4.2 TWO OPPOSITE SIDES SS

There are six combinations of boundary conditions for which two opposite sides are SS. One of these (for the plate with all sides SS which has a simple, exact solution) has already been discussed. The remaining five cases also have exact (although more difficult) solutions. When the edges $x=0$ and $x=a$ are SS, it is seen that the conditions at these boundaries, as well as the differential equation of the problem (eq. (1.4)), are exactly satisfied by using the first half of equation (1.37) with $\alpha=m\pi/a$; that is,

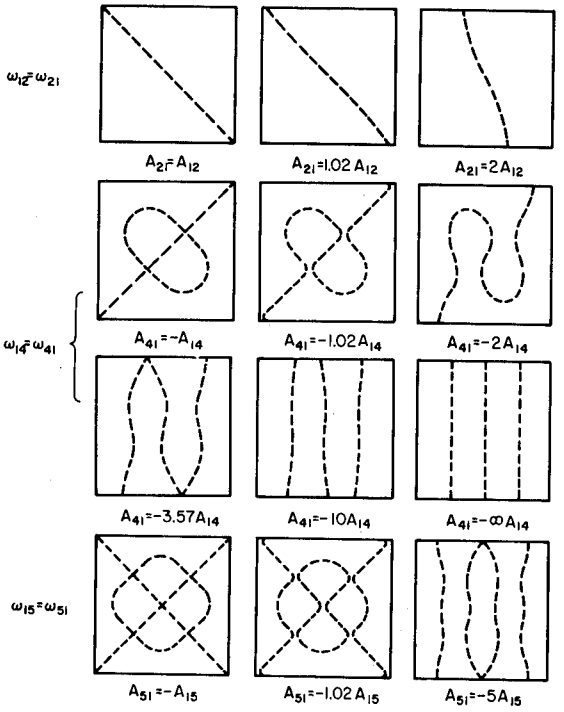


FIGURE 4.3.—Combined nodal patterns for a SS square plate. (After ref. 4.5)

$$W(x,y)=\sum_{m=1}^{\infty}[A_m\sin\sqrt{k^2-\alpha^2}y+B_m\cos\sqrt{k^2-\alpha^2}y+C_m\sinh\sqrt{k^2+\alpha^2}y+D_m\cosh\sqrt{k^2+\alpha^2}y]\sin\alpha x \quad (4.21)$$

Applying the remaining four homogeneous boundary conditions results in a set of fourth-order characteristic determinants, one for each value of α. Each determinant has an infinity of solutions for the eigenvalues k. Any of the four edges being free is a necessary and sufficient condition for the frequency parameter to depend upon Poisson's ratio.

The first straightforward, comprehensive solution of these five cases by the method outlined above was given by Fletcher, Woodfield, and Larsen in reference 4.7 and in reference 4.8. In reference 4.7 an excellent analysis is made of the conditions which lead to $k^2<\alpha^2$ requiring

that $\sin\sqrt{k^2-\alpha^2}y$ and $\cos\sqrt{k^2-\alpha^2}y$ be replaced in equation (1.36) by $\sinh\sqrt{\alpha^2-k^2}y$ and $\cosh\sqrt{\alpha^2-k^2}y$, respectively. They formulated the characteristic determinants and solved for the eigenfunctions for all five cases and published the first six frequencies of a square plate in each case.

Iguchi (ref. 4.9) solved the problems involving one edge C and the opposite either C or SS and presented extensive numerical results for them. Das (ref. 4.10) formulated characteristic equations and eigenfunctions for the two cases of opposite edges either F or C. Pertinent discussion can also be found in reference 4.11.

It has been shown (e.g., refs. 4.9 and 4.12) that a useful analogy exists between the vibration and buckling of rectangular plates having two opposite sides SS. The deflection of a rectangular plate loaded by compressive inplane forces is given by (see the appendix)

$$D\nabla^4 w=-N_x\frac{\partial^2 w}{\partial x^2}+2N_{xy}\frac{\partial^2 w}{\partial x\partial y}-N_y\frac{\partial^2 w}{\partial y^2} \tag{4.22}$$

where $N_x=N_x(x,y)$ and N_y are compressive forces per unit length acting in the x- and y-directions, respectively, and N_{xy} is the inplane shearing force per unit length. Taking the case $N_{xy}=N_y=0$ and assuming that $w(x,\ y)=\sum_m Y_m(y)\sin\frac{m\pi x}{a}$ (where $m=1,\ 2,\ \ldots$) satisfy the SS boundary conditions at $x=0$ and $x=a$ and reduce equation (4.22) to the two homogeneous equations

$$\left.\begin{aligned}\frac{d^2Y_{m_1}}{dy^2}+\left(\alpha\sqrt{\frac{N_x}{D}}-\alpha^2\right)Y_{m_1}=0\\ \frac{d^2Y_{m_2}}{dy^2}-\left(\alpha\sqrt{\frac{N_x}{D}}+\alpha^2\right)Y_{m_2}=0\end{aligned}\right\} \tag{4.23}$$

where $\alpha=m\pi/a$, as before. When equations (4.23) are compared with equations (1.34), it is seen that the solution for buckling also solves the vibration problem if $N_x\alpha^2/D$ is replaced by $\rho\omega^2/D$ and the boundary conditions on the remaining two edges are the same. Thus the critical buckling load N_x gives vibration frequencies according to

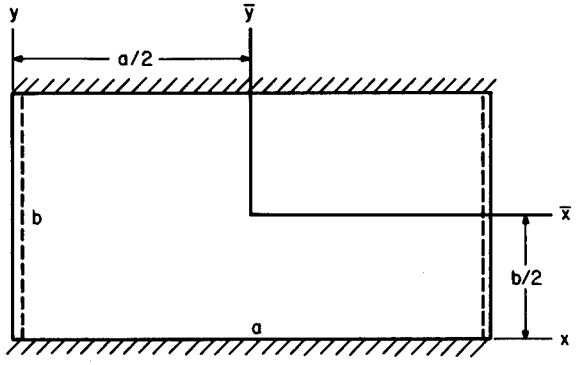


FIGURE 4.4.—SS–C–SS–C plate.

$$N_x\sim\frac{\rho\omega^2}{\alpha^2} \tag{4.24}$$

4.2.1 SS–C–SS–C

Recognizing that the solution for SS–C–SS–C plates (fig. 4.4) given by equation (1.37) must be valid for all independent values of x and substituting into the boundary conditions

$$W(x,0)=\frac{\partial W}{\partial y}(x,0)=W(x,b)=\frac{\partial W}{\partial y}(x,b)=0 \tag{4.25}$$

results in the four homogeneous equations

$$\left.\begin{aligned}&B_m+D_m=0\\ &A_m\lambda_1+C_m\lambda_2=0\\ &A_m\sin\lambda_1 b+B_m\cos\lambda_1 b+C_m\sinh\lambda_2 b\\ &\qquad\qquad+D_m\cosh\lambda_2 b=0\\ &A_m\lambda_1\cos\lambda_1 b-B_m\lambda_1\sin\lambda_1 b+C_m\lambda_2\cosh\lambda_2 b\\ &\qquad\qquad+D_m\lambda_2\sinh\lambda_2 b=0\end{aligned}\right\} \tag{4.26}$$

where

$$\left.\begin{aligned}\lambda_1&\equiv\sqrt{k^2-\alpha^2}\\ \lambda_2&\equiv\sqrt{k^2+\alpha^2}\end{aligned}\right\} \tag{4.27}$$

For a nontrivial solution the determinant of the coefficients of equations (4.26) must vanish; that is,

$$\begin{vmatrix}0 & 1 & 0 & 1\\ \lambda_1 & 0 & \lambda_2 & 0\\ \sin\lambda_1 b & \cos\lambda_1 b & \sinh\lambda_2 b & \cosh\lambda_2 b\\ \lambda_1\cos\lambda_1 b & -\lambda_1\sin\lambda_1 b & \lambda_2\cosh\lambda_2 b & \lambda_2\sinh\lambda_2 b\end{vmatrix}=0 \tag{4.28}$$

TABLE 4.3.—*First 6 Frequency Parameters* $\lambda=\omega a^2\sqrt{\rho/D}$ *for SS–C–SS–C Square Plate*

λ	28.946	54.743	69.320	94.584	102.213	129.086
Mode	ω_{11}	ω_{21}	ω_{12}	ω_{22}	ω_{31}	ω_{13}

which, when expanded, yields the characteristic equation

$$2\lambda_1\lambda_2(\cos\lambda_1 b\cosh\lambda_2 b-1)+(\lambda_1^2-\lambda_2^2)\sin\lambda_1 b\sinh\lambda_2 b=0 \quad (4.29)$$

Iguchi (ref. 4.9) solved this problem in essentially the same manner and obtained the first six frequency parameters for the case of the square. They are presented in table 4.3.

For the frequency ω_{mn}, the subscript m identifies the number of half-sine waves in the x-direction and the subscript n identifies the nth lowest root for a fixed value of m. The results of table 4.3 are also verified in references 4.7 and 4.13.

TABLE 4.4.—*12 Higher Frequency Parameters* $\lambda=\omega a^2(\sqrt{\rho/D})$ *(not a Complete Set) for SS–C–SS–C Square Plate*

λ	Mode	λ	Mode
140.189	ω_{32}	307.300	ω_{15}
154.765	ω_{23}	333.926	ω_{25}
199.797	ω_{33}	379.274	ω_{35}
208.373	ω_{14}	425.885	ω_{16}
234.578	ω_{24}	452.877	ω_{26}
279.627	ω_{34}	498.501	ω_{36}

In addition, reference 4.9 gives 12 more roots as listed in table 4.4. It must be emphasized that other frequencies exist (e.g., ω_{41}, ω_{42}, and ω_{51}) which would separate some of the values in table 4.4 if a complete, sequential list were available. These can be obtained from the work of Ödman (ref. 4.13) who solved equation (4.29) with less accuracy than did Iguchi but extracted the first six roots for $m=1, 2, \ldots, 6$. The corresponding frequency parameters are listed in table 4.5.

Nishimura (ref. 4.14) achieved accurate results for the square using relatively coarse finite difference grids. He obtained $\omega a^2\sqrt{\rho/D}=28.974$ for the fundamental mode by solving only third-order finite-difference determinants.

For nonsquare plates, fundamental frequencies are available for various aspect ratios. These are listed in table 4.6 (see also ref. 4.9). Hamada (ref. 4.15) used a variational approach and Kanazawa and Kawai (ref. 4.16) used an

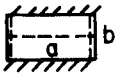
TABLE 4.5.—*Frequency Parameters* $\omega a^2\sqrt{\rho/D}$ *for SS–C–SS–C Square Plate*

m	$\omega a^2\sqrt{\rho/D}$ for values of n of—					
	1	2	3	4	5	6
1	28.9	69.2	129.1	208.6	307.4	426.1
2	54.8	94.6	154.8	234.5	333.9	452.9
3	102.2	140.2	199.9	279.5	379.1	498.4
4	170.3	206.6	265.2	344.6	443.8	563.5
5	258.5	293.8	351.1	429.8	529.0	647.9
6	366.8	400.9	457.4	535.1	633.7	752.2

TABLE 4.6.—*Fundamental Frequency Parameters for a SS–C–SS–C Rectangular Plate*

Parameter	λ for values of b/a and λ^* for values of a/b of—					
	1	1.5	2	2.5	3	∞
$\lambda=\omega a^2(\sqrt{\rho/D})$	28.946	17.369	13.688	12.129	11.359	9.869
$\lambda^*=\omega b^2(\sqrt{\rho/D})$	28.946	24.047	23.814	23.271	22.985	22.373

TABLE 4.7.—*Frequency Parameter* $\omega b^2(\sqrt{\rho/D})$ *for the Second Antisymmetric Mode of a SS–C–SS–C Rectangular Plate*

Boundary conditions	$\omega b^2(\sqrt{\rho/D})$ for value of a/b of—					
	1	1.5	2	2.5	3	∞
	68. 181	65. 118	63. 641	62. 967	62. 602	61. 178

integral formulation to obtain confirming results for several a/b ratios. In reference 4.16, results are also obtained for the mode antisymmetric about $\bar{y}=0$, for $a/b \geqq 1$. Unfortunately, this is the *second* antisymmetric mode shape of the plate. These frequency parameters are given in table 4.7.

The first six roots of equation (4.29) for $m=1, 2, \ldots, 6$ and for $a/b=0.5$, 1.5, and 2.0 were found in reference 4.13. The corresponding frequency parameters are listed in table 4.8.

By using equation (4.24), one can apply stability results to this problem. Fundamental frequencies are listed in table 4.9 for various a/b ratios as given on page 367 of reference 4.17.

Eliminating three of the constants (e.g., B_n, C_n, and D_n) in equations (4.26) in favor of a fourth (e.g., A_n) leaves one equation giving the eigenfunctions, or mode shapes, for this case. From reference 4.7 it is known to be:

$$w(x,y)=[(\cosh \lambda_2 b-\cos \lambda_1 b)(\lambda_1 \sinh \lambda_2 y - \lambda_2 \sin \lambda y) - (\lambda_1 \sinh \lambda_2 \sin \lambda_1 b)(\cosh \lambda_2 y-\cos \lambda_1 y)] \sin \alpha x \quad (4.30)$$

Substitution of λ_1 and λ_2 determined from equations (4.27) into equation (4.30), using the frequencies from the tables of this section, completely determines the mode shapes. Mode

TABLE 4.8.—*Frequency Parameters* $\omega b^2\sqrt{\rho/D}$ *for SS–C–SS–C Rectangular Plate*

$\frac{a}{b}$	m	$\omega b^2\sqrt{\rho/D}$ for values of n of—					
		1	2	3	4	5	6
0.5	1	54. 8	94. 6	154. 8	234. 5	333. 9	452. 9
	2	170. 3	206. 6	265. 2	344. 6	443. 8	563. 5
	3	366. 8	400. 9	457. 4	535. 1	633. 7	752. 2
	4	642. 8	675. 9	730. 5	806. 9	904. 2	1021
	5	997. 7	1030	1084	1159	1257	1375
	6	1432	1464	1517	1592	1686	1802
1.5	1	25. 0	64. 9	124. 5	203. 7	302. 4	420. 9
	2	35. 1	75. 6	135. 7	215. 1	314. 1	432. 8
	3	54. 8	94. 6	154. 8	234. 5	333. 9	452. 9
	4	84. 1	122. 3	182. 6	262. 5	362: 0	481. 1
	5	122. 6	160. 0	219. 3	298. 9	398. 5	518. 0
	6	170. 3	206. 6	265. 2	344. 6	443. 8	563. 5
2.0	1	23. 8	63. 4	123. 0	202. 1	300. 7	419. 0
	2	28. 9	69. 2	129. 1	208. 6	307. 4	426. 1
	3	39. 0	79. 5	139. 7	219. 3	318. 2	437. 1
	4	54. 8	94. 6	154. 8	234. 5	333. 9	452. 9
	5	75. 9	114. 7	174. 6	254. 7	354. 1	473. 3
	6	102. 2	140. 2	199. 9	279. 5	379. 1	498. 4

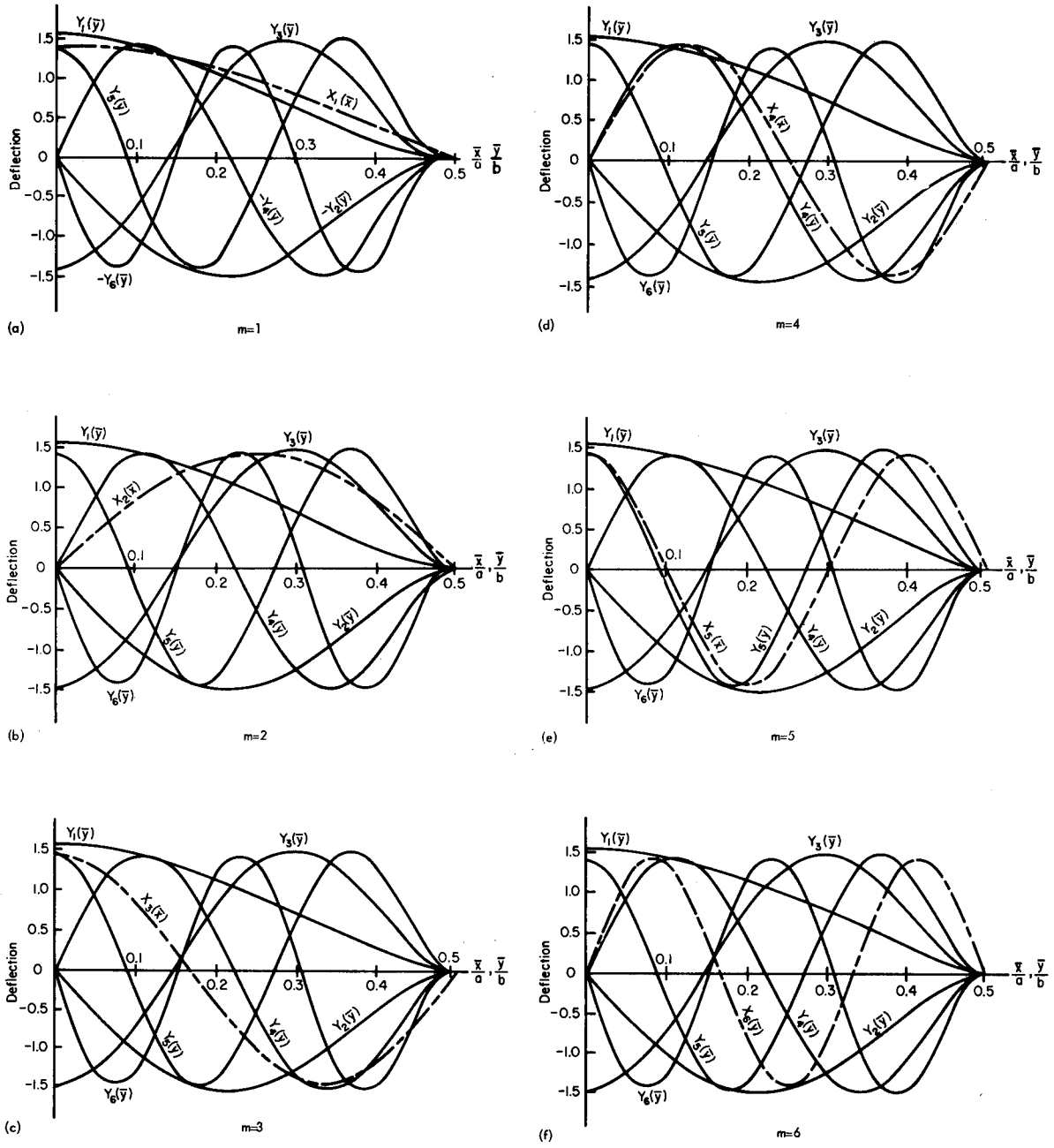


FIGURE 4.5.—Mode shapes $W_{mn}(\bar{x}, \bar{y}) = X_m(\bar{x})\, Y_n(\bar{y})$ for 36 modes of a SS–C–SS–C square plate. $m, n = 1, 2, \ldots 6$. (After ref. 4.13)

TABLE 4.9.—*Fundamental Frequency Parameters for SS–C–SS–C Rectangular Plate*

a/b	0.4	0.5	0.6	0.7	0.8	0.9
$\omega a^2\sqrt{\rho/D}$	12. 139	13. 718	15. 692	18. 258	20. 824	24. 080

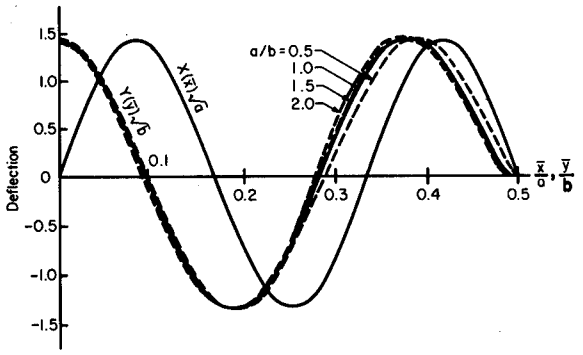


FIGURE 4.6.—Variation in $Y_n(\bar{y})$ with a/b for the mode $m=6$, $n=5$ for a SS–C–SS–C rectangular plate. (After ref. 4.13)

shapes were computed and plotted in reference 4.13 for the first six roots of equation (4.29) for $m=1, 2, \ldots, 6$. Plots were made for $a/b=0.5$, 1.0, 1.5, and 2.0. These are reproduced in figure 4.5 for $a/b=1.0$ alone. The mode shapes are represented as the products $W_{mn}(\bar{x},\bar{y})=X_m(\bar{x})Y_n(\bar{y})$. Each of the six parts of figure 4.5 corresponds to one value of m. The first six modes having that value of m are then determined from the separate curves $Y_n(\bar{y})$. The curves for $Y_n(\bar{y})$ do not change markedly for variation of a/b in the range $0.5<a/b<2.0$. The maximum variations for the 36 modes shown in reference 4.13 are illustrated by figure 4.6, which is for the mode $m=6$, $n=5$.

When $k^2+\alpha^2>>1$, then $\cosh\sqrt{k^2+\alpha^2}b\rightarrow\sinh\sqrt{k^2+\alpha^2}b$ and equation (4.29) reduces to the following asymptotic formula (ref. 4.7):

$$\omega=\pi^2\left[\left(\frac{m}{a}\right)^2+\left(\frac{n+\frac{1}{2}}{b}\right)^2\right]\sqrt{\frac{D}{\rho}} \qquad (m,n \text{ integers}) \quad (4.31)$$

Other approximate formulas are given previously in equations (4.16) and (4.17). Frequency parameters obtained from equation (4.16) are given in reference 4.4 and are reproduced as figure 4.7.

The problem was also studied in references 4.18 to 4.21.

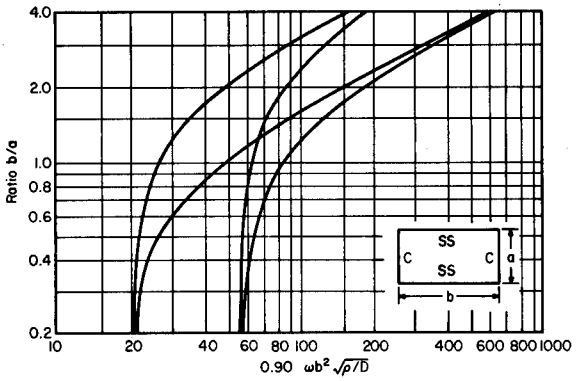


FIGURE 4.7.—Frequency parameter $0.90\omega b^2\sqrt{\rho/D}$ for a SS–C–SS–C rectangular plate. (After ref. 4.4)

4.2.2 SS–C–SS–SS

The boundary conditions for SS–C–SS–SS rectangular plates (fig. 4.8) at $y=0, b$ are

$$W(x,0)=M_y(x,0)=W(x,b)=\frac{\partial W}{\partial y}(x,b)=0 \qquad (4.32)$$

Substituting equation (1.37) into equation (4.32) as in the previous section yields the characteristic equation (ref. 4.7)

$$\lambda_2\cosh\lambda_2 b\sin\lambda_1 b=\lambda_1\sinh\lambda_2 b\cos\lambda_1 b \qquad (4.33)$$

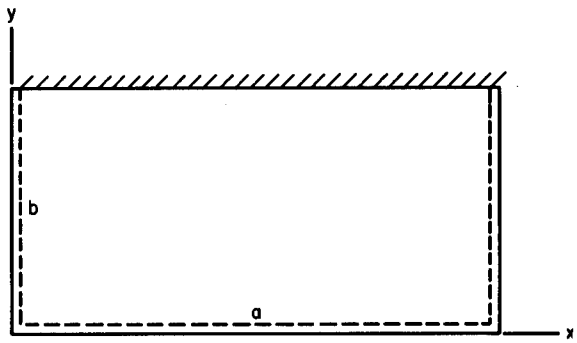


FIGURE 4.8.—SS–C–SS–SS plate.

TABLE 4.10—*First 6 Frequency Parameters* $\lambda=\omega a^2\sqrt{\rho/D}$ *for SS–C–SS–SS Square Plate*

λ	23. 646	51. 674	58. 641	86. 126	100. 259	113. 217
Mode	ω_{11}	ω_{21}	ω_{12}	ω_{22}	ω_{31}	ω_{13}

where λ_1 and λ_2 are defined in equations (4.27).

Iguchi (ref. 4.9) also obtained equation (4.33) and presented the first six frequencies for the case of the square. They are given in table 4.10. These results are verified in reference 4.7. Three additional frequencies listed in reference 4.9 are given in table 4.11. Explanation of the significance of these roots appears in the preceding section (4.2.1).

TABLE 4.11.—*3 High-Frequency Parameters* $\lambda=\omega a^2\sqrt{\rho/D}$ *for SS–C–SS–SS Square Plate*

λ	133. 784	140. 840	188. 102
Mode	ω_{32}	ω_{23}	ω_{33}

Ungar (ref. 4.22) presented an interesting table which shows the ratio of the frequencies of the SS–C–SS–SS plate to those of the SS–SS–SS–SS plate when $a=b$. This is given here as table 4.12, where m denotes the number of half-sine waves in the x-direction (fig. 4.8) and n denotes the mode number for a given value of m.

TABLE 4.12.—*Ratio of Frequencies of a SS–C–SS–SS Plate to Those of SS–SS–SS–SS Plate When* a=b

m	Frequency ratio for value of n—					
	1	2	3	4	5	6
1	1. 19	1. 06	1. 02	1. 01	1. 00	1. 00
2	1. 21	1. 09	1. 05	1. 02	1. 02	1. 01
3	1. 14	1. 09	1. 06	1. 03	1. 02	1. 02
4	1. 11	1. 09	1. 06	1. 04	1. 03	1. 02
5	1. 10	1. 08	1. 06	1. 05	1. 03	1. 02
6	1. 08	1. 07	1. 06	1. 05	1. 04	1. 02

For nonsquare plates, fundamental frequencies are available for various aspect ratios as listed in table 4.13 (ref. 4.9). Hamada (ref. 4.15) used a variational approach and Kanazawa and Kawai (ref. 4.16) used an integral equation formulation to obtain confirming results for several a/b ratios.

TABLE 4.13—*Fundamental Frequency Parameters for SS–C–SS–SS Rectangular Plate*

Frequency parameter	λ for values of b/a or λ^* for values of a/b of—					
	1	1. 5	2	2. 5	3	∞
$\lambda=\omega a^2(\sqrt{\rho/D})$	23. 646	15. 573	12. 918	11. 754	11. 142	9. 869
$\lambda^*=\omega b^2(\sqrt{\rho/D})$	23. 646	18. 899	17. 330	16. 629	16. 254	15. 425

The mode shapes are (ref. 4.7)

$$W(x, y)=(\sin\lambda_1 b\sinh\lambda_2 y-\sinh\lambda_2 b\sin\lambda_1 y)\sin\alpha x \tag{4.34}$$

When $k^2+\alpha^2>>1$, equation (4.33) reduces to (ref. 4.7)

$$\omega=\pi^2\left\{\left(\frac{m}{a}\right)^2+\left[\frac{n+(1/4)}{b}\right]^2\right\}\sqrt{\frac{D}{\rho}} \quad (m, n \text{ integers}) \tag{4.35}$$

Other approximate formulas are given in equations (4.16) and (4.17). Frequency parameters obtained from equation (4.16) are given in figure 4.9 (ref. 4.4). The problem was also discussed in references 4.23 and 4.24.

4.2.3 SS–C–SS–F

The boundary conditions for SS–C–SS–F rectangular plates (fig. 4.10) at $y=0, b$ are

$$W(x, 0)=\frac{\partial W}{\partial y}(x, 0)=M_y(x, b)=V_y(x, b)=0 \tag{4.36}$$

All results reported in this section are from reference 4.7.

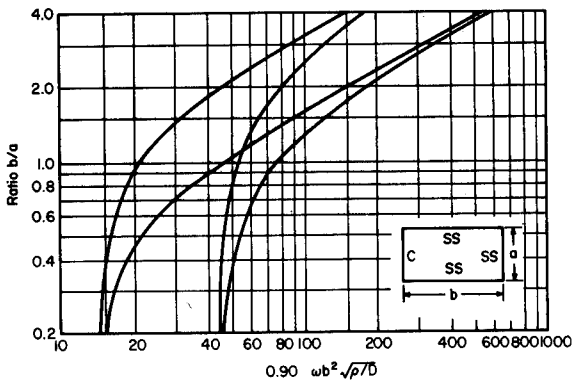


FIGURE 4.9.—Frequency parameter $0.90\omega b^2\sqrt{\rho/D}$ for a SS–C–SS–SS rectangular plate. (After ref. 4.4)

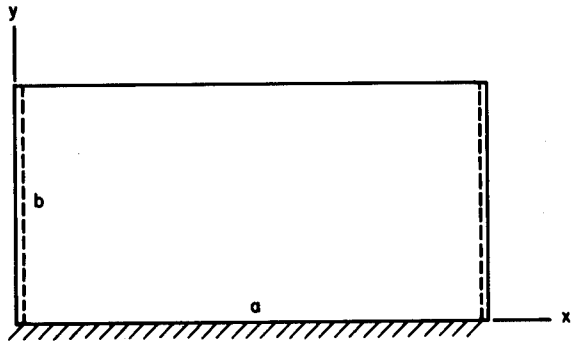


FIGURE 4.10.—SS–C–SS–F plate.

Substituting equation (1.37) into equation (4.36) yields the characteristic equation

$$2\lambda_1\lambda_2\left[\left(\frac{k}{\alpha}\right)^4-(1-\nu)^2\right]+2\lambda_1\lambda_2\left[\left(\frac{k}{\alpha}\right)^4+(1-\nu)^2\right]\cos\lambda_1 b\cosh\lambda_2 b+(\lambda_2^2-\lambda_1^2)\left[\left(\frac{k}{\alpha}\right)^4(1-2\nu)-(1-\nu)^2\right]\sin\lambda_1 b\sinh\lambda_2 b=0 \quad (4.37)$$

where λ_1 and λ_2 are defined in equations (4.27).

The first six frequencies for the case of the square and $\nu=0.3$ are listed in table 4.14, with ω_{mn} as described in the section covering SS–C–SS–C plates (sec. 4.2.1). The mode shapes are

$$W(x,y)=\Bigg(\left\{\left[\left(\frac{k}{\alpha}\right)^2+(1-\nu)\right]\cosh\lambda_2 b+\left[\left(\frac{k}{\alpha}\right)^2-(1-\nu)\right]\cos\lambda_1 b\right\}(\lambda_2\sin\lambda_1 y-\lambda_1\sinh\lambda_2 y)+\left\{\left[\left(\frac{k}{\alpha}\right)^2+(1-\nu)\right]\lambda_1\sinh\lambda_2 b+\left[\left(\frac{k}{\alpha}\right)^2-(1-\nu)\right]\lambda_2\sin\lambda_1 b\right\}(\cosh\lambda_2 y-\cos\lambda_1 y)\Bigg)\sin\alpha x \quad (4.38)$$

TABLE 4.14—*First 6 Frequency Parameters* $\lambda=\omega a^2\sqrt{\rho/D}$ *for SS–C–SS–F Square Plate;* $\nu=0.3$

λ	12. 69	33. 06	41. 70	63. 01	72. 40	90. 61
Mode	ω_{11}	ω_{12}	ω_{21}	ω_{22}	ω_{13}	ω_{31}

When $k^2=\alpha^2>>1$, equation (4.37) reduces to

$$\omega=\pi^2\left\{\left(\frac{m}{a}\right)^2+\left[\frac{n+(1/2)}{b}\right]^2\right\}\sqrt{\frac{D}{\rho}} \quad (m,n \text{ integers}) \quad (4.39)$$

Another approximate formula is given by equation (4.17).

By using equation (4.24), one can apply stability results to this problem. Fundamental frequencies given in reference 4.17 (p. 364) and reference 4.25 (p. 298) are listed in table 4.15 for various a/b ratios for $\nu=0.25$.

4.2.4 SS–SS–SS–F

The boundary conditions for SS–SS–SS–F rectangular plates (fig. 4.11) at $y=0, b$ are

$$W(x,0)=M_y(x,0)=M_y(x,b)=V_y(x,b)=0 \quad (4.40)$$

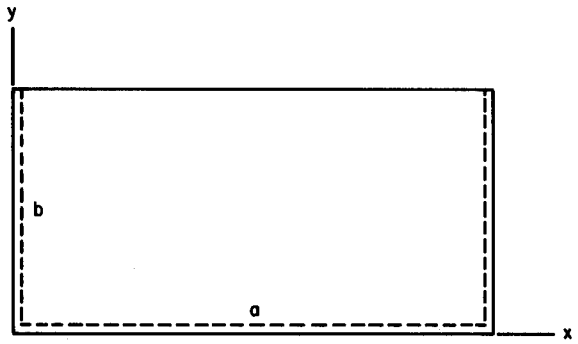


FIGURE 4.11.—SS–SS–SS–F plate.

TABLE 4.15.—*Fundamental Frequency Parameters for SS–C–SS–F Rectangular Plate; $\nu=0.25$*

a/b	$\omega a^2\sqrt{\rho/D}$	a/b	$\omega a^2\sqrt{\rho/D}$
1.0	12. 859	1.6	18. 258
1.1	13. 520	1.7	19. 343
1.2	14. 310	1.8	20. 527
1.3	15. 198	1.9	21. 910
1.4	16. 086	2.0	23. 192
1.5	17. 172	2.2	26. 153

All results reported in this section are from reference 4.7.

Substituting equation (1.37) into equation (4.40) yields the characteristic equation

$$\lambda_2\left[\left(\frac{k}{\alpha}\right)^2-(1-\nu)\right]^2\cosh\lambda_2 b\sin\lambda_1 b =\lambda_1\left[\left(\frac{k}{\alpha}\right)^2+(1-\nu)\right]^2\sinh\lambda_2 b\cos\lambda_1 b \quad (4.41)$$

where λ_1 and λ_2 are defined in equations (4.27).

The first six frequencies for the case of the square and $\nu=0.3$ are listed in table 4.16, with ω_{mn} as described in the section covering SS–C–SS–C plates (sec. 4.2.1).

The mode shapes are

$$W(x,y)=\left\{\left[\left(\frac{k}{\alpha}\right)^2-(1-\nu)\right]\sin\lambda_2 y +\left[\left(\frac{k}{\alpha}\right)^2+(1-\nu)\right]\sinh\lambda_2 b\sin\lambda_1 y\right\}\sin\alpha x \quad (4.42)$$

When $k^2+\alpha^2>>1$, equation (4.41) reduces to

$$\omega=\pi^2\left\{\left(\frac{m}{a}\right)^2+\left[\frac{n+(1/2)}{b}\right]^2\right\}\sqrt{\frac{D}{\rho}} \quad (m,n \text{ integers}) \quad (4.43)$$

Other approximate formulas are given by equations (4.16) and (4.17).

By using equation (4.24), one can apply stability results to this problem. Fundamental frequencies given in reference 4.17 (p. 362) and reference 4.25 (p. 297) are listed in table 4.17 for various a/b ratios for $\nu=0.25$.

4.2.5 SS–F–SS–F

The boundary conditions for SS–F–SS–F rectangular plates (fig. 4.12) at $y=0$, b are

$$M_y(x,0)=V_y(x,0)=M_y(x,b)=V_y(x,b)=0 \quad (4.44)$$

Substituting equation (1.37) into equations (4.44) yields the characteristic equation

$$\left\{\lambda_2^2\left[\left(\frac{k}{\alpha}\right)^2-(1-\nu)\right]^4-\lambda_1^2\left[\left(\frac{k}{\alpha}\right)^2+(1-\nu)\right]^4\right\}\times\sin\lambda_1 b\sinh\lambda_2 b=2\lambda_1\lambda_2\left[\left(\frac{k}{\alpha}\right)^4-(1-\nu)^2\right]^2\times(\cos\lambda_2 b\cosh\lambda_2 b-1) \quad (4.45)$$

where λ_1 and λ_2 are defined in equation (4.27).

TABLE 4.16.—*First 6 Frequency Parameters $\lambda=\omega a^2(\sqrt{\rho/D})$ for SS–SS–SS–F Square Plate; $\nu=0.3$*

λ	11.68	27.76	41.20	59.07	61.86	90.29
Mode	ω_{11}	ω_{12}	ω_{21}	ω_{22}	ω_{13}	ω_{31}

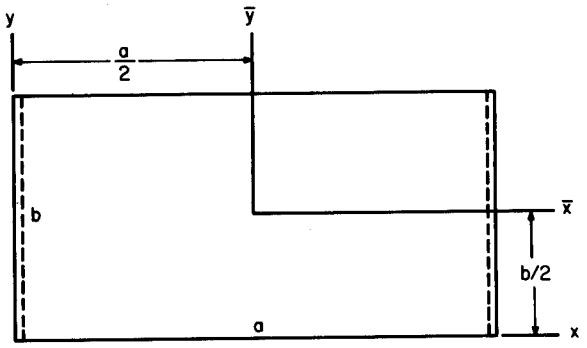


FIGURE 4.12.—SS–F–SS–F plate.

TABLE 4.17.—*Fundamental Frequency Parameters for SS–SS–SS–F Rectangular Plate; ν=0.25*

a/b	$\omega a^2\sqrt{\rho/D}$	a/b	$\omega a^2\sqrt{\rho/D}$
0.50	10.362	1.8	15.396
0.60	11.349	2.0	16.481
0.80	11.547	2.5	19.244
1.0	11.843	3.0	22.205
1.2	12.632	4.0	28.324
1.4	13.520	5.0	35.133
1.6	14.409		

The first exact solution to this problem was achieved by Voigt (ref. 4.26) in 1893. The first six frequencies for the case of the square and ν=0.3 are taken from reference 4.7 and listed in table 4.18, with ω_{mn} as described in the section covering SS–C–SS–C plates (sec. 4.2.1). The frequencies ω_{11} and ω_{21} are the only frequencies among the first six frequencies for each of the six cases of plates having two opposite edges simply supported for which $k^2<\alpha^2$.

For non-square plates, a complete set of lowest frequencies for $m^2\pi^2<\omega a^2\sqrt{\rho/D}<160$ has been calculated by Jankovic (ref. 4.27) for various aspect ratios and for ν=0.3 and ν=0.16. These are given in tables 4.19 and 4.20. In these tables the notation ω_{mn} is the same as before; that is, m gives the number of half-sine waves in the x-direction, and n is the nth lowest frequency for a given value of m. Ödman (ref. 4.13) also obtained frequency parameters for ν=1/6 and a/b=0.5, 1.0, 1.5, and 2.0. He gave 36 values, but he assumed that for n=1 the plate behaves exactly like a beam. His results, where applicable, are essentially verified in table 4.19. Roots obtained from reference 4.13 which supplement those of reference 4.27 are also shown in the column for a/b=1.0 in table 4.19. It must be remembered that the frequencies ω_{m1} are omitted in these portions of the table.

When the results of table 4.20, when a/b=1, are compared with those of table 4.18, it can be seen that disagreement exists for values of ω_{11} and ω_{21}. The problem appears to be the assumption in reference 4.27 that $k^2>\alpha^2$ for all roots. In reference 4.7 it is shown that $k^2<\alpha^2$ if

$$m\left(\frac{b}{a}\right)<\frac{\sqrt{2}}{\pi}\left(\frac{2}{\nu}-1\right)^2 \qquad (4.46)$$

This gives critical constants for various values of Poisson's ratio as listed in table 4.21. Thus, for a square plate, if ν=0.3, negative values of $k^2-\alpha^2$ exist for $m<15$. Even though the roots for which $k^2<\alpha^2$ are not handled correctly in reference 4.27, the frequencies arising from these roots should not differ markedly from those given in tables 4.19 and 4.20.

Zeissig in an early piece of work (ref. 4.28, published in 1898) also set up the frequency determinant for an exact solution and achieved a comprehensive set of solutions which are shown in figure 4.13. In this figure, solid curves identify symmetric modes in y and broken curves identify antisymmetric modes in y. The 10 numbered points indicate interesting intersections or "transition points"

TABLE 4.18.—*First 6 Frequency Parameters $\lambda=\omega a^2(\sqrt{\rho/D})$ for SS–F–SS–F Square Plate; ν=0.3*

λ	9.631	16.13	36.72	38.94	46.74	70.75
Mode	ω_{11}	ω_{12}	ω_{13}	ω_{21}	ω_{22}	ω_{23}

TABLE 4.19.—*Values of* $\omega a^2\sqrt{\rho/D}$ *for SS–F–SS–F Rectangular Plate;* $\nu=0.16$

$\omega a^2\sqrt{\rho/D}$ for aspect ratio a/b of—

0.5		0.6		0.667		0.75		0.8		1		1.333		1.5		2	
Value	Mode	Value	Mode	Value	Mode	Value	Mode	Value	Mode	Value	Mode	Value	Mode	Value	Mode	Value	Mode
9.87	ω_{11}	9.87	ω_{11}	9.87	ω_{11}	9.87	ω_{11}	9.87	ω_{11}	9.87	ω_{11}	9.87	ω_{11}	9.87	ω_{11}	9.87	ω_{11}
12.01	ω_{12}	12.87	ω_{12}	13.51	ω_{12}	14.33	ω_{12}	14.85	ω_{12}	17.06	ω_{12}	21.10	ω_{12}	23.21	ω_{12}	29.77	ω_{12}
18.21	ω_{13}	21.39	ω_{13}	23.21	ω_{13}	26.90	ω_{13}	28.92	ω_{13}	37.95	ω_{13}	39.48	ω_{13}	39.48	ω_{13}	39.48	ω_{13}
28.37	ω_{14}	35.69	ω_{14}	39.48	ω_{21}	39.48	ω_{21}	39.48	ω_{21}	39.48	ω_{21}	53.96	ω_{22}	57.27	ω_{22}	68.24	ω_{22}
39.48	ω_{21}	39.48	ω_{21}	41.19	ω_{14}	44.44	ω_{22}	45.10	ω_{22}	48.09	ω_{22}	56.46	ω_{13}	67.42	ω_{13}	88.83	ω_{31}
41.69	ω_{22}	42.68	ω_{22}	43.42	ω_{22}	48.77	ω_{14}	53.70	ω_{14}	72.88	ω_{23}	88.83	ω_{31}	88.83	ω_{31}	107.35	ω_{13}
43.03	ω_{15}	52.49	ω_{23}	55.36	ω_{23}	59.26	ω_{23}	61.76	ω_{23}	76.36	ω_{14}	94.99	ω_{23}	107.63	ω_{23}	121.40	ω_{32}
48.66	ω_{23}	56.62	ω_{15}	67.00	ω_{15}	81.41	ω_{15}	88.78	ω_{24}	88.83	ω_{31}	104.28	ω_{32}	108.11	ω_{32}	151.81	ω_{23}
60.01	ω_{24}	68.42	ω_{24}	74.70	ω_{24}	83.26	ω_{24}	88.83	ω_{31}	97.69	ω_{32}	124.77	ω_{14}	154.00	ω_{14}	157.91	ω_{41}
62.43	ω_{16}	84.60	ω_{16}	88.83	ω_{31}	88.83	ω_{31}	90.86	ω_{15}	113.60	ω_{24}	149.60	ω_{33}	157.91	ω_{41}		
75.67	ω_{25}	88.83	ω_{31}	92.78	ω_{32}	93.83	ω_{32}	94.53	ω_{32}	124.56	ω_{33}	157.91	ω_{41}				
86.81	ω_{17}	90.49	ω_{25}	101.57	ω_{16}	109.49	ω_{33}	112.22	ω_{33}	134.58	ω_{15}						
88.83	ω_{31}	92.02	ω_{32}	101.61	ω_{25}	116.91	ω_{25}	126.82	ω_{25}	157.91	ω_{41}						
91.02	ω_{32}	102.22	ω_{33}	105.27	ω_{33}	125.24	ω_{16}	140.77	ω_{16}	[a] 166.8	ω_{42}						
95.77	ω_{26}	118.97	ω_{34}	125.74	ω_{34}	135.03	ω_{34}	141.03	ω_{34}	[a] 167.8	ω_{34}						
98.17	ω_{33}	119.01	ω_{26}	136.58	ω_{26}	157.91	ω_{41}	157.91	ω_{41}	[a] 171.9	ω_{25}						
109.99	ω_{34}	119.76	ω_{17}	145.23	ω_{17}					[a] 194.5	ω_{43}						
116.15	ω_{18}	142.12	ω_{35}	153.99	ω_{35}					[a] 213.0	ω_{16}						
120.44	ω_{27}	154.24	ω_{27}	157.91	ω_{41}					[a] 228.0	ω_{35}						
126.34	ω_{35}	157.91	ω_{41}							[a] 239.8	ω_{44}						
147.21	ω_{36}									[a] 249.9	ω_{26}						
149.85	ω_{28}									[a] 255.5	ω_{52}						
150.47	ω_{19}									[a] 283.7	ω_{53}						
157.91	ω_{41}									[a] 302.3	ω_{45}						

[a] Roots from ref. 4.13.

TABLE 4.20—*Values of* $\omega a^2\sqrt{\rho/D}$ *for SS–F–SS–F Rectangular Plate;* $\nu=0.30$

$\omega a^2\sqrt{\rho/D}$ for aspect ratio a/b of—																	
0.5		0.6		0.667		0.75		0.8		1		1.333		1.5		2	
Value	Mode	Value	Mode	Value	Mode	Value	Mode	Value	Mode	Value	Mode	Value	Mode	Value	Mode	Value	Mode
9. 87	ω_{11}	9. 87	ω_{11}	9. 87	ω_{11}	9. 87	ω_{11}	9. 87	ω_{11}	9. 87	ω_{11}	9. 87	ω_{11}	9. 87	ω_{11}	9. 87	ω_{11}
11. 66	ω_{12}	12. 43	ω_{12}	12. 98	ω_{12}	13. 71	ω_{12}	14. 17	ω_{12}	16. 13	ω_{12}	19. 73	ω_{12}	21. 62	ω_{12}	27. 52	ω_{12}
17. 66	ω_{13}	20. 69	ω_{13}	22. 95	ω_{13}	25. 99	ω_{13}	27. 94	ω_{13}	36. 71	ω_{13}	39. 48	ω_{21}	39. 48	ω_{21}	39. 48	ω_{21}
27. 73	ω_{14}	34. 93	ω_{14}	39. 48	ω_{21}	39. 48	ω_{21}	39. 48	ω_{21}	39. 48	ω_{21}	51. 93	ω_{22}	54. 84	ω_{22}	64. 54	ω_{22}
39. 48	ω_{21}	39. 48	ω_{21}	40. 33	ω_{14}	43. 56	ω_{22}	44. 15	ω_{22}	46. 73	ω_{22}	54. 62	ω_{13}	65. 79	ω_{13}	88. 83	ω_{31}
41. 18	ω_{22}	42. 04	ω_{22}	42. 67	ω_{22}	47. 85	ω_{14}	52. 73	ω_{14}	70. 73	ω_{23}	88. 83	ω_{31}	88. 83	ω_{31}	105. 48	ω_{13}
42. 35	ω_{15}	51. 54	ω_{23}	54. 23	ω_{23}	57. 89	ω_{23}	60. 24	ω_{23}	75. 72	ω_{14}	91. 81	ω_{23}	103. 97	ω_{23}	116. 83	ω_{32}
47. 73	ω_{23}	55. 90	ω_{15}	66. 21	ω_{15}	80. 59	ω_{15}	86. 82	ω_{24}	88. 83	ω_{31}	101. 80	ω_{32}	105. 16	ω_{32}	146. 90	ω_{23}
59. 06	ω_{24}	67. 14	ω_{24}	73. 19	ω_{24}	81. 47	ω_{24}	88. 83	ω_{31}	96. 29	ω_{32}	123. 56	ω_{14}	152. 77	ω_{14}	157. 91	ω_{41}
61. 85	ω_{16}	83. 97	ω_{16}	88. 83	ω_{31}	88. 83	ω_{31}	90. 03	ω_{15}	111. 02	ω_{24}	145. 57	ω_{33}	157. 91	ω_{41}		
74. 51	ω_{25}	88. 83	ω_{31}	91. 76	ω_{32}	92. 67	ω_{32}	93. 28	ω_{32}	122. 04	ω_{33}	157. 91	ω_{41}	159. 16	ω_{33}		
86. 27	ω_{17}	88. 99	ω_{25}	99. 88	ω_{25}	107. 92	ω_{33}	110. 47	ω_{33}	133. 69	ω_{15}						
88. 83	ω_{13}	91. 12	ω_{32}	100. 91	ω_{16}	114. 93	ω_{25}	124. 70	ω_{25}	157. 91	ω_{41}						
90. 26	ω_{32}	101. 11	ω_{33}	103. 98	ω_{33}	124. 55	ω_{16}	138. 65	ω_{16}								
94. 46	ω_{26}	117. 39	ω_{26}	123. 99	ω_{34}	132. 89	ω_{34}	140. 07	ω_{34}								
97. 33	ω_{33}	117. 50	ω_{34}	134. 78	ω_{26}	157. 91	ω_{41}	157. 91	ω_{41}								
108. 91	ω_{34}	119. 19	ω_{17}	144. 44	ω_{17}	158. 91	ω_{26}										
115. 67	ω_{18}	140. 29	ω_{35}	151. 81	ω_{35}												
119. 10	ω_{27}	152. 63	ω_{27}	157. 91	ω_{41}												
125. 01	ω_{35}	157. 91	ω_{41}														
145. 63	ω_{36}																
148. 49	ω_{28}																
150. 05	ω_{19}																
157. 91	ω_{41}																

TABLE 4.21.—*Critical Constants Determining When* $k^2 < \alpha^2$ *for SS–F–SS–F Plate*

ν	0	0.1	0.2	0.3	0.4	0.5
$m\left(\frac{b}{a}\right)$	∞	162. 507	36. 463	14. 455	7. 202	4. 051

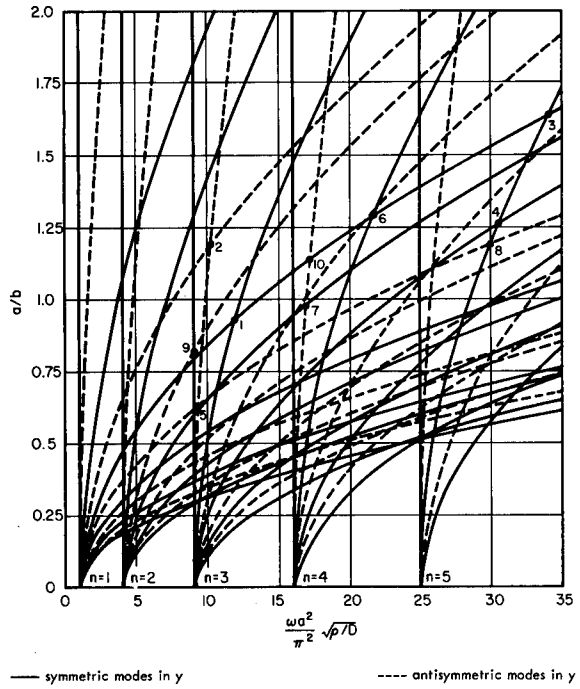


FIGURE 4.13.—Frequency parameters $\omega a^2/\pi^2\sqrt{\rho/D}$ for various a/b ratios of a rectangular SS–F–SS–F plate. Numbered points are intersections where two modes can exist simultaneously. (After ref. 4.28)

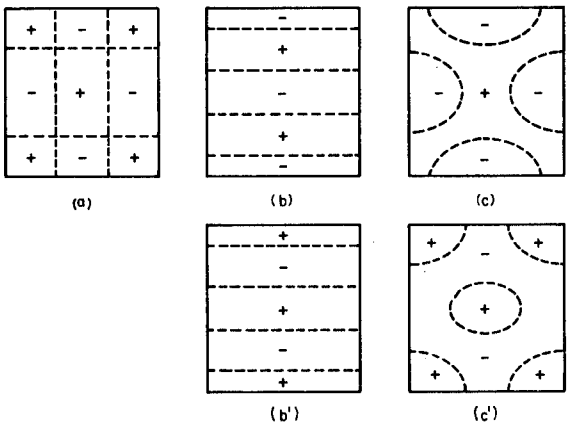


FIGURE 4.14.—Superposition of two modes having the same frequency. (*a*) Nodal pattern for 3/2 mode. (*b*) Nodal pattern for 1/4 mode. (*c*) Nodal pattern for (*a*) superimposed on (*b*). (b^1) Nodal pattern when initial amplitude of 1/4 mode is 180° out of phase. (c^1) Nodal pattern for (*a*) superimposed on (b^1). (After ref. 4.28)

where two modes can exist simultaneously. For example, at point 1 the fifth root for $m=1$ (called 1/4 mode) and the third root for $m=3$ (3/2 mode) can exist simultaneously for a plate having an a/b ratio of approximately 0.9. Figures 4.14(*a*) and 4.14(*b*) (reprinted from ref. 4.28) show the nodal patterns for these two modes. The areas denoted by plus signs can be taken as positive (upward) displacements and the others, as negative. If the initial conditions are chosen so as to excite each mode with the same amplitude, the resulting nodal pattern of the superimposed modes is shown in figure 4.14(*c*). If the initial amplitude of the 1/4 mode is taken 180° out of phase as in figure 4.14(*b'*), the superimposed motion is as in figure 4.14(*c'*). Stepwise superposition of varying ratios of the modes 3/2 and 1/4 yields nodal patterns as shown in figure 4.15 (from ref. 4.13).

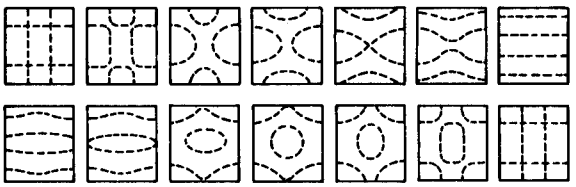


FIGURE 4.15.—Stepwise superposition of two modes having the same frequency. (After ref. 4.28)

The detailed mode shapes are (ref. 4.7):

$$W(x,y)=\Bigg(-(\cosh\lambda_2 b-\cos\lambda_1 b)\left[\left(\frac{k}{\alpha}\right)^4-(1-\nu)^2\right]\left\{\lambda_1\left[\left(\frac{k}{\alpha}\right)^2+(1-\nu)\right]\sinh\lambda_2 y+\lambda_2\left[\left(\frac{k}{\alpha}\right)^2-(1-\nu)\right]\sin\lambda_1 y\right\}+\left\{\lambda_1\left[\left(\frac{k}{\alpha}\right)^2+(1-\nu)\right]^2\sinh\lambda_2 b-\lambda_2\left[\left(\frac{k}{\alpha}\right)^2-(1-\nu)\right]^2\sin\lambda_1 b\right\}\left\{\left[\left(\frac{k}{\alpha}\right)^2-(1-\nu)\right]\cosh\lambda_2 y+\left[\left(\frac{k}{\alpha}\right)^2+(1-\nu)\right]\cos\lambda_1 y\right\}\Bigg)\sin\alpha x \tag{4.47}$$

Mode shapes were computed and plotted in reference 4.13 for the six roots of equation (4.45) for $m=1, 2, \ldots, 6$ and $\nu=1/6$. Unfortunately, it was assumed that for the lowest root (symmetry about $\bar{y}=0$) for each value of m, the plate behaves exactly like a beam and, consequently, these cases were omitted in the results. Thus, the plotted mode shapes begin with those antisymmetrical about $\bar{y}=0$. Plots are given in reference 4.13 for $a/b=0.5$, 1.0, 1.5, and 2.0 and those for $a/b=1.0$ reproduced in figure 4.16. The mode shapes are represented as the products $W_{mn}(\bar{x}, \bar{y})=X_m(\bar{x})Y_n(\bar{y})$, where $\bar{x}$ and $\bar{y}$ are measured with the point at the center of the plate taken as origin (see fig. 4.12). Each of the six parts of figure 4.16 corresponds to one value of m. The first six modes having that value of m are then determined from the separate curves $Y_n(\bar{y})$. The curves for $Y_n(\bar{y})$ do not change markedly for variations in a/b in the range $0.5<a/b<2.0$. The maximum variations for the 36 modes shown are illustrated in figure 4.17, which corresponds to $m=5$ and $n=5$.

When $k^2/\alpha^2>>1$, equation (4.45) reduces to (ref. 4.7)

$$\omega=\pi^2\left\{\left(\frac{m}{a}\right)^2+\left[\frac{n+(1/2)}{b}\right]^2\right\}\sqrt{\frac{D}{\rho}} \qquad (m, n \text{ integers}) \tag{4.48}$$

Other approximate formulas are given in equations (4.16) and (4.17).

Zeissig (ref. 4.28) reported many experimental results which essentially substantiated his analytical calculations. The problem was also formulated in references 4.10 and 4.24.

4.3 OTHER SIMPLE EDGE CONDITIONS

4.3.1 All Sides Clamped (C–C–C–C)

The problem of C–C–C–C rectangular plates (fig. 4.18) has received a voluminous treatment in the literature, especially for the case of the square plate. The first reasonably accurate results for the square plate were given in 1931 by Sezawa (ref. 4.21), who used the series method. He used functions which exactly satisfied the differential equation (eq. (1.1)) and the boundary condition of zero deflection along all edges and required the slope to be zero only at the midpoints of the edges. This initial work has been followed by a host of Japanese publications on the problem; for example, see references 4.9, 4.15, 4.16, 4.20, and 4.29 to 4.33.

Some variation of the series method was used in references 4.9, 4.20, 4.21, 4.29, 4.30, 4.32, and 4.34 to 4.40. Particularly notable is Tomotika's work (refs. 4.30 and 4.41); he determined the fundamental frequency for the square plate with extreme accuracy. Like Sezawa, he chose functions which satisfied the deflection conditions exactly and set up an infinite characteristic determinant for the slope conditions. Convergence of results from a sequence of determinants obtained by truncating the infinite case was used to get extreme accuracy. He also used the Rayleigh and Weinstein methods to obtain the frequency bounds $35.9855<(\omega a^2\sqrt{\rho/D})<36.09$ for a square of dimension a x a.

Finite difference techniques were used in references 4.14, 4.38, 4.42, and 4.43; the Galerkin technique, in references 4.13, 4.33, 4.44, 4.45, and 4.46; the Rayleigh or Rayleigh-Ritz method, in references 4.1, 4.2, 4.47, and 4.48; Weinstein's method, in reference 4.49; integral equations, in reference 4.16; and a variational approach, in reference 4.15. Other publications include references 4.18, 4.31, and 4.50 to 4.56. A notable lack of experimental results exists.

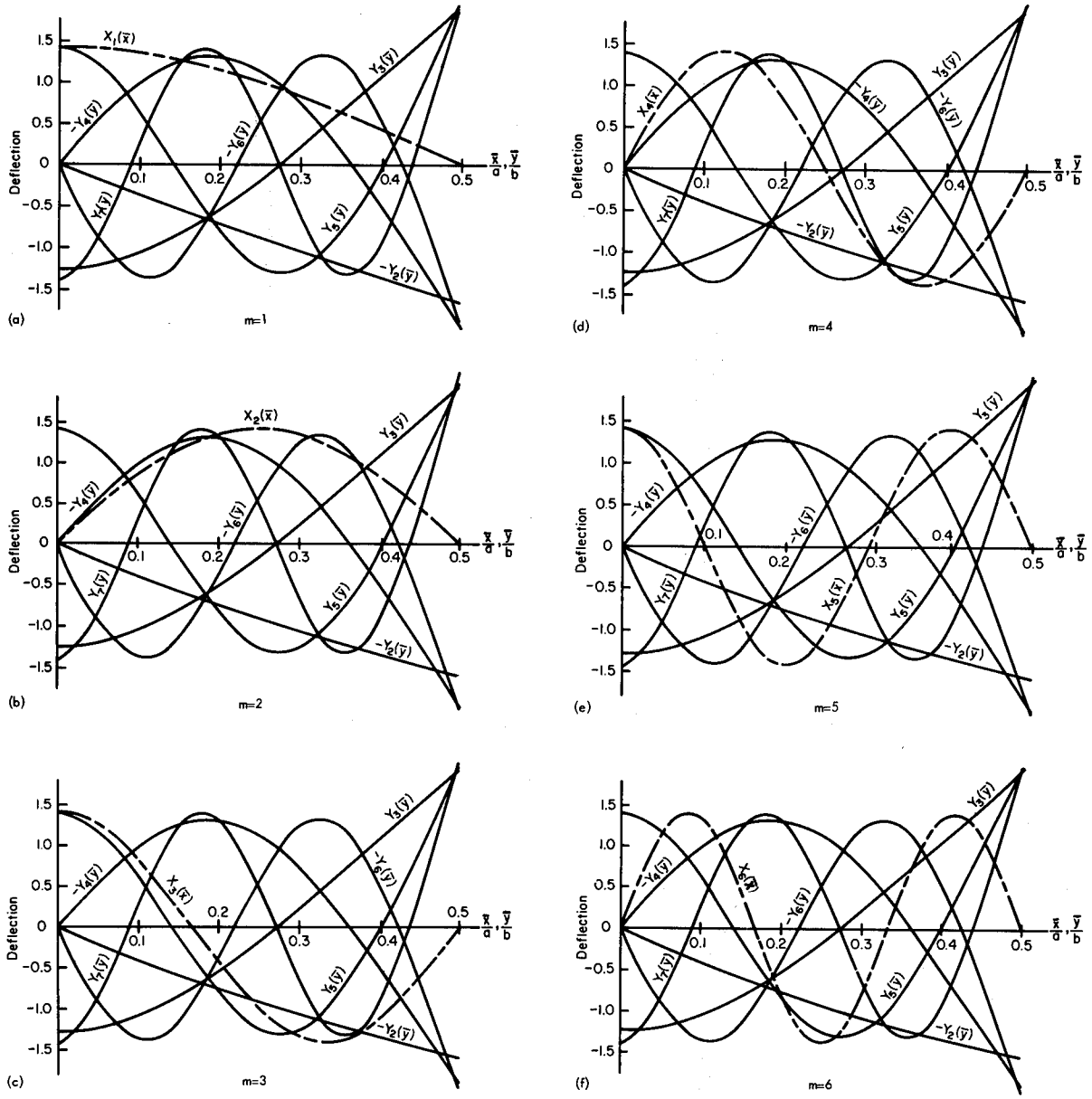


FIGURE 4.16.—Mode shapes $W_{mn}(\bar{x}, \bar{y}) = X_m(\bar{x})\, Y_n(\bar{y})$ for 36 modes of a SS–F–SS–F square plate. $n=2, 3, \ldots 7$. (After ref. 4.13)

Table 4.22 summarizes the first six sets of frequencies, nodal lines, and amplitude coefficients for a square plate having side length a. Iguchi (ref. 4.9) did not find the fourth mode in his work. Young (ref. 4.47) used the products of beam functions (i.e., eigenfunctions for C–C beams) and the Rayleigh-Ritz method to obtain accurate upper bounds. The resulting mode shapes are of the form

$$W(x,y)=\sum_{m=1}^{p}\sum_{n=1}^{q}A_{mn}\left[\cosh\frac{\epsilon_m x}{a}-\cos\frac{\epsilon_m x}{a}-\alpha_m\left(\sinh\frac{\epsilon_m x}{a}-\sin\frac{\epsilon_m x}{a}\right)\right]\left[\cosh\frac{\epsilon_n y}{a}-\cos\frac{\epsilon_n y}{a}-\alpha_n\left(\sinh\frac{\epsilon_n y}{a}-\sin\frac{\epsilon_n y}{a}\right)\right] \quad (4.49)$$

where the values of A_{mn} are given in table 4.22, those of α and ϵ are given in table 4.23, and

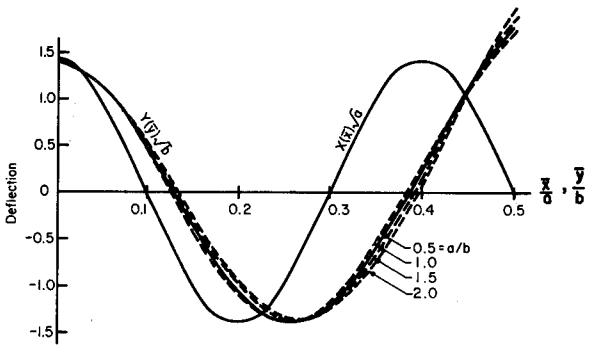


FIGURE 4.17.—Variation in $Y_n(\bar{y})$ with a/b for the mode $m=5$, $n=5$ for a SS–F–SS–F rectangular plate. (After ref. 4.13)

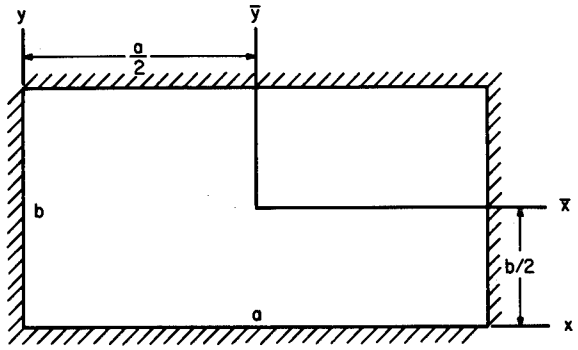


FIGURE 4.18.—C–C–C–C rectangular plate.

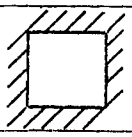
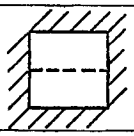
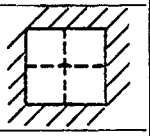
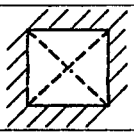
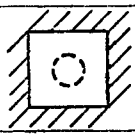
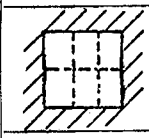
the origin of the xy-coordinate system is taken at one corner of the plate as shown in figure 4.18.

Further results were obtained by Bolotin (ref. 4.57), who used a variation of the series method to obtain approximate results for the square. These are summarized in table 4.24. In table 4.24 odd values of m yield modes symmetric about the $\bar{y}$-axis, even values of m yield modes antisymmetric about the $\bar{y}$-axis, and similarly for n with respect to the $\bar{x}$-axis. It is

TABLE 4.23.—*Eigenfunction Parameters for a C–C Beam*

m, n	α_m, α_n	ϵ_m, ϵ_n
1	0. 98250222	4. 7300408
2	1. 00077731	7. 8532046
3	0. 99996645	10. 9956078
4	1. 00000145	14. 1371655
5	0. 99999994	17. 2787596
6	1. 00000000	20. 4203522
$r>6$	1. 0	$(2r+1)\pi/2$

TABLE 4.22.—*First 6 Sets of Frequency Parameters, Nodal Lines, and Amplitude Coefficients for a C–C–C–C Square Plate*

Mode	1	2	3	4	5	6
$\omega a^2\sqrt{\frac{\rho}{D}}$	[a] 35. 9866 [b] 35. 99	[c] 73. 40 [b] 73. 41	[c] 108. 22 [b] 108. 27	---------- [b] 131. 64	[c] 132. 18 [b] 132. 25	[c] 164. 99 [b] 165. 15
Nodal lines						
Amplitude coefficient [b]	$A_{11}=1.0000$ $A_{13}=0.0142$ $A_{15}=0.0020$ $A_{31}=0.0142$ $A_{33}=-0.0031$ $A_{35}=-0.0009$ $A_{51}=0.0020$ $A_{53}=-0.0009$ $A_{55}=-0.0004$	$A_{12}=1.0000$ $A_{14}=0.0101$ $A_{16}=0.0020$ $A_{32}=0.0406$ $A_{34}=-0.0022$ $A_{36}=-0.0007$ $A_{52}=0.0070$ $A_{54}=-0.0011$ $A_{56}=-0.0005$	$A_{22}=1.0000$ $A_{24}=0.0326$ $A_{26}=0.0073$ $A_{42}=0.0326$ $A_{44}=-0.0019$ $A_{46}=-0.0010$ $A_{62}=0.0073$ $A_{64}=-0.0010$ $A_{66}=-0.0006$	$A_{13}=1.0000$ $A_{15}=0.0085$ $A_{31}=-1.0000$ $A_{35}=-0.0141$ $A_{51}=-0.0085$ $A_{53}=0.0141$	$A_{11}=-0.0280$ $A_{13}=1.0000$ $A_{15}=0.0055$ $A_{31}=1.0000$ $A_{33}=0.1267$ $A_{35}=0.0118$ $A_{51}=0.0055$ $A_{53}=0.0118$ $A_{55}=-0.0018$	$A_{12}=-0.0406$ $A_{14}=-0.0105$ $A_{16}=-0.0017$ $A_{32}=1.0000$ $A_{34}=0.0560$ $A_{36}=0.0141$ $A_{52}=0.0238$ $A_{54}=-0.0011$ $A_{56}=-0.0009$

[a] Work of Tomotika (ref. 4.30).
[b] Work of Young (ref. 4.47).
[c] Work of Iguchi (ref. 4.9).

TABLE 4.24.—*Approximate Frequencies for a C–C–C–C Square Plate*

m	n	$\omega a^2\sqrt{\rho/D}$
1	1	35. 10
2	1	72. 90
2	2	107. 47
3	1	131. 63
3	2	164. 39
4	1	210. 35
3	3	219. 32
4	2	242. 20
4	3	295. 69
4	4	370. 66

noted that only one root is given in this table in the vicinity of 132. The general formula for frequency for a square when $m=n$ is (ref. 4.57)

$$\omega_{mn}=2\left(m+\frac{1}{3}\right)^2\frac{\pi^2}{a^2}\sqrt{\frac{D}{\rho}} \qquad (4.50)$$

Bazley, Fox, and Stadter (ref. 4.58) used a method developed in reference 4.59 to compute lower bounds for the first 15 frequencies of the following symmetry class of a square: With an $\bar{x}\bar{y}$-coordinate system having its origin at the plate center and axes parallel to the edges, the modes are symmetric with respect to both $\bar{x}$ and $\bar{y}$ and are unaltered by interchange of $\bar{x}$ and $\bar{y}$ (fourfold symmetry). (Thus, the first and fifth modes of table 4.22 would be the only modes shown which would fall into this symmetry class.) They also obtained extremely accurate upper bounds by the Rayleigh-Ritz method by taking the first 50 admissible products of C–C beam functions. Double-precision arithmetic (16 significant figures) was used in the computations where necessary. Results are listed in table 4.25. In this table results from the Rayleigh-Ritz method are given using both 25 and 50 admissible functions to show the rate of convergence.

Another significant contribution was made by Aronszajn (ref. 4.49), who used Weinstein's method to obtain accurate lower bounds for the first 10 frequencies of a square plate. The Rayleigh-Ritz method was used to obtain upper bounds. These results are summarized in table 4.26.

TABLE 4.25.—*Bounds on Frequency Parameters* $\omega a^2\sqrt{\rho/D}$ *for Fourfold Symmetric Modes of a C–C–C–C Square Plate*

Mode	$\omega a^2\sqrt{\rho/D}$		
	Lower bound	Upper bound	
		25 terms	50 terms
1	35. 982	35. 986	35. 986
2	132. 18	132. 21	132. 21
3	219. 73	220. 06	220. 04
4	309. 08	309. 17	309. 17
5	393. 00	393. 98	393. 92
6	558. 58	562. 38	562. 18
7	565. 39	565. 56	565. 54
8	646. 62	648. 58	648. 46
9	806. 51	814. 84	814. 48
10	900. 70	901. 00	900. 97
11	979. 55	----------	982. 93
12	1017. 5	----------	1062. 5
13	1127. 4	----------	1147. 1
14	1235. 1	----------	1315. 4
15	1314. 9	----------	1393. 4

Ödman (ref. 4.13) used a variation of the Galerkin method and mode shapes of the form $W(\bar{x},\bar{y})=X(\bar{x})Y(\bar{y})$, where

$$\left.\begin{aligned} X(\bar{x})&=A_1\cosh\mu_1\bar{x}+A_2\sinh\mu_1\bar{x}\\ &\quad+A_3\cosh\mu_2\bar{x}+A_4\sinh\mu_2\bar{x}\\ Y(\bar{y})&=B_1\cosh\mu_3\bar{y}+B_2\sinh\mu_3\bar{y}\\ &\quad+B_3\cosh\mu_4\bar{y}+B_4\sinh\mu_4\bar{y}\end{aligned}\right\} \qquad (4.51)$$

and where $\mu_1, \ldots, \mu_4$ are determined by applying the Galerkin formula to the differential equation of motion for the plate. The 36 frequencies $\omega_{mn}(m, n=1, \ldots, 6)$ computed by this method in reference 4.13 are upper bounds and are given in table 4.27. It is interesting to note that, in spite of apparent numerical precision, Ödman did not detect two separate frequencies for ω_{13}, as did Young (table 4.22).

For computing fundamental frequencies of clamped rectangular plates of arbitrary a/b ratio, there exists, in addition, Warburton's (ref. 4.1) and Janich's (ref. 4.2) formulas, equations (4.16) and (4.17). Frequencies obtained from Warburton's formula were plotted in reference 4.4.

TABLE 4.26.—*Frequency Parameters for a C–C–C–C Square Plate*

Mode symmetry	$\omega a^2\sqrt{\rho/D}$			
	Lower bound	Upper bound	Mean value	Maximum error, percent
Symmetric about both $\bar{x}$ and $\bar{y}$	35. 9693	36. 1074	36. 0384	0. 19
	131. 55	133. 20	132. 38	. 63
	131. 8	134. 1	132. 9	. 87
	218	231	224. 5	2. 98
Symmetric about $\bar{x}$, antisymmetric about $\bar{y}$ (or conversely)	73. 354	74. 226	73. 790	. 59
	164. 39	171. 39	167. 89	2. 13
	210	216	213	1. 43
Antisymmetric about both $\bar{x}$ and $\bar{y}$	108. 119	109. 936	109. 027	. 84
	241. 924	246. 118	244. 021	. 87
	242. 071	251. 033	246. 552	1. 85

TABLE 4.27.—*Frequency Parameters* $\omega a^2\sqrt{\rho/D}$ *for a C–C–C–C Square Plate*

[Values in parentheses were obtained by interpolation; table is symmetric]

m	$\omega a^2\sqrt{\rho/D}$ for values of n of—					
	1	2	3	4	5	6
1	35. 998965	73. 405	131. 902	210. 526	309. 038	(428)
2		108. 237	165. 023	242. 66	340. 59	458. 27
3			220. 06	296. 35	393. 36	509. 9
4				371. 38	467. 29	583. 83
5					562. 18	(676)
6						792. 5

A simple formula derived by Galin (ref. 4.45) for this case is

$$\omega=12\sqrt{\frac{7}{2}\left(\frac{1}{a^4}+\frac{4}{7}\frac{1}{a^2b^2}+\frac{1}{b^4}\right)}\sqrt{\frac{D}{\rho}} \quad (4.52)$$

For a square this reduces to $\omega a^2\sqrt{\rho/D}=36$, which compares favorably with the accurate value of 35.9866 from table 4.22.

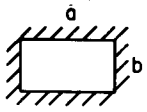
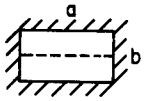
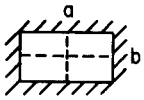
A summary of the literature for frequencies of nonsquare C–C–C–C rectangular plates is presented in table 4.28. Neither Iguchi (ref. 4.9) nor Kanazawa and Kawai (ref. 4.16) recognized the existence of the other mode having one symmetry axis and one antisymmetry axis which is not shown in the table.

Sixteen frequency parameters for $a/b=0.25$ and 0.50 are computed in reference 4.60. These are given in table 4.29, with m and n as explained previously. More extensive results are obtained in reference 4.13 and are also listed in table 4.29.

Mode shapes in the form $W_{mn}(\bar{x}, \bar{y})=X_m(\bar{x})Y_n(\bar{y})$ corresponding to ω_{mn} were found in reference 4.13. The components $X_m(\bar{x})\sqrt{a}$ and $Y_n(\bar{y})\sqrt{b}$ are shown in figure 4.19 for $a/b=1.0$. Variation in these curves with a/b is very small for the range $0.5\leqq a/b\leqq 2.0$. The magnitude of this variation is shown by figure 4.20 for the components $X_4(\bar{x})\sqrt{a}$ and $Y_4(\bar{y})\sqrt{b}$. Figure 4.21, taken from reference 4.60, shows the frequency parameter $\frac{\lambda}{\pi^2}=\omega a^2(\sqrt{\rho/D})/\pi^2$ plotted as a function of a/b and b/a. For $a/b=0$, the frequencies are given by reference 4.60:

$$\omega_m=\frac{\pi^2}{a^2}\left(m+\frac{1}{2}\right)^2\sqrt{\frac{D}{\rho}} \quad (4.53)$$

TABLE 4.28.—$\omega b^2\sqrt{\rho/D}$ *for C–C–C–C Rectangular Plates*

Source	Mode ($a>b$)	$\omega b^2\sqrt{\rho/D}$ for values of a/b of—				
		1.5	2	2.5	3	∞
Iguchi (ref. 4.9)_____		27. 00	24. 56	23. 76	23. 19	22. 37
Kanazawa and Kawai (ref. 4.16).		67. 58	65. 41	64. 49	64. 02	61. 78
Kanazawa and Kawai (ref. 4.16).		81. 57	72. 66	68. 89	66. 96	61. 78

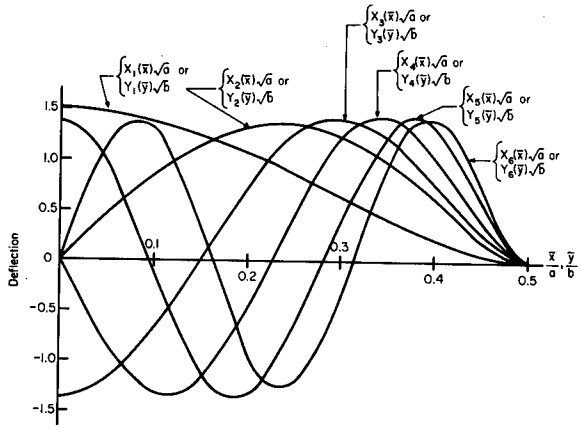


FIGURE 4.19.—Mode shape components $X_m(\bar{x})\sqrt{a}$ or $Y_n(\bar{y})\sqrt{b}$ for a C–C–C–C rectangular plate. (After ref. 4.13)

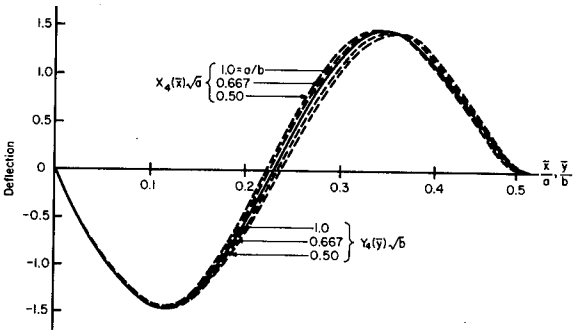


FIGURE 4.20.—Variation in mode shape components $X_4(\bar{x})\sqrt{a}$ and $Y_4(\bar{y})\sqrt{b}$ with a/b for a C–C–C–C rectangular plate. (After ref. 4.13)

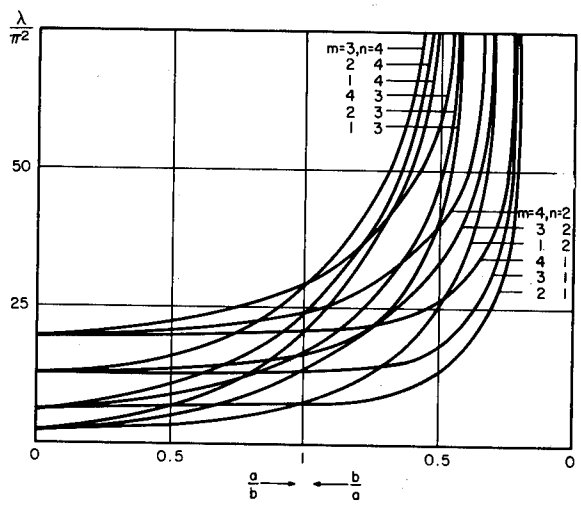


FIGURE 4.21.—$\lambda/\pi^2=\omega a^2/\pi^2(\sqrt{\rho/D})$ for a C–C–C–C rectangular plate.

Claassen and Thorne (refs. 4.35 and 4.36) used a most straightforward application of the series method which represented the deflection form as a double Fourier sine series; that is,

$$W(x,y)=\sum_{m=1}^{\infty}\sum_{n=1}^{\infty}A_{mn}\sin\frac{m\pi x}{a}\sin\frac{n\pi y}{b} \quad (4.54)$$

When the homogeneous boundary conditions are written for all edges, they result in an infinite determinant, the zeros of which are the desired eigenvalues. Numerical convergence

TABLE 4.29.—*Frequency Parameters* $\omega a^2\sqrt{\rho/D}$ *for a C–C–C–C Rectangular Plate*

[Values in parentheses are interpolated]

m	n	$\omega a^2\sqrt{\rho/D}$ for value of a/b of—			
		0.25 (ref. 4.60)	0.50		0.667 (ref. 4.13)
			Ref. 4.60	Ref. 4.13	
1	1	23. 19	24. 09	24. 58	27. 01
	2	23. 94	31. 40	31. 83	41. 72
	3	26. 32	44. 35	44. 78	66. 53
	4	30. 01	63. 00	63. 34	100. 81
	5	--------	--------	87. 26	144. 21
	6	--------	--------	(117)	(195)
2	1	62. 17	63. 93	(64. 1)	(65. 5)
	2	63. 70	70. 90	71. 08	79. 81
	3	66. 23	82. 90	(83. 2)	(103)
	4	69. 97	100. 18	100. 80	136. 10
	5	--------	--------	(124. 2)	(178)
	6	--------	--------	151. 91	230. 04
3	1	121. 59	123. 07	(124)	(126)
	2	122. 98	130. 13	130. 35	138. 64
	3	125. 74	142. 12	142. 38	161. 23
	4	129. 81	156. 47	159. 49	193. 24
	5	--------	--------	181. 79	234. 65
	6	--------	--------	(209. 6)	(285. 4)
4	1	200. 33	202. 02	(204)	(206)
	2	202. 00	209. 18	(210)	(218)
	3	204. 72	231. 02	(221)	(241)
	4	208. 83	238. 01	238. 35	271. 17
	5	--------	--------	(261)	(312)
	6	--------	--------	287. 54	361. 90
5	1	--------	--------	(302)	(303)
	2	--------	--------	308. 12	316. 11
	3	--------	--------	(320)	(339)
	4	--------	--------	337. 08	369. 34
	5	--------	--------	358. 0	(409)
	6	--------	--------	(382)	(456)
6	1	--------	--------	(421)	(422)
	2	--------	--------	(427)	(436)
	3	--------	--------	(439)	(457)
	4	--------	--------	(456)	(488)
	5	--------	--------	(478)	(529)
	6	--------	--------	504. 3	576. 6

is established by successive truncation of the infinite determinant. The method is also discussed in reference 4.39.

The frequency as a function of the a/b ratio for the 10 lowest modes is plotted in reference 4.35. These curves are reproduced as figures 4.22 to 4.25. In table 4.30 the accurate values

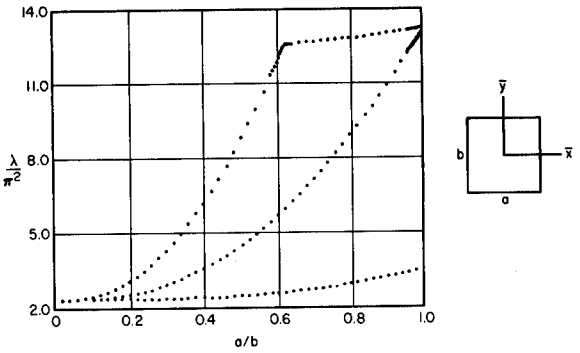


FIGURE 4.22.—Frequency parameters $\lambda/\pi^2=\omega a^2/\pi^2(\sqrt{\rho/D})$ for modes symmetric about both $\bar{x}$- and $\bar{y}$- axes for a C–C–C–C rectangular plate. (After ref. 4.35)

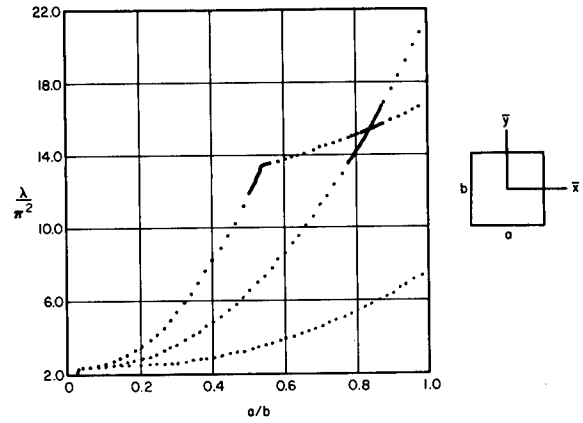


FIGURE 4.23.—Frequency parameter $\lambda/\pi^2=\omega a^2/\pi^2(\sqrt{\rho/D})$ for modes symmetric about $\bar{x}=0$ and antisymmetric about $\bar{y}=0$ for a C–C–C–C rectangular plate. (After ref. 4.35)

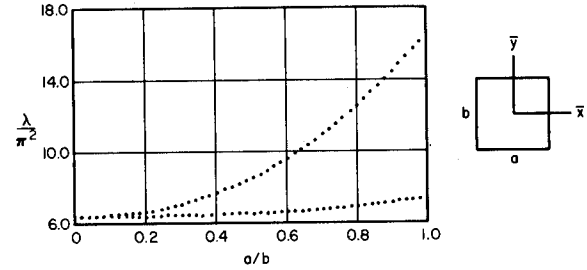


FIGURE 4.24.—Frequency parameters $\lambda/\pi^2=\omega a^2/\pi^2(\sqrt{\rho/D})$ for modes antisymmetric about $\bar{x}=0$ and symmetric about $\bar{y}=0$ for a C–C–C–C rectangular plate. (After ref. 4.35)

of frequency used in the preceding plots are displayed for a/b increments of 0.02 in the range $1.00 \geqq a/b \geqq 0$ (ref. 4.36).

When one looks, for example, at figure 4.23, it appears that the curves for the second and

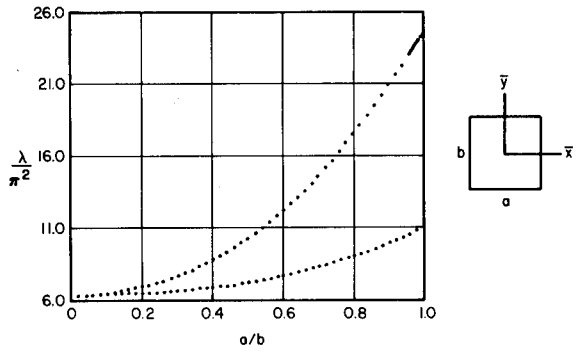


FIGURE 4.25.—Frequency parameters $\lambda/\pi^2=\omega a^2/\pi^2(\sqrt{\rho/D})$ for modes antisymmetric about both $\bar{x}$- and $\bar{y}$-axes for a C–C–C–C rectangular plate. (After ref. 4.35)

third symmetric-antisymmetric frequencies cross in the vicinity of $a/b=0.84$. Such an intersection point is termed a "transition point." It is the contention of Claassen and Thorne that these curves do not actually cross at transition points but only approach each other closely before "veering away" or being "repelled." Very small increments of a/b are taken in reference 4.36 in the vicinity of these transition points and corresponding values of frequency parameter λ are computed which appear to substantiate this. The details of this phenomenon can be seen in table 4.31. From the table it is seen that the two curves approach each other most closely at $a/b=0.834$. It is the opinion of the writer that, although extremely precise work was performed in reference 4.36, certain questions of convergence of the series approach used need to be answered before the transition-point phenomena described above can be accepted.

In figure 4.26 are shown nodal lines for one quadrant of the plate for various a/b ratios in the vicinity of transition points (ref. 4.36). In these figures the center of the plate is at $(0, 0)$ and the $\bar{x}$ and $\bar{y}$ coordinates have been nondimensionalized to $\bar{x}/a$ and $\bar{y}/b$, respectively. The rapid change from one mode form to another with small variation in a/b is interesting. Precise node-line coordinates used for figure 4.26 and other nodal patterns are given in reference 4.36.

Accurate upper and lower bounds for the doubly symmetric modes of a rectangle (see discussion earlier in this section) are reported in reference 4.58. These results are given in table 4.32. Upper bounds were computed using 50 admissible beam modes. It is noteworthy that the second and third doubly symmetric modes for the square are for distinct frequencies, as reported earlier in references 4.36 and 4.47.

4.3.2 C–C–C–SS

Three sources of numerical data are available for the problem of the C–C–C–SS plate (fig. 4.27). Results are listed in table 4.33 for the case of the square.

Some higher frequencies for the square were obtained by Kaul and Cadambe (ref. 4.61) as a special case of the parallelogram plate by using the Rayleigh-Ritz method and beam functions (see sec. 5.1.1). Frequencies for four higher modes are presented in table 4.34.

For a general rectangle, a spectrum of fundamental frequency parameters is given in table 4.35.

Frequencies for the first antisymmetric mode with respect to $x=a/2$ are given in table 4.36 (ref. 4.16). However, it is obvious that this is at least the third mode of all mode shapes of a plate for $a/b \leqq 1$. No detailed mode shapes are available in the literature, but for $a/b \leqq 1$ the second mode clearly must have a nodal line essentially parallel to the x-axis and located above $y=b/2$.

Approximate formulas for frequencies are given previously in equations (4.16) and (4.17). Frequency parameters obtained from equation (4.6) are plotted in figure 4.28 (from ref. 4.4).

For more information on this problem, see the discussion of the antisymmetric modes of a C–C–C–C rectangular plate in the preceding section (sec. 4.3.1). Straight nodal lines of antisymmetry duplicate SS boundary conditions.

4.3.3 C–C–C–F

The only known results for the problem of the C–C–C–F plate (fig. 4.29) are the approximate formulas, equations (4.16) and (4.17).

4.3.4 C–C–SS–SS

Four sources of numerical data are available for fundamental frequencies of C–C–SS–SS rectangular plates (fig. 4.30). The results are

TABLE 4.30.—*10 Frequencies* $\omega a^2(\sqrt{\rho/D})$ *for a C–C–C–C Rectangular Plate*

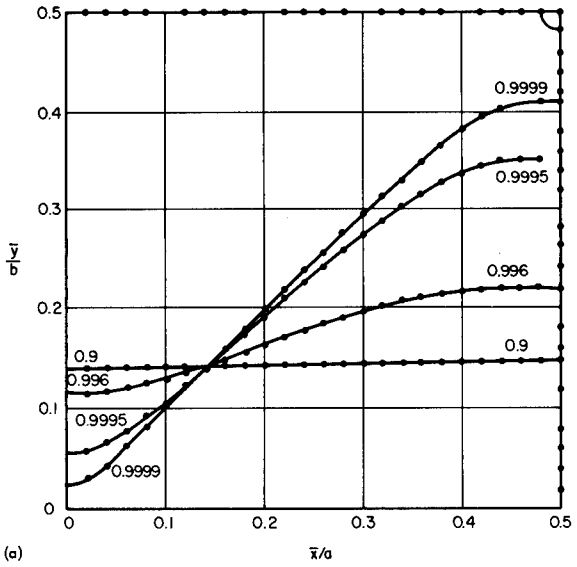
[Table reprinted with permission from ref. 4.36]

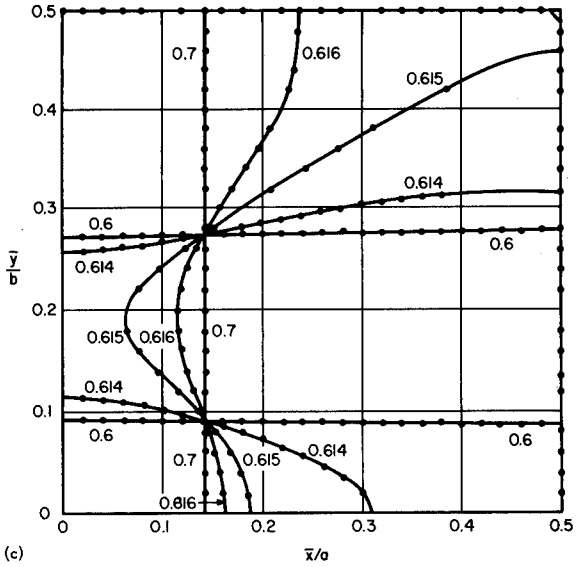
$\frac{a}{b}$	$\omega a^2\sqrt{\rho/D}$ for—									
	Modes symmetric about both $\bar{x}=0$ and $\bar{y}=0$			Modes symmetric about $\bar{x}=0$, antisymmetric about $\bar{y}=0$			Modes antisymmetric about $\bar{x}=0$, symmetric about $\bar{y}=0$		Modes antisymmetric about both $\bar{x}=0$ and $\bar{y}=0$	
	1st	2d	3d	1st	2d	3d	1st	2d	1st	2d
1.00	35. 9852	131. 5808	132. 2048	73. 3938	165. 0004	210. 5218	73. 3938	165. 0004	108. 2165	242. 1539
0.98	35. 2765	127. 1541	131. 4130	71. 0595	163. 0206	202. 659	72. 8282	160. 4586	106. 0800	234. 8886
0.96	34. 5900	122. 5488	130. 9143	68. 7792	161. 0931	194. 9597	72. 2803	156. 0217	103. 9993	227. 3558
0.94	33. 9257	118. 0362	130. 4374	66. 5530	159. 2177	187. 4225	71. 7500	151. 6896	101. 9741	219. 9772
0.92	33. 2834	113. 6220	129. 9765	64. 3813	157. 3939	180. 0481	71. 2369	147. 4627	100. 0048	212. 7632
0.90	32. 6631	109. 3081	129. 5303	62. 2643	155. 6212	172. 8373	70. 7410	143. 3414	98. 0908	205. 7163
0.88	32. 0647	105. 0947	129. 0981	60. 2022	153. 8982	165. 7906	70. 2617	139. 3258	96. 0908	198. 8375
0.86	31. 4881	100. 9822	128. 6797	58. 1954	152. 2222	158. 9113	69. 7990	135. 4162	94. 4293	192. 1276
0.84	30. 9333	96. 9713	128. 2748	56. 2442	150. 5557	152. 2364	69. 3526	131. 6129	92. 6813	185. 5883
0.82	30. 4001	93. 0622	127. 8829	54. 3488	145. 5856	149. 0788	68. 9228	127. 9160	90. 9884	179. 2169
0.80	29. 8881	89. 2553	127. 5041	52. 5095	139. 2082	147. 5424	68. 5075	124. 3257	89. 3501	173. 0170
0.78	29. 3975	85. 5510	127. 1382	50. 7266	132. 9827	146. 0480	68. 1083	120. 8423	87. 7663	166. 9883
0.76	28. 9277	81. 9499	126. 7847	49. 0004	126. 9195	144. 6443	67. 7242	117. 4658	86. 2369	161. 1310
0.74	28. 4787	78. 4522	126. 4436	47. 3314	121. 0206	143. 2698	67. 3550	114. 1963	84. 7612	155. 4458
0.72	28. 0502	75. 0586	126. 1147	45. 7196	115. 2870	141. 9435	67. 0005	111. 0339	83. 3390	149. 9331
0.70	27. 6418	71. 7697	125. 7978	44. 1654	109. 7195	140. 6645	66. 6603	107. 9788	81. 9700	144. 5934
0.68	27. 2532	68. 5858	125. 4925	42. 6691	104. 3185	139. 4323	66. 3341	105. 0307	80. 6535	139. 4272
0.66	26. 8840	65. 5075	125. 1988	41. 2308	99. 0846	138. 2463	66. 0217	102. 1896	79. 3892	134. 4349
0.64	26. 5338	62. 5358	124. 9162	39. 8508	94. 0187	137. 1059	65. 7227	99. 4553	78. 1764	129. 6168
0.62	26. 2023	59. 6710	124. 6389	38. 5292	89. 1215	136. 0104	65. 4370	96. 8276	77. 0147	124. 9736

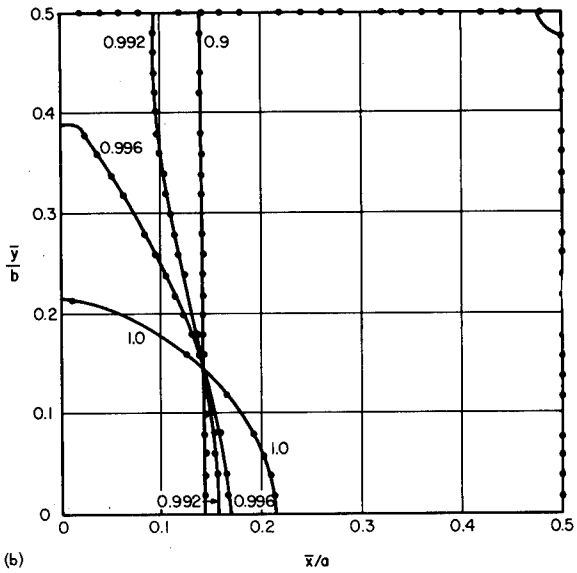
0.60	25. 8890	56. 9140	119. 3510	37. 2661	84. 3938	134. 9591	65. 1641	94. 3061	75. 9033	120. 5052
0.58	25. 5933	54. 2654	112. 4335	36. 0617	79. 8364	133. 9516	64. 9038	91. 8904	74. 8415	116. 2120
0.56	25. 3148	51. 7258	105. 7632	34. 9156	75. 5403	132. 9861	64. 6559	89. 5800	73. 8287	112. 0942
0.54	25. 0531	49. 2963	99. 3420	33. 8278	71. 2362	132. 0485	64. 4199	87. 3740	72. 8641	108. 1517
0.52	24. 8075	46. 9772	93. 1714	32. 9981	67. 1963	124. 7195	64. 1958	85. 2719	71. 9468	104. 3844
0.50	24. 5777	44. 7696	87. 2526	31. 8260	63. 3308	116. 3570	63. 9831	83. 2727	71. 0763	100. 7921
0.48	24. 3629	42. 6738	81. 5874	30. 9110	59. 6412	108. 3391	63. 7816	81. 3753	70. 2513	97. 3742
0.46	24. 1628	40. 6904	76. 1770	30. 0526	56. 1291	100. 6687	63. 5911	79. 5785	69. 4712	94. 1300
0.44	23. 9765	38. 8197	71. 0234	29. 2498	52. 7958	93. 3476	63. 4113	77. 8810	68. 7348	91. 0586
0.42	23. 8037	37. 0619	66. 1287	28. 5015	49. 6427	86. 3781	63. 2419	76. 2814	68. 0414	88. 1589
0.40	23. 6438	35. 4171	61. 4950	27. 8068	46. 6713	79. 7625	63. 0826	74. 7780	67. 3901	85. 4293
0.38	23. 4962	33. 8847	57. 1247	27. 1643	43. 8828	73. 5036	62. 9331	73. 3692	66. 7796	82. 8680
0.36	23. 3602	32. 4641	53. 0200	26. 5724	41. 2784	67. 6043	62. 7934	72. 0529	66. 2092	80. 4728
0.34	23. 2355	31. 1541	49. 1837	26. 0296	38. 8589	62. 0682	62. 6631	70. 8272	65. 6777	78. 2414
0.32	23. 1214	29. 9530	45. 6181	25. 5340	36. 6245	56. 8988	62. 5418	69. 6901	65. 1841	76. 1708
0.30	23. 0175	28. 8584	42. 2530	25. 0837	34. 5750	52. 1002	62. 4296	68. 6393	64. 7275	74. 2577
0.28	22. 9231	27. 8679	39. 3070	24. 6767	32. 7091	47. 6761	62. 3261	67. 6726	64. 3069	72. 4989
0.26	22. 8380	26. 9778	36. 5638	24. 3109	31. 0244	43. 6306	62. 2309	66. 7876	63. 9212	70. 8902
0.24	22. 7614	26. 1842	34. 0950	23. 9840	29. 5175	39. 9663	62. 1441	65. 9820	63. 5695	69. 4279
0.22	22. 6931	25. 4825	31. 8983	23. 6941	28. 1835	36. 6849	62. 0652	65. 2534	63. 2507	68. 1075
0.20	22. 6325	24. 8681	29. 9683	23. 4388	27. 0158	33. 7854	61. 9942	64. 5993	62. 9641	66. 9244
0.18	22. 5793	24. 3356	28. 2974	23. 2162	26. 0064	31. 2634	61. 9309	64. 0175	62. 7086	65. 8743
0.16	22. 5330	23. 8795	26. 8742	23. 0240	25. 1461	29. 1094	61. 8749	63. 5057	62. 4835	64. 9525
0.14	22. 4933	23. 4944	25. 6847	22. 8604	24. 4245	27. 3083	61. 8262	63. 0613	62. 2876	64. 1540
0.12	22. 4599	23. 1747	24. 7114	22. 7233	23. 8307	25. 8388	61. 7845	62. 6824	62. 1202	63. 4747
0.10	22. 4323	22. 9155	23. 9356	22. 6112	23. 3534	24. 6742	61. 7497	62. 3668	61. 9806	62. 9101
0.08	22. 4103	22. 7118	23. 3374	22. 5224	22. 9819	23. 7839	61. 7215	62. 1126	61. 8680	62. 4560
0.06	22. 3938	22. 5613	22. 8979	22. 4556	22. 7062	23. 1360	61. 6999	----------	61. 7815	62. 1088
0.04	22. 3822	----------	22. 5996	22. 4091	22. 5174	22. 7007	61. 6849	61. 7806	61. 7206	61. 8645
0.02	22. 3755	----------	22. 4285	16. 2699	22. 3830	22. 4541	61. 6758	61. 6993	61. 6847	61. 7205
0	22. 3733	----------	22. 3722	----------	22. 3733	22. 3733	61. 6728	61. 6728	61. 6728	61. 6728

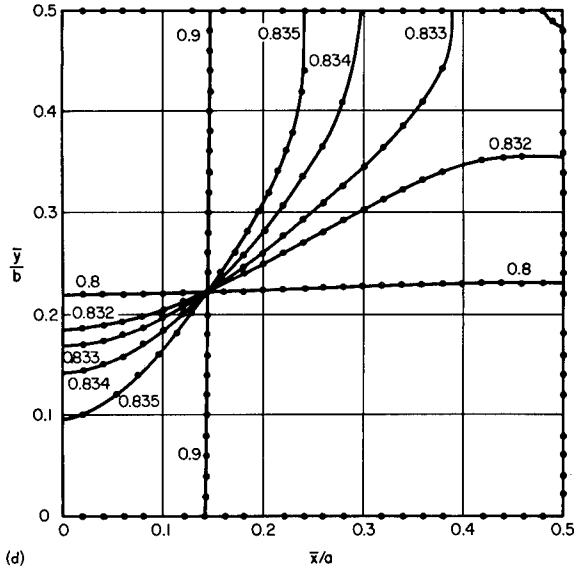
TABLE 4.31.—*Frequency Parameters* $\omega a^2\sqrt{\rho/D}$ *for the Second and Third Modes Symmetric About* $\bar{x}=0$ *and Antisymmetric About* $\bar{y}=0$ *in Vicinity of a Transition Point*

Mode	$\omega a^2\sqrt{\rho/D}$ for values of a/b of—						
	0. 837	0. 836	0. 835	0. 834	0. 833	0. 832	0. 831
Second	150. 2685	150. 1544	150. 0184	149. 8461	149. 6269	149. 3663	149. 0791
Third	151. 2909	150. 9951	150. 7217	150. 4853	150. 2963	150. 1492	150. 0029
Difference	1. 0224	. 8407	. 7033	. 6392	. 6694	. 7829	. 9238









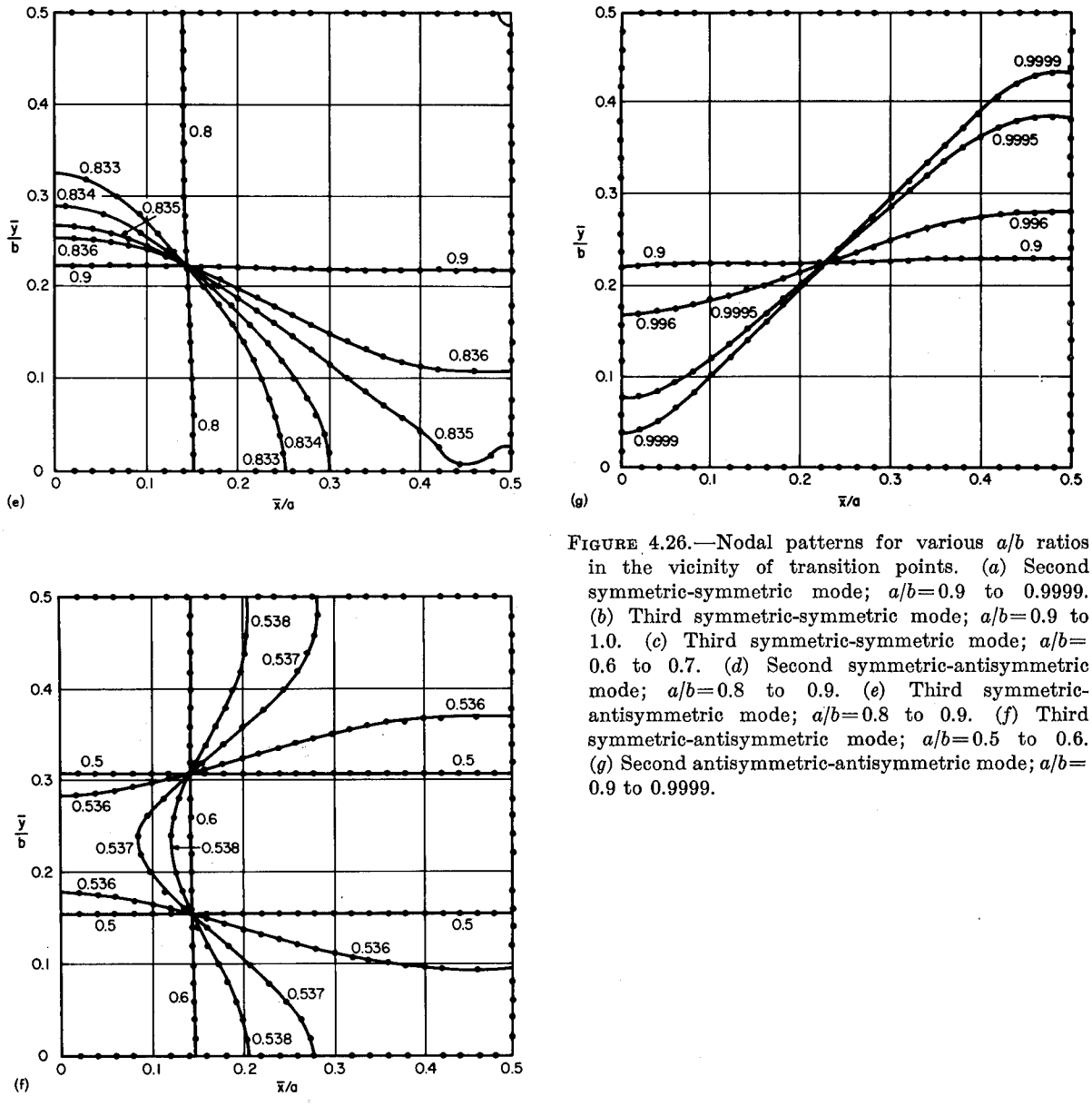


FIGURE 4.26.—Nodal patterns for various a/b ratios in the vicinity of transition points. (*a*) Second symmetric-symmetric mode; $a/b=0.9$ to 0.9999. (*b*) Third symmetric-symmetric mode; $a/b=0.9$ to 1.0. (*c*) Third symmetric-symmetric mode; $a/b=0.6$ to 0.7. (*d*) Second symmetric-antisymmetric mode; $a/b=0.8$ to 0.9. (*e*) Third symmetric-antisymmetric mode; $a/b=0.8$ to 0.9. (*f*) Third symmetric-antisymmetric mode; $a/b=0.5$ to 0.6. (*g*) Second antisymmetric-antisymmetric mode; $a/b=0.9$ to 0.9999.

summarized in table 4.37. Kanazawa and Kawai (ref. 4.16) used an integral equation formulation. Hamada (ref. 4.15) used a variational approach. Iwato (ref. 4.62) used the Rayleigh-Ritz method and mode shapes of the form

$$W(x,y)=\sum_m\sum_n C_{mn}\left(\cos\frac{m\pi x}{2a}-\cos\frac{3m\pi x}{2a}\right)\left(\cos\frac{n\pi y}{2b}-\cos\frac{3n\pi y}{2b}\right) \quad (4.55)$$

and retained C_{11}, C_{13}, C_{31}, and C_{33}. Nishimura (ref. 4.14) used finite difference equations. Approximate formulas, equations (4.16) and (4.17), may also be used. Frequency parameters obtained from equation (4.16) are plotted in figure 4.31 (from ref. 4.4) for four modes.

For more information on this problem, see the discussion of the doubly antisymmetric modes of a C–C–C–C rectangular plate (sec. 4.3.1). Straight node lines of antisymmetry duplicate simply supported boundary conditions.

TABLE 4.32.—*Bounds on Frequency Parameters* $\omega a^2\sqrt{\rho/D}$ *for the Doubly Symmetric Modes of a C–C–C–C Rectangular Plate*

Mode	$\omega a^2\sqrt{\rho/D}$ for values of b/a of—											
	1.00		1.25		1.50		2.00		4.00		8.00	
	Lower bound	Upper bound	Lower bound	Upper bound	Lower bound	Upper bound	Lower bound	Upper bound	Lower bound	Upper bound	Lower bound	Upper bound
1	35. 976	35. 985	29. 882	29. 888	27. 000	27. 005	24. 574	24. 578	22. 798	22. 799	22. 467	22. 468
2	131. 50	131. 58	89. 190	89. 256	66. 523	66. 523	44. 725	44. 771	26. 551	26. 569	23. 243	23. 249
3	132. 13	132. 21	127. 45	127. 51	125. 25	125. 30	87. 090	87. 257	35. 214	25. 297	24. 904	24. 936
4	219. 08	220. 06	180. 55	181. 29	144. 00	144. 21	123. 22	123. 25	49. 359	49. 615	27. 609	27. 715
5	308. 60	308. 91	201. 85	202. 07	160. 24	161. 24	141. 98	142. 37	68. 939	69. 454	31. 455	31. 755
6	308. 99	309. 17	286. 83	289. 72	232. 18	234. 68	150. 18	150. 56	93. 787	94. 607	36. 507	37. 158
7	388. 74	392. 85	304. 86	305. 02	257. 34	257. 75	180. 06	181. 81	121. 44	121. 45	43. 024	43. 958
8	391. 40	393. 98	354. 85	357. 14	302. 82	302. 93	233. 43	234. 00	123. 93	124. 95	51. 003	52. 186
9	544. 75	562. 38	365. 55	365. 96	336. 52	338. 22	236. 41	242. 19	125. 71	125. 82	60. 412	61. 763
10	564. 99	565. 40	443. 96	451. 22	338. 57	345. 38	300. 88	300. 95	134. 17	134. 73	71. 209	72. 689
11	565. 12	565. 56	448. 94	462. 48	399. 26	406. 63	306. 53	320. 16	145. 94	148. 39	83. 358	84. 939
12	640. 82	647. 79	540. 49	561. 58	406. 09	409. 76	319. 22	323. 41	158. 62	160. 37	96. 817	98. 493
13	640. 89	648. 58	561. 34	580. 55	450. 87	492. 46	336. 68	337. 36	159. 24	167. 01	111. 49	113. 34
14	719. 16	813. 67	580. 04	613. 15	473. 57	518. 04	352. 60	359. 09	169. 56	190. 74	121. 03	121. 03
15	719. 38	814. 84	608. 55	621. 14	547. 46	559. 54	371. 97	418. 22	186. 43	200. 81	122. 00	122. 08

TABLE 4.33.—*Frequency Parameters* $\omega a^2\sqrt{\rho/D}$ *for a C–C–C–SS Square Plate*

Source	$\omega a^2\sqrt{\rho/D}$ for mode—				
	1	2	3	4	5
Dill and Pister (ref. 4.24)	31. 83	63. 33	71. 08	100. 8	116. 4
Kanazawa and Kawai (ref. 4.16)	31. 88	------	71. 26	------	------
Hamada (ref. 4.15)	31. 83	------	------	------	------

TABLE 4.34.—*Frequency Parameters for Higher Mode Shapes of a C–C–C–SS Square Plate*

Mode	6	7	8	9
$\omega a^2\sqrt{\rho/D}$	130. 84	152. 75	160. 00	209. 97

4.3.5 C–C–SS–F

The only known results for the problem of the C–C–SS–F plate (fig. 4.32) are the approximate formulas, equations (4.16) and (4.17).

TABLE 4.35.—*Fundamental Frequency Parameters* $\omega a^2\sqrt{\rho/D}$ *for a C–C–C–SS Rectangular Plate*

Source	$\omega a^2\sqrt{\rho/D}$ for values of a/b of—							
	0	0.333	0.4	0.5	0.667	1	1.5	2
Dill and Pister (ref. 4.24)	------	------	------	24. 49	------	31. 83	------	73. 07
Kanazawa and Kawai (ref. 4.16)	22. 39	23. 40	23. 76	24. 48	26. 23	31. 87	------	------
Hamada (ref. 4.15)	------	------	------	------	25. 85	31. 83	48. 1	------

TABLE 4.36.—*Fundamental Frequency Parameters* $\omega a^2\sqrt{\rho/D}$ *for the First Antisymmetric Mode of a C–C–C–SS Rectangular Plate*

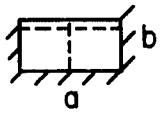
Mode shape	$\omega a^2\sqrt{\rho/D}$ for values of a/b of—					
	0	0.333	0.4	0.5	0.667	1
	61. 781	63. 947	64. 366	65. 161	66. 971	71. 259

TABLE 4.37.—*Fundamental Frequency Parameters* $\omega a^2\sqrt{\rho/D}$ *for a C–C–SS–SS Rectangular Plate*

Source	$\omega a^2\sqrt{\rho/D}$ for values of a/b of—						
	0	0.333	0.4	0.5	0.667	1	1.5
Kanazawa and Kawai (ref. 4.16)	15. 45	16. 74	17. 22	18. 16	20. 39	27. 10	------
Hamada (ref. 4.15)	------	------	------	------	------	27. 00	44. 90
Iwato (ref. 4.62)	------	------	------	------	------	28. 357	------
Nishimura (ref. 4.14)	------	------	------	------	------	27. 234	------

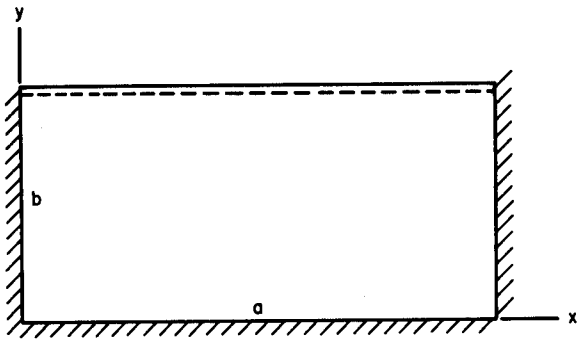


FIGURE 4.27.—C–C–C–SS plate.

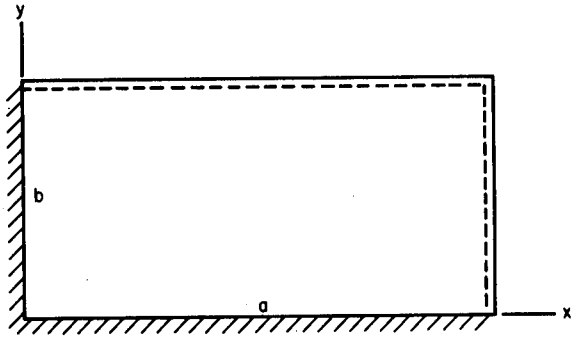


FIGURE 4.30.—C–C–SS–SS plate.

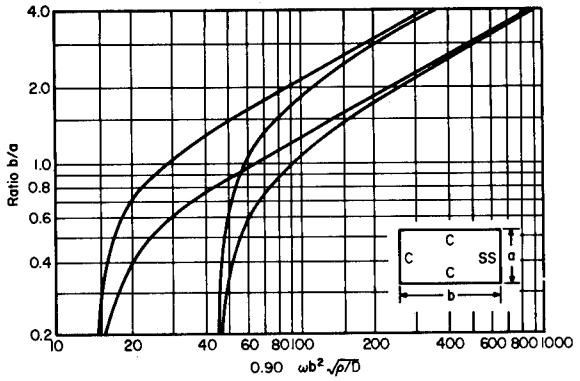


FIGURE 4.28.—Frequency parameter $0.90\omega b^2\sqrt{\rho/D}$ for a C–C–C–SS rectangular plate. (After ref. 4.4)

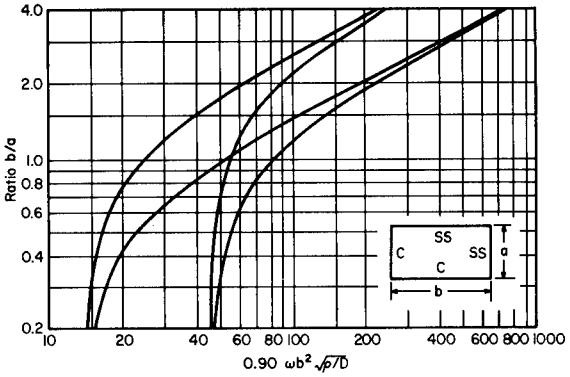


FIGURE 4.31.—Frequency parameters $0.90\omega b^2\sqrt{\rho/D}$ for a C–C–SS–SS rectangular plate. (After ref. 4.4)

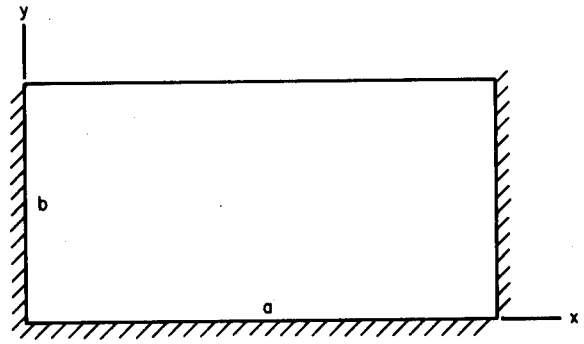


FIGURE 4.29.—C–C–C–F plate.

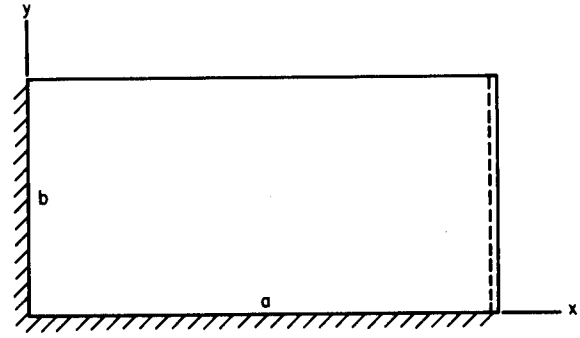


FIGURE 4.32.—C–C–SS–F plate.

4.3.6 C–C–F–F

The problem of the C–C–F–F rectangular plate (fig. 4.33) was investigated by Young (ref. 4.47), who used the products of beam functions and the Rayleigh-Ritz method to obtain accurate upper bounds for frequencies in the case of the square plate for $\nu=0.3$. These results are summarized in table 4.38. The resulting mode shapes are of the form of equation (4.49) where the values of A_{mn} are given in table 4.38 and α and ϵ are given in table 4.39 (from ref. 4.47).

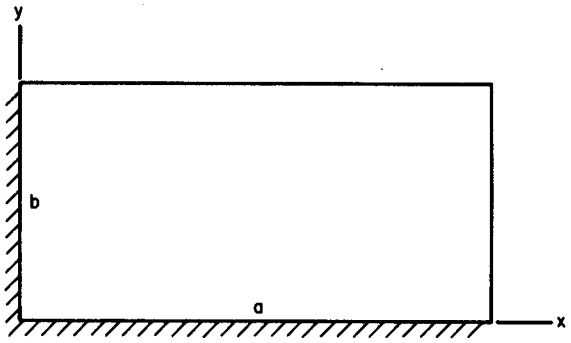


FIGURE 4.33.—C–C–F–F plate.

A fundamental frequency of large error is also computed in reference 4.48 by use of the Rayleigh-Ritz method.

Results from using the Galerkin method are given in reference 4.46; these results also appear to have considerable error, particularly for the fundamental mode. Approximate formulas, equations (4.16) and (4.17), may also be used.

4.3.7 C–SS–C–F

The approximate formulas, equations (4.16) and (4.17), may be used for the problem of a C–SS–C–F rectangular plate (fig. 4.34). Additional information can be obtained from an antisymmetric mode of the case of the C–F–C–F plate (sec. 4.3.10). Straight node lines of antisymmetry duplicate SS boundary conditions.

TABLE 4.39.—*Eigenfunction Parameters for a C–F Beam*

m, n	α_m, α_n	ϵ_m, ϵ_n
1	0. 7340955	1. 8751041
2	1. 01846644	4. 6940911
3	. 99922450	7. 8547574
4	1. 00003355	10. 9955407
5	. 99999855	14. 1371684
$r>5$	1. 0	$(2r-1)\pi/2$

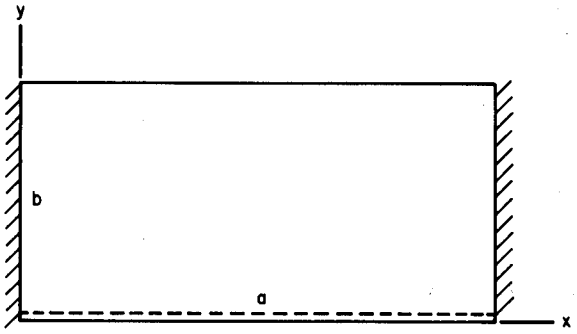
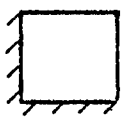
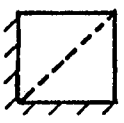
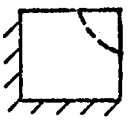
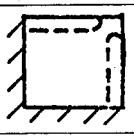
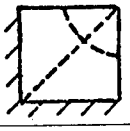


FIGURE 4.34.—C–SS–C–F plate.

TABLE 4.38.—*First Five Sets of Frequency Parameters, Nodal Lines, and Amplitude Coefficients for a C–C–F–F Square Plate; $\nu=0.3$*

Mode	1	2	3	4	5
$\omega a^2\sqrt{\rho/D}$	6.958	24.80	26.80	48.05	63.14
Nodal lines					
Amplitude coefficients.	$A_{11}=1.0000$ $A_{12}=0.0604$ $A_{13}=-0.0030$ $A_{21}=0.0604$ $A_{22}=-0.0101$ $A_{23}=-0.0003$ $A_{31}=-0.0030$ $A_{32}=-0.0003$ $A_{33}=-0.0017$	$A_{11}=0$ $A_{12}=1.0000$ $A_{13}=0.00003$ $A_{21}=-1.0000$ $A_{22}=0$ $A_{23}=-0.0221$ $A_{31}=-0.00003$ $A_{32}=0.0221$ $A_{33}=0$	$A_{11}=-0.1172$ $A_{12}=1.0000$ $A_{13}=0.0553$ $A_{21}=1.0000$ $A_{22}=0.3223$ $A_{23}=0.0111$ $A_{31}=0.0553$ $A_{32}=0.0111$ $A_{33}=0.0022$	$A_{11}=0.0286$ $A_{12}=-0.1566$ $A_{13}=-0.0825$ $A_{21}=-0.1566$ $A_{22}=1.0000$ $A_{23}=-.1458$ $A_{31}=-0.0825$ $A_{32}=0.1458$ $A_{33}=-0.0019$	$A_{11}=0$ $A_{12}=0.0030$ $A_{13}=1.0000$ $A_{21}=-0.0030$ $A_{22}=0$ $A_{23}=0.1350$ $A_{31}=-1.0000$ $A_{32}=-0.1350$ $A_{33}=0$

4.3.8 C–SS–SS–F

The only known results for the problem of the C–SS–SS–F rectangular plate (fig. 4.35) are the approximate formulas, equations (4.16) and (4.17). Additional information can be obtained from the doubly antisymmetric modes of the C–F–C–F plate (sec. 4.3.10). Straight node lines of antisymmetry duplicate SS boundary conditions.

4.3.9 C–SS–F–F

The only known results for the problem of the C–SS–F–F rectangular plate (fig. 4.36) are the approximate formulas, equations (4.16) and (4.17). Additional results can be obtained from the antisymmetric modes of the C–F–F–F plate (sec. 4.3.12). Straight node lines of antisymmetry duplicate SS boundary conditions.

4.3.10 C–F–C–F

Claassen and Thorne (ref. 4.36) used the series method described in the section for the C–C–C–C rectangular plate (sec. 4.3.1) to obtain frequencies for 11 modes and varying a/b ratios for the C–F–C–F rectangular plate (fig. 4.37). These modes will be classified as symmetric-symmetric, symmetric-antisymmetric, antisymmetric-symmetric, and antisymmetric-antisymmetric, according to the symmetry or antisymmetry exhibited about the axes $\bar{x}=0$ and $\bar{y}=0$, respectively, as shown in figure 4.37. The first mode of each class is illustrated in figure 4.38. Frequency results are summarized in tables 4.40 to 4.43. Poisson's ratio is not known, but is assumed to be 0.3 as in reference 4.63.

A question arises about the foregoing results in one of the limiting cases. It would appear

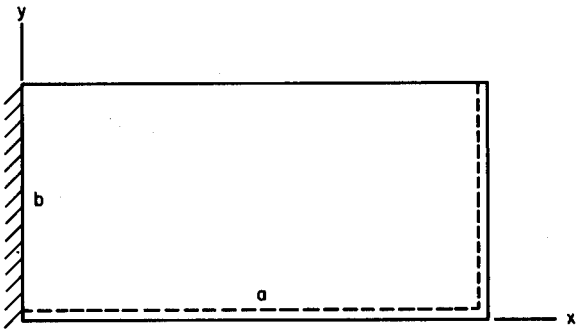


FIGURE 4.35.—C–SS–SS–F plate.

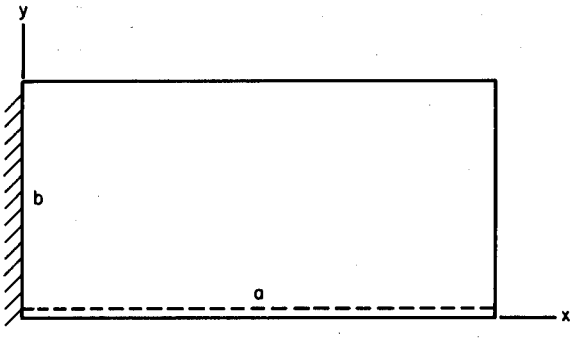


FIGURE 4.36.—C–SS–F–F plate.

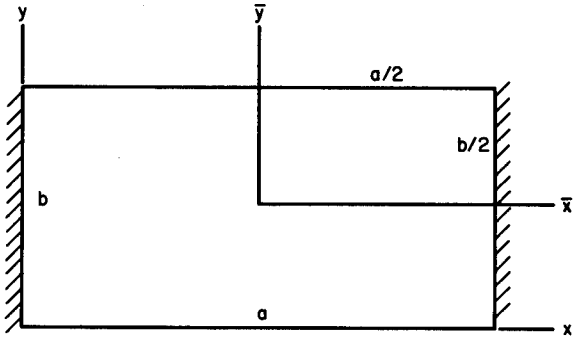


FIGURE 4.37.—C–F–C–F plate.

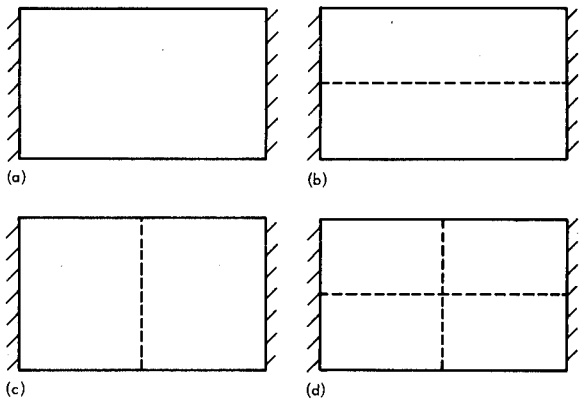


FIGURE 4.38.—Lowest nodal patterns in the four classes of symmetry for a C–F–C–F plate. (*a*) First symmetric-symmetric mode. (*b*) First symmetric-antisymmetric mode. (*c*) First antisymmetric-symmetric mode. (*d*) First antisymmetric-antisymmetric mode.

from table 4.40 that the doubly symmetric frequencies all vanish as $b/a \to 0$. However, as b is held fixed and a becomes infinite, it is obvious that the boundary conditions at $x=0$ and $x=\infty$ are no longer significant, and the fundamental frequency becomes that of an infinite strip having two node lines parallel to the x-axis. Additional frequency parameters in the vicinity of "transition points" (see sec. 4.3.1) and detailed coordinates of nodal lines are given in reference 4.36.

Approximate values of frequency parameters are given by equations (4.16) and (4.17).

TABLE 4.40.—*Frequency Parameters* $\lambda = \omega a^2\sqrt{\rho/D}$ *and* $\lambda^* = \omega b^2\sqrt{\rho/D}$ *for the Doubly Symmetric Modes of a C–F–C–F Rectangular Plate*

Ratio a/b	Mode 1	2	3	4	5
	λ				
1.0	22. 17	43. 6	120. 1	136. 9	149. 3
0.9	22. 19	39. 5	114. 2	120. 1	143. 9
0.8	22. 20	35. 8	94. 1	120. 2	139. 1
0.7	22. 22	32. 6	76. 3	120. 3	134. 8
0.6	22. 24	29. 8	61. 1	120. 4	122. 5
0.5	22. 26	27. 5	48. 6	90. 3	120. 4
0.4	22. 28	25. 6	38. 5	64. 3	103. 6
0.3	22. 3	24. 1	31. 0	44. 6	65. 9
0.2	22. 3	23. 1	26. 0	31. 4	40. 0
0.1	22. 3	22. 5	23. 1	24. 3	26. 1
0	22. 4	22. 4	22. 4	22. 4	22. 4
b/a	λ^*				
1.0	22. 17	43. 6	120. 1	136. 9	149. 3
0.9	18. 93	39. 5	97. 2	126. 1	133. 6
0.8	14. 16	35. 7	76. 8	105. 5	130. 8
0.7	10. 83	32. 5	58. 7	87. 0	128. 3
0.6	7. 95	29. 7	43. 1	70. 9	106. 7
0.5	5. 51	27. 3	29. 9	56. 9	74. 0
0.4	3. 51	19. 0	25. 5	45. 3	47. 3
0.3	1. 97	10. 7	24. 1	26. 5	35. 7
0.2	. 87	4. 7	11. 7	21. 9	23. 1
0.1	. 217	1. 2	2. 9	5. 4	8. 7
0	. 00	. 0	. 0	. 0	------

TABLE 4.41.—*Frequency Parameters* $\lambda = \omega a^2\sqrt{\rho/D}$ *and* $\lambda^* = \omega b^2\sqrt{\rho/D}$ *for the Symmetric-Antisymmetric Modes of a C–F–C–F Rectangular Plate*

a/b for λ, b/a for λ^*	Mode 1		2	
	λ	λ^*	λ	λ^*
1.0	26. 40	26. 40	79. 8	79. 8
0.9	25. 67	22. 10	68. 4	76. 1
0.8	24. 99	18. 22	58. 2	72. 9
0.7	24. 38	14. 75	49. 3	65. 2
0.6	23. 84	11. 68	41. 8	49. 5
0.5	23. 36	8. 99	35. 5	36. 2
0.4	23. 0	6. 65	30. 6	25. 1
0.3	22. 7	4. 63	26. 8	16. 3
0.2	22. 5	2. 88	24. 2	9. 4
0.1	22. 3	1. 36	22. 7	4. 1
0	22. 4	. 0	22. 4	. 0

TABLE 4.42.—*Frequency Parameters* $\lambda = \omega a^2\sqrt{\rho/D}$ *and* $\lambda^* = \omega b^2\sqrt{\rho/D}$ *for the Antisymmetric-Symmetric Modes of a C–F–C–F Rectangular Plate*

a/b for λ, b/a for λ^*	Mode 1		2	
	λ	λ^*	λ	λ^*
1.0	61. 2	61. 2	87. 5	87. 5
0.9	61. 2	49. 5	82. 8	75. 7
0.8	61. 3	39. 1	78. 4	64. 9
0.7	61. 3	29. 9	74. 5	55. 4
0.6	61. 4	21. 9	71. 1	47. 0
0.5	61. 4	15. 2	68. 2	39. 8
0.4	61. 4	9. 7	65. 7	31. 6
0.3	61. 5	5. 4	63. 9	17. 7
0.2	61. 2	2. 3	62. 6	7. 8
0.1	--------	. 6	61. 8	2. 0
0	--------	. 0	61. 7	. 0

4.3.11 C–F–SS–F

The first four frequencies for the C–F–SS–F rectangular plate (fig. 4.39) in the case of the square for $\nu=0.3$ are given in table 4.44 (refs. 4.24 and 4.64). Additional results for this

TABLE 4.43.—*Frequency Parameters* $\lambda=\omega a^2\sqrt{\rho/D}$ *and* $\lambda^*=\omega b^2\sqrt{\rho/D}$ *for the Doubly Antisymmetric Modes of a C–F–C–F Rectangular Plate*

a/b for λ, b/a for λ^*	Mode 1		Mode 2	
	λ	λ^*	λ	λ^*
1.0	67. 2	67. 2	124. 5	124. 5
0.9	66. 1	55. 5	112. 6	112. 6
0.8	65. 1	45. 0	102. 0	102. 0
0.7	64. 3	35. 7	92. 5	92. 6
0.6	63. 5	27. 5	84. 3	78. 3
0.5	62. 9	20. 5	77. 4	56. 3
0.4	62. 4	14. 7	71. 7	38. 2
0.3	62. 0	9. 87	67. 2	24. 0
0.2	61. 2	5. 90	64. 1	13. 3
0.1		2. 80	62. 1	5. 6
0		. 0	61. 7	. 0

TABLE 4.44.—*Frequency Parameters for a C–F–SS–F Square Plate;* $\nu=0.3$

Mode	1	2	3	4
$\omega a^2\sqrt{\rho/D}$	15. 16	20. 50	50. 21	56. 38

problem are given by the approximate formulas, equations (4.16) and (4.17).

Further information on this problem can be obtained by considering antisymmetric modes of the C–F–C–F plate (see preceding section). Straight node lines of antisymmetry duplicate SS boundary conditions.

4.3.12 C–F–F–F (Cantilever)

Young (ref. 4.47) in his investigation of rectangular C–F–F–F plates (fig. 4.40) used the products of beam functions and the Rayleigh-Ritz method to obtain accurate upper bounds for frequencies in the case of the square canti-

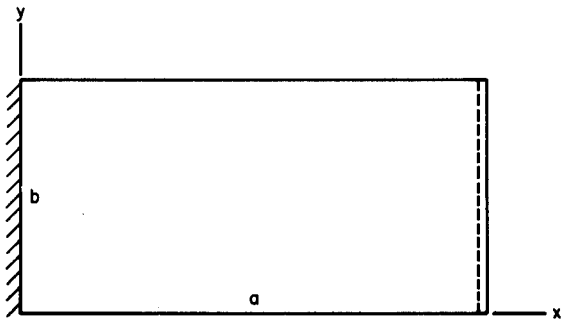


FIGURE 4.39.—C–F–SS–F plate.

TABLE 4.45.—*First Five Sets of Frequency Parameters, Nodal Lines, and Amplitude Coefficients for a Square Cantilever Plate;* $\nu=0.3$

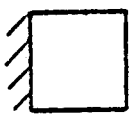
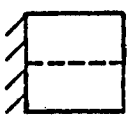
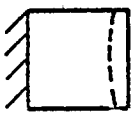
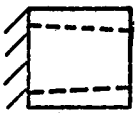
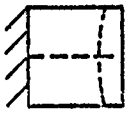
Mode	1	2	3	4	5
$\omega a^2\sqrt{\rho/D}$	3. 494	8. 547	21. 44	27. 46	31. 17
Nodal lines					
Amplitude coefficients.	$A_{11}=$ 1. 0000 $A_{13}=-$0. 0087 $A_{15}=-$0. 0008 $A_{21}=-$0. 0026 $A_{23}=-$0. 0050 $A_{25}=-$0. 0011 $A_{31}=$ 0. 0001 $A_{33}=-$0. 0014 $A_{35}=-$0. 0006	$A_{12}=$ 1. 0000 $A_{14}=-$0. 0134 $A_{16}=-$0. 0011 $A_{22}=$ 0. 1212 $A_{24}=$ 0. 0044 $A_{26}=$ 0. 0006 $A_{32}=-$0. 0020 $A_{34}=-$0. 0011 $A_{36}=-$0. 0006	$A_{11}=$ 0. 0054 $A_{13}=$ 0. 2731 $A_{15}=$ 0. 0092 $A_{21}=$ 1. 0000 $A_{23}=$ 0. 0713 $A_{25}=$ 0. 0079 $A_{31}=-$0. 0118 $A_{33}=$ 0. 0050 $A_{35}=-$0. 0003	$A_{11}=$ 0. 0090 $A_{13}=$ 1. 0000 $A_{15}=-$0. 0120 $A_{21}=-$0. 2866 $A_{23}=$ 0. 1786 $A_{25}=$ 0. 0009 $A_{31}=-$0. 0451 $A_{33}=$ 0. 0125 $A_{35}=-$0. 0023	$A_{12}=-$0. 1201 $A_{14}=$ 0. 0627 $A_{16}=$ 0. 0080 $A_{22}=$ 1. 0000 $A_{24}=-$0. 0388 $A_{26}=-$0. 0013 $A_{32}=$ 0. 0776 $A_{34}=$ 0. 0086 $A_{36}=$ 0. 0024

TABLE 4.46.—*Eigenfunction Parameters for C–F and F–F Beams*

m, n	α_m	α_n	ϵ_m	ϵ_n
1	0. 7340955		1. 8751041	
2	1. 01846644		4. 6940911	
3	. 99922450	0. 98250222	7. 8547574	4. 7300408
4	1. 00003355	1. 00077731	10. 9955407	7. 8532046
5	. 99999855	. 99996645	14. 1371684	10. 9956078
6	1. 0	1. 00000145	$(2m-1)\pi/2$	14. 1371655

lever for $\nu=0.3$. These results are summarized in table 4.45. The mode shapes are given by

$$W(x,y)=\sum_{m=1}^{p}\left\{A_{m1}+A_{m2}\sqrt{3}\left(1-2\frac{y}{a}\right)+\sum_{n=3}^{q}A_{mn}\left[\cosh\frac{\epsilon_n y}{b}+\cos\frac{\epsilon_n y}{b}-\alpha_n\left(\sinh\frac{\epsilon_n y}{b}+\sin\frac{\epsilon_n y}{b}\right)\right]\right\}\left[\cosh\frac{\epsilon_m x}{a}-\cos\frac{\epsilon_m x}{a}-\alpha_m\left(\sinh\frac{\epsilon_m x}{a}-\sin\frac{\epsilon_m x}{a}\right)\right] \quad (4.56)$$

where the values of A_{mn} are given in table 4.45 and those of α and ϵ are given in table 4.46.

In references 4.65 to 4.68, Reissner's variational principle (ref. 4.69) is modified and applied to the square plate. As in the Rayleigh-Ritz method, generalized force boundary conditions may or not be satisfied here. In reference 4.66, moment boundary conditions were satisfied at discrete points and four degrees of satisfaction of shear boundary conditions were considered; the best results were obtained when the transverse shear conditions on the free edges were ignored. Theoretical frequencies for the first three modes, along with experimental data from reference 4.66, are presented in table 4.47. Mode shapes corresponding to these frequencies are shown in figure 4.41.

Electrical analogies were developed in reference 4.70 for solution of the problem on a passive element analog computer. Five sets of frequencies and mode shapes for a square are given. In reference 4.71, simple difference and higher order difference equations were written and solved by means of electronic analog computer for the first six frequencies of a square. The problem is also discussed in references 4.48 and 4.72.

TABLE 4.47.—*Frequency Parameters* $\omega a^2\sqrt{\rho/D}$ *for a Square Cantilever Plate*

Type of data	$\omega a^2\sqrt{\rho/D}$ for mode—		
	1	2	3
Theoretical	3. 44	8. 21	21. 09
Experimental	3. 33	8. 17	19. 97

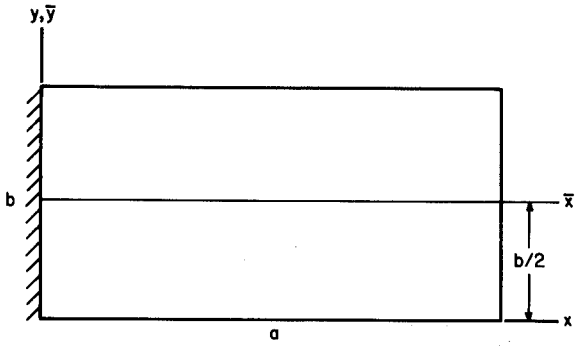


FIGURE 4.40.—C–F–F–F plate.

Barton (refs. 4.73 and 4.74) extended the Rayleigh-Ritz analysis of reference 4.47 to obtain results for the nonsquare cantilever. Five sets of mode shapes and frequencies for $a/b=\frac{1}{2}$, 2, and 5 are reproduced as table 4.48. The amplitude coefficients A_{mn} refer to equation (4.56). These frequencies are approximately plotted as solid lines in figure 4.42.

Bazley, Fox, and Stadter (ref. 4.75) used a method developed in reference 4.61 to compute frequency lower bounds for the first 10 symmetric modes. They also obtained accurate upper

TABLE 4.48.—*Frequency Parameters, Mode Shapes and Amplitude Coefficients of Rectangular Cantilever Plates;* $\nu=0.3$

First mode

a/b	1/2	2	5	Mode shape
$\omega a^2\sqrt{\rho/D}$	3.508	3.472	3.450	
A_{11}	1.0000	1.0000	1.0000	
A_{13}	−.0151	−.0027	−.0004	
A_{14}	−.0028	−.0002	.0000	
A_{21}	−.0011	−.0040	−.0048	
A_{23}	−.0040	−.0032	−.0008	
A_{25}	−.0023	−.0004	−.0001	
A_{31}	.0001	−.0003	−.0010	
A_{33}	−.0005	−.0015	−.0005	
A_{35}	−.0008	−.0003	−.0001	

Second mode

a/b	1/2	2	5	Mode shape
$\omega a^2\sqrt{\rho/D}$	5.372	14.93	34.73	
A_{12}	1.0000	1.0000	1.0000	
A_{14}	−.0509	−.0027	−.0004	
A_{16}	−.0056	−.0001	.0000	
A_{22}	.0436	.2040	.2555	
A_{24}	.0045	.0011	.0001	
A_{26}	.0007	.0002	.0000	
A_{32}	−.0012	.0059	.0215	
A_{34}	−.0014	−.0005	−.0001	
A_{36}	−.0010	−.0002	.0000	

Third mode

a/b	1/2	2	5	Mode shape
$\omega a^2\sqrt{\rho/D}$	21.96	21.61	21.52	
A_{11}	0.0008	0.0042	0.0048	
A_{13}	−.0465	.0346	.0054	
A_{15}	.0725	.0027	.0004	
A_{21}	1.0000	1.0000	1.0000	
A_{23}	.0271	.0206	.0050	
A_{25}	.0196	.0024	.0005	
A_{31}	−.0011	−.0058	−.0068	
A_{33}	.0001	.0010	−.0007	
A_{35}	.0024	−.0003	−.0001	

Fourth mode

a/b	1/2	2	5	Mode shape
$\omega a^2\sqrt{\rho/D}$	10.26	94.49	563.9	
A_{11}	0.0155	0.0034	0.0006	
A_{13}	1.0000	1.0000	1.0000	
A_{15}	−.0357	−.0031	−.0004	
A_{21}	.0459	−.0389	−.0065	
A_{23}	.1120	.2359	.2469	
A_{25}	.0088	.0009	.0001	
A_{31}	−.0091	.1025	.0104	
A_{33}	.0020	.0351	.0381	
A_{35}	−.0018	−.0003	−.0002	

Fifth mode

a/b	1/2	2	5	Mode shape
$\omega a^2\sqrt{\rho/D}$	24.85	48.71	105.9	
A_{12}	−0.0529	−0.2053	−0.2639	
A_{14}	−.1989	.0128	.0016	
A_{16}	.0448	.0017	.0002	
A_{22}	1.0000	1.0000	1.0000	
A_{24}	−.1069	−.0168	−.0028	
A_{26}	.0000	−.0005	−.0001	
A_{32}	.0261	.2222	.3893	
A_{34}	.0001	.0048	.0004	
A_{36}	.0040	.0012	.0002	

bounds by the Rayleigh-Ritz method by taking the first 50 admissible products of beam functions. Double-precision arithmetic (16 significant figures) was used in the computations where necessary. Results are listed in table 4.49 for seven a/b ratios. Sigillito (ref. 4.76) showed that even more precise upper bounds can be obtained with the Rayleigh-Ritz procedure by using deflection functions which are products of beam functions and Legendre functions. Results obtained using 30 admissible functions constructed in this manner are also listed in table 4.49. All values in table 4.49 are for $\nu=0.3$.

Gontkevich (ref. 4.55) used Southwell's method to get lower bounds of frequency param-

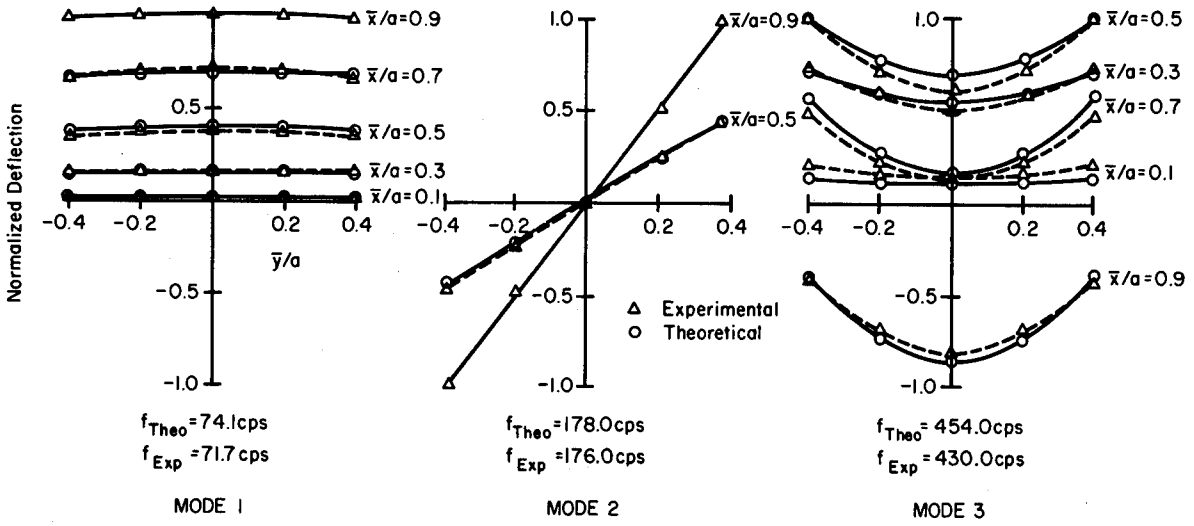


FIGURE 4.41.—Theoretical and experimental mode shapes for a square cantilever plate.

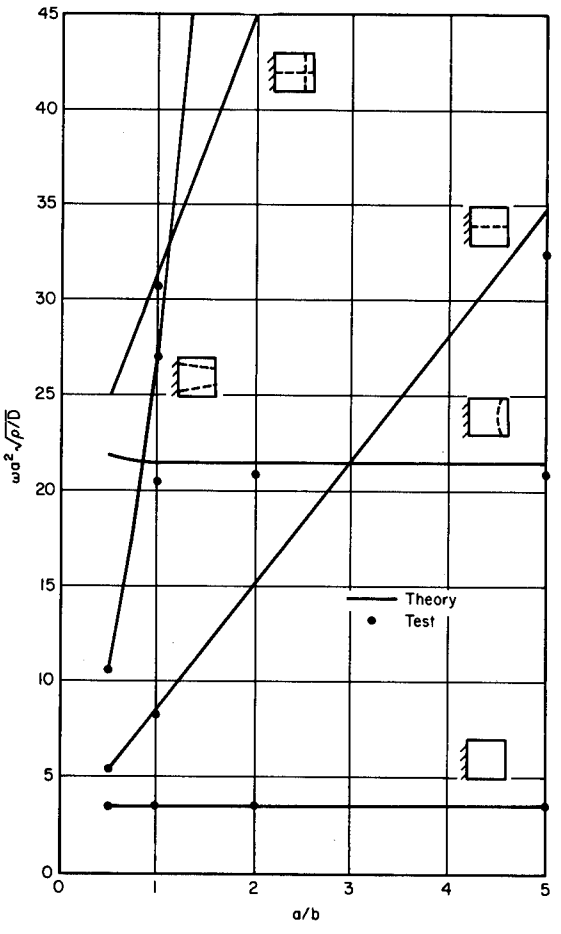


FIGURE 4.42.—Frequency parameter $\omega a^2\sqrt{\rho/D}$ for a rectangular cantilever plate; $\nu=0.3$. (After ref. 4.73)

eters for the first five modes. These are summarized in table 4.50 for $\nu=0.3$. The mode numbers agree with those of table 4.48.

Claassen and Thorne (refs. 4.63 and 4.77) used the series method described in the discussion of the C–C–C–C plate (sec. 4.3.1) to obtain precise frequencies for small variations in a/b ratio. Figure 4.43 gives the lowest five symmetric frequencies and the lowest four antisymmetric frequencies as functions of a/b, with $a<b$. Figure 4.44 shows the variation with b/a for $a>b$. Poisson's ratio $\nu=0.3$ was used.

Detailed tabular data for the above curves are given in tables 4.51 and 4.52. Additional frequencies in the vicinity of "transition points" (see discussion of the C–C–C–C plate, sec. 4.3.1) and the detailed coordinates of nodal lines are given in reference 4.63.

Martin (ref. 4.78) devised a variational procedure similar to the Rayleigh-Ritz method and used it to compute the frequencies of a mild steel plate of dimensions $a=5.12$ inches, $b=2.76$ inches, and $h=0.053$ inch. These are compared with experimental data found by Grinsted (ref. 4.79) in table 4.53. The upper values are taken from reference 4.78 and the lower, from reference 4.79, and the percent difference is given. The indicators m and n correspond to the number of nodal lines running "parallel" to the y- and x-axes, respectively;

TABLE 4.49.—*Bounds on Frequency Parameter* $\omega a^2\sqrt{\rho/D}$ *for Symmetric Modes of a Rectangular Cantilever Plate;* $\nu=0.3$

Mode	$\omega a^2\sqrt{\rho/D}$					
	Lower bounds	Upper bounds		Lower bounds	Upper bounds	
		Ref. 4.75	Ref. 4.76		Ref. 4.75	Ref. 4.76
	$a/b=0.125$			$a/b=0.250$		
1	3.4926	3.5134	3.5113	3.4835	3.5094	3.5059
2	3.9425	4.0448	4.0406	5.2559	5.5171	5.5141
3	5.3402	5.6095	5.6076	10.583	11.313	11.318
4	7.6439	8.2204	8.2204	20.106	21.465	21.455
5	11.050	11.995	11.996	21.900	22.309	22.308
6	15.576	17.008	17.018	24.040	24.857	24.816
7	20.827	21.977	21.955	30.755	32.500	32.489
8	21.869	22.618	22.606	35.142	37.669	37.890
9	22.381	23.431	23.599	41.738	44.481	44.520
10	24.067	24.909	24.901	53.987	58.218	60.738
	$a/b=0.500$			$a/b=1.000$		
1	3.4608	3.5001	3.4944	3.4305	3.4823	3.4729
2	9.7605	10.210	10.208	20.874	21.367	21.304
3	21.529	21.891	21.848	26.501	27.278	27.291
4	29.927	31.522	31.491	51.502	54.301	54.262
5	32.906	34.160	34.180	60.249	61.450	61.276
6	55.061	58.195	58.184	92.143	97.321	97.208
7	60.256	61.560	61.440	115.68	119.51	119.24
8	68.292	71.346	71.217	121.11	124.63	125.14
9	74.355	77.717	78.936	143.98	150.24	156.67
10	93.740	99.722	99.925	149.47	158.25	161.13
	$a/b=2.000$			$a/b=4.000$		
1	3.3856	3.4575	3.4415	3.3306	3.4332	3.4131
2	21.062	21.550	21.447	20.822	21.475	21.340
3	58.946	60.477	60.191	58.356	60.292	59.937
4	91.165	93.390	94.245	114.57	118.59	117.98
5	115.77	119.00	118.67	189.63	196.62	195.80
6	122.53	127.22	128.44	283.02	293.96	293.03
7	170.71	179.29	181.56	354.30	361.12	364.43
8	193.19	198.94	198.20	384.46	394.02	400.44
9	234.60	294.00	252.59	401.04	415.19	416.66
10	287.76	297.09	296.00	443.26	459.58	520.04
	$a/b=8.000$					
1	3.3025	3.4297	3.3885			
2	20.683	21.481	21.220			
3	57.940	60.208	59.472			
4	113.67	118.20	116.79			
5	188.20	195.83	193.60			
6	281.60	293.22	290.08			
7	393.91	410.42	406.38			
8	525.11	547.45	542.54			
9	675.15	704.29	698.58			
10	842.90	880.88	874.46			

TABLE 4.50.—*Lower Bounds of* $\omega a^2\sqrt{\rho/D}$ *for Rectangular Cantilever Plates;* $\nu=0.3$

Mode	Lower bounds of $\omega a^2\sqrt{\rho/D}$ for values of a/b of—			
	0.5	1.0	2.0	5.0
1	3. 35407	3. 35407	3. 35407	3. 35407
2	4. 6490	7. 2595	13. 3064	32. 3660
3	21. 0195	21. 0195	21. 0195	21. 0195
4	9. 0096	25. 151	86. 402	534. 55
5	23. 110	28. 546	43. 977	98. 836

thus, n must be even for symmetric modes and odd for antisymmetric modes.

Forsyth and Warburton (ref. 4.80) used the Rayleigh-Ritz method with a deflection function having two terms involving the products of beam functions to obtain the frequencies of a rectangular steel plate having $a=16$ inches, $b=7.5$ inches, and $h=0.282$ inch and compared them with experimental results. These results are listed in table 4.54.

Much experimental information is available on this problem. Dalley and Ripperger (refs. 4.81 and 4.82) gave results determined from

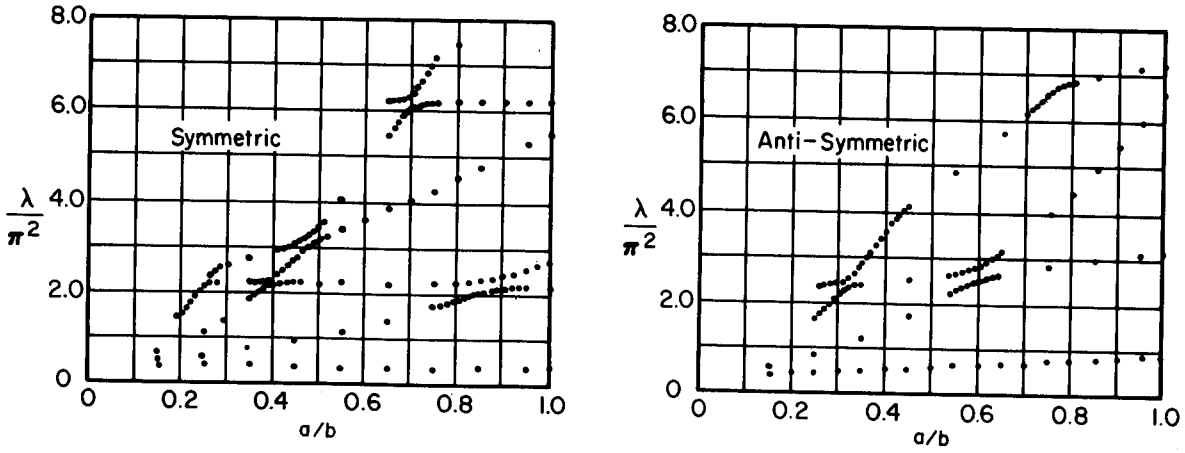


FIGURE 4.43.—Frequency parameter $\lambda/\pi^2=\omega a^2\sqrt{\rho/D}\,(\pi^2)$ for a rectangular cantilever plate; $\nu=0.3$. (After ref. 4.77)

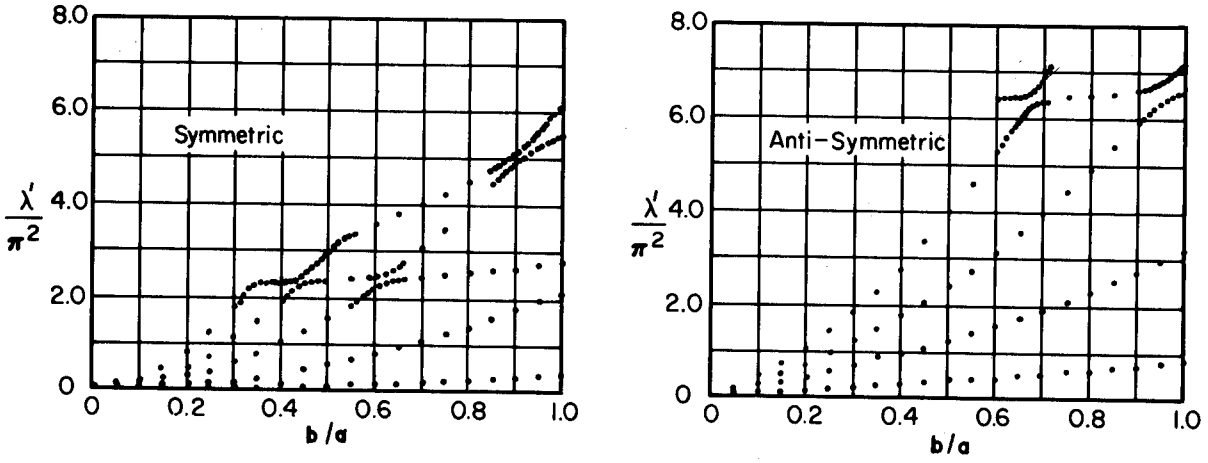


FIGURE 4.44.—Frequency parameter $\lambda'/\pi^2=\omega b^2\sqrt{\rho/D}\,(\pi^2)$ for a rectangular cantilever plate; $\nu=0.3$. (After ref. 4.77)

TABLE 4.51.—*Frequency Parameters* $\lambda=\omega a^2\sqrt{\rho/D}$ *and* $\lambda^*=\omega b^2\sqrt{\rho/D}$ *for Symmetric Modes of a Rectangular Cantilever Plate;* $\nu=0.3$

Aspect ratio	λ and λ* for mode—				
	1	2	3	4	5
a/b	λ				
1.00	3.472	21.29	27.2	54.3	61.3
0.95	3.474	21.13	25.3	51.8	61.2
0.90	3.476	20.74	23.7	49.2	61.2
0.85	3.477	19.85	22.7	46.9	61.1
0.80	3.479	18.49	22.2	44.5	61.1
0.75	3.481	16.98	22.1	42.1	61.0
0.70	3.484	15.48	22.0	40.0	60.3
0.65	3.486	14.06	21.9	37.9	54.0
0.60	3.488	12.68	21.9	35.7	46.7
0.55	3.491	11.41	21.9	33.7	40.1
0.50	3.493	10.22	21.9	31.5	34.1
0.45	3.496	9.13	21.8	27.6	30.7
0.40	3.498	8.11	21.5	22.0	28.8
0.35	3.501	7.18	18.3	21.9	27.2
0.30	3.503	6.32	14.52	21.4	25.8
0.25	3.506	5.57	11.31	15.3	-----
0.20	3.508	4.85	8.65	-----	-----
0.15	3.511	4.28	6.5	-----	-----
0.10	-----	-----	-----	-----	-----
0.05	-----	-----	-----	-----	-----
0.00	3.5160	-----	-----	-----	-----
b/a	λ*				
1.00	3.472	21.29	27.2	54.3	61.3
0.95	3.132	19.30	26.6	51.5	55.5
0.90	2.809	17.36	26.1	48.3	50.4
0.85	2.504	15.51	25.6	43.8	47.0
0.80	2.217	13.75	25.2	39.0	44.3
0.75	1.946	12.09	24.7	34.3	41.8
0.70	1.694	10.53	24.2	30.0	39.6
0.65	1.459	9.08	23.5	26.3	37.3
0.60	1.242	7.73	21.4	24.3	35.2
0.55	1.042	6.49	18.2	23.7	33.2
0.50	.861	5.37	15.03	23.3	29.6
0.45	.696	4.34	12.18	22.7	24.5
0.40	.549	3.42	9.61	18.9	23.0
0.35	.419	2.63	7.35	14.47	22.5
0.30	.307	1.92	5.39	10.63	17.6
0.25	.213	1.33	3.73	7.36	12.20
0.20	.135	.85	2.39	4.70	7.79
0.15	.076	.47	1.34	2.64	4.36
0.10	.034	.21	.59	1.16	1.92
0.05	.008	.05	.15	.29	.47
0.00	.000	.00	.00	.00	.00

TABLE 4.52.—*Frequency Parameters* $\lambda=\omega a^2\sqrt{\rho/D}$ *and* $\lambda^*=\omega b^2\sqrt{\rho/D}$ *for Antisymmetric Modes of a Rectangular Cantilever Plate;* $\nu=0.3$

Aspect ratio	λ and λ* for mode—			
	1	2	3	4
a/b	λ			
1.00	8.55	31.1	64.2	71.1
0.95	8.23	30.3	58.6	69.8
0.90	7.92	29.5	53.2	68.7
0.85	7.60	28.7	48.0	67.7
0.80	7.27	28.0	43.0	66.6
0.75	6.96	27.2	38.5	64.1
0.70	6.63	26.5	34.1	59.8
0.65	6.32	25.7	30.3	55.4
0.60	6.00	24.4	27.2	51.1
0.55	5.68	22.0	25.6	47.1
0.50	5.38	19.0	24.8	43.2
0.45	5.07	16.4	24.1	39.6
0.40	4.79	13.8	23.6	34.6
0.35	4.51	11.5	23.1	27.7
0.30	4.26	9.62	21.0	23.2
0.25	4.04	7.91	15.8	-----
0.20	3.85	6.42	11.58	-----
0.15	3.70	5.20	-----	-----
0.10	3.64	-----	-----	-----
0.05	-----	-----	-----	-----
0	-----	-----	-----	-----
b/a	λ*			
1.00	8.55	31.1	64.2	71.1
0.95	8.01	28.8	62.3	66.6
0.90	7.49	26.6	57.9	64.8
0.85	6.98	24.6	52.8	64.2
0.80	6.47	22.5	47.9	63.7
0.75	5.99	20.6	43.0	63.2
0.70	5.51	18.8	38.6	62.5
0.65	5.04	17.0	34.3	58.7
0.60	4.59	15.3	30.4	51.7
0.55	4.15	13.7	26.6	44.7
0.50	3.71	12.1	23.2	38.3
0.45	3.29	10.7	19.9	32.5
0.40	2.87	9.21	17.0	27.0
0.35	2.48	7.86	14.2	22.3
0.30	2.09	6.56	11.7	18.0
0.25	1.72	5.34	9.36	14.05
0.20	1.35	4.16	7.19	10.60
0.15	.997	3.06	5.20	7.52
0.10	.66	1.99	3.36	4.78
0.05	.33	.98	1.64	2.30
0.00	.00	.00	.00	.00

TABLE 4.53.—*Theoretical and Experimental Frequencies (cps) for a Mild Steel Cantilever Plate; a=5.12 inches, b=2.76 inches, and h=0.053 inch*

n	Type	Frequency, cps, for values of m of—					
		0	1	2	3	4	5
0	Theoretical	69. 5	436	1, 220	2, 390	3, 940	5, 900
	Experimental	64	405	1, 120	2, 233	3, 736	5, 573
	Percent difference	8. 6	7. 7	8. 9	7. 0	5. 5	5. 9
1	Theoretical	276	905	1, 743	2, 970	4, 530	----------
	Experimental	260	----------	1, 676	2, 804	4, 335	----------
	Percent difference	6. 2	----------	4. 0	5. 9	4. 5	----------
2	Theoretical	1, 610	2, 260	3, 280	4, 660	6, 350	8, 350
	Experimental	1, 606	----------	3, 160	4, 428	6, 009	7, 859
	Percent difference	0. 2	----------	3. 8	5. 3	5. 7	5. 9
3	Theoretical	4, 250	4, 810	5, 950	7, 450	9, 200	11, 280
	Experimental	4, 235	4, 773	5, 739	7, 069	----------	----------
	Percent difference	0. 4	0. 8	3. 7	5. 4	----------	----------
4	Theoretical	8, 260	8, 870	9, 750	10, 620	13, 150	15, 300
	Experimental	8, 238	8, 685	9, 651	----------	----------	----------
	Percent difference	0. 3	2. 1	1. 0	----------	----------	----------

TABLE 4.54.—*Theoretical and Experimental Cyclic Frequencies for a Rectangular Cantilever Steel Plate Having* a/b=*2.13*

m	Type	Frequency, cps, for values of n of—		
		1	2	3
1	Theoretical	37. 7	169. 8	1166
	Experimental	35. 6	162	1115
2	Theoretical	236. 3	542. 9	1563
	Experimental	219	529	1451
3	Theoretical	662. 3	1030. 5	2149
	Experimental	618	996	1996
4	Theoretical	1298	--------	--------
	Experimental	1216	--------	--------

TABLE 4.55.—*Experimentally Determined Frequency Parameters* $\omega a^2\sqrt{\rho/D}$ *for a Rectangular Cantilever Aluminum Plate*

a/b	$\omega a^2\sqrt{\rho/D}$ for mode—				
	1	2	3	4	5
½	3. 34	5. 38	10. 31	-------	------
1	3. 37	8. 26	20. 55	27. 15	29. 75
2	3. 36	14. 43	20. 86	-------	------
5	3. 32	20. 84	32. 40	-------	------

aluminum plates as listed in table 4.55. The foregoing results are also shown as circles in figure 4.42. Photographs showing nodal lines formed by the soap powder used in the experiment are shown for a square plate in figure 4.45.

Heiba (ref. 4.83) tested a series of ⅛-inch-thick mild steel plates of width $b=10$ inches and $a/b=1.0$, 0.8, 0.6, and 0.4, and obtained the frequencies and nodal patterns shown in figure 4.46.

Plunkett and Wilson (refs. 4.84 and 4.85) measured the frequencies of steel plates with $a=5.00$ inches, $h=0.100$ inch, and $a/b=2.00$, 2.50, 3.33, and 5.00. Results are listed in table 4.56. The significance of m and n is the same as it is in table 4.53.

Craig, Plass, and Caughfield (ref. 4.86) experimentally obtained the first four frequencies and mode shapes of a 6061–T6 aluminum cantilever plate 7.5 inches by 7.5 inches by 0.125 inch. Frequencies and corresponding frequency parameters are listed in table 4.57. Mode shapes are also given in reference 4.86 but are inaccurate, apparently because of the influence of the shaker position. Neverthe-

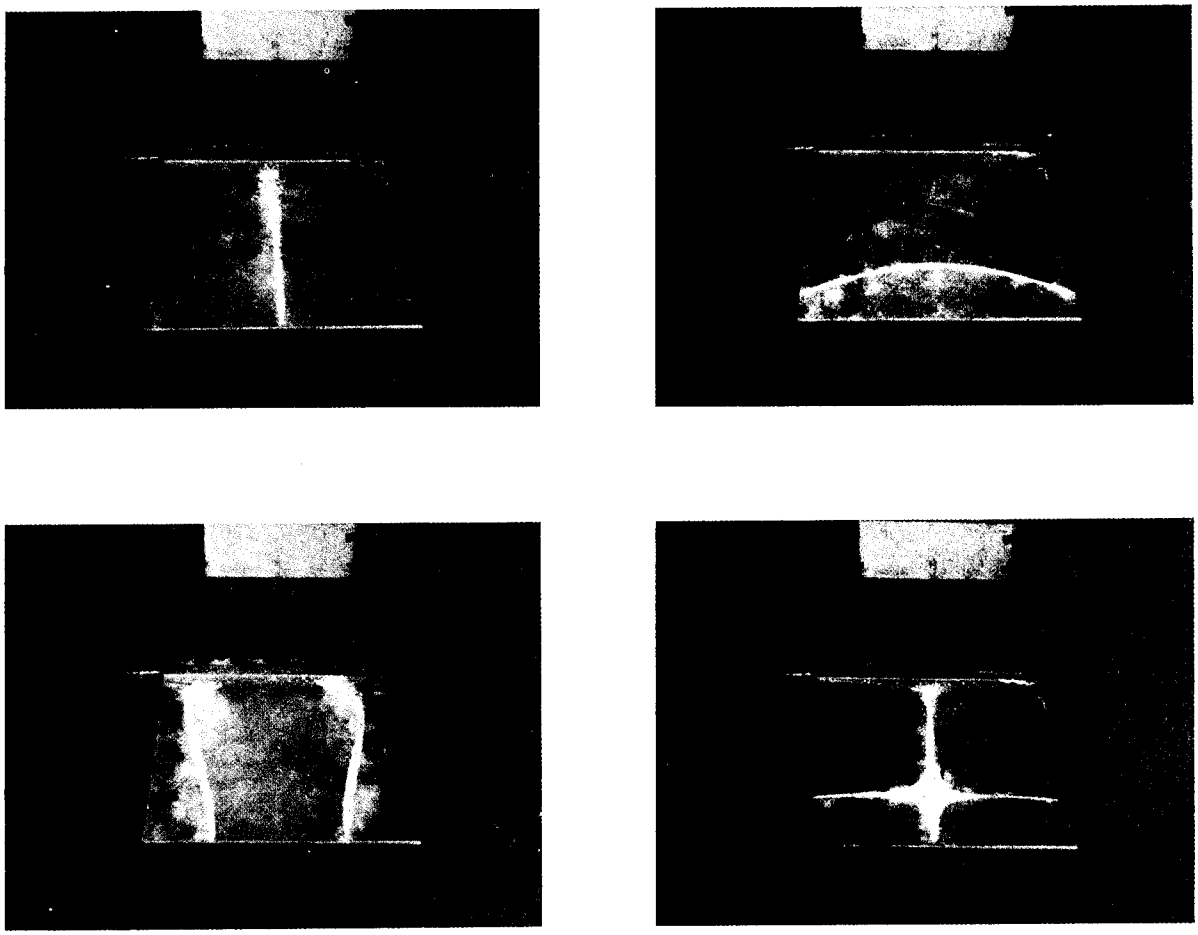


FIGURE 4.45.—Photographs of nodal patterns on a square cantilever plate. (From ref. 4.81)

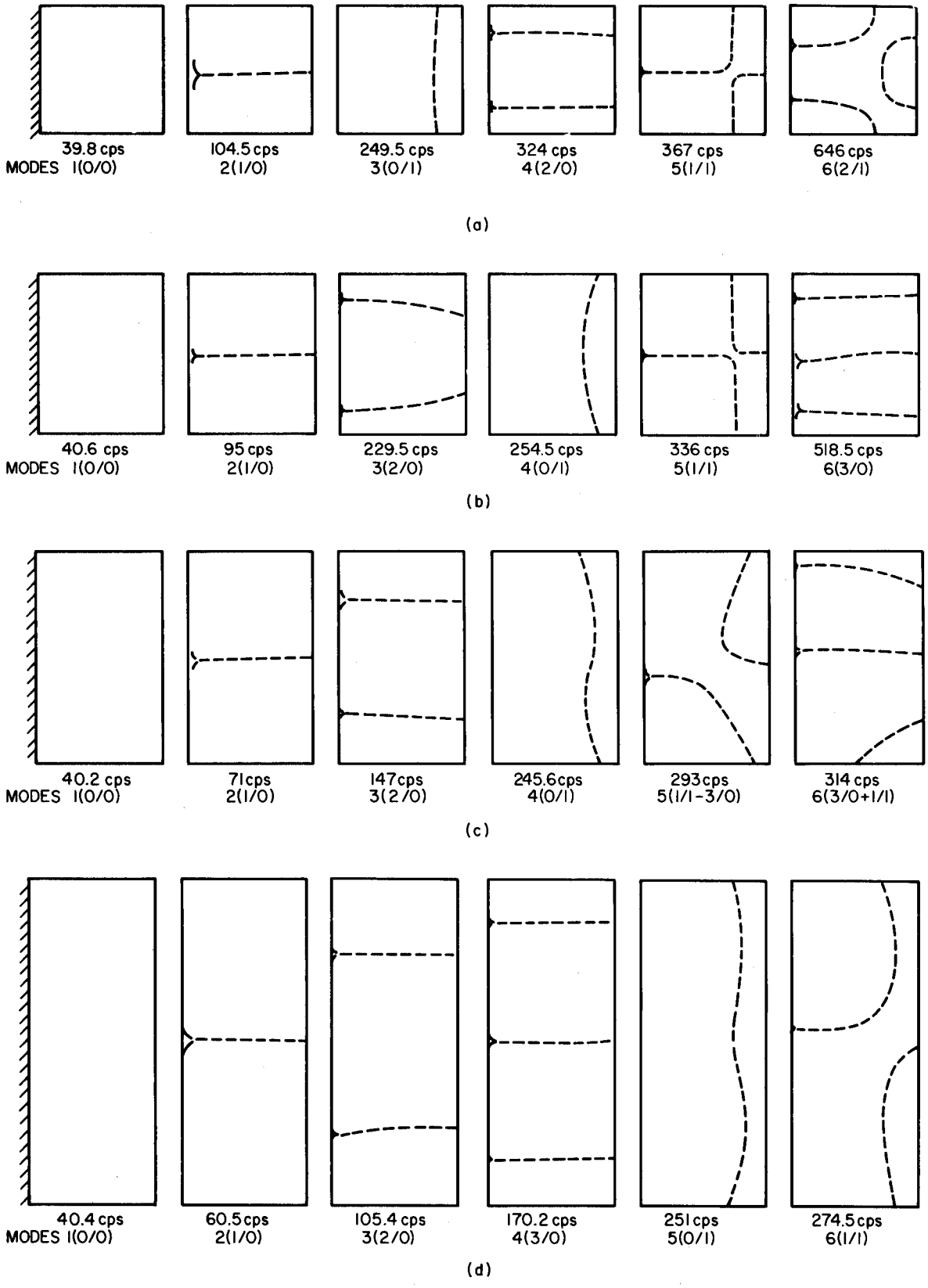


FIGURE 4.46.—Experimentally determined cyclic frequencies and nodal patterns for rectangular cantilever plates. (*a*) $a/b=1.0$. (*b*) $a/b=0.8$. (*c*) $a/b=0.6$. (*d*) $a/b=0.4$.

TABLE 4.56—*Experimental Values of* $\omega a^2\sqrt{\rho/D}$ *for a Rectangular Cantilever Steel Plate*

n/m	$\omega a^2\sqrt{\rho/D}$ for values of a/b of—			
	2.00	2.50	3.33	5.00
0/0	3. 50	3. 50	3. 50	3. 45
0/1	21. 7	21. 6	21. 5	21. 1
0/2	60. 5	60. 4	59. 8	59. 3
0/3	118. 7	117. 5	116. 5	115. 2
0/4	196. 0		195. 0	190. 0
0/5	292. 0			281. 0
1/0	14. 5	17. 3	22. 5	32. 0
1/1	48. 1	54. 8	69. 6	98. 0
1/2	92. 3	101. 5	125. 0	169. 0
1/3	154. 0		187. 0	248. 0
1/4	228. 0			
1/5	319–324			
2/0	92. 8	139. 1	246. 0	
2/1	125. 1			
2/2	176. 0			
2/3	244. 0			
3/0	246. 0			
3/1	274. 0			
3/2	319–324			

less, figure 4.47 showing the nodal lines is reproduced, partly as an estimate of accuracy for further results on parallelogram and triangular plates.

Gustafson, Stokey, and Zorowski (ref. 4.87) experimentally determined the first five frequencies of a square steel plate having dimensions 10 inches by 10 inches by 0.0627 inch and the following material properties:

Modulus of elasticity in x-direction: 29.3×10^6 psi

Modulus of elasticity in y-direction: 31.5×10^6 psi

Weight density: 0.282 16/in.^{3}

Poisson's ratio (assumed): 0.29

Frequency parameters $\omega a^2\sqrt{\rho/D}$ are listed in table 4.58. The arithmetic mean of the two moduli given above was used as E in the flexural rigidity D.

Grinsted (ref. 4.79) obtained considerable experimental data. Frequencies and nodal patterns

TABLE 4.57.—*Experimentally Determined Frequency Parameters and Cyclic Frequencies for a C–F–F–F Square Plate*

Mode	1	2	3	4
Frequency, cps	71. 9	175	437	552
$\omega a^2\sqrt{\rho/D}$	3. 34	8. 23	20. 56	25. 97

TABLE 4.58.—*Experimentally Determined Frequency Parameters for a Square Cantilever Plate*

Mode	1	2	3	4	5
$\omega a^2\sqrt{\rho/D}$	3. 35	8. 53	20. 90	26. 72	30. 61

for a mild steel plate having $a/b=1.86$ are shown in figure 4.48.

Walton (ref. 4.88) used the method developed by Houbolt (ref. 4.89) to determine the first five frequencies for the cantilevered square. This method is a numerical development of the Rayleigh-Ritz method in which derivatives are replaced by finite differences and area integrals are replaced by double summations. In table 4.59 are given the first five cyclic frequencies for an aluminum-alloy plate as determined: (1) Experimentally, (2) by the method of reference 4.89, using 30 internal grid points in the finite-difference mesh, and (3) by using Warburton's formula (eq. (4.16)). No plate dimensions are given in reference 4.88.

TABLE 4.59.—*Theoretical and Experimental Cyclic Frequencies for a Square Aluminum-Alloy Cantilever Plate;* $\nu=0.28$

Mode	Frequency, cps		
	Experimental	Method of ref. 4.89	Eq. (4.16)
1	23	21	21
2	48	50	56
3	118	121	132
4	162	163	171
5	173	177	190

For a comparison of frequencies of a rectangular cantilever plate in air, water, or vacuum, see the chapter entitled "Other Considerations" (ch. 12).

The problem was also discussed in references 4.90 to 4.94.

4.3.13 SS-SS-F-F

The only specific result directly available for the problem of the SS–SS–F–F plate (fig. 4.49) is the approximate formula, equation (4.16). For more information on this problem, see the discussion of the doubly antisymmetric modes of a completely free rectangular plate (sec. 4.3.15). Straight node lines of antisymmetry duplicate SS boundary conditions.

4.3.14 SS-F-F-F

The only specific result directly available for the problem of the SS–F–F–F plate (fig. 4.50) is the approximate formula, equation (4.16).

4.3.15 F-F-F-F

The problem of the completely free plate (fig. 4.51) has a rich history. The first significant work examining nodal patterns on rectangular plates of any kind was produced by Chladni in 1787 (ref. 4.95) for completely free boundaries and extended in references 4.96 to 4.98. Other early experimental work on this problem was performed by Strehlke (refs. 4.99 to 4.103), König (ref. 4.104), and Tanaka (ref. 4.105). Wheatstone (ref. 4.106) in 1833 made an attempt to explain the Chladni patterns in terms of the modes of F–F beams, and these geometrical studies were extended by Rayleigh (ref. 4.107).

Ritz (ref. 4.108) in 1909 used the problem to demonstrate his famous method for extending the Rayleigh principle for obtaining upper bounds on vibration frequencies. This innovation resulted in several following papers (e.g., refs. 4.109 to 4.112) which used the method to solve the problem in great detail.

Lemke (ref. 4.110) computed frequencies and mode shapes for the six modes of a square. Functions of the type

$$W(\bar{x},\bar{y})=\sum A_{mn}X_m(\bar{x})Y_n(\bar{y}) \qquad (4.57)$$

were used, where $X_m(\bar{x})$ and $Y_m(\bar{y})$ are the F–F beam functions expressed in terms of a normalized (i.e., $x=x/a$, where $a=1$) xy coordinate system having the origin at the plate center (fig. 4.51); that is,

$$\left.\begin{aligned} X_m(\bar{x})&=\frac{\cosh k_m\cos k_m\bar{x}+\cos k_m\cosh k_m\bar{x}}{\sqrt{\cosh^2 k_m+\cos^2 k_m}} \qquad (m \text{ even})\\ X_m(\bar{x})&=\frac{\sinh k_m\sin k_m\bar{x}+\sin k_m\sinh k_m\bar{x}}{\sqrt{\sinh^2 k_m-\sin^2 k_m}} \qquad (m \text{ odd}) \end{aligned}\right\} \qquad (4.58)$$

The function $Y_n(\bar{y})$ is obtained from equations (4.58) by replacing $\bar{x}$ by $\bar{y}$ and m by n. The values k_m are the roots of the equations

$$\left.\begin{aligned} \tan k_m+\tanh k_m&=0 \qquad (m \text{ even})\\ \tan k_m-\tanh k_m&=0 \qquad (m \text{ odd}) \end{aligned}\right\} \qquad (4.59)$$

and are listed in table 4.60.

Results were obtained in reference 4.110 by using six or more terms of equation (4.57) and four different values of Poisson's ratio. These data are given in table 4.61.

Ritz (ref. 4.108) himself computed many more frequencies for the square. Table 4.62 lists frequency parameters, nodal patterns, and the approximate mode shapes used, again in terms of equations (4.57) and (4.58). All the nodal patterns in table 4.62 are either doubly symmetric or doubly antisymmetric about the bisectors of the square $\bar{x}=0$, $\bar{y}=0$.

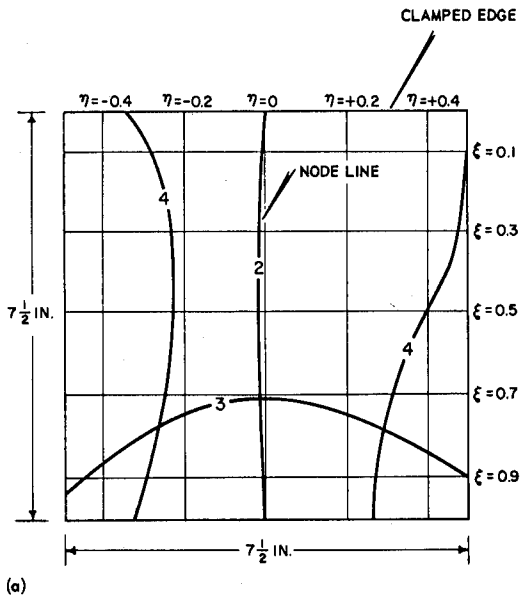
Frequencies and mode shapes are computed for $\nu=0.225$, using the number of terms listed for $W(\bar{x},\bar{y})$. Small variations in ν from the

TABLE 4.60.—*Eigenvalues of a F–F Beam*

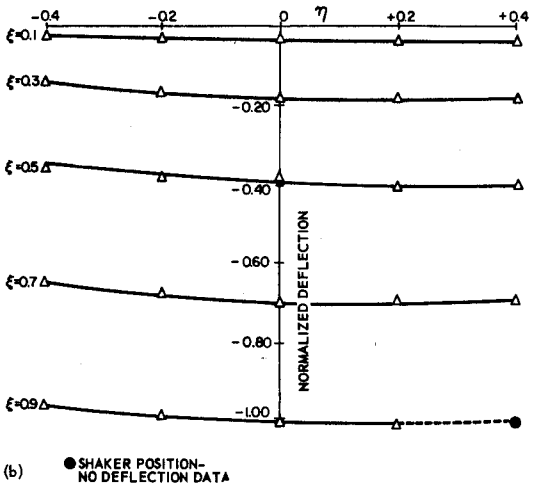
m	k_m	m	k_m
0	0	1	0
2	2. 36502	3	3. 92660
4	5. 49780	5	7. 06858
6	8. 63938	7	10. 21017
8	11. 78096	9	13. 35175
10	14. 92255	m	$(2m-1)\pi/4$
m	$(2m-1)\pi/4$		

value of 0.225 can be taken into account by the terms $\delta\nu$, where given. It must be remembered that these are upper bounds on the exact frequencies and that the higher frequencies and mode shapes may be quite inaccurate. In reference 4.108 frequencies and mode shapes are also listed for modes symmetric about one axis and antisymmetric about the other. Some interesting superpositions of these modes are also presented. These are given in table 4.63.

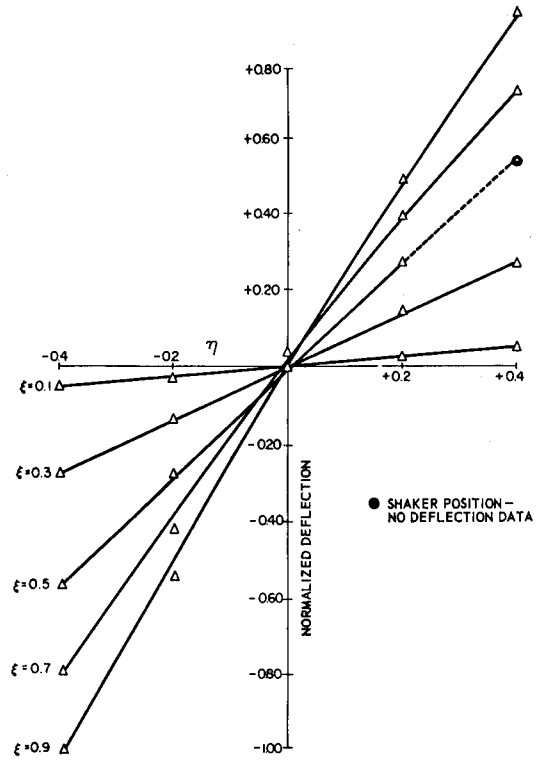
Ödman (ref. 4.13) used a variation of the Galerkin method to obtain extensive results for this problem. Unfortunately, his results for the cases when nodal lines lie in only one



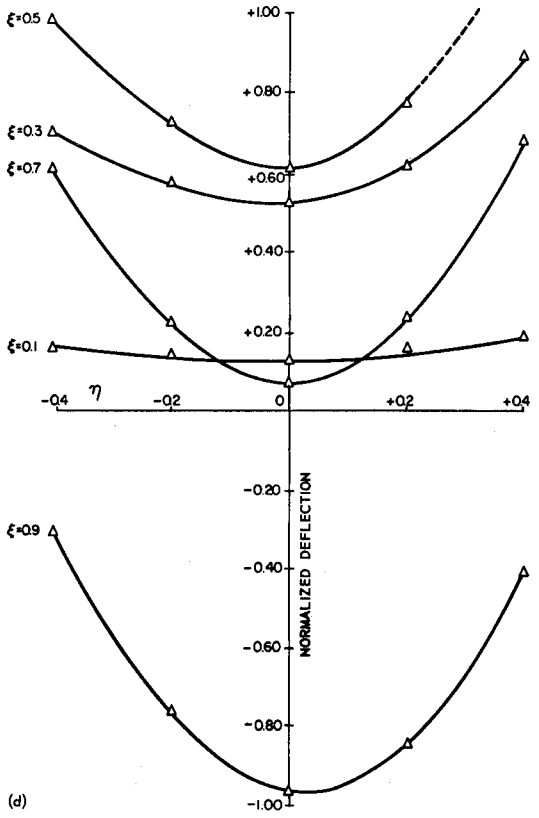
(a)



(b)



(c)



(d)

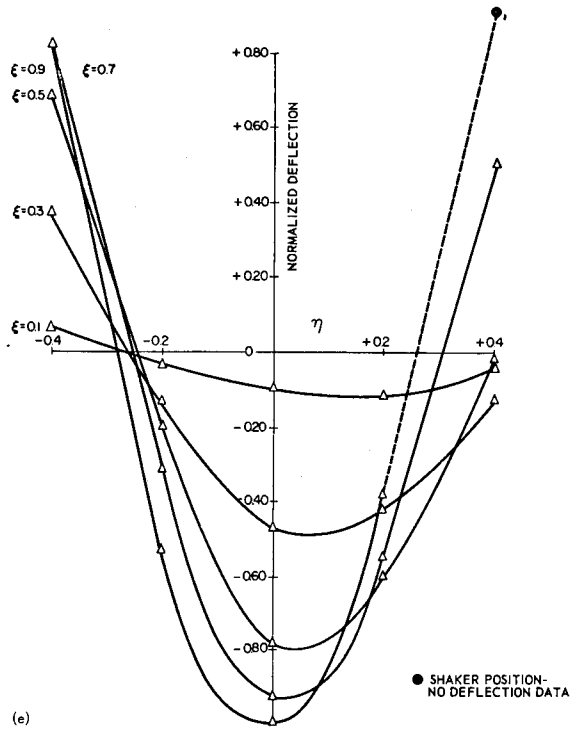


FIGURE 4.47.—Experimentally determined nodal patterns for the first four modes of a C–F–F–F square plate; material, 6061–T6 aluminum ⅛-inch thick. (*a*) Experimental node lines and data points. (*b*) Mode 1; $f_1=71.9$ cps. (*c*) Mode 2; $f_2=175$ cps. (*d*) Mode 3; $f_3=437$ cps. (*e*) Mode 4; $f_4=552$ cps.

direction are those of a F–F beam and do not consider anticlastic bending effects. The numerical error in these frequencies is not large, however. Results for ω_{mn} (m, $n=0$, 1, . . ., 6) are given in table 4.64, where m and n denote the number of nodal lines approximately parallel to the y- and x-directions, respectively. The cases when $m=0$ or $n=0$ are then the beam modes just described. Values in parentheses were obtained by interpolation. Poisson's ratio is 1/6.

Iguchi (ref. 4.113) used the series method to solve the problem. He formulated the problem for the general rectangle with solutions to equation (1.4) in the form

$$W(\bar{x},\bar{y})=\sum_{n=0}^{\infty}X_n\cos n\pi\left[\left(\frac{1}{2}\right)+\eta\right]+\sum_{m=0}^{\infty}Y_m\cos m\pi\left[\left(\frac{1}{2}\right)+\xi\right] \quad (4.60)$$

in terms of figure 4.51, where $\xi=\bar{x}/a$, $\eta=\bar{y}/b$, and

$$\left.\begin{aligned}X_n&=A_n\frac{\cosh\pi\lambda_{\alpha n}\xi}{\sinh\frac{\pi}{2}\lambda_{\alpha n}}+A_n^*\frac{\cosh\pi\lambda_{\alpha n}^*\xi}{\sinh\frac{\pi}{2}\lambda_{\alpha n}^*}\\&\quad+A_n^{**}\frac{\sinh\pi\lambda_{\alpha n}\xi}{\cosh\frac{\pi}{2}\lambda_{\alpha n}}+A_n^{***}\frac{\sinh\pi\lambda_{\alpha n}^*\xi}{\cosh\frac{\pi}{2}\lambda_{\alpha n}^*}\\Y_m&=B_m\frac{\cosh\pi\lambda_{\beta m}\eta}{\sinh\frac{\pi}{2}\lambda_{\beta m}}+B_m^*\frac{\cosh\pi\lambda_{\beta m}^*\eta}{\sinh\frac{\pi}{2}\lambda_{\beta m}^*}\\&\quad+B_m^{**}\frac{\sinh\pi\lambda_{\beta m}\eta}{\cosh\frac{\pi}{2}\lambda_{\beta m}}+B_m^{***}\frac{\sinh\pi\lambda_{\beta m}^*\eta}{\cosh\frac{\pi}{2}\lambda_{\beta m}^*}\end{aligned}\right\} \quad (4.61)$$

with

$$\left.\begin{aligned}\lambda_{\alpha n},\lambda_{\alpha n}^*&=\sqrt{\alpha^2n^2\pm\mu}\qquad\left(\mu=\frac{\omega a^2}{\pi^2}\sqrt{\frac{\rho}{D}},\ \alpha=\frac{a}{b}\right)\\\lambda_{\beta m},\lambda_{\beta m}^*&=\sqrt{\beta^2m^2\pm\mu^*}\qquad\left(\mu^*=\frac{\omega b^2}{\pi^2}\sqrt{\frac{\rho}{D}},\ \beta=\frac{b}{a}\right)\end{aligned}\right\} \quad (4.62)$$

The boundary conditions are

$$\frac{\partial^2W}{\partial\bar{x}^2}+\nu\frac{\partial^2W}{\partial\bar{y}^2}=0 \qquad \left(\text{on }\bar{x}=\pm\frac{a}{2}\right) \quad (4.63(a))$$

$$\frac{\partial^2W}{\partial\bar{y}^2}+\nu\frac{\partial^2W}{\partial\bar{x}^2}=0 \qquad \left(\text{on }\bar{y}=\pm\frac{b}{2}\right) \quad (4.63(b))$$

$$\frac{\partial}{\partial\bar{x}}\left[\frac{\partial^2W}{\partial\bar{x}^2}+(2-\nu)\frac{\partial^2W}{\partial\bar{y}^2}\right]=0 \qquad \left(\text{on }\bar{x}=\pm\frac{a}{2}\right) \quad (4.63(c))$$

$$\frac{\partial}{\partial\bar{y}}\left[\frac{\partial^2W}{\partial\bar{y}^2}+(2-\nu)\frac{\partial^2W}{\partial\bar{x}^2}\right]=0 \qquad \left(\text{on }\bar{y}=\pm\frac{b}{2}\right) \quad (4.63(d))$$

$$\frac{\partial^2W}{\partial\bar{x}\partial\bar{y}}=0 \quad \text{(at the corners)} \quad (4.63(e))$$

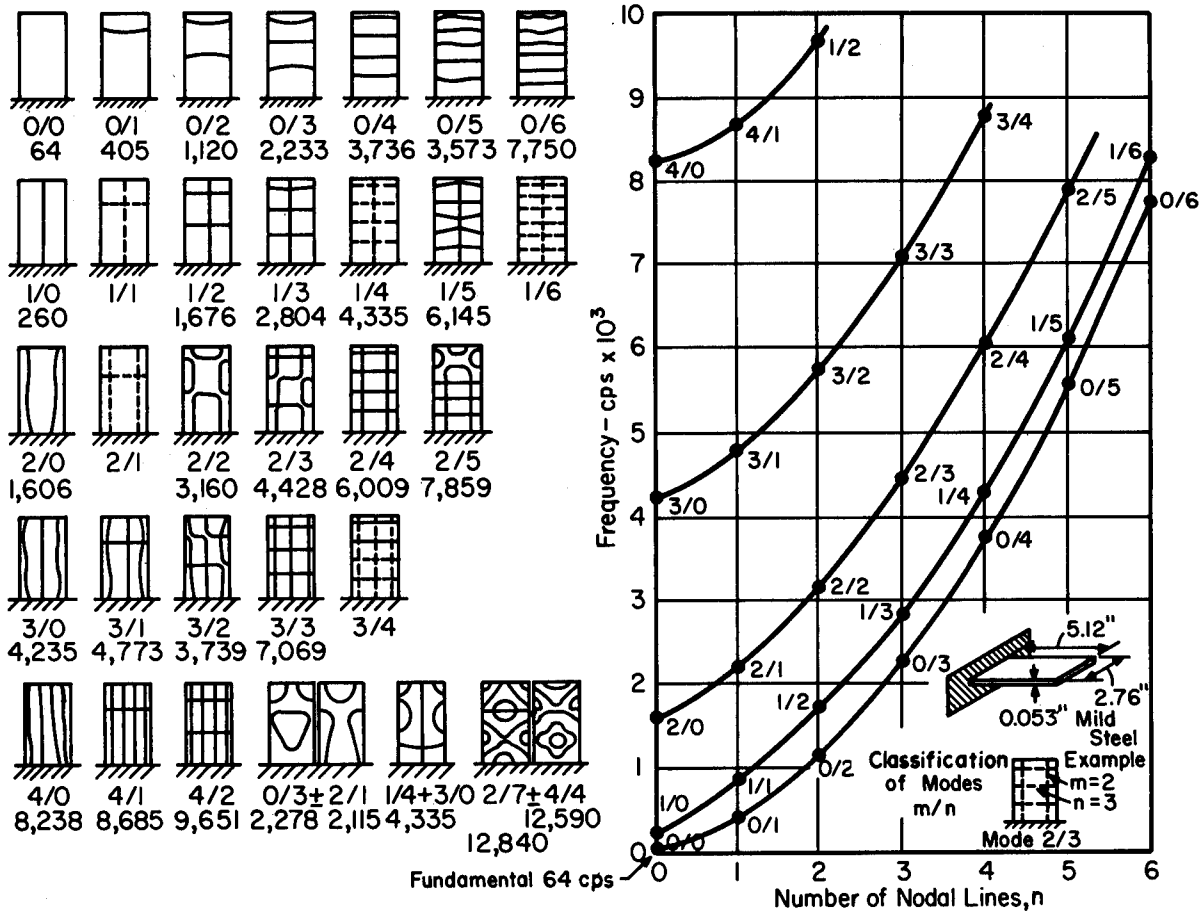


FIGURE 4.48.—Experimental frequencies and nodal patterns for a rectangular cantilever plate; $a/b=1.86$. (After ref. 4.79)

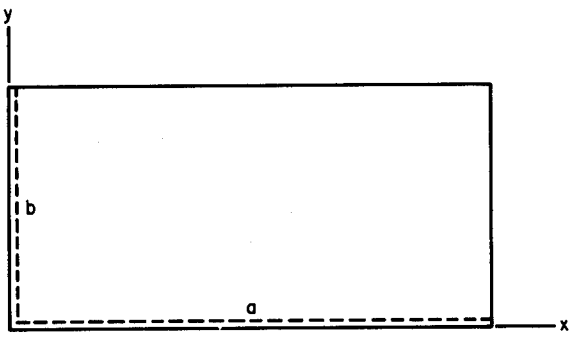


FIGURE 4.49.—SS–SS–F–F plate.

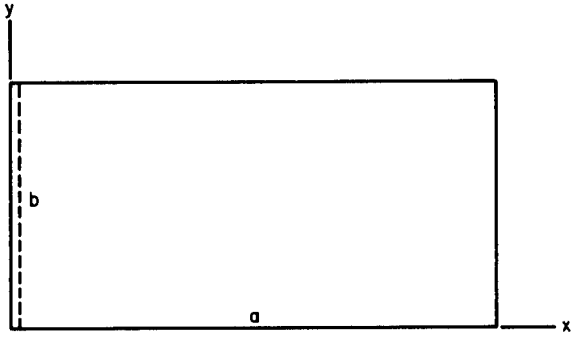


FIGURE 4.50.—SS–F–F–F plate.

The last of these is identically satisfied by equation (4.60). Applying equations (4.63(c)) and (4.63(d)) gives

$$
\left.
\begin{aligned}
&X_n = a_n u_{\alpha n}(\xi) + a_n^* v_{\alpha n}(\xi) \\
&Y_m = b_m u_{\beta m}(\eta) + b_m^* v_{\beta m}(\eta) \\
&u_{\alpha n}(\xi) = \frac{1}{\lambda_{\alpha n}}(\lambda_{\alpha n}^2 - \nu\alpha^2 n^2)\frac{\cosh \pi\lambda_{\alpha n}\xi}{\sinh \frac{\pi}{2}\lambda_{\alpha n}} \\
&\qquad\qquad - \frac{1}{\lambda_{\alpha n}^*}(\lambda_{\alpha n}^{*2} - \nu\alpha^2 n^2)\frac{\cosh \pi\lambda_{\alpha n}^*\xi}{\sinh \frac{\pi}{2}\lambda_{\alpha n}^*} \\
&v_{\alpha n}(\xi) = \frac{1}{\lambda_{\alpha n}}(\lambda_{\alpha n}^2 - \nu\alpha^2 n^2)\frac{\sinh \pi\lambda_{\alpha n}\xi}{\cosh \frac{\pi}{2}\lambda_{\alpha n}} \\
&\qquad\qquad - \frac{1}{\lambda_{\alpha n}^*}(\lambda_{\alpha n}^{*2} - \nu\alpha^2 n^2)\frac{\sinh \pi\lambda_{\alpha n}^*\xi}{\cosh \frac{\pi}{2}\lambda_{\alpha n}^*} \\
&u_{\beta m}(\eta) = \frac{1}{\lambda_{\beta m}}(\lambda_{\beta m}^2 - \nu\beta^2 m^2)\frac{\cosh \pi\lambda_{\beta m}\eta}{\sinh \frac{\pi}{2}\lambda_{\beta m}} \\
&\qquad\qquad - \frac{1}{\lambda_{\beta m}^*}(\lambda_{\beta m}^{*2} - \nu\beta^2 m^2)\frac{\cosh \pi\lambda_{\beta m}^*\eta}{\sinh \frac{\pi}{2}\lambda_{\beta m}^*} \\
&v_{\beta m}(\eta) = \frac{1}{\lambda_{\beta m}}(\lambda_{\beta m}^2 - \nu\beta^2 m^2)\frac{\sinh \pi\lambda_{\beta m}\eta}{\cosh \frac{\pi}{2}\lambda_{\beta m}} \\
&\qquad\qquad - \frac{1}{\lambda_{\beta m}^*}(\lambda_{\beta m}^{*2} - \nu\beta^2 m^2)\frac{\sinh \pi\lambda_{\beta m}^*\eta}{\cosh \frac{\pi}{2}\lambda_{\beta m}^*} \\
&u_{\alpha 0}(\xi) = \sqrt{\mu}\left(\frac{\cosh \pi\sqrt{\mu}\xi}{\sinh \frac{\pi}{2}\sqrt{\mu}} - \frac{\cosh \pi\sqrt{\mu}\xi}{\sin \frac{\pi}{2}\sqrt{\mu}}\right) \\
&u_{\alpha 0}(\eta) = \sqrt{\mu^*}\left(\frac{\cosh \pi\sqrt{\mu^*}\eta}{\sinh \frac{\pi}{2}\sqrt{\mu^*}} - \frac{\cos \pi\sqrt{\mu^*}\eta}{\sin \frac{\pi}{2}\sqrt{\mu^*}}\right) \\
&v_{\beta 0}(\eta) = \sqrt{\mu^*}\left(\frac{\sinh \pi\sqrt{\mu^*}\eta}{\cosh \frac{\pi}{2}\sqrt{\mu^*}} + \frac{\sin \pi\sqrt{\mu^*}\eta}{\cos \frac{\pi}{2}\sqrt{\mu^*}}\right)
\end{aligned}
\right\} \tag{4.64}
$$

where a_n, a_n^*, b_m, and b_m^* are undetermined constants.

Applying equations (4.63(a)) and (4.63(b)) results in an infinite characteristic determinant

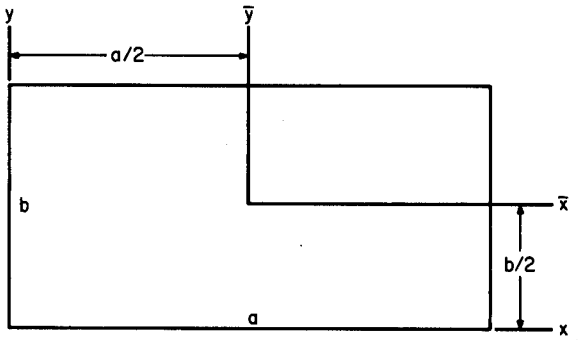


FIGURE 4.51.—F–F–F–F plate.

for the frequencies. When the determinant is truncated to a finite order of terms, the eigenvalues are found to converge rapidly with increasing order of determinant. Frequencies, nodal patterns, and numerical constants for mode shapes are given in table 4.65 (from ref. 4.113) for the case of the square having $\nu = 0.3$. For modes having symmetry about both coordinate axes and both diagonals, the mode shapes are

$$
\begin{aligned}
W(\bar{x}, \bar{y}) = {} & \alpha_0[u_0(\xi) + u_0(\eta)] \\
& + \sum_{n=2,4,\ldots} (-1)^{n/2}\alpha_n[u_n(\xi)\cos n\pi\eta \\
& \qquad + u_n(\eta)\cos n\pi\xi]
\end{aligned} \tag{4.65}
$$

For mode shapes symmetric about the coordinate axes and antisymmetric about the diagonals:

$$
\begin{aligned}
W(\bar{x}, \bar{y}) = {} & \alpha_0[u_0(\xi) - u_0(\eta)] \\
& + \sum_{n=2,4,\ldots} (-1)^{n/2}\alpha_n[u_n(\xi)\cos n\pi\eta \\
& \qquad - u_n(\eta)\cos n\pi\xi]
\end{aligned} \tag{4.66}
$$

For mode shapes antisymmetric about the coordinate axes and symmetric about the diagonals:

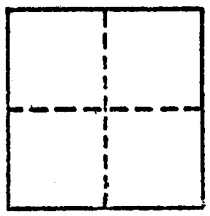
$$
\begin{aligned}
W(\bar{x}, \bar{y}) = {} & \sum_{n=1,3,\ldots} \alpha_n(-1)^{\frac{n-1}{2}}[v_n(\xi)\sin n\pi\eta \\
& \qquad + v_n(\eta)\sin n\pi\xi]
\end{aligned} \tag{4.67}
$$

For mode shapes antisymmetric about the coordinate axes and the diagonals:

$$
\begin{aligned}
W(\bar{x}, \bar{y}) = {} & \sum_{n=1,3,\ldots} \alpha_n(-1)^{\frac{n-1}{2}}[v_n(\xi)\sin n\pi\eta \\
& \qquad - v_n(\eta)\sin n\pi\xi]
\end{aligned} \tag{4.68}
$$

where u_n and v_n are given in equation (4.64) and α_n, λ_n, λ_n^*, and so forth are given in table 4.65.

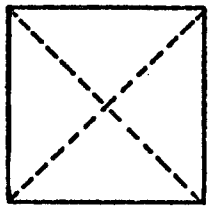
TABLE 4.61.—*6 Frequency Parameters and Mode Shapes for a Completely Free Square Plate*



(a) First mode: $W(\bar{x},\bar{y}) = A_{11}X_1Y_1 + A_{13}(X_1Y_3 + X_3Y_1) + A_{33}X_3Y_3 + A_{15}(X_1Y_5 + X_5Y_1) + A_3(X_3Y_5 + X_5Y_3) + A_{55}X_5Y_5 + \ldots$

ν	0.225	0.343		0.360		0.390
No. terms	6	6	15	6	15	15
$\omega a^2\sqrt{\rho/D}$	14.14	13.10	13.086	12.94	12.927	12.64
Amplitude coefficients:						
A_{11}	1. 0000	1. 0000	1. 0000	1. 0000	1. 0000	1. 0000
A_{13}	. 0378	. 0328	. 0325	. 0320	. 0318	. 0306
A_{33}	−. 00435	−. 00541	−. 0050	−. 00555	−. 00514	−. 00537
A_{15}	−. 0034	−. 00265	−. 00257	−. 00255	−. 00246	−. 002285
A_{35}	. 00118	. 00139	. 00121	. 00141	. 001235	. 001276
A_{55}	−. 00045	−. 000474	−. 000365	−. 00048	−. 000366	−. 000370
A_{17}			. 000413		. 000382	. 000328
A_{37}			−. 000431		−. 000440	−. 000456
A_{57}			. 000148		. 000149	. 000150
A_{77}			−. 0000703		−. 0000701	−. 000070
A_{19}			−. 0000767		−. 0000638	−. 0000413
A_{39}			. 000196		. 000201	. 0002086
A_{59}			. 0000720		−. 0000727	. 0000733
A_{79}			. 0000382		. 0000382	. 00003805
A_{99}			−. 000023		−. 0000230	−. 0000228

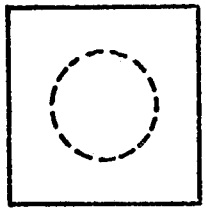
TABLE 4.61.—*6 Frequency Parameters and Mode Shapes for a Completely Free Square Plate*—Con.



(b) Second mode: $W(\bar{x}, \bar{y}) = A_{02}(X_0Y_2 - X_2Y_0) + A_{04}(X_0Y_4 - X_4Y_0)$
$+ A_{24}(X_2Y_4 - X_4Y_2) + A_{06}(X_0Y_6 - X_6Y_0) + A_{26}(X_2Y_6 - X_6Y_2) + \ldots$

ν	0.225	0.343		0.360		0.390
No. terms	3	4	11	4	11	11
$\omega a^2\sqrt{\rho/D}$	20. 49	19. 306	19. 231	19. 129	19. 045	18. 707
Amplitude coefficients:						
A_{02}	1. 0000	1. 0000	1. 0000	1. 0000	1. 0000	1. 0000
A_{04}	−. 131	−. 0204	−. 02042	−. 02142	−. 02146	−. 023312
A_{24}	−. 0043	−. 00643	−. 006105	−. 00675	−. 00642	−. 006976
A_{06}		. 00522	. 00518	. 00549	. 00545	. 005927
A_{26}			. 00207		. 00217	. 00235
A_{46}			. 000098		. 0001006	. 000105
A_{08}			−. 002042		−. 00215	−. 002337
A_{28}			−. 000929		−. 000975	−. 001054
A_{48}			−. 0000613		−. 0000631	−. 0000658
A_{68}			. 0000080		. 0000083	. 0000087
A_{010}			. 001008		. 00106	. 001154

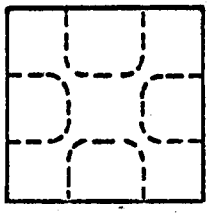
TABLE 4.61.—*6 Frequency Parameters and Mode Shapes for a Completely Free Square Plate*—Con.



(c) Third mode: $W(\bar{x}, \bar{y}) = A_{02}(X_0Y_2 + X_2Y_0) + A_{22}X_2Y_2 + A_{04}(X_0Y_4 + X_4Y_0) + A_{24}(X_2Y_4 + X_4Y_2) + A_{44}X_4Y_4 + \ldots$

ν	0.225	0.343		0.360		0.390
No. terms	5	6	15	6	15	15
$\omega a^2\sqrt{\rho/D}$	23.97	24.64	24.58	24.73	24.66	24.80
Amplitude coefficients:						
A_{02}	1. 0000	1. 0000	1. 0000	1. 0000	1. 0000	1. 0000
A_{22}	−. 0236	−. 0447	−. 0449	−. 0484	−. 0488	−. 0563
A_{04}	. 00132	. 02011	. 0202	. 02115	. 0213	. 02324
A_{24}	. 0022	. 00384	. 00363	. 00409	. 00385	. 00426
A_{44}	. 00166	. 00282	. 00252	. 00302	. 00271	. 00306
A_{06}		−. 00503	−. 00505	−. 00529	−. 00531	−. 00580
A_{26}			−. 00194		−. 00206	−. 00229
A_{08}			. 00199		. 00209	. 00228
A_{46}			−. 000822		−. 000884	−. 000994
A_{28}			. 000987		. 00105	. 001166
A_{010}			−. 000976		−. 00103	−. 001121
A_{66}			. 000293		. 000316	. 000353
A_{48}			. 000355		. 000382	. 0004303
A_{68}			−. 000138		−. 000146	−. 000163
A_{88}			. 000069		. 000073	. 000081

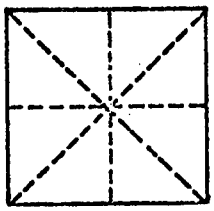
TABLE 4.61.—*6 Frequency Parameters and Mode Shapes for a Completely Free Square Plate*—Con.



(d) Fourth mode: $W(\bar{x}, \bar{y}) = A_{02}(X_0Y_2 + X_2Y_0) + A_{22}X_2Y_2 + A_{04}(X_0Y_4 + X_4Y_0) + A_{24}(X_2Y_4 + X_4Y_2) + A_{44}X_4Y_4 + \ldots$

ν	0.225	0.343		0.360		0.390
No. terms	5	6	15	6	15	15
$\omega a^2\sqrt{\rho/D}$	66.402	63.160	62.676	62.664	62.196	61.329
Amplitude coefficients:						
A_{02}	0. 0118	0. 02266	0. 0228	0. 0246	0. 0248	0. 02864
A_{22}	1. 0000	1. 0000	1. 0000	1. 0000	1. 0000	1. 0000
A_{04}	−. 020	−. 0288	−. 0275	−. 03005	−. 02875	−. 0310
A_{24}	. 0876	. 0730	. 0690	. 0709	. 06704	. 06350
A_{44}	−. 0047	−. 00951	−. 00674	−. 01015	−. 007355	−. 00841
A_{06}		. 00529	. 00540	. 00556	. 00568	. 00619
A_{26}			−. 00971		−. 00921	−. 00830
A_{46}			. 00314		. 00330	. 003574
A_{66}			−. 00148		−. 00151	−. 00158
A_{08}			−. 00211		−. 00222	−. 002425
A_{28}			. 00204		. 00183	. 00147
A_{48}			−. 00153		−. 00160	−. 00172
A_{68}			. 00076		. 000778	. 000808
A_{88}			−. 000435		−. 000441	−. 000452
A_{010}			. 001006		. 00106	. 00116

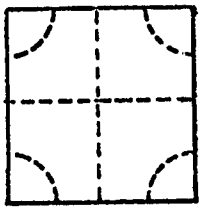
TABLE 4.61.—*6 Frequency Parameters and Mode Shapes for a Completely Free Square Plate*—Con.



(e) Fifth mode: $W(\bar{x}, \bar{y})=A_{13}(X_1Y_3-X_3Y_1)+A_{15}(X_1Y_5-X_5Y_1)$
$+A_{35}(X_3Y_5-X_5Y_3)+A_{17}(X_1Y_7-X_7Y_1)+\ldots$

ν	0.225	0.343		0.360		0.390
No. terms	3	3	10	3	10	10
$\omega a^2\sqrt{\rho/D}$	71.830	68.50	68.346	67.993	67.804	66.820
Amplitude coefficients:						
A_{13}	1. 0000	1. 0000	1. 0000	1. 0000	1. 0000	1. 0000
A_{15}	. 00024	—. 01394	—. 01423	—. 0160	—. 01634	—. 02008
A_{35}	. 00216	—. 005895	—. 00511	—. 00707	—. 00623	—. 008235
A_{17}	----------	----------	. 00643	----------	. 00709	. 00826
A_{37}	----------	----------	. 004255	----------	. 00470	. 005495
A_{57}	----------	----------	. 00031	----------	. 000315	. 000322
A_{19}	----------	----------	—. 00338	----------	—. 00367	—. 00419
A_{39}	----------	----------	—. 002713	----------	—. 002934	—. 00333
A_{59}	----------	----------	—. 000232	----------	—. 000236	—. 000241
A_{79}	----------	----------	. 000415	----------	. 0000421	. 000043

TABLE 4.61.—*6 Frequency Parameters and Mode Shapes for a Completely Free Square Plate*—Con.



(f) Sixth mode: $W(\bar{x}, \bar{y}) = A_{11}X_1Y_1 + A_{13}(X_1Y_3 + X_3Y_1) + A_{33}X_3Y_3 + A_{15}(X_1Y_5 + X_5Y_1) + A_{35}(X_3Y_5 + X_5Y_3) + \ldots$

ν	0.225	0.343		0.360		0.390
No. terms	6	6	15	6	15	15
$\omega a^2\sqrt{\rho/D}$	77.881	77.730	77.380	77.683	77.309	77.162
Amplitude coefficients:						
A_{11}	−0. 0746	−0. 06456	−0. 0641	−0. 0631	−0. 0627	−0. 06035
A_{13}	1. 0000	1. 0000	1. 0000	1. 0000	1. 0000	1. 0000
A_{33}	. 171	. 1295	. 1252	. 1227	. 1184	. 10562
A_{15}	. 0431	. 05066	. 0489	. 0518	. 0500	. 05194
A_{35}	−. 0084	−. 00480	−. 00347	−. 00419	−. 00285	−. 00172
A_{55}	. 00546	. 00814	. 00645	. 00856	. 00684	. 00755
A_{17}			−. 01286		−. 01321	−. 01384
A_{37}			−. 001936		−. 00229	−. 00295
A_{57}			−. 00290		−. 003052	−. 00334
A_{77}			. 00139		. 00146	. 001575
A_{19}			. 00515		. 00531	. 00560
A_{39}			. 00184		. 002046	. 00242
A_{59}			. 00150		. 00158	. 001724
A_{79}			−. 000766		−. 000798	−. 000858
A_{99}			. 000448		. 000466	. 000497

TABLE 4.62.—*Doubly Symmetric and Doubly Antisymmetric Frequencies and Mode Shapes for a Completely Free Square Plate; $\nu=0.225$*

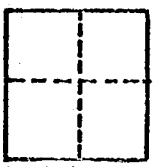
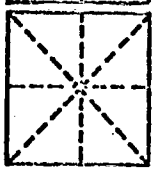
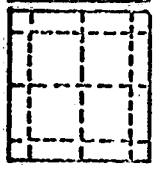
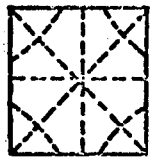
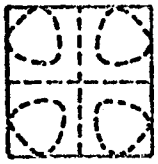
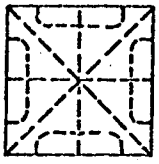
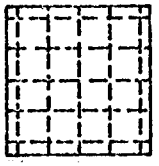
Nodal pattern	$\omega^2 a^4 \rho/16D$	$W(\bar{x}, \bar{y})$
Doubly antisymmetric modes		
	12. 43−18. 0 $\delta\nu$	$X_1Y_1+0.0394(X_1Y_3+X_3Y_1)-0.0040X_3Y_3-0.0034(X_1Y_5+X_5Y_1)$ $+0.0011(X_3Y_5+X_5Y_3)-0.0019X_5Y_5$
	316. 1−270 $\delta\nu$	$(X_1Y_3-X_3Y_1)+0.0002(X_1Y_5-X_5Y_1)+0.0033(X_3Y_5-X_5Y_3)$
	378−57 $\delta\nu$	$-0.075X_1Y_1+(X_1Y_3+X_3Y_1)+0.173X_3Y_3+0.045(X_1Y_5+X_5Y_1)$ $-0.015(X_3Y_5+X_5Y_3)-0.029X_5Y_5$
	1554	$0.009X_1Y_1-0.075(X_1Y_3+X_3Y_1)+X_3Y_3-0.057(X_1Y_5+X_5Y_1)$ $+0.121(X_3Y_5+X_5Y_3)-0.007X_5Y_5$
	2713	$X_1Y_5-X_5Y_1$
	2945	$X_1Y_5+X_5Y_1$
	5570	$X_3Y_5 \rightharpoonup X_5Y_3$
	6303	$X_3Y_5+X_5Y_3$
	13 674	X_5Y_5

TABLE 4.62.—*Doubly Symmetric and Doubly Antisymmetric Frequencies and Mode Shapes for a Completely Free Square Plate; $\nu=0.225$*—Continued

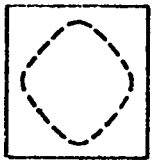
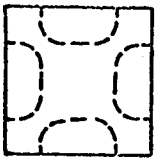
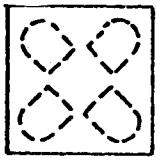
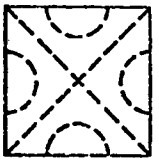
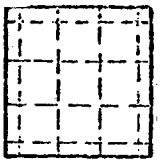
Nodal pattern	$\omega^2 a^4 \rho/16D$	$W(\bar{x}, \bar{y})$
	Doubly symmetric modes	
	26. 40	$(X_0Y_2-X_2Y_0)-0.0129(X_0Y_4-X_4Y_0)-0.0045(X_2Y_4-X_4Y_2)$
	35. 73+20. 8 $\delta\nu$	$(X_0Y_2-X_2Y_0)-0.0238X_2Y_2+0.0130(X_0Y_4+X_4Y_0)+0.0026$ $(X_2Y_4+X_4Y_2)+0.0016X_4Y_4$
	266. 0−274 $\delta\nu$	$0.0122(X_0Y_2+X_2Y_0)+X_2Y_2-0.0188(X_0Y_4+X_4Y_0)+0.0880$ $(X_2Y_4+X_4Y_2)-0.0044X_4Y_4$
	886	$X_0Y_4-X_4Y_0$
	941	$X_0Y_4+X_4Y_0$
	1702	$X_2Y_4+X_4Y_2$
	2020	$X_2Y_4+X_4Y_2$
	5480	X_4Y_4

TABLE 4.62.—*Doubly Symmetric and Doubly Antisymmetric Frequencies and Mode Shapes for a Completely Free Square Plate; $\nu=0.225$*—Continued

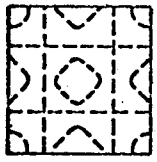
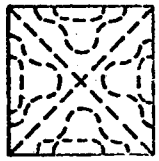
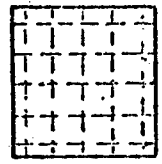
Nodal pattern	$\omega^2 a^4 \rho/16D$	$W(\bar{x}, \bar{y})$
Doubly symmetric modes—Continued		
	5500	$X_0Y_6-X_6Y_0$
	5640	$X_0Y_6+X_6Y_0$
	7310	$X_2Y_6-X_6Y_2$
	7840	$X_2Y_6+X_6Y_2$
	13 840	$X_4Y_6-X_6Y_4$
	15 120	$X_4Y_6+X_6Y_4$
	28 740	X_6Y_6

TABLE 4.63.—*Symmetric-Antisymmetric Frequencies and Mode Shapes for a Completely Free Square Plate; $\nu = 0.225$*

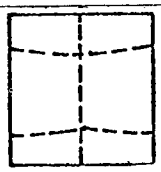
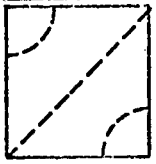
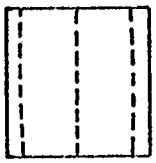
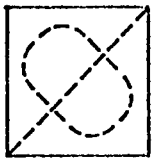
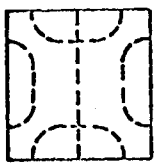
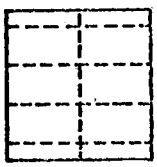
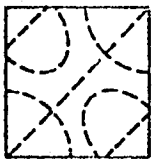
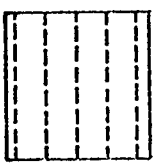
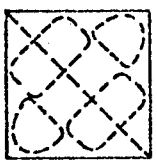
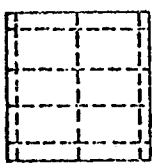
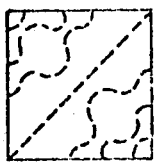
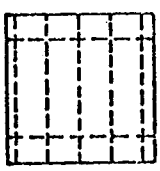
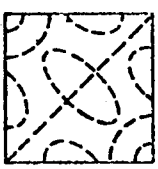
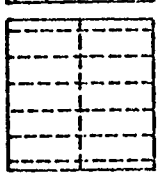
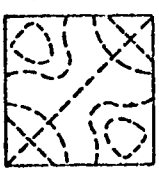
$\frac{\omega^2 a^4 \rho}{16D}$	$W(\bar{x}, \bar{y})$ Mode shape	$W(\bar{x}, \bar{y})$ Nodal pattern	$W(\bar{x}, \bar{y}) - W(\bar{y}, \bar{x})$ nodal pattern
80.8 − 73 $\delta\nu$	$X_1Y_2 - 0.0682X_3Y_0 + 0.0760X_3Y_2 + 0.0260X_1Y_4 + 0.0073X_5Y_0 - 0.0027X_3Y_4 - 0.0112X_5Y_2 + 0.0030X_5Y_4$		
237.1	$0.0678X_1Y_2 + X_3Y_0 - 0.0150X_3Y_2 + 0.0355X_1Y_4 + 0.0000X_5Y_0 + 0.0100X_3Y_4 - 0.0007X_5Y_2 + 0.0016X_5Y_4$		
746	$-0.0709X_1Y_2 + 0.0214X_3Y_0 + X_3Y_2 - 0.1260X_1Y_4 - 0.0038X_5Y_0 + 0.1234X_3Y_4 - 0.0095\ X_5Y_2 - 0.0100\ X_5Y_4$		
1131	X_1Y_4		
2497	X_5Y_0		
3240	X_3Y_4		
3927	X_5Y_2		
6036	X_1Y_6		

TABLE 4.63.—*Symmetric-Antisymmetric Frequencies and Mode Shapes for a Completely Free Square Plate; $\nu = 0.225$*—Contineud

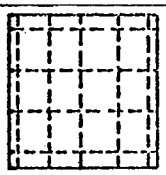
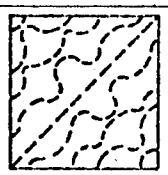
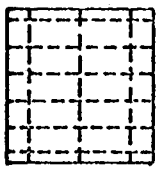
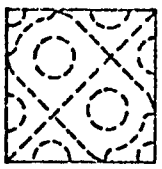
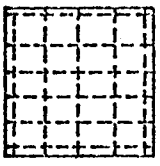
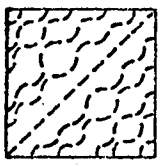
$\frac{\omega^2 a^4 \rho}{16D}$	$W(\bar{x}, \bar{y})$		$W(\bar{x}, y) - W(\bar{y}, \bar{x})$ nodal pattern
	Mode shape	Nodal pattern	
9030	X_5Y_4		
10 380	X_3Y_6		
20 400	X_5Y_6		

TABLE 4.64.—*Frequency Parameters $\omega a^2\sqrt{\rho/D}$ for F–F–F–F Square Plate; $\nu = 1/6$*

[Table is symmetric; values in parentheses are interpolated]

m	$\omega a^2\sqrt{\rho/D}$ for values of n of—						
	0	1	2	3	4	5	6
0			22. 373	61. 673	120. 903	199. 860	298. 556
1		14. 920	37. 284	75. 948	134. 107	214. 138	(292. 4)
							(309. 06)
2			67. 591	110. 599	169. 998	248. 064	345. 669
3				159. 324	222. 700	302. 831	(399. 2)
							(396. 8)
4					290. 427	373. 952	474. 596
5						460. 964	(562. 6)
							(565. 5)
6							670. 958

For modes symmetric with respect to $\bar{x}=0$ (fig. 4.51) and antisymmetric about $\bar{y}=0$ (asymmetric with respect to the diagonals):

$$W(\bar{x}, \bar{y}) = \sum_{n=1,3,\ldots} \alpha_n u_n(\xi)(-1)^{\frac{n-1}{2}} \sin n\pi\eta + \beta_0^* v_0(\eta) + \sum_{m=2,4,\ldots} \beta_m^* v_m(\eta)(-1)^{m/2} \cos m\pi\xi \quad (4.69)$$

The first four of these frequencies and the amplitude parameters are listed in table 4.66 (ref. 4.113).

The four nodal patterns corresponding to table 4.66 are shown in figure 4.52; also shown are interesting patterns which arise by taking the linear combinations:

$$W(\bar{x}, \bar{y}) - KW(\bar{y}, \bar{x})$$

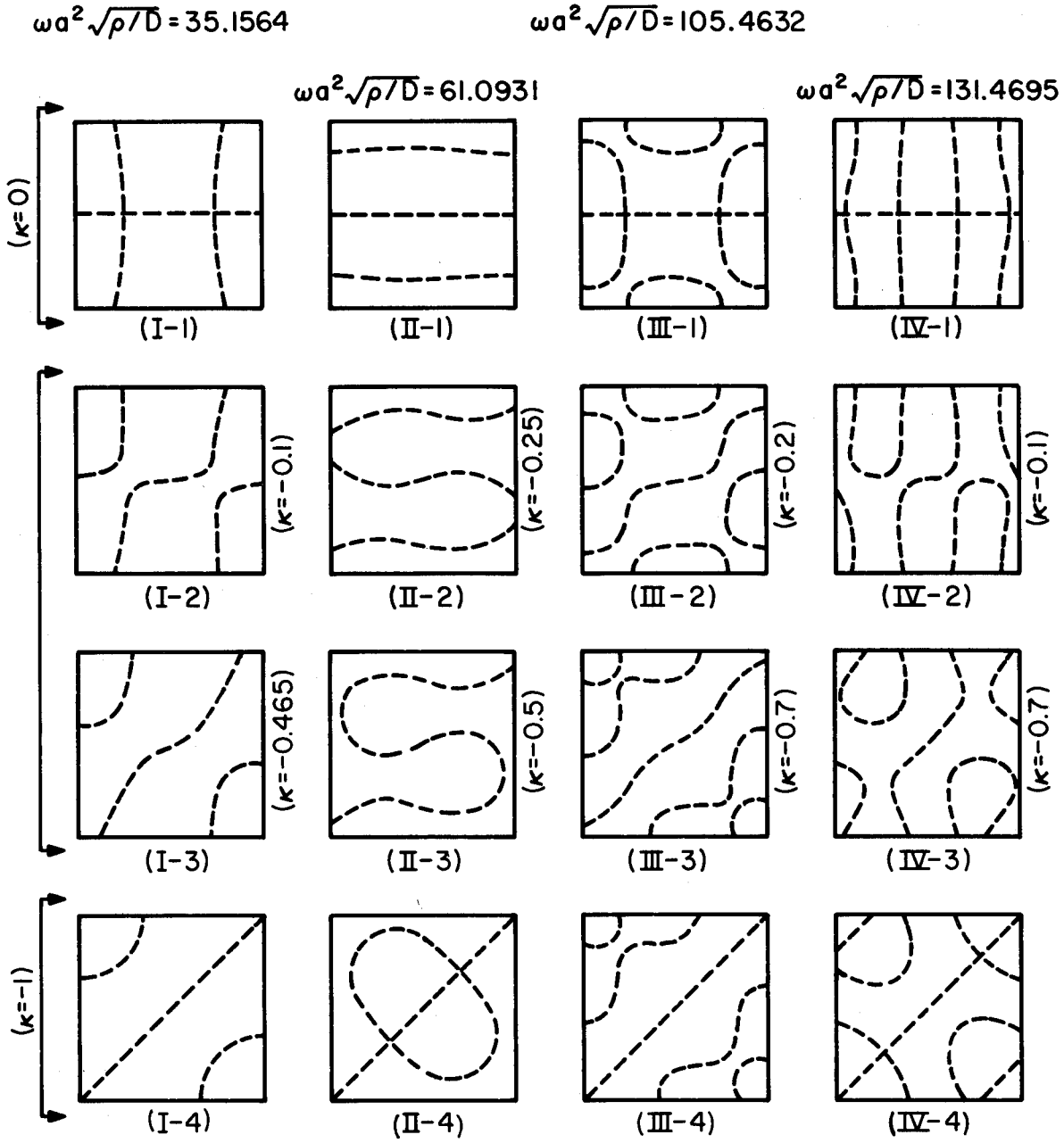
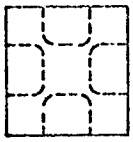


FIGURE 4.52.—Superposition of mode shapes for a completely free square plate; $\nu=0.3$. (After ref. 4.113)

TABLE 4.65.—*Frequency Parameters and Mode Shapes for a Completely Free Square Plate; $\nu=0.3$*

Nodal pattern	$\omega a^2\sqrt{\rho/D}$	n	α_n	λ_n	λ_n^*
Modes symmetric about coordinate axes, symmetric about diagonals					
	24. 2702	0	8. 51935		
		2	[a]1. 00000	2. 54147	1. 24133
		4	. 04225	4. 29641	3. 67990
		6	. 01173	6. 20154	5. 79145
		8	. 00494	8. 15225	7. 84480
	63. 6870	0	−. 11966		
		2	1. 0000	3. 23309	[a]1. 56615i
		4	. 03422	4. 73844	3. 08985
		6	. 01065	6. 51558	5. 43573
		8	. 00473	8. 39362	7. 58598
	122. 4449	0	−8. 81714		
		2	1. 00000	4. 05046	2. 89935i
		4	−1. 19356	5. 32975	1. 89572
		6	−. 08213	6. 95746	4. 85734
		8	−. 02402	8. 74107	7. 18288
	168. 4888	0	−. 07482		
		2	1. 00000	4. 59037	3. 61545i
		4	. 44885	5. 75078	1. 03513i
		6	. 03590	7. 28502	4. 35069
		8	. 01347	9. 00397	6. 85044
	299. 9325	0	−8. 90424		
		2	1. 00000	5. 86426	5. 13707i
		4	−. 59521	6. 81099	3. 79335i
		6	−1. 39192	8. 14998	2. 36864
		8	−. 13703	9. 71543	5. 79745

[a] $i=\sqrt{-1}$.

Detailed mode shapes showing contour lines for 16 of the modes described in the foregoing paragraphs are shown in figure 4.53 (ref. 4.113).

Grauers (ref. 4.114) in an early work also attempted to solve the problem using solutions to the differential equation but obtained inaccurate results.

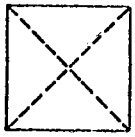
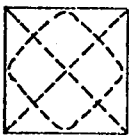
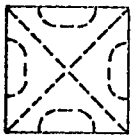
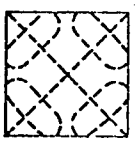
Upper and lower bounds for the fundamental frequency were obtained in references 4.115 and 4.116 and were improved to extreme accuracy in reference 4.117. For $\nu=0.225$, these bounds are

$$14.1028<\omega a^2\sqrt{\rho/D}<14.1165$$

Bazley, Fox, and Stadter (ref. 4.118) used a method developed in reference 4.59 to compute lower bounds for the first 10 frequencies of the following symmetry class of a square: Taking a coordinate system as in figure 4.51, the modes are antisymmetric with respect to both $\bar{x}$ and $\bar{y}$ and are unaltered by interchange of $\bar{x}$ and $\bar{y}$ (symmetric about the diagonals). Five nodal patterns of this type are shown in the third part of table 4.65. They also obtained extremely accurate upper bounds by the Rayleigh-Ritz method, using the first 50 admissible products of free-free beam functions. Double precision arithmetic was used in the computations where necessary. Results are listed in table 4.67 for $\nu=0.225$ and $\nu=0.3$. Herein results from the Rayleigh-Ritz procedure are given; both 25 and 50 admissible functions are used to show the rate of convergence.

Sigillito (ref. 4.76) showed that more precise upper bounds can be obtained with the Ray-

TABLE 4.65.—*Frequency Parameters and Mode Shapes for a Completely Free Square Plate; $\nu=0.3$*—Con.

Nodal pattern	$\omega a^2\sqrt{\rho/D}$	n	α_n	λ_n	λ_n^*
Modes symmetric about coordinate axes, antisymmetric about diagonals					
	19.5961	0	−19.46060		
		2	1.00000	2.44653	1.41933
		4	.00264	4.24093	3.74359
		6	−.00487	6.16324	5.83219
		8	−.00290	8.12315	7.87493
	65.3680	0	3.93698		
		2	1.00000	3.25932	[a]1.61926i
		4	−.09935	4.75638	3.06216
		6	−.01507	6.52864	5.42004
		8	−.00451	8.40376	7.57475
	117.1093	0	3.84826		
		2	1.00000	3.98317	2.80458i
		4	−.48091	5.27879	2.03331
		6	−.02845	6.91850	4.91267
		8	−.00453	8.71009	7.22041
	161.5049	0	−.02833		
		2	1.00000	4.51264	3.51623i
		4	−.24428	5.68893	.60322i
		6	−.01363	7.23629	4.43127
		8	−.00297	8.96459	6.90189
	293.7190	0	5.79354		
		2	1.00000	5.81033	5.07543i
		4	.66331	6.76461	3.70944i
		6	−.61699	8.10925	2.49801
		8	−.05732	9.68297	5.85150

[a] $i=\sqrt{-1}$.

leigh-Ritz procedure by using Legendre functions rather than beam functions. Results from this approach are also listed in table 4.67.

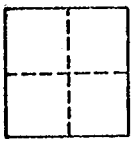
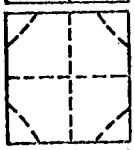
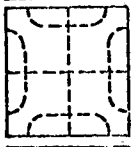
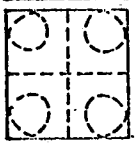
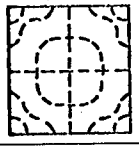
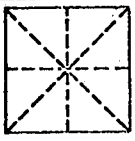
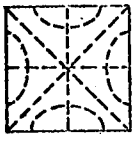
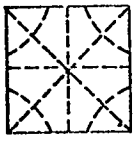
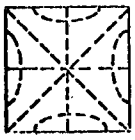
Waller (ref. 4.119) obtained experimental frequencies and mode shapes for square brass plates ($\nu=1/3$). Consider the mode shapes as being approximated by free membrane mode shapes; for example,

$$W(\bar{x},\bar{y})=\cos\frac{m\pi\bar{x}}{a}\cos\frac{n\pi\bar{y}}{a}\pm\cos\frac{n\pi\bar{x}}{a}\cos\frac{m\pi\bar{y}}{a} \tag{4.70}$$

in terms of figure 4.51. Theratio of frequencies relative to the fundamental are given in table 4.68 for various m/n ratios. The plus or minus signs after m/n in the table correspond to plus or minus signs in equation (4.70). Values given above the main diagonal of the array are for the minus sign, and values below the diagonal are for the plus sign. Numbers on the diagonal of the table are then for $m=n$. In reference 4.79 are plotted the experimental frequency ratios of reference 4.119. This plot is reproduced as figure 4.54. Experimentally observed mode shapes corresponding to many of these frequencies are shown in figure 4.55 (ref. 4.119). Other experimental results for the square are given in references 4.110, 4.113, 4.120, and 4.121.

Waller (ref. 4.122) observed the transition points in sudden nodal pattern change in the fundamental mode as a/b varies for the completely free plate. This had been observed

TABLE 4.65.—*Frequency Parameters and Mode Shapes for a Completely Free Square Plate; $\nu=0.3$*—Concluded

Nodal pattern	$\omega a^2\sqrt{\rho/D}$	n	α_n	λ_n	λ_n^*
Modes antisymmetric about coordinate axes, symmetric about diagonals					
	13. 4728	1	1. 00000	1. 53788	[a] 0. 060422i
		3	. 00766	3. 21949	2. 76314
		5	. 00100	5. 13469	4. 86158
		7	. 00041	7. 09684	6. 90181
	77. 5897	1	1. 00000	2. 97685	2. 61947i
		3	. 23339	4. 10632	1. 06694
		5	. 00888	5. 73251	4. 13985
		7	. 00178	7. 54066	6. 41392
	156. 2387	1	1. 00000	4. 10247	3. 85101i
		3	−4. 56065	4. 98299	2. 61348i
		5	−. 05491	6. 38986	3. 02815
		7	−. 01457	8. 05176	5. 75931
	214. 1914	1	1. 00000	4. 76468	4. 54996i
		3	−. 07613	5. 54095	3. 56400i
		5	. 17938	6. 83389	1. 81600
		7	. 01181	8. 40846	5. 22474
	301. 5724	1	1. 00000	5. 61744	5. 43651i
		3	−6. 10581	6. 28933	4. 64281i
		5	−2. 80175	7. 45357	2. 35705i
		7	−. 12231	8. 91940	4. 29469
Modes antisymmetric about coordinate axes and diagonals					
	69. 5020	1	1. 00000	2. 83585	[a] 2. 45805i
		3	−. 12827	4. 00525	1. 39928
		5	−. 00557	5. 66057	4. 23769
		7	−. 00101	7. 48612	6. 47750
	173. 6954	1	1. 00000	4. 31266	4. 07419i
		3	2. 68336	5. 15742	2. 93241i
		5	−. 13566	6. 52679	2. 72047
		7	−. 02103	8. 16082	5. 60366
	204. 6527	1	1. 00000	4. 66215	4. 44248i
		3	. 15411	5. 45304	3. 42573i
		5	−. 13841	6. 76282	2. 06503
		7	−. 01080	8. 35079	5. 31642
	294. 9247	1	1. 00000	5. 55717	5. 37421i
		3	1275. 527	6. 23555	4. 56970i
		5	−346. 402	7. 40825	2. 20955i
		7	−20. 133	8. 88156	4. 37240

[a] $i=\sqrt{-1}$.

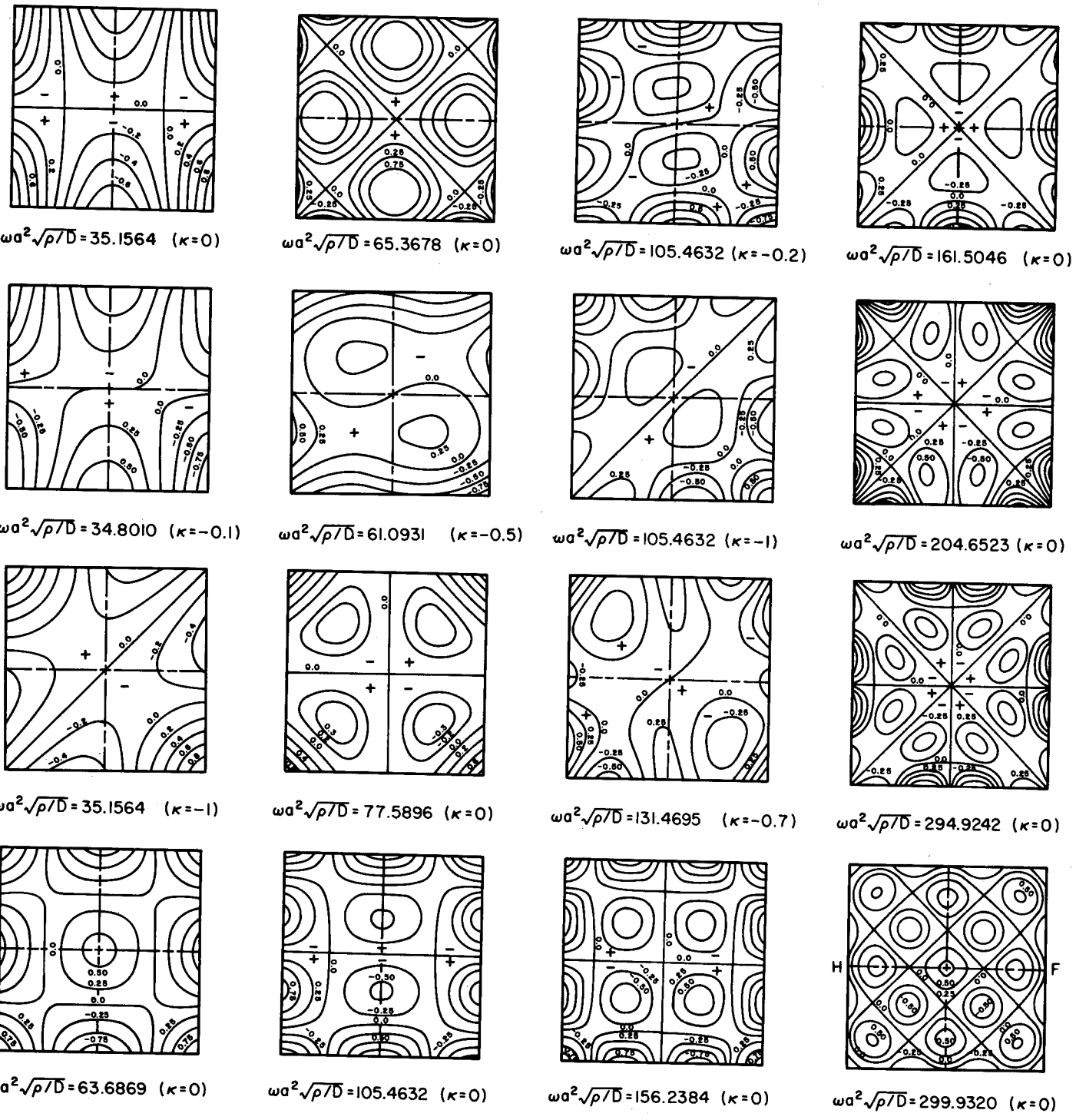


FIGURE 4.53.—Contour lines for 16 modes of a completely free square plate; $\nu = 0.3$. (After ref. 4.113)

TABLE 4.66.—*Frequencies and Amplitude Parameters for a Completely Free Square Plate; $\nu=0.3$; Modes Symmetric to $\bar{x}=0$; antisymmetric to $\bar{y}=0$; $i=\sqrt{-1}$*

$\omega a^2\sqrt{\rho/D}$	n	α_n	λ_n	λ_n^*	m	β_m	λ_m	λ_m^*
34.8011	1	−1.00000	2.12746	1.58937i	0	−0.18568	----------	----------
	3	.01182	3.53922	2.33964	2	.29218	2.74337	0.68841
	5	.00430	5.34098	4.63399	4	.01218	4.41884	3.53184
	7	.00183	7.24749	6.74343	6	.00321	6.28698	5.69859
					8	.00133	8.21743	7.77650
61.0932	1	1.00000	2.68145	2.27819	0	−7.62932	----------	----------
	3	−.86028	3.89746	1.67626	2	−.56588	3.19221	1.47992i
	5	−.04348	5.58482	4.33703	4	−.01392	4.71065	3.13207
	7	−.00974	7.42901	6.54292	6	−.01076	6.49540	5.45984
					8	−.00595	8.37796	7.60328
105.4634	1	1.00000	3.41843	3.11218i	0	.14106	----------	----------
	3	−1.43311	4.43685	1.29834i	2	−3.03882	3.83219	2.58567i
	5	−.07788	5.97375	3.78343	4	−.01973	5.16582	2.30528
	7	−.02391	7.72565	6.18986	6	−.02166	6.83269	5.03133
					8	−.01136	8.64209	7.30167
131.4697	1	1.00000	3.78427	3.51008i	0	−.07630	----------	----------
	3	.09333	3.72448	2.07863i	2	−.07815	4.16181	3.05298i
	5	.00250	6.19037	3.41750	4	.17972	5.41486	1.63687i
	7	.00245	7.89434	5.97322	6	.01323	7.02287	4.76227
					8	.00382	8.79322	7.11894

theoretically for other boundary conditions (see secs. 4.3.1 and 4.3.12). In figures 4.56(a) and 4.56(b) are shown the nodal patterns of two brass plates having the same width, but the length in figure 4.56(a) is slightly greater. The a/b ratio is approximately 1.93. The cyclic frequencies in figures 4.56(a) and 4.56(b) were 548.8 and 558 cps, respectively. It was found that by gradually filing down the longer side the nodal patterns in figures 4.56(c), 4.56(d), and 4.56(e) could be produced. It is estimated that the transition between figures 4.56(b) and 4.56(f) occurs at $a/b=3.9$.

Pavlik (refs. 4.111 and 4.112) extended Ritz' work to nonsquare rectangular plates. Frequencies and mode shapes for three aspect ratios are presented in tables 4.69 to 4.71 for $\nu=0.25$. The functions X_m and Y_n are as defined previously in equation (4.58).

In reference 4.13, extensive results are obtained for $a/b=\frac{1}{2}$ and $\frac{2}{3}$ and $\nu=\frac{1}{4}$. These are listed in table 4.72. Values in parentheses are interpolated.

Mode shapes in the form $W_{mn}(\bar{x}, y)=X_m(\bar{x})$ $Y_n(\bar{y})$ corresponding to ω_{mn} were found in reference 4.13. The shape of the components $X_m(\bar{x})$ and $Y_n(\bar{y})$ are shown in figure 4.57 for $a/b=1.0$. The curves of figure 4.57 do change slightly between the different modes and with varying a/b ratio. Thirty-six precise sets of curves for $W_{mn}(\bar{x}, \bar{y})$ are plotted in reference 4.13, but is is not felt that the variations are sufficient to justify their detailed repetition here. An estimate of this variation can be obtained by looking at the edges where the variation is usually the greatest. One of the mode components having *relatively* large change in shape due to change in the other component or a/b is $X_2(\bar{x})$. Deflection values to be used at $x/a=0.5$ in figure 4.57 for varying values of $Y_n(\bar{y})$ are given in table 4.73 for $a/b=1.0$. Increasing n also increases the magnitude of the negative curvature in the range $0.3<x/a<0.5$.

Variation in edge deflection of $X_2(\bar{x})$ with a/b ratio is shown in table 4.74 for $Y_2(\bar{y})$.

Accurate upper and lower bounds for the doubly antisymmetric modes of a rectangle (see discussion earlier in this section) are reported in reference 4.118. These results are given in table 4.75 for $\nu=0.3$. Upper bounds from reference 4.78 for doubly antisymmetric

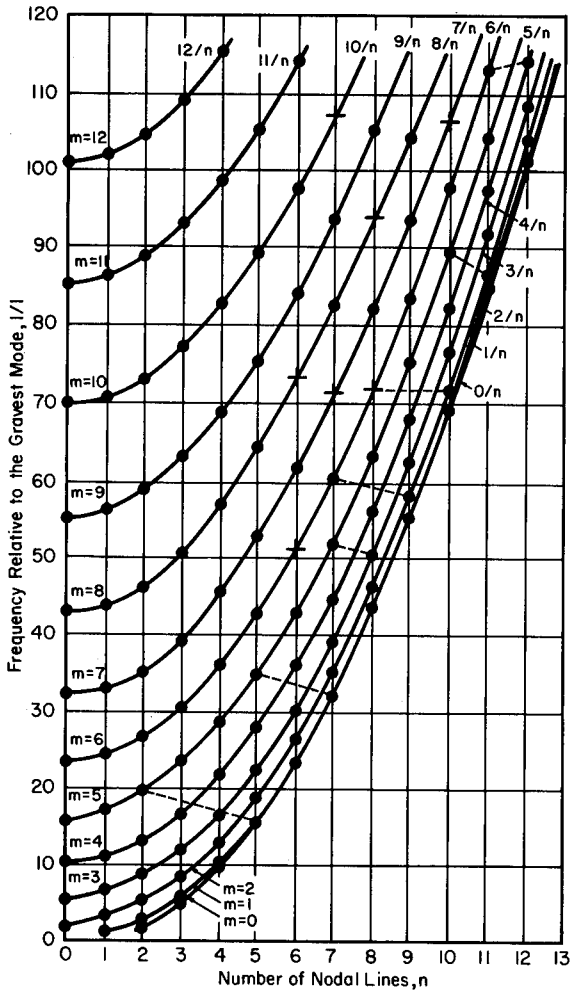


FIGURE 4.54.—Experimentally determined frequency ratios for a completely free square plate; $\nu=\frac{1}{3}$. (After ref. 4.79)

modes for $b/a=4.0$ are given in table 4.76 for $\nu=0.3$.

Waller (ref. 4.123) measured experimental frequencies and mode shapes for brass plates having several aspect ratios. Relative frequencies for three aspect ratios are given in table 4.77. The letter m indicates the number of nodal lines approximately parallel to the y-axis (or width), and, similarly, n indicates those for the $\bar{x}$ axis.

TABLE 4.67.—*Bounds on Frequency Parameters* $\omega a^2\sqrt{\rho/D}$ *for Modes of a Completely Free Square Plate Which Are Antisymmetric About the Coordinate Axes and Symmetric About the Diagonals*

Mode	$\omega a^2\sqrt{\rho/D}$			
	Lower bounds	Upper bounds		
		25 terms (ref. 4.118)	50 terms (ref. 4.118)	50 terms (ref. 4.76)
	$\nu=0.225$			
1	13. 851	14. 119	14. 118	14. 111
2	76. 245	77. 621	77. 576	77. 154
3	151. 54	156. 41	156. 36	156. 26
4	210. 90	214. 79	214. 67	214. 29
5	293. 27	302. 49	302. 24	301. 94
6	421. 26	430. 94	430. 76	430. 03
7	438. 47	456. 82	456. 37	456. 05
8	504. 41	519. 43	519. 03	518. 40
9	654. 62	683. 94	682. 76	682. 03
10	710. 70	727. 35	726. 97	725. 85
	$\nu=0.300$			
1	13. 201	13. 474	13. 473	13. 464
2	75. 735	77. 430	77. 354	76. 904
3	147. 71	153. 13	153. 07	152. 80
4	209. 46	214. 85	214. 62	213. 94
5	288. 72	299. 31	299. 05	298. 51
6	416. 00	430. 68	430. 33	428. 96
7	432. 13	451. 06	450. 71	450. 19
8	498. 77	516. 68	516. 19	515. 01
9	645. 60	677. 35	676. 35	675. 27
10	701. 20	727. 79	727. 08	724. 92

Nodal patterns (ref. 4.123) are shown in figure 4.58 for $a/b=4.0$, 2.0, 1.5, and 1.09. Other experimental results for free rectangular plates are given in references 4.111 and 4.112. Other approximate analytical results for the problem are in references 4.109, 4.114, and 4.124 to 4.126.

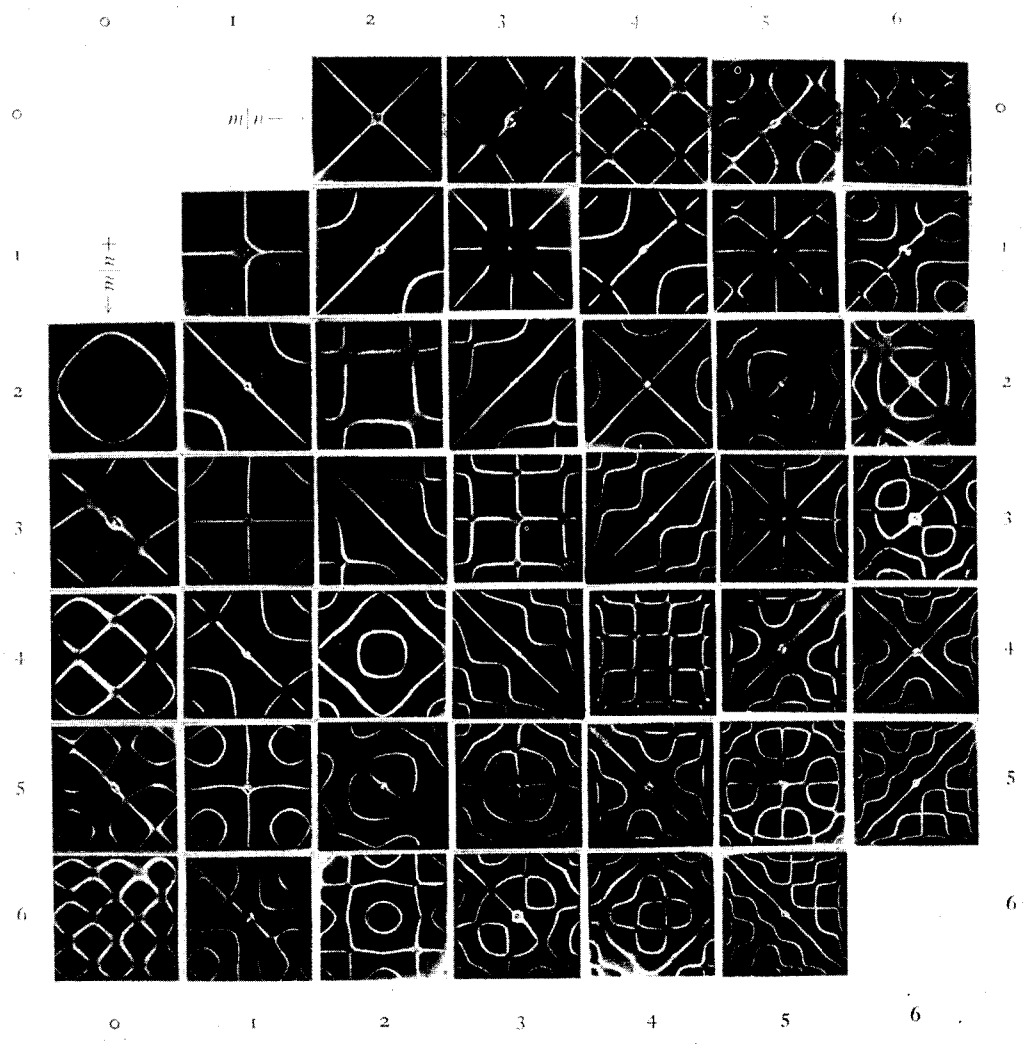


FIGURE 4.55.—Experimentally determined mode shapes for a completely free square plate. (From ref. 4.119)

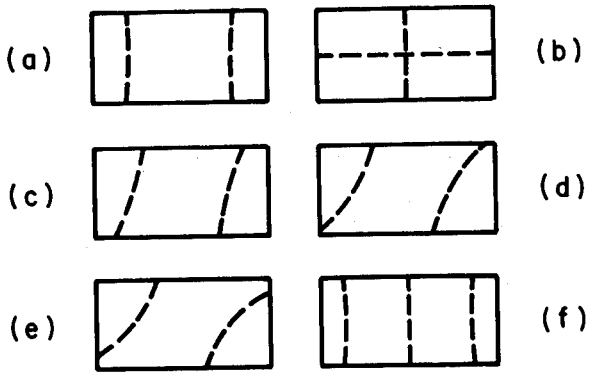


FIGURE 4.56.—Nodal patterns in the vicinity of a transition point for a completely free rectangular plate. (After ref. 4.122)

TABLE 4.68.—*Experimentally Determined Relative Frequencies for a Completely Free Square Brass Plate; $\nu=1/3$*

m/n +	Relative frequency for values of m/n minus—														
	0	1	2	3	4	5	6	7	8	9	10	11	12	13	14
0	-------	-------	1.52	5.10	9.14	15.8	23.0	32.5	43	55.2	70	84	101	119	141
1	-------	1	2.71	5.30	10.3	15.8	23.9	32.2	43	55.8	71	86.1	102	121	---
2	1.94	2.71	4.81	8.52	12.4	19.0	26.4	34	46.6	59	73	89	105	124	---
3	5.10	6.00	8.52	11.8	16.6	22.6	30.0	39.5	50.5	63.4	77.5	92.4	110	128	---
4	9.9	10.3	13.2	16.6	21.5	28.7	35.5	45.4	55.9	69.7	82.9	99	116	132	---
5	15.8	16.6	19.0	23.3	28.7	35	43	52.1	64.5	75.9	90	106	122	136	---
6	23.8	23.9	27.1	30.0	35.9	43	51	61.7	73	84	99	115	130	---	---
7	32.5	32.4	34.0	39.8	45.4	53	61.7	70.3	84	93	108	124	---	---	---
8	43.0	43.0	46.6	50.5	57.2	64.5	73	84	94.4	106	120	136	---	---	---
9	55.2	55.8	59	63.4	69.7	76.2	84	93.2	106	120	133	------	---	---	---
10	70.0	71.0	73	77.5	82.9	90	99	108	120	133	------	------	---	---	---
11	84.0	86.1	89	92.4	99	106	115	124	136	------	------	------	---	---	---
12	101	102	105	110	116	122	130	------	------	------	------	------	---	---	---
13	119	121	124	128	132	136	147	------	------	------	------	------	---	---	---
14	141	-------	-------	-------	-------	------	------	------	------	------	------	------	---	---	---

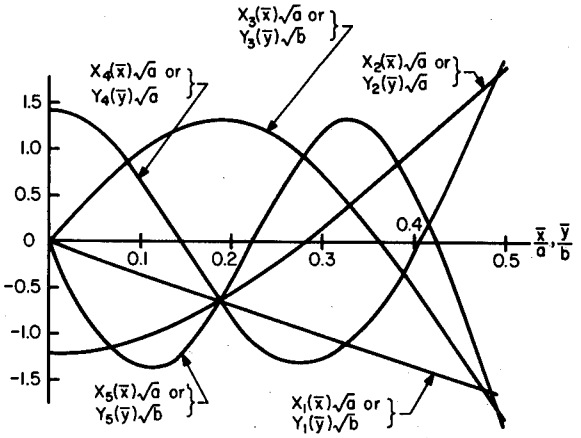


FIGURE 4.57.—Mode shape components $X_m(\bar{x})\sqrt{a}$ or $Y_n(\bar{y})\sqrt{b}$ for a F–F–F–F rectangular plate of dimensions a and b. (After ref. 4.13)

TABLE 4.69.—*Frequencies and Mode Shapes for a Completely Free Rectangular Plate;* a/b=*1.041;* $\nu=\frac{1}{4}$

$\omega a^2\sqrt{\rho/D}$	$W(\bar{x}, \bar{y})$
189.6	$X_1Y_1+0.050X_3Y_1+0.045X_1Y_3-0.012X_3Y_3-0.0064X_5Y_1-0.0055X_1Y_5+0.0034X_5Y_3+0.0032X_3Y_5$
280.6	$X_2Y_0-0.66X_0Y_2-0.0043X_2Y_2-0.011X_4Y_0+0.013X_0Y_4-0.0034X_4Y_2+0.0045X_2Y_4+0.00077X_4Y_4$
343.9	$0.66X_2Y_0+X_0Y_2-0.022X_2Y_2+0.016X_4Y_0+0.0090X_0Y_4+0.0046X_4Y_2+0.0027X_2Y_4+0.00038X_4Y_4$
494.9	$X_2Y_1-0.066X_0Y_3+0.083X_2Y_3+0.042X_4Y_1+0.0094X_0Y_5-0.016X_4Y_3$
511.9	$X_1Y_2-0.088X_3Y_0+0.082X_3Y_2+0.036X_1Y_4+0.011X_5Y_0-0.015X_3Y_4$
832.0	$0.094X_1Y_2+X_3Y_0-0.024X_3Y_2+0.028X_1Y_4+0.010X_3Y_4$
902.6	$0.070X_2Y_1+X_0Y_3-0.024X_2Y_3+0.035X_4Y_1+0.011X_4Y_3$
909.2	$0.016X_2Y_0-0.016X_0Y_2+X_2Y_2-0.026X_4Y_0-0.021X_0Y_4+0.10X_4Y_2+0.096X_2Y_4-0.024X_4Y_4$
987.5	$-0.020X_1Y_1+X_3Y_1-0.64X_1Y_3+0.029X_3Y_3+0.010X_5Y_1+0.0099X_1Y_5-0.0047X_5Y_3-0.0053X_3Y_5$
1098	$-0.074X_1Y_1+0.65X_3Y_1+X_1Y_3+0.15X_3Y_3+0.052X_5Y_1+0.043X_1Y_5-0.025X_5Y_3-0.023X_3Y_5$
1502	$-0.094X_1Y_2+0.028X_3Y_0+X_3Y_2-0.16X_1Y_4-0.010X_5Y_0+0.13X_3Y_4+0.085X_5Y_2-0.024X_5Y_4$
1552	$-0.091X_2Y_1+0.027X_0Y_3+X_2Y_3-0.28X_4Y_1-0.0084X_0Y_5+0.14X_4Y_3$
1624	$-0.016X_0Y_2+0.029X_2Y_2+X_4Y_0-0.19X_0Y_4-0.030X_4Y_2+0.032X_2Y_4+0.015X_4Y_4$
1772	$-0.013X_2Y_0+0.022X_2Y_2+0.20X_4Y_0+X_0Y_4+0.044X_4Y_2-0.031X_2Y_4+0.015X_4Y_4$
1824	$-0.042X_2Y_1-0.038X_0Y_3+0.35X_2Y_3+X_4Y_1-0.035X_0Y_5+0.0016X_4Y_3$
1951	$-0.037X_1Y_2-0.028X_3Y_0+0.19X_3Y_2+X_1Y_4-0.053X_5Y_0+0.0018X_3Y_4$
2165	$0.013X_1Y_1-0.098X_3Y_1-0.10X_1Y_3+X_3Y_3-0.097X_5Y_1-0.071X_1Y_5+0.15X_5Y_3+0.14X_3Y_5$
2306	$X_4Y_2-0.65X_2Y_4$
2484	$0.65X_4Y_2+X_2Y_4$
2698	X_5Y_0

TABLE 4.70.—*Frequencies and Mode Shapes for a Completely Free Rectangular Plate;* a/b=*1.073;* $\nu=\frac{1}{4}$

$\omega a^2\sqrt{\rho/D}$	$W(\bar{x}, \bar{y})$
174.1	$X_1Y_1+0.052X_3Y_1+0.043X_1Y_3-0.012X_3Y_3-0.0067X_5Y_1-0.0052X_1Y_5+0.0034X_5Y_3+0.0031X_3Y_5$
255.4	$X_2Y_0-0.44X_0Y_2-0.013X_2Y_2+0.0075X_4Y_0+0.013X_0Y_4-0.00030X_4Y_2+0.0043X_2Y_4+0.00023X_4Y_4$
320.3	$0.50X_2Y_0+X_0Y_2-0.028X_2Y_2+0.017X_4Y_0+0.0064X_0Y_4+0.0051X_4Y_2+0.0019X_2Y_4-0.000097X_4Y_4$
449.2	$X_2Y_1-0.061X_0Y_3+0.081X_2Y_3+0.044X_4Y_1+0.0089X_0Y_5-0.016X_4Y_3$
475.3	$X_1Y_2-0.098X_3Y_0+0.084X_3Y_2+0.034X_1Y_4+0.012X_5Y_0-0.014X_3Y_4$
742.1	$0.11X_1Y_2+X_3Y_0-0.024X_3Y_2+0.026X_1Y_4+0.010X_3Y_4$
840.2	$0.015X_2Y_0+0.016X_0Y_2+X_2Y_2-0.029X_4Y_0-0.019X_0Y_4+0.11X_4Y_2+0.095X_2Y_4-0.024X_4Y_4$
853.1	$0.064X_2Y_1+X_0Y_3-0.024X_2Y_3+0.038X_4Y_1+0.011X_4Y_3$
887.4	$-0.059X_1Y_1+X_3Y_1-0.44X_1Y_3+0.083X_3Y_3+0.032X_5Y_1+0.025X_1Y_5-0.015X_5Y_3-0.014X_3Y_5$
1028	$-0.074X_1Y_1+0.65X_3Y_1+X_1Y_3+0.15X_3Y_3+0.056X_5Y_1+0.041X_1Y_5-0.025X_5Y_3-0.022X_3Y_5$
1370	$-0.095X_1Y_2+0.027X_3Y_0+X_3Y_2-0.14X_1Y_4-0.011X_5Y_0+0.13X_3Y_4+0.088X_5Y_2-0.024X_5Y_4$
1432	$-0.090X_2Y_1+0.027X_0Y_3+X_2Y_3-0.34X_4Y_1-0.0078X_0Y_5+0.14X_4Y_3$
1450	$-0.017X_0Y_2+0.031X_2Y_2+X_4Y_0-0.11X_0Y_4-0.030X_4Y_2+0.029X_2Y_4+0.015X_4Y_4$
1637	$-0.044X_2Y_1-0.039X_0Y_3+0.48X_2Y_3+X_4Y_1-0.031X_0Y_5+0.0015X_4Y_3$
1676	$-0.013X_2Y_0+0.020X_2Y_2+0.12X_4Y_0+X_0Y_4+0.051X_4Y_2-0.031X_2Y_4+0.016X_4Y_4$
1836	$-0.035X_1Y_2-0.026X_3Y_0+0.16X_3Y_2+X_1Y_4-0.064X_5Y_0+0.0016X_3Y_4$
1991	$0.013X_1Y_1-0.098X_3Y_1-0.10X_1Y_3+X_3Y_3-0.11X_5Y_1-0.064X_1Y_5+0.15X_5Y_3+0.14X_3Y_5$
2084	$+X_4Y_2-0.44X_2Y_4$
2314	$+0.65X_4Y_2+X_2Y_4$
2405	$+X_5Y_0$

TABLE 4.71.—*Frequencies and Mode Shapes for a Completely Free Rectangular Plate;* a/b=*1.499;* $\nu=1/4$

$\omega a^2\sqrt{\rho/D}$	$W(\bar{x}, \bar{y})$
498.7	$X_1Y_1+0.072X_3Y_1+0.024X_1Y_3$
525.7	$X_2Y_0-0.098X_0Y_2-0.011X_2Y_2$
1208	$0.085X_2Y_0+X_0Y_2-0.014X_2Y_2+0.039X_4Y_0$
1212	$X_2Y_1-0.026X_0Y_3$
1434	$X_3Y_0-0.42X_1Y_2$
1623	$0.55X_3Y_0+X_1Y_2+0.1X_3Y_2+0.025X_5Y_0-0.020X_5Y_2$
2160	$-0.074X_1Y_1+X_3Y_1-0.10X_1Y_3$
2611	$0.012X_2Y_0+0.014X_0Y_2+X_2Y_2-0.20X_4Y_0$
2904	$-0.039X_0Y_2+0.20X_2Y_2+X_4Y_0-0.03X_4Y_2-0.019X_0Y_4+0.014X_2Y_4+0.0039X_0Y_6$
3332	$0.026X_2Y_1+X_0Y_3-0.025X_2Y_3$

TABLE 4.72.—*Frequency Parameters* $\omega a^2\sqrt{\rho/D}$ *for a F–F–F–F Rectangular Plate;* $\nu=1/6$

[Values in parentheses are interpolated]

$\frac{a}{b}$	m	$\omega a^2\sqrt{\rho/D}$ for values of n of—						
		0	1	2	3	4	5	6
1/2	0	----------	----------	5. 593	15. 418	30. 223	49. 965	74. 639
	1	----------	7. 374	(17. 61)	27. 032	(42. 25)	61. 628	(85. 56)
	2	22. 373	(26. 52)	37. 585	(51. 70)	70. 007	(91. 78)	(117. 29)
	3	61. 673	(65. 17)	(75. 05)	91. 963	(111. 58)	135. 794	(162. 56)
	4	120. 903	(123. 34)	(132. 94)	(149. 57)	170. 974	(196. 56)	(223. 50)
	5	199. 860	(200. 70)	(210. 02)	(226. 41)	248. 876	274. 639	(303. 18)
	6	298. 556	(298. 94)	(307. 30)	(324. 72)	(345. 96)	(372. 88)	402. 968
2/3	0	----------	----------	9. 944	27. 410	53. 735	88. 826	132. 691
	1	----------	9. 905	22. 245	40. 339	66. 309	100. 928	(144. 5)
	2	22. 373	(30. 36)	46. 654	(68. 39)	97. 822	(133. 40)	177. 606
	3	61. 673	(69. 56)	86. 028	111. 510	143. 532	182. 204	(226. 20)
	4	120. 903	(127. 7)	(145. 2)	(160. 5)	204. 804	(245. 9)	294. 258
	5	199. 860	(205. 1)	222. 088	(250. 0)	283. 715	326. 580	(374. 8)
	6	298. 556	(302. 1)	(320. 4)	(347. 8)	(382. 6)	(425. 6)	476. 853

TABLE 4.73.—*Variation in Edge Deflection of a Mode Component Due to Change in the Other Component;* $\nu=1/6$

n	1	2	3	4	5	6
Edge deflection	1. 95	1. 81	1. 71	1. 66	1. 62	1. 60

TABLE 4.74—*Variation in Edge Deflection of a Mode Component Due to Change in* a/b; $\nu=1/6$

a/b	1	2/3	1/2
Edge deflection	1. 81	1. 72	1. 67

TABLE 4.75.—*Bounds on Frequency Parameters* $\omega a^2\sqrt{\rho/D}$ *for the Doubly Antisymmetric Modes of a Completely Free Rectangular Plate;* $\nu=0.3$

Mode	$\omega a^2\sqrt{\rho/D}$					
	Lower bound	Upper bound	Lower bound	Upper bound	Lower bound	Upper bound
	$b/a=1.00$		$b/a=1.25$		$b/a=1.50$	
1	13. 092	13. 474	10. 479	10. 761	8. 6667	8. 9351
2	66. 508	69. 576	48. 352	50. 487	36. 651	38. 294
3	75. 146	77. 411	67. 665	69. 746	64. 844	66. 965
4	145. 57	153. 12	117. 68	124. 15	94. 147	98. 648
5	196. 46	205. 17	132. 77	138. 41	103. 32	108. 18
6	207. 87	214. 81	197. 36	205. 77	166. 83	176. 56
7	277. 72	292. 37	208. 75	220. 03	184. 44	193. 73
8	285. 47	299. 27	249. 46	262. 66	198. 62	205. 35
9	393. 93	420. 99	264. 27	277. 23	234. 75	244. 80
10	410. 74	430. 66	339. 96	358. 87	261. 14	275. 96
	$b/a=2.00$		$b/a=4.00$		$b/a=8.00$	
1	6. 4563	6. 6464	3. 1463	3. 2604	1. 5330	1. 6158
2	24. 417	25. 455	10. 284	10. 728	4. 7291	4. 9941
3	56. 151	59. 051	19. 809	20. 821	8. 2953	8. 7915
4	63. 726	65. 392	32. 952	34. 783	12. 436	13. 237
5	85. 647	89. 263	49. 920	53. 194	17. 323	18. 514
6	107. 66	113. 81	60. 830	62. 394	23. 095	24. 766
7	125. 15	131. 73	67. 133	69. 099	29. 845	32. 089
8	174. 88	186. 73	71. 408	76. 824	37. 617	40. 542
9	178. 26	190. 04	78. 658	82. 051	46. 410	50. 150
10	195. 26	202. 79	94. 076	99. 291	56. 017	60. 602

TABLE 4.76.—*Frequencies for Doubly Antisymmetric Modes of a Completely Free Rectangular Plate;* b/a= *4.0;* $\nu=0.3$

Mode	1	2	3	4	5	6	7	8	9	10
$\omega a^2\sqrt{\rho/D}$	3. 2597	10. 711	20. 749	34. 622	53. 092	64. 080	71. 048	77. 232	84. 532	102. 87

4.4 ELASTIC, DISCONTINUOUS, AND POINT SUPPORTS

4.4.1 Elastic Edge Supports

Consider first the rectangular plate simply supported (SS) along the sides $x=0$ and $x=a$ and elastically restrained (ES) against both translation and rotation along the other sides as shown in figure 4.59. The solution equation (eq. (1.37)) satisfies the boundary conditions along $x=0$ and $x=a$. The remaining boundary conditions are

$$\left.\begin{aligned} M_y(x,0)&=-K_1\frac{\partial W}{\partial y}(x,0)\\ M_y(x,b)&=K_2\frac{\partial W}{\partial y}(x,b)\\ V_y(x,0)&=K_3W(x,0)\\ V_y(x,b)&=-K_4W(x,b)\end{aligned}\right\} \tag{4.71}$$

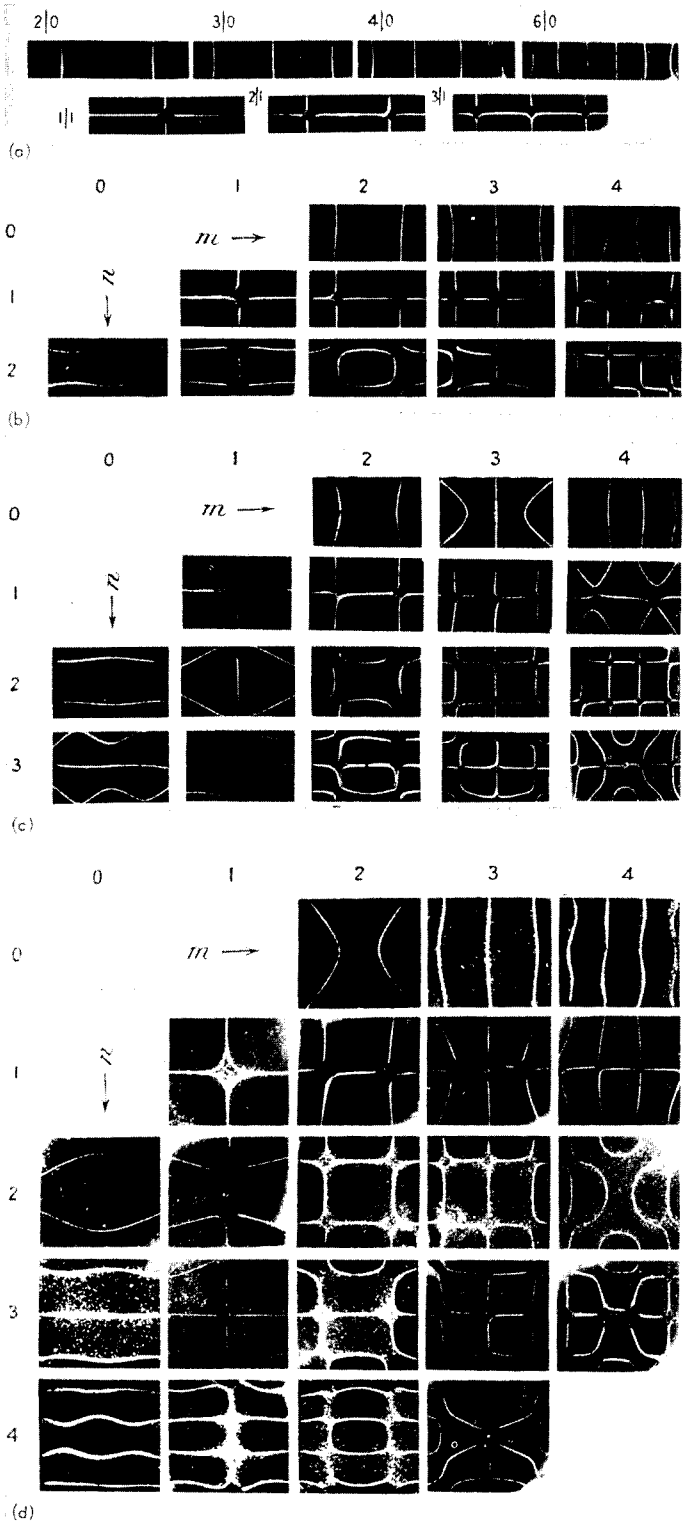


FIGURE 4.58.—Experimentally observed nodal patterns for completely free rectangular brass plates. (*a*) $a/b=4$. (*b*) $a/b=2$. (*c*) $a/b=1.5$. (*d*) $a/b=1.09$. (From ref. 4.123)

TABLE 4.77.—*Experimentally Determined Frequency Ratios for Completely Free Rectangular Brass Plates*

n	Frequency ratio for values of m of—					
	0	1	2	3	4	5
	$a/b=1.09$					
0			1. 53	4. 55	9. 3	
1		[a]1	2. 67	5. 16	10	
2	2. 23	2. 78	5. 1	8	13	
3	5. 35	6. 4	8. 8	11. 5	16	
4	10. 8	11. 8	14	17	21	
	$a/b=1.5$					
0			1. 08	2. 93	5. 53	9. 96
1		[b]1	2. 49	4. 47	7. 09	11
2	2. 62	3. 42	5	7. 60	10. 5	14. 9
3	7. 5	7. 9	9. 6	12. 3	15. 5	20
4	13. 6	14. 4	16. 5	19. 3	22. 7	27
	$a/b=2.0$					
0			[c]1	2. 88	5. 42	
1		1. 20	2. 30	3. 62	6. 2	
2	4. 37	4. 87	6. 7	8. 2	10. 8	

[a] Fundamental frequency of a 3.94- by 3.62- by 0.720-in. plate was 423 cps. For a 6.15- by 5.67- by 0.0906-in. plate, it was 220 cps.

[b] Fundamental frequency of a 9.81- by 6.38- by 0.934-in. plate was 134 cps.

[c] Fundamental frequency of a 2.36- by 1.172- by 0.0807-in. plate was 1730 cps. For a 5.55- by 2.78- by 0.1240-in. plate, it was 482 cps.

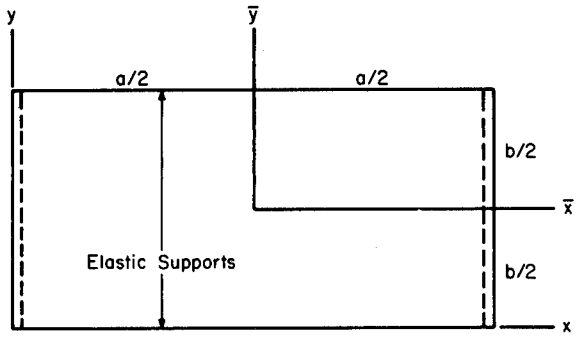


FIGURE 4.59.—SS–ES–SS–ES plate.

where $K_{1,2,3,4}$ are the stiffness coefficients of distributed translational and rotational springs acting along the edges $y=0$ and $y=b$. For simplicity it will be assumed that these coefficients do not vary with x. The constants K_1 and K_2 have dimensions of moment/(unit length) and K_3 and K_4 have dimensions of force/(unit length)^2. Substituting equation (1.37) into equations (4.71) results in a characteristic determinant, the zeros of which yield the vibration frequencies.

Das (ref. 4.10) showed that the characteristic equation for the case $K_1=K_2=K$, $K_3=K_4=\infty$ becomes

$$\frac{\cos\lambda_1 b\cosh\lambda_2 b-1}{\sin\lambda_1 b\sinh\lambda_2 b}=\frac{\lambda_2^2-\lambda_1^2}{2\lambda_1\lambda_2}+\left(\frac{(\lambda_1^2+\lambda_2^2)D}{K}\right)\left[\frac{\coth\lambda_2 b}{\lambda_1}-\frac{\cot\lambda_1 b}{\lambda_2}+\frac{D}{K}\left(\frac{\lambda_1^2+\lambda_2^2}{2\lambda_1\lambda_2}\right)\right] \tag{4.72}$$

with λ_1 and λ_2 as defined in equations (4.27) and that the mode shapes are given by

$$W(x,y)=\left\{(\cosh\lambda_2 y-\cos\lambda_1 y)+\left[\frac{(\lambda_1^2+\lambda_2^2)\sin\lambda_1 b+(K\lambda_1/D)(\cosh\lambda_2 b-\cos\lambda_1 b)}{(K/D)(\lambda_2\sin\lambda_1 b-\lambda_1\sinh\lambda_2 b)}\right]\sinh\lambda_2 y-\frac{(\lambda_1^2+\lambda_2^2)\sinh\lambda_2 b+(K\lambda_2/D)(\cosh\lambda_2 b-\cos\lambda_1 b)}{(K/D)(\lambda_2\sin\lambda_1 b-\lambda_1\sinh\lambda_2 b)}\sin\lambda_1 y\right\}\sin\alpha x \tag{4.73}$$

In reference 4.10 the characteristic equation for $K_1=K_2=\infty$, $K_3=K_4=K$ is given as

$$\frac{\cos\lambda_1 b\cosh\lambda_2 b-1}{\sin\lambda_1 b\sinh\lambda_2 b}=\frac{(g_2h_1)^2-(g_1h_2)^2}{2g_1g_2h_1h_2}+\left(\frac{K}{D}(h_1+h_2)\right)\left[\frac{\cot\lambda_1 b}{g_2h_1}-\frac{\coth\lambda_2 b}{g_1h_2}+\left(\frac{K}{D}\right)\frac{h_1+h_2}{2g_1g_2h_1h_2}\right] \tag{4.74}$$

with $g_{1,2}$ and $h_{1,2}$ defined as

$$\left.\begin{aligned} g_1&=\lambda_1[\lambda_1^2+(2-\nu)\alpha^2]\\ g_2&=\lambda_2[\lambda_2^2-(2-\nu)\alpha^2]\\ h_1&=\lambda_1(\lambda_1^2+\nu\alpha^2)\\ h_2&=\lambda_2(\lambda_2^2-\nu\alpha^2)\end{aligned}\right\} \tag{4.75}$$

and the mode shapes are

$$W(x,y)=\left[\cosh\lambda_2 y+\frac{(K/D)(h_1+h_2)\sin\lambda_1 b+g_1h_2(\cos\lambda_1 b-\cosh\lambda_2 b)}{g_1h_2\sinh\lambda_2 b-g_2h_1\sin\lambda_1 b}\sinh\lambda_2 y+\frac{h_2}{h_1}\cos\lambda_1 y+\frac{(K/D)h_2(h_1+h_2)\sinh\lambda_2 b-g_2h_1h_2(\cosh\lambda_2 b-\cos\lambda_1 b)}{h_1(g_1h_2\sinh\lambda_2 b-g_2h_1\sin\lambda_1 b}\sin\lambda_1 y\right]\sin\alpha x \tag{4.76}$$

The buckling results obtained by Lundquist and Stowell (ref. 4.127) can be applied here by use of equation (4.24). For the case given by equation (4.71) when $K_3=K_4=\infty$ and K_1 and K_2 are separate and distinct, the characteristic equation is given as

$$\left[(\lambda_1^2+\lambda_2^2)+(K_1/D)\left(\lambda_2\tanh\frac{\lambda_2 b}{2}+\lambda_1\tan\frac{\lambda_1 b}{2}\right)\right]\times\left[(\lambda_1^2+\lambda_2^2)+(K_2/D)\left(\lambda_2\coth\frac{\lambda_2 b}{2}-\lambda_1\cot\frac{\lambda_1 b}{2}\right)\right]=-\left[(\lambda_1^2+\lambda_2^2)+(K_2/D)\left(\lambda_2\tanh\frac{\lambda_2 b}{2}+\lambda_1\tan\frac{\lambda_1 b}{2}\right)\right]\times\left[(\lambda_1^2+\lambda_2^2)+(K_1/D)\left(\lambda_2\coth\frac{\lambda_2 b}{2}-\lambda_1\cot\frac{\lambda_1 b}{2}\right)\right] \tag{4.77}$$

It is apparent that for $K_1=K_2=K$, equation (4.77) reduces to one of its sides set equal to zero. Furthermore, for $K_1=K_2=K$, modes symmetric with respect to $\bar{x}$ (fig. 4.59) give rise to the characteristic equation

$$\lambda_1^2+\lambda_2^2+(K/D)\left(\lambda_2\tanh\frac{\lambda_2 b}{2}+\lambda_1\tan\frac{\lambda_1 b}{2}\right)=0 \tag{4.78}$$

and the antisymmetric modes

$$\lambda_1^2+\lambda_2^2+(K/D)\left(\lambda_2\coth\frac{\lambda_2 b}{2}-\lambda_1\cot\frac{\lambda_1 b}{2}\right)=0 \tag{4.79}$$

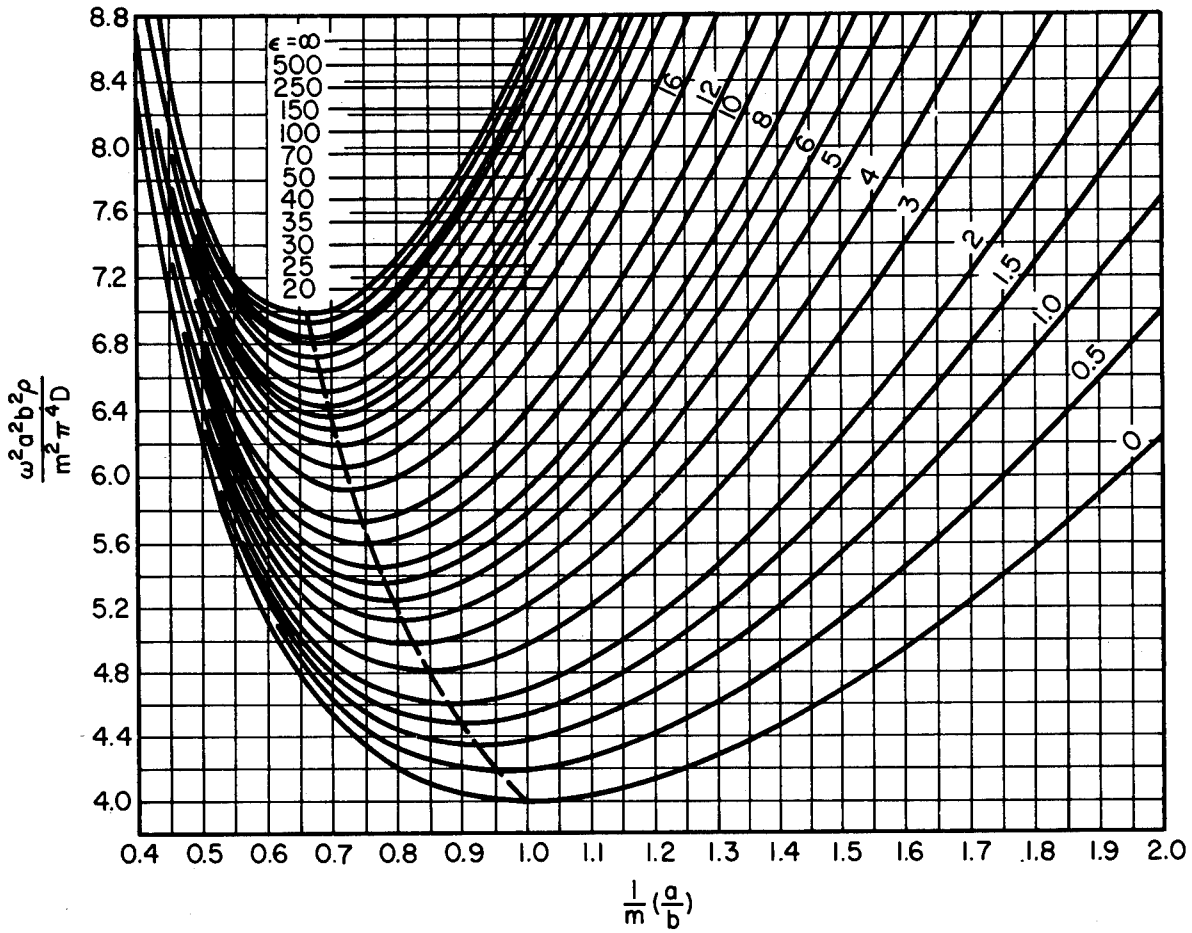


FIGURE 4.60.—Frequency parameters $\omega^2a^2b^2\rho/m^2\pi^4D$ for a SS–ES–SS–ES rectangular plate with symmetrical slope restraints.

In reference 4.127 the problem is also solved by the Rayleigh method. A mode shape is chosen as

$$W(\bar{x},\bar{y})=\left[\frac{4A}{b^2}\left(\bar{y}^2-\frac{b^2}{4}\right)+\left(\frac{4A}{\pi}+B\right)\cos\frac{\pi\bar{y}}{b}\right]\cos\alpha\bar{x} \quad (4.80)$$

where A and B are arbitrary amplitude coefficients. The coefficients A and B are chosen so that $A=0$ represents the condition of simply supported edges at $\bar{y}=\pm b/2$, and $B=0$ represents the condition of clamped edges. The ratio A/B is then a measure of edge restraint and is determined from

$$-D\left(\frac{\partial^2W}{\partial\bar{y}^2}+\nu\frac{\partial^2W}{\partial\bar{x}^2}\right)_{\bar{y}=b/2}=K\left(\frac{\partial W}{\partial\bar{y}}\right)_{\bar{y}=b/2} \quad (4.81)$$

which gives $A=(\pi Kb/8D)B$. Formulating the Rayleigh quotient yields the frequency parameter

$$\frac{\omega^2a^4\rho}{D}=m^2\pi^4\left(\frac{a}{b}\right)^2\left\{\left[\left(\frac{\alpha^2b^2}{120}+\frac{1}{\alpha^2b^2}+\frac{1}{6}\right)\left(\frac{Kb}{D}\right)^2+\left(1+\frac{Kb}{2D}\right)\left(\frac{mb}{a}+\frac{a}{mb}\right)^2\left(\frac{1}{2}+\frac{Kb}{4D}-\frac{4Kb}{\pi^2D}\right)+\frac{2Kb}{\alpha^2b^2D}\right]\div\left[\frac{\pi^2K^2b^2}{120D^2}-\frac{4Kb}{\pi^2D}\left(1+\frac{Kb}{D}\right)+\frac{1}{2}\left(1+\frac{Kb}{2D}\right)^2\right]\right\} \quad (4.82)$$

Results obtained from equation (4.82) are given in table 4.78 in the columns denoted by (*a*). Realizing that these values must be upper bounds, correction factors were established based upon exact solutions of equation

(4.78) for fundamental roots at selected points. Column (*b*) lists the corrected values. Values marked by an asterisk identify the exact values obtained. The values of column (*b*) are plotted as figure 4.60.

Figure 4.60 gives valuable design information if properly used. The fundamental frequency is obtained by letting $m=1$. While frequencies higher than the fundamental can be obtained from it by increasing m, it must be remembered that all higher mode shapes considered have nodal lines parallel to only the y-axis. Other mode shapes are not considered in figure 4.60. The dashed line locates the minima of the various curves.

It is suggested in reference 4.127 that, when the two side moment restraints are unequal, a reasonably good approximation to the true frequency value can be obtained by averaging the results obtained from the separate symmetric problems by considering first one magnitude of edge restraint and then the other. If the frequency parameter Γ is defined by

$$\Gamma=\frac{\omega^2a^2b^2\rho}{m^2\pi^4D} \tag{4.83}$$

then the average used may be either the arithmetic mean, $(\Gamma_1+\Gamma_2)/2$, or the geometric mean, $\sqrt{\Gamma_1\Gamma_2}$.

Carmichael (ref. 4.128) used the Rayleigh-Ritz method to compute frequencies for a rectangular plate having $w=0$ and uniform slope restraint along pairs of opposite edges. Mode shapes of the type

$$W(x,y)=\sum_{m,n}X_m(x)Y_n(y)$$

were used, where $X_m(x)$ and $Y_n(y)$ are the characteristic functions of a vibrating beam having zero deflection and rotational restraint at its ends; that is,

$$X_m=A_m\left(\cosh\frac{\epsilon_m x}{a}-\cos\frac{\epsilon_m x}{a}\right)+B_m\left(\sinh\frac{\epsilon_m x}{a}+\sin\frac{\epsilon_m x}{a}\right) \tag{4.84}$$

and similarly for Y_n, by replacing m, x, and a in equation (4.84) by n, y, and b, respectively. Values of ϵ_m, A_m, and B_m are given in table 4.79 for varying spring constant parameters ξ, with

$$\left.\begin{aligned}\xi_A&=\frac{Ka}{D}\quad(\text{for } X_m)\\ \xi_B&=\frac{Kb}{D}\quad(\text{for } Y_n)\end{aligned}\right\} \tag{4.85}$$

and K defined as in equation 4.81.

The strain energy of the system is (fig. 4.59)

$$V=\frac{D}{2}\int_0^a\int_0^b\left[\left(\frac{\partial^2W}{\partial x^2}\right)^2+\left(\frac{\partial^2W}{\partial y^2}\right)^2+2\nu\frac{\partial^2W}{\partial x^2}\frac{\partial^2W}{\partial y^2}+2(1-\nu)\left(\frac{\partial^2W}{\partial x\,\partial y}\right)^2\right]dx\,dy-\frac{D}{2}\left[\int_0^a\left(\frac{\partial^2W}{\partial y^2}\frac{\partial W}{\partial y}\right)_0^b dx+\int_0^b\left(\frac{\partial^2W}{\partial x^2}\frac{\partial W}{\partial x}\right)_0^a dy\right] \tag{4.86}$$

where the second term represents the energy stored in the rotational springs along the edges.

Calculations were based upon a 36-term series for the deflection function taking m, $n=1$, 2, 3, 4, 5, 6. Because the diagonal terms of the resulting frequency determinant are much greater than the others, an approximate solution for the (mn)th mode can be obtained by taking only the (mn)th term of $W(x,y)$. The approximate frequency can then be written as

$$\omega_{mn}=\frac{1}{b^2}\sqrt{\frac{D}{\rho}\left[\left(\frac{b}{a}\right)^4\epsilon_m^4+\epsilon_n^4+2\left(\frac{b}{a}\right)^2\phi_m\phi_n\right]} \tag{4.87}$$

where

$$\phi_m=\frac{\epsilon_m^2[\epsilon_m(B_m^2+1)+2A_m(B_m-1)]}{\epsilon_m(2A_m^2-B_m^2+1)+2A_m(B_m+1)} \tag{4.88}$$

and similarly for ϕ_n by replacing m by n in equation (4.88). Values of $\phi_{m,n}$ are given in table 4.79.

Frequencies and approximate nodal patterns are shown in table 4.80 for ranges of b/a and $\xi_a=\xi_b=\xi$. Values in parentheses are those found from equation (4.87). Other results for $\xi=20$ and ∞ are obtained from the 36-term series. Values for $\xi=0$ found from equation (4.20) are included for comparison. It is seen that the approximate solution in the table

TABLE 4.78.—*Frequency Parameters* $\omega^2a^2b^2\rho/m^2\pi^4D$ *for a SS–ES–SS–ES Rectangular Plate With Symmetrical Slope Restraints*

[(*a*), values obtained from energy method; (*b*), corrected values]

Kb/D	$\omega^2a^2b^2\rho/m^2\pi^4D$ for values of *a/mb* of—															
	0.4		0.5		0.6		0.7		0.8		0.9		1.0		1.1	
	(*a*)	(*b*)	(*a*)	(*b*)	(*a*)	(*b*)	(*a*)	(*b*)	(*a*)	(*b*)	(*a*)	(*b*)	(*a*)	(*b*)	(*a*)	(*b*)
0	8.410	[a] 8.410	6.250	[a] 6.250	5.138	[a] 5.138	4.531	[a] 4.531	4.203	[a] 4.203	4.045	[a] 4.045	4.000	[a] 4.000	4.036	[a] 4.036
0.5	8.442	8.438	6.299	6.291	5.208	5.206	4.627	4.627	4.327	4.326	4.202	4.202	4.194	4.194	4.271	4.271
1	8.473	8.468	6.346	6.333	5.275	5.271	4.716	4.715	4.443	4.441	4.348	4.347	4.374	4.373	4.488	4.487
1.5	8.503	8.497	6.390	6.375	5.337	5.331	4.799	4.797	4.550	4.547	4.483	4.481	4.539	4.538	4.687	4.685
2	8.531	[a] 8.525	6.432	6.414	5.395	5.387	4.876	4.873	4.650	4.646	4.608	4.605	4.693	4.691	4.872	4.870
3	8.585	8.572	6.510	6.487	5.501	5.491	5.017	5.012	4.831	4.825	4.833	4.829	4.968	4.965	5.203	5.200
4	8.634	8.611	6.579	6.551	5.596	5.584	5.141	5.134	4.989	4.982	5.030	5.025	5.208	5.205	5.490	5.487
5	8.679	8.649	6.642	6.611	5.680	5.666	5.251	5.243	5.128	5.120	5.203	5.198	5.419	5.415	5.743	5.739
6	8.720	[a] 8.694	6.699	6.665	5.756	[a] 5.741	5.369	5.359	5.253	5.244	5.357	5.351	5.605	5.601	5.965	5.960
7	-------	--------	6.750	6.714	5.825	5.809	5.438	5.427	5.364	5.355	5.494	5.487	5.771	5.766	6.164	6.159
8	8.793	8.746	6.797	6.758	5.886	5.868	5.517	5.505	5.464	5.454	5.617	5.609	5.920	5.914	6.341	6.335
10	8.854	8.801	6.879	6.837	5.994	5.974	5.655	5.640	5.636	5.625	5.829	5.820	6.176	6.169	6.646	6.639
12	-------	--------	6.949	6.904	6.085	6.063	5.770	5.752	5.780	5.768	6.005	5.995	6.388	6.380	6.897	6.889
16	8.991	8.927	7.060	7.012	6.228	6.203	5.951	5.929	6.005	5.992	6.279	6.268	6.718	6.708	7.289	7.280
20	9.057	[a] 8.989	7.145	[a] 7.095	6.336	6.309	6.087	6.063	6.173	6.159	6.484	6.472	6.963	[a] 6.952	7.579	7.569
25	-------	--------	7.226	7.174	6.439	6.410	6.216	6.190	6.331	6.316	6.676	6.663	7.193	7.181	7.850	7.839
30	9.168	9.092	7.288	7.234	6.517	6.487	6.314	6.287	6.451	6.435	6.821	6.807	7.367	7.354	8.056	8.044
35	-------	--------	7.337	7.281	6.579	6.548	6.391	6.363	6.546	6.529	6.935	6.920	7.503	7.489	8.216	8.203
40	9.239	9.158	7.377	7.320	6.629	6.597	6.453	6.424	6.622	6.605	7.027	7.011	7.612	7.597	8.345	8.332
50	9.287	9.204	7.438	7.380	6.705	6.671	6.547	6.517	6.737	6.719	7.166	7.149	7.777	7.761	8.538	8.524
70	-------	--------	7.515	7.456	6.802	6.766	6.666	6.635	6.882	6.863	7.340	7.322	7.984	7.967	8.782	8.767
100	9.401	9.312	7.580	7.519	6.882	6.845	6.765	6.733	7.001	6.981	7.484	7.465	8.155	8.137	8.983	8.907
150	-------	--------	7.634	7.572	6.950	6.912	6.848	6.815	7.102	7.082	7.604	7.584	8.298	8.279	9.150	9.134
200	-------	--------	7.663	7.600	6.985	6.946	6.891	6.858	7.155	7.134	7.668	7.648	8.373	8.353	9.238	9.221
500	-------	--------	7.719	7.655	7.053	7.013	6.974	6.940	7.255	7.234	7.788	7.767	8.515	8.494	9.405	9.387
∞	9.545	[a] 9.448	7.757	[a] 7.692	7.101	7.059	7.032	6.997	7.326	[a] 7.304	7.872	7.850	8.615	[a] 8.593	-------	-------

Kb/D	1.2		1.3		1.4		1.5		1.6		1.8		2.0	
	(a)	(b)	(a)	(b)	(a)	(b)	(a)	(b)	(a)	(b)	(a)	(b)	(a)	(b)
0	4. 134	[a] 4. 134	4. 282	[a] 4. 282	4. 470	[a] 4. 470	4. 694	[a] 4. 694	4. 951	[a] 4. 951	5. 549	[a] 5. 549	6. 250	[a] 6. 250
0.5	4. 414	4. 414	4. 610	4. 610	4. 850	4. 850	5. 131	5. 131	5. 447	5. 447	6. 176	6. 176	7. 025	7. 025
1	4. 671	4. 670	4. 911	4. 911	5. 199	5. 199	5. 530	5. 530	5. 901	5. 901	6. 751	6. 751	7. 733	7. 732
1.5	4. 908	4. 906	5. 188	5. 187	5. 520	5. 520	5. 898	5. 897	6. 320	6. 320	7. 279	7. 278	8. 384	8. 383
2	5. 126	5. 121	5. 444	5. 443	5. 816	5. 816	6. 237	6. 236	6. 705	6. 704	7. 765	7. 764	8. 984	8. 983
3	5. 518	5. 516	5. 901	5. 899	6. 345	6. 344	6. 843	6. 842	7. 392	7. 391	8. 632	8. 631	10. 051	10. 050
4	5. 858	5. 855	6. 298	6. 296	6. 803	6. 802	7. 366	7. 365	7. 980	7. 984	9. 380	9. 378	----	----
5	6. 155	6. 151	6. 645	6. 643	7. 203	7. 202	7. 824	7. 822	8. 504	8. 502	----	----	----	----
6	6. 418	6. 414	6. 951	[a] 6. 948	7. 555	7. 553	8. 226	8. 224	8. 961	8. 959	10. 607	[a] 10. 605	----	----
7	6. 651	6. 646	7. 222	7. 219	7. 865	7. 863	8. 584	8. 582	9. 366	9. 364	----	----	----	----
8	6. 860	6. 855	7. 465	7. 461	8. 147	8. 144	8. 903	8. 900	----	----	----	----	----	----
10	7. 218	7. 212	7. 881	7. 877	8. 626	8. 623	9. 448	9. 444	----	----	----	----	----	----
12	7. 513	7. 507	8. 224	8. 220	9. 020	9. 017	9. 897	9. 893	----	----	----	----	----	----
16	7. 972	7. 965	8. 755	8. 750	9. 630	9. 626	----	----	----	----	----	----	----	----
20	8. 311	8. 303	9. 148	[a] 9. 143	----	----	----	----	----	----	----	----	----	----
25	8. 628	8. 619	9. 515	9. 509	----	----	----	----	----	----	----	----	----	----
30	8. 868	8. 859	9. 791	9. 785	----	----	----	----	----	----	----	----	----	----
35	9. 055	9. 046	----	----	----	----	----	----	----	----	----	----	----	----
40	9. 205	9. 195	----	----	----	----	----	----	----	----	----	----	----	----
50	9. 430	9. 420	----	----	----	----	----	----	----	----	----	----	----	----
70	9. 709	9. 698	----	----	----	----	----	----	----	----	----	----	----	----

[a] Values obtained from exact solution of differential equation.

308-337 O—70——9

TABLE 4.79.—*Eigenfunction Parameters for a Beam With*

ξ	$m, n=1$				$m, n=2$				$m, n=3$		
	ϵ_1	A_1	$-B_1$	ϕ_1	ϵ_2	A_2	$-B_2$	ϕ_2	ϵ_3	$A_3=-B_3$	ϕ_3
0	3. 1416	0	0	9. 8697	6. 2832	0	0	39. 479	9. 4248	0	88. 827
0.25	3. 2166	. 0375	. 0346	9. 8710	6. 3220	. 0194	. 0195	39. 482	9. 4909	. 0131	88. 827
0.5	3. 2836	. 0711	. 0668	9. 8750	6. 3588	. 0378	. 0380	39. 485	9. 4762	. 0257	88. 830
0.75	3. 3440	. 1015	. 0946	9. 8806	6. 3939	. 0554	. 0556	39. 495	9. 5007	. 0380	88. 833
1	3. 3988	. 1293	. 1210	9. 8880	6. 4273	. 0722	. 0724	39. 505	9. 5245	. 0499	88. 839
1.5	3. 4949	. 1785	. 1680	9. 9074	6. 4896	. 1036	. 1039	39. 534	9. 5699	. 0727	88. 853
2	3. 5768	. 2211	. 2091	9. 9320	6. 5466	. 1325	. 1328	39. 572	9. 6127	. 0942	88. 874
2.5	3. 6477	. 2586	. 2454	9. 9604	6. 5989	. 1592	. 1596	39. 614	9. 6531	. 1146	88. 901
3	3. 7097	. 2919	. 2780	9. 9908	6. 6472	. 1840	. 1845	39. 652	9. 6913	. 1340	88. 934
3.5	3. 7646	. 3220	. 3074	10. 023	6. 6918	. 2072	. 2077	39. 718	9. 7274	. 1525	88. 971
4	3. 8135	. 3492	. 3341	10. 057	6. 7332	. 2289	. 2294	39. 775	9. 7617	. 1700	89. 022
5	3. 8974	. 3970	. 3812	10. 126	6. 8077	. 2684	. 2690	39. 900	9. 8250	. 2028	89. 108
6	3. 9666	. 4376	. 4214	10. 196	6. 8728	. 3037	. 3043	40. 028	9. 8824	. 2329	89. 218
7	4. 0250	. 4729	. 4563	10. 265	6. 9303	. 3353	. 3360	40. 162	9. 9345	. 2605	89. 257
8	4. 0748	. 5037	. 4869	10. 332	6. 9814	. 3640	. 3647	40. 297	9. 9821	. 2861	89. 466
10	4. 1557	. 5555	. 5383	10. 459	7. 0683	. 4140	. 4147	40. 564	10. 066	. 3322	89. 729
12	4. 2185	. 5973	. 5800	10. 573	7. 1394	. 4563	. 4570	40. 819	10. 137	. 3718	90. 021
15	4. 2905	. 6472	. 6297	10. 726	7. 2248	. 5090	. 5097	41. 176	10. 225	. 4231	90. 447
20	4. 3737	. 7080	. 6904	10. 932	7. 3293	. 5766	. 5774	41. 695	10. 339	. 4917	91. 123
25	4. 4304	. 7514	. 7337	11. 095	7. 4040	. 6275	. 6283	42. 097	10. 423	. 5453	91. 735
30	4. 4714	. 7840	. 7663	11. 223	7. 4601	. 6673	. 6681	42. 486	10. 489	. 5885	92. 358
45	4. 5467	. 8467	. 8289	11. 487	7. 5673	. 7477	. 7485	43. 268	10. 618	. 6794	93. 539
60	4. 5880	. 8828	. 8650	11. 648	7. 6286	. 7966	. 7974	43. 775	10. 695	. 7372	94. 418
80	4. 6208	. 9124	. 8946	11. 785	7. 6735	. 8460	. 8467	44. 185	10. 760	. 7880	95. 233
100	4. 6413	. 9313	. 9135	11. 875	7. 7103	. 8657	. 8665	44. 523	10. 801	. 8224	95. 802
150	4. 6697	. 9582	. 9404	12. 005	7. 7550	. 9056	. 9064	44. 970	10. 861	. 8735	96. 671
200	4. 6843	. 9723	. 9544	12. 074	7. 7784	. 9271	. 9279	45. 214	10. 892	. 9184	97. 092
300	4. 6992	. 9869	. 9691	12. 146	7. 8025	. 9498	. 9506	45. 475	10. 925	. 9320	97. 693
500	4. 7114	. 9990	. 9812	12. 207	7. 8224	. 9689	. 9697	45. 696	10. 953	. 9581	98. 152
1000	4. 7207	1. 0083	. 9905	12. 254	7. 8377	. 9838	. 9846	45. 870	10. 974	. 9785	98. 515
∞	4. 7300	1. 0178	1. 0000	12. 302	7. 8532	. 9992	1. 0000	46. 050	10. 996	1. 000	98. 905

nowhere differs from the series solution by more than 0.7 percent. It must be noted from equations (4.81) and (4.85) that choosing equal values of ξ_a and ξ_b does *not* give equal slope restraint along all edges except for the case of the square.

The case of uniform slope restraint and $W=0$ along all edges was studied by Bolotin et al. (ref. 4.60), who used a variation of the series method to obtain frequencies for the first 10 modes of a square having variable restraint. These results are shown in figure 4.61. Results for this problem were also presented in reference 4.129 for the case of the square by using the same procedure as in reference 4.128. These are shown in figure 4.62.

In reference 4.130, the problem is also solved by using the Rayleigh-Ritz method and algebraic polynomials.

In reference 4.131, the typical electronic chassis which is formed by bending the edges of a plate down is treated as a plate with elastic edge supports. An eigenfunction is used to solve the problem which is an average of the eigenfunctions for plates with simply supported edges and those having clamped edges. The Rayleigh-Ritz method is employed. Theoretical and experimental results are obtained for particular chassis.

Ends Elastically Restrained Against Rotation

$m, n=4$			$m, n=5$			$m, n=6$		
ϵ_4	$A_4=-B_4$	ϕ_4	ϵ_5	$A_5=-B_5$	ϕ_5	ϵ_6	$A_6=-B_6$	ϕ_6
12. 566	0	157. 91	15. 708	0	246. 74	18. 850	0	355. 31
12. 566	. 0098	157. 92	15. 724	. 0079	246. 74	18. 863	. 0066	355. 31
12. 605	. 0194	157. 92	15. 739	. 0156	246. 74	18. 876	. 0131	355. 31
12. 624	. 0288	157. 92	15. 755	. 0232	246. 74	18. 889	. 0195	355. 31
12. 642	. 0380	157. 92	15. 769	. 0307	246. 74	18. 901	. 0258	355. 31
12. 678	. 0558	157. 93	15. 799	. 0454	246. 75	18. 926	. 0381	355. 32
12. 712	. 0729	157. 94	15. 827	. 0594	246. 76	18. 950	. 0501	355. 32
12. 745	. 0893	157. 96	15. 854	. 0731	246. 78	18. 973	. 0618	355. 34
12. 776	. 1051	157. 99	15. 880	. 0863	246. 79	18. 996	. 0732	355. 34
12. 806	. 1202	158. 01	15. 906	. 0991	246. 82	19. 018	. 0842	355. 36
12. 834	. 1348	158. 04	15. 930	. 1115	246. 83	19. 039	. 0951	355. 38
12. 889	. 1625	158. 12	15. 977	. 1353	246. 89	19. 080	. 1158	355. 42
12. 939	. 1882	158. 21	16. 021	. 1577	246. 96	19. 119	. 1356	355. 48
12. 985	. 2123	158. 31	16. 062	. 1788	247. 05	19. 156	. 1545	355. 55
13. 028	. 2349	158. 42	16. 101	. 1990	247. 14	19. 191	. 1724	355. 63
13. 105	. 2762	158. 84	16. 172	. 2362	247. 36	19. 256	. 2061	355. 81
13. 173	. 3129	158. 94	16. 235	. 2698	247. 61	19. 315	. 2370	356. 04
13. 260	. 3613	159. 38	16. 318	. 3149	248. 02	19. 394	. 2789	356. 41
13. 375	. 4278	160. 12	16. 431	. 3783	248. 77	19. 503	. 3393	357. 15
13. 464	. 4814	160. 84	16. 521	. 4307	249. 54	19. 592	. 3895	357. 91
13. 534	. 5257	161. 51	16. 595	. 4748	250. 28	19. 666	. 4327	358. 68
13. 679	. 6219	163. 17	16. 749	. 5733	252. 25	19. 827	. 5316	360. 86
13. 768	. 6854	164. 41	16. 847	. 6404	253. 80	19. 932	. 6008	362. 68
13. 844	. 7428	165. 62	16. 933	. 7026	255. 38	20. 025	. 6664	364. 61
13. 894	. 7825	166. 48	16. 990	. 7464	256. 55	20. 089	. 7134	366. 08
13. 967	. 8430	167. 85	17. 075	. 8145	258. 47	20. 184	. 7880	368. 55
14. 007	. 8771	168. 65	17. 121	. 8538	259. 10	20. 237	. 8317	370. 07
14. 048	. 9144	169. 53	17. 171	. 8973	260. 89	20. 294	. 8808	371. 84
14. 082	. 9476	170. 29	17. 212	. 9356	262. 04	20. 342	. 9248	373. 40
14. 109	. 9726	170. 92	17. 254	. 9667	262. 98	20. 380	. 9608	374. 71
14. 137	1. 0000	171. 59	17. 279	1. 0000	264. 00	20. 240	1. 0000	376. 15

Hoppmann and Greenspon (ref. 4.132) presented a method for experimentally simulating elastic edge supports by means of sharp V-grooves machined along the edges of a clamped plate, the degree of slope restraint being determined by the depth of the grooves. A curve showing the frequency parameter for a clamped square plate as a function of the notch ratio R is shown in figure 4.63; R is the ratio of the depth of the notch to the thickness of the plate. Experimentally determined points are shown as circles. The curve was drawn through endpoints determined by the theoretical results of Iguchi (ref. 4.9) and fitted to the four experimental points.

4.4.2 Discontinuous Edge Conditions

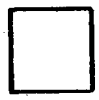
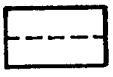
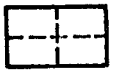
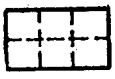
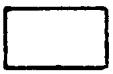
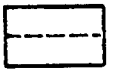
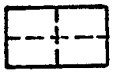
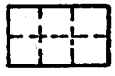
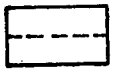
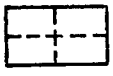
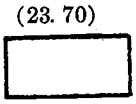
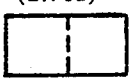
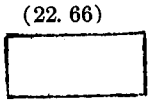
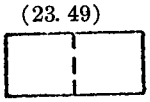
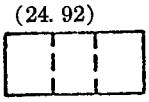
Some interesting results are available for the case of a square plate which is simply supported but clamped along segments of its edges.

Consider first the square which is clamped along four symmetrically located segments of length l_1, and simply supported along the remainder of the boundary as in figure 4.64. Ota and Hamada (refs. 4.133 and 4.134) solved the problem by assuming a deflection function which satisfies the simply supported boundary conditions everywhere (eq. (4.19)), and applying distributed edge moments of the type, for example,

$$(M_y)_{y=0}=\left(\sum_{m=1}^{m^*} K_m \sin m\pi x\right)\cos \omega t \quad (4.89)$$

TABLE 4.80.—*Frequency Parameters* $\omega b^2\sqrt{\rho/D}$ *and Approximate Nodal Patterns for a Rectangular Plate Elastically Restrained Against Rotation Along All Edges*

[Values in parentheses are found from eq. (4.87)]

b/a	ξ	$\omega b^2\sqrt{\rho/D}$ for mode—					
		1	2	3	4	5	6
1.0	0	19. 74	49. 35	78. 96	98. 70	98. 70	128. 3
	20	31. 09	64. 31	95. 85	117. 3	116. 8	147. 6
		(31. 16)	(64. 52)	(96. 17)	(117. 8)	(116. 9)	(148. 0)
	∞	35. 99	73. 41	108. 3	131. 6	132. 3	165. 2
		(36. 11)	(73. 74)	(108. 9)	(131. 7)	(132. 4)	(165. 4)
							
0.9	0	17. 86	41. 85	47. 47	71. 46	81. 82	111. 4
	20	28. 21	54. 57	61. 97	86. 85	97. 03	123. 0
		(28. 28)	(54. 77)	(62. 17)	(87. 15)	(97. 34)	(123. 3)
	∞	32. 67	62. 29	70. 76	98. 14	109. 4	143. 5
		(32. 78)	(62. 71)	(71. 06)	(98. 66)	(109. 8)	(144. 1)
							
0.8	0	16. 19	35. 14	45. 79	64. 74	66. 72	96. 33
	20	25. 80	46. 02	59. 98	79. 06	79. 24	111. 2
		(25. 86)	(46. 17)	(60. 16)	(79. 32)	(79. 50)	(111. 5)
	∞	29. 08	52. 52	68. 52	89. 40	89. 29	124. 5
		(29. 18)	(52. 76)	(68. 80)	(89. 86)	(89. 69)	(125. 0)
							
0.6	0	13. 42	24. 08	41. 85	43. 03	53. 69	
	20	22. 30	32. 58	50. 48	56. 97	66. 96	
		(22. 34)	(32. 68)	(50. 63)	(57. 11)	(67. 17)	
	∞	25. 90	37. 28	56. 93	65. 18	75. 94	
		(25. 97)	(37. 43)	(57. 20)	(65. 39)	(76. 31)	
							
0.4	0	11. 45	16. 19	24. 08			
	20	20. 30	24. 15	31. 20			
		(20. 33)	(24. 20)	(31. 26)			
	∞	23. 65	27. 81	35. 45			
		(23. 70)	(27. 91)	(35. 56)			
							
0.2	0	10. 26	11. 45	13. 42			
	20	19. 38	20. 15	21. 52			
		(19. 39)	(20. 17)	(21. 54)			
	∞	22. 64	23. 45	24. 89			
		(22. 66)	(23. 49)	(24. 92)			
							

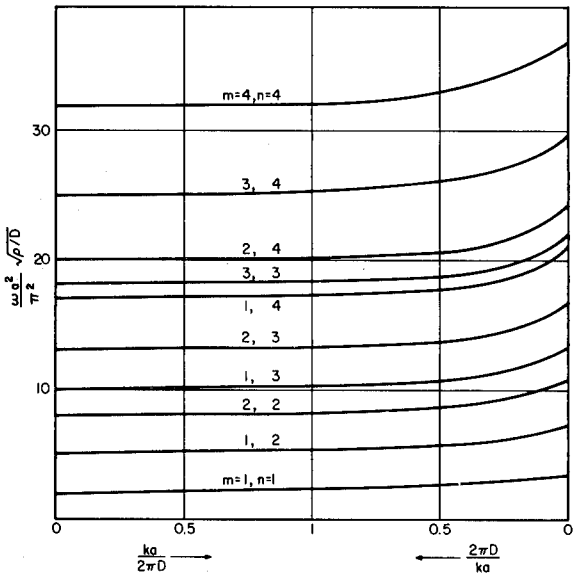


FIGURE 4.61.—Frequency parameters for a square plate having uniform slope restraint along all edges derived by Bolotin (ref. 4.60)

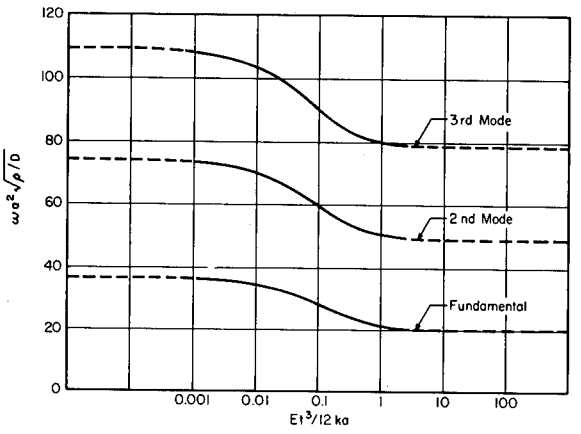


FIGURE 4.62.—Frequency parameters for a square plate having uniform slope restraint along all edges derived by procedure of reference 4.128. (After ref. 4.129)

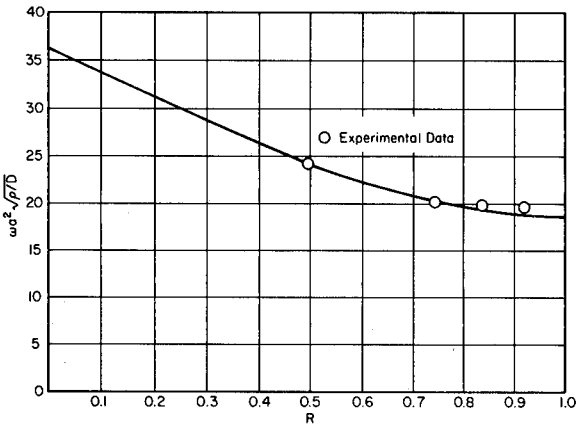


FIGURE 4.63.—Variation in frequency parameter with notch ratio for a square plate. (After ref. 4.132)

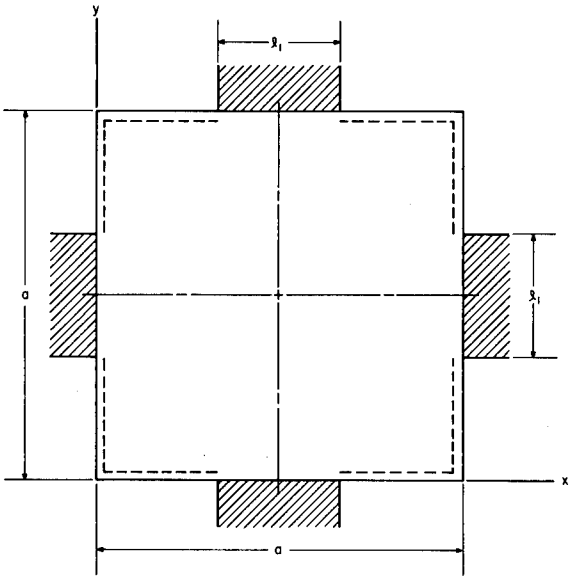


FIGURE 4.64.—SS–SS–SS–SS square plate clamped along four symmetrically located segments.

The coefficients K_m are then chosen for each edge such that the normal moments are zero along the simply supported segments and the normal slopes are zero along the clamped segments. These conditions, along with the principle of stationary total energy, are used to formulate a characteristic determinant for the problem, the roots of which yield the vibration frequencies. The accuracy of the results depends upon the number of terms kept in the summations and, hence, the orders of the characteristic determinants used. The problem was solved at essentially the same time by Kurata and Okamura (ref. 4.135), who used a very similar method.

Fundamental frequency parameters for several values of l_1 are shown in figure 4.65 (ref. 4.133) and tabulated in table 4.81. Experimental data shown in figure 4.65 were obtained on mild steel plates having edge

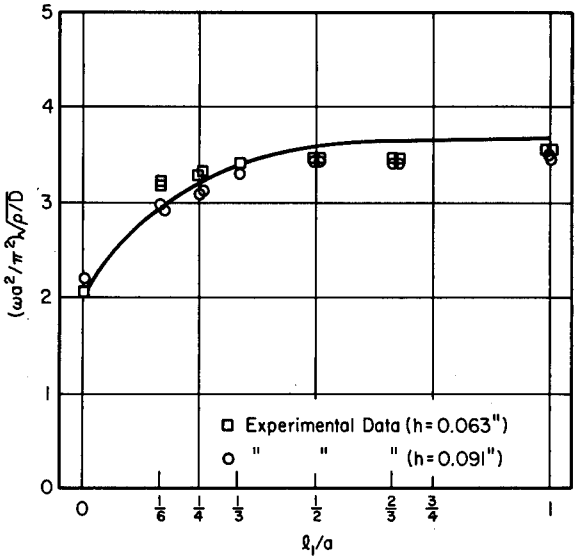


FIGURE 4.65.—Frequency parameters for SS–SS–SS–SS square plate clamped along four symmetrically located segments. (After ref. 4.133)

lengths of 6.50 inches and thicknesses of 0.063 and 0.091 inch.

Experimental frequencies and nodal patterns for the first three modes for an aluminum plate 11.8 inches long, 0.012 inch thick, and having $l_1/a=⅓$ were obtained in reference 4.135 and are presented as table 4.82.

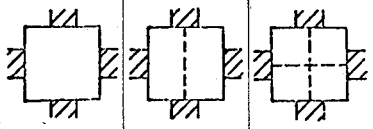
The cases when only two opposite edges have symmetrically located clamped segments as shown in figure 4.66 were also studied in references 4.133 and 4.135. Fundamental frequency parameters for several values of l_2 are shown in figure 4.67 (ref. 4.133) and tabulated in table 4.83. Additional experimental frequencies are given in table 4.84 (ref. 4.135) for $l_2/a=⅓$. Experimental results shown in figure 4.67 and table 4.84 were obtained on the same plates described earlier in this section.

The case when two unsymmetrically located segments of opposite edges are clamped is shown in figure 4.68 and was discussed in reference 4.133. Fundamental frequency parameters for several values of l_3 are shown in figure 4.69 and tabulated in table 4.85. Ex-

TABLE 4.81.—*Fundamental Frequency Parameters* $\omega a^2\sqrt{\rho/D}$ *for a Simply Supported Square Plate Clamped Along 4 Symmetrically Located Segments,* $\nu=0.3$

Source	$\omega a^2\sqrt{\rho/D}$ for values of l_1/a of—			
	0	⅓	½	1
Ref. 4.133	19.74	33.9	35.5	35.98
Ref. 4.135	19.74	33.97	----------	35.98

TABLE 4.82.—*Experimental Cyclic Frequencies and Nodal Patterns for a Simply Supported Square Plate Clamped Along 4 Symmetrically Located Segments*

Nodal pattern			
Frequency, cps	280	535	725

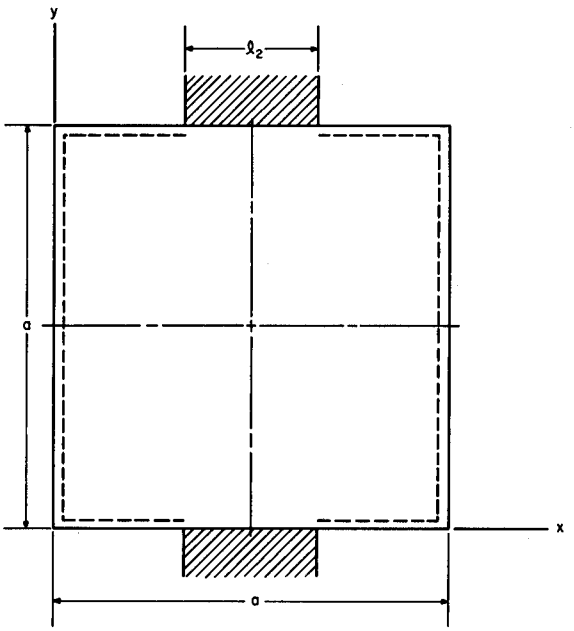


FIGURE 4.66.—SS–SS–SS–SS square plate clamped along two symmetrically located segments of opposite edges.

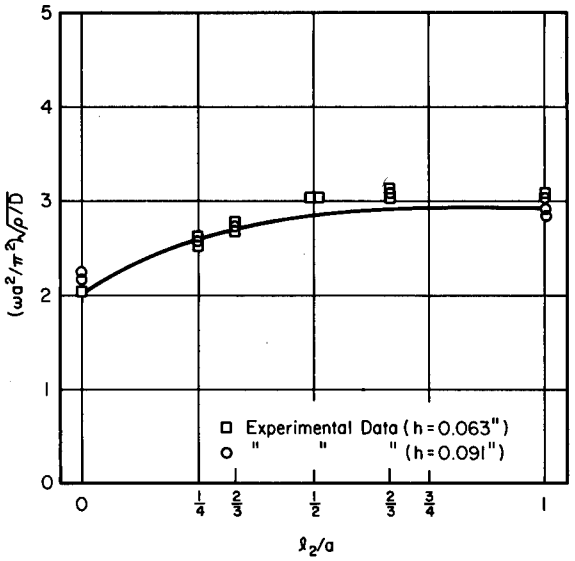


FIGURE 4.67.—Frequency parameters for SS–SS–SS–SS square plate clamped along two symmetrically located segments of opposite edges. (After ref. 4.133)

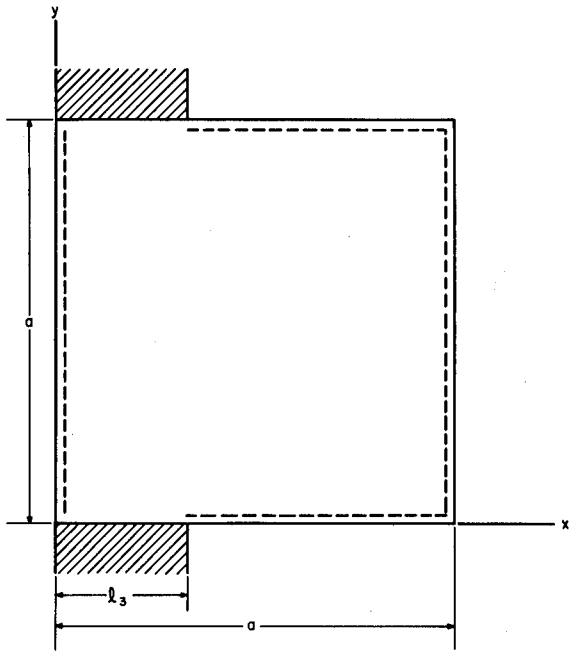


FIGURE 4.68.—SS–SS–SS–SS square plate clamped along two unsymmetrically located segments of opposite edges.

perimental data shown in figure 4.69 were obtained on the plates described earlier in this section.

The case when one symmetrically located segment of an edge is clamped is shown in figure 4.70. The numerical solution to this problem was obtained in reference 4.133 and is given in figure 4.71 and table 4.86. Experimental frequencies and approximate nodal pat-

TABLE 4.83.—*Fundamental Frequency Parameters* $\omega a^2\sqrt{\rho/D}$ *for a Simply Supported Square Plate Clamped Along 2 Symmetrically Located Segments of Opposite Edges,* $\nu=0.3$

Source	$\omega a^2\sqrt{\rho/D}$ for values of l_2/a of—				
	0	1/3	1/2	2/3	1
Ref. 4.133	19. 74	27. 1	28. 3	28. 8	28. 95
Ref. 4.135	19. 74	27. 31			

TABLE 4.84.—*Experimental Cyclic Frequencies and Nodal Patterns for a Simply Supported Square Plate Clamped Along 2 Symmetrically Located Segments of Opposite Edges*

Nodal pattern						
Frequency, cps	225	420	500	660	785	955

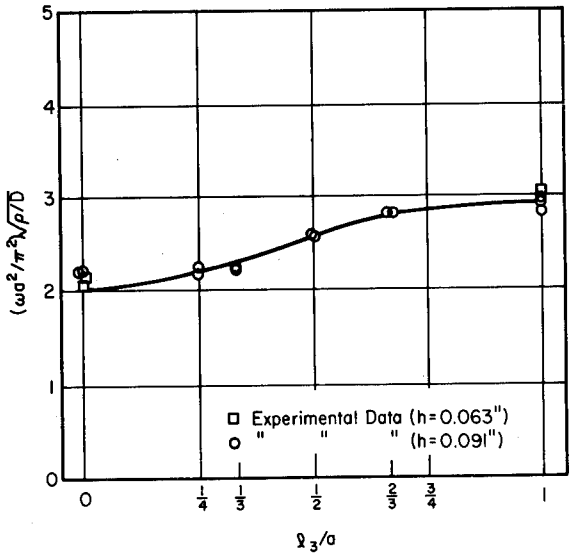


FIGURE 4.69.—Frequency parameters for SS–SS–SS–SS square plate clamped along two unsymmetrically located segments of opposite edges. (After ref. 4.133)

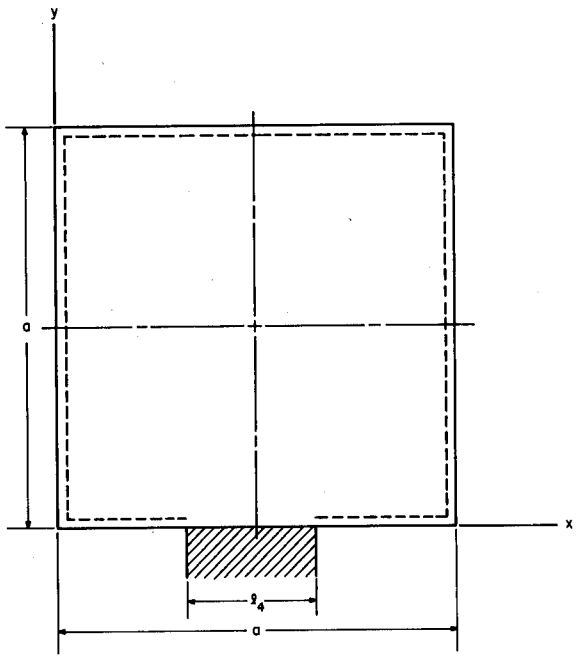


FIGURE 4.70.—SS–SS–SS–SS square plate clamped along one symmetrically located segment of an edge.

terns obtained in reference 4.135 are given in table 4.87 for $l_4/a = \frac{1}{3}$. Experimental results shown in figure 4.71 and table 4.87 were ob-

TABLE 4.85.—*Fundamental Frequency Parameters for a Simply Supported Square Plate Clamped Along 2 Unsymmetrically Located Segments of Opposite Edges;* $\nu = 0.3$

l_3/a	0	⅓	½	⅔	1
$\omega a^2\sqrt{\rho/D}$	19.74	22.2	25.5	27.8	28.95

TABLE 4.86.—*Fundamental Frequency Parameters for a Simply Supported Square Plate Clamped Along 1 Symmetrically Located Segment of an Edge;* $\nu = 0.3$

l_4/a	0	⅓	½	⅔	1
$\omega a^2\sqrt{\rho/D}$	19.74	23.0	23.4	23.6	23.65

tained on the same plates as those described earlier in this section.

The case when the plate is clamped along one segment at the end of one edge is shown in figure 4.72. Nowacki (refs. 4.136 and 4.137) expressed a unit moment acting at a point along the clamped interval in terms of a trigo-

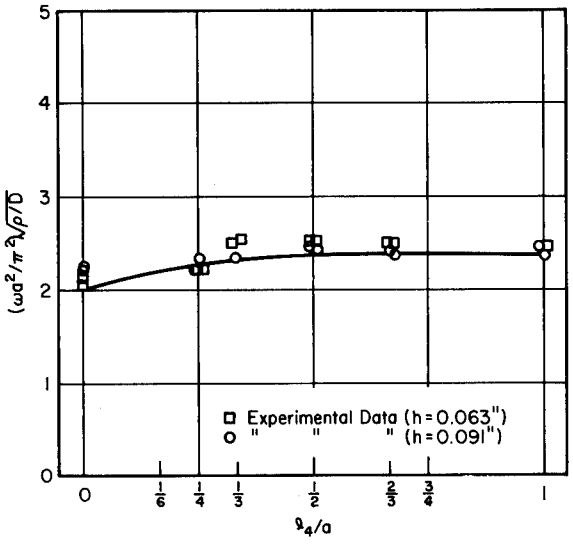


FIGURE 4.71.—Frequency parameters for SS–SS–SS–SS square plate clamped along one symmetrically located segment of an edge. (After ref. 4.133)

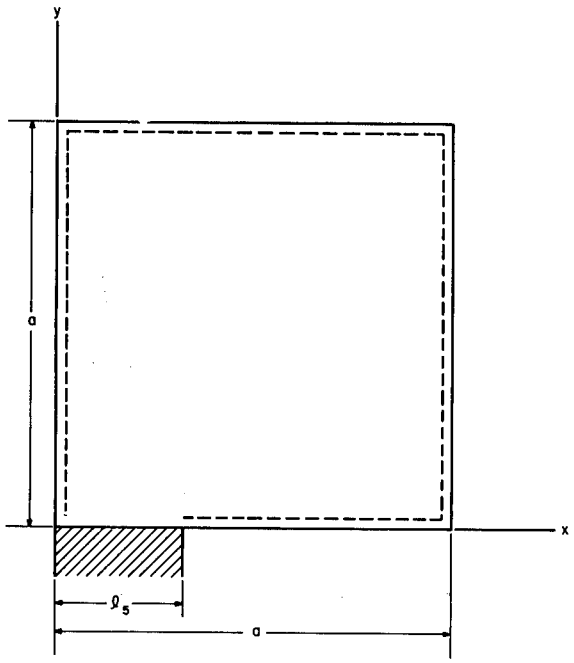


FIGURE 4.72.—SS–SS–SS–SS square plate clamped along one segment at the end of an edge.

nometric series and formulated an integral equation involving a Green's function along the clamped interval. The integral equation was replaced by a finite summation carried out over discrete segments of the interval, which resulted in a system of equations, each term of which is an infinite series of transcendental functions containing the eigenvalues. Truncating the series and solving the resulting characteristic determinant yielded the vibration frequencies.

Numerical results from reference 4.133 are given in figure 4.73. Data from references 4.133 and 4.136 are also given in table 4.88. By looking at the results of reference 4.136 in table 4.88, it is seen that they are clearly inaccurate, the frequency parameter listed for the case when $l_5/a=\frac{1}{2}$ being greater than the well-known result for the case when $l_5/a=1$ (see discussion on SS–C–SS–SS plate, sec. 4.2.2).

The solution is also given in reference 4.136 for the case when the interval $0<x<l_5$ is clamped along the edge $y=0$ (fig. 4.72), the interval $l_5<x<a$ is free, and the remaining edges are simply supported. It was found for $l_5/a=\frac{1}{2}$ that $\omega a^2\sqrt{\rho/D}=14.8$.

The case obtained when the simply supported portions of the edges of the plate shown in figure 4.72 are replaced by clamped edge conditions and the remaining portion has zero slope and shear is included in reference 4.138.

TABLE 4.87.—*Experimental Cyclic Frequencies and Nodal Patterns for a Simply Supported Square Plate Clamped Along 1 Symmetrically Located Segment of an Edge*

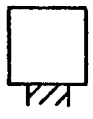
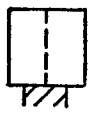
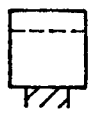
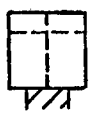
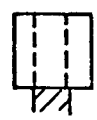
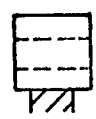
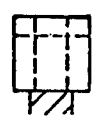
Nodal pattern							
Frequency, cps	200	425	480	680	835	900	1000

TABLE 4.88.—*Frequency Parameters* $\omega a^2\sqrt{\rho/D}$ *for a Simply Supported Square Plate Clamped Along 1 Segment at the End of an Edge*

Source	$\omega a^2\sqrt{\rho/D}$ for values of l_5/a of—					
	0	⅙	⅓	½	⅔	1
Ref. 133	19. 74	----------	21. 1	22. 4	23. 3	23. 65
Ref. 136	----------	21. 0	23. 2	23. 8	----------	----------

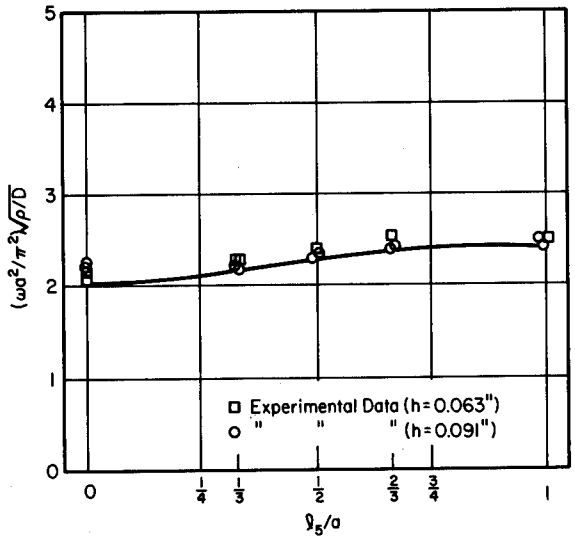


FIGURE 4.73.—Frequency parameters for SS–SS–SS–SS square plate clamped along one segment at the end of an edge. (After ref. 4.133)

The necessary integral equations are completely formulated but no numerical results are obtained.

4.4.3 Point Supports

Throughout this section the term "point support" will be used to denote a constraint of zero deflection at a point. Unless otherwise stated, there will be no constraint on the slopes at such points.

Consider first the problem of the rectangular plate free along all edges and supported at the four corner points (fig. 4.74). Cox and Boxer (ref. 4.139) solved the problem by means of finite difference equations. Fundamental frequencies for $a/b=1$, 1.5, 2, and 3 for $\nu=0.3$ are listed in table 4.89 and plotted in figure 4.75. The mesh widths Δa and Δb

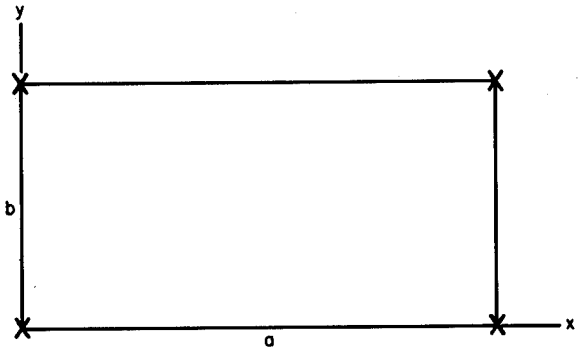


FIGURE 4.74.—Free rectangular plate point supported at the four corners.

are shown in figure 4.76. The extrapolated values of table 4.89 were obtained from the extrapolation formula

$$\lambda_e^2=\frac{(6\lambda_6)^2-(4\lambda_4)^2}{(6)^2-(4)^2} \tag{4.90}$$

where $\lambda\equiv\omega a^2\sqrt{\rho/D}$ and the subscripts 4 and 6 identify the two meshes used.

The mode shapes $W(x,y)$ corresponding to the fundamental frequencies are given in table 4.90, where the grid locations are those shown in figure 4.76.

Higher frequencies for the square supported at the corners were also given in reference 4.139. These are listed in table 4.91 for two mesh widths. Extrapolated values using equation (4.90) are also given.

Mode shapes corresponding to these frequencies are shown in figure 4.77, and the amplitudes of $W(x, y)$ at the grid locations shown in figure 4.78 are listed in table 4.92 for $\nu=0.3$. Two independent mode shapes corresponding to the second frequency were found. They are identified as $2a$ and $2b$. As can be seen from figure

TABLE 4.89.—*Frequency Parameters* $\omega a^2\sqrt{\rho/D}$ *for a Free Rectangular Plate Point Supported at the 4 Corners;* $\nu=0.3$

Mesh width	$\omega a^2\sqrt{\rho/D}$ for values of a/b of—			
	1	1.5	2	3
$\Delta a=\Delta b=b/4$	6. 97939	8. 78632	9. 18688	9. 35971
$\Delta a=\Delta b=b/6$	7. 05598	8. 86492	9. 24590	9. 39803
	[a]7. 117	[a]8. 927	[a]9. 293	[a]9. 429

[a] Extrapolated value from eq. (4.90).

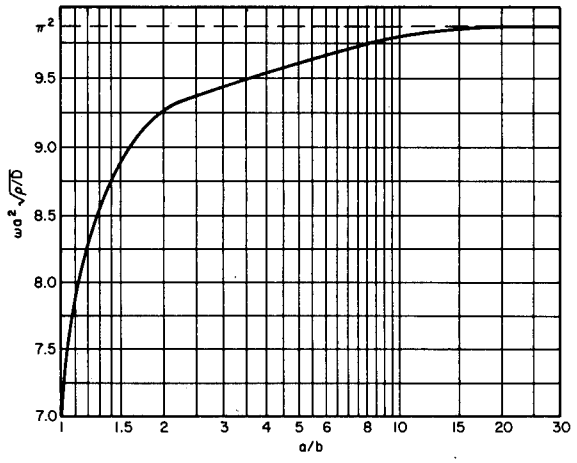


FIGURE 4.75.—Frequency parameters $\omega a^2\sqrt{\rho/D}$ for a free rectangular plate point supported at the four corners; $\nu=0.3$. (After ref. 4.139)

4.77, the third mode shape and frequency are identical to those of the fundamental mode of a completely free square plate (sec. 4.3.15).

Variation in the frequency parameter $\omega a^2\sqrt{\rho/D}$ with Poisson's ratio is shown in figure 4.79. However, it must be remembered that D depends upon ν. Substituting equation (1.2) for D into the frequency parameters permits the variation of the frequency itself with Poisson's ratio to be seen. This is shown in figure 4.80.

Nishimura (ref. 4.14) used the finite-difference method and a relatively coarse grid (characteristic determinants of order no larger than six) to obtain the first 10 frequencies and nodal patterns of a free square plate point supported at the four corners. He also obtained experimental results on a steel plate 10.1 by 10.1 inches by 0.087 inch. These results are shown in figure 4.81, with experimental values given in parentheses. It is noted that the third, sixth, and ninth mode shapes and frequencies also exist for the completely free square plate.

Reed (ref. 4.140) obtained extensive analytical and experimental results for the rectangular plate supported at its four corners. Analytical results were achieved by two methods—the Rayleigh-Ritz and series methods. The deflection function

$$W(x,y)=\sum_{n=1}\left(a_{0n}\sin\frac{n\pi y}{b}+b_{0n}\sin\frac{n\pi x}{a}\right)+\sum_{m=1}\sum_{n=1}\left(a_{mn}\cos\frac{m\pi x}{a}\sin\frac{n\pi y}{b}+b_{mn}\cos\frac{m\pi y}{b}\sin\frac{n\pi x}{a}\right) \quad (4.91)$$

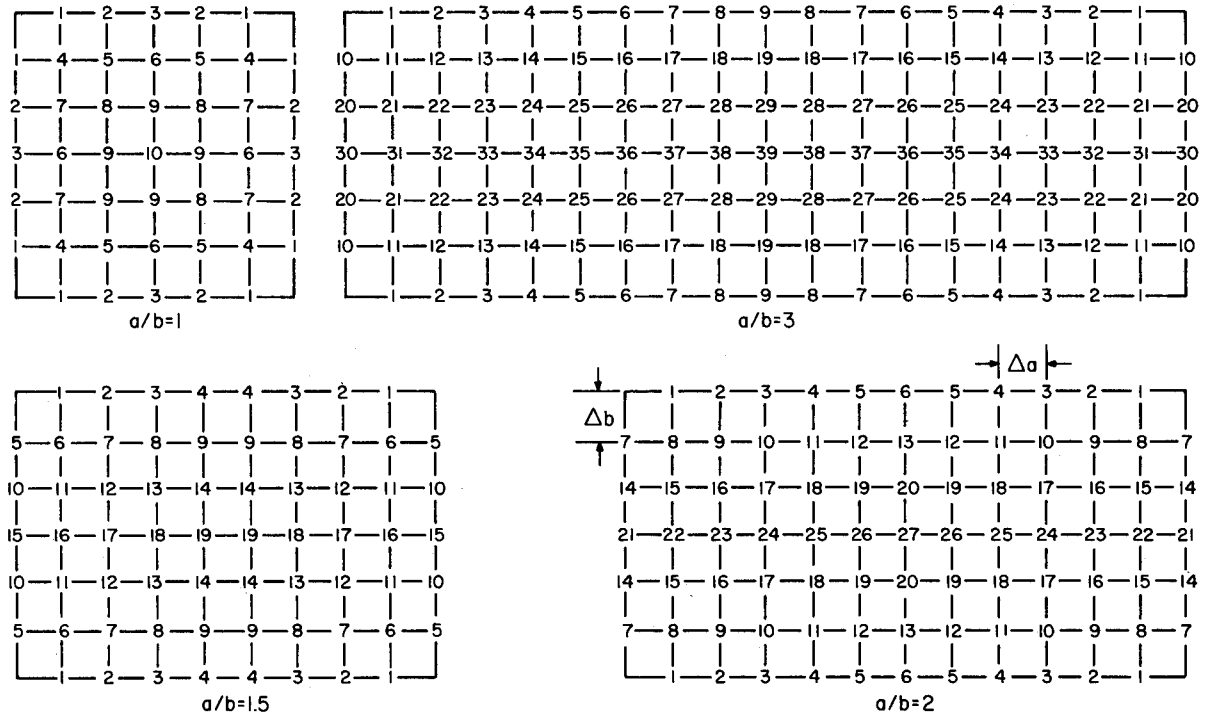


FIGURE 4.76.—Finite difference meshes. (After ref. 4.139)

TABLE 4.90.—*Fundamental Mode Shapes* W(x, y) *for Free Rectangular Plates Point Supported at the 4 Corners;* $\nu=0.3$

Grid location	$W(x, y)$ for values of a/b of—			
	1.0	1.5	2.0	3.0
1	0.34407	0.35177	0.26141	0.17474
2	.58825	.65713	.50327	.34364
3	.67600	.88141	.70970	.50168
4	.58026	1.0	.86743	.64423
5	.75981	.11297	.96631	.76711
6	.82616	.41240	1.0	.86668
7	.75981	.67951	.04188	.94000
8	.89905	.87885	.28042	.98489
9	.95183	.98513	.50445	1.0
10	1.0	.19186	.69753	.01135
11		.45973	.84592	.17900
12		.70293	.93928	.34210
13		.88653	.97113	.49540
14		.98502	.07094	.63408
15		.21992	.29562	.75387
16		.47731	.50849	.85106
17		.71244	.69315	.92268
18		.89066	.83569	.96655
19		.98649	.92561	.98132
20			.95632	.01919
21			.08124	.18251
22			.30131	.34197
23			.51040	.49228
24			.69218	.62855
25			.83274	.74642
26			.92148	.84216
27			.95181	.91275
28				.95600
29				.97057
30				.02196
31				.18384
32				.34205
33				.49135
34				.62681
35				.74403
36				.83927
37				.90952
38				.95257
39				.96707

was used with the Rayleigh-Ritz method. Poisson's ratio was taken to be 0.3. Frequency parameters, nodal patterns, and normalized mode shape coefficients are shown in table 4.93 for the first seven modes of plates having a/b ratios of 1.0, 1.5, 2.0, and 2.5.

The second analytical method in reference 4.140 used the series given in equation (4.21) as half of the solution, the other half being a similar series obtained by interchanging x and y. Frequency parameters obtained in keeping 24 terms of the series are listed in parentheses in table 4.93. In table 4.94 the theoretical cyclic

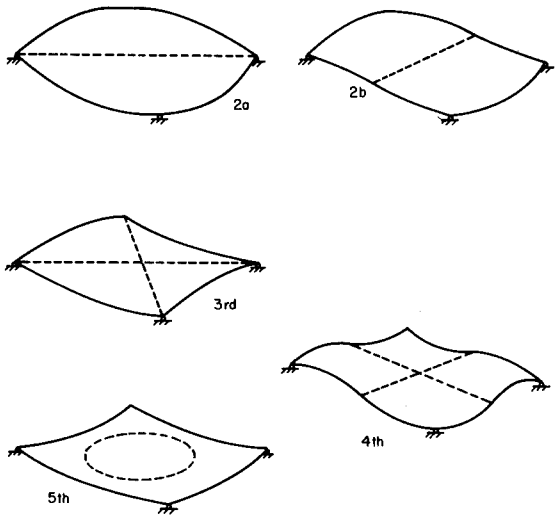


FIGURE 4.77.—Higher mode shapes for the free square plate point supported at the four corners. (After ref. 4.139)

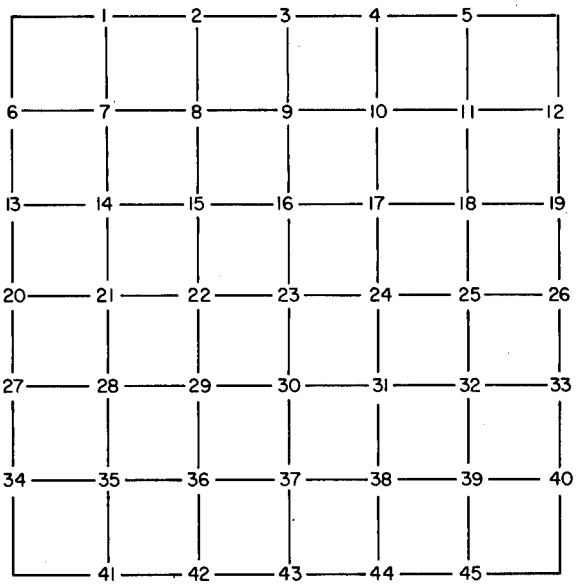


FIGURE 4.78.—General finite difference mesh for a square. (After ref. 4.139)

TABLE 4.91.—*Higher Frequency Parameters* $\omega a^2\sqrt{\rho/D}$ *for a Free Square Plate Point Supported at the 4 Corners;* $\nu=0.3$

Mesh width	$\omega a^2\sqrt{\rho/D}$ for mode—			
	2	3	4	5
$\Delta a=\Delta b=a/5$	15. 0541	16. 8311	35. 5951	38. 7292
$\Delta a=\Delta b=a/6$	15. 2650	17. 5659	36. 4827	40. 2638
	[a] 15. 73	[a] 19. 13	[a] 38. 42	[a] 43. 55

[a] Extrapolated values.

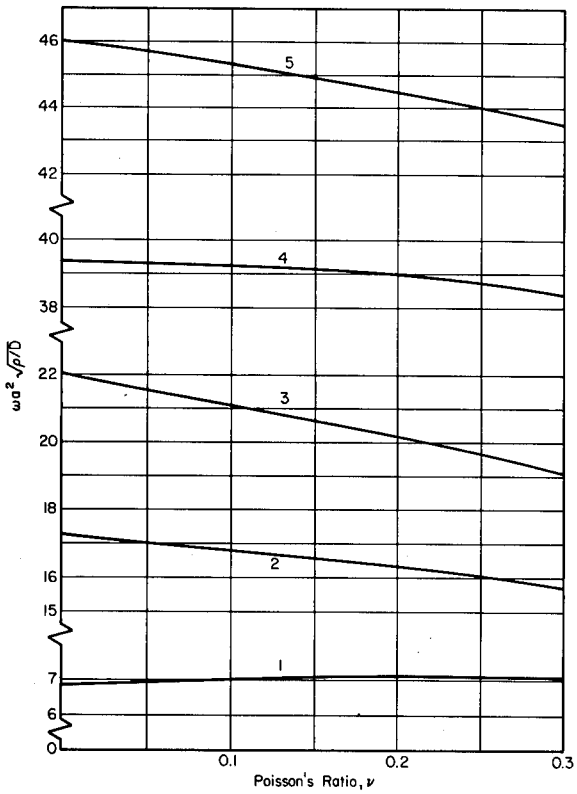


FIGURE 4.79.—Variation of frequency parameter with Poisson's ratio for a free square plate point supported at the four corners. (After ref. 4.139)

frequencies determined by the series method and by adapting the results of reference 4.139 are compared with experimental results obtained with two aluminum plates.

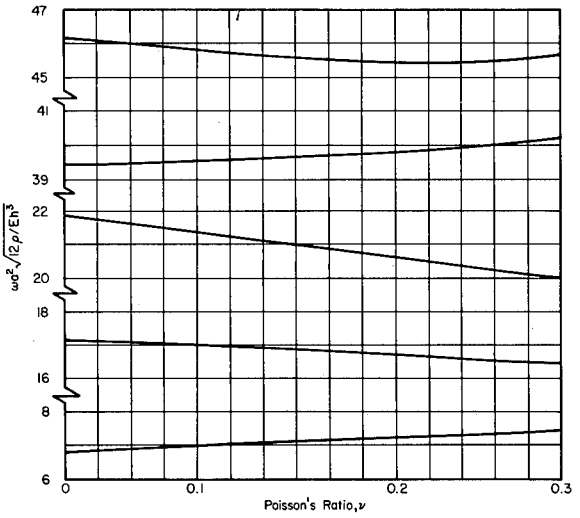


FIGURE 4.80.—Variation in the modified frequency parameter with Poisson's ratio for a free square plate point supported at the four corners. (After ref. 4.139)

Kirk (ref. 4.141) used the Rayleigh-Ritz method and a mode shape

$$W(x,y)=A\left(\sin\frac{\pi x}{a}+\sin\frac{\pi y}{b}\right)+(1-2A)\sin\frac{\pi x}{a}\sin\frac{\pi y}{b} \quad (4.92)$$

to obtain a fundamental frequency for the problem when $\nu=0.3$. Minimizing the Rayleigh quotient with respect to A yields $A=0.6956$ and $\omega a^2\sqrt{\rho/D}=7.224$.

The Rayleigh method and a mode shape of the form

$$W(x,y)=A\sin\frac{\pi x}{a}+B\sin\frac{\pi y}{b} \quad (4.93)$$

TABLE 4.92.—*Higher Mode Shapes* W(x, y) *for a Free Square Plate Point Supported at the 4 Corners;* $\nu=0.3$

Grid location	$W(x, y)$ for mode—				
	2*a*	2*b*	3	4	5
1	0. 42800	0. 50302	0. 48159	0. 82466	−0. 49310
2	. 79707	. 86736	. 85688	. 79791	−. 73475
3	1. 0	1. 0	1. 0	0	−. 78861
4	. 93765	. 86736	. 85688	−. 79791	−. 73475
5	. 57804	. 50302	. 48159	−. 82466	−. 49310
6	−. 42800	. 07502	−. 48159	. 82466	−. 49310
7	0	. 37920	0	1. 0	−. 35047
8	. 39652	. 60887	. 36362	. 73369	−. 13858
9	. 69381	. 69381	. 50055	0	−. 02813
10	. 82122	. 60887	. 36362	−. 73369	−. 13858
11	. 75841	. 37920	0	−1. 0	−. 35047
12	. 57804	. 07502	−. 48159	−. 82466	−. 49310
13	−. 79707	. 07029	−. 85688	. 79791	−. 73475
14	−. 39652	. 21235	−. 36362	. 73369	−. 13858
15	0	. 32296	0	. 47978	. 44086
16	. 36438	. 36438	. 13585	0	. 69261
17	. 64592	. 32296	0	−. 47978	. 44086
18	. 82122	. 21235	−. 36362	−. 73369	−. 13858
19	. 93765	. 07029	−. 85688	−. 79791	−. 73475
20	−1. 0	0	−1. 0	0	−. 78861
21	−. 69381	0	−. 50055	0	−. 02813
22	−. 36438	0	−. 13585	0	. 69261
23	0	0	0	0	1. 0
24	. 36438	0	−. 13585	0	. 69261
25	. 69381	0	−. 50055	0	−. 02813
26	1. 0	0	−1. 0	0	−. 78861
27	−. 93765	−. 07029	−. 85688	−. 79791	−. 73475
28	−. 82122	−. 21235	−. 36362	−. 73369	−. 13858
29	−. 64592	−. 32296	0	−. 47978	. 44086
30	−. 36438	−. 36438	. 13585	0	. 69261
31	0	−. 32296	0	. 47978	. 44086
32	. 39652	−. 21235	−. 36362	. 73369	−. 13858
33	. 79707	−. 07029	−. 85688	. 79791	−. 73475
34	−. 57804	−. 07502	−. 48159	−. 82466	−. 49310
35	−. 75841	−. 37920	0	−1. 0	−. 35047
36	−. 82122	−. 60887	. 36362	−. 73369	−. 13858
37	−. 69381	−. 69381	. 50055	0	−. 02813
38	−. 39652	−. 60887	. 36362	. 73369	−. 13858
39	0	−. 37920	0	1. 0	−. 35047
40	. 42800	−. 07502	−. 48159	. 82466	−. 49310
41	−. 57804	−. 50302	. 48159	−. 82466	−. 49310
42	−. 93765	−. 86736	. 85688	−. 79791	−. 73475
43	−1. 0	−1. 0	1. 0	0	−. 78861
44	−. 79707	−. 86736	. 85688	. 79791	−. 73475
45	−. 42800	−. 50302	. 48159	. 82466	−. 49310

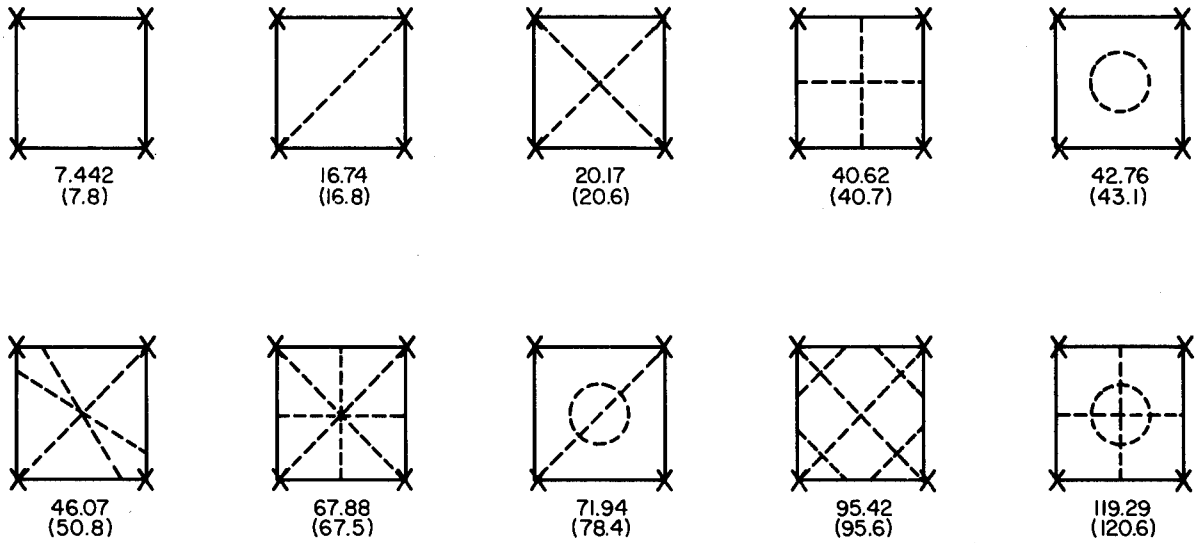


FIGURE 4.81.—Theoretical and experimental frequency parameters and nodal patterns for a free steel square plate point supported at the four corners. Experimental values are given in parentheses. (After ref. 4.14)

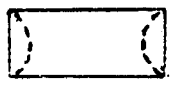
TABLE 4.93.—*Frequency Parameters, Nodal Patterns, and Amplitude Coefficients for a Rectangular Plate Supported at Its 4 Corners; $\nu=0.3$*

[Values in parentheses are obtained by keeping 24 terms of the series]

a/b	Mode 1: □			Mode 2: □		
	$\omega a^2\sqrt{\rho/D}$	Normalized mode-shape coefficients		$\omega a^2\sqrt{\rho/D}$	Normalized mode-shape coefficients	
1.0	7. 46 (7.12)	$a_{01}=1.000$ $a_{03}=-.0663$ $a_{21}=.1737$ $a_{23}=.0329$ $a_{41}=-.0267$	$b_{01}=1.000$ $b_{03}=-.0663$ $b_{21}=.1737$ $b_{23}=.0329$ $b_{41}=-.0267$	16. 80 (15.77)	$a_{02}=-0.1248$ $a_{04}=-.0075$ $a_{22}=.1695$ $a_{24}=-.0055$ $a_{42}=-.0146$	$b_{11}=1.000$ $b_{13}=-.0671$ $b_{31}=-.0574$ $b_{33}=.0348$ $b_{51}=-.0083$
1.5	9.21 (8.92)	$a_{01}=.0869$ $a_{03}=-.0150$ $a_{21}=.0950$ $a_{23}=.0056$ $a_{41}=-.0102$	$b_{01}=1.000$ $b_{03}=-.0320$ $b_{21}=.0281$ $b_{23}=.0161$ $b_{41}=-.0068$	22.78 (21.53)	$a_{02}=-.1753$ $a_{04}=.0002$ $a_{22}=.1530$ $a_{24}=-.0059$ $a_{42}=.0012$ $a_{06}=.0009$	$b_{11}=1.000$ $b_{13}=-.0499$ $b_{31}=-.0748$ $b_{33}=.0205$ $b_{51}=.0032$ $b_{15}=-.0065$
2.0	9.46 (9.29)	$a_{01}=-.0054$ $a_{03}=-.0052$ $a_{21}=.570$ $a_{23}=.0013$ $a_{41}=-.0035$	$b_{01}=1.000$ $b_{03}=-.0179$ $b_{21}=.0046$ $b_{23}=.0080$ $b_{41}=-.0025$	29.03 (27.50)	$a_{02}=-.1915$ $a_{04}=.0067$ $a_{22}=.1537$ $a_{24}=-.0088$ $a_{42}=.0080$ $a_{06}=.0007$	$b_{11}=1.000$ $b_{13}=-.0460$ $b_{31}=-.0893$ $b_{33}=.0159$ $b_{51}=-.0028$ $b_{15}=-.0093$
2.5	9.48 (9.39)	$a_{01}=-.0197$ $a_{03}=-.0020$ $a_{21}=.0372$ $a_{23}=.0002$ $a_{41}=-.0007$	$b_{01}=1.000$ $b_{03}=-.0108$ $b_{21}=-.0014$ $b_{23}=.0042$ $b_{41}=-.0011$	35.5	$a_{02}=-.1984$ $a_{04}=.0100$ $a_{22}=.1550$ $a_{24}=-.0103$ $a_{42}=.0120$ $a_{06}=.0005$	$b_{11}=1.000$ $b_{13}=-.0451$ $b_{31}=-.0967$ $b_{33}=.0135$ $b_{51}=-.0009$ $b_{15}=-.0113$

TABLE 4.93.—*Frequency Parameters, Nodal Patterns, and Amplitude Coefficients for a Rectangular Plate Supported at Its 4 Corners; $\nu=0.3$*—Continued

[Values in parentheses are obtained by keeping 24 terms of the series]

a/b	Mode 3: 			Mode 4:  		
	$\omega a^2\sqrt{\rho/D}$	Normalized mode-shape coefficients		$\omega a^2\sqrt{\rho/D}$	Normalized mode-shape coefficients	
1.0	16.80 (15.77)	$a_{11}=1.000$ $a_{13}=-.0671$ $a_{31}=-.0574$ $a_{33}=.0348$ $a_{51}=-.0083$	$b_{02}=-0.1248$ $b_{04}=-.0075$ $b_{22}=.1695$ $b_{24}=-.0055$ $b_{42}=-.0146$	19.60 (19.60)	$a_{01}=1.000$ $a_{03}=-.0244$ $a_{21}=-.0802$ $a_{23}=.0112$ $a_{41}=.0049$	$b_{01}=-1.000$ $b_{03}=.0244$ $b_{21}=.0802$ $b_{23}=-.0112$ $b_{41}=-.0049$
1.5	27.74 (25.82)	$a_{11}=1.000$ $a_{13}=-.0817$ $a_{31}=.0205$ $a_{33}=.0428$ $a_{51}=-.0209$	$b_{02}=0.1539$ $b_{04}=-.0380$ $b_{22}=.1850$ $b_{24}=.0115$ $b_{42}=-.0230$	34.8 (33.69)	$a_{01}=1.000$ $a_{03}=-.0536$ $a_{21}=.0756$ $a_{23}=.0255$ $a_{41}=-.0107$	$b_{01}=-0.8108$ $b_{03}=.0002$ $b_{21}=.1693$ $b_{23}=.0171$ $b_{41}=-.0191$
2.0	34.7 (32.83)	$a_{11}=0.7924$ $a_{13}=-.0877$ $a_{31}=.1496$ $a_{33}=.0426$ $a_{51}=-.0304$	$b_{02}=1.000$ $b_{04}=-.0808$ $b_{22}=.1713$ $b_{24}=.0334$ $b_{42}=-.0272$	56.2 (52.0)	$a_{01}=1.000$ $a_{03}=-.0726$ $a_{21}=.2048$ $a_{23}=.0322$ $a_{41}=.0011$	$b_{01}=-0.742$ $b_{03}=.0903$ $b_{21}=.2277$ $b_{23}=.0341$ $b_{41}=-.0277$
2.5	3.72	$a_{11}=0.1928$ $a_{13}=-.0337$ $a_{31}=.1130$ $a_{33}=.0150$ $a_{51}=-.0109$	$b_{02}=1.000$ $b_{04}=-.0479$ $b_{22}=.0536$ $b_{24}=.0191$ $b_{42}=-.0112$	101.7	$a_{01}=0.8438$ $a_{03}=-.3091$ $a_{21}=-.8536$ $a_{23}=.2419$ $a_{41}=.0530$	$b_{01}=-0.8072$ $b_{03}=.1068$ $b_{21}=1.000$ $b_{23}=-.1570$ $b_{41}=-.1440$

were used in reference 4.2 to obtain approximate fundamental frequencies for general values of a/b and $\nu=0.25$. The frequency may be computed from equation (4.17) with

$$\left.\begin{aligned} K&=\frac{1}{2}\left(\frac{1}{a^2}+\frac{1}{b^2}\right)\\ N&=\frac{1}{2}\left(a^2+\frac{16}{\pi}ab+b^2\right)\end{aligned}\right\} \tag{4.94}$$

Cox (ref. 4.142) also used the finite-difference method to solve the problem of the free square plate supported at the midpoints of its sides (see fig. 4.82). Frequencies obtained from two mesh widths and from the extrapolation formula equation (4.90) are listed in table 4.95 for $\nu=0.3$.

Plass (ref. 4.143) used a variational method described later in this section to solve the problem of a free square plate clamped at one midpoint as shown in figure 4.83. A deflection function

$$W(\bar{x},\bar{y})=A_1\left(\frac{\bar{x}}{a}\right)^2-\frac{1}{2}\left(\frac{\bar{y}}{a}\right)^2\left[C_1+C_2\left(\frac{\bar{x}}{a}\right)\right] \tag{4.95}$$

was used to yield a fundamental frequency parameter $\omega a^2\sqrt{\rho/D}=2.580$. In this case the point clamp at (0, 0) permits rotation about the $\bar{x}$-axis, but not about the $\bar{y}$-axis.

The square plate having two adjacent edges both either clamped or simply supported and a point support at the opposite corner (see fig. 4.84) was also analyzed by Cox (ref. 4.144). The finite difference method and $\nu=0.3$ was used. Frequency parameters for both problems are listed in table 4.96 for two mesh

TABLE 4.93.—*Frequency Parameters, Nodal Patterns, and Amplitude Coefficients for a Rectangular Plate Supported at Its 4 Corners; $\nu=0.3$*—Continued

a/b	Mode 5: 		Mode 6: 	
	$\omega a^2\sqrt{\rho/D}$	Normalized mode-shape coefficients	$\omega a^2\sqrt{\rho/D}$	Normalized mode-shape coefficients
1.0	41.5 (38.44)	$a_{12}=1.000$ $a_{14}=-.1458$ $a_{32}=.2107$ $a_{34}=.0645$ $a_{52}=-.0433$ $a_{16}=-.0053$	$b_{12}=1.000$ $b_{14}=-.1458$ $b_{32}=.2107$ $b_{34}=.0645$ $b_{52}=-.0433$ $b_{16}=-.0053$	51.6 (50.3)	$a_{11}=1.000$ $a_{13}=-.0629$ $a_{31}=-.2789$ $a_{33}=-.0007$ $a_{51}=.0318$	$b_{02}=-0.9796$ $b_{04}=.0944$ $b_{22}=.0337$ $b_{24}=-.0492$ $b_{42}=-.0000$
1.5	56.0 (52.7)	$a_{12}=-.0666$ $a_{14}=-.0342$ $a_{32}=.1809$ $a_{34}=.0119$ $a_{52}=-.0049$ $a_{16}=.0014$	$b_{12}=1.000$ $b_{14}=-.0797$ $b_{32}=-.0153$ $b_{34}=.0326$ $b_{52}=-.0190$ $b_{16}=-.0101$	57.7 (57.7)	$a_{11}=1.000$ $a_{13}=-.0446$ $a_{31}=-.1487$ $a_{33}=.0225$ $a_{51}=.0084$	$b_{02}=-0.8072$ $b_{04}=.0477$ $b_{22}=.1222$ $b_{24}=-.0232$ $b_{42}=-.0078$
2.0	67.1 (63.8)	$a_{12}=-.1869$ $a_{14}=-.0122$ $a_{32}=.1764$ $a_{34}=.0011$ $a_{52}=.0068$ $a_{16}=.0015$	$b_{12}=1.000$ $b_{14}=-.0671$ $b_{32}=-.0548$ $b_{34}=.0238$ $b_{52}=-.0114$ $b_{16}=-.0134$	73.0 (71.3)	$a_{11}=1.000$ $a_{13}=-.0597$ $a_{31}=-.0626$ $a_{33}=.0316$ $a_{51}=-.0013$	$b_{02}=-0.6479$ $b_{04}=.0324$ $b_{22}=.1557$ $b_{24}=-.0051$ $b_{42}=-.0151$
2.5	78.5	$a_{12}=-.2238$ $a_{14}=-.0021$ $a_{32}=.1772$ $a_{34}=-.0038$ $a_{52}=.0134$ $a_{16}=.0013$	$b_{12}=1.000$ $b_{14}=-.0630$ $b_{32}=-.0717$ $b_{34}=.0195$ $b_{52}=-.0074$ $b_{16}=-.0160$	97.5	$a_{11}=1.000$ $a_{13}=-.0705$ $a_{31}=-.0104$ $a_{33}=.0364$ $a_{51}=.0059$	$b_{02}=-0.5687$ $b_{04}=.0720$ $b_{22}=.1772$ $b_{24}=.0027$ $b_{42}=-.0195$

a/b	Mode 7: 		
	$\omega a^2\sqrt{\rho/D}$	Normalized mode-shape coefficients	
1.0	48.3 (44.4)	$a_{01}=0.1555$ $a_{03}=-.1950$ $a_{21}=1.000$ $a_{23}=.1088$ $a_{41}=-.0988$	$b_{01}=0.1555$ $b_{03}=-.1950$ $b_{21}=1.000$ $b_{23}=.1088$ $b_{41}=-.0988$
1.5	75.4 (70.1)	$a_{01}=-0.4491$ $a_{03}=-.1209$ $a_{21}=1.000$ $a_{23}=.0468$ $a_{41}=-.0658$	$b_{01}=0.6498$ $b_{03}=-.0355$ $b_{21}=.5491$ $b_{23}=.1078$ $b_{41}=-.0590$

308-337 O - 70 - 10

TABLE 4.94.—*Comparison Between Experimental and Theoretical Results for Cyclic Frequencies of Rectangular Plates Point Supported in the Corners*

Mode	Cyclic frequencies, cps, for—					
	Plate 1: 12- by 12- by 0.129-in. 2024 aluminum $E=10.6\times10^6$ psi (book value)			Plate 2: 10- by 20- by 0.173-in. 2024 aluminum $E=10.6\times10^6$ psi (book value)		
	Solution from ref. 4.139	Experiment	Series solution	Solution from ref. 4.139	Experiment	Series solution
1	61. 4	62	61. 4	38. 8	38. 3	38. 8
2	136	134	136	----------	113	115
3	136	134	136	----------	136	137
4	166	169	170	----------	214	218
5	333	330	333	----------	261	267
6	----------	434	436	----------	294	298
7	375	383	385	----------	----------	----------

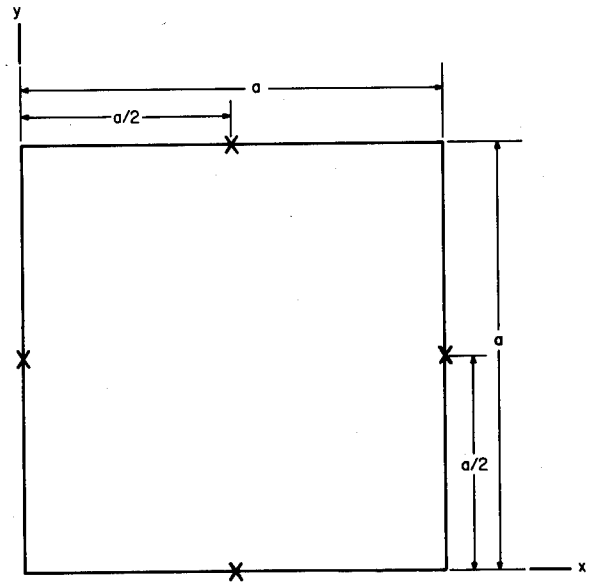


FIGURE 4.82.—Free square plate supported at the midpoints of its sides.

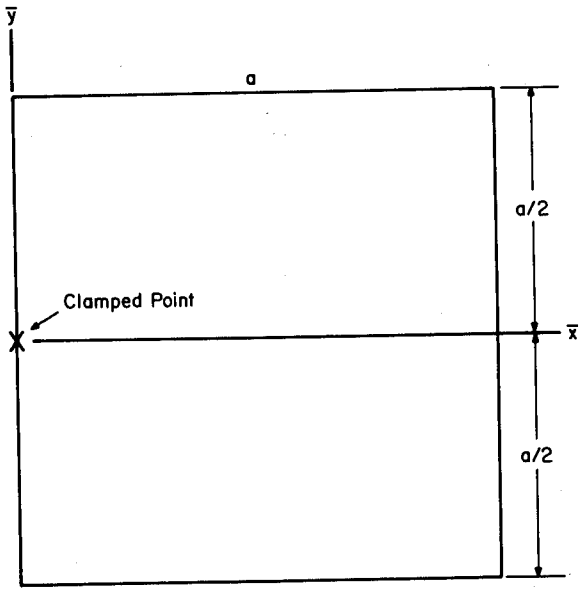


FIGURE 4.83.—Free square plate clamped at one midpoint.

widths. Extrapolated values are derived from equation (4.90).

The second mode shapes for these two problems have node lines $y=x$, and thereby duplicate the second modes that exist when the corner point is not supported. (See secs. 4.3.6 and 4.3.13 for relevant information.) First and second mode shapes and frequencies can also be obtained directly from the results of the free square plate point supported at its four corners given earlier in this section. Straight node lines duplicate simply supported boundary conditions.

Consider next the problem of the rectangular plate simply supported on all edges and supported at a point located at the coordinates ξ, η (fig. 4.85). Nowacki (refs. 4.137 and 4.145)

TABLE 4.95.—*Fundamental Frequency Parameter* $\omega a^2\sqrt{\rho/D}$ *for a Free Square Plate Supported at the Midpoints of Its Sides;* $\nu=0.3$

$\omega a^2\sqrt{\rho/D}$		
Mesh width		Extrapolated value
$a/8$	$a/10$	
17. 129	17. 443	18. 002

TABLE 4.96.—*Frequency Parameters* $\omega a^2\sqrt{\rho/D}$ *for a Square Plate Simply Supported or Clamped on 2 Adjacent Edges and Supported at the Opposite Corner;* $\nu=0.3$

Adjacent edge conditions	$\omega a^2\sqrt{\rho/D}$			
	Mesh width			Extrapolated value
	$a/4$	$a/5$	$a/6$	
Simply supported	8. 22	8. 50	-------	9. 00
Clamped	------	12. 55	12. 90	13. 68

solved the problem by dividing the plate into two sections by the line $y=\xi$, assuming a solution of the form

$$W(x,y)=\sum_m (A_m \sinh \lambda_3 y + B_m \sinh \lambda_4 y)\sin\frac{m\pi x}{a} \tag{4.96}$$

where

$$\lambda_3, \lambda_4=\sqrt{\left(\frac{m\pi}{a}\right)^2 \pm \frac{\rho\omega^2}{D}} \tag{4.97}$$

for each section, and satisfying the boundary conditions along $y=0$ and $y=b$ and the continuity conditions along $y=\eta$ exactly. Continuity of transverse shear along $y=\eta$ requires expanding the point load at ξ, η into a Fourier sine series. These conditions lead to the characteristic equation

$$\sum_{m=1,2,\ldots}^{\infty} \frac{\sin^2\alpha\xi}{(\lambda_3^2-\lambda_4^2)}\left[\frac{\sinh\lambda_4\eta\sinh\lambda_4(b-\eta)}{\lambda_4\sinh\lambda_4 b} - \frac{\sinh\lambda_3\eta\sinh\lambda_3(b-\eta)}{\lambda_3\sinh\lambda_3 b}\right]=0 \tag{4.98}$$

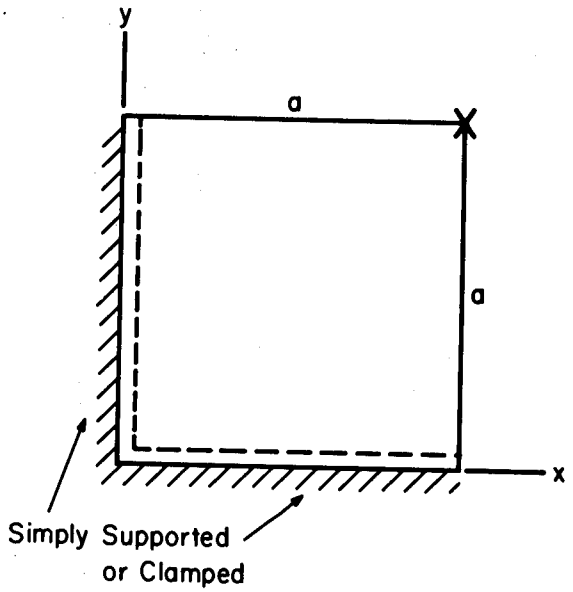


FIGURE 4.84.—Square plate simply supported or clamped on two adjacent edges and supported at the opposite corner.

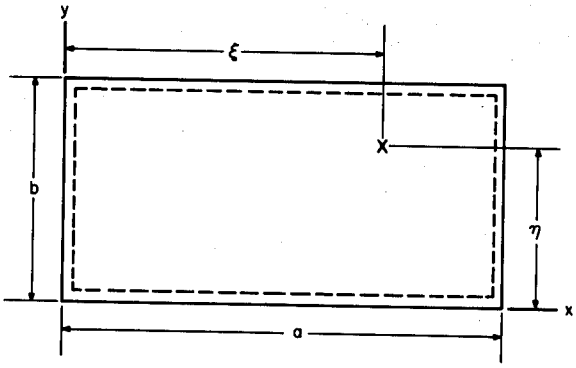


FIGURE 4.85.—SS–SS–SS–SS rectangular plate with point support along one symmetry axis.

where $\alpha=m\pi/a$. The roots λ_3 and λ_4 of equation (4.98) yield the frequencies.

The fundamental frequency parameters for three a/b ratios and with the point support at the center ($\xi=a/2, \eta=b/2$) are listed in table 4.97. Frequencies were also determined (ref. 4.137) for the case of the square when the support point was allowed to relocate along the line $y=a/2=b/2$. Results are given in table 4.98. It is noted that corresponding values ($\xi/a=\frac{1}{2}$, $a/b=1$) of tables 4.97 and 4.98 show considerable disagreement.

TABLE 4.97.—*Fundamental Frequency Parameters for a SS–SS–SS–SS Rectangular Plate Having a Point Support at the Center*

a/b	1.0	1.5	2.0
$\omega a^2\sqrt{\rho/D}$	52. 6	73. 1	91. 1

TABLE 4.98.—*Fundamental Frequency Parameters for a SS–SS–SS–SS Square Plate Having a Point Support Along a Symmetry Axis*

ξ/a	0	⅛	¼	⅜	½
$\omega a^2\sqrt{\rho/D}$	19. 7	25. 5	30. 4	38. 9	49. 3

The case when the plate is supported at a point by a spring, with or without added mass, is discussed in the section entitled "Point Masses" (sec. 4.5.2).

The square hub-pin plate (fig. 4.86) consists of a hub support attached to the edge of a plate and having an axis of rotation parallel to the adjacent edges and a pin support at another point along the same edge. For the particular locations shown in figure 4.87, the boundary conditions at the hub are for $W(x,y)$

$$W\left(0,\frac{a}{2}\right)=\frac{\partial W}{\partial x}\left(0,\frac{a}{2}\right)=0 \qquad (4.99)$$

and at the pin

$$W\left(0,\frac{3}{4}a\right)=M_x\left(0,\frac{3}{4}a\right)=0 \qquad (4.100)$$

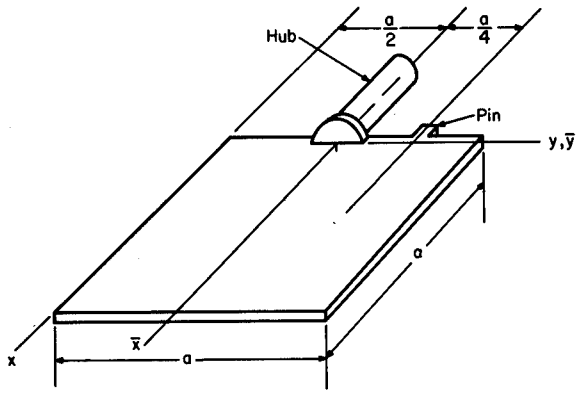


FIGURE 4.86.—Square hub-pin plate.

Free-edge boundary conditions apply everywhere else.

This problem was treated in references 4.66 and 4.143 by using a modification of Reissner's variational method (ref. 4.71) and a deflection function

$$\begin{aligned}W(\bar{x},\bar{y})=&A_1\left[\left(\frac{\bar{x}}{a}\right)^2-\frac{1}{3}\left(\frac{\bar{x}}{a}\right)^3\right]\\&+A_2\left[\left(\frac{\bar{x}}{a}\right)^2-\frac{91}{75}\left(\frac{\bar{x}}{a}\right)^3\right]\\&+A_3\left[\left(\frac{\bar{x}}{a}\right)^2-\frac{14}{5}\left(\frac{\bar{x}}{a}\right)^3+\frac{28}{15}\left(\frac{\bar{x}}{a}\right)^4\right]\\&+B_1\left\{\frac{\bar{y}}{a}-\frac{96}{23}\left[\left(\frac{\bar{\eta}}{a}\right)^2-\frac{2}{3}\left(\frac{\bar{y}}{a}\right)^4\right]\right\}\\&+B_2\left(\frac{\bar{x}}{a}\right)\left(\frac{\bar{\eta}}{a}\right)+B_3\left(\frac{\bar{x}}{a}\right)^2\left(\frac{\bar{\eta}}{a}\right)\\&+C_2\left(\frac{1}{2}\right)\left(\frac{\bar{x}}{a}\right)\left[\left(\frac{\bar{y}}{a}\right)^2-\frac{2}{3}\left(\frac{\bar{y}}{a}\right)^4\right]\\&+C_3\left(\frac{1}{2}\right)\left(\frac{\bar{x}}{a}\right)^2\left[\left(\frac{\bar{\eta}}{a}\right)^2-\frac{2}{3}\left(\frac{\bar{\eta}}{a}\right)^4\right] \qquad (4.101)\end{aligned}$$

Moment boundary conditions were exactly satisfied at discrete points and four degrees of approximate satisfaction of the shear boundary conditions were considered; the best results were obtained when the transverse shear conditions on the free edges were ignored. Frequency parameters from reference 4.66 compared with the experimental data of reference 4.72 are presented in table 4.99 for an aluminum plate 7.5 by 7.5 inches by 0.25 inch. Experimental methods used to get these results are described in reference 4.146.

Mode shapes corresponding to the first three frequencies are shown in figure 4.87, where

TABLE 4.99.—*Frequency Parameters* $\omega a^2\sqrt{\rho/D}$ *and Nodal Patterns for a Square Hub-Pin Plate*

Type	$\omega a^2\sqrt{\rho/D}$ for mode—				
	1	2	3	4	5
Theoretical	2. 67	5. 86	15. 87	-------	------
Experimental	2. 76	5. 59	15. 95	21. 73	26. 81

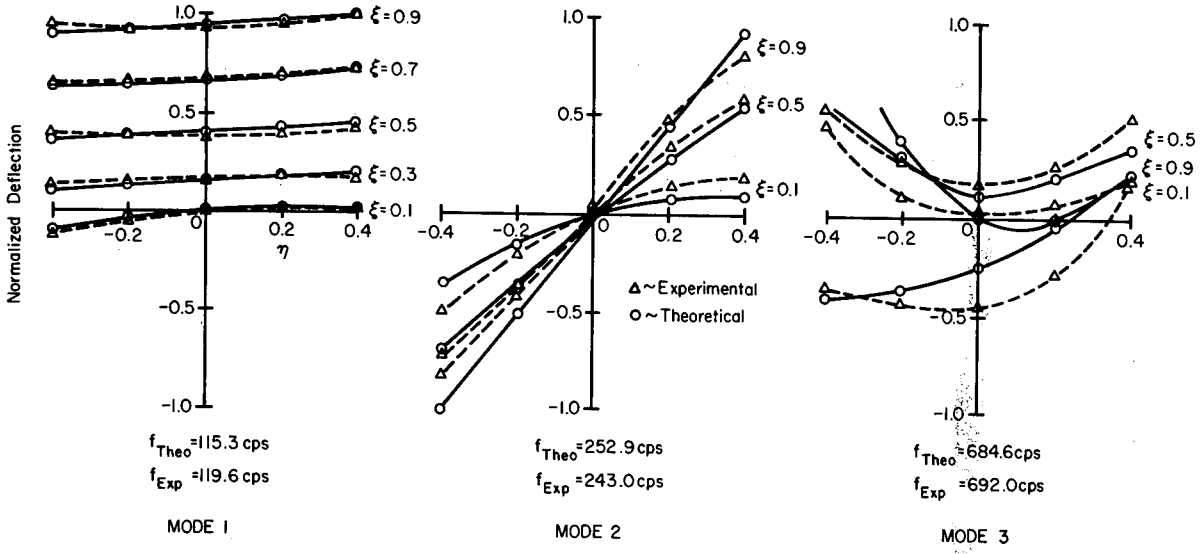


FIGURE 4.87.—Theoretical and experimental mode shapes for a square hub-pin plate.

$\xi=\bar{x}/a$ and $\eta=\bar{y}/a$. Further experimental results (ref. 4.86) for a thinner plate are shown in figure 4.88. More work on point-supported plates is contained in reference 4.147.

4.5 ADDED MASS

4.5.1 Rigid Strip Mass

The problem of the rectangular plate, simply supported on two opposite edges, free on the other two, and carrying a rigid mass of finite width l running across the center of the plate (fig. 4.89) was studied by Cohen and Handelman (ref. 4.148). In reference 4.148, the Rayleigh-Ritz method is used with a fundamental mode shape

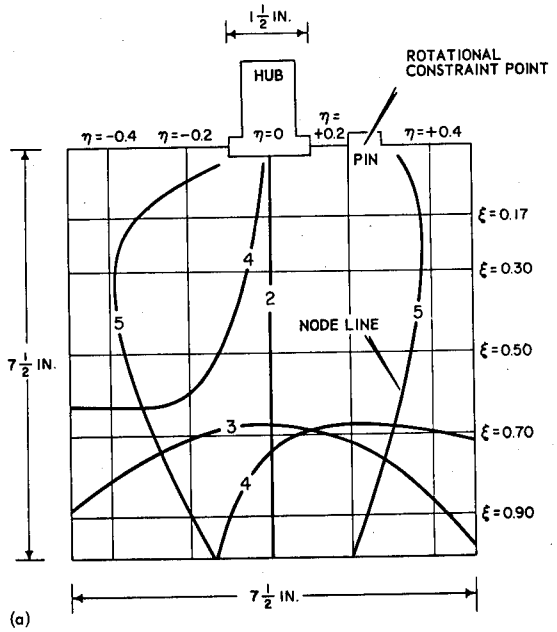
$$W(x,y)=\sin\frac{\pi x}{(a-l)}+Ab^3x\left(x-\frac{a}{2}+\frac{l}{2}\right)^2\sin\frac{\pi y}{b} \tag{4.102}$$

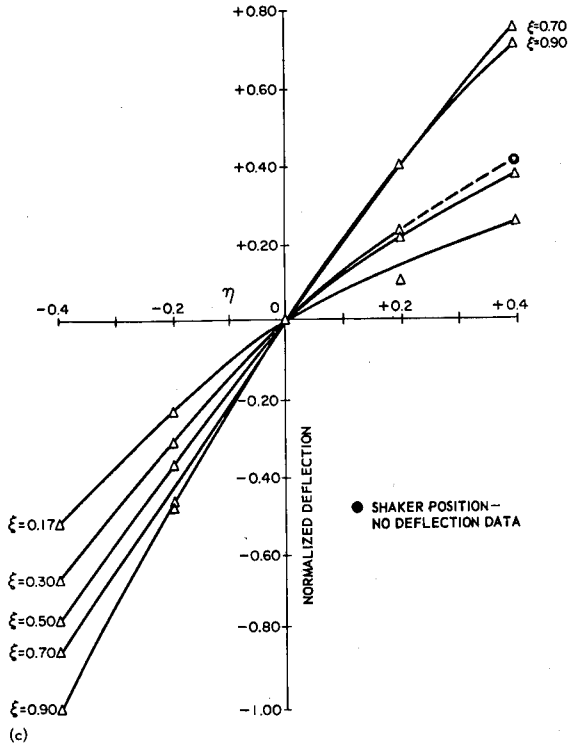
where A is an undetermined coefficient to be found from the minimization process. An explicit formula for the frequency parameter is found to be

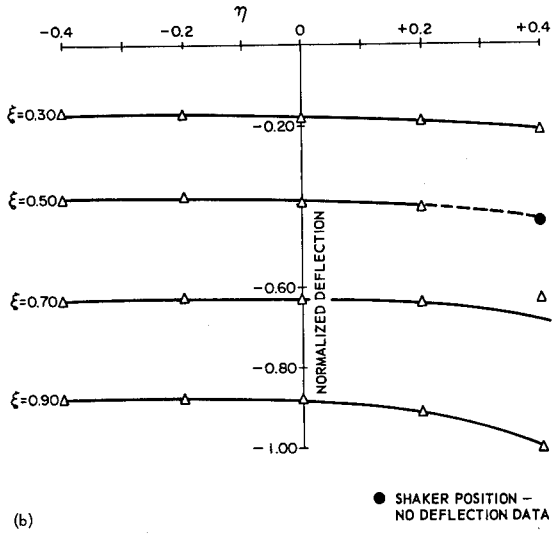
$$\lambda^2=\frac{C_2C_5-2(C_3C_4+C_1C_6)+2\sqrt{(C_3C_4-C_1C_6)^2-C_2C_5(C_3C_4+C_1C_6)+C_2^2C_4C_6+C_1C_3C_5^2}}{C_5^2-4C_4C_6} \tag{4.103}$$

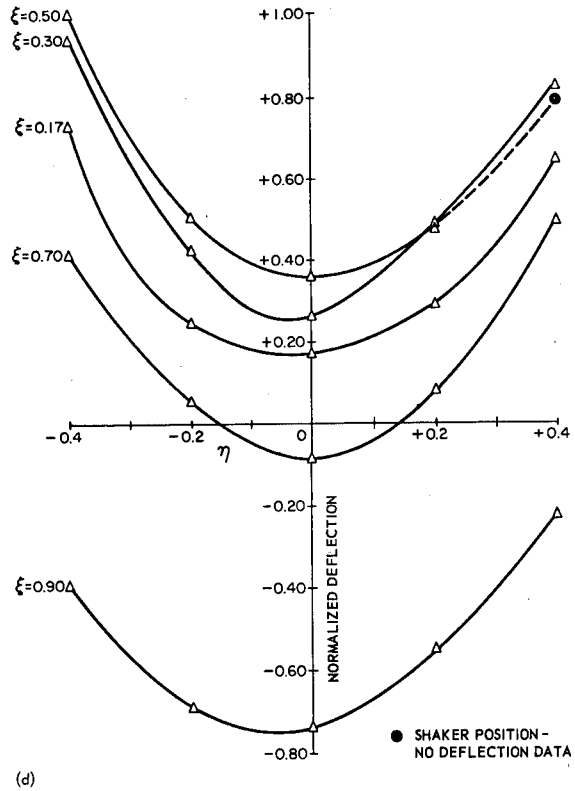
where

$$\left.\begin{aligned}
&\lambda=\omega a^2\sqrt{\rho/D}\\
&C_1=\frac{\pi^4}{16\left(\frac{a}{b}\right)\left(1-\frac{l}{a}\right)^3}\\
&C_2=16\left(\frac{b}{a}\right)^4\left(1-\frac{3}{\pi}\right)\left[1+\nu\left(\frac{a}{b}\right)^2\left(1-\frac{l}{a}\right)^2\right]\\
&C_3=\left(\frac{b}{a}\right)^3\left(1-\frac{l}{a}\right)^3\left[4\left(\frac{b}{a}\right)^4+\frac{\pi^4}{1680}\left(1-\frac{l}{a}\right)^4+\frac{\pi^2}{15}\left(\frac{b}{a}\right)^2\left(1-\frac{l}{a}\right)^2\right]\\
&C_4=\left(\frac{b}{a}\right)\left[1-\frac{l}{a}+2\left(\frac{l}{a}\right)\left(\frac{\rho'}{\rho}\right)\right]\\
&C_5=\frac{256}{\pi^4}\left(\frac{b}{a}\right)^4\left(1-\frac{l}{a}\right)^4\left(1-\frac{3}{\pi}\right)\\
&C_6=\frac{1}{105}\left(\frac{b}{a}\right)^7\left(1-\frac{l}{a}\right)^7
\end{aligned}\right\} \tag{4.104}$$


1½ IN.
HUB
ROTATIONAL CONSTRAINT POINT
η=-0.4
η=-0.2
η=0
η=+0.2
η=+0.4
PIN
ξ=0.17
ξ=0.30
ξ=0.50
ξ=0.70
ξ=0.90
NODE LINE
7½ IN.
7½ IN.
(a)


+0.80
+0.60
+0.40
+0.20
-0.20
-0.40
-0.60
-0.80
-1.00
-0.4
-0.2
0
+0.2
+0.4
η
ξ=0.70
ξ=0.90
ξ=0.17
ξ=0.30
ξ=0.50
ξ=0.70
ξ=0.90
NORMALIZED DEFLECTION
SHAKER POSITION—
NO DEFLECTION DATA
(c)


η
-0.4
-0.2
0
+0.2
+0.4
ξ=0.30
ξ=0.50
ξ=0.70
ξ=0.90
-0.20
-0.60
-0.80
-1.00
NORMALIZED DEFLECTION
SHAKER POSITION—
NO DEFLECTION DATA
(b)


ξ=0.50
ξ=0.30
ξ=0.17
ξ=0.70
ξ=0.90
+1.00
+0.80
+0.60
+0.40
+0.20
-0.20
-0.40
-0.60
-0.80
-0.4
-0.2
0
+0.2
+0.4
η
NORMALIZED DEFLECTION
SHAKER POSITION—
NO DEFLECTION DATA
(d)

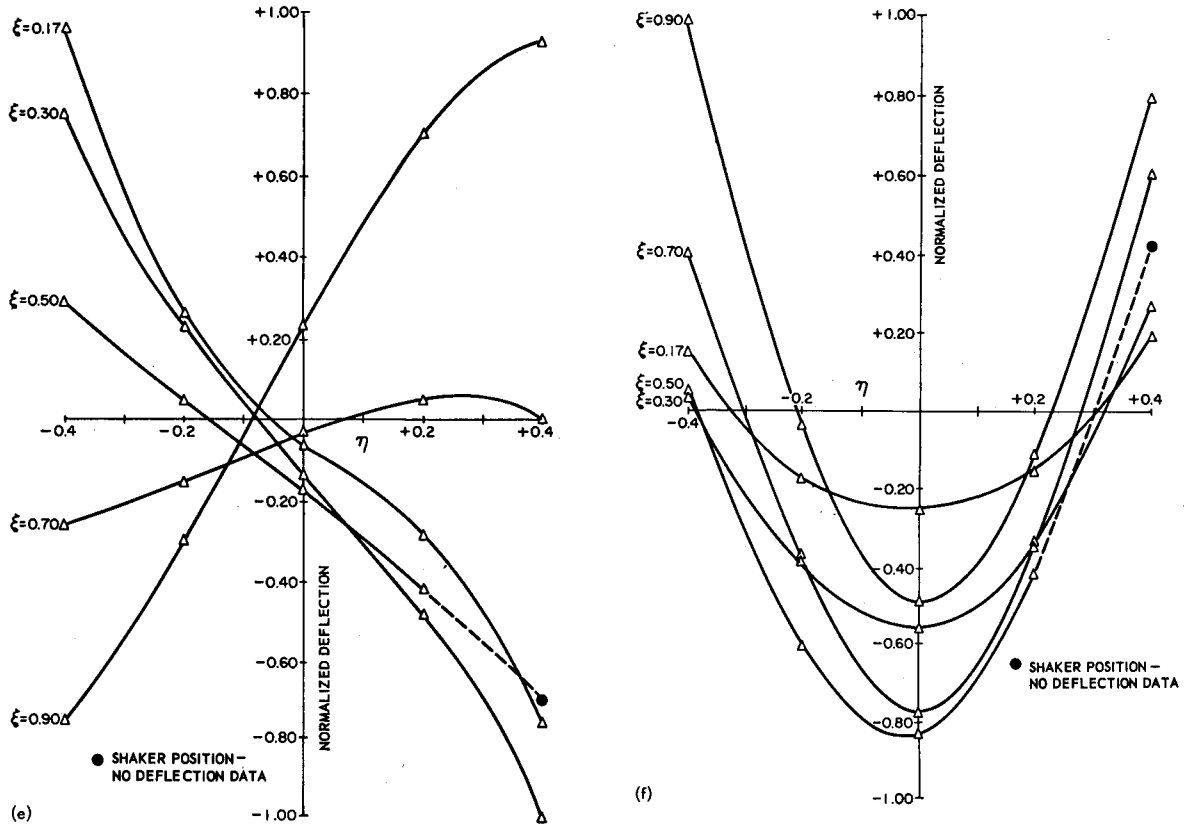


FIGURE 4.88.—Experimental node lines and normalized deflection of a square hub-pin plate; material, 6061–T6 aluminum ⅛ inch thick. (*a*) Experimental node lines and data points. (*b*) First mode; $f_1=58.8$ cps. (*c*) Second mode; $f_2=119$ cps. (*d*) Third mode; $f_3=339$ cps. (*e*) Fourth mode; $f_4=462$ cps. (*f*) Fifth mode; $f_5=570$ cps.

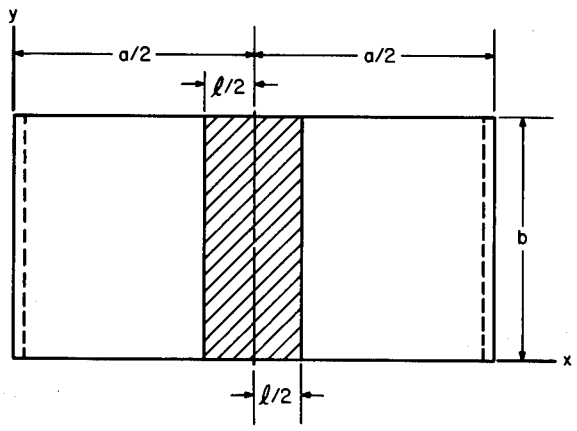


FIGURE 4.89.—SS–F–SS–F plate carrying a rigid mass.

and where ρ' is the mass density per unit area of the plate plus the additional mass in the region $[(a/2)-(l/2)]<x<[(a/2)+(l/2)]$. For large values of a/b, equation (4.104) can be simplified by retaining terms of order $(b/a)^2$, but no higher powers, giving:

$$\lambda^2=\frac{\frac{\pi^6}{60}\left[\frac{\pi^2}{112}\left(1-\frac{l}{a}\right)^2+\left(\frac{b}{a}\right)^2\right]-16\nu\left(1-\frac{3}{\pi}\right)^2\left[\nu\left(1-\frac{l}{a}\right)^2+2\left(\frac{b}{a}\right)^2\right]}{\frac{4\pi^2}{15}\left(1-\frac{l}{a}\right)^3\left[1-\left(\frac{l}{a}\right)\left(1-2\frac{\rho'}{\rho}\right)\right]\left[\frac{\pi^2}{112}\left(1-\frac{l}{a}\right)^2+\frac{1}{15}\left(\frac{b}{a}\right)^2\right]-\frac{8192}{\pi^4}\nu\left(1-\frac{l}{a}\right)^4\left(1-\frac{3}{\pi}\right)^2\left(\frac{b}{a}\right)^2} \tag{4.105}$$

Numerical results were evaluated in reference 4.148 for $\nu=0.25$. For the square, equation (4.103) was used. Frequency variation with l/a ratio for several values of ρ'/ρ is shown in figure 4.90. For $a/b=10$, equation (4.105) was used. Results are shown in figure 4.91. It is interesting to note that in both figures for $\rho'/\rho<2$ the frequency always increases as l/a increases, whereas for $\rho'/\rho>2$ there exist crossover points where the frequency of the plate with the added strip is the same as that of the unloaded plate.

In reference 4.149 the technique of reference 4.148 was extended to the lowest antisymmetrical mode. A function

$$W(x,y)=\sin\frac{\beta x}{a}+A\frac{b^3}{a^6}x(x-a+l)^2\sin\frac{\pi y}{b} \tag{4.106}$$

is used where β is the fundamental root of the equation

$$\tan\beta\left(1-\frac{l}{a}\right)+\beta\frac{l}{a}=0 \tag{4.107}$$

The explicit form for the frequency parameter is found to be

$$\lambda^2=\frac{D_1-2D_2+2\sqrt{D_3^2+D_4D_5}}{} \tag{4.108}$$

where

$$\left.\begin{aligned}
&\lambda=\omega a^2\sqrt{\rho/D}\\
&D_1=E_2\left(\frac{b}{a}\right)^3\left[E_5\left(\frac{b}{a}\right)^3+E_6\left(\frac{b}{a}\right)\right]\\
&D_2=E_1\left[E_7\left(\frac{b}{a}\right)^6+E_8\left(\frac{b}{a}\right)^4+E_9\left(\frac{b}{a}\right)^2\right]\\
&\qquad\qquad+E_3E_4\left(\frac{b}{a}\right)^6\\
&D_3=D_2-2E_3E_4\left(\frac{b}{a}\right)^6\\
&D_4=E_3\left(\frac{b}{a}\right)^6\left[E_5\left(\frac{b}{a}\right)^3+E_6\left(\frac{b}{a}\right)\right]\\
&\qquad-E_2\left(\frac{b}{a}\right)^3\left[E_7\left(\frac{b}{a}\right)^6+E_8\left(\frac{b}{a}\right)^4+E_9\left(\frac{b}{a}\right)^2\right]\\
&D_5=E_1\left[E_5\left(\frac{b}{a}\right)^3+E_6\left(\frac{b}{a}\right)\right]-E_2E_4\left(\frac{b}{a}\right)^3\\
&D_6=\left(\frac{b}{a}\right)^6[E_2^2-4E_1E_3]
\end{aligned}\right\} \tag{4.109}$$

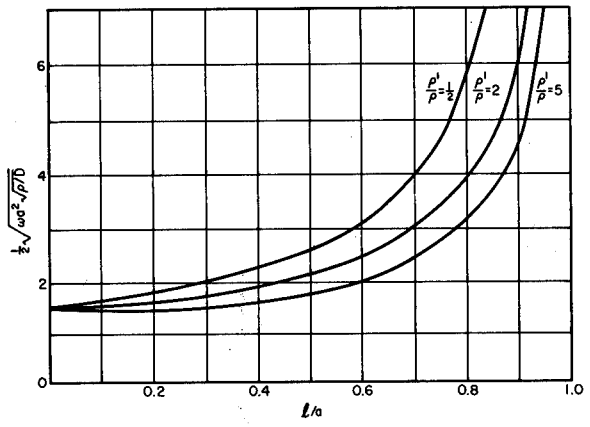


FIGURE 4.90.—Fundamental frequency variation for a SS–F–SS–F square plate carrying a rigid strip mass; $\nu=0.25$. (After ref. 4.148)

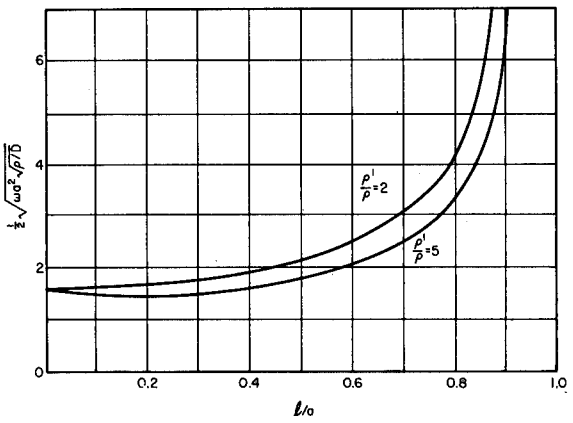


FIGURE 4.91.—Frequency variation for a SS–F–SS–F rectangular plate ($a/b=10$) carrying a rigid strip mass; $\nu=0.25$. (After ref. 4.148)

and where

$$
\left.
\begin{aligned}
E_1&=\frac{1+\beta^2\left(\frac{l}{a}\right)^2\left(1-\frac{l}{a}\right)+\left(\frac{2}{3}\right)\beta^2\left(\frac{\rho'}{\rho}\right)\left(\frac{l}{a}\right)^3}{1+\beta^2\left(\frac{l}{a}\right)^2}\\
E_2&=E_5/\beta^4\\
E_3&=\frac{1}{105}\left(1-\frac{l}{a}\right)^7\\
E_4&=\beta^4\left[\frac{1+\beta^2\left(\frac{l}{a}\right)^2\left(1-\frac{l}{a}\right)}{1+\beta^2\left(\frac{l}{a}\right)^2}\right]\\
E_5&=\frac{16\beta}{\pi}\left[2\left(1-\frac{l}{a}\right)-\frac{1+2\left(\frac{l}{a}\right)}{\sqrt{1+\beta^2\left(\frac{l}{a}\right)^2}}\right]\\
E_6&=\frac{\pi^2\nu}{4\beta^2}E_5\\
E_7&=4\left(1-\frac{l}{a}\right)^3\\
E_8&=\frac{\pi^2}{15}\left(1-\frac{l}{a}\right)^5\\
E_9&=\frac{\pi^4}{1680}\left(1-\frac{l}{a}\right)^7
\end{aligned}
\right\} \qquad (4.110)
$$

For large values of a/b, equation (4.108) simplifies to

$$\lambda^2=\frac{4E_4E_9-E_6^2}{4E_1E_9}+\frac{E_6}{8E_1^2E_9^2}\left(\frac{b}{a}\right)^2[2E_1(E_6E_8-2E_5E_9)-E_2(E_6^2-4E_4E_9)] \qquad (4.111)$$

Numerical results were evaluated in reference 4.149. For the square, equation (4.108) was used. Frequency variation with l/a ratio for several values of ρ'/ρ is shown in figure 4.92. For $a/b=10$, equation (4.111) was used. Results are shown in figure 4.93.

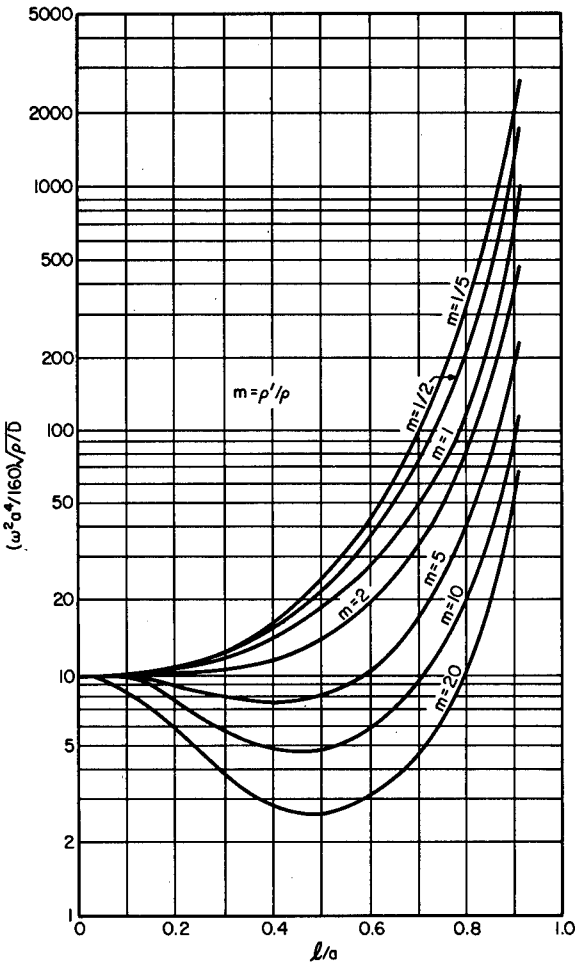


FIGURE 4.92.—Variation of the first antisymmetric frequency for a SS–F–SS–F square plate carrying a rigid strip mass. (After ref. 4.149)

4.5.2 Point Masses

A rectangular plate simply supported all around and having a concentrated mass M attached at the coordinates ξ, η is shown in figure 4.94. Gershgorin (ref. 4.150) solved the problem by dividing the plate into two regions $0<y<\eta$ and $\eta<y<b$ and assuming a solution (eq. (1.37)) for each region. Eight homogeneous equations are written, four for the boundary conditions at $y=0$ and $y=b$, and four for the continuity conditions across the line $y=\eta$. The continuity condition for transverse shear takes into account the concentrated mass by expanding a point load into a Fourier sine series. This procedure leads to a characteristic equation, the roots of which are the desired eigenvalues.

Numerical results are presented in implicit form in reference 4.150 for the doubly symmet-

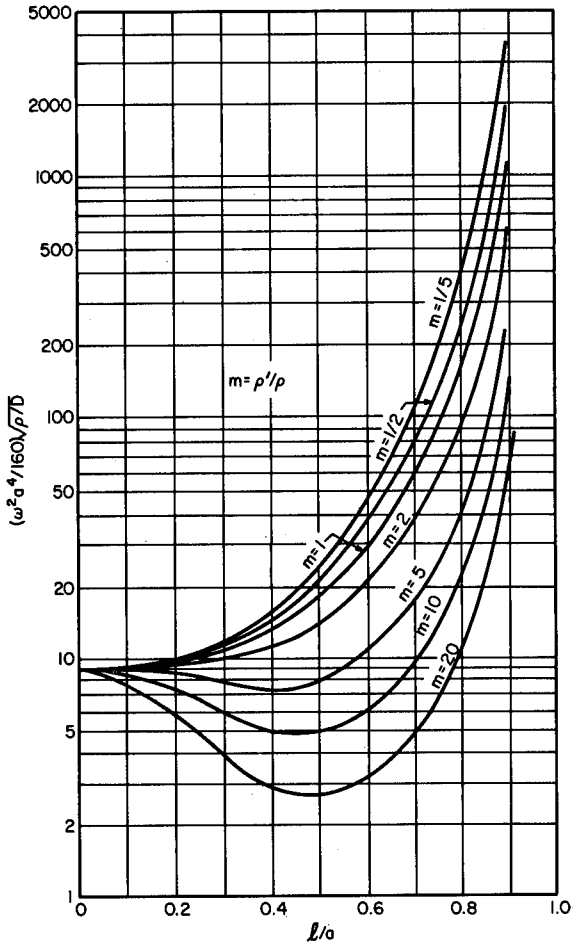


FIGURE 4.93.—Variation of the first antisymmetric frequency for a SS–F–SS–F rectangular plate carrying a rigid strip mass; $a/b=10$. (After ref. 4.149)

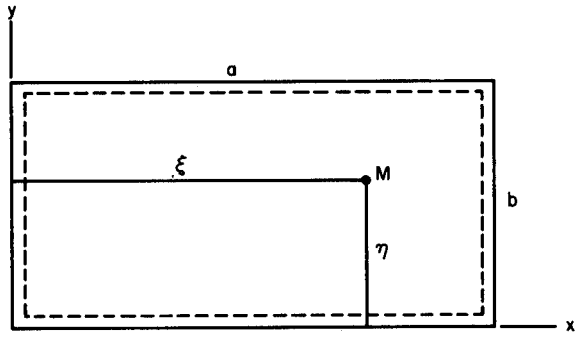


FIGURE 4.94.—SS–SS–SS–SS rectangular plate with a point mass M.

ric modes of a square ($a=b$) when the mass is at the center ($\xi=a/b$, $\eta=a/2$). It is obvious that for modes having an axis of antisymmetry the mass M will fall on a node line and, hence, will not affect the plate. The frequencies may be obtained from the characteristic equation

$$f_1(\lambda)=\lambda\sum_{m=0}^{\infty}\frac{\tanh\frac{\pi}{2}\sqrt{(2m+1)^2-\lambda}}{\sqrt{(2m+1)^2-\lambda}}-\frac{\tanh\frac{\pi}{2}\sqrt{(2m+1)^2+\lambda}}{\sqrt{(2m+1)^2+\lambda}}=\frac{2\rho a^2}{\pi M} \quad (4.112)$$

where

$$\lambda=\frac{\omega a^2}{\pi^2}\sqrt{\rho/D} \quad (4.113)$$

The function $f_1(\lambda)$ is given in table 4.100 and plotted in figure 4.95.

TABLE 4.100.—*Characteristic Functions for a SS–SS–SS–SS Square Plate Having a Mass at the Center*

λ	$f_1(\lambda)$	λ	$f_1(\lambda)$	λ	$f_1(\lambda)$
0	0	2.0	$-\infty$	10	$-\infty$
0.2	.0289	2.1	−26.9900	10.1	−264.8749
0.4	.1197	2.2	−13.9576	10.2	−129.7239
0.6	.2818	2.5	−6.5248	10.5	−61.1816
0.8	.5382	3.0	−3.7910	11.0	−33.3897
1.0	.9323	4.0	−1.7000	12.0	−13.6614
1.2	1.3698	5.0	−.5124	13.0	−7.6301
1.4	2.6115	6.0	−1.2861	14.0	−3.5239
1.6	4.7415	7.0	3.7948	15.0	.6548
1.7	7.4900	8.0	8.5774	16.0	6.4283
1.8	11.1529	9.0	22.0731	17.0	19.7349
1.9	24.3803	9.5	45.3092	17.5	42.6325
2.0	∞	9.8	124.2640	17.8	113.0580
		10.0	∞	18.0	∞

The method of obtaining frequencies is shown in figure 4.95. For a given problem, the right-hand side of equation (4.112) is computed. This is represented by the broken line in figure 4.95. The intersections of this line with the curves $f_1(\lambda)$ yield the values of λ on the abscissa. The frequency is then determined from equation (4.113). It is seen that $f_1(\lambda)$ becomes infinite at values of λ corresponding to the natural frequencies of the unloaded plate. Also, as the mass is increased, $f_1(\lambda)$ always remains positive. Thus, for infinite mass M the higher frequencies are not zero.

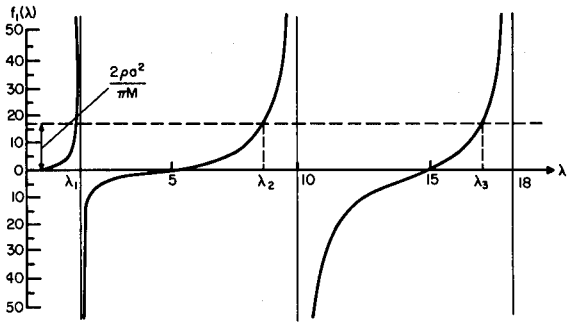


FIGURE 4.95.—Characteristic functions for a SS–SS–SS–SS square plate having a mass at the center.

The doubly symmetric mode shapes are given by

$$W(x,y)=\sum_{m=0}^{\infty}(-1)^m\left[\frac{\sinh\left(\frac{\pi y}{a}\sqrt{(2m+1)^2-\lambda_i}\right)}{\sqrt{(2m+1)^2-\lambda_i}\cosh\left(\frac{\pi}{2}\sqrt{(2m+1)^2-\lambda_i}\right)}-\frac{\sinh\left(\frac{\pi y}{a}\sqrt{(2m+1)^2+\lambda_i}\right)}{\sqrt{(2m+1)^2+\lambda_i}\cosh\left(\frac{\pi}{2}\sqrt{(2m+1)^2+\lambda_i}\right)}\right]\sin\left[(2m+1)\frac{\pi x}{a}\right] \quad (4.114)$$

where λ_i are the associated frequency parameters.

Wah (ref. 4.151) and Amba-Rao (ref. 4.152) solved the problem by using a solution for the plate without an added mass (eq. (4.19)) and representing the concentrated force resulting from the point mass by a Dirac delta function. In reference 4.152, the frequencies for modes which do not have nodes at (ξ, η) are determined from the characteristic equation

$$1=\frac{4M\omega^2}{Dab}\sum_{m=1}^{\infty}\sum_{n=1}^{\infty}\left\{\frac{\sin^2\frac{m\pi\xi}{a}\sin^2\frac{n\pi\eta}{b}}{\left[\left(\frac{m\pi}{a}\right)^2+\left(\frac{n\pi}{b}\right)^2\right]^2-\frac{\omega^2\rho}{D}}\right\} \quad (4.115)$$

Frequency parameters for doubly symmetric modes of a square having the mass $M=\rho a^2/4$ at the center are listed in table 4.101.

In reference 4.151, an approximate formula for the square of the fundamental frequency of the simply supported rectangle having a point mass M at the center is given as

$$\omega^2=\frac{\frac{\pi^4 D}{4}ab\left(\frac{1}{a^2}+\frac{1}{b^2}\right)^2}{M+\frac{\rho ab}{4}} \quad (4.116)$$

and an independently derived approximation for the square of the fundamental frequency of a massless plate having the point mass is

$$\omega^2=\frac{\frac{\pi^4 D}{4}ab\left(\frac{1}{a^2}+\frac{1}{b^2}\right)^2}{M} \quad (4.117)$$

Thus the practical rule results that the fundamental frequency of the plate-mass system in this case may be approximated by adding one-fourth of the mass of the plate to the central concentrated mass and calculating the frequency by equation (4.117) as if the plate itself were massless.

Stokey and Zorowski (refs. 4.153 and 4.131) and Lee (ref. 4.154) developed a general method for determining the frequencies of a rectangular plate with arbitrary edge conditions and any number of arbitrarily located masses having both translational and rotational inertia. Deflections are expressed in terms of

TABLE 4.101.—*Frequency Parameters* $\omega a^2\sqrt{\rho/D}$ *for a SS–SS–SS–SS Square Plate Having a Point Mass* $M=\rho a^2/4$ *at the Center*

Mode No.	Number of terms in eq. (4.115)—			
	1	2	3	4
1	13. 96	13. 89	13. 81	13. 79
2	--------	80. 999	70. 511	68. 996
3	--------	--------	--------	162. 65

the eigenfunctions of the plate without masses, and the equations of motion of the plate-mass system are determined from Lagrange's equation

$$\frac{d}{dt}\left(\frac{\partial T}{\partial \dot{q}_i}\right)-\frac{\partial T}{\partial q_i}+\frac{\partial U}{\partial q_i}=0 \qquad (4.118)$$

where T is the kinetic energy of the plate-mass system, U is the potential energy of the system, q_i are the generalized coordinates corresponding to the eigenfunctions used, and t is time. The resulting infinite set of ordinary differential equations in the q_i are solved for the frequencies of the system in the usual manner.

Numerical results were obtained for a simply supported aluminum plate 20 by 20 inches by 0.091 inch with a concentrated mass having negligible rotational inertia at the center. By assuming a specific weight of 0.0955 pound per cubic inch for aluminum, this gives the weight of the plate as 3.48 pounds. Theoretical and experimental fundamental cyclic frequencies were obtained and are given in table 4.102. Only the first four eigenfunctions of the SS–SS–SS–SS plate were used in the calculation of the frequencies.

Table 4.103 (ref. 4.153) lists the results for the effect of adding various numbers of cylindrical masses having equal rotational inertias about all axes in the xy plane at different locations (the axis of the cylinder is perpendicular to the plate). Moments of inertia listed are relative to axes lying in the middle plane of the plate.

The case when an externally connected translational spring of stiffness k (force/length) is attached to the plate at the same location as that of a concentrated mass is studied in

TABLE 4.102.—*Fundamental Cyclic Frequencies for a SS–SS–SS–SS Square Plate With Varying Point Mass at the Center*

Concentrated weight, lb	Cyclic frequency, cps	
	Theoretical	Experimental
2	23. 5	23. 4
4	18. 0	17. 5
6	15. 1	15. 0
8	13. 2	13. 2
10	11. 9	12. 0
12	11. 0	11. 0

reference 4.155. The characteristic equation for the simply supported square having a mass and a spring at its center is equation (4.112) with the right-hand side modified to become

$$f_1(\lambda)=\frac{2\rho a^2}{\pi\left(M-\frac{k}{\omega^2}\right)} \qquad (4.119)$$

for doubly symmetric modes. Again, values of $f_1(\lambda)$ may be taken directly from table 4.100 and figure 4.95. From equation (4.119) and figure 4.95 it is seen that for $\omega=\sqrt{k/M}$ the vibrations of the spring-mass system and the plate become uncoupled. As $k\to\infty$, $f_1(\lambda)\to 0$ and the solution is that of a rigid point support at the center.

Consider next the simply supported square plate having four equal masses symmetrically located along its diagonals as shown in figure 4.96. For modes symmetric with respect to $x=a/2$ and antisymmetric with respect to $y=a/2$, the frequencies may be determined from the characteristic equation (ref. 4.150)

$$f_2(\lambda)=\lambda\sum_m\left[\frac{\tanh\frac{\pi}{4}\sqrt{(2m+1)^2-\lambda}}{\sqrt{(2m+1)^2-\lambda}}-\frac{\tanh\frac{\pi}{4}\sqrt{(2m+1)^2+\lambda}}{\sqrt{(2m+1)^2+\lambda}}\right]=\frac{2\rho a^2}{\pi M} \qquad (4.120)$$

with λ given in equation (4.113). The function $f_2(\lambda)$ is given in table 4.104 and plotted in figure 4.97.

TABLE 4.103.—*Fundamental Cyclic Frequencies for a SS-SS-SS-SS Square Plate Having Various Numbers and Locations of Added Masses*

Location		Weight, lb	I, lb in. sec^2	Cyclic frequency, cps	
ξ	η			Theoretical	Experimental
		2. 75	0. 021	25. 1	26. 0
$a/4$	$a/2$	2. 75	. 021	28. 7	28. 5
$a/4$	$a/4$	2. 70	. 020	17. 9	15. 5
$a/2$	$a/2$	2. 75	. 021		
$a/4$	$a/2$	2. 70	. 020	20. 1	18. 0
$a/2$	$a/4$	2. 75	. 021		
$a/4$	$a/2$				

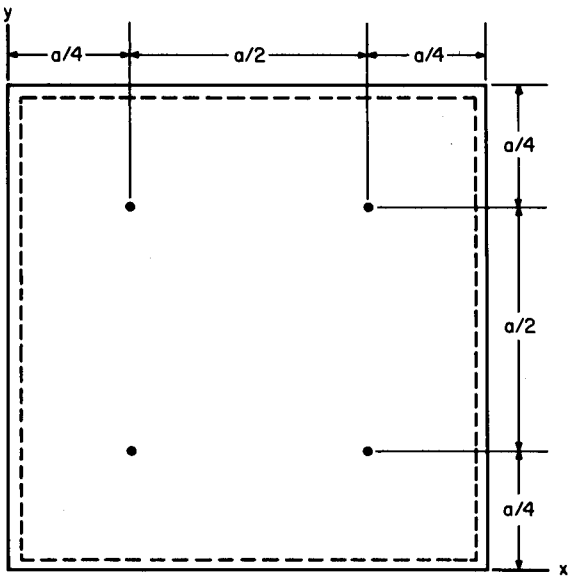


FIGURE 4.96.—Simply supported plate with four symmetrical masses.

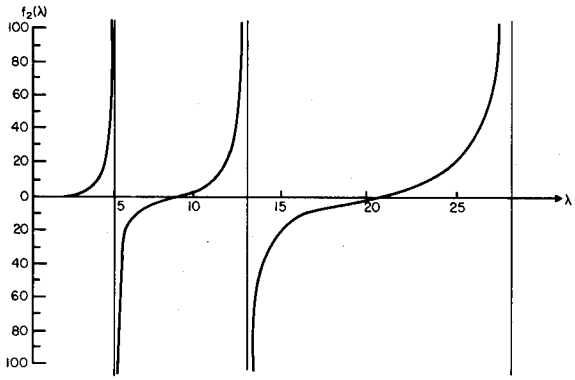


FIGURE 4.97.—Characteristic functions for a SS–SS–SS–SS square plate having four symmetrically located masses.

TABLE 4.104.—*Characteristic Functions for a SS–SS–SS–SS Square Plate Having 4 Symmetrically Located Masses*

λ	$f_2(\lambda)$	λ	$f_2(\lambda)$	λ	$f_2(\lambda)$
0	0	5.0	$-\infty$	13.0	$-\infty$
1.0	. 2650	5.1	−153. 5112	13.5	−71. 4574
2.0	1. 1836	5.2	−66. 4149	14.0	−37. 8496
3.0	3. 3561	5.5	−27. 5738	15.0	−20. 3772
4.0	9. 9930	6.0	−14. 4680	16.5	−11. 7206
4.5	22. 5453	7.0	−7. 1951	18.0	−7. 0385
4.8	61. 1634	8.5	−1. 5711	20.0	−2. 2286
4.9	125. 1397	10.0	2. 9591	23.0	6. 5164
5.0	∞	11.0	8. 9760	25.0	15. 8490
		12.0	26. 6930	26.5	29. 6535
		12.5	60. 2381	28.0	77. 1999
		12.8	159. 6640	28.5	152. 1900
		12.9	211. 6283	29.0	∞
		13.0	∞		

The mode shapes corresponding to these frequencies are given by

$$W(x,y)=\sum\left\{\left[(-1)^m\cos\frac{(2m+1)\pi}{4}\sin\frac{(2m+1)\pi x}{a}\right]\right.$$
$$\left.\left[\frac{\sinh\frac{\pi y\sqrt{(2m+1)^2-\lambda}}{a}}{\sqrt{(2m+1)^2-\lambda}\cosh\frac{\pi\sqrt{(2m+1)^2-\lambda}}{4}}-\frac{\sinh\frac{\pi y\sqrt{(2m+1)^2+\lambda}}{a}}{\sqrt{(2m+1)^2+\lambda}\cosh\frac{\pi\sqrt{(2m+1)^2+\lambda}}{4}}\right]\right\} \quad (4.121)$$

In references 4.156 and 4.157, Solecki gives the fundamental frequency of a square plate clamped all around and having a point mass at the center of twice its own mass. The frequency is found to be

$$\omega=\frac{0.99\pi^2}{a^2}\sqrt{\frac{D}{\rho}} \quad (4.122)$$

The problem of the rectangular plate having three sides simply supported and the other clamped and having a mass M and a spring of stiffness k attached at a given point (fig. 4.98) was solved in reference 4.158. The method used was essentially that given in reference 4.153 and discussed previously in this section. Ratios of the fundamental frequency of the system to that of the plate alone as functions of the stiffness ratio k/k_c and the mass ratio $M/\rho ab$ are shown in figure 4.99 for the case of the square, and $\xi=\eta=0.2a$. The quantity k_c may be thought of as a generalized spring constant corresponding to a uniformly loaded SS–SS–SS–C square plate of negligible mass; that is, $k_c=D/0.00279a^2$.

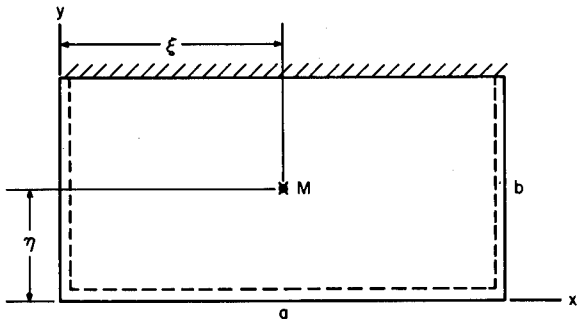


FIGURE 4.98.—SS–SS–SS–C plate with a point mass and point spring.

The problem of the SS–SS–SS–C square plate having two point masses, one at $\xi_1=\eta_1=0.2a$ and the other at $\xi_2=\eta_2=0.4a$, was also solved by Das and Navaratna (ref. 4.158). Frequency ratios are shown in figure 4.100.

A method for determining frequencies of rectangular plates having added masses and elastic edge constraints is given in reference 4.131. Theoretical and experimental frequencies are given for specific plates used as electronic chassis.

For a specific case of a rectangular cantilever plate having added mass at the tip ($x=a$), see the discussion under parallelogram plates entitled "Other Supports and Conditions" (sec. 5.2).

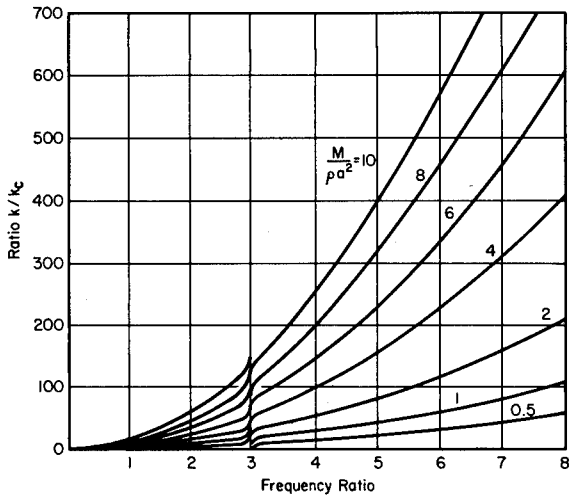


FIGURE 4.99.—Ratio of the fundamental frequency of a SS–SS–SS–C square plate having a point mass and a spring at $\xi=\eta=0.2a$ to that of the plate alone.

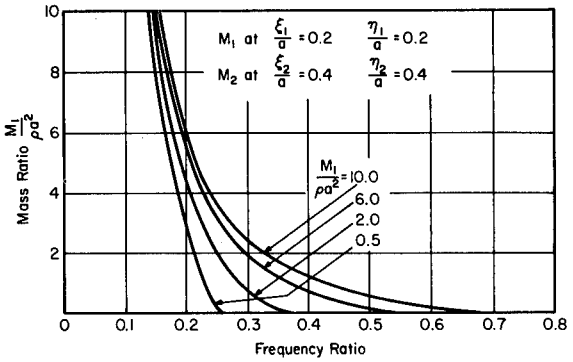


FIGURE 4.100.—Ratio of the fundamental frequency of a SS–SS–SS–C square plate having point masses M_1 and M_2 at $\xi_1=\eta_1=0.2a$ and $\xi_2=\eta_2=0.4a$, respectively, to that of the plate alone.

4.6 INTERNAL CUTOUTS

4.6.1 Circular Holes

A rectangular plate either clamped or simply supported on the outer edges and having a centrally located circular hole is shown in figure 4.101. Takahashi (ref. 4.159) solved the problem in the case when all edges are clamped by using the Rayleigh-Ritz method and deflection functions which are products of beam functions. Variation in fundamental frequency parameter as a function of R/a ratio is given in figure 4.102 for several a/b ratios and $\nu=0.3$. The frequency scale is amplified in figure 4.103 and theoretical and experimental values are given for the case when $a/b=0.5$.

Kumai (ref. 4.160) used the point-matching method to find the first three frequencies for

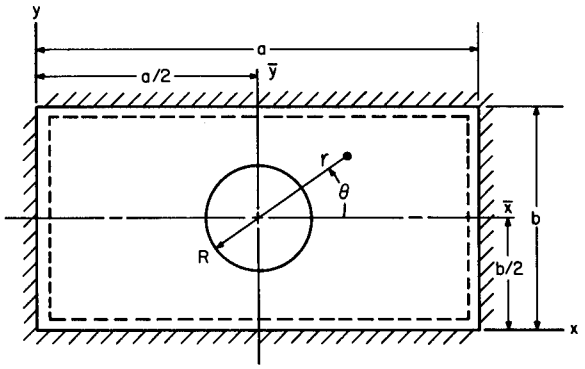


FIGURE 4.101.—Rectangular plate having a centrally located circular hole.

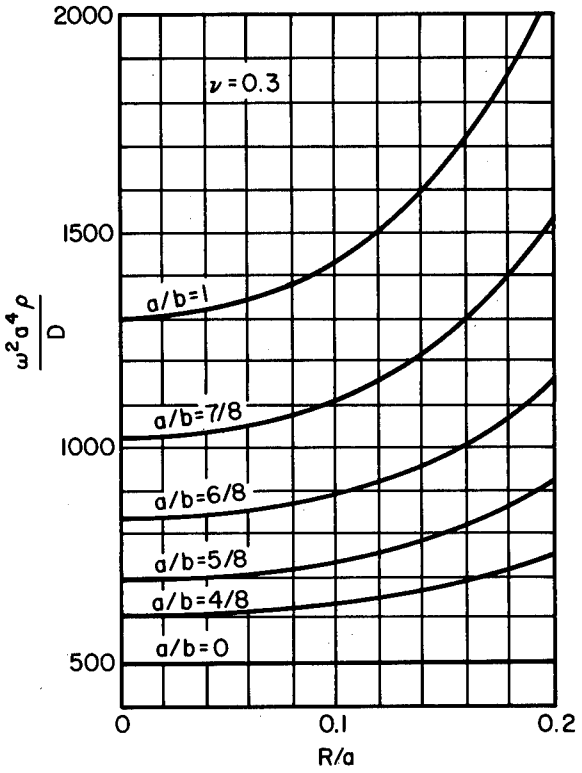


FIGURE 4.102.—Frequency parameters $\omega^2a^4\rho/D$ for a rectangular plate clamped all around having a central circular hole. (After ref. 4.159)

the previous problem when $a/b=0.5$. Theoretical and experimental cyclic frequencies were obtained for celluloid plates 2.75 by 2.75 inches by 0.020 inch having various R/a ratios and are shown in figure 4.104. In table 4.105 are listed the ratios of the frequencies of clamped square plates having central circular holes to those of plates without holes.

The case when the outer boundary is simply supported was also studied in reference 4.160 and cyclic frequency variations are shown in figure 4.105. Frequency ratios for this problem are also shown in table 4.105.

Joga-Rao and Pickett (ref. 4.37) used the Rayleigh-Ritz method with algebraic polynomials and a biharmonic singular function to obtain

$$\omega a^2\sqrt{\rho/D}=5.6148 \qquad (4.123)$$

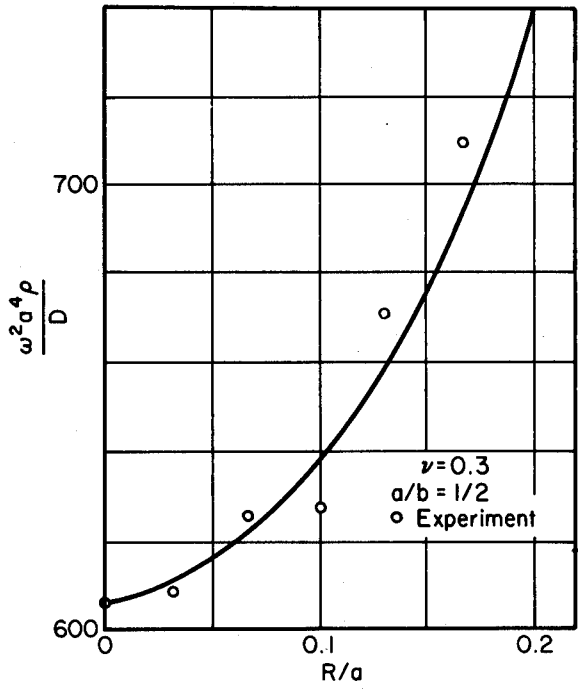


FIGURE 4.103.—Theoretical and experimental frequency parameters $\omega^2 a^4 \rho/D$ for a clamped rectangular plate having a central circular hole. (After ref. 4.159)

for a SS–SS–SS–SS square plate having a central circular hole, $R/a=0.5$, and $\nu=0.3$. The function used was (see fig. 4.101)

$$W(\bar{x},\bar{y})=\left(1-\frac{\bar{x}^2}{a^2}\right)\left(1-\frac{\bar{y}^2}{a^2}\right)\left[A_1+A_2\left(\frac{r}{a}\right)^2+A_3\ln\frac{r}{a}\right] \quad (4.124)$$

Frequency parameters for various numbers and combinations of coefficients retained in equation (4.124) are listed in table 4.106. Because all results are upper bounds, the lowest value is the most accurate one.

The frequency parameter for the square plate having a central circular hole in the case when the outer edge is completely free was given in reference 4.37 as

$$\omega a^2\sqrt{\rho/D}=2.8963 \quad (4.125)$$

when $R/a=0.5$ and $\nu=0.3$. The Rayleigh-Ritz method and the function

$$W(r,\theta)=(A_1r^2+A_2r^4+A_3+A_4r^{-2})\sin 2\theta \quad (4.126)$$

(see fig. 4.101) was used. Frequency parameters for various numbers and combinations of coefficients retained in equation (4.126) are listed in table 4.107.

TABLE 4.105.—*Frequency Ratios and Nodal Patterns for Square Plates With Central Circular Holes*

Nodal pattern	$\frac{R}{a}$	Frequency ratio	
		Clamped edge	SS edge
	0	1. 000	1. 000
	.2	. 986	. 985
	.4	1. 118	. 965
	0	1. 000	1. 000
	.2	. 916	. 913
	.4	. 876	. 804
	0	1. 000	1. 000
	.2	1. 040	1. 024
	.4	1. 195	1. 228

4.6.2 Other Cutouts

The case of the completely free square plate (fig. 4.106) having a centrally located square hole was investigated in reference 4.37. The Rayleigh-Ritz method and functions given in equation (4.126) were used for $c/a=0.5$. Frequency parameters for various numbers and combinations of coefficients retained in equa-

TABLE 4.106.—*Frequency Parameters* $\omega a^2\sqrt{\rho/D}$ *for a SS–SS–SS–SS Square Plate Having a Central Circular Hole;* $\nu=0.3$

Coefficients retained	A_1	A_2	A_3	A_1A_2	A_1A_3	$A_1A_2A_3$
$\omega a^2\sqrt{\rho/D}$	6. 743	24. 21	20. 003	5. 955	5. 629	5. 615

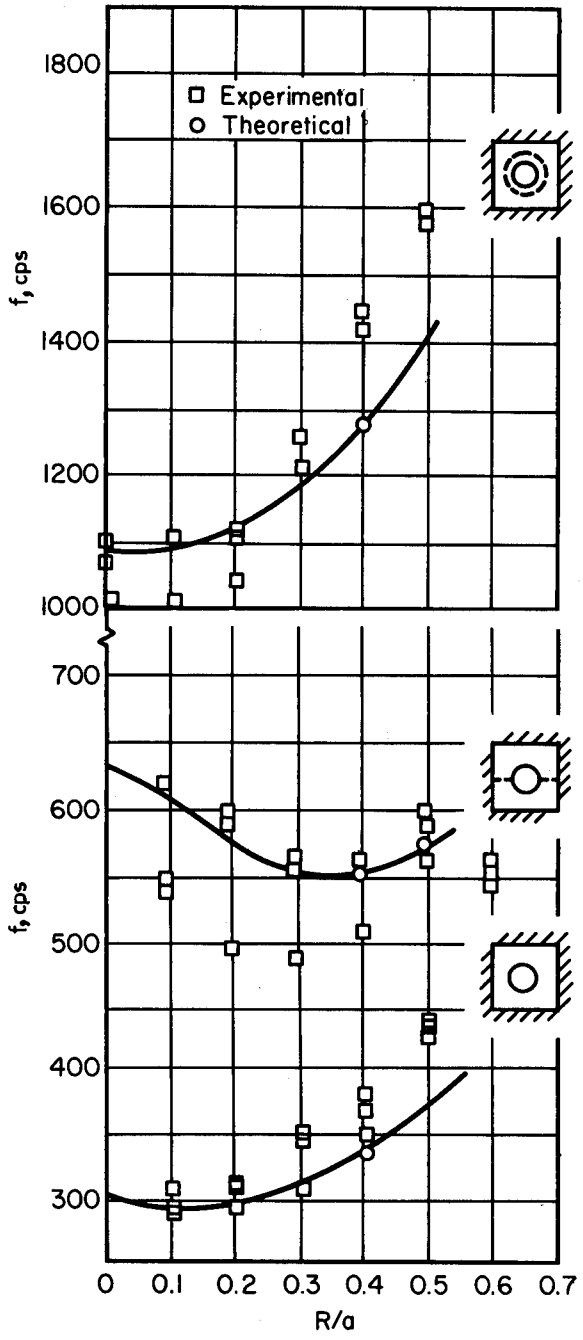


FIGURE 4.104.—Cyclic frequencies for C–C–C–C square plate having a central circular hole. (After ref. 4.160)

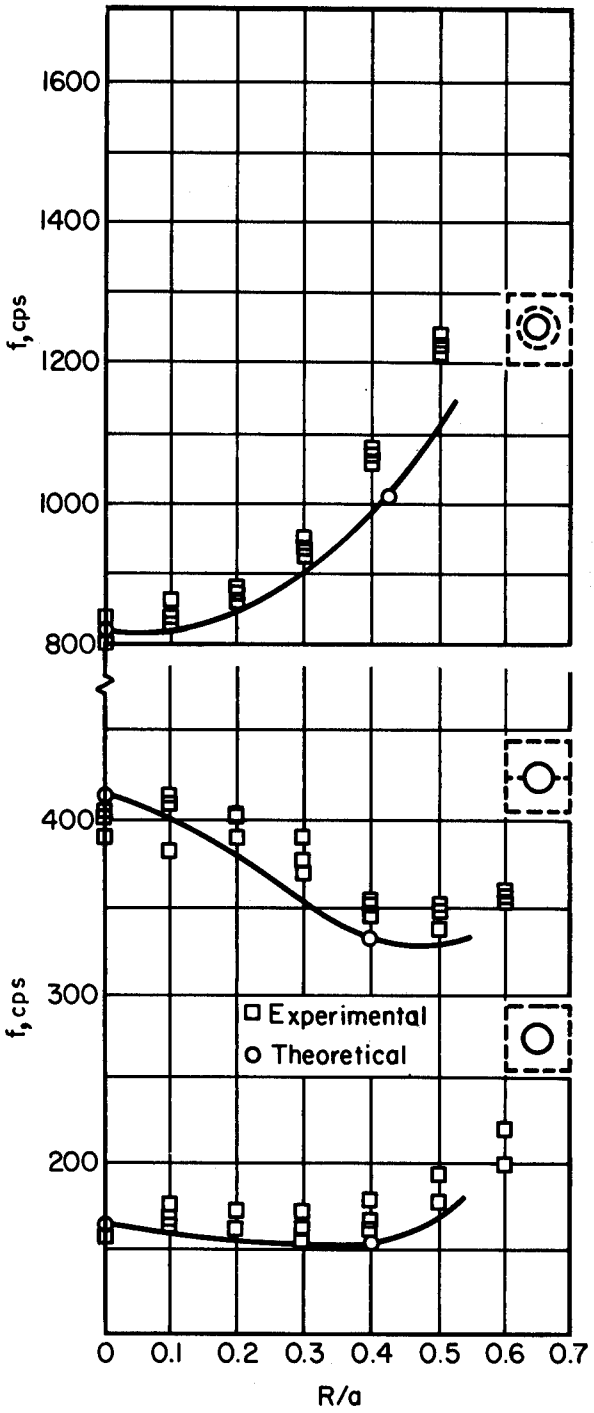


FIGURE 4.105.—Cyclic frequencies for SS–SS–SS–SS square plate having a central circular hole. (After ref. 4.160)

308-337 O - 70 - 11

TABLE 4.107.—*Frequency Parameters* $\omega a^2\sqrt{\rho/D}$ *for a F–F–F–F Square Plate Having a Central Circular Hole*

Coefficients retained	A_1	A_2	A_3	A_4	A_1A_3	$A_1A_2A_3$	$A_1A_3A_4$	$A_1A_2A_3A_4$
$\omega a^2\sqrt{\rho/D}$	3. 189	9. 478	7. 617	25. 45	3. 026	2. 914	2. 962	2. 896

TABLE 4.108.—*Frequency Parameters* $\omega a^2\sqrt{\rho/D}$ *for a F–F–F–F Square Plate Having a Central Square Hole;* $\nu=0.3$

Coefficients retained	A_1	A_2	A_3	A_4	A_1A_3	$A_1A_2A_3$	$A_1A_3A_4$	$A_1A_2A_3A_4$
$\omega a^2\sqrt{\rho/D}$	3. 1	10. 21	6. 754	17. 13	2. 931	2. 845	2. 887	2. 845

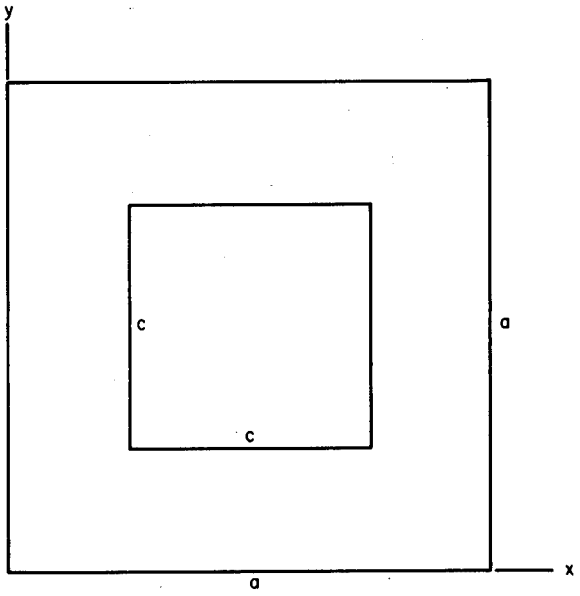


FIGURE 4.106.—F–F–F–F square plate with a central square hole.

tion (4.126) are listed in table 4.108. The lowest value is the most accurate.

Consider next the rectangular plate simply supported on all external edges and having a narrow slit of length c along one axis of symmetry as shown in figure 4.107. This problem is studied in reference 4.136. One numerical result is given but it is highly inaccurate. The case when the slit is completely internal is formulated in reference 4.161, but no numerical results for vibration are given.

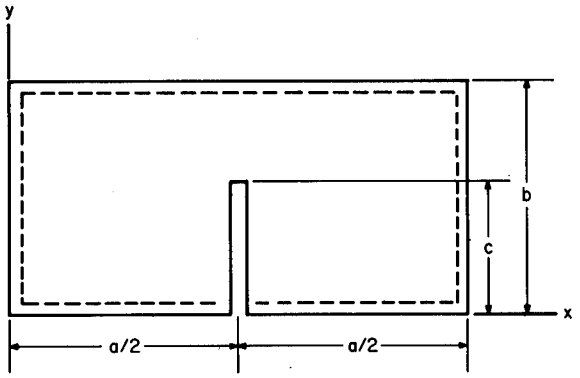


FIGURE 4.107.—SS–SS–SS–SS rectangular plate with a symmetrically located slit.

REFERENCES

4.1. WARBURTON, G. B.: The Vibration of Rectangular Plates. Proc. Inst. Mech. Eng., ser. A, vol. 168, no. 12, 1954, pp. 371–384.

4.2. JANICH, R.: Die näherungsweise Berechnung der Eigenfrequenzen von rechteckigen Platten bei verschiedenen Randbedingungen. Die Bautechnik, vol. 3, Mar. 1962, pp. 93–99.

4.3. HEARMON, R. F. S.: The Frequency of Vibration of Rectangular Isotropic Plates. J. Appl. Mech., vol. 19, 1952, pp. 402–403.

4.4. VET, MAARTEN: Natural Frequencies of Thin Rectangular Plates. Mach. Design, vol. 37, no. 13, June 1965, pp. 183–185.

4.5. NADAI, A.: Die Elastiche Platten. Julius Springer (Berlin), 1925, pp. 164–173.

4.6. LECKIE, F. A.: The Application of Transfer Matrices to Plate Vibrations. Ingr.-Arch., vol. 32, no. 2, Feb. 1963, pp. 100–111.

4.7. FLETCHER, H. J.; WOODFIELD, N.; AND LARSEN, K.: Natural Frequencies of Plates With Opposite Edges Supported. Contract DA-04-495-ORD-560 (CFSTI No. AD 107 224), Brigham Young Univ., Sept. 1956.

4.8. FLETCHER, H. J.: The Frequency of Vibration of Rectangular Isotropic Plates. J. Appl. Mech., vol. 26, no. 2, June 1959, p. 290.

4.9. IGUCHI, S.: Die Eigenwertprobleme für die elastische rechteckige Platte. Mem. Fac. Eng., Hokkaido Univ., 1938, pp. 305–372.

4.10. DAS, Y. C.: On the Transverse Vibrations of Rectangular Isotropic Plates. J. Aeron. Soc. India, vol. 13, no. 4, Nov. 1961, pp. 111–117.

4.11. VELETSOS, A. S.; AND NEWMARK, N. M.: Determination of Natural Frequencies of Continuous Plates Hinged Along Two Opposite Edges. J. Appl. Mech., vol. 23, no. 1, Mar. 1956, pp. 97–102.

4.12. LURIE, H.: Vibrations of Rectangular Plates. J. Aeron. Sci., vol. 18, no. 2, Feb. 1951, pp. 139–140.

4.13. ÖDMAN, S. T. A.: Studies of Boundary Value Problems. Part II. Characteristic Functions of Rectangular Plates. Proc. NR 24, Swedish Cement and Concrete Res. Inst., Roy. Inst. Tech. (Stockholm), 1955, pp. 7–62.

4.14. NISHIMURA, T.: Studies on Vibration Problems of Flat Plates by Means of Difference Calculus. Proc. 3d Jap. Natl. Congr. Appl. Mech., 1953, pp. 417–420.

4.15. HAMADA, M.: A Method for Solving Problems of Vibration, Deflection and Buckling of Rectangular Plates With Clamped or Supported Edges. Bull. JSME, vol. 2, no. 5, 1959, pp. 92–97.

4.16. KANAZAWA, T.; AND KAWAI, T.: On the Lateral Vibration on Anisotropic Rectangular Plates. Proc. 2d Jap. Natl. Congr. Appl. Mech., 1952, pp. 333–338.

4.17. TIMOSHENKO, S.; AND GERE, J. M.: Theory of Elastic Stability. McGraw-Hill Book Co., Inc., 1961.

4.18. KIST'YAN, K. YA: An Approximate Determination of the Frequencies of Vibrations of Plates and Their Subsequent Improvement. Str-vo Arkhitekt., no. 9, 1959, pp. 67–70. (In Russian.)

4.19. SONNEMAN, GEORGE: On Correlation of Buckling and Vibration of Plates. Proc. 1st Midwest. Conf. Solid Mech., Eng. Exp. Sta., Univ. Michigan, Apr. 1953, pp. 124–126.

4.20. KATO, H.: On the Bending and Vibration of Rectangular Plates. J. Soc. Nav. Architect., vol. 50, 1932, pp. 209–230. (In Japanese.)

4.21. SEZAWA, K.: On the Lateral Vibration of a Rectangular Plate Clamped at Four Edges. Rept. No. 70, Aeron. Res. Inst., Tokyo Univ., 1931, pp. 61–70.

4.22. UNGAR, E. E.: Free Oscillations of Edge-Connected Simply Supported Plate Systems. J. Eng. Ind., vol. 4, Nov. 1961, pp. 434–440.

4.23. KIST'YAN, K. YA: Approximate Determination of the Frequencies of Rectangular Plates. Prikl. Mekh., vol. 8, no. 2, 1962, pp. 219–222. (In Ukrainian.)

4.24. DILL, E. H.; AND PISTER, K. S.: Vibration of Rectangular Plates and Plate Systems. Proc. 3d U.S. Natl. Congr. Appl. Mech., 1958, pp. 123–132.

4.25. VOLMIR, A. S.: Stability of Elastic Systems. Gos. Izd. Phys.-Mat. Lit. (Moscow), 1963. (In Russian.)

4.26. VOIGT, W.: Bemerkungen zu dem Problem der transversalen Schwingungen rechteckiger Platten. Nachr. Ges. Wiss. (Göttingen), no. 6, 1893, pp. 225–230.

4.27. JANKOVIC, V.: The Solution of the Frequency Equation of Plates Using Digital Computers. Stavebnicky Casopis, vol. 12, no. 6, 1964, pp. 360–365. (In Czech.)

4.28. ZEISSIG, C.: Ein einfacher Fall der transversalen Schwingungen einer rechteckigen elastischen Platte. Ann. Physik, Bd. 64, 1898, pp. 361–397.

4.29. NARUOKA, M.: On Transverse Vibration of Rectangular Flat Plates Clamped at Four Edges. Trans. JSME, vol. 17, no. 57, 1951, pp. 26–30. (In Japanese.)

4.30. TOMOTIKA, S.: The Transverse Vibration of a Square Plate Clamped at Four Edges. Phil. Mag., ser. 7, vol. 21, no. 142, Apr. 1936, pp. 745–760.

4.31. SUZUKI, S.: On the Transverse Vibrations of Rectangular Flat Plates Clamped at Four Edges. Trans. JSME, vol. 13, no. 44, pp. I–50—I–58. (In Japanese.)

4.32. HABATA, Y.: On the Lateral Vibration of a Rectangular Plate Clamped at Four Edges. Trans. JSME, vol. 13, no. 44, 1947, pp. 67–83. (In Japanese.)

4.33. MUNAKATA, K.: On the Vibration and Elastic Stability of a Rectangular Plate Clamped at Its Four Edges. J. Math. & Phys., vol. 31, no. 1, Apr. 1952, pp. 69–74.

4.34. DEVERALL, L. I.: Modified Method of Collocations for Vibrating Plate Problems. Int. Conf. on Partial Differential Equations and Continuum Mechanics (Univ. Wisconsin, 1960), Univ. Press, 1961.

4.35. CLAASSEN, R. W.; AND THORNE, C. J.: Vibrations of Thin Rectangular Isotropic Plates. J. Appl. Mech., vol. 28, no. 2, June 1961, pp. 304–305.

4.36. CLAASSEN, R. W.; AND THORNE, C. J.: Transverse Vibrations of Thin Rectangular Isotropic Plates. NOTS Tech. Pub. 2379, NAVWEPS Rept. 7016 U.S. Naval Ordnance Test Sta.,

China Lake, Calif., Aug. 1960. (Errata available from CFSTI as AD 245 000.)

4.37. Joga-Rao, C. V.; and Pickett, Gerald: Vibrations of Plates of Irregular Shapes and Plates With Holes. J. Aeron. Soc. India, vol. 13, no. 3, 1961, pp. 83–88.

4.38. Hidaka, K.: Vibration of a Square Plate Clamped at Four Edges. Math. Jap., vol. 2, 1951, pp. 97–101.

4.39. Green, A. E.: Double Fourier Series and Boundary Value Problems. Proc. Cambridge Phil. Soc., 1944.

4.40. Leissa, A. W.: A Method for Analyzing the Vibration of Plates. J. Aerospace Sci., vol. 29, no. 4, Apr. 1962, p. 475.

4.41. Tomotika, S.: On the Transverse Vibration of a Square Plate With Clamped Edges. Aeron. Res. Inst. Rept., Tokyo Univ., vol. 10, 1935, p. 301.

4.42. Hersch, J.: Contribution à la Méthode des Équations aux Différences. ZAMP, vol. 9a, no. 9, 1958, pp. 129–180.

4.43. Abramowitz, M.; and Cahill, W. F.: On the Vibration of a Square Clamped Plate. J. Assoc. Comput. Mach., vol. 2, no. 3, 1955, pp. 162–168.

4.44. Aynola, L. Ya.: Methods of Investigating Elastic Plate Vibrations. Inz. Zhurnal, vol. 3, no. 2, 1963, pp. 312–321. (In Russian.)

4.45. Galin, M. P.: On the Transverse Vibrations of Plates. Prikl. Mat. Mekh., vol. 12, no. 3, 1947, pp. 387–388. (In Russian.)

4.46. Stanisic, M.: An Approximate Method Applied to the Solution of the Problem of Vibrating Rectangular Plates. J. Aeron. Sci., vol. 24, no. 2, Feb. 1957, pp. 159–160.

4.47. Young, D.: Vibration of Rectangular Plates by the Ritz Method. J. Appl. Mech., vol. 17, no. 4, Dec. 1950, pp. 448–453.

4.48. Nagaraja, J.; and Rao, S. S.: Vibration of Rectangular Plates. J. Aeron. Sci., vol. 20, no. 12, Dec. 1953, pp. 855–856.

4.49. Aronszajn, N.: The Rayleigh-Ritz and the Weinstein Methods for Approximation of Eigenvalues—III: Application of Weinstein's Method With an Auxiliary Problem of Type I. Tech. Rept. no. 3, Proj. NR 041, 090, Oklahoma A. and M. College (Stillwater, Okla.), 1950.

4.50. Hopkins, H. G.: The Solution of Small Displacement, Stability, or Vibration Problems Concerning a Flat Rectangular Panel When the Edges Are Either Clamped or Simply Supported. R.A.E. Rept. No. SME 3331, R. & M. No. 2234, British A.R.C., June 1945.

4.51. Gontkevich, V. S.: Natural Vibrations of Plates and Shells. A. P. Filippov, ed., Nauk. Dumka (Kiev), 1964. (Transl. by Lockheed Missiles & Space Co. (Sunnyvale, Calif.).)

4.52. Sorokin, E. S.: Dynamics of Between-Floors Ceilings. Stroiizdat (Moscow), 1941. (In Russian.)

4.53. Eschler, H.: Zur Ermittlung der Eigenschwingungszahlen der in ihrer Mittelebene belasteten Rechteckplatte. Ingr.-Arch., Bd. 18, 1950, pp. 330–337.

4.54. Collatz, L.: Das Mehrstellverfahren bei Plattenaufgaben. ZAMM, vol. 30, 1950, pp. 385–388.

4.55. Gontkevich, V. S.: The Lower Bounds of Natural Frequencies of a Plate in Flexural Vibrations. Prikl. Mekh., AN UkrSSR, vol. 6, no. 3, 1960, pp. 346–350. (In Ukrainian.)

4.56. Sezawa, K.: Free Vibration of a Clamped Square Plate. J. Aeron. Res. Inst., no. 6, 1924, pp. 29–42.

4.57. Bolotin, V. V.: Dynamic Edge Effect in the Elastic Vibrations of Plates. Inshen. Sbornik., vol. 31, 1961, pp. 3–14. (In Russian.)

4.58. Bazley, N. W.; Fox, D. W.; and Stadter, J. T.: Upper and Lower Bounds for the Frequencies of Rectangular Clamped Plates. Tech. Memo. TG–626, Appl. Phys. Lab., The Johns Hopkins Univ., May 1965.

4.59. Bazley, N. W.; and Fox, D. W.: Methods for Lower Bounds to Frequencies of Continuous Elastic Systems. Rept. TG–609, Appl. Phys. Lab., The Johns Hopkins Univ., Oct. 1964.

4.60. Bolotin, V. V.; Makarov, B. P.; Mishenkov, G. V.; and Shveiko, Yu Yu: Asymptotic Method of Investigating the Natural Frequency Spectrum of Elastic Plates. Raschet na Prochnost, Mashgiz (Moscow), no. 6, 1960, pp. 231–253. (In Russian.)

4.61. Kaul, R. K.; and Cadambe, V.: The Natural Frequencies of Thin Skew Plates. Aeron. Quart., vol. 7, 1956, pp. 337–352.

4.62. Iwato: Approximate Calculation for the Frequency of Natural Vibration of a Thin Rectangular Plate the Two Adjacent Edges of Which Are Clamped While the Other Two Edges Are Freely Supported. Trans. JSME, vol. 17, no. 57, 1951, pp. 30–33. (In Japanese.)

4.63. Claassen, R. W.; and Thorne, C. J.: Vibrations of a Rectangular Cantilever Plate. Tech. Rept. PMR–TR–61–1, Pacific Missile Range, Aug. 1962.

4.64. Dill, E. H.: The Vibration of Plates and Plate Systems. Ph. D. Thesis, Univ. Calif. (Berkeley, Calif.), Jan. 1957.

4.65. Plass, H. J., Jr.; Gaines, J. H.; and Newsom, C. D.: Application of Reissner's Variational Principle to Cantilever Plate Deflection and Vibration Problems. J. Appl. Mech., vol. 29, no. 1, Mar. 1962, pp. 127–135.

4.66. Austin, R. N.; Caughfield, D. A.; and Plass, H. J., Jr.: Application of Reissner's Variational Principle to the Vibration Analysis of Square Flat Plates With Various Root Sup-

port Conditions. Developments in Theoretical and Applied Mechanics. Vol. 1. Plenum Press (New York, N.Y.), 1963, pp. 1–24.

4.67. GAINES, J. H.: Application of the Modified Reissner Variational Principle to a Cantilever Plate Problem. Def. Res. Lab. Rept. DRL–440, CF 2766, Univ. Texas, Mar. 1959. Also, M. Sc. Thesis, Univ. Texas, June 1959.

4.68. CAUGHFIELD, D. A.: Application of the Modified Reissner Variational Principle to a Cantilever Plate Problem Using the Techniques of Numerical Integration and Finite Differences. Def. Res. Lab. Rept. DRL–457, CF 2902, Univ. Texas, Jan. 1961. Also, M. Sc. thesis, Univ. Texas, Jan. 1961.

4.69. REISSNER, E.: On a Variational Theorem in Elasticity. J. Math. Phys., vol. 29, 1950, pp. 90–95.

4.70. MACNEAL, R. H.: The Solution of Elastic Plate Problems by Electrical Analogies. J. Appl. Mech., vol. 18, no. 1, Mar. 1951, pp. 59–67.

4.71. GREENWOOD, DONALD: Some Difference Methods of Plate Vibration Analysis. NASA Grant NsG–63–60; CFSTI No. N62–14018.

4.72. CRAIG, R. R.; AND PLASS, H. J.: Vibration of Hub-Pin Plates. AIAA J., vol. 3, no. 6, June 1965, pp. 1177–1178.

4.73. BARTON, M. V.: Vibration of Rectangular and Skew Cantilever Plates. J. Appl. Mech., vol. 18, no. 1, June 1951, pp. 129–134.

4.74. BARTON, M. V.: Free Vibration Characteristics of Cantilever Plates. Defense Res. Lab. Rept. DRL–222, CM 570, Univ. Texas, Dec. 1949.

4.75. BAZLEY, N. W.; FOX, D. W; AND STADTER, J. T.: Upper and Lower Bounds for Frequencies of Rectangular Cantilever Plates. Tech. Memo. TG–705, Appl. Phys. Lab., The Johns Hopkins Univ., July 1965.

4.76. SIGILITO, V. G.: Improved Upper Bounds for Frequencies of Rectangular Free and Cantilever Plates. Eng. Memo. EM–4012, Appl. Phys. Lab., The Johns Hopkins Univ., Dec. 1965.

4.77. CLAASSEN, R. W.; AND THORNE, C. J.: Vibrations of a Rectangular Cantilever Plate. J. Aerospace Sci., vol. 29, no. 11, Nov. 1962, pp. 1300–1305.

4.78. MARTIN, A. I.: On the Vibration of a Cantilever Plate. Quart. J. Mech. Appl. Math., vol. 9, pt. 1, 1956, pp. 94–102.

4.79. GRINSTED, B.: Nodal Pattern Analysis. Proc. Inst. Mech. Eng., ser. A, vol. 166, 1952, pp. 309–326.

4.80. FORSYTH, E. M.; AND WARBURTON, G. B.: Transient Vibration of Rectangular Plates. J. Mech. Eng. Sci., vol. 2, no. 4, Dec. 1960, pp. 325–330.

4.81. DALLEY, J. W.; AND RIPPERGER, E. A.: Experimental Values of Natural Frequencies for Skew and Rectangular Cantilever Plates. Proc. Soc. Exp. Stress Anal., vol. 9, no. 2, 1952, pp. 51–66.

4.82. DALLEY, J. W.; AND RIPPERGER, E. A.: Experimental Values of Natural Frequencies for Skew and Rectangular Cantilever Plates. Def. Res. Lab. Rept. DRL–231, CF–1354, Univ. Texas, Dec. 1949.

4.83. HEIBA, A. E.: Vibration Characteristics of a Cantilever Plate With Sweptback Leading Edge. Rept. No. 82, Cranfield College of Aeron., Oct. 1954.

4.84. PLUNKETT, R.: Natural Frequencies of Uniform and Non-uniform Rectangular Cantilever Plates. J. Mech. Eng. Sci., vol. 5, no. 2, 1963, pp. 146–156.

4.85. WILSON, R. E.; AND PLUNKETT, R.: Vibration of Cantilever Plates With Rectangular and Wedge-Shaped Cross-Sections. Rept. DF 53GL17, Gen. Elec. Co., Mar. 1953.

4.86. CRAIG, R. R.; PLASS, H. J., JR.; AND CAUGHFIELD, D. A.: Experimental Determination of Frequencies and Mode Shapes of Cantilever and Hub-Pin Plates. Def. Res. Lab. Rept. DRL–518, CR–13, Univ. Texas, June 1964.

4.87. GUSTAFSON, P. N.; STOKEY, W. F.; AND ZOROWSKI, C. F.: The Effect of Tip Removal on the Natural Vibrations of Uniform Cantilevered Triangular Plates. J. Aeron. Sci., vol. 21, no. 9, Sept. 1954, pp. 621–633.

4.88. WALTON, W. C., JR.: Applications of a General Finite-Difference Method for Calculating Bending Deformations of Solid Plates. NASA TN D–536, 1960.

4.89. HOUBOLT, J. C.: A Study of Several Aerothermoelastic Problems of Aircraft Structures in High Speed Flight. Ph. D. Thesis, Zürich E.T.H., 1958.

4.90. DRAPER, K. J.; IRONS, B.; AND BAZELEY, G.: Comment on Vibration of a 45° Right Triangular Cantilever Plate by a Gridwork Method. AIAA J., vol. 2, no. 10, Oct. 1964, pp. 1870–1871.

4.91. HALL, A. H.: The Nature and Stiffness of Swept Wing Deformations With Reference to the Prediction of Normal Modes and Frequencies. Preprint no. 494, Can. Aeron. Inst. of Aeron. Sci., presented at CAI–IAS Int. Meeting, Oct. 1954. In CASI J., Sept. 1955.

4.92. BARTON, M. V.: Free Vibration Characteristics of Cantilever Plates. Def. Res. Lab. Rept. DRL–212, CF–1258, Univ. Texas, May 1949.

4.93. DALLEY, J. W.: Experimental Studies on Vibration Characteristics of Some Idealized Missile Fins. Def. Res. Lab. Rept. DRL–402, CF–2643, Univ. Texas, Sept. 1957.

4.94. REISSNER, E.; AND STEIN, M.: Torsion and Transverse Bending of Cantilever Plates. NACA TN 2369, 1951.

4.95. CHLADNI, E. F. F.: Entdeckungen über die Theorie des Klanges. Leipzig, 1787.
4.96. CHLADNI, E. F. F.: Die Akustik. Leipzig, 1802.
4.97. CHLADNI, E. F. F.: Ann. Physik, Leipzig, vol. 5, 1825, p. 345.
4.98. CHLADNI, E. F. F.: Neue Beitrage zur Akustik. Leipzig, 1817.
4.99. STREHLKE: Ann. Physik (Leipzig), vol. 4, 1825, p. 205.
4.100. STREHLKE: Ann. Physik (Leipzig), vol. 18, 1830, p. 198.
4.101. STREHLKE: Ann. Physik (Leipzig), vol. 27, 1833, p. 505.
4.102. STREHLKE: Ann. Physik (Leipzig), vol. 95, 1855, p. 577.
4.103. STREHLKE: Ann. Physik (Leipzig), vol. 146, 1872, p. 319.
4.104. KÖNIG, R.: Pogg. Ann., vol. 122, 1864.
4.105. TANAKA, S.: Ann. Physik (Leipzig), vol. 32 1887, p. 670.
4.106. WHEATSTONE, CHARLES: On the Figures Obtained by Strewing Sand on Vibrating Surfaces, Commonly Called Acoustic Figures. Phil. Trans. Roy. Soc. (London), 1833, pp. 593–633.
4.107. RAYLEIGH, Lord: On the Nodal Lines of a Square Plate. Phil. Mag., ser. 4, vol. 46, no. 304, Aug. 1873, pp. 166–171.
4.108. RITZ, W.: Theorie der Transversalschwingungen, einer quadratischen Platte mit freien Rändern. Ann. Physik, Bd. 28, 1909, pp. 737–786.
4.109. GOLDMANN, ELLA: Anwendung der Ritzschen Methode auf die Theorie der Transversalschwingungen freischwingender Platten von rechteckiger, rhombischer, dreieckiger und elliptischer Begrenzung. Dissertation, Breslau Univ., 1918.
4.110. LEMKE, A.: Experimentelle Untersuchungen zur W. Ritzschen Theorie der Transversalschwingungen Quadratischer Platten. Ann. Physik, Bd. 4, ser. 86, 1928, pp. 717–750.
4.111. PAVLIK, B.: Beitrag zur Theoretischen und Experimentellen Untersuchung der Biegungsschwingungen bei rechteckigen Platten mit freien Rändern. Ann. Physik, 1936, pp. 532–542.
4.112. PAVLIK, B.: Beitrag zur Untersuchung des Zusammenhanges der bei Beigungsschwingungen an rechteckigen und quadratischen Platten beobachteten Staubfiguren. Ann. Physik, Bd. 28, Heft 5, ser. 632, 1937, pp. 632–648.
4.113. IGUCHI, S.: Die Eigenschwingungen und Klangfiguren der vierseitig freien rechteckigen Platte. Ingr.-Arch., Bd. 21, ser. 303, Heft 5–6, 1953, pp. 304–322.
4.114. GRAUERS, H.: Transversalschwingungen rechteckiger Platten mit besonderer Rucksicht der Knickung. Ingeniorsvetenskapsakademien, Handlingar, 98, Stockholm, 1929.
4.115. NAKATA, Y.; AND FUJITA, H.: On Upper and Lower Bounds of the Eigenvalues of a Free Plate. J. Phys. Soc. Japan, vol. 10, 1955, pp. 823–824.
4.116. PAYNE, L. E.: Inequalities for Eigenvalues of Supported and Free Plates. Quart. J. Appl. Math., vol. 16, no. 2, 1958, pp. 111–120.
4.117. KATO, T.; FUJITA, H.; NAKATA, Y.; AND NEWMAN, M.: Estimation of the Frequencies of Thin Elastic Plates With Free Edges. J. Res. Natl. Bur. Std., vol. 59, no. 3, Sept. 1957, pp. 169–186.
4.118. BAZLEY, N. W.; FOX, D. W.; AND STADTER, J. T.: Upper and Lower Bounds for the Frequencies of Rectangular Free Plates. Tech. Memo TG–707, Appl. Physics Lab., The Johns Hopkins Univ., Aug. 1965.
4.119. WALLER, MARY D.: Vibrations of Free Square Plates. Proc. Phys. Soc. (London), vol. 51, Jan. 1939, pp. 831–844.
4.120. PAVLIK, B.: Biegungsschwingungen bei magnetostriktiv erregten Kreisplatten. Ann. Physik, Bd. 26, Heft 5, 1936, p. 625.
4.121. WALLER, MARY D.: Concerning Combined and Degenerate Vibrations of Plates. Acustica, vol. 3, 1953, pp. 370–374.
4.122. WALLER, MARY D.: Fundamental Vibration of a Rectangular Plate. Nature, vol. 143, no. 3610, Jan. 1939, pp. 27–28.
4.123. WALLER, MARY D.: Vibration of Free Rectangular Plates. Proc. Phys. Soc. (London), ser. B, vol. 62, no. 353, 1949, pp. 277–285.
4.124. PFEIFFER, F.: Ubergang zu Systemen mit unendlich vielen Freiheitsgraden. Ch. 4, Handbuch der Phys., Julius Springer (Berlin), 1928, pp. 337–402.
4.125. RAYLEIGH, Lord: On the Calculation of Chladni Figures for a Square Plate. Phil. Mag., vol. 22, 1911, pp. 225–229.
4.126. TANAKA, S.: Ann. Physik (Leipzig), vol. 32, 1887, p. 670.
4.127. LUNDQUIST, E. E.; AND STOWELL, E.: Critical Compressive Stress for Flat Rectangular Plates Supported Along All Edges and Elastically Restrained Against Rotation Along the Unloaded Edges. NACA Rept. 733, 1942.
4.128. CARMICHAEL, T. E.: The Vibration of a Rectangular Plate With Edges Elastically Restrained Against Rotation. Quart. J. Mech. Appl. Math., vol. 12, pt. 1, 1959, pp. 29–42.
4.129. JOGA-RAO, C. V.; AND KANTHAM, C. L.: Natural Frequencies of Rectangular Plates With Edges Elastically Restrained Against Rotation. J. Aeron. Sci., vol. 24, no. 4, Nov. 1957, pp. 855–856.
4.130. CHULAY, S. J.: Vibration of Elastically Restrained Rectangular Plates. M.S. Thesis, Univ. Wisconsin, 1957.
4.131. STOKEY, W. F.; ZOROWSKI, C. F.; AND APPL, F. C.: Prevention of Mechanical Vibrations

in Electronic Chassis-Design Manual. Rept. to Rome Air Develop. Center, Contract AF30(602)-913, Sept. 1955.

4.132. Hoppmann, W. H., II; and Greenspon, J.: An Experimental Device for Obtaining Elastic Rotational Constraints on the Boundary of a Plate. Proc. 2d U.S. Natl. Congr. Appl. Mech., 1954, pp. 187–191.

4.133. Ota, T.; and Hamada, M.: Fundamental Frequencies of Simply Supported but Partially Clamped Square Plates. Bull. JSME, vol. 6, no. 23, Aug. 1963, pp. 397–403.

4.134. Ota, T.; and Hamada, M.: Bending and Vibration of a Simply Supported but Partially Clamped Rectangular Plate. Proc. 8th Jap. Natl. Congr. Appl. Mech., 1958, pp. 103–106.

4.135. Kurata, M.; and Okamura, H.: Natural Vibrations of Partially Clamped Plates. J. Eng. Mech. Div., Proc. Am. Soc. Civil Eng., June 1963, pp. 169–186.

4.136. Nowacki, W.: Free Vibrations and Buckling of a Rectangular Plate With Discontinuous Boundary Conditions. Bull. Acad. Pol. Sci., cl. 4, vol. 3, no. 4, 1955, pp. 159–167.

4.137. Nowacki, W.: Dynamics of Elastic Systems. John Wiley & Sons, Inc., 1963.

4.138. Kurlandzki, J.: A Method for Solving Problems of Rectangular Plates With Mixed Boundary Conditions. Proc. Vibration Probl., vol. 2, no. 4, 1961, pp. 377–396.

4.139. Cox, H. L.; and Boxer, J.: Vibration of Rectangular Plates Point-Supported at the Corners. Aeron. Quart., vol. 11, no. 1, Feb. 1960, pp. 41–50.

4.140. Reed, R. E., Jr.: Comparison of Methods in Calculating Frequencies of Corner-Supported Rectangular Plates. NASA TN D-3030, 1965.

4.141. Kirk, C. L.: A Note on the Lowest Natural Frequency of a Square Plate Point-Supported at the Corners. J. Roy. Aeron. Soc., vol. 66, no. 616, Apr. 1962, pp. 240–241.

4.142. Cox, H. L.: Vibration of a Square Plate, Point Supported at Midpoints of Sides. J. Acoust. Soc. Am., vol. 27, no. 1, 1955, pp. 791–792.

4.143. Plass, H. J., Jr.: Application of Reissner's Variational Principle to Cantilever Plate Deflection and Vibration Problems. Def. Res. Lab. Rept. DRL-418, CM-921, Univ. Texas, Aug. 1958.

4.144. Cox, H. L.: Vibration of Certain Square Plates Having Similar Adjacent Edges. Quart. J. Mech. Appl. Math., vol. 8, pt. 4, 1955, pp. 454–456.

4.145. Nowacki, W.: Vibration and Buckling of Rectangular Plates Simply-Supported at the Periphery and at Several Points Inside. Arch. Mech. Stos., vol. 5, no. 3, 1953, p. 437. (In Polish.)

4.146. Beck, C. W.: An Excitation and Instrumentation System for Vibrating Plate Studies. Def. Res. Lab. Rept. DRL-467, CF-2930, Univ. Texas, June 1961.

4.147. Plass, H. J.: Theoretical Studies on Vibration Characteristics of Several Missile Fin Models. Def. Res. Lab. Rept. DRL-401, CF-2642, Univ. Texas, July 1957.

4.148. Cohen, H.; and Handelman, G.: Vibrations of a Rectangular Plate With Distributed Added Mass. J. Franklin Inst., vol. 261, no. 3, Mar. 1956, pp. 319–329.

4.149. Subramanian, N. R.; and Kumaraswamy, M. P.: Antisymmetric Vibrations of a Rectangular Plate With Distributed Added Mass. J. Aeron. Soc. India, vol. 12, no. 3, Aug. 1960, pp. 63–68.

4.150. Gershgorin, S.: Vibrations of Plates Loaded by Concentrated Masses. Prikl. Mat. Mekh., vol. 1, no. 1, 1933, pp. 25–37. (In Russian.)

4.151. Wah, T.: Natural Frequencies of Plate-Mass Systems. Proc. Indian Soc. Theor. and Appl. Mech., 1961, pp. 157–168.

4.152. Amba-Rao, C. L.: On the Vibration of a Rectangular Plate Carrying a Concentrated Mass. J. Appl. Mech., vol. 31, no. 3, Sept. 1964, pp. 550–551.

4.153. Stokey, W. F.; and Zorowski, C. F.: Normal Vibrations of a Uniform Plate Carrying Any Number of Finite Masses. J. Appl. Mech., vol. 26, no. 2, June 1959, pp. 210–216.

4.154. Lee, W. F. Z.: Free and Forced Vibrations of Constrained Beams and Plates. Ph. D. thesis, Carnegie Inst. Tech., 1952.

4.155. Filippov, A. P.: Vibrations of Elastic Systems. AN UkrSSR Press, 1956. (In Russian.)

4.156. Solecki, R.: Vibration of Plates With Concentrated Masses. Bull. Acad. Pol. Sci., Ser. Sci. Tech., vol. 9, no. 4, 1961, pp. 209–215.

4.157. Solecki, R.: Vibrations of Straight Bars and Plates With Concentrated Masses. Rozprawy Inzh. CC II, vol. 9, no. 3, 1961, pp. 497–511. (In Polish.)

4.158. Das, Y. C.; and Navaratna, D. R.: Vibrations of a Rectangular Plate With Concentrated Mass, Spring, and Dashpot. J. Appl. Mech., vol. 30, no. 1, Mar. 1963, pp. 31–36.

4.159. Takahashi, S.: Vibration of Rectangular Plates With Circular Holes. Bull. JSME, vol. 1, no. 4, 1958, 380–385.

4.160. Kumai, T.: The Flexural Vibrations of a Square Plate With a Central Circular Hole. Proc. 2d Jap. Natl. Congr. Appl. Mech., 1952, pp. 339–342.

4.161. Solecki, R.: Bending and Vibration of an Isotropic Rectangular Plate With a Hinged Slot. Acta Polytech. Scandinavica, no. 12, 1962, pp. 3–19.

Chapter 5

Parallelogram Plates

Because no exact solutions to equation (1.4) expressed in skew coordinates by equation (1.39) are known to exist in variables separable form, no significant exact solutions exist for parallelogram plates. Even the case when all edges are simply supported requires an intricate solution, unlike the case of the rectangle (sec. 4.1). Some solutions have been obtained by approximate methods for a few of the many possible combinations of boundary conditions. Particular emphasis exists in the literature for the case of the cantilevered parallelogram because of its importance as an aerodynamic lifting or stabilizing surface.

5.1 SIMPLE EDGE CONDITIONS

Results for plates with clamped (C), simply supported (SS), and free (F) edges are given in the following subsections.

5.1.1 C–C–C–C

Kaul and Cadambe (ref. 5.1) proposed a solution to the problem of the C–C–C–C parallelogram plate which used the Rayleigh-Ritz method and the products of characteristic beam functions; that is,

$$W(\xi, \eta)=\sum_m \sum_n A_{mn}\phi_m(\xi)\psi_n(\eta) \qquad (5.1)$$

where

$$\phi_m(\xi)=\frac{1}{\sqrt{a}}\left(\frac{\sin\{k_m[\xi-(a/2)]\}}{\sin(k_m a/2)}-\frac{\sinh\{k_m[\xi-(a/2)]\}}{\sinh(k_m a/2)}\right)\cos^2\frac{m\pi}{2}+\frac{1}{\sqrt{a}}\left(\frac{\cos\{k_m[\xi-(a/2)]\}}{\cos(k_m a/2)}-\frac{\cosh\{k_m[\xi-(a/2)]\}}{\cosh(k_m a/2)}\right)\sin^2\frac{m\pi}{2} \qquad m=1, 2, 3, \ldots \qquad (5.2)$$

where $k_m a$ is the mth positive root of the transcendental equation

$$\tan(k_m a/2)=(-1)^m \tanh(k_m a/2) \qquad (5.3)$$

The functions $\psi_n(\eta)$ are obtained by replacing ξ, a, and m in equation (5.2) by η, b, and n, respectively.

Results were obtained in reference 5.1 by using only one term of equation (5.1) and the Rayleigh method to obtain upper bounds for frequency parameters for the case of the rhombus ($a=b$). These results are given in table 5.1; the notation m/n is used to indicate the number of approximate half sine waves in the ξ/η directions, respectively (at least for small values of α). Combined modes of the form $(m/n \pm n/m)$ having nearly equal frequencies exist, as in the case of the square. (See sec. 4.3.1.)

Lower bounds were obtained in reference 5.1 for some of the modes by use of the Kato-

TABLE 5.1.—*Frequency Parameters* $\omega a^2\sqrt{\rho/D}$ *cos*^{2} α *for a C–C–C–C Rhombic Plate*

Mode type	$\omega a^2\sqrt{\rho/D}\cos^2\alpha$ for values of skew angle, α, deg, of—			
	0	15	30	45
1/1	36. 11	36. 67	38. 15	40. 08
1/2	73. 74	74. 76	77. 48	81. 06
2/2	108. 85	111. 43	118. 19	126. 84
(1/3) − (3/1)	131. 77	132. 90	135. 96	140. 02
(1/3) + (3/1)	133. 20	133. 71	138. 03	142. 70
3/2	165. 92	169. 56	179. 12	191. 41
3/3	220. 91	226. 76	242. 04	261. 46
(2/4) − (4/2)	242. 82	246. 91	258. 02	272. 36
(2/4) + (4/2)	245. 23	249. 67	261. 40	276. 64

TABLE 5.2.—*Upper and Lower Bounds of* $\omega a^2\sqrt{\rho/D}\cos^2\alpha$ *for a C–C–C–C Rhombic Plate*

Skew angle, α, deg	Mode type	$\omega a^2\sqrt{\rho/D}\cos^2\alpha$			
		Lower bound	Upper bound	Mean value	Maximum possible percentage deviation from mean value
0	1/1	35. 333	36. 109	35. 721	1. 07
	1/2	71. 768	73. 737	72. 752	1. 33
	2/2	104. 988	108. 850	106. 919	1. 77
15	1/1	34. 690	36. 666	35. 678	2. 69
	1/2	63. 686	74. 759	69. 222	7. 41
30	1/1	32. 959	38. 147	35. 55	6. 80
45	1/1	30. 638	40. 082	35. 36	11. 36

TABLE 5.3.—*Fundamental Frequency Parameters* $\omega a^2\sqrt{\rho/D}\cos^2\alpha$ *for a C–C–C–C Parallelogram Plate*

$\frac{a}{b}$	Source	$\omega a^2\sqrt{\rho/D}\cos^2\alpha$ for values of skew angle, α, deg, of—					
		15	20	30	35	45	60
1	Ref. 5.5	35. 636	35. 376	34. 624	34. 172	----------	----------
	Ref. 5.2	35. 625	----------	34. 788	----------	32. 795	30. 323
0.5	Ref. 5.5	24. 484	24. 388	24. 196	24. 096	----------	----------

Temple method. These are given in table 5.2 along with a mean value of frequency parameter determined from the lower and upper bounds and a computation of the maximum possible error which can arise from using the mean value.

It is clear from table 5.2 that the accuracies of the solutions decrease as (1) the mode number increases and (2) the skew angle increases.

Further results for this problem were obtained by Hamada (refs. 5.2 and 5.3) who used the method of Trefftz (ref. 5.4) and deflection functions

$$W(\xi,\eta)=\sum_{m=0}\sum_{n=0}\left(A_{mn}\cos\frac{m\pi\xi}{a}\cos\frac{n\pi\eta}{b}+B_{mn}\cos\frac{m\pi\xi}{a}\sin\frac{n\pi\eta}{b}+C_{mn}\sin\frac{m\pi\xi}{a}\cos\frac{n\pi\eta}{b}+D_{mn}\sin\frac{m\pi\xi}{a}\sin\frac{n\pi\eta}{b}\right) \quad (5.4)$$

and by Hasegawa (ref. 5.5) who used the Rayleigh-Ritz method and deflection functions (see fig. 5.1)

$$W(\bar{\xi},\bar{\eta})=[\bar{\xi}^2-(a/2)^2]^2[\bar{\eta}^2-(b/2)^2]^2(A_{00}+A_{11}\bar{\xi}\bar{\eta}+A_{20}\bar{\xi}^2+A_{02}\bar{\eta}^2+A_{31}\bar{\xi}^3\bar{\eta}+A_{13}\bar{\xi}\bar{\eta}^3+A_{22}\bar{\xi}^2\bar{\eta}^2) \quad (5.5)$$

These results are summarized in table 5.3 for $a/b=1$ and $a/b=0.5$. The problem is also discussed in reference 5.6.

In references 5.2 and 5.3, experimental results for the rhombic plate were also given. Mild steel plates with $a=b=2.36$ inches and $h=0.035$ inch were used. Figure 5.2 shows the ratio of the frequency of the rhombic plate to that of the square as a function of the skew angle. The curve shown is from the theoretical results. Plotted points are experimental data.

Conway and Farnham (ref. 5.7) analyzed

TABLE 5.4.—*Frequency Parameters for a C–C–C–C Rhombic Plate*

β, deg	45	40	37.5	35	30	27.5	25	22.5	20	15
$\omega c^2\sqrt{\rho/D}$	18. 00	21. 70	24. 05	26. 90	34. 66	40. 03	47. 05	56. 02	67. 91	107. 27

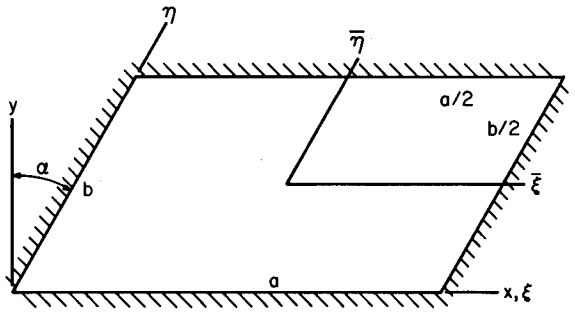


FIGURE 5.1.—C–C–C–C parallelogram plate.

the case of the rhombus by the point-matching method. In terms of the coordinate system shown in figure 5.3, the deflection functions

$$W(r,\theta)=\sum_{n=0,4,8}^{\infty}[A_nJ_n(kr)+B_nI_n(kr)]\cos n\theta \quad (5.6)$$

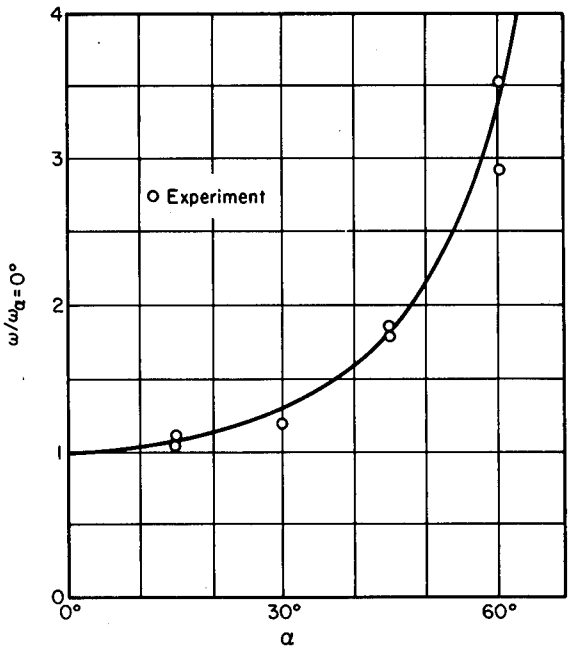


FIGURE 5.2.—Ratio of the frequency of a C–C–C–C rhombic plate to that of a square. (After ref. 5.2)

which exactly satisfy the differential equation (1.4) were taken. Boundary conditions of $w=\partial w/\partial r=0$ at $\theta=0°$, 30°, 60°, and 90° were matched, thus giving an eighth-order characteristic determinant. Frequency parameters for various values of β are listed in table 5.4.

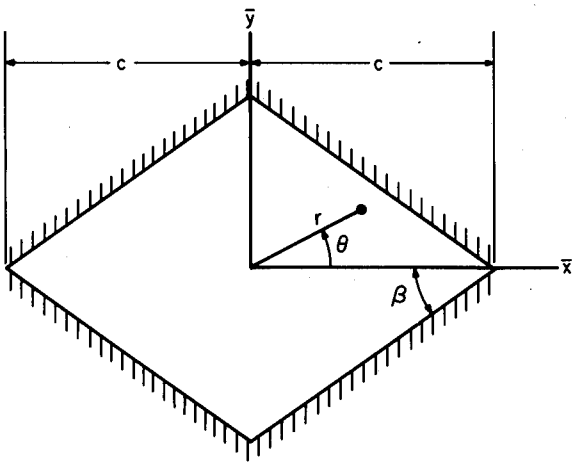


FIGURE 5.3.—C–C–C–C rhombic plate.

TABLE 5.5.—*Frequency Parameters* $\omega a^2\sqrt{\rho/D}\cos^2\alpha$ *for a C–C–C–SS Rhombic Plate*

Mode type	$\omega a^2\sqrt{\rho/D}\cos^2\alpha$ for values of skew angle, α, deg, of—			
	0	15	30	45
1/1	31. 95	32. 54	34. 09	36. 11
1/2	63. 66	64. 76	67. 68	71. 47
2/1	71. 43	72. 40	75. 04	78. 46
2/2	101. 26	103. 83	110. 58	119. 18
1/3	116. 97	118. 29	121. 81	126. 47
3/1	130. 84	132. 03	135. 11	139. 25
2/3	152. 75	156. 50	166. 32	178. 87
3/2	160. 00	163. 51	172. 75	184. 62
3/3	209. 97	215. 82	231. 06	250. 37

TABLE 5.6.—*Upper and Lower Bounds of* $\omega a^2\sqrt{\rho/D}\cos^2\alpha$ *for a C–C–C–SS Rhombic Plate*

Skew angle, α, deg	Mode type	$\omega a^2\sqrt{\rho/D}\cos^2\alpha$			
		Lower bound	Upper bound	Mean value	Maximum possible percentage deviation from mean value
0	1/1	31. 460	31. 953	31. 707	0. 77
	1/2	62. 227	63. 659	62. 943	1. 13
15	1/1	31. 467	32. 541	32. 004	1. 65
	1/2	60. 881	64. 761	62. 821	2. 99
30	1/1	30. 351	34. 094	32. 222	5. 49
45	1/1	29. 464	36. 108	32. 786	9. 20

5.1.2 C–C–C–SS

The problem of the C–C–C–SS parallelogram plate (fig. 5.4) is solved in reference 5.1 by using the Rayleigh method and a single term which is the product of beam functions expressed in terms of the skew coordinates. (See preceding sec. 5.1.1.) Frequency parameters for the case $a=b$ are given in table 5.5. Lower bounds from reference 5.1 are given in table 5.6 along with a mean value of frequency parameter determined from its lower and upper bounds. Also given is the maximum possible error which can arise from using the mean value. Accuracies of the solutions decrease as (1) the mode number increases and (2) the skew angle increases.

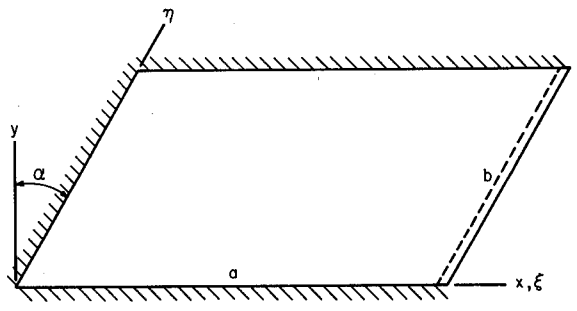


FIGURE 5.4.—C–C–C–SS parallelogram plate.

TABLE 5.7.—*Frequency Parameters* $\omega a^2\sqrt{\rho/D}\cos^2\alpha$ *for a C–C–SS–SS Rhombic Plate*

Mode type	$\omega a^2\sqrt{\rho/D}\cos^2\alpha$ for values of skew angle, α, deg, of—			
	0	15	30	45
1/1	27. 19	27. 84	29. 52	31. 68
(1/2)−(2/1)	60. 69	61. 73	64. 48	68. 06
(1/2)+(2/1)	61. 29	62. 40	65. 33	69. 13
2/2	93. 13	95. 74	102. 33	111. 15
(1/3)−(3/1)	115. 06	116. 29	119. 60	124. 44
(1/3)+(3/1)	115. 31	116. 57	119. 96	124. 44
(2/3)−(3/2)	145. 98	149. 58	159. 00	171. 04
(2/3)+(3/2)	146. 81	150. 50	160. 15	172. 46
3/3	198. 55	204. 43	219. 69	238. 97

5.1.3 C–C–SS–SS

The problem of the C–C–SS–SS parallelogram plate (fig. 5.5) is solved in reference 5.1 by using the Rayleigh method and a single term which is the product of beam functions expressed in terms of skew coordinates. (See sec. 5.1.1.) Frequency parameters for the case $a=b$ are given in table 5.7. Lower bounds from reference 5.1 are given in table 5.8 along with a mean value of frequency parameter determined from its lower and upper bounds. Also given is the maximum possible error that can arise from using the mean value. Accu-

TABLE 5.8.—*Upper and Lower Bounds of* $\omega a^2\sqrt{\rho/D}\cos^2\alpha$ *for a C–C–SS–SS Rhombic Plate*

Skew angle, α, deg	Mode type	$\omega a^2\sqrt{\rho/D}\cos^2\alpha$			
		Lower bound	Upper bound	Mean value	Maximum possible percentage deviation from mean value
0	1/1	26. 225	27. 195	26. 710	1. 78
	(1/2)−(2/1)	59. 407	60. 690	60. 048	1. 06
15	1/1	24. 913	27. 838	26. 375	5. 25
30	1/1	21. 450	29. 523	25. 487	13. 67

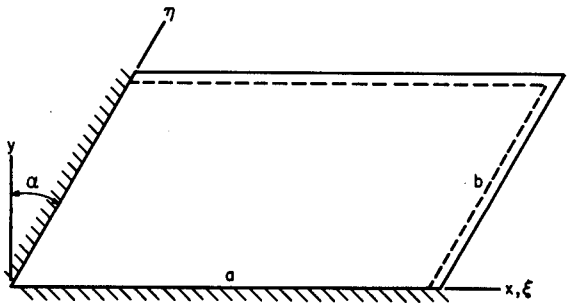


FIGURE 5.5.—C–C–SS–SS parallelogram plate.

racies of the solutions decrease as (1) the mode number increases and (2) the skew angle increases.

5.1.4 SS–SS–SS–SS

Tsydzik (ref. 5.8) solved the problem of the SS–SS–SS–SS parallelogram plate (fig. 5.6) by using the perturbation method. Equation (1.4) can be expressed as

$$\nabla^4 W-\lambda W=\epsilon L_1(W)-\epsilon^2 L_2(W)+\epsilon^3 L_3(W)-\epsilon^4 L_4(W) \tag{5.7}$$

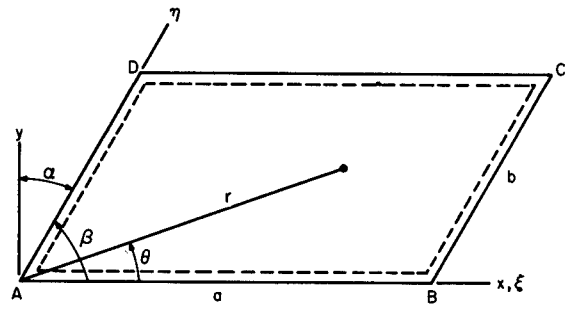


FIGURE 5.6.—SS–SS–SS–SS parallelogram plate.

where $\epsilon=\tan\alpha$, $\lambda=\omega^2\rho/D$, $W=W(\xi,\eta)$,

$$\left.\begin{aligned} L_1&\equiv 4\left(\frac{\partial^4 W}{\partial\xi^3\partial\eta}+\frac{\partial^4 W}{\partial\xi\partial\eta^3}\right)\\ L_2&=6\frac{\partial^4 W}{\partial\xi^2\partial\eta^2}+2\frac{\partial^4 W}{\partial\eta^4}\\ L_3&=4\frac{\partial^4 W}{\partial\xi\partial\eta^3}\\ L_4&=\frac{\partial^4 W}{\partial\eta^4}\end{aligned}\right\} \tag{5.8}$$

and ϵ may be considered as a perturbation parameter. Solutions for W and λ are then assumed in the form

$$\left.\begin{aligned} W_{mn}&=W_{mn}^{(0)}+\epsilon W_{mn}^{(1)}+\epsilon^2 W_{mn}^{(2)}+\cdots\\ \lambda_{mn}&=\lambda_{mn}^{(0)}+\epsilon\lambda_{mn}^{(1)}+\epsilon^2\lambda_{mn}^{(2)}+\cdots\end{aligned}\right\} \tag{5.9}$$

Substituting equations (5.9) into equation (5.7) and equating powers of ϵ yield

$$\nabla^4 W_{mn}^{(0)}-\lambda_{mn}^{(0)}W_{mn}^{(0)}=0 \tag{5.10}$$

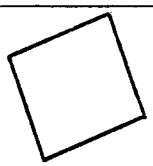
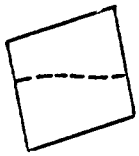
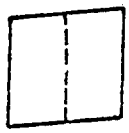
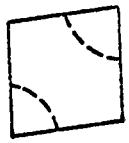
$$\nabla^4 W_{mn}^{(1)}-\lambda_{mn}^{(0)}W_{mn}^{(1)}=L_1(W_{mn}^{(0)})+\lambda_{mn}^{(1)}W_{mn}^{(0)} \tag{5.11}$$

$$\nabla^4 W_{mn}^{(2)}-\lambda_{mn}^{(0)}W_{mn}^{(2)}=L_1(W_{mn}^{(1)})-L_2(W_{mn}^{(0)})+\lambda_{mn}^{(1)}W_{mn}^{(1)}+\lambda_{mn}^{(2)}W_{mn}^{(0)} \tag{5.12}$$

Thus $W_{mn}^{(0)}$ and $\lambda_{mn}^{(0)}$ are taken to be

$$\left.\begin{aligned} W_{mn}^{(0)}&=\frac{2}{\sqrt{ab}}\sin\frac{m\pi\xi}{a}\sin\frac{n\pi\eta}{b}\\ \lambda_{mn}^{(0)}&=\pi^4\left(\frac{m^2}{a^2}+\frac{n^2}{b^2}\right)^2\end{aligned}\right\} \tag{5.13}$$

TABLE 5.9.—*Frequency Parameters, Nodal Patterns, and Mode Shape Coefficients for a SS–SS–SS–SS Rhombic Plate; tan $\alpha=0.1$*

Mode	1	2(*a*)	2(*b*)	3
$\omega a^2\sqrt{\rho/D}$	19.87	49.27	49.27	78.67
Nodal pattern				
Amplitude coefficients	$A_{11}=1.00000$ $A_{22}=-.00963$ $A_{24}=-.00058$ $A_{26}=-.00019$ $A_{42}=-.00058$ $A_{44}=-.00009$ $A_{46}=-.00004$ $A_{62}=-.00019$ $A_{64}=-.00004$ $A_{66}=-.00001$	$A_{12}=1.00000$ $A_{21}=0$ $A_{23}=-.09020$ $A_{25}=-.00126$ $A_{41}=.00219$ $A_{43}=-.00173$ $A_{45}=-.00025$ $A_{61}=.00028$ $A_{63}=-.00033$ $A_{65}=-.00007$	$A_{21}=1.00000$ $A_{12}=0$ $A_{14}=.00219$ $A_{16}=.00028$ $A_{32}=-.09020$ $A_{34}=-.00173$ $A_{36}=-.00033$ $A_{52}=-.00126$ $A_{54}=-.00025$ $A_{56}=-.00007$	$A_{22}=1.00000$ $A_{11}=.03850$ $A_{13}=.11540$ $A_{15}=.00269$ $A_{31}=.11540$ $A_{33}=-.02880$ $A_{35}=-.00274$ $A_{51}=.00269$ $A_{53}=-.00274$ $A_{55}=-.00048$

and the solution to equation (5.11) is assumed to be

$$W_{mn}^{(i)}=\sum_{p=1}^{r}\sum_{q=1}^{s}A_{pq}W_{pq}^{(i)} \qquad p\neq m,\ q\neq n \qquad (5.14)$$

This is substituted in equation (5.11) to yield A_{pq} and $\lambda_{mn}^{(i)}$, and the procedure is continued.

Results for the first three independent modes of a rhombus ($a=b$) are given in reference 5.8 for $\epsilon=\tan\alpha=0.1$. Frequency parameters and mode shapes for this plate are given in table 5.9. Fundamental frequencies ω_{11} may be obtained for other skew angles α and other a/b ratios from the curves of figure 5.7, where

$$\left.\begin{aligned}\Phi_{11}&=\frac{\omega_{11}ab}{2\pi}\sqrt{\frac{\rho}{D}}\\ \beta&=\frac{b}{a}\cos\alpha\end{aligned}\right\} \qquad (5.15)$$

Seth (ref. 5.9) gave an exact solution for the parallelogram bounded by the sides $x=0$, $x=a$, $y=x/\sqrt{3}$, and $y=(x/\sqrt{3})+(2a/\sqrt{3})$ as shown in figure 5.8. Frequencies are given by

$$\omega_{mn}=\frac{\pi^2}{4a^2}(m^2+mn+n^2)\sqrt{\frac{D}{\rho}} \qquad m,n=1,2,\ldots \qquad (5.16)$$

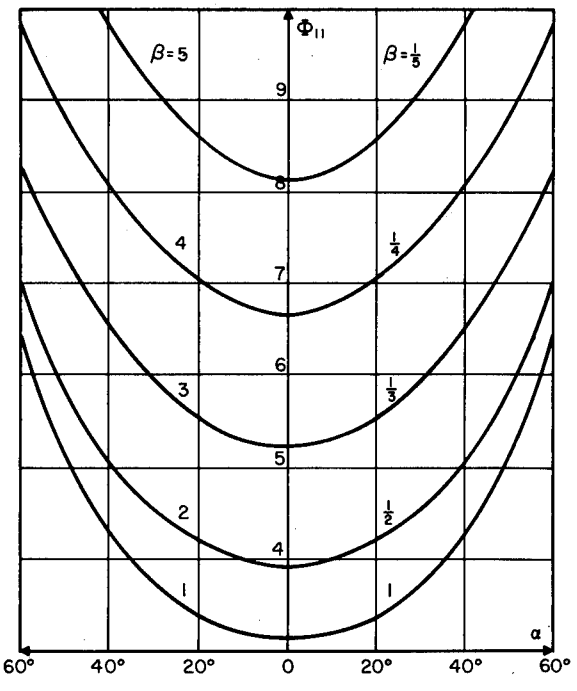


FIGURE 5.7.—Fundamental frequency parameters $\Phi_{11}=\omega_{11}ab\sqrt{\rho/D}/2\pi$ as a function of skew angle α and aspect ratio parameter $(b/a)\cos\alpha$ for a SS–SS–SS–SS parallelogram plate.

and the mode shapes by

$$W_{mn}(x,y)=2\sin\frac{(m-n)\pi x}{a}\cos\frac{(m+n)\pi\sqrt{3}y}{a}$$
$$-2\sin\frac{(2m+n)\pi x}{a}\cos\frac{n\pi\sqrt{3}y}{a}$$
$$+2\sin\frac{(2n+m)\pi x}{a}\cos\frac{m\pi\sqrt{3}y}{a} \quad (5.17)$$

Conway and Farnham (ref. 5.7) solved the problem by using the point-matching method.

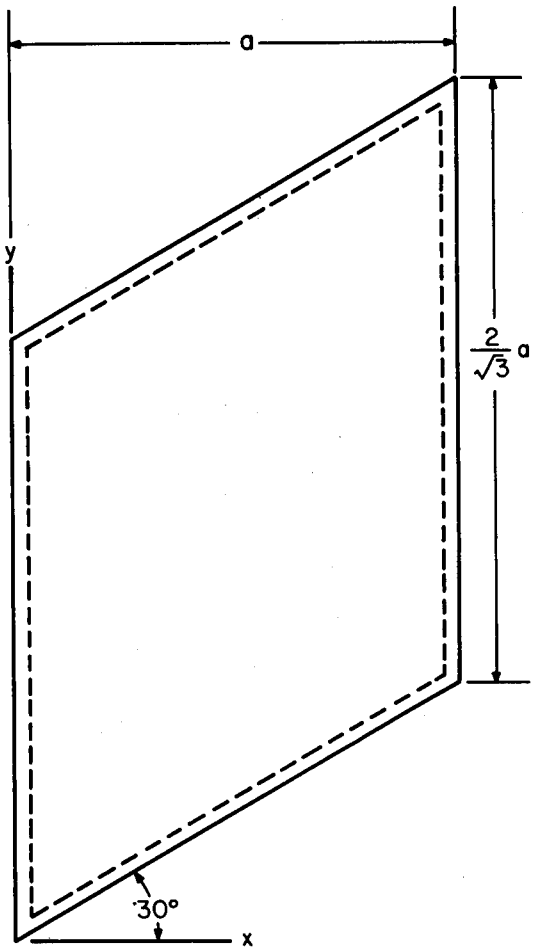


FIGURE 5.8.—SS–SS–SS–SS parallelogram plate having an exact solution.

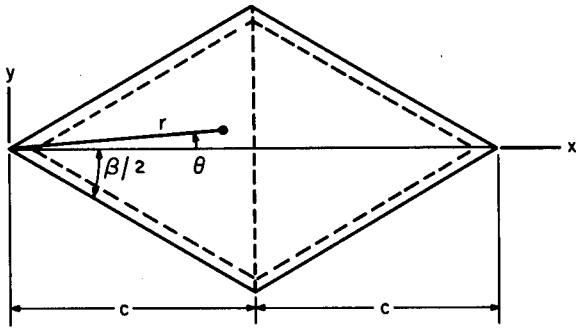


FIGURE 5.9.—SS–SS–SS–SS rhombic plate.

Fundamental frequencies for the rhombus (fig. 5.9) were derived by choosing a solution for the bending moment M in the form

$$M=\sum_{n=1,3,\ldots}^{\infty}A_nJ_q(kr)\cos q\theta \quad (5.18)$$

where $q=n\pi/\beta$ and M is defined by

$$M\equiv\frac{M_x+M_y}{1+\nu}=D\nabla^2w \quad (5.19)$$

The function in equation (5.18) satisfies exactly the differential equation (eq. (1.4)) and the boundary conditions along the edges $\theta=\pm\beta$. Symmetry conditions require that the transverse shear Q_x be zero along the line $x=c$. Satisfying this boundary condition at N discrete points along $x=c$ in the interval $0\leq y<c\tan\theta$ results in an N-by-N characteristic determinant for frequencies. Frequency parameters obtained by using various numbers of points are given in table 5.10.

In reference 5.7 the case of the general parallelogram (fig. 5.6) was also studied. In this case the functions

$$M=\sum_{n=1,2,\ldots}^{\infty}A_nJ_q(kr)\sin q\theta \quad (5.20)$$

were chosen and a characteristic determinant was derived by satisfying symmetry conditions

along the diagonal AC having the length c. Pointwise symmetry conditions employed were

$$\left.\begin{aligned} w|_{r=c/3} &= w|_{r=5c/3} \\ w|_{r=2c/3} &= w|_{r=4c/3} \\ \frac{1}{r}\frac{\partial w}{\partial \theta}\Big|_{r=c/3} &= -\frac{1}{r}\frac{\partial w}{\partial \theta}\Big|_{r=5c/3} \\ \frac{1}{r}\frac{\partial w}{\partial \theta}\Big|_{r=2c/3} &= -\frac{1}{r}\frac{\partial w}{\partial \theta}\Big|_{r=4c/3} \end{aligned}\right\} \quad (5.21)$$

Solutions of the resulting fourth-order characteristic determinants are given in table 5.11 for various angles β and a/b ratios.

Accuracy of the results can be estimated by comparing values for $\beta=90°$ with the known exact ones (section entitled "All Sides SS" under "Rectangular Plates" (4.1)) and the parameters for $a/b=1$ with those of table 5.10.

TABLE 5.10.—*Frequency Parameters* $\omega c^2\sqrt{\rho/D}$ *for SS–SS–SS–SS Rhombic Plates*

β, deg	$\omega c^2\sqrt{\rho/D}$ for determinant of size—	
	3 by 3	6 by 6
10	116. 92	
15	58. 06	58. 14
20	35. 87	
25	24. 95	
30	18. 65	18. 654
35	14. 62	
40	11. 87	
45	9. 872	

TABLE 5.11.—*Frequency Parameters* $\omega b^2\sqrt{\rho/D}$ *for SS–SS–SS–SS Parallelogram Plates*

β, deg	$\omega b^2\sqrt{\rho/D}$ for values of a/b of—		
	1	1.5	2
90	19. 8	14. 2	11. 97
75	20. 4	14. 3	12. 0
60	23. 7	16. 1	13. 3
45	31. 9	21. 2	16. 6

Analogies which permit one to obtain frequencies for polygonal plates simply supported all around from the problems of either (*a*) membrane vibration or (*b*) plate buckling due to hydrostatic pressure are discussed in the chapter entitled "Plates of Other Shapes" (ch. 8).

5.1.5 C–F–F–F

Barton (ref. 5.10) obtained the first comprehensive set of results for the problem of C–F–F–F parallelograms (fig. 5.10) by using the Rayleigh-Ritz method with deflection functions which are products of characteristic beam functions; that is,

$$W(\xi,\eta)=\sum_{m=1}^{p}\sum_{n=1}^{q} A_{mn}\phi_m(\xi)\psi_n(\eta) \quad (5.22)$$

where

$$\phi_m=\cosh\frac{\epsilon_m\xi}{a}-\cos\frac{\epsilon_m\xi}{a} - \alpha_m\left(\sinh\frac{\epsilon_m\xi}{a}-\sin\frac{\epsilon_m\xi}{a}\right)$$

$$\psi_1=1$$

$$\psi_2=\sqrt{3}(1-2\eta/b)$$

$$\psi_n=\cosh\frac{\epsilon_n\eta}{b}+\cos\frac{\epsilon_n\eta}{b} - \alpha_n\left(\sinh\frac{\epsilon_n\eta}{b}+\sin\frac{\epsilon_n\eta}{b}\right) \qquad n>2 \quad (5.23)$$

and where ϵ_m, ϵ_n, α_m, and α_n are found from table 4.46.

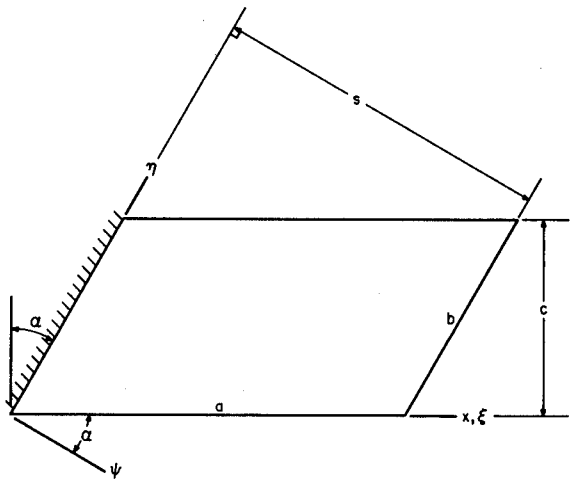


FIGURE 5.10.—C–F–F–F parallelogram plate.

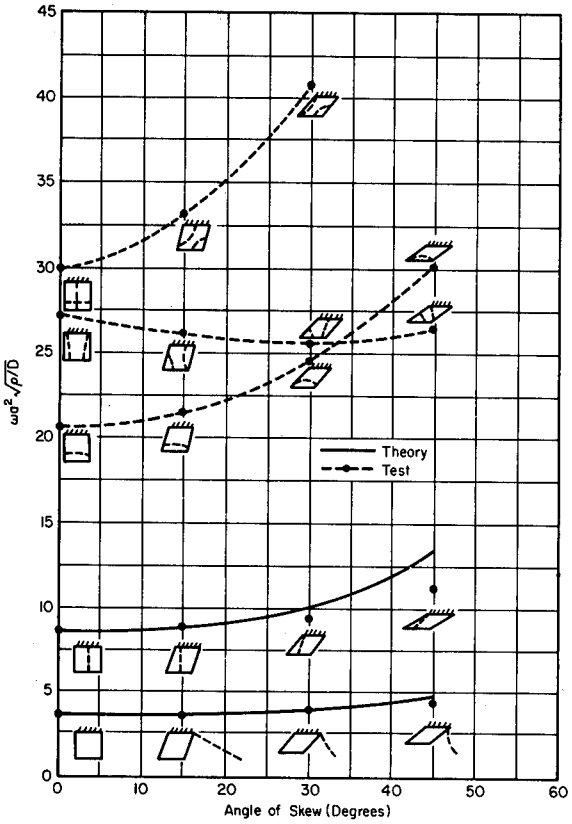
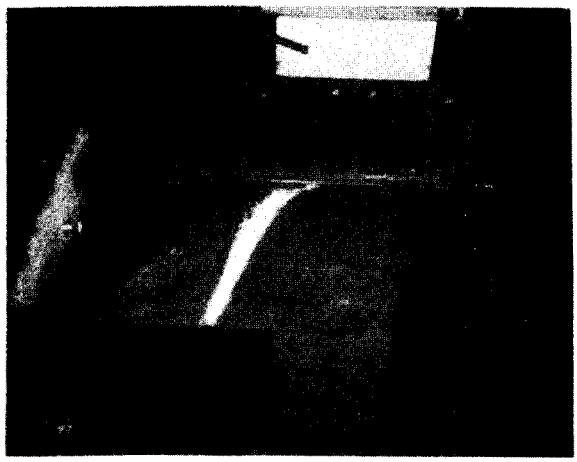
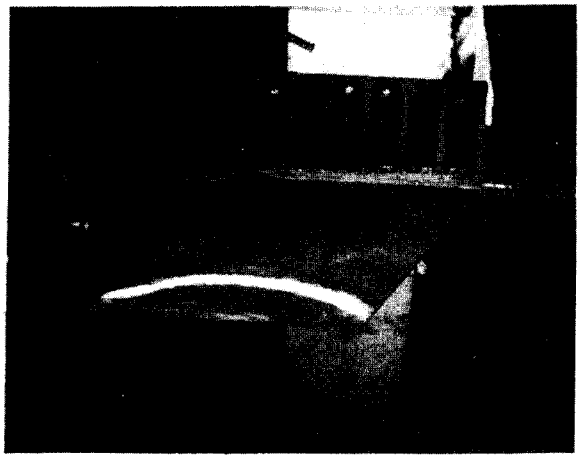
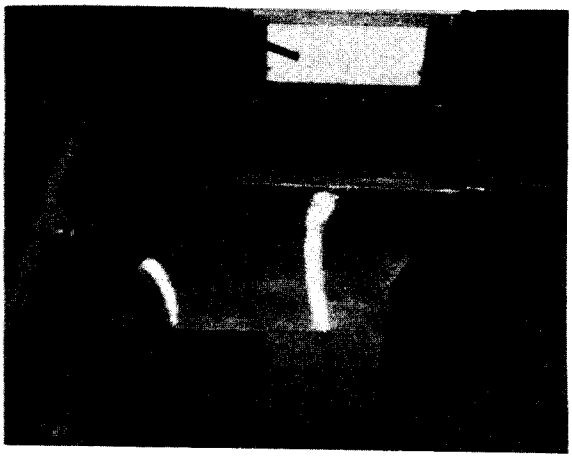


FIGURE 5.11.—Experimental and theoretical frequency parameters $\omega a^2\sqrt{\rho/D}$ for a C–F–F–F parallelogram; $a/b=1$; material, 24 S–T aluminum alloy.







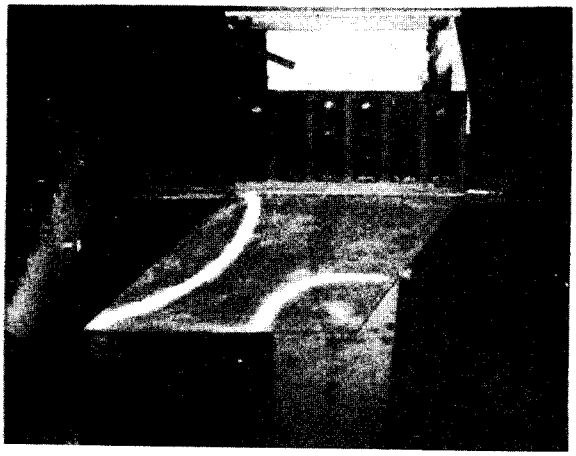


FIGURE 5.12.—Nodal patterns on a C–F–F–F parallelogram; $\alpha=30°$; material, 24 S–T aluminum alloy.

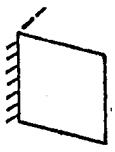
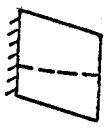
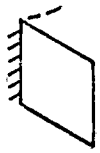
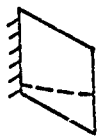
308-337 O—70——12

Results were computed by using 18 terms in equation (5.22), and frequency parameters, nodal lines, and mode shape amplitude coefficients are given in table 5.12 for $\alpha=15°$, 30°, and 45°, $a/b=1$, and $\nu=0.3$.

Experimental frequency parameters for the first five modes were also determined in references 5.10, 5.11, and 5.12. Test results and corrected results are shown and compared with theoretical results in table 5.13. Corrected results include an approximation of the effect of air-mass in order to estimate the equivalent frequency in a vacuum. (See chapter entitled "Other Considerations" (ch. 12).) A plot of the foregoing results, including approximate nodal patterns, is shown in figure 5.11. Photographs of nodal patterns obtained when $\alpha=30°$ are shown in figure 5.12.

Claassen (refs. 5.13 and 5.14) extended the work of reference 5.10 by using the same analytical procedure. A detailed Fortran program statement listing for the procedure is also given in reference 5.13. The first nine frequency parameters for $\alpha=0°$, 5°, 10°, . . ., 35°, and $a/b=1$ are given in table 5.14. In reference 5.13, extensive frequency and node line data are given in the vicinity of "transition curves"; i.e., the frequencies at which the basic form of the nodal pattern changes into another. This phenomenon is discussed in the section on rectangular plates entitled "All Sides Clamped" (4.3.1). In this case the mode shapes vary

TABLE 5.12.—*Frequency Parameters, Nodal Lines, and Amplitude Coefficients for C–F–F–F Parallelograms;* a/b=*1;* $\nu=0.3$

α, deg	15		30		45	
Mode	1	2	1	2	1	2
$\omega a^2\sqrt{\rho/D}$	3.601	8.872	3.961	10.190	4.824	13.75
Nodal lines						
Amplitude coefficients:						
A_{11}	1. 0000	0. 1162	1. 0000	0. 2387	1. 0000	0. 3534
A_{12}	−. 1134	1. 0000	−. 2288	1. 0000	−. 3302	1. 0000
A_{13}	−. 0041	−. 0721	. 0089	−. 1447	. 0231	−. 2173
A_{14}	−. 0007	−. 0145	−. 0006	−. 0179	. 0013	−. 0237
A_{15}	−. 0006	−. 0049	. 0001	−. 0093	. 0010	−. 0116
A_{21}	−. 0102	. 0892	−. 0339	. 1785	−. 0704	. 2685
A_{22}	−. 0223	. 1035	−. 0399	. 0489	−. 0488	−. 0411
A_{23}	−. 0016	−. 0384	. 0074	−. 0708	. 0197	−. 0970
A_{24}	−. 0015	. 0057	−. 0028	. 0103	−. 0038	. 0203
A_{25}	−. 0006	−. 0035	. 0002	−. 0049	. 0007	−. 0040
A_{31}	−. 0001	−. 0043	−. 0006	−. 0138	−. 0003	−. 0337
A_{32}	−. 0011	−. 0081	. 0010	−. 0254	. 0082	−. 0511
A_{33}	−. 0006	−. 0074	. 0017	−. 0078	. 0036	. 0027
A_{34}	−. 0003	−. 0005	−. 0008	. 0024	−. 0021	. 0074
A_{41}	−. 0005	−. 0034	−. 0014	. 0057	−. 0021	. 0064
A_{42}	−. 0007	. 0032	−. 0010	. 0020	−. 0008	. 0046
A_{43}	−. 0001	−. 0020	. 0002	−. 0009	−. 0007	. 0039
A_{51}	. 0001	−. 0010	. 0002	−. 0026	. 0005	−. 0044

with skew angle α as well as with the a/b ratio, and the "transition points" of section 4.3.1 consequently become "transition curves" in a three-dimensional plot.

Plass, Gaines, and Newsom (refs. 5.15 and 5.16) used a variational method (see the section for C–F–F–F cantilever rectangular plates (4.3.12)) to obtain the first three frequencies and mode shapes for the case when $\alpha=45°$ and $a=b$. Theoretical and experimental frequency parameters are listed in table 5.15. Mode shapes are shown in figure 5.13. Experimental results are taken from reference 5.12.

Hall, Pinckney, and Tulloch (ref. 5.17 used) statically determined influence functions to obtain frequencies and mode shapes for three cantilevered skew plates. The plates were given six degrees of freedom—three points along $\eta=b/2$ were allowed transverse displacement, and the corresponding three stations were allowed to rotate about an axis normal to the η-direction. The first three cyclic frequencies for $\alpha=30°$, 45°, and 60° are given in table 5.16 for aluminum-alloy plates 0.613 inch thick ($\rho=0.0001561$ lb-sec^2/in.^{3}) having varying dimensions as indicated. The experiments were conducted with accelerometers, each with a mass of 0.0005135 lb-sec^2/in. Five accelerometers were equally spaced along the leading edge ($\eta=0$) and five along the trailing edge ($\eta=b$). The effects of the accelerometer masses were included in the theoretical calculations. In figure 5.14 are shown the mode shapes corresponding to the frequencies of table 5.16. The deflections W^* are defined as the mean of the leading and trailing edge deflections measured at points intersecting $\psi=$constant (see fig. 5.10); the angles θ refer to rotations about axes parallel to the ψ-axis. The quantity θ is defined as the difference between the deflections at the leading and trailing edges divided by b.

Extensive numerical results for frequencies and mode shapes are obtained and presented in reference 5.18 by use of the same theoretical procedure as that in reference 5.17. Sweep angles are taken as 0°, 15°, 30°, 37½°, 45°, 50°, 55°, and 60°. Ratios c/a of 1.5, 2.0, 2.5, 3.0, 4.0, 5.0, 6.0, 10.0, and 20.0 were used. Ratios EI/GJ of ⅝, 1, and 1½ were taken, where EI and GJ are the flexural and torsional moduli of rigidity, respectively, in a plane normal to

TABLE 5.13.—*Experimental and Theoretical Frequency Parameters* $\omega a^2\sqrt{\rho/D}$ *for a C–F–F–F Parallelogram;* a/b=*1; Material, 24 S–T Aluminum Alloy*

α, deg	Mode	$\omega a^2\sqrt{\rho/D}$				
		Test results	Corrected test results	Theoretical results	Uncorrected percent difference	Corrected percent difference
15	1	3. 38	3. 44	3. 60	6. 2	4. 6
	2	8. 63	8. 68	8. 87	2. 7	2. 1
	3	21. 49				
	4	26. 04				
	5	33. 01				
30	1	3. 82	3. 88	3. 96	3. 6	2. 0
	2	9. 23	9. 33	10. 19	9. 4	8. 4
	3	24. 51				
	4	25. 54				
	5	40. 64				
45	1	4. 26	4. 33	4. 82	11. 8	10. 3
	2	11. 07	11. 21	13. 75	19. 5	18. 5
	3	26. 52				
	4	30. 13				
	5	50. 19				

the swept centerline (or normal to the ξ-axis). Cyclic frequency parameters $fa^2\sqrt{m_0/EI}\cos\alpha$, where m_0 is mass (slugs) per unit length measured along the ξ-direction, are shown in figure 5.15. Translational and rotational mode shape deflections are listed in reference 5.18 for 12 values of ψ and the sweep angle, c/a, and EI/GJ variations just described. The volume of these results (47 pages of tables) is too great to be included here.

Craig, Plass, and Caughfield (ref. 5.19) measured the first four frequencies and mode shapes on aluminum rhombic plates having sweep angles α of 15°, 30°, 45°, and 60°. Cyclic frequencies, nodal patterns, and mode shapes for these four configurations are shown in figures 5.16 to 5.19, respectively. An estimate of the accuracy of the nodal patterns can be obtained from figure 4.47.

TABLE 5.14.—*Frequency Parameters* $\omega a^2\sqrt{\rho/D}\cos^2\alpha$ *for a C–F–F–F Parallelogram;* a/b=*1;* ν=*0.3*

α, deg	$\omega a^2\sqrt{\rho/D}\cos^2\alpha$ for mode—								
	1	2	3	4	5	6	7	8	9
0	3.48	8.52	21.3	27.2	31.1	54.3	61.4	64.3	71.3
5	3.46	8.48	21.3	26.8	31.2	53.6	61.3	64.3	71.6
10	3.42	8.36	21.1	26.0	31.6	51.6	60.9	64.0	72.3
15	3.36	8.16	20.8	24.7	31.9	48.8	60.3	63.0	73.4
20	3.25	7.91	20.4	23.1	32.1	45.6	59.2	61.4	74.0
25	3.12	7.60	19.8	21.4	32.1	42.1	57.7	59.2	70.5
30	2.96	7.24	19.1	19.6	31.8	38.7	55.2	56.3	66.5
35	2.76	6.87	17.8	18.4	31.2	35.3	51.2	53.4	63.7

TABLE 5.16.—*Theoretical and Experimental Cyclic Frequencies for C–F–F–F Parallelogram Plates; Material, 65 S Aluminum Alloy*

α, deg		30	45	60
a, in		29.00	36.55	28.70
c, in		10.00	10.00	10.00
f_1, cps	Theory	25.38	17.56	37.79
	Test	24.2	16.5	32.6
	Test/theory	0.954	0.940	0.853
f_2, cps	Theory	114.0	85.59	126.8
	Test	116	83.3	122
	Test/theory	1.02	0.970	0.962
f_3, cps	Theory	156.8	113.8	224.0
	Test	162	127.6	227
	Test/theory	1.03	1.12	1.01

TABLE 5.15.—*Frequency Parameters* $\omega a^2\sqrt{\rho/D}$ *for a C–F–F–F Parallelogram Plate;* $\alpha=45°$; a=b; $\nu=0.3$

Mode	$\omega a^2\sqrt{\rho/D}$	
	Theoretical	Experimental
1	4. 12	4. 26
2	11. 26	11. 07
3	27. 72	26. 52

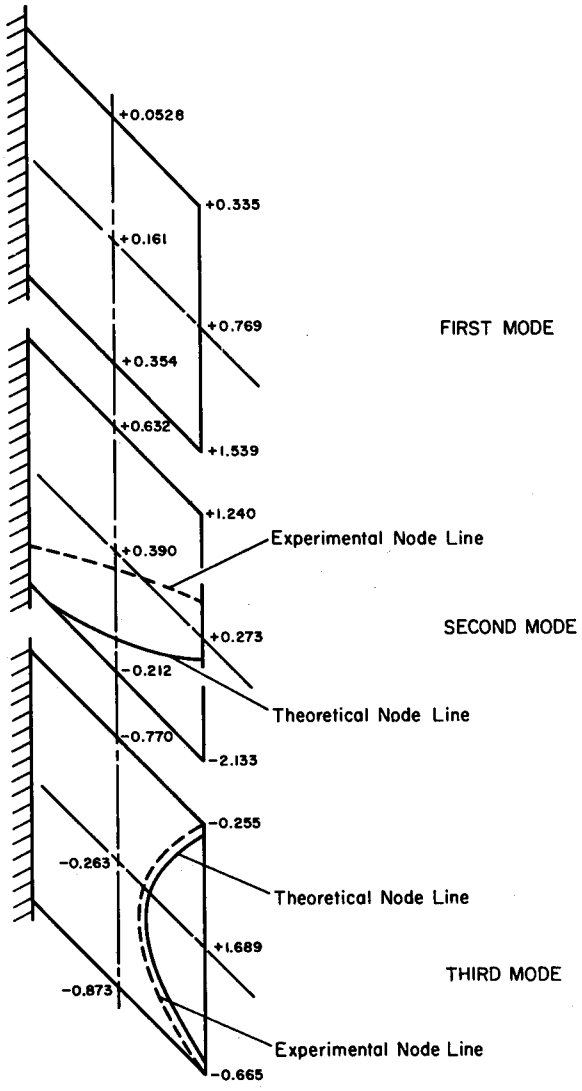


FIGURE 5.13.—Mode shapes for a C–F–F–F parallelogram plate; $\alpha=45°$; $a=b$; $\nu=0.3$. (After refs. 5.15 and 5.16)

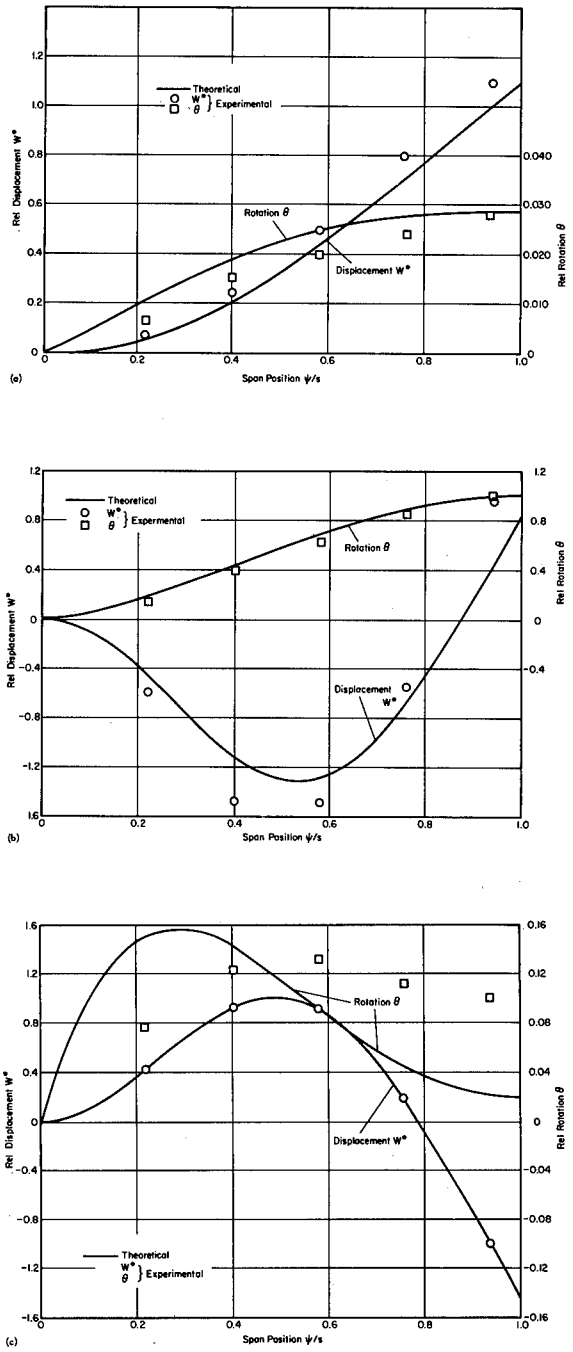


FIGURE 5.14.—Theoretical and experimental mode shapes for C–F–F–F parallelogram plates; material, 65 S aluminum alloy. (*a*) Fundamental mode; $\alpha=30°$. (*b*) First overtone mode; $\alpha=30°$. (*c*) Second overtone mode; $\alpha=30°$. (*d*) Fundamental mode; $\alpha=45°$. (*e*) First overtone mode; $\alpha=45°$. (*f*) Second overtone mode; $\alpha=45°$. (*g*) Fundamental mode; $\alpha=60°$. (*h*) First overtone mode; $\alpha=60°$. (*i*) Second overtone mode; $\alpha=60°$.

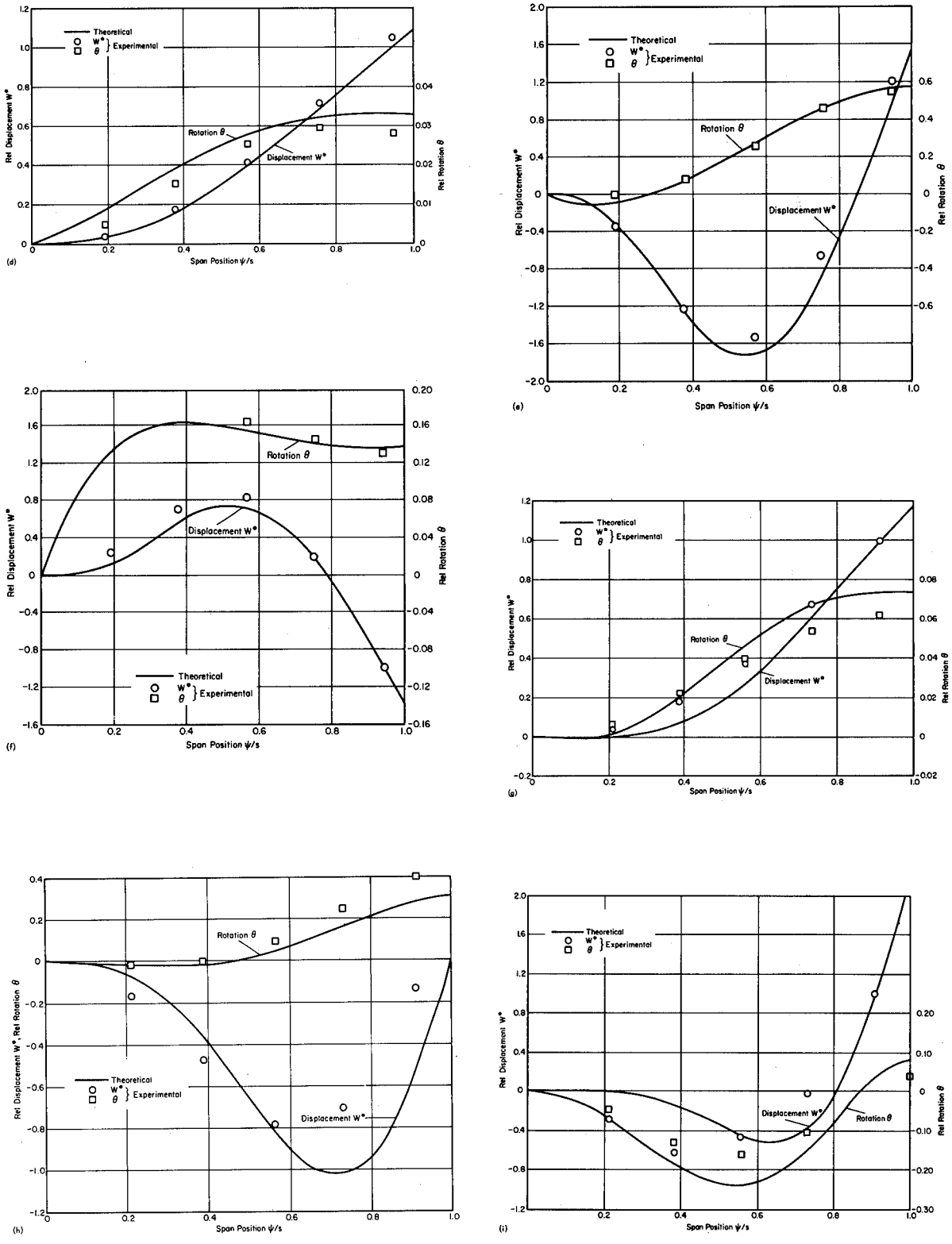


FIGURE 5.14—Concluded.

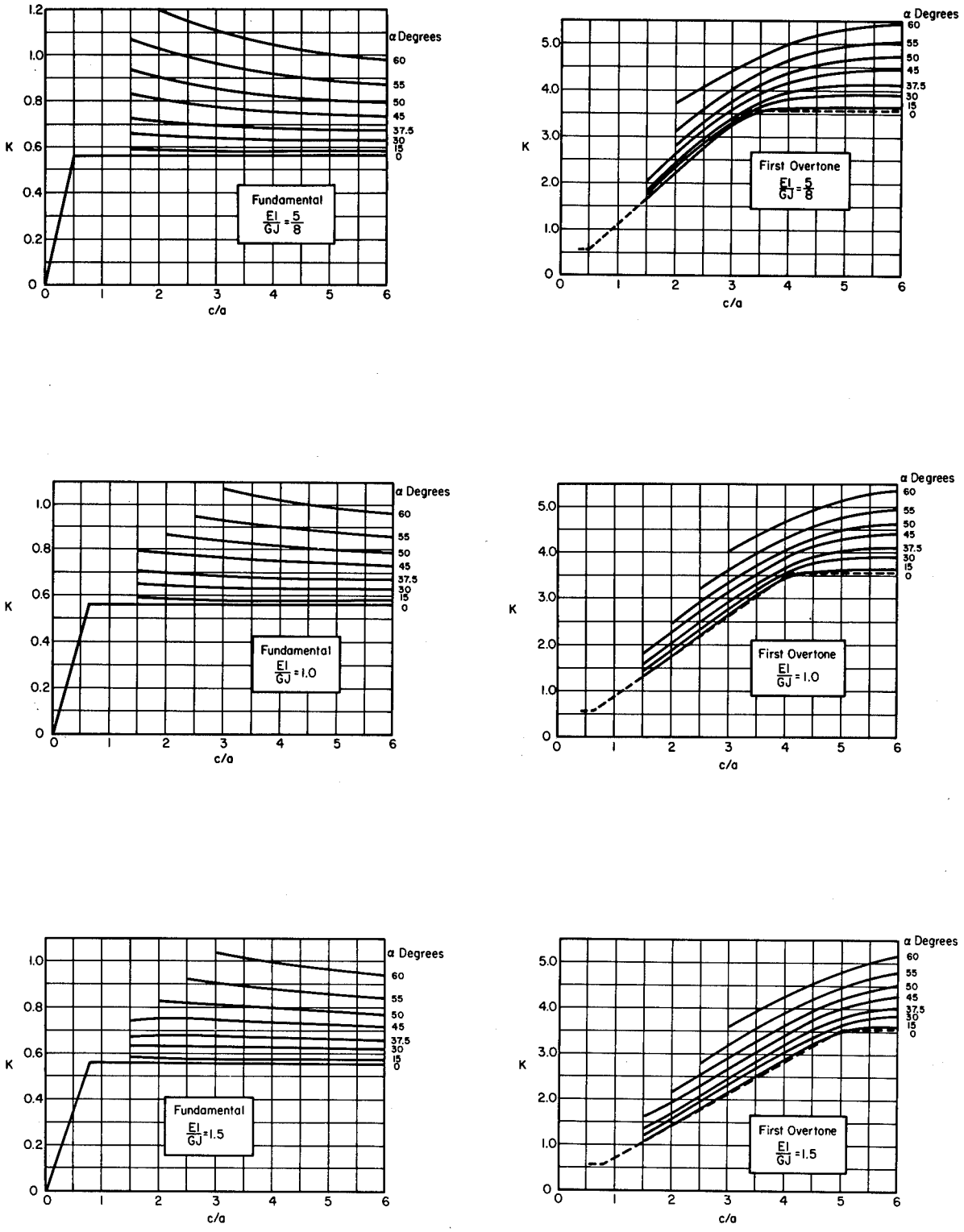
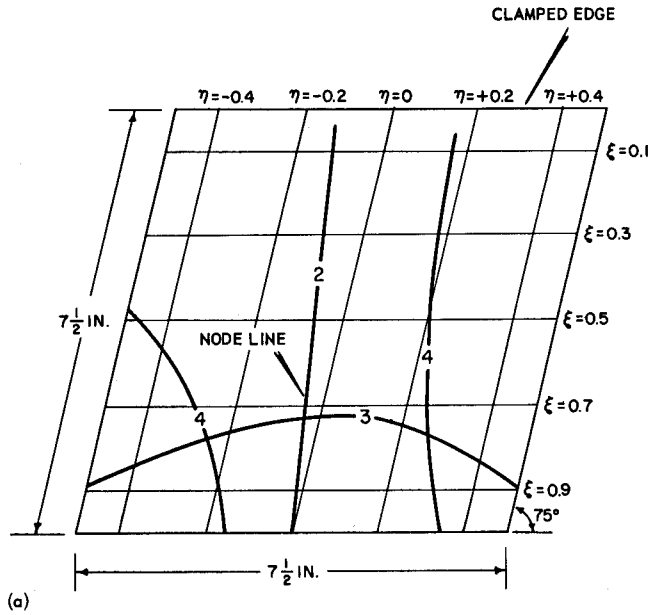
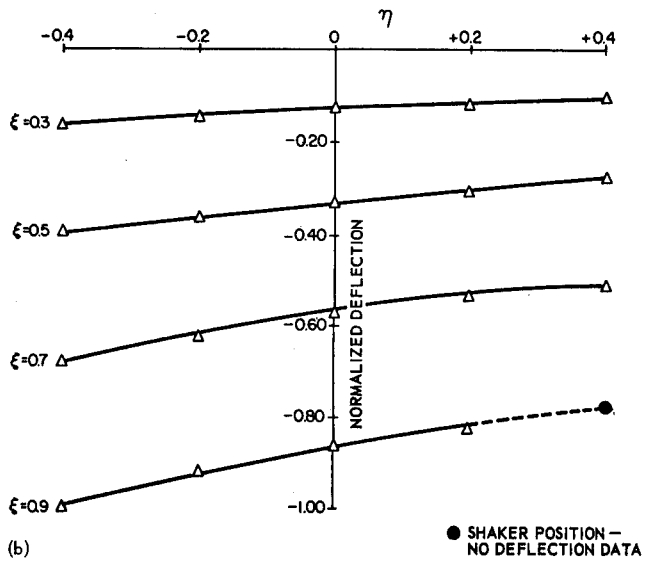


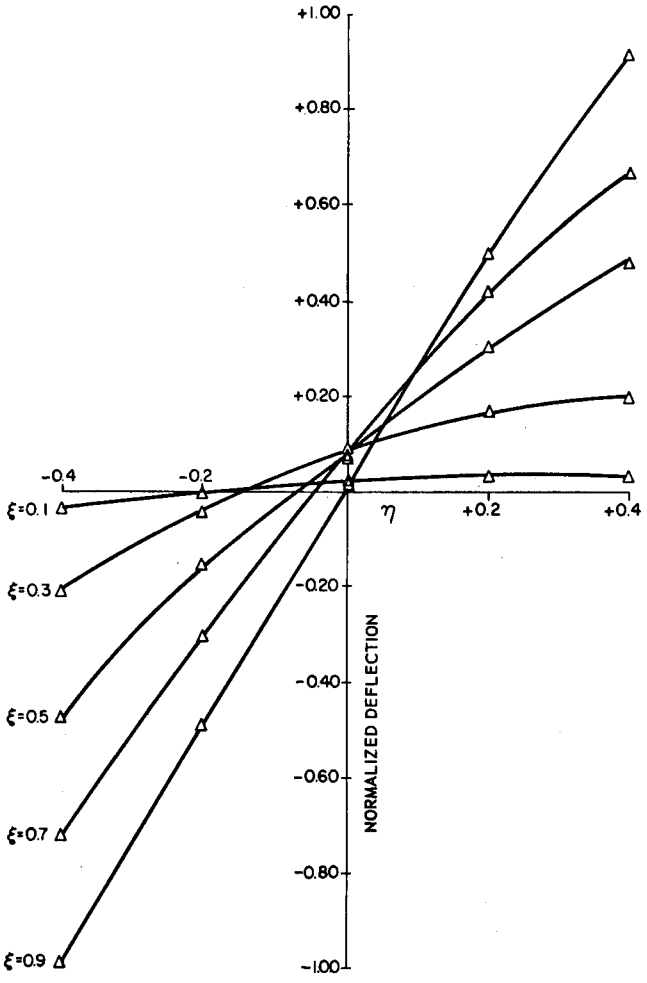
FIGURE 5.15.—Cyclic frequency parameters $K=fa^2\sqrt{m_0/EI}\cos\alpha$; material, 65 S aluminum alloy.


CLAMPED EDGE
η=-0.4
η=-0.2
η=0
η=+0.2
η=+0.4
ξ=0.1
ξ=0.3
ξ=0.5
ξ=0.7
ξ=0.9
7½ IN.
NODE LINE
2
3
4
4
75°
7½ IN.

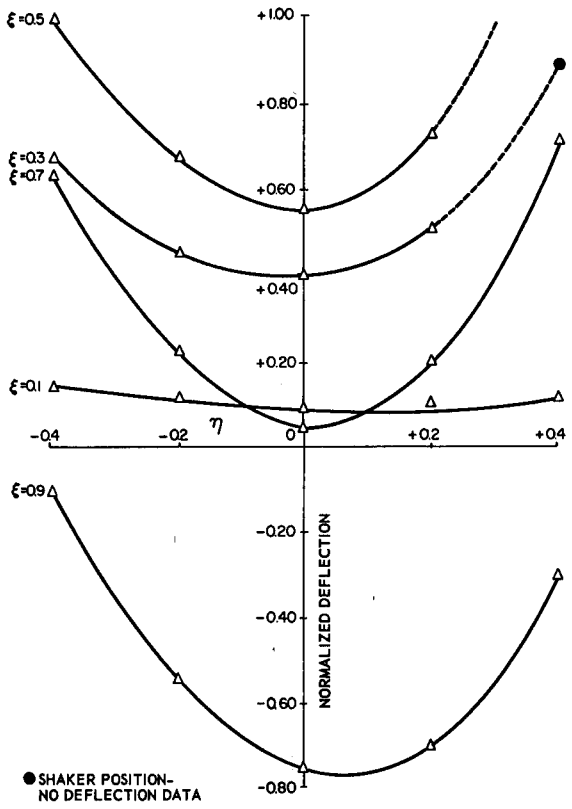
(a)


η
-0.4
-0.2
0
+0.2
+0.4
ξ=0.3
ξ=0.5
ξ=0.7
ξ=0.9
-0.20
-0.40
-0.60
-0.80
-1.00
NORMALIZED DEFLECTION
SHAKER POSITION — NO DEFLECTION DATA

(b)


+1.00
+0.80
+0.60
+0.40
+0.20
-0.20
-0.40
-0.60
-0.80
-1.00
-0.4
-0.2
η
+0.2
+0.4
ξ=0.1
ξ=0.3
ξ=0.5
ξ=0.7
ξ=0.9
NORMALIZED DEFLECTION

(c)



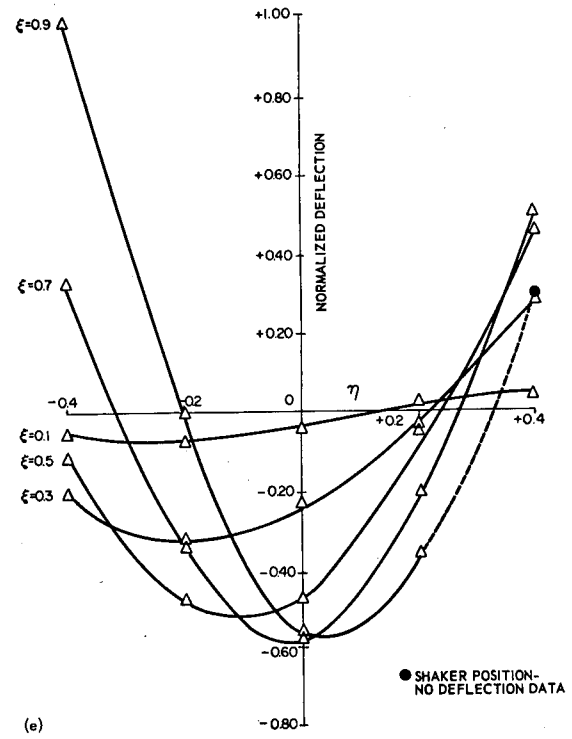
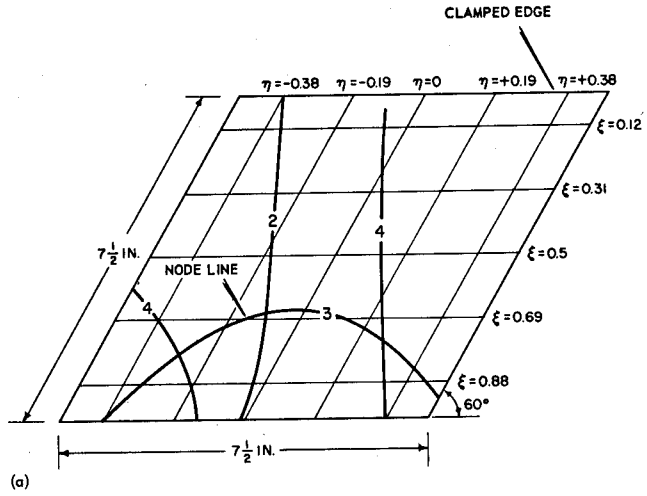
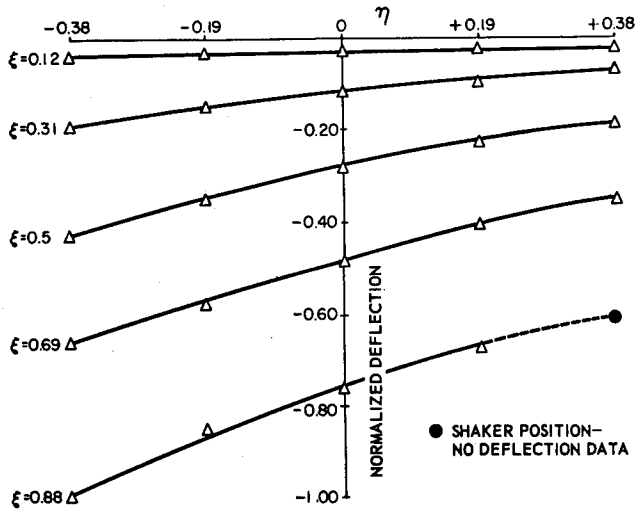


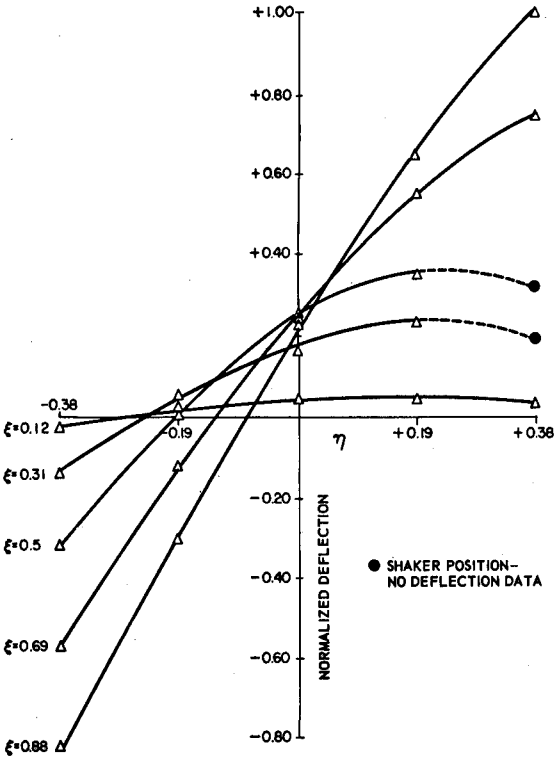
FIGURE 5.16.—Experimentally determined cyclic frequencies, nodal patterns, and mode shapes for a C–F–F–F rhombic plate; $\alpha=15°$; material, 6061–T6 aluminum alloy $\frac{1}{8}$ inch thick. (*a*) Experimental node lines and data points. (*b*) Mode 1; $f_1=76.6$ cps. (*c*) Mode 2; $f_2=179$ cps. (*d*) Mode 3; $f_3=469$ cps. (*e*) Mode 4; $f_4=566$ cps.


CLAMPED EDGE
η=-0.38
η=-0.19
η=0
η=+0.19
η=+0.38
ξ=0.12
ξ=0.31
ξ=0.5
ξ=0.69
ξ=0.88
60°
7½ IN.
NODE LINE
2
4
4
3
7½ IN.

(a)


η
-0.38
-0.19
0
+0.19
+0.38
ξ=0.12
ξ=0.31
ξ=0.5
ξ=0.69
ξ=0.88
-0.20
-0.40
-0.60
-0.80
-1.00
NORMALIZED DEFLECTION
SHAKER POSITION–
NO DEFLECTION DATA

(b)


+1.00
+0.80
+0.60
+0.40
-0.20
-0.40
-0.60
-0.80
-0.38
-0.19
+0.19
+0.38
η
ξ=0.12
ξ=0.31
ξ=0.5
ξ=0.69
ξ=0.88
NORMALIZED DEFLECTION
SHAKER POSITION–
NO DEFLECTION DATA

(c)

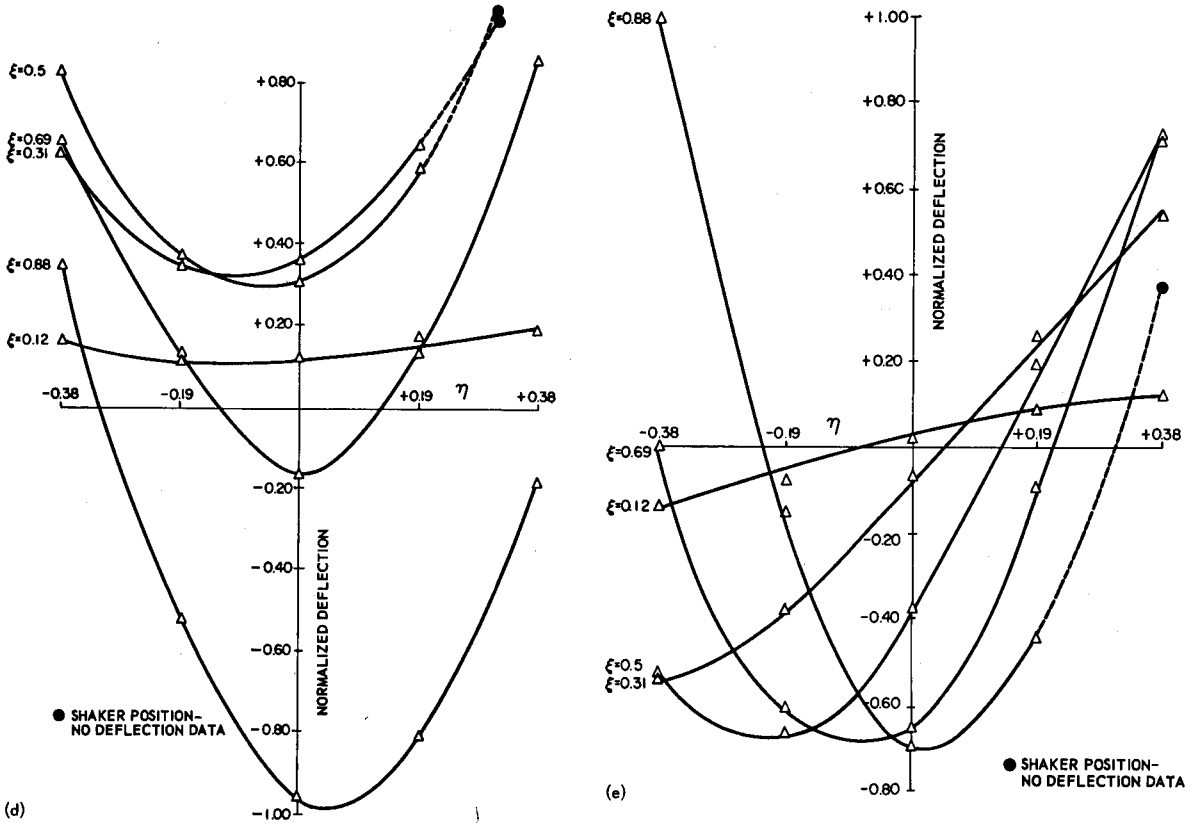
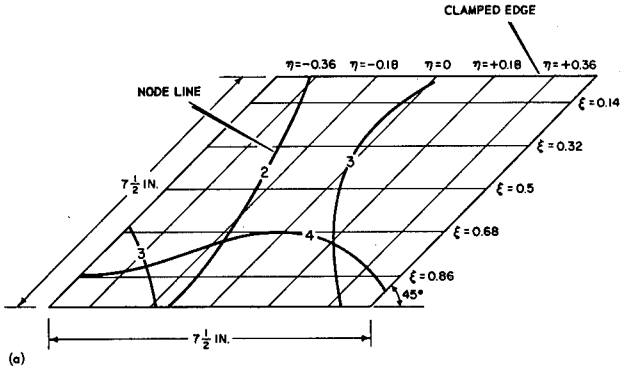
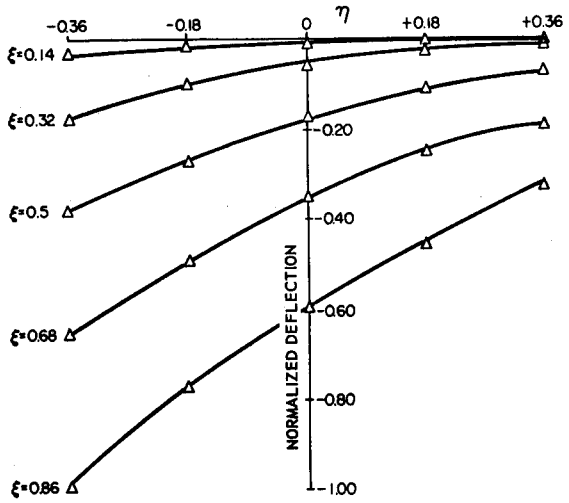


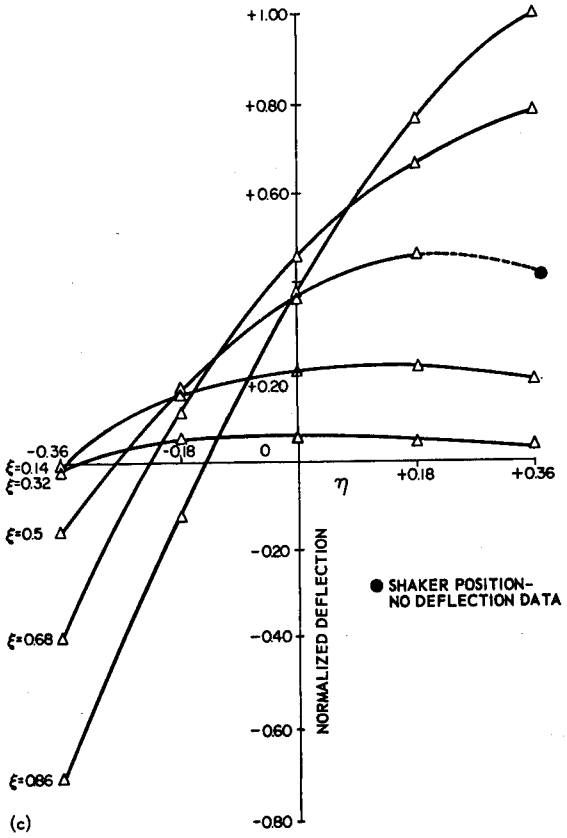
FIGURE 5.17.—Experimentally determined cyclic frequencies, nodal patterns, and mode shapes for a C–F–F–F rhombic plate; $\alpha=30°$; material, 6061–T6 aluminum alloy $\frac{1}{8}$ inch thick. (*a*) Experimental node lines and data points. (*b*) Mode 1; $f_1=83.5$ cps. (*c*) Mode 2; $f_2=195$ cps. (*d*) Mode 3; $f_3=521$ cps. (*e*) Mode 4; $f_4=556$ cps.


CLAMPED EDGE
η=-0.36
η=-0.18
η=0
η=+0.18
η=+0.36
NODE LINE
ξ=0.14
ξ=0.32
ξ=0.5
ξ=0.68
ξ=0.86
45°
7½ IN.
7½ IN.
2
3
3
4

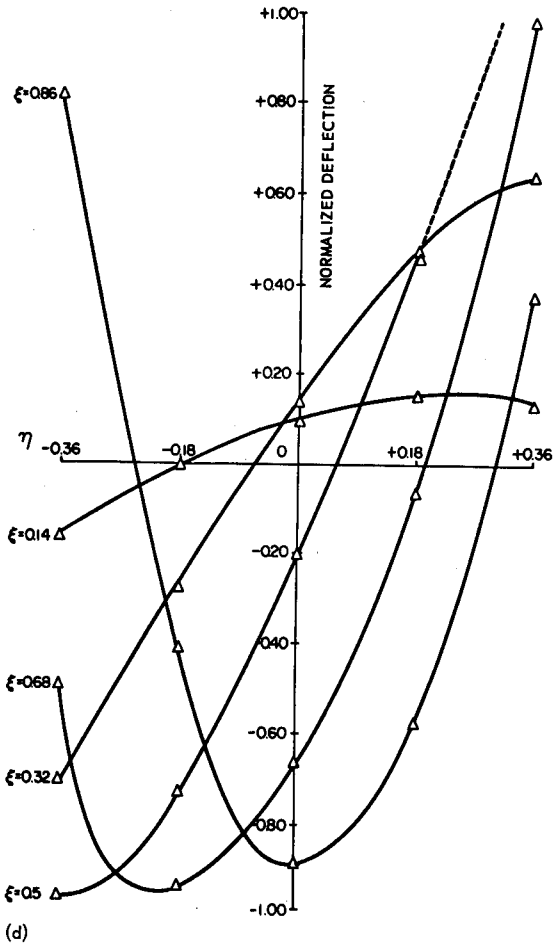
(a)


η
-0.36
-0.18
0
+0.18
+0.36
ξ=0.14
ξ=0.32
ξ=0.5
ξ=0.68
ξ=0.86
-0.20
-0.40
-0.60
-0.80
-1.00
NORMALIZED DEFLECTION

(b)


+1.00
+0.80
+0.60
+0.20
-0.20
-0.40
-0.60
-0.80
-0.36
-0.18
0
+0.18
+0.36
η
ξ=0.14
ξ=0.32
ξ=0.5
ξ=0.68
ξ=0.86
NORMALIZED DEFLECTION
SHAKER POSITION-
NO DEFLECTION DATA

(c)



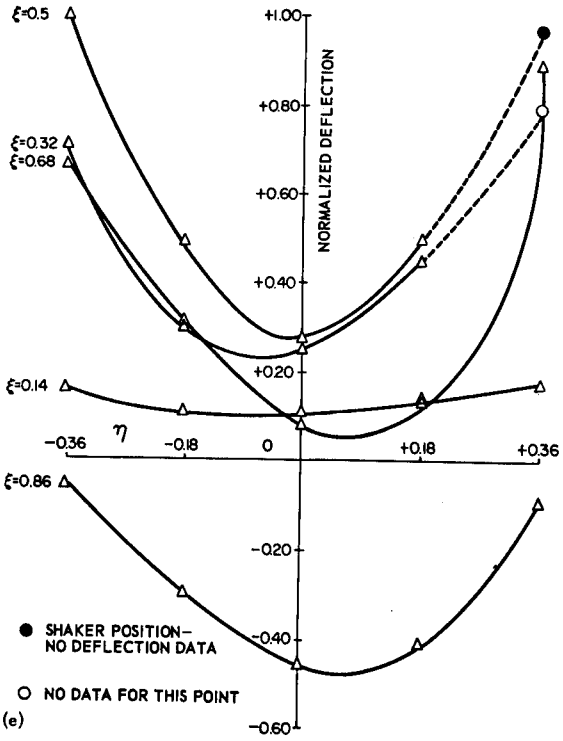


FIGURE 5.18.—Experimentally determined cyclic frequencies, nodal patterns, and mode shapes for a C–F–F–F rhombic plate; $\alpha=45°$; material, 6061–T6 aluminum alloy $\frac{1}{8}$ inch thick. (*a*) Experimental node lines and data points. (*b*) Mode 1; $f_1=97.4$ cps. (*c*) Mode 2; $f_2=231$ cps. (*d*) Mode 3; $f_3=560$ cps. (*e*) Mode 4; $f_4=669$ cps.

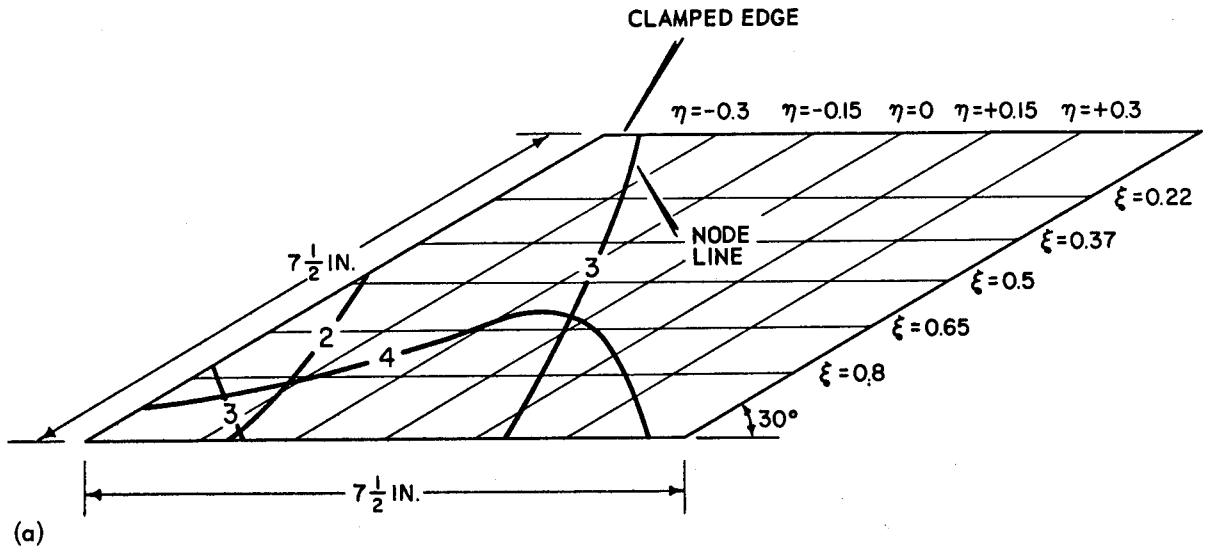
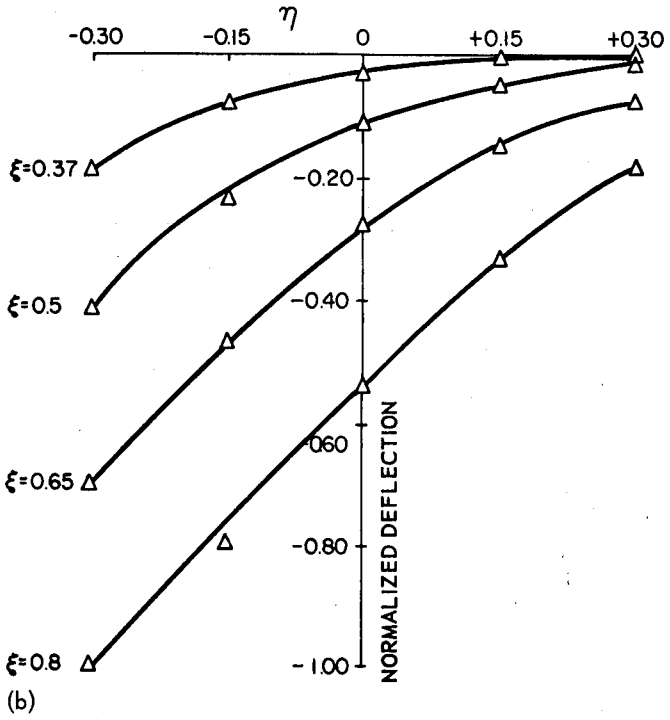
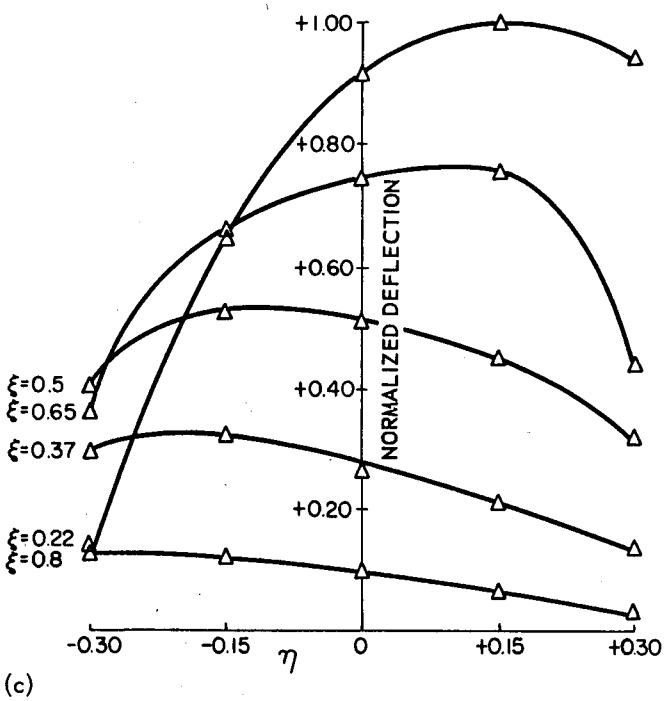


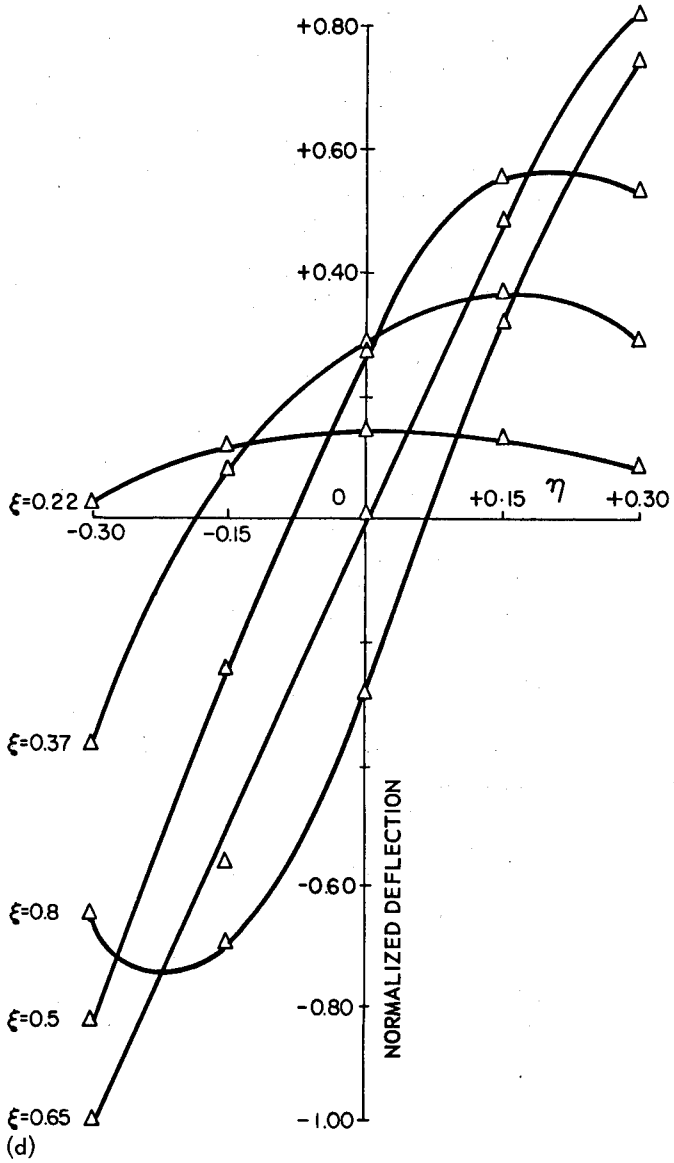
FIGURE 5.19.—Experimentally determined cyclic frequencies, nodal patterns, and mode shapes for a C–F–F–F rhombic plate; $\alpha=60°$; material, 6061–T6 aluminum alloy ⅛ inch thick. (*a*) Experimental node lines and data points. (*b*) Mode 1; $f_1=97$ cps. (*c*) Mode 2; $f_2=305$ cps. (*d*) Mode 3; $f_3=570$ cps.


η
-0.30
-0.15
0
+0.15
+0.30
ξ=0.37
ξ=0.5
ξ=0.65
ξ=0.8
-0.20
-0.40
-0.60
-0.80
-1.00
NORMALIZED DEFLECTION

(b)


+1.00
+0.80
+0.60
+0.40
+0.20
ξ=0.5
ξ=0.65
ξ=0.37
ξ=0.22
ξ=0.8
NORMALIZED DEFLECTION
-0.30
-0.15
η
0
+0.15
+0.30

(c)


+0.80
+0.60
+0.40
ξ=0.22
-0.30
-0.15
0
+0.15
η
+0.30
ξ=0.37
ξ=0.8
ξ=0.5
ξ=0.65
-0.60
-0.80
-1.00
NORMALIZED DEFLECTION

(d)

Hanson and Tuovila (ref. 5.20) used a method "called the 1-g method" to determine experimental mode shapes. In this method the plate is sprinkled with sand, and the sand particles themselves are used as accelerometers. At any given frequency, particles having equal accelerations will also have equal amplitudes. An acceleration corresponding to that of gravity occurs when a particle placed on a vibrating plate just begins to rise from the surface. In this way "1-g lines" of constant amplitude may be located, in addition to the nodal lines. Varying the magnitude of the exciting force allows one to find other 1-g lines.

Experimental results were obtained on four plate configurations made of 0.041-inch-thick magnesium having a weight density of 0.064 lb/in.^{3} The plate dimensions in terms of figure 5.10 are given in table 5.17.

Frequencies and mode shapes for the first three modes of each plate are shown in figures 5.20 to 5.23 and the deflections are given in tables 5.18 to 5.21, respectively. In these figures the heavy solid lines indicate the position of the plate at rest. The broken lines indicate the deflected shape in its mode of vibration. Vertical lines measure the relative amplitudes of points on the plate surface.

5.1.6 F–F–F–F

Very little information is known on the problem of the F–F–F–F parallelogram plate (see fig. 5.24). Waller (ref. 5.21) obtained the nodal patterns shown in figure 5.25.

5.2 OTHER SUPPORTS AND CONDITIONS

No results are available for parallelogram plates having elastic or discontinuous edge conditions, or being supported at discrete points. Some results for plates with added mass were discussed earlier for the cantilever (sec. 5.1.5) as obtained in reference 5.17. The accelerometer masses added there were small and well distributed and so had small effect upon the problem.

TABLE 5.17.—*Dimensions of 4 Experimental Plate Specimens*

Plate no.	s, in.	b, in.	α, deg
1	5.52	2.05	15
2	4.80	2.28	30
3	3.90	2.93	45
4	2.77	4.10	60

TABLE 5.18.—*Deflections for First 3 Modes of Plate 1*

Mode	η/b	Normalized deflection at ξ/a of—					
		0.1	0.3	0.5	0.7	0.9	1.0
1[a]	0.00	0.039	0.160	0.316	0.547	0.800	
	.25	.043	.175	.338	.569	.817	0.952
	.50	.048	.185	.360	.569	.840	.966
	.75	.053	.200	.383	.608	.856	.983
	1.00	.056	.225	.406	.631	.875	1.000
2[b]	.00	−.088	−.361	−.579	−.485	−.207	−.055
	.25	−.080	−.289	−.407	−.297	−.008	.117
	.50	−.069	−.210	−.260	−.106	.180	.310
	.75	−.044	−.135	−.120	.100	.386	.524
	1.00	−.014	−.062	.014	.331	.758	1.000
3[c]	.00	.099	.106	.162	.401	.788	1.000
	.25	.021	−.035	−.021	.176	.472	.654
	.50	−.042	−.190	−.225	−.085	.190	.352
	.75	−.099	−.345	−.451	−.338	−.099	.085
	1.00	−.155	−.556	−.831	−.746	−.373	−.162

[a] f_1=36 cps. [b] f_2=205 cps. [c] f_3=238 cps.

TABLE 5.19.—*Deflections for First 3 Modes of Plate 2*

Mode	η/b	Normalized deflection at ξ/a of—					
		0.1	0.3	0.5	0.7	0.9	1.0
1[a]	0.00	0.011	0.052	0.126	0.233	0.383	0.472
	.25	.015	.067	.148	.267	.420	.509
	.50	.018	.080	.170	.296	.461	.635
	.75	.025	.098	.195	.328	.518	.778
	1.00	.030	.118	.226	.370	.604	1.000
2[b]	.00	−.025	−.264	−.494	−.563	−.500	−.361
	.25	−.031	−.264	−.405	−.400	−.228	−.028
	.50	−.033	−.228	−.295	−.160	.110	.300
	.75	−.028	−.125	−.117	.147	.458	.630
	1.00	−.011	−.022	.111	.458	.818	1.000
3[c]	.00	.010	.028	.071	.361	.787	1.000
	.25	−.006	−.061	−.123	.150	.600	.830
	.50	−.019	−.232	−.335	−.110	.380	.613
	.75	−.074	−.445	−.600	−.380	.070	.355
	1.00	−.168	−.677	−.910	−.658	−.193	.097

[a] f_1=39 cps. [b] f_2=212 cps. [c] f_3=272 cps.

TABLE 5.20.—*Deflections for First 3 Modes of Plate 3*

Mode	η/b	Normalized deflection at ξ/a of—					
		0.1	0.3	0.5	0.7	0.9	1.0
1[a]	0.00	0.007	0.054	0.124	0.210	0.350	0.467
	.25	.017	.070	.155	.259	.418	.557
	.50	.021	.091	.191	.313	.510	.673
	.75	.028	.117	.238	.395	.640	.810
	1.00	.039	.159	.307	.500	.812	1.000
2[b]	.00	.007	.132	.578	.872	.904	.857
	.25	.021	.286	.625	.718	.668	.607
	.50	.046	.300	.471	.403	.014	−.143
	.75	.050	.179	.057	−.282	−.678	−.786
	1.00	−.036	−.196	−.518	−.793	−.947	−1.000
3[c]	.00	.000	−.017	−.071	.063	.622	1.000
	.25	−.004	−.059	−.185	−.029	.520	.840
	.50	−.008	−.201	−.374	−.200	.416	.735
	.75	−.050	−.470	−.676	−.412	.310	.681
	1.00	−.214	−1.000	−1.000	−.504	.250	.651

[a] f_1=38 cps. [b] f_2=184 cps. [c] f_3=263 cps.

308-837 O—70——13

TABLE 5.21.—*Deflections for First 3 Modes of Plate 4*

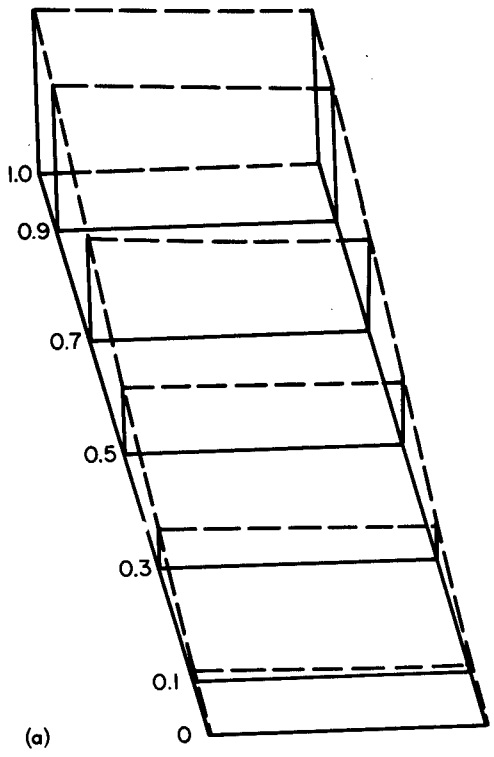
Mode	η/b	Normalized deflection at ξ/a of—					
		0.1	0.3	0.5	0.7	0.9	1.0
1[a]	0.00	0.012	0.040	0.085	0.164	0.286	0.380
	.25	.015	.058	.116	.215	.376	.475
	.50	.022	.091	.171	.315	.510	.620
	.75	.040	.135	.272	.458	.665	.800
	1.00	.062	.211	.400	.618	.830	1.000
2[b]	.00	−.008	−.039	−.156	−.383	−.495	−.515
	.25	−.016	−.078	−.258	−.433	−.445	−.390
	.50	−.022	−.133	−.312	−.328	−.156	.047
	.75	−.034	−.159	−.180	.019	.350	.515
	1.00	−.055	−.089	.109	.484	.867	1.000
3[c]	.00	−.024	−.111	−.347	−.606	−.667	−.650
	.25	−.045	−.125	−.202	−.303	−.505	−.707
	.50	−.071	.000	.238	.216	−.252	−.666
	.75	.101	.545	.808	.657	−.162	−.656
	1.00	.465	.980	1.000	.657	−.353	−1.000

[a] f_1=47 cps. [b] f_2=207 cps. [c] f_3=380 cps.

The case of a cantilevered parallelogram with an added mass at the tip is discussed in reference 5.22. An aluminum-alloy plate having dimensions a=30 inches, c=10 inches, h=⅝ inch and having a total mass of 0.0468 lb-sec²/in. is loaded by a mass at the tip ($\xi=a$, $\eta=b/2$, in terms of fig. 5.10) which has the following inertial properties: mass=0.0330 lb-sec²/in., I_θ=6.483 lb-in.-sec², I_ϕ=0.1242 lb-in.-sec². The mass moments of inertia I_θ and I_ϕ are about axes in the ψ- and η-directions, respectively. These axes pass through $\xi=a$ and $\eta=b/2$. The first three theoretical frequencies for α=0°, 30°, 45°, and 60° are given in table 5.22. In figure 5.26 are shown the nodal lines for the fundamental and second modes of vibration for α=30°, 45°, and 60° with and without the tip mass.

TABLE 5.22.—*Cyclic Frequencies for a C–F–F–F Parallelogram Plate With Added Tip Mass; Material, 65 S Aluminum Alloy*

Mode	Cyclic frequency, cps, for values of skew angle, α, deg, of—			
	0	30	45	60
1	11.33	12.40	10.91	15.35
2	--------	23.07	27.39	40.83
3	101.7	114.9	111.1	153.5



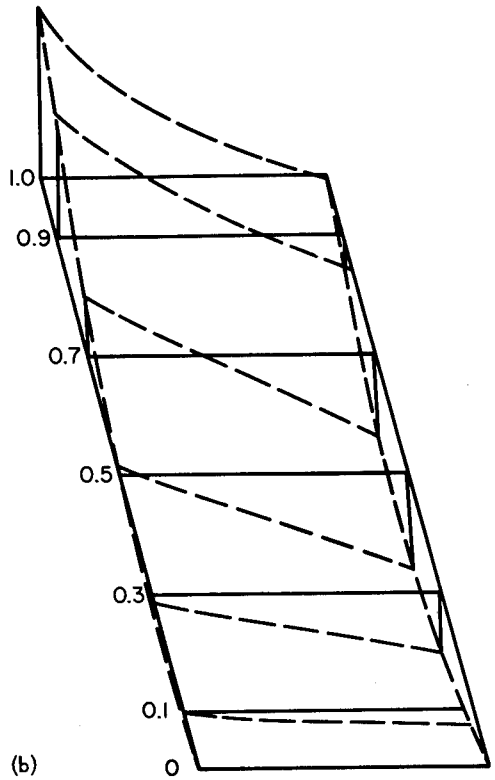
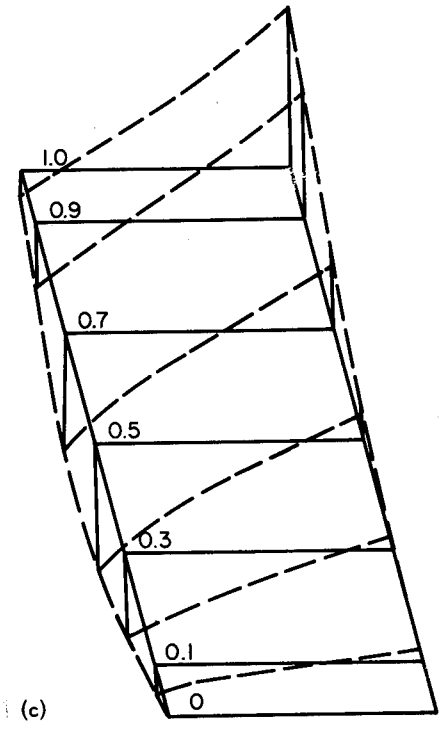


FIGURE 5.20.—First three mode shapes and frequencies for a C–F–F–F plate; $\alpha = 15°$; material, magnesium. (*a*) Mode 1; $f_1 = 36$ cps. (*b*) Mode 2; $f_2 = 205$ cps. (*c*) Mode 3; $f_3 = 238$ cps.



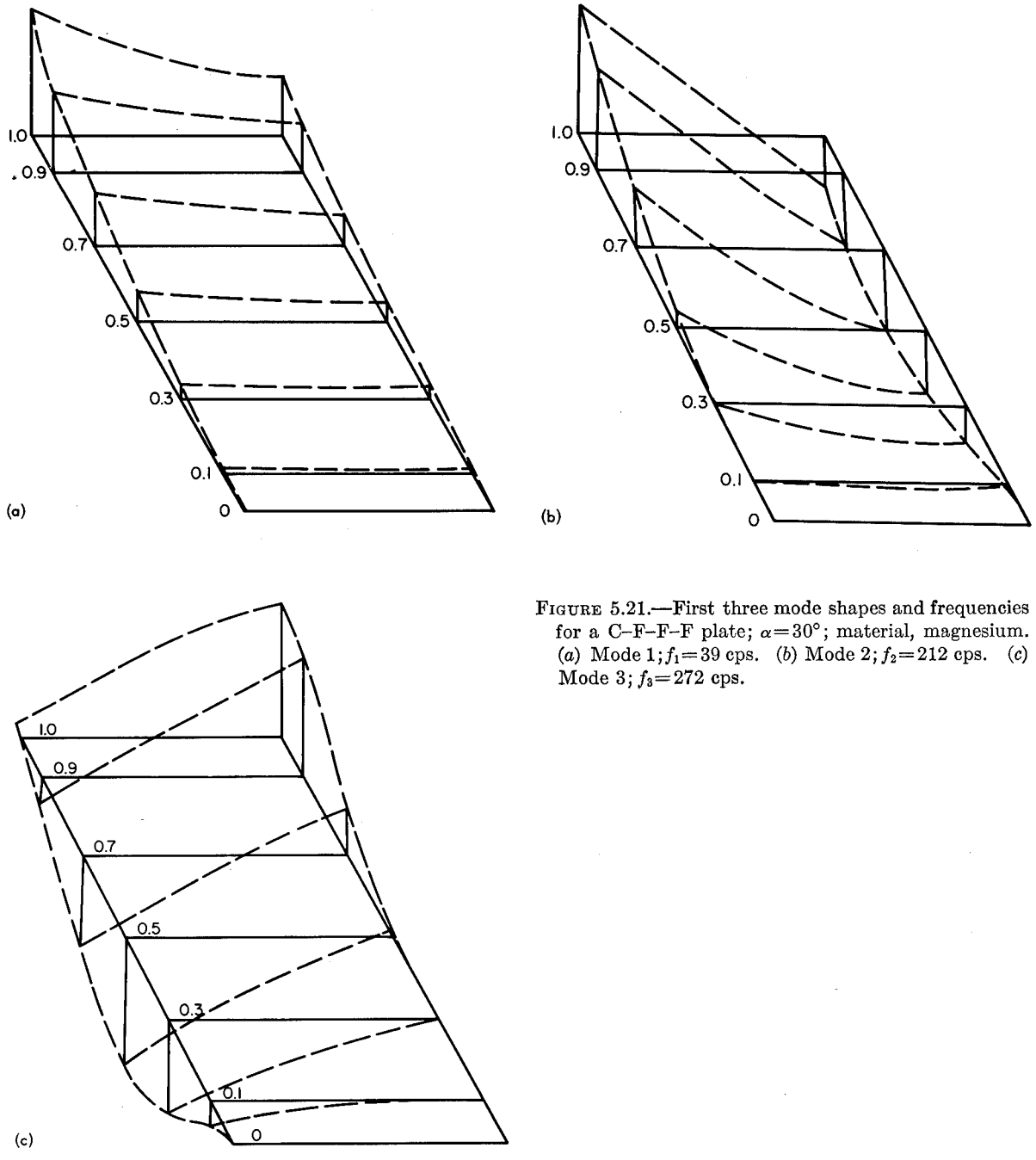


FIGURE 5.21.—First three mode shapes and frequencies for a C–F–F–F plate; $\alpha=30°$; material, magnesium. (*a*) Mode 1; $f_1=39$ cps. (*b*) Mode 2; $f_2=212$ cps. (*c*) Mode 3; $f_3=272$ cps.

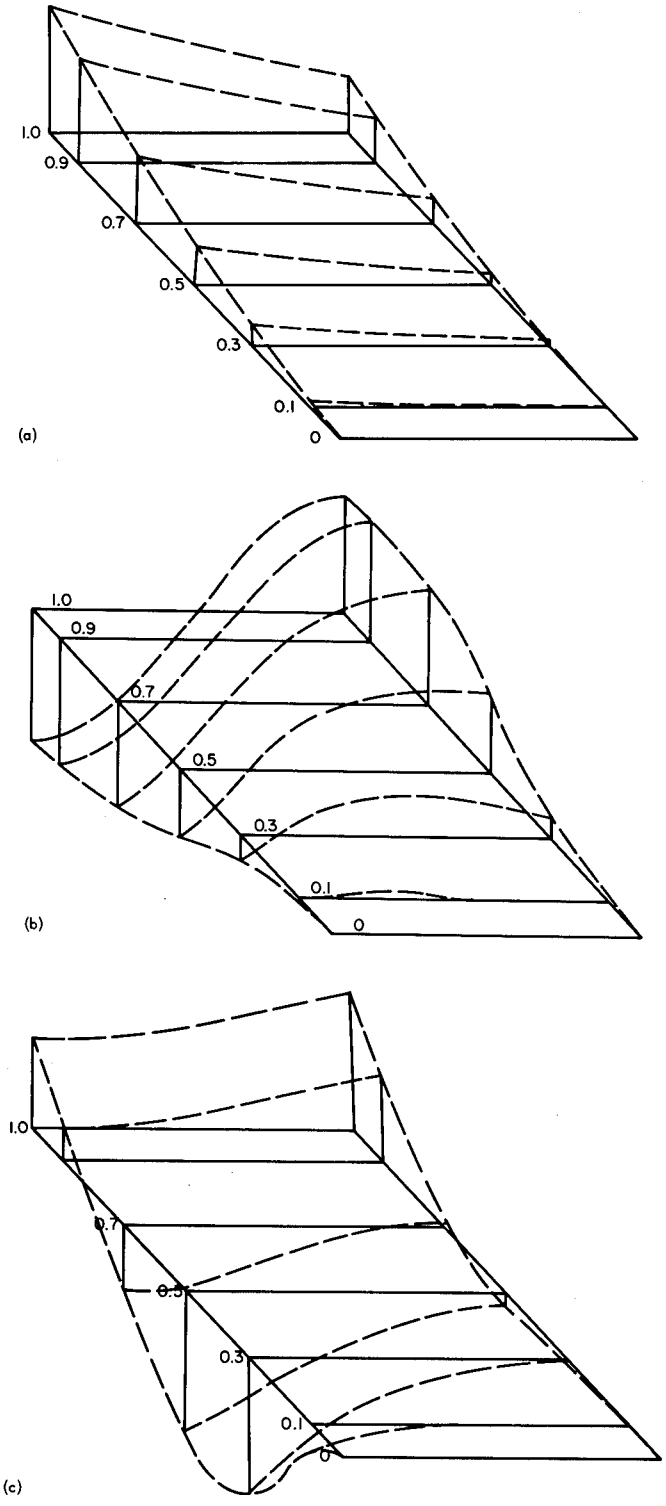


FIGURE 5.22.—First three mode shapes and frequencies for a C–F–F–F plate; $\alpha=45°$; material, magnesium. (*a*) Mode 1; $f_1=38$ cps. (*b*) Mode 2; $f_2=184$ cps. (*c*) Mode 3; $f_3=263$ cps.

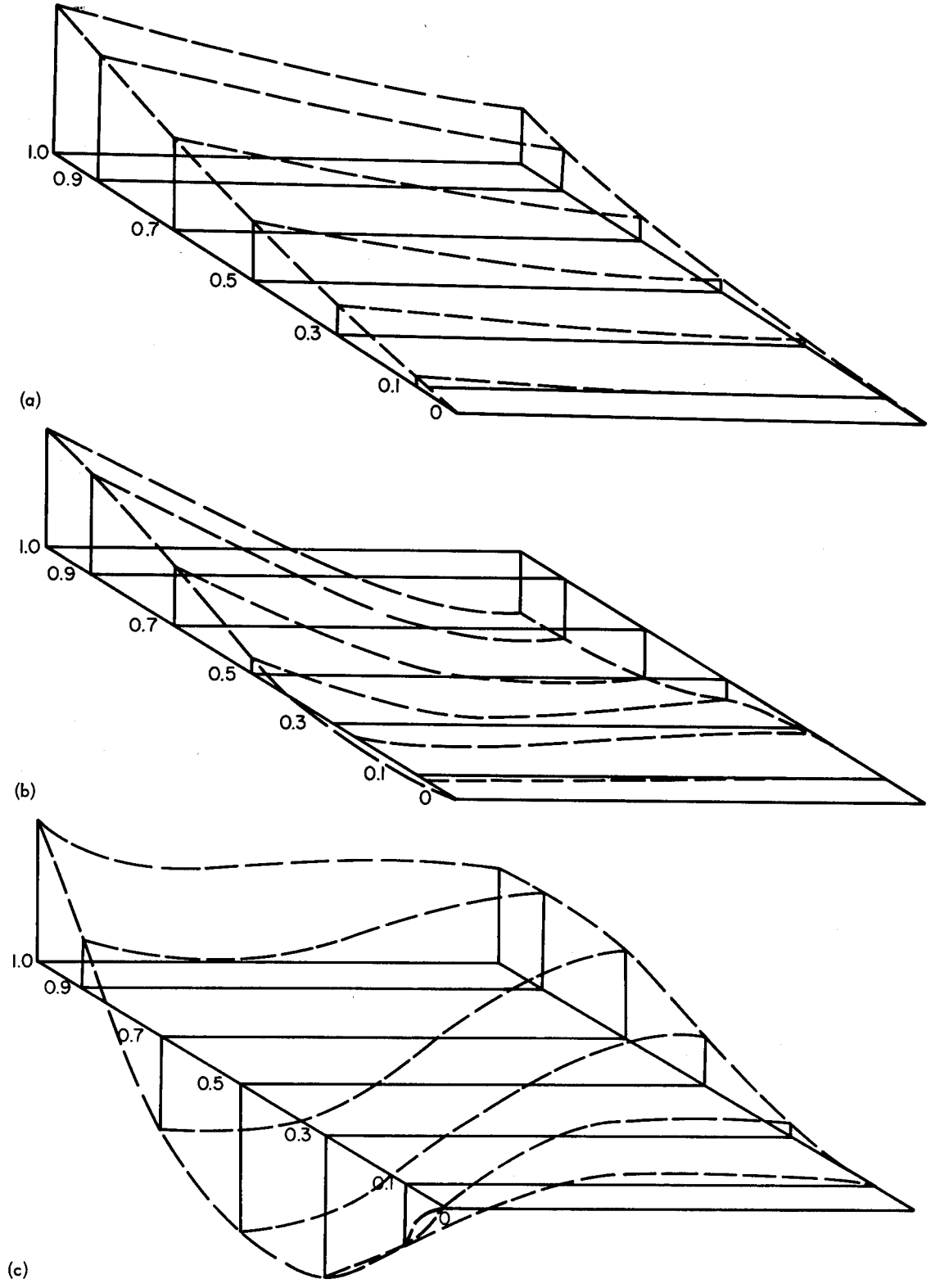


FIGURE 5.23.—First three mode shapes and frequencies for a C–F–F–F plate; $\alpha=60°$; material, magnesium. (*a*) Mode 1; $f_1=47$ cps. (*b*) Mode 2; $f_2=207$ cps. (*c*) Mode 3; $f_3=380$ cps.

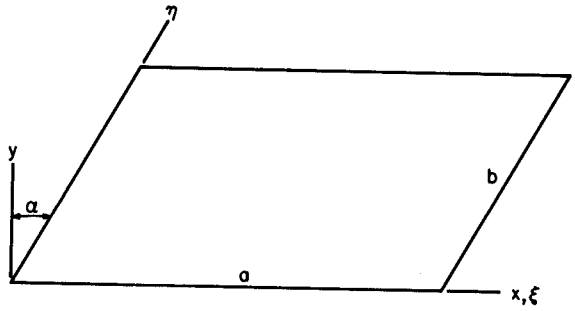


FIGURE 5.24.—F–F–F–F parallelogram plate.

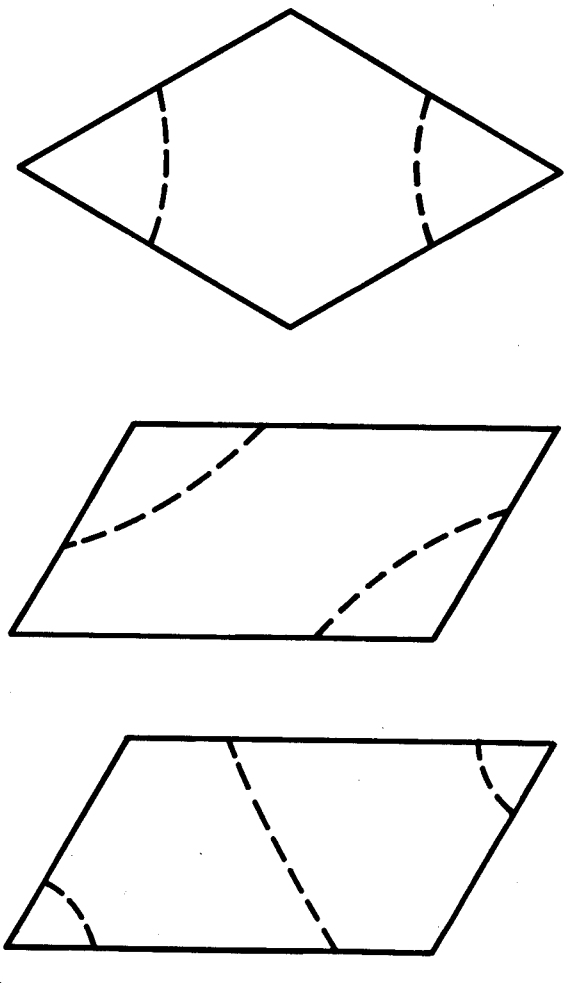


FIGURE 5.25.—Nodal patterns of F–F–F–F parallelogram plates. (After ref. 5.21)

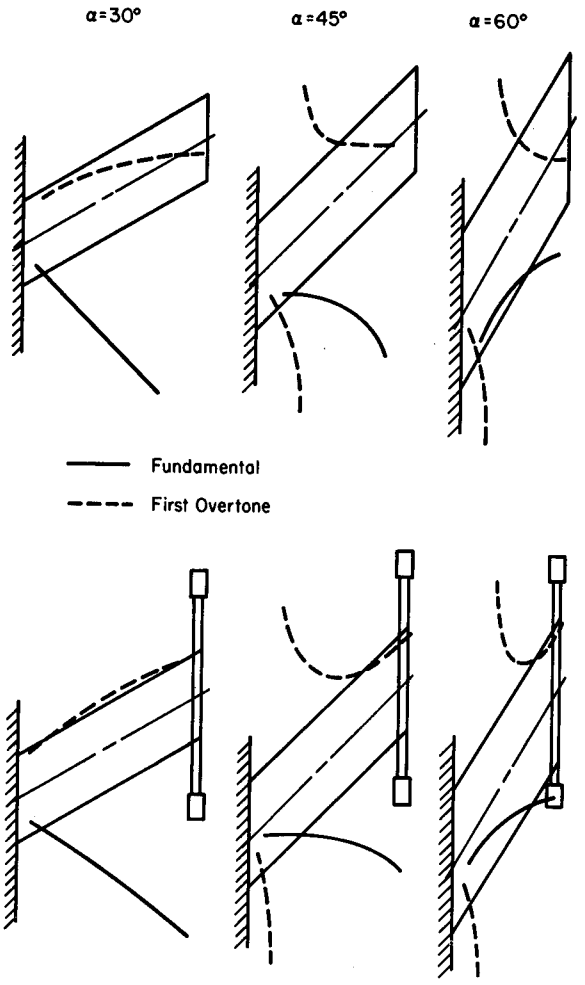


FIGURE 5.26.—Nodal lines for C–F–F–F parallelogram plates with and without tip mass; material. 65 S aluminum alloy.

REFERENCES

5.1. KAUL, R. K., AND CADAMBE, V.: The Natural Frequencies of Thin Skew Plates. Aeron. Quart., vol. 7, 1956, pp. 337–352.

5.2. HAMADA, M.: Compressive or Shearing Buckling Load and Fundamental Frequency of a Rhomboidal Plate With All Edges Clamped. Bull. JSME, vol. 2, no. 8, Nov. 1959, pp. 520–526.

5.3. HAMADA, M.; AND KONDO, H.: Fundamental Frequency of a Rhomboidal Plate With All Edges Clamped. Trans. JSME, vol. 23, no. 131, 1957, pp. 522–528.

5.4. TREFFTZ, E.: Calculation of Buckling Loads of Rectangular Plates. ZAMM, vol. 15, 1935, pp. 339–344. (In German.)

5.5. HASEGAWA, M.: Vibration of Clamped Parallelogrammic Isotropic Flat Plates. J. Aeron. Sci., vol. 24, no. 2, Feb. 1957, pp. 145–146.

5.6. HASEGAWA, M.: On the Vibration of Clamped Rhombic Isotropic Plates. Bull. Shimane Univ., vol. 6, 1956, p. 21.

5.7. CONWAY, H. D.; AND FARNHAM, K. A.: The Free Flexural Vibrations of Triangular, Rhombic and Parallelogram Plates and Some Analogies. Int. J. Mech. Sci., vol. 7, 1965, pp. 811–816.

5.8. TSYDZIK, P. V.: Application of the Perturbation Method To Solve Problems of the Natural Vibrations of Nearly Rectangular Plates. Prikl. Mat. Mekh., vol. 16, no. 3, 1952. (In Russian.)

5.9. SETH, B. R.: Transverse Vibrations of Rectilinear Plates. Proc. Indian Acad. Sci., sec. A, vol. 25, Jan. 1947, pp. 25–29.

5.10. BARTON, M. V.: Vibration of Rectangular and Skew Cantilever Plates. J. Appl. Mech., vol. 18, no. 1, June 1951, pp. 129–134.

5.11. DALLEY, J. W.; AND RIPPERGER, E. A.: Experimental Values of Natural Frequencies for Skew and Rectangular Cantilever Plates. Proc. Soc. Exp. Stress Anal., vol. 9, no. 2, 1952, pp. 51–66.

5.12. DALLEY, J. W.; AND RIPPERGER, E. A.: Experimental Values of Natural Frequencies for Skew and Rectangular Cantilever Plates. Def. Res. Lab. Rept. DRL–231, CF–1354, Univ. Texas, Dec. 1949.

5.13. CLAASSEN, R. W.: Vibration of Skew Cantilever Plate. Pacific Missile Range Tech. Rept. PMR–TR–62–1, Pacific Missile Range, May 1963.

5.14. CLAASSEN, R. W.: Vibrations of Skew Cantilever Plates. AIAA J., vol. 1, no. 5, May 1963, p. 1222.

5.15. PLASS, H. J., JR.; GAINES, J. H.; AND NEWSOM, C. D.: Application of Reissner's Variational Principle to Cantilever Plate Deflection and Vibration Problems. J. Appl. Mech., vol. 29, no. 1, Mar. 1962, pp. 127–135.

5.16. NEWSOM, C. D.: Application of the Modified Reissner Variational Principle to a Forty-Five Degree Skew Cantilever Plate Problem. Def. Res. Lab. Rept. DRL–443, CF–2769, Univ. Texas, Jan. 1960. Also, M. Sc. thesis, Univ. Texas, Jan. 1960.

5.17. HALL, A. H.; PINCKNEY, H. F. L.; AND TULLOCH, H. A.: On the Analytical Determination of the Normal Modes and Frequencies of Swept Cantilever Vibrations. Rept. LR–76, Natl. Aeron. Estab. Can., July 1953.

5.18. HALL, A. H.; TULLOCH, H. A.; PINCKNEY, H. F. L.; AND SARAZIN, A. C.: Graphical and Tabulated Data on the Frequency and Modal Characteristics of Swept Cantilevers. Rept. 23, LR–193, Natl. Aeron. Estab. Can., 1958.

5.19. CRAIG, R. R.; PLASS, H. J., JR.; AND CAUGHFIELD, D. A.: Experimental Determination of Frequencies and Mode Shapes of Cantilever and Hub-Pin Plates. Def. Res. Lab. Rept. DRL–518, CR–13, Univ. Texas, June 1964.

5.20. HANSON, P. W.; AND TUOVILA, W.: Experimentally Determined Natural Vibration Modes of Some Cantilever Wing Flutter Models by Using an Acceleration Method. NACA TN 4010, 1957.

5.21. WALLER, MARY D.: Vibrations of Free Plates, Line Symmetry: Corresponding Modes. Proc. Roy. Soc. (London), ser. A, vol. 211, 1952, pp. 265–276.

5.22. HALL, A. H.: The Nature and Stiffness of Swept Wing Deformations With Reference to the Prediction of Normal Modes and Frequencies. Preprint 494, Can. Inst. Aeron. Sci., presented at CAI–IAS Int. Meeting, Oct. 1954. Also in CASI J., Sept. 1955.

Other Quadrilateral Plates

6.1 TRAPEZOIDS

6.1.1 All Edges Simply Supported

The problem of the trapezoidal plate simply supported all around (SS–SS–SS–SS) (see fig. 6.1) was solved by Klein (ref. 6.1) by using the collocation method for the case $\alpha_1=\alpha_2=\alpha$. A function

$$W(x,y)=\left[A_1\sin\frac{\pi(x-c)}{a}+A_2\sin\frac{2\pi(x-c)}{a}+A_3\sin\frac{3\pi(x-c)}{a}\right]\left(\cos\frac{\pi y}{2x}\cot\alpha\right) \quad (6.1)$$

was used. This function guarantees that—

(1) The deflections are zero on all edges

(2) The bending moment M_x is zero at $(c,\ 0)$ and $(c+a,\ 0)$.

(3) The bending moment M_n is zero at some point in the region $h/3\leqq x\leqq 2h/3$ along the edges $y=\pm x\tan\alpha$

(4) Symmetry exists about $y=0$

The differential equation (eq. (1.4)) is satisfied at the three points along the line $y=0$ given by $(x-c)/a=1/3,\ 1/2,\ 2/3$. This leads to a third-order characteristic determinant for the frequencies, the elements of which are listed in reference 6.1.

Fundamental frequencies for varying values of α and average width $\bar{b}=(b_1+b_2)/2$ are shown in figures 6.2 and 6.3.

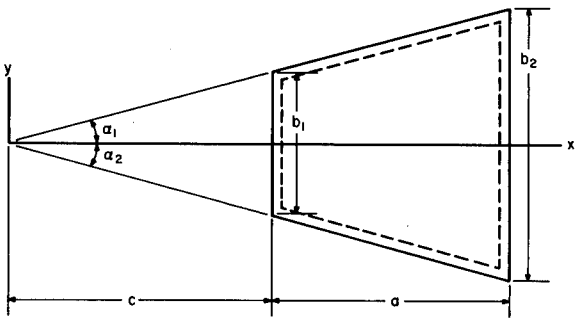


FIGURE 6.1.—SS–SS–SS–SS trapezoidal plate.

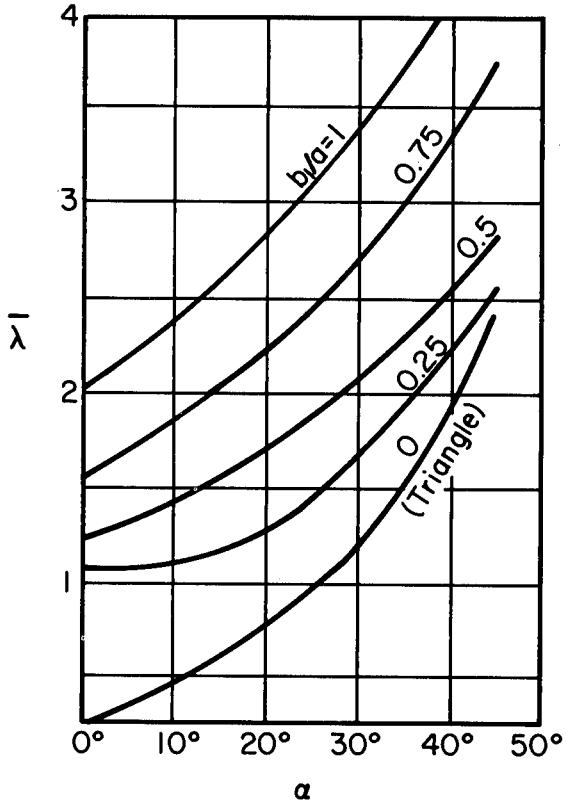


FIGURE 6.2.—Fundamental frequency parameter $\bar{\lambda}=\frac{\omega\bar{b}^2\sqrt{\rho/D}}{\pi^2}$, where $\bar{b}=(b_1+b_2)/2$, against α for an isosceles SS–SS–SS–SS trapezoidal plate. (After ref. 6.1)

A method of perturbing the solution for the rectangle simply supported all around in order to solve this problem is discussed in reference 6.2.

Reipert (ref. 6.3) formulated a solution in terms of functions (eq. (1.37)) which satisfy the differential equation (eq. (1.4)) and the parallel edge boundary conditions exactly. Satisfaction of the remaining boundary conditions yielded a characteristic determinant for the frequencies. A first approximation yields the following formula for fundamental fre-

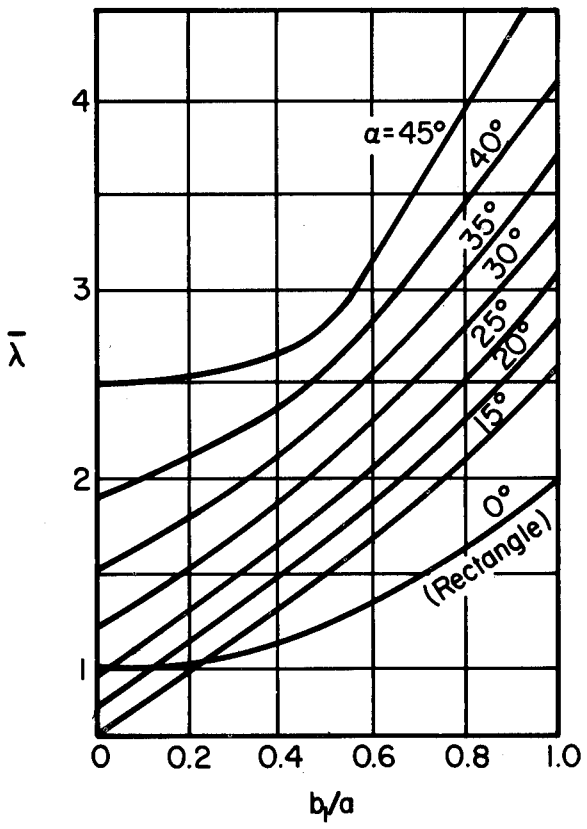


FIGURE 6.3.—Fundamental frequency parameter $\bar{\lambda}=\frac{\omega\bar{b}^2\sqrt{\rho/D}}{\pi^2}$, where $\bar{b}=(b_1+b_2)/2$, against b_1/a for an isosceles SS–SS–SS–SS trapezoidal plate. (After ref. 6.1)

quency parameters of isosceles trapezoids ($\alpha_1=\alpha_2=\alpha$):

$$\omega a^2\sqrt{\frac{\rho}{D}}=\pi^2\left[1+\frac{a^2}{\left(\frac{b_2}{2}+c\tan\alpha\right)^2}\right] \qquad (6.2)$$

Numerical values for $\alpha=45°$ are given in table 6.1 as determined from equation (6.2) and from a second approximation.

6.1.2 Cantilever (C–F–F–F)

The problem of the C–F–F–F trapezoidal plate is depicted in figure 6.4. Nagaraja (ref. 6.4) used the Rayleigh-Ritz method and the nonorthogonal right triangular coordinates shown in figure 6.5 to solve the problem in the special case when $\alpha_2=0$. The coordinates u, v are related to the x, y coordinates by:

$$u=\frac{x}{l} \qquad v=\frac{y}{x}\cot\alpha \qquad (6.3)$$

TABLE 6.1.—*Fundamental Frequency Parameters* $\omega a^2\sqrt{\rho/D}$ *for a SS–SS–SS–SS Isosceles Trapezoidal Plate;* $\alpha=45°$

$\frac{a}{b_2}$	$\omega a^2\sqrt{\rho/D}$	
	First approximation	Second approximation
1/8	10. 11	10. 09
1/4	10. 96	11. 177
3/8	13. 4	14. 311
1/2	19. 7	24. 7

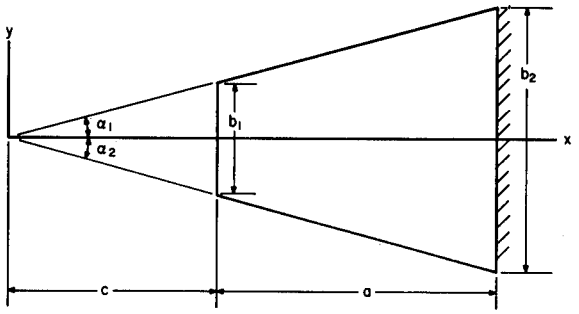


FIGURE 6.4.—C–F–F–F trapezoidal plate.

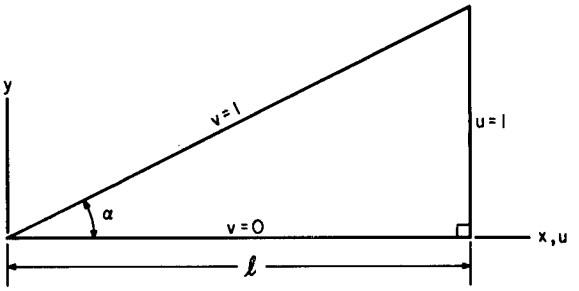


FIGURE 6.5.—Right triangular coordinates.

Using the chain rule of differentiation and substituting equation (6.3) into equation (1.32) yield the following expression for the strain energy of the plate (ref. 6.4):

$$V=\frac{D\tan\alpha}{2l^2}\iint\left\{u\left(\frac{\partial^2 w}{\partial u^2}\right)^2+\frac{1}{u^3}(v^2+\cot^2\alpha)^2\left(\frac{\partial^2 w}{\partial v^2}\right)^2+\frac{2}{u}(v^2+\nu\cot^2\alpha)\frac{\partial^2 w}{\partial u^2}\frac{\partial^2 w}{\partial v^2}-4v\frac{\partial^2 w}{\partial u^2}\frac{\partial^2 w}{\partial u\,\partial v}\right.$$

$$-4\frac{v}{u^2}(v^2+\cot^2\alpha)\frac{\partial^2 w}{\partial v^2}\frac{\partial^2 w}{\partial u\,\partial v}$$
$$+\frac{2}{u}[2v^2+(1-\nu)\cot^2\alpha]\left(\frac{\partial^2 w}{\partial u\,\partial v}\right)^2$$
$$+4\frac{v}{u}\frac{\partial^2 w}{\partial u^2}\frac{\partial w}{\partial v}+4\frac{v}{u^2}(v^2+\cot^2\alpha)\frac{\partial^2 w}{\partial v^2}\frac{\partial w}{\partial v}$$
$$-\frac{4}{u^2}[2v^2+(1+\nu)\cot^2\alpha]\frac{\partial^2 w}{\partial u\,\partial v}\frac{\partial w}{\partial v}$$
$$+\frac{2}{u^3}[2v^2-(1-\nu)\cot^2\alpha]\left(\frac{\partial w}{\partial v}\right)^2\Bigg\}\,du\,dv \quad (6.4)$$

The kinetic energy of translation is

$$T=\frac{l^2\rho\tan\alpha}{2}\omega^2\iint uw^2\,du\,dv \quad (6.5)$$

Deflection functions of the form

$$W(u,v)=\sum_m^r\sum_n^s A_{mn}\phi_m(u)\psi_n(v) \quad (6.6)$$

were used, where $\phi_m(u)$ and $\psi_n(v)$ are the characteristic beam functions deduced from equation (5.23). Because the limits of integration of equation (6.4) give considerable algebraic complication, the integration was performed numerically. Results for the first two modes for $\tan\alpha=1/2$ and for various c/l ratios are given in table 6.2.

TABLE 6.2.—*Frequency Parameters* $\omega l^2\sqrt{\rho/D}$ *for a C–F–F–F Trapezoidal Plate;* $\nu=0.3$

$\frac{c}{l}$	$\omega l^2\sqrt{\rho/D}$ for—			
	Mode 1			Mode 2 upper bound (beam functions)
	Upper bound		Lower bound	
	Beam functions	Polynomial		
0	7. 152	7. 163	6. 880	21. 209
0.2	8. 465	8. 150	8. 042	23. 996
0.4	13. 121	12. 291	11. 160	26. 625
0.6	18. 397	----------	----------	30. 965

In order to determine another set of upper bounds for the problem, the polynomial

$$W(u,v)=(1-u^2)^2(A_{00}+A_{10}u+A_{21}u^2v) \quad (6.7)$$

was also used in reference 6.4 with the Rayleigh-Ritz method. Resulting fundamental frequency parameters are tabulated in table 6.2. Lower bounds appearing in the table are obtained by application of the Kato-Temple method (refs. 6.5 and 6.6).

Rather extensive experimental results are available for this problem. Gustafson, Stokey, and Zorowski (ref. 6.7) took three series of steel plates obtained by cutting the tips off of cantilevered triangles. These series are shown in figure 6.6. Measured material properties for the three series are given in table 6.3. The weight density for all series was $\rho g=0.281$ pound per cubic inch and ν was taken as 0.29. Experimentally measured cyclic frequencies for the three series of plates are given in table 6.4.

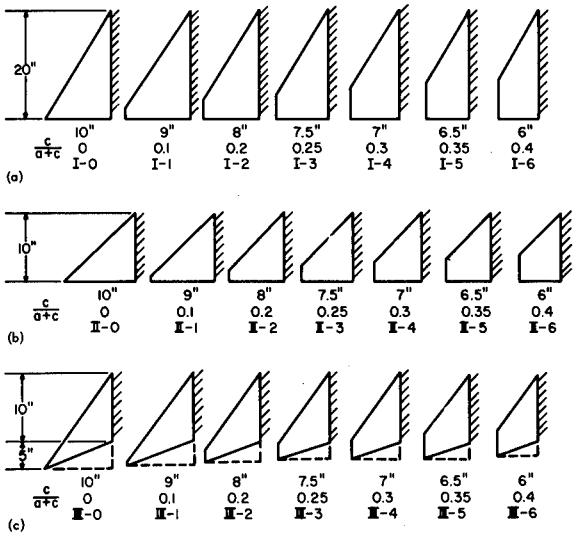


FIGURE 6.6.—C–F–F–F trapezoidal plate configurations. (*a*) Series I plates. (*b*) Series II plates. (*c*) Series III plates. (After ref. 6.7)

TABLE 6.3.—*Material Properties for 3 Series of Trapezoidal Cantilever Plates;* $\nu=0.29$

Series	Modulus of elasticity, psi		Thickness, in.
	x-direction	y-direction	
I	29.3×10^6	31.5×10^6	0. 0622
II	29. 2	27. 8	. 0613
III	29. 0	27. 8	. 0613

TABLE 6.4.—*Experimentally Measured Cyclic Frequencies for C–F–F–F Trapezoidal Plates; $\nu=0.29$*

Series	$\frac{c}{a+c}$	Cyclic frequencies, cps, for mode—					
		1	2	3	4	5	6
I	0	32. 8	91	164	181	283	348
	. 1	34	93	179	181	293	352
	. 2	38. 5	97. 6	184	212	302	362
	. 25	41. 9	99. 4	186	235	304	366
	. 3	48. 3	103. 4	190	266	308	379
	. 35	53. 7	107. 4	196	299	314	404
	. 4	60	112	202	350	312	436
II	0	34. 5	136	190	325	441	578
	. 1	37	142	198	335	482	583
	. 2	42	153	223	364	561	598
	. 25	46	157	243	374	596	621
	. 3	50. 5	161	268	385	606	660
	. 35	56	169	300	410	629	695
	. 4	64	175	339	434	639	718
III	0	26. 3	101	171	259	346	522
	. 1	27. 9	110	184	274	376	525
	. 2	31. 5	122	198	289	438	542
	. 25	34. 8	130	215	300	476	567
	. 3	38. 5	136	243	312	505	623
	. 35	44. 9	143	277	327	540	674
	. 4	51. 7	151	314	347	573	699

Nodal patterns corresponding to most of the frequencies of table 6.4 are shown in figures 6.7, 6.8, and 6.9. Plate designations are shown on the fundamental modes and refer to those of figure 6.6.

Heiba (ref. 6.8) experimentally determined frequencies and mode shapes for 12 trapezoidal plates of various aspect ratios and having $\alpha_1=15°$, 30°, and 45° and $\alpha_2=0$ (fig. 6.10). Aspect ratios of 2.0, 1.6, 1.2, and 0.8 were used, where the aspect ratio $\equiv 4a/(b_1+b_2)$. The plates were made of ⅛-inch-thick steel. Cyclic frequencies and nodal patterns for the first six modes of each plate are shown in figure 6.10. Planform dimensions are given on the fundamental mode in each case. The mode labels (m/n) identify the number of nodal lines approximately parallel to the x- and y-directions, respectively. Modes having double labels (e.g., $(0/1)+(2/0)$) can be thought of as being the superposition of two simple modes, each of the designated label. The variation in frequency with $\tan \alpha_1$ is shown in figure 6.11. It is seen that this choice of parameters yields small variations. Frequencies for $\alpha_1=0$ for the rectangle, as well as nodal patterns, are listed in section 4.3.12.

6.2 OTHER QUADRILATERALS OF GENERAL SHAPE

No published results exist for quadrilaterals of general shape.

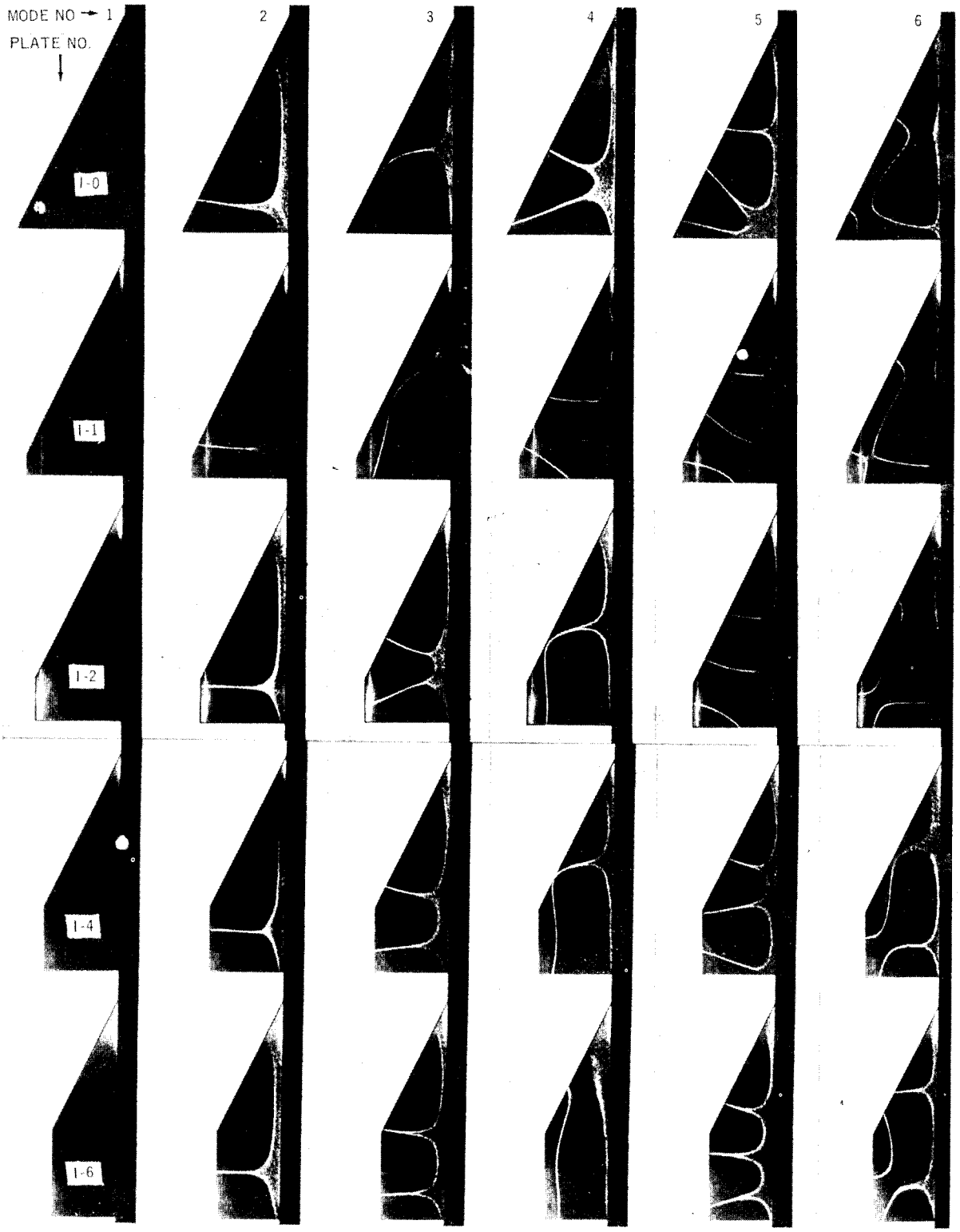


FIGURE 6.7.—Nodal patterns for series I plates; $\nu = 0.3$. (From ref. 6.7)

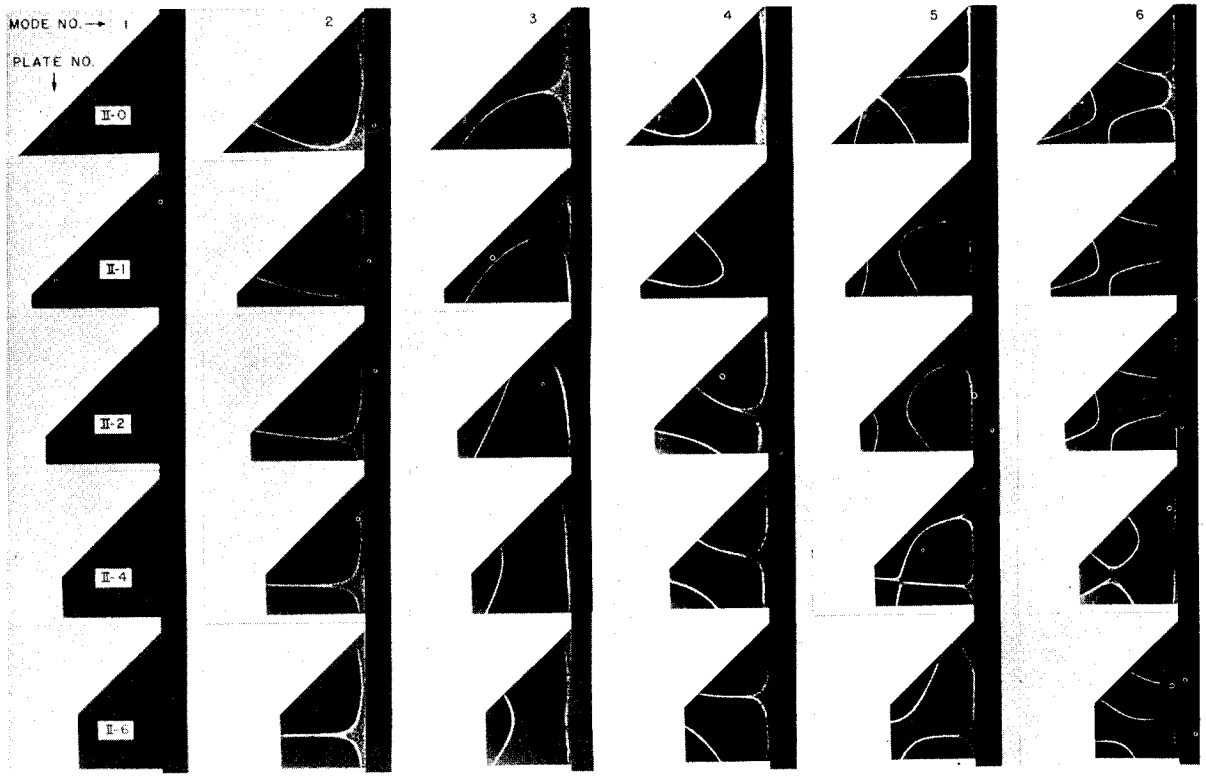


FIGURE 6.8.—Nodal patterns for series II plates; $\nu = 0.3$. (From ref. 6.7)

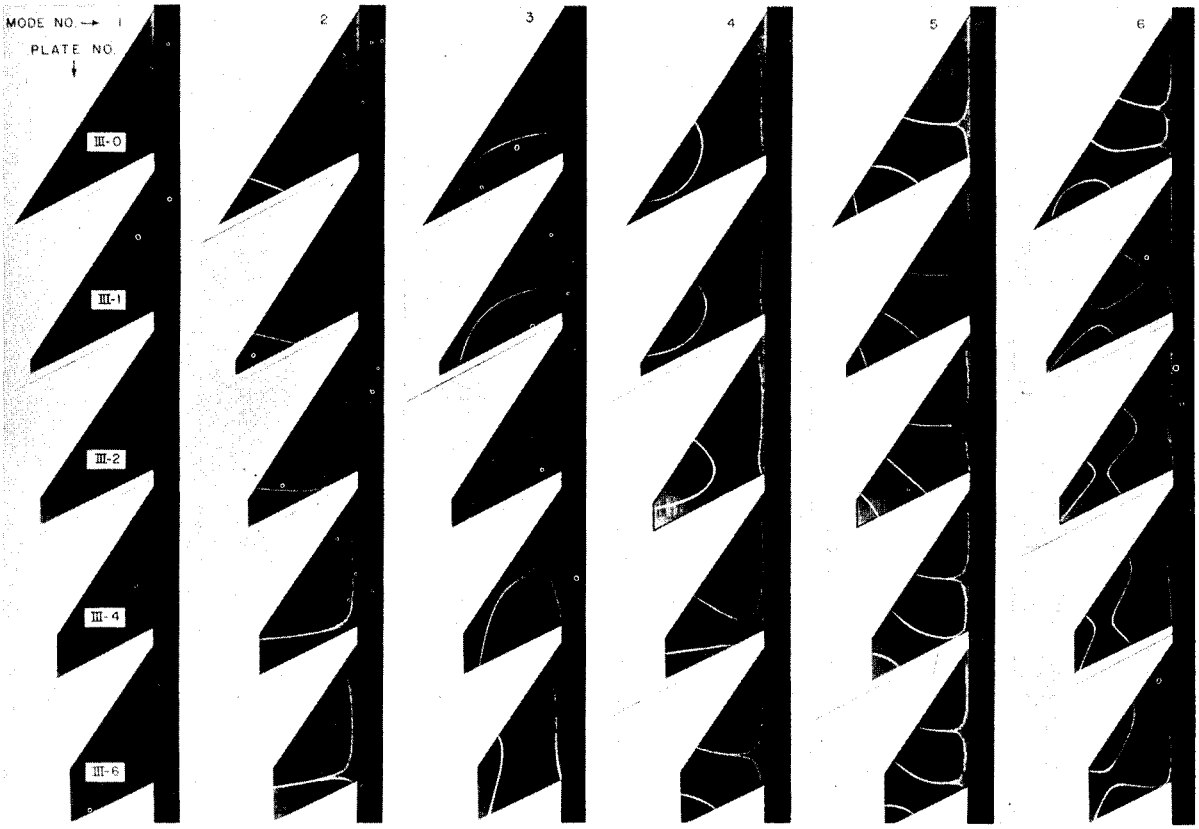
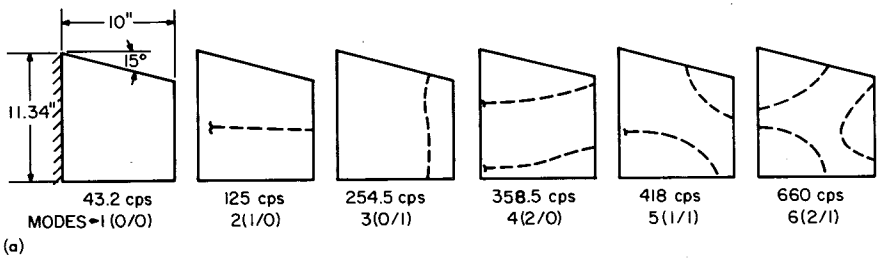
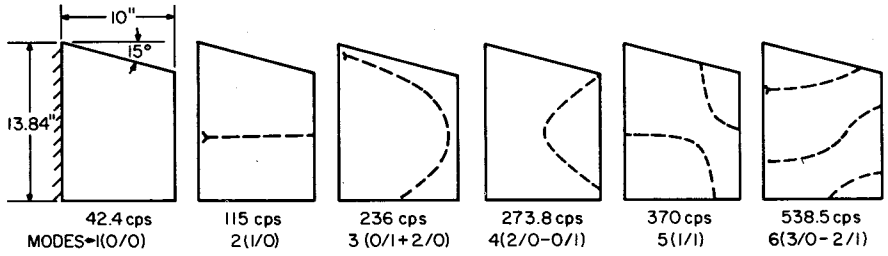


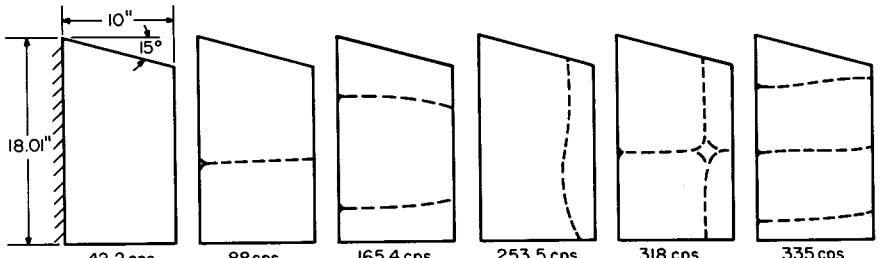
FIGURE 6.9.—Nodal patterns for series III plates; $\nu = 0.3$. (From ref. 6.7)


10"
15°
11.34"
43.2 cps
MODES ➡ 1 (0/0)
125 cps
2(1/0)
254.5 cps
3(0/1)
358.5 cps
4(2/0)
418 cps
5(1/1)
660 cps
6(2/1)

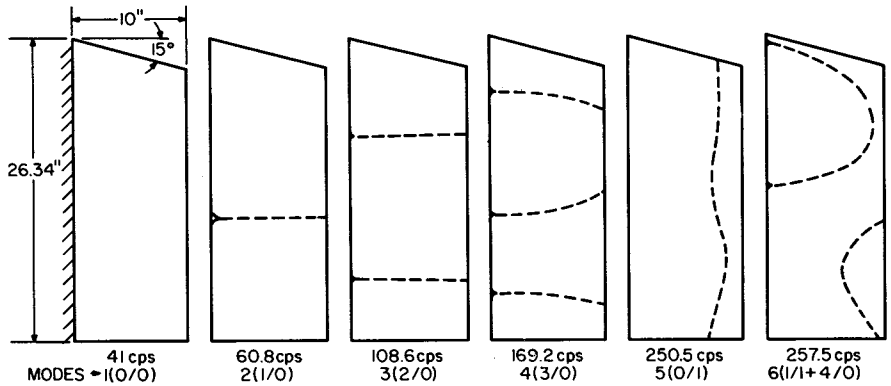
(a)


10"
15°
13.84"
42.4 cps
MODES ➡ 1(0/0)
115 cps
2(1/0)
236 cps
3 (0/1+2/0)
273.8 cps
4(2/0-0/1)
370 cps
5(1/1)
538.5 cps
6(3/0-2/1)

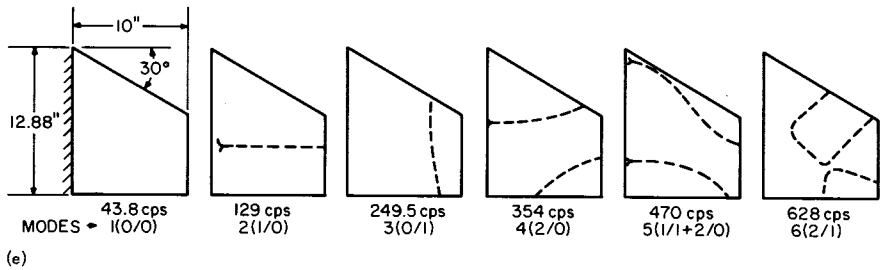
(b)


10"
15°
18.01"
42.2 cps
MODES ➡ 1(0/0)
88 cps
2(1/0)
165.4 cps
3(2/0)
253.5 cps
4(0/1)
318 cps
5(1/1)
335 cps
6(3/0)

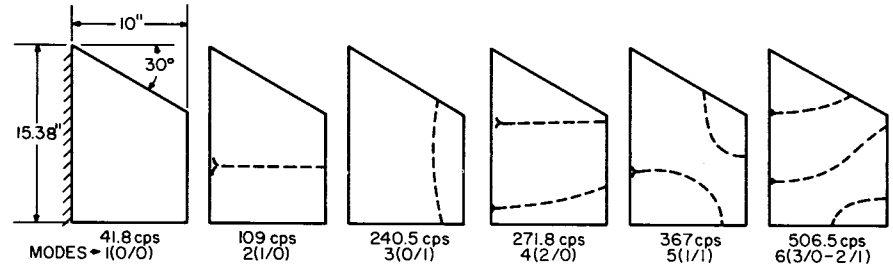
(c)


10"
15°
26.34"
41 cps
MODES ➡ 1(0/0)
60.8 cps
2(1/0)
108.6 cps
3(2/0)
169.2 cps
4(3/0)
250.5 cps
5(0/1)
257.5 cps
6(1/1+4/0)

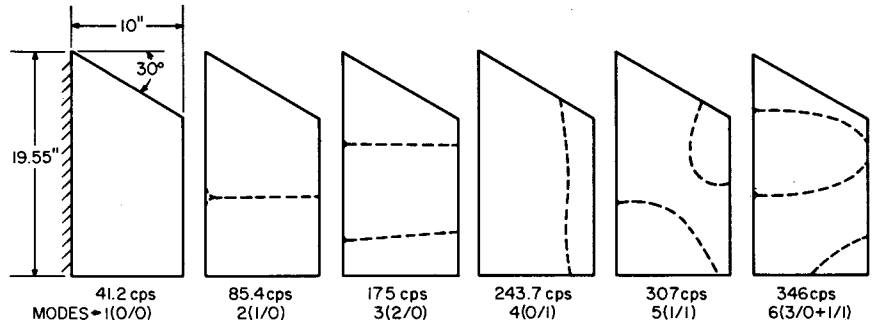
(d)


10"
30°
12.88"
43.8 cps
MODES ➡ 1(0/0)
129 cps
2(1/0)
249.5 cps
3(0/1)
354 cps
4(2/0)
470 cps
5(1/1+2/0)
628 cps
6(2/1)

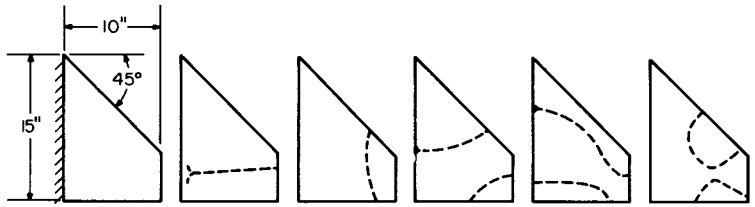
(e)


10"
30°
15.38"
41.8 cps
MODES ➡ 1(0/0)
109 cps
2(1/0)
240.5 cps
3(0/1)
271.8 cps
4(2/0)
367 cps
5(1/1)
506.5 cps
6(3/0-2/1)

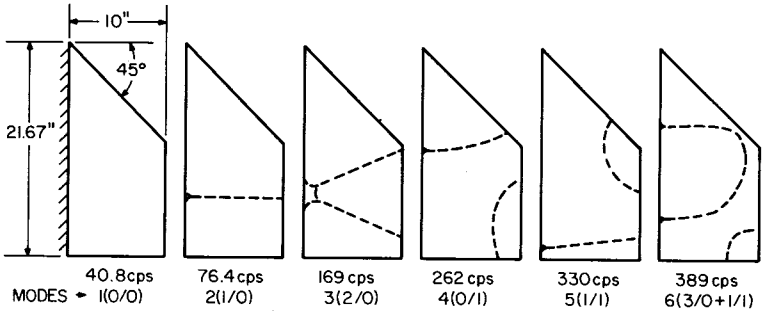
(f)



(g)



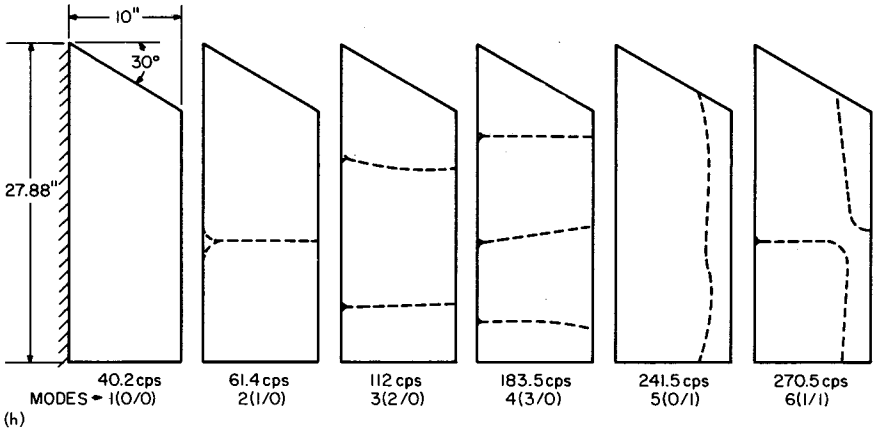
(i)



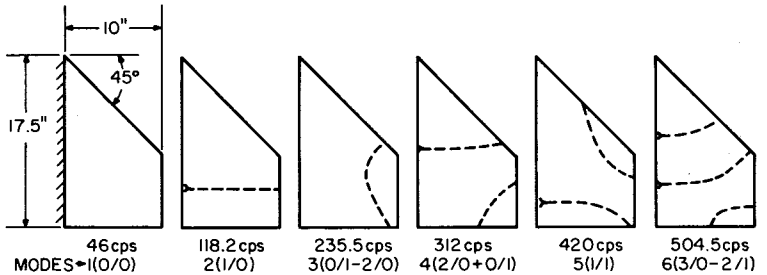
(k)

FIGURE 6.10.—Experimentally determined cylic frequencies and nodal patterns for cantilevered trapezoidal plates; material, steel.

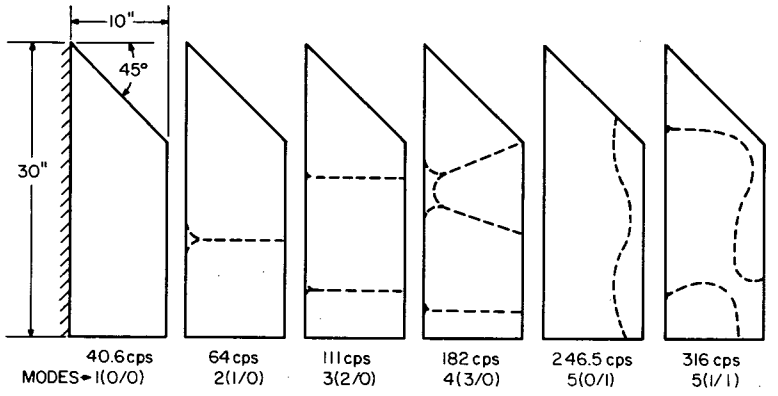
(a) $b_2/a=1.134$; $\alpha_2=15°$.
(b) $b_2/a=1.384$; $\alpha_2=15°$.
(c) $b_2/a=1.801$; $\alpha_2=15°$.
(d) $b_2/a=2.634$; $\alpha_2=15°$.
(e) $b_2/a=1.288$; $\alpha_2=30°$.
(f) $b_2/a=1.538$; $\alpha_2=30°$.
(g) $b_2/a=1.955$; $\alpha_2=30°$.
(h) $b_2/a=2.788$; $\alpha_2=30°$.
(i) $b_2/a=1.5$; $\alpha_2=45°$.
(j) $b_2/a=1.75$; $\alpha_2=45°$.
(k) $b_2/a=2.167$; $\alpha_2=45°$.
(l) $b_2/a=3.00$; $\alpha_2=45°$.



(h)



(j)



(l)

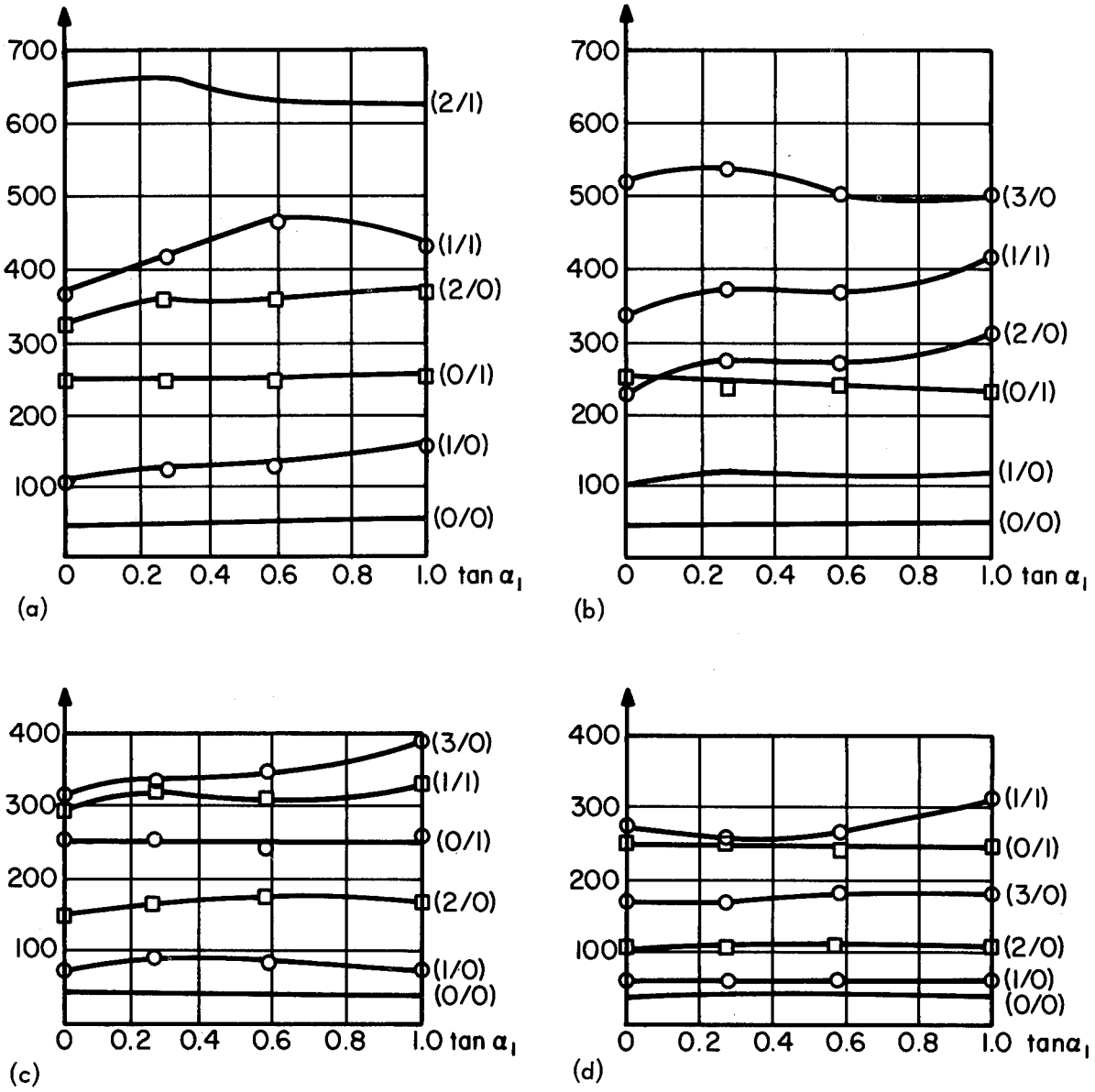


FIGURE 6.11.—Variation of frequency (cps) with tangent of sweep angle for a trapezoidal C–F–F–F plate; material, steel. (*a*) Aspect ratio=2.0. (*b*) Aspect ratio=1.6. (*c*) Aspect ratio=1.2. (*d*) Aspect ratio=0.8.

REFERENCES

6.1. KLEIN, B.: Vibration of Simply Supported Isosceles Trapezoidal Flat Plates. J. Acoust. Soc. Am., vol. 27, no. 6, Nov. 1955, pp. 1059–1060.

6.2. TSYDZIK, P. V.: Application of the Perturbation Method To Solve Problems of the Natural Vibrations of Nearly Rectangular Plates. Prikl. Mat. Mekh., vol. 16, no. 3, 1952. (In Russian.)

6.3. REIPERT, ZBIGNIEW: Application of Simple Functional Series to the Solution of Problems Concerning Statics, Stability, and Vibration of Plates Having Non-Typical Forms. Arch. Mech. Stos., vol. 6, no. 15, 1963, pp. 791–815.

6.4. NAGARAJA, J. V.: Effect of Tip Removal Upon the Frequency of Natural Vibrations of Triangular Plates. J. Sci. Ind. Res. India, vol. 20B, no. 5, May 1961, pp. 193–197.

6.5. KATO, T.: On the Upper and Lower Bounds of Eigenvalues. J. Phys. Soc. Japan, vol. 4, no. 1, 1949, pp. 334–339.

6.6. TEMPLE, G.: The Accuracy of Rayleigh's Method of Calculating the Natural Frequencies of Vibrating Systems. Proc. Roy. Soc. (London), ser. A, vol. 211, 1952, pp. 204–224.

6.7. GUSTAFSON, P. N.; STOKEY, W. F.; AND ZOROWSKI, C. F.: The Effect of Tip Removal on the Natural Vibrations of Uniform Cantilevered Triangular Plates. J. Aeron. Sci., vol. 21, no. 9, Sept. 1954, pp. 621–633, 648.

6.8. HEIBA, A. E.: Vibration Characteristics of a Cantilever Plate With Sweptback Leading Edge. Rept. No. 82, Cranfield College of Aeron., Oct. 1954.

Chapter 7

Triangular Plates

7.1 SIMPLE EDGE CONDITIONS

Ten combinations of simple (i.e., clamped (C), simply supported (SS), or free (F)) boundary conditions exist for a triangular plate. Of these, only six have a significant amount of results. One, the case when one edge is simply supported and the others free, has absolutely no results in the published literature and will not be discussed herein.

7.1.1 C-C-C

In terms of the ξ, η skew coordinates for the C–C–C triangular plate shown in figure 7.1, the differential equation (eq. (1.4)) for the region becomes

$$\frac{\partial^4 W}{\partial \eta^4}+2(1+2\sin^2\phi)\frac{\partial^4 W}{\partial \eta^2 \partial \xi^2}+\frac{\partial^4 W}{\partial \xi^4} -4\sin\phi\left(\frac{\partial^4 W}{\partial \eta^3 \partial \xi}+\frac{\partial^4 W}{\partial \eta \partial \xi^3}\right)=\frac{\rho\omega^2}{D}W \quad (7.1)$$

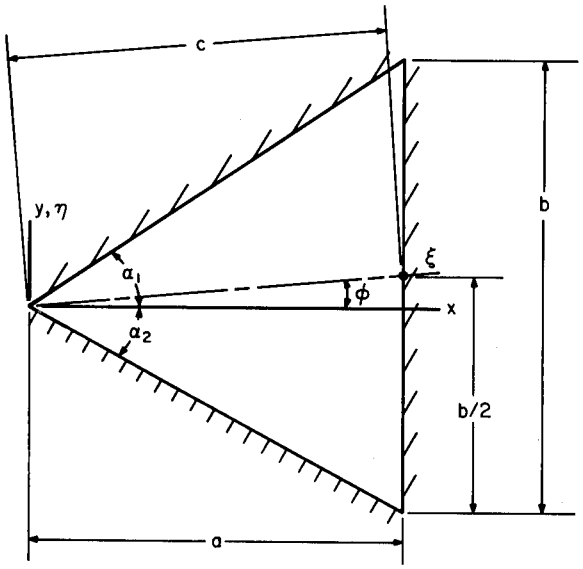


FIGURE 7.1.—C–C–C triangular plate.

Cox and Klein (ref. 7.1) took a deflection function

$$W(\xi,\eta)=\left(A_1\xi^2\sin^2\frac{\pi\xi}{c}+A_2\xi^2\sin\frac{\pi\xi}{c}\sin\frac{2\pi\xi}{c}\right)\left(1-\frac{4c^2\eta^2}{b^2\xi^2}\right)\cos\frac{mc\eta\pi}{b\xi} \qquad (m=1,3\ldots) \quad (7.2)$$

where A_1 and A_2 are undetermined constants. Equation (7.2) satisfies the boundary conditions exactly. Equation (7.1) was satisfied at the two points $\xi=c/2$ and $2c/3$ and $\eta=0$; this yielded a second-order characteristic determinant. Fundamental frequency parameters are shown in figure 7.2 for $\phi=0°$ and 25°. As discussed later in this section, the limiting case as $2c/b\to 0$ is $\omega c^2\sqrt{\rho/D}=22.4$, an exact solution, which indicates a lack of accuracy for small values of $2c/b$ in figure 7.2. According to reference 7.1, the results are not sufficiently accurate for use when $\phi>25°$, but, by suitable choice of coordinates, ϕ can almost always be kept less than 25°. The mode shape components arising from equation (7.2) are shown in figure 7.3.

The results were also checked in reference 7.2 for the case when $\phi=0$ and the triangle is equilateral by using the finite difference method. The two triangular meshes shown in figure 7.4 were used. For the fundamental mode, only one sextile of the triangle is required; this results in independent deflections of one point in figure 7.4(*a*) and eight points in figure 7.4(*b*). Results from using these two meshes and the extrapolation formula (eq. 4.90)) are given in table 7.1.

In reference 7.3 the solution for the rhombus given in reference 7.4 (see discussion on the C–C–C–C rhombic plate, sec. 5.1.1) is extended to yield the solution for the isosceles triangle clamped all around. Fundamental frequency parameters $\omega l^2\sqrt{\rho/D}$ for $\alpha_1=\alpha_2=\alpha$, where l is

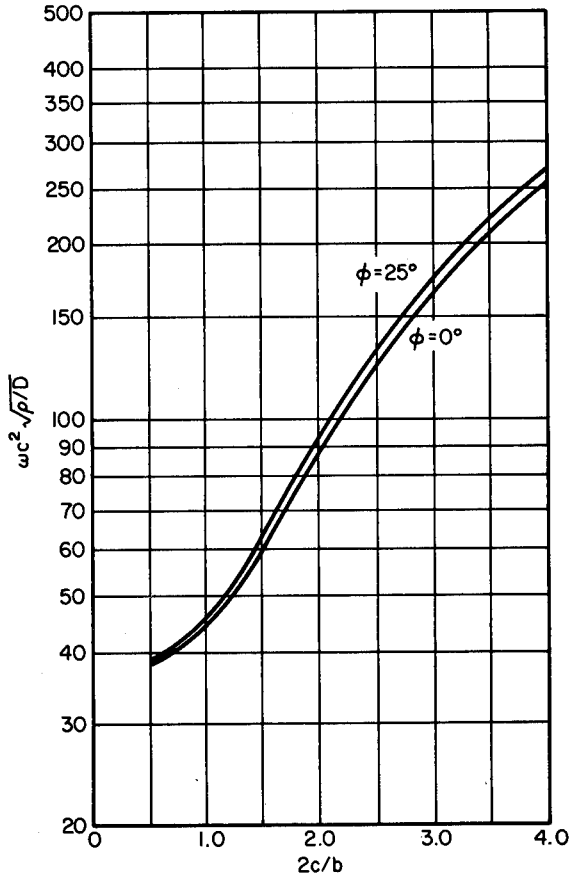


FIGURE 7.2—Fundamental frequency parameters for a C–C–C triangular plate. (After ref. 7.1)

TABLE 7.1.—*Fundamental Frequency Parameters* $\omega c^2\sqrt{\rho/D}$ *for a C–C–C Equilateral Triangle*

Solution	1 point	8 points	Extrapolation
$\omega c^2\sqrt{\rho/D}$	42. 31	65. 85	70. 34

the length of one of the equal sides, are given in table 7.2.

These results are also plotted as a solid line in figure 7.5 along with experimental data obtained on two mild steel plates having l=2.95 inches and thicknesses h=0.091 and 0.063 inch.

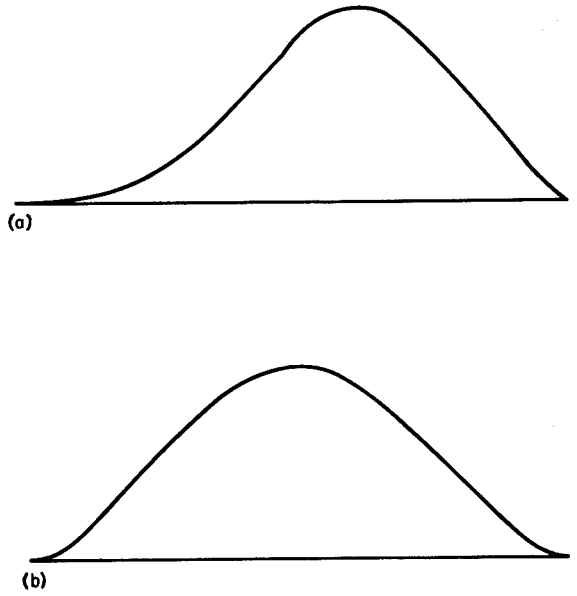


FIGURE 7.3.—Fundamental mode shape components for a C–C–C triangular plate. (*a*) Shape along ξ-axis. (*b*) Shape parallel to η-axis. (After ref. 7.1)

The limiting values as $\alpha_1=\alpha_2=\alpha\rightarrow 0$ and $\alpha_1=\alpha_2=\alpha\rightarrow 90°$ are both well-known exact solutions. Both cases become, in the limit, that of an infinite strip having its opposite edges clamped; that is, $\omega b^2\sqrt{\rho/D}=22.4$. This limiting value is used to plot the curves of figures 7.6 and 7.7 which were taken from reference 7.3.

Hersch (ref. 7.5) showed that a lower bound for the frequency of an equilateral triangle clamped all around is given by $\omega b^2\sqrt{\rho/D}>82.20$.

7.1.2 C–C–SS

The only known solutions to the problem of the C–C–SS triangular plate are for the case when the triangle is isosceles, as shown in figure 7.8.

TABLE 7.2.—*Fundamental Frequency Parameters* $\omega l^2\sqrt{\rho/D}$ *for C–C–C Isosceles Triangle Plates*

2α, deg	30	60	90
$\omega l^2\sqrt{\rho/D}$	199. 6	99. 2	93. 6

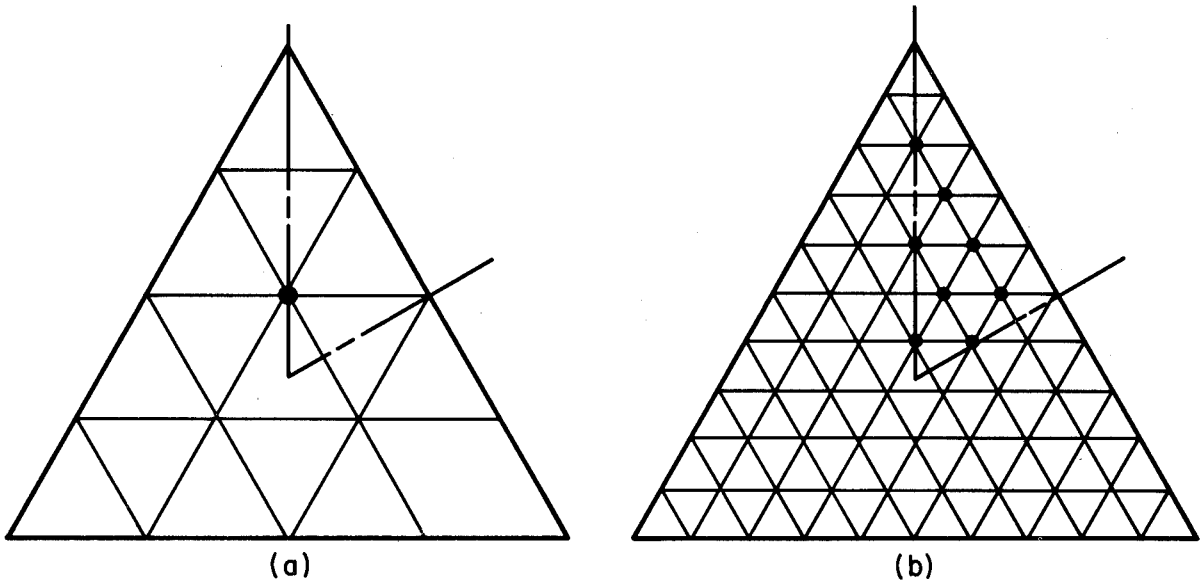


FIGURE 7.4.—Triangular finite difference meshes. (*a*) Coarse grid. (*b*) Fine grid.

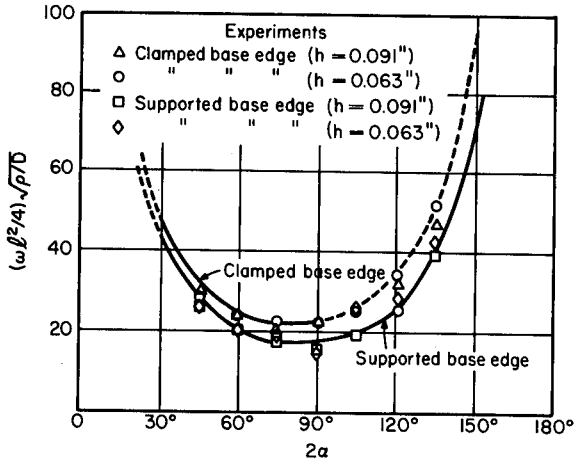


FIGURE 7.5.—Theoretical and experimental fundamental frequency parameters for C–C–C and C–C–SS isosceles triangular plates. (After ref. 7.3)

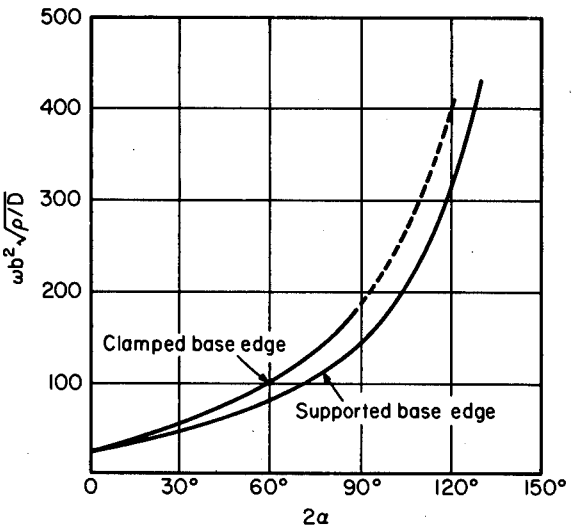


FIGURE 7.6.—Fundamental frequency parameters $\omega b^2\sqrt{\rho/D}$ for C–C–C and C–C–SS isosceles triangular plates. (After ref. 7.3)

Cox and Klein (ref. 7.6) solved the problem by using the collocation method and the deflection function

$$W(x,y)=\left(A_1\sin\frac{\pi x}{a}+A_2\sin\frac{2\pi x}{a}+A_3\sin\frac{3\pi x}{a}\right)\left(1-\frac{4a^2y^2}{b^2x^2}\right)\sin^2\frac{\pi x}{2a}\cos\left(\frac{\pi a}{b}\frac{y}{x}\right) \quad (7.3)$$

Equation (7.3) satisfies all the boundary conditions exactly except that for zero bending moment M_x along $x=a$. It satisfies this condition only at the midpoint of the side (i.e., at $y=0$). The differential equation (eq. (1.4)) was satisfied at the three points $(a/2, 0)$, $(2a/3, 0)$, and $(3a/4, 0)$, thus giving a third-order characteristic determinant for the frequencies. Results for the fundamental frequency parameter obtained directly from the collocation procedure are shown as the broken curve in figure

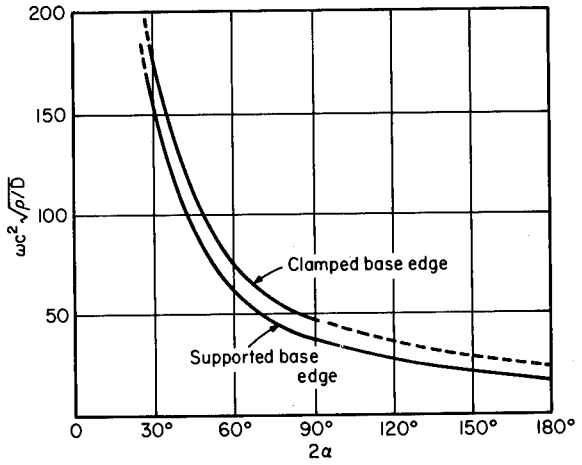


FIGURE 7.7.—Fundamental frequency parameters $\omega c^2\sqrt{\rho/D}$ for C–C–C and C–C–SS isosceles triangular plates. (After ref. 7.3)

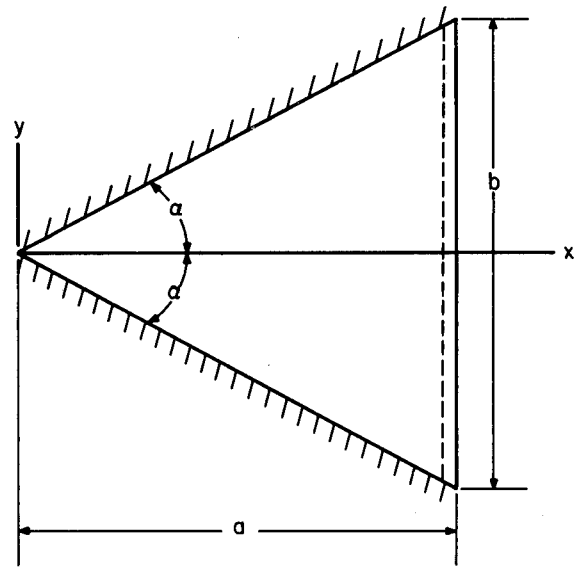


FIGURE 7.8.—C–C–SS isosceles triangular plate.

7.9. The solid curve, which is indicated in reference 7.6 as being more accurate, was found from an extrapolation of finite difference solutions.

Ota, Hamada, and Tarumoto (ref. 7.3) used the solution for the rhombus given in reference 7.4 (see sec. 5.1.1 of the present work) to solve the problem of the isosceles triangle. Fundamental frequency parameters are given in table 7.3, where l is the length of the equal sides. These frequency parameters are plotted

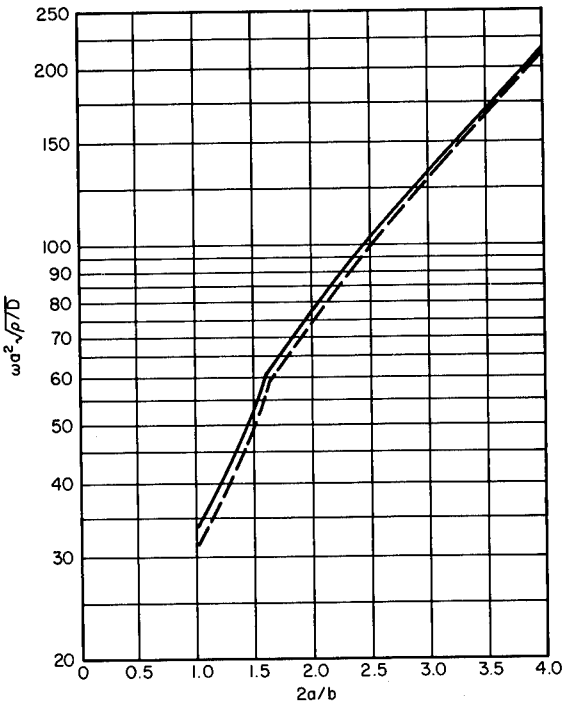


FIGURE 7.9.—Fundamental frequency parameters for a C–C–SS isosceles triangular plate. (After ref. 7.6)

TABLE 7.3.—*Fundamental Frequency Parameters for a C–C–SS Isosceles Triangular Plate*

2α, deg	30	60	90	120	150
$\omega l^2\sqrt{\rho/D}$	178.8	81.6	73.6	105.2	304.0

in figure 7.5 along with experimental results obtained on mild steel plates. In figures 7.6 and 7.7 they are plotted again in terms of other length dimensions, including the limiting cases as $2\alpha \to 0$ and as $2\alpha \to 180°$, for which there are exact solutions.

For more results on the problem, including those for higher frequencies, see the discussion of the antisymmetric modes of a C–C–C–C rhombus (sec. 5.1.1) and of a C–C–C–C square (sec. 4.3.1).

7.1.3 C–C–F

There are no specific solutions of the problem of the C–C–F triangular plate. Westmann (ref. 7.7) proposes for the case of the isosceles triangle having its equal sides clamped that

the frequency is bounded by those of the inscribed and circumscribing C–C–F sectorial plates as shown in figure 7.10. Results for the sectorial plates are given in the chapter entitled "Plates of Other Shapes" (sec. 8.2).

7.1.4 C–SS–SS

Cox and Klein (ref. 7.8) solved the problem of the C–SS–SS triangular plate for the case of an isosceles shape; that is, $\alpha_1=\alpha_2$ in figure 7.11. The collocation method was used, with a deflection function

$$W(x,y)=\left(A_1x^2\sin^2\frac{\pi x}{a}+A_2x^2\sin\frac{\pi x}{a}\sin\frac{2\pi x}{a}+A_3\frac{x^4}{a^4}(x-a)^4\right)\cos\left(\frac{\pi a y}{bx}\right) \quad (7.4)$$

The differential equation (eq. (1.4)) is satisfied at the three points $(a/2, 0)$, $(2a/3, 0)$, and $(3a/4, 0)$, thus giving a third-order characteristic determinant for the frequencies. Resulting fundamental frequency parameters are shown in figure 7.12.

For the case when $\alpha_1=\alpha_2=45°$, the fundamental frequency may be found quite accurately from the fourth mode of a square plate clamped all around (sec. 4.3.1). Using the value from reference 7.9 yields $\omega a^2\sqrt{\rho/D}=32.91$ as a close upper bound. The value from figure 7.12 is 34.7 (ref. 7.8).

Solecki (ref. 7.10) solved the problem for the case $\alpha_1=60°$, $\alpha_2=30°$. A solution for the SS–SS–SS case (see sec. 7.1.6) is taken, and a Fredholm integral equation of the first kind is formulated to satisfy the condition of zero slope along $x=a$. The fundamental frequency is found to be $\omega=(120.0\sqrt{D/\rho})/c^2$.

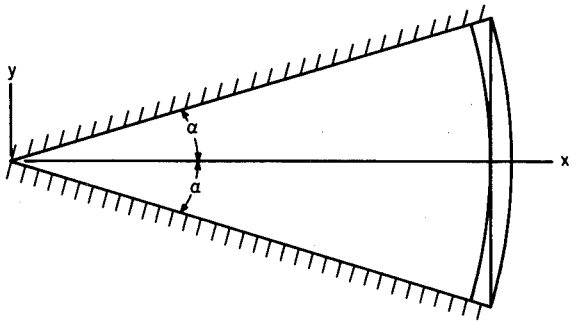


FIGURE 7.10.—C–C–F isosceles triangular plate with inscribed and circumscribing sectors.

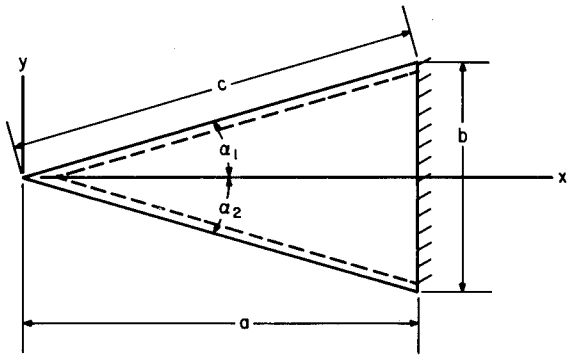


FIGURE 7.11.—C–SS–SS triangular plate.

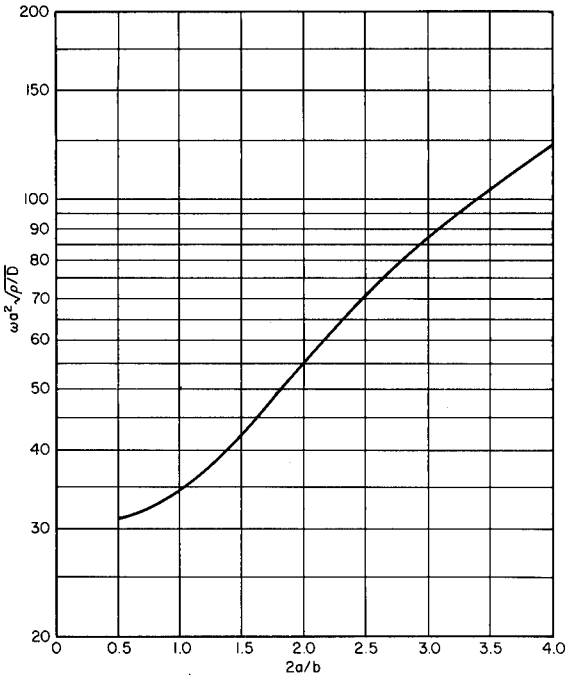


FIGURE 7.12.—Fundamental frequency parameters for a C–SS–SS isosceles triangular plate. (After ref. 7.8)

7.1.5 C–SS–F

No solutions of the specific problem of the C–SS–F triangular plate are known. In the case of the right triangular plate (see fig. 7.13) having the hypotenuse free, a considerable amount of information can be obtained from the antisymmetric modes of a symmetric C–F–F triangular plate (sec. 7.1.8).

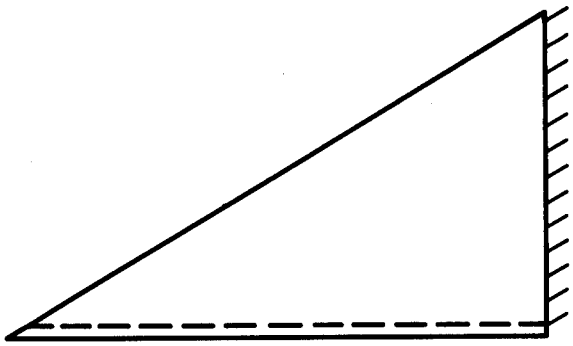


FIGURE 7.13.—C–SS–F right triangular plate.

7.1.6 SS–SS–SS

Conway and Farnham (ref. 7.11) solved the problem for the SS–SS–SS isosceles triangle ($\alpha_1=\alpha_2=\alpha$ in fig. 7.14) by using the method employed on the SS–SS–SS–SS rhombus (sec. 5.1.4). Functions given in equation (5.18) were used and boundary conditions of zero bending moment were satisfied at N points along the edge $x=a$ (fig. 7.14). Frequency parameters arising from various N^{th}-order characteristic determinants are displayed in table 7.4. For a first-order determinant, the single point used was at $x=a$, $y=0$.

Cox and Klein (ref. 7.2) solved the case of the isosceles triangle by the collocation method using a deflection function

$$W(x,y)=\left(A_1\sin\frac{\pi x}{a}+A_2\sin\frac{2\pi x}{a}+A_3\sin\frac{3\pi x}{a}\right)\left(\sin^2\frac{\pi x}{2a}\cos\frac{\pi a y}{bx}\right) \quad (7.5)$$

This function satisfies the condition of zero deflection exactly on all boundaries. It also gives zero normal moment at $(a, 0)$ and at some point in the interval $a/2\leqq x\leqq 3a/4$ along the equal sides. The differential equation (eq. (1.4)) is satisfied at the three points $(h/2, 0)$, $(2h/3, 0)$, and $(3h/4, 0)$, giving a third-order characteristic determinant to solve for the frequencies. Fundamental frequency parameters are given in figure 7.15. When $2\alpha=90°$ the frequency parameter is found by the foregoing method to be $\omega a^2\sqrt{\rho/D}=24.028$. This is in error by 2.61 percent (ref. 7.2) from the exact value of 24.674 obtained from the second mode of a SS–SS–SS–SS square plate. It must be

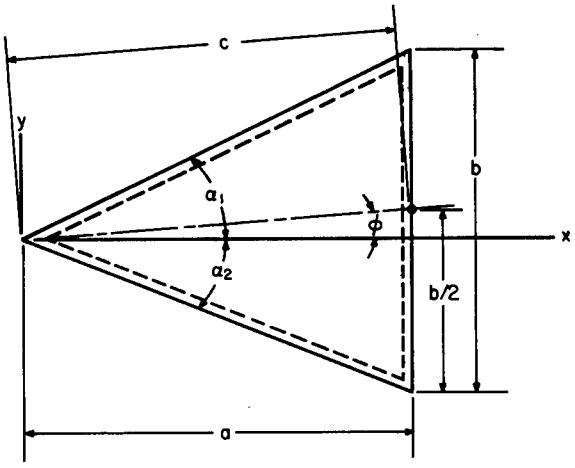


FIGURE 7.14.—SS–SS–SS triangular plate.

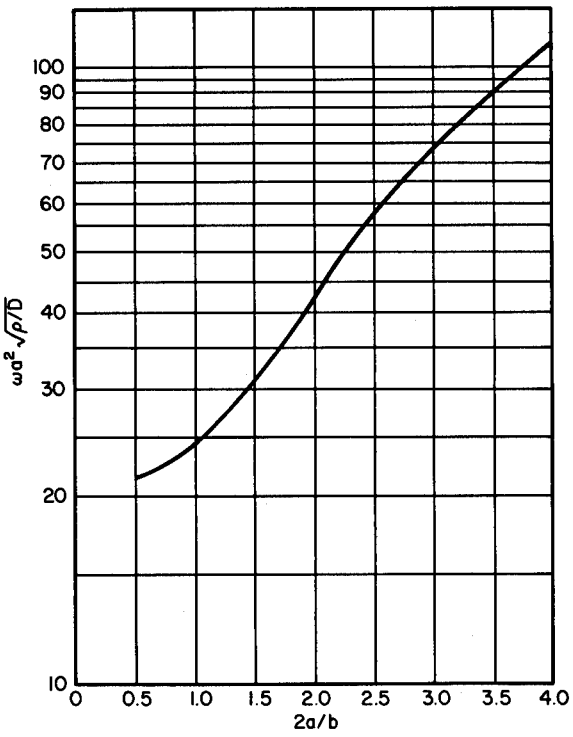


FIGURE 7.15.—Fundamental frequency parameters for a SS–SS–SS isosceles triangular plate. (After ref. 7.2)

observed that the curve of figure 7.15 is clearly inaccurate for small values of $2a/b$, for in the limiting case $2a/b\to 0$ the exact solution for the case of a SS–SS strip, which is $\omega a^2\sqrt{\rho/D}=\pi^2=9.87$, applies.

The results of reference 7.2 were extended in reference 7.12 to estimate the frequencies of non-

TABLE 7.4—*Frequency Parameters* $\omega a^2\sqrt{\rho/D}$ *for SS–SS–SS Isosceles Triangular Plates*

α, deg	$\omega a^2\sqrt{\rho/D}$ for determinant of size—	
	1 by 1	3 by 3
10		177. 69
15	98. 72	97. 93
20		66. 34
25		49. 45
30	40. 70	39. 48
35		32. 87
40		28. 18
45	26. 38	24. 67

isosceles triangles. This was done by taking the results of reference 7.2 and redefining the dimensions a and b so that one of the equal angles becomes the vertex angle and its opposite side becomes the base of length b. This gives some points on the curves of figure 7.16. Other points are determined from the relationship

$$\left(\omega\sqrt{\frac{\rho}{D}}\right)_{\phi_1}=\left(\omega\sqrt{\frac{\rho}{D}}\right)_{\phi_2}=\left(\omega\sqrt{\frac{\rho}{D}}\right)_{\phi_3} \quad (7.8)$$

relating the frequency parameters $\omega c^2\sqrt{\rho/D}$ corresponding to the medians of the triangle which have lengths c_1, c_2, and c_3. Again, the curves are inaccurate for small values of $2c/b$.

Solecki (ref. 7.10) gave the frequencies and mode shapes for the 30°–60°–90° triangle shown in figure 7.17. Mode shapes were taken as

$$W_{mn}(x,y)=\left(\sin\frac{(2m+n)\pi x}{3b}\sin\frac{n\pi y}{a}\right)-\left[(-1)^{m+n}\sin\frac{(m+2n)\pi x}{3b}\sin\frac{m\pi y}{a}\right]+\left[(-1)^{m}\sin\frac{(m-n)\pi x}{3b}\sin\frac{(m+n)\pi y}{a}\right]$$
$$(m=2,3,\ldots;n=1,2,\ldots;m>n) \quad (7.7)$$

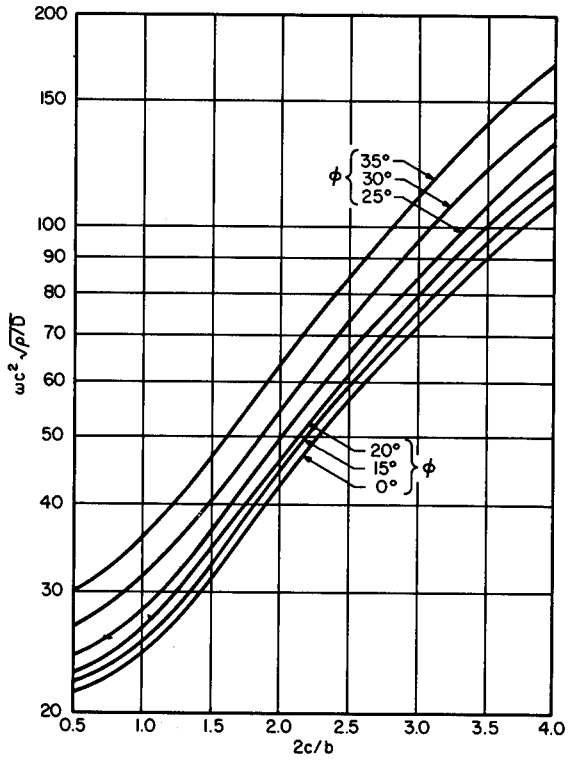


FIGURE 7.16.—Fundamental frequency parameters for a SS–SS–SS triangular plate. (After ref. 7.12)

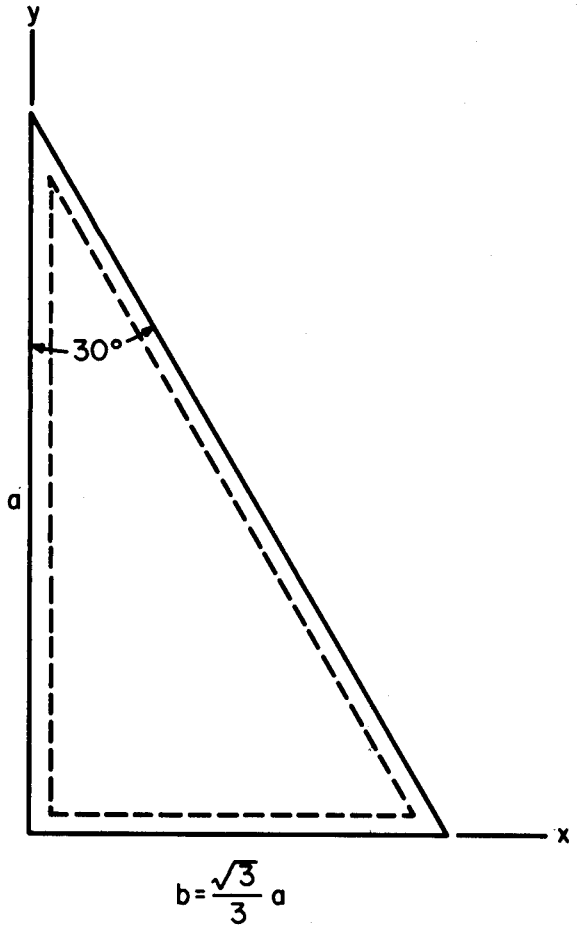


FIGURE 7.17.—30°–60°–90° SS–SS–SS triangular plate.

in terms of figure 7.17. Corresponding frequencies are found from substituting equation (7.7) into equation (1.4), giving

$$\omega_{mn}=\frac{4\pi^2(m^2+mn+n^2)}{3a^2}\sqrt{\frac{D}{\rho}} \quad (m=2, 3, \ldots; n=1, 2, 3, \ldots; m>n) \quad (7.8)$$

Thus the fundamental frequency is found from equation (7.8) to be $\omega_{21}a^2\sqrt{\rho/D}=92.113$.

This was also found in reference 7.13 by using the solution for the SS–SS–SS–SS rectangle and the method of images. Nodal patterns for the first six modes are shown in figure 7.18. The case of the 30°–60°–90° triangle is also discussed in reference 7.14.

Schaefer and Havers (ref. 7.15) found the fundamental frequency of the equilateral triangle of altitude a to be $\omega a^2\sqrt{\rho/D}=39.478$. The problem was also solved by Conway by analogy in reference 7.16 and by the point-matching method in reference 7.11. The problem is also solved in references 7.17 and 7.18.

The case when $\alpha_1=\alpha_2=45°$ (fig. 7.14) can be deduced from the higher mode shapes of a SS–SS–SS–SS square plate. The fundamental frequency parameter is $\omega a^2\sqrt{\rho/D}=24.674$.

The case when $\alpha_1=\alpha_2=60°$ was examined by Seth (ref. 7.17), who gave a fundamental frequency parameter of $\omega a^2\sqrt{\rho/D}=17.272$.

Much more information is available for this problem from an analogy that exists between a vibrating membrane and a simply supported polygonal plate (see the chapter entitled "Plates of Other Shapes" (ch. 8)).

7.1.7 SS–SS–F

There are no specific solutions of the problem of SS–SS–F triangular plates. Westmann (ref. 7.7) proposed obtaining bounds from SS–SS–F sectorial plates. (See sec. 7.1.3.)

7.1.8 C–F–F

Consider first the symmetric cantilevered triangle depicted in figure 7.19. Andersen (refs. 7.19 and 7.20) solved the problem by using the Rayleigh-Ritz method and the triangular u-v coordinates shown in figure 7.19 (see also the discussion for the C–F–F–F trapezoidal plate, sec. 6.1.2). For symmetric modes, the four-term series

$$W(u,v)=[A_{11}+A_{31}u^2\psi_3(v)]\phi_1(u)+[A_{12}+A_{32}u^2\psi_3(v)]\phi_2(u) \quad (7.9)$$

was used, and for antisymmetric modes the series

$$W(u,v)=[A_{21}v+A_{41}\psi_4(v)]u^2\phi_1(u)+[A_{22}v+A_{42}\psi_4(v)]u^2\phi_2(u) \quad (7.10)$$

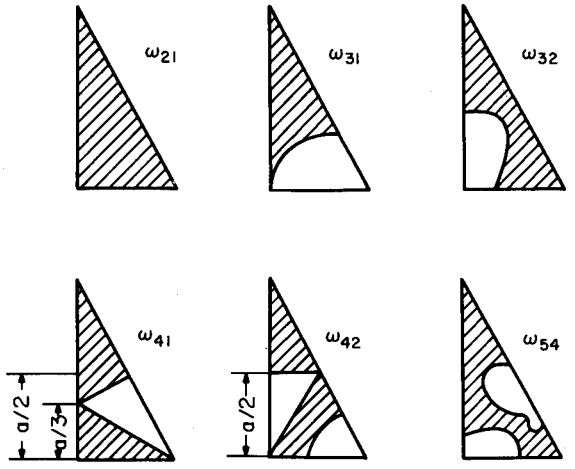


FIGURE 7.18.—Nodal patterns for a 30°–60°–90° SS–SS–SS triangular plate.

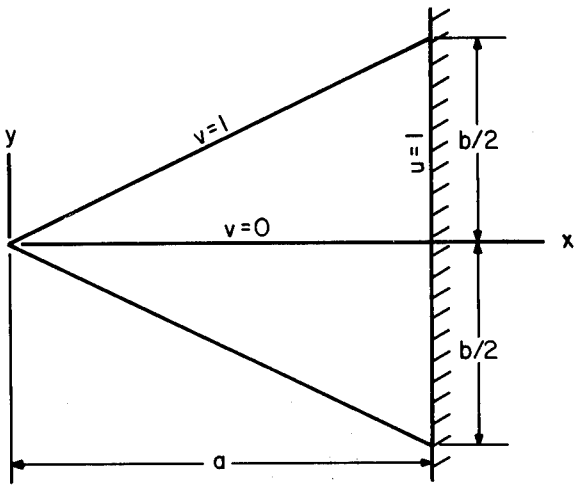


FIGURE 7.19.—Symmetric C–F–F triangular plate.

was used, where ϕ_1 and ϕ_2 represent the first two modes of a cantilever beam free at $u=0$ and clamped at $u=1$. (See discussion of the rectangular cantilever beam, sec. 4.3.12.) The functions ψ_3 and ψ_4 represent the first symmetric and antisymmetric modes, respectively, of a beam free at $v=\pm 1$. The expression for the strain energy in triangular coordinates is given in equation (6.4). Integration was performed numerically. Frequency parameters, nodal patterns, and amplitude coefficients for the first four modes and several a/b ratios are given in table 7.5. Poisson's ratio is 0.3.

Variation of frequency parameter with a/b ratio for the two antisymmetric modes is shown in figure 7.20. It is seen that the frequency parameters increase linearly with a/b, as was the case for the C–F–F–F rectangle (sec. 4.3.12). Frequency variations for the first two modes are shown in figure 7.21 where the frequency parameters $\omega a^2\sqrt{12\rho/Eh^3}$ obtained from beam theory are also plotted as horizontal broken lines. It must be remembered that the plate and beam frequency parameters differ by the factor $1-\nu^2$. Thus, when Poisson's ratio is considered, the plate frequencies themselves are slightly higher than those predicted by beam theory.

Duffin, Gustafson, and Warner (ref. 7.21) also used the Rayleigh-Ritz method to analyze the triangular plate of symmetric shape. A partial summary of deflection functions used and frequency parameters obtained is given in table 7.6, where the notation used is that of figure 7.19 and $\nu=1/4$. Because modes 1 and 2 are symmetric and antisymmetric, respectively, the frequency parameters listed for these modes are guaranteed to be upper bounds on the exact frequencies, and improvement in bounds with the various functions used is clearly indicated in the table. Further results were obtained which showed the variation in fundamental frequency parameter and mode shape with a/b ratio and Poisson's ratio by using the deflection function.

$$w=\left(\frac{x}{a}-1\right)^2\left(\frac{3x}{a}+5\right)+A_1\left(\frac{x}{a}-1\right)^2\frac{y^2}{a^2} \qquad (7.11)$$

These are shown in table 7.7.

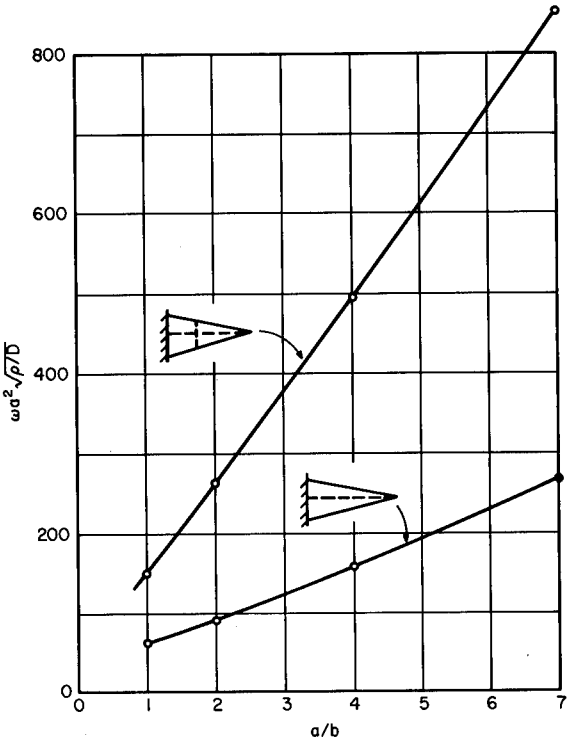


FIGURE 7.20.—Variation in antisymmetric frequency parameters with a/b for a C–F–F symmetric triangular plate; $\nu=0.3$. (After ref. 7.20)

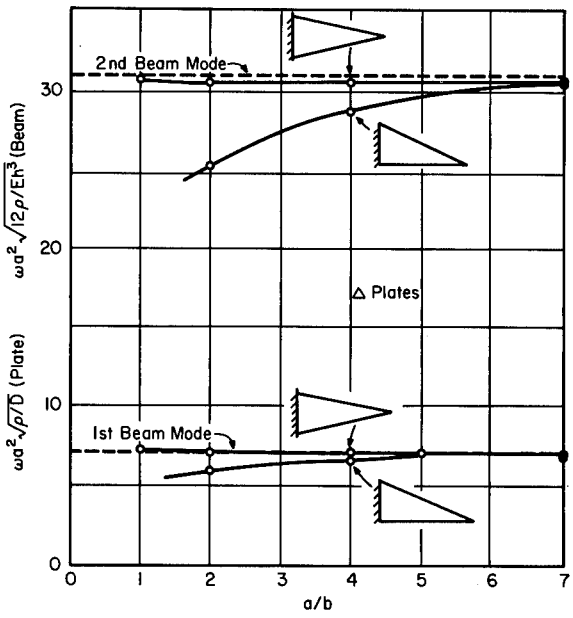


FIGURE 7.21.—Variation in symmetric frequency parameters with a/b for a C–F–F symmetric triangular plate; $\nu=0.3$. (After ref. 7.20)

TABLE 7.5.—*Frequency Parameters, Nodal Patterns, and Amplitude Coefficients for a C–F–F Symmetric Triangular Plate; $\nu=0.3$*

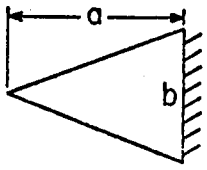
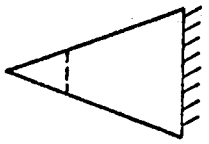
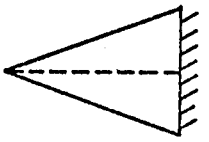
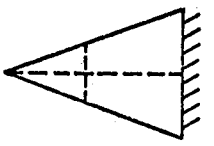
Mode	Nodal lines	Amplitude coefficient	a/b			
			1	2	4	7
			$\omega a^2\sqrt{\rho/D}$			
1			7.149	7.122	7.080	7.068
		A_{11}	1. 000000	1. 000000	1. 000000	1. 000000
		A_{12}	−. 013453	−. 018583	−. 020249	−. 020664
		A_{31}	. 000887	−. 000068	−. 000026	−. 000008
		A_{32}	. 002312	−. 001362	−. 000498	−. 000176
			$\omega a^2\sqrt{\rho/D}$			
2			30.803	30.718	30.654	30.638
		A_{11}	−0. 77460	−0. 76682	−0. 76427	−0. 76368
		A_{12}	1. 00000	1. 00000	1. 00000	1. 00000
		A_{31}	−. 02305	. 00527	. 00208	. 00073
		A_{32}	. 04645	. 01022	. 00241	. 00077
			$\omega a^2\sqrt{\rho/D}$			
3			61.131	90.105	157.70	265.98
		A_{21}	1. 64125	0. 60941	0. 33684	0. 27432
		A_{22}	1. 00000	1. 00000	1. 00000	1. 00000
		A_{41}	. 00581	. 00155	. 00038	. 00012
		A_{42}	−. 00380	−. 00079	−. 00019	−. 00006
			$\omega a^2\sqrt{\rho/D}$			
4			148.8	259.4	493.4	853.6
		A_{21}	1. 00000	1. 00000	1. 00000	1. 00000
		A_{22}	−. 32893	−. 31823	−. 31430	−. 31330
		A_{41}	−. 00808	−. 00156	−. 00036	−. 00012
		A_{42}	. 00586	. 00122	. 00029	. 00009

TABLE 7.6.—*Deflection Functions and Frequency Parameters for a Rayleigh-Ritz Analysis of a C–F–F Symmetric Triangular Plate; $\nu=1/4$*

a/b	Mode no.	Deflection function, $W(x, y)$	Amplitude coefficients	$\omega a^2\sqrt{\rho/D}$
1/2	1	$\left(\frac{x}{a}-1\right)^2\left(\frac{x}{a}+A_0\right)$	$A_0=5/3$	7. 15
		$\left(\frac{x}{a}-1\right)^2\left(\frac{3x}{a}+5\right)+A_1\left(\frac{x}{a}-1\right)^2\frac{y^2}{a^2}$	$A_1=-4.85$	6. 55
	2	$\left(\frac{x}{a}-1\right)^2\frac{y}{a}$	----------	26. 5
		$\left(\frac{x}{a}-1\right)^2\left(\frac{y}{a}+A_2\frac{y^3}{a^3}\right)$	$A_2=-1$	23. 8
		$\left(\frac{x}{a}-1\right)^2\left(\frac{x}{a}+A_3\right)\frac{y}{a}$	$A_3=0.462$	23. 0
	3	$\left(\frac{x}{a}-1\right)^2\left(\frac{x}{a}-A_4\right)$	$A_4=49/164$	37. 1
1	1	$\left(\frac{x}{a}-1\right)^2\left(\frac{x}{a}+A_5\right)$	$A_5=5/3$	7. 15
		$\left(\frac{x}{a}-1\right)^2\left(\frac{3x}{a}+5\right)+A_6\left(\frac{x}{a}-1\right)^2\frac{y^2}{a^2}$	$A_6=-3.61$	7. 02

TABLE 7.7.—*Frequency Parameters and Amplitude Coefficients for C–F–F Symmetric Triangular Plates*

a/b	$\nu=0$		$\nu=1/4$		$\nu=1/2$	
	A_1	$\omega a^2\sqrt{\rho/D}$	A_1	$\omega a^2\sqrt{\rho/D}$	A_1	$\omega a^2\sqrt{\rho/D}$
1/2	−3. 95	6. 733	−4. 85	6. 555	−5. 92	6. 320
1	−2. 27	7. 101	−3. 61	7. 002	−5. 09	6. 888
2	−. 725	7. 154	−2. 25	7. 122	−3. 83	7. 032

Kumaraswamy and Cadambe (ref. 7.22) experimentally determined the first 18 modes and frequencies of a symmetric triangular cantilever plate made of commercial mild steel. Pertinent dimensions and physical constants were: $a=6.00$ inches, $b=6.00$ inches, $h=0.0895$ inch, $\rho g=0.282$ pound per cubic inch, lengthwise $E=29.83\times10^6$ psi, breadthwise $E=29.18\times10^6$ psi, and $\nu=0.29$ (assumed). Cyclic frequencies and frequency parameters are given in table 7.8. The disagreement in values of $\omega a^2\sqrt{\rho/D}$ between tables 7.5 and 7.8 for $a/b=1$ is readily apparent. Nodal patterns are shown in figure 7.22.

Further experimental results from reference 7.23 for $a/b=1$ are given later in this section.

Consider next the delta cantilever plate depicted in figure 7.23. This problem was solved in reference 7.20 for the first two modes by the method described earlier in this section. The following six-term series was used for the deflection function:

$$W(u,v)=(A_{11}+A_{21}u^2v+A_{31}u^2\psi_3(v))\phi_1(u)+(A_{12}+A_{22}u^2v+A_{32}u^2\psi_3(v))\phi_2(u) \quad (7.12)$$

Frequency parameters, nodal patterns, and amplitude coefficients are listed in table 7.9 for

$\nu=0.3$. Variation of frequency parameter with a/b ratio is seen in figure 7.21.

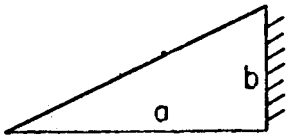
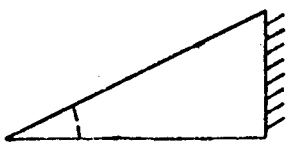
In reference 7.24 the method of reference 7.20 given previously was duplicated by using only the four terms of equation (7.12) associated with A_{11}, A_{21}, A_{12}, and A_{22}. The fundamental frequency for the plate of figure 7.23 was found to be $\omega a^2\sqrt{\rho/D}=5.045$ for $a/b=1$. A corroborating experimental value of $\omega a^2\sqrt{\rho/D}=5.36$ was determined for a steel plate ($a=6.00$ in., $b=6.00$ in., $h=0.0895$ in., $\rho g=0.282$ lb/in.^{3}, and $E=29.5\times10^6$ psi). Tabular values of the integrals obtained from equation (6.4) are also given in reference 7.24.

In reference 7.21 the delta plate having $\alpha=45°$ was also analyzed by the Rayleigh-

TABLE 7.8.—*Experimentally Determined Frequencies and Frequency Parameters for a C–F–F Symmetric Triangular Plate;* a/b=*1;* $\nu=0.29$

Mode	f, cps	$\omega a^2\sqrt{\rho/D}$	Mode	f, cps	$\omega a^2\sqrt{\rho/D}$	Mode	f, cps	$\omega a^2\sqrt{\rho/D}$
1	137	5.76	7	28.40	119.10	13	6499	272.4
2	642	26.91	8	3133	131.30	14	6526	273.5
3	655	27.45	9	3924	164.40	15	6884	288.5
4	1442	60.42	10	3988	167.1	16	7627	319.7
5	1725	72.30	11	4929	206.5	17	8498	356.1
6	2080	87.18	12	5939	249	18	9875	413.8

TABLE 7.9.—*Frequency Parameters, Nodal Patterns, and Amplitude Coefficients for a C–F–F Right Triangular Plate;* $\nu=0.3$

Mode	Nodal lines	Amplitude coefficient	a/b		
			2	4	7
			$\omega a^2\sqrt{\rho/D}$		
			5.887	6.617	6.897
1		A_{11}	1.00000	1.00000	1.00000
		A_{12}	.02030	−.00077	−.01287
		A_{21}	−.31370	−.09379	−.03234
		A_{22}	−.14370	−.07012	−.02783
		A_{31}	−.00073	−.00005	−.00002
		A_{32}	−.00598	−.00198	−.00070
			$\omega a^2\sqrt{\rho/D}$		
			25.40	28.80	30.28
2		A_{11}	−0.81541	−0.77842	−0.77340
		A_{12}	1.00000	1.00000	1.00000
		A_{21}	3.1448	1.11722	.40809
		A_{22}	−1.25112	−.50815	−.19731
		A_{31}	.05200	.01065	.00320
		A_{32}	.01845	.00748	.00028

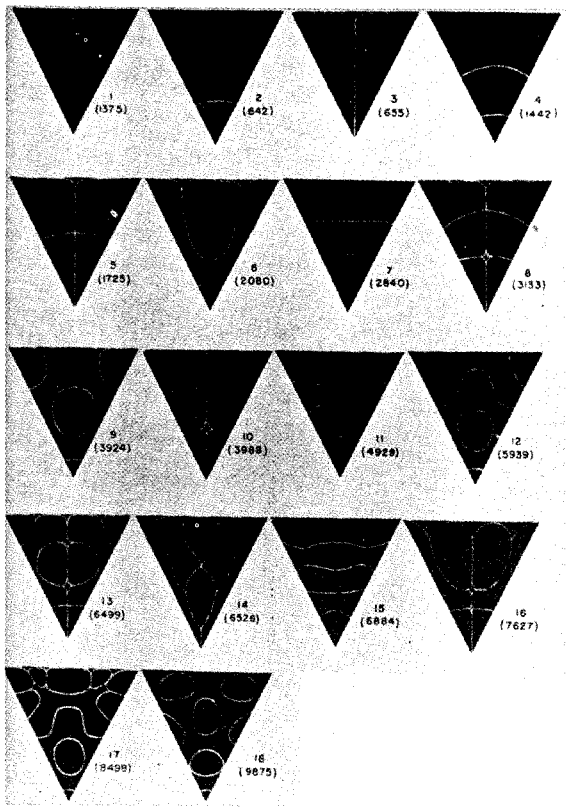


FIGURE 7.22.—Nodal patterns for a C–F–F symmetric triangular plate, $a/b=1$; material, steel. (From ref. 7.22)

Ritz method, using $\nu=1/4$. A summary of deflection functions used and the frequency parameters obtained is given in table 7.10. (See fig. 7.23.)

Gustafson, Stokey, and Zorowski (ref. 7.23) obtained experimental mode shapes and frequencies for the delta configurations shown in figure 7.24. The plates were cut from sheet steel averaging 0.061 inch in thickness. Observed nodal patterns and cyclic frequencies for the first six mode shapes of each plate are shown in figure 7.25, where the designations A1, A2, etc., refer to figure 7.24. Variation in cyclic frequency with b/a ratio for each mode is shown in figure 7.26.

Christensen (ref. 7.25) used the method of replacing plate elements by equivalent beam networks as developed by Hrennikoff (ref. 7.26) to analyze the delta plate when $\alpha=45°$. The 10 grid points shown in figure 7.27 were used. Each grid point is allowed rotation about axes parallel to the x- and y-axes and a w displacement, and a thirtieth-order characteristic determinant results. Frequency parameters and grid-point deflections associated with each of the first 10 vibration modes are given in table 7.11 for $\nu=0.3$. Experimental frequency parameters converted in reference 7.25 from reference 7.23 (discussed previously) and values obtained from reference 7.27 by using the Rayleigh-Ritz method and polynomials are also listed for comparison. The total mass of the plate is M. Nodal patterns compared with the experimental results of reference 7.23 are shown in figure 7.28.

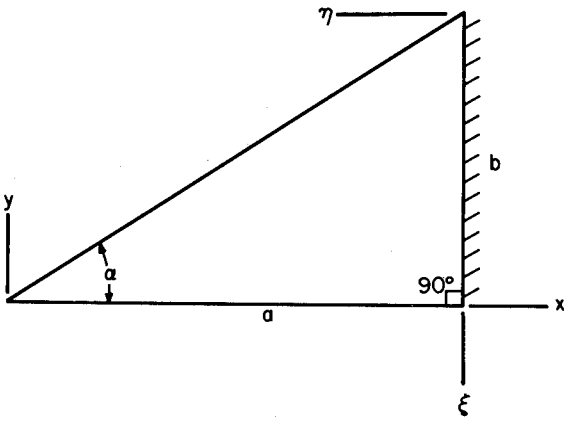


FIGURE 7.23.—C–F–F right triangular plate.

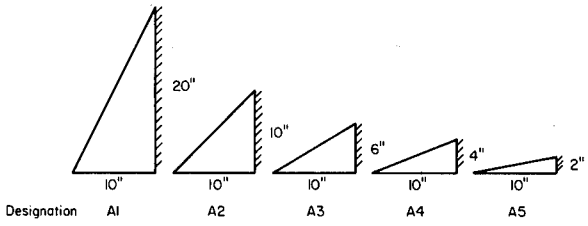


FIGURE 7.24.—C–F–F delta configurations. (After ref. 7.23)

TABLE 7.10.—*Deflection Functions and Frequency Parameters for a Rayleigh-Ritz Analysis of a C–F–F 45° Delta Triangular Plate; $\nu=1/4$*

Mode no.	Deflection function, $W(x,y)$	Amplitude coefficients	$\omega a^2\sqrt{\rho/D}$
1	$\left(\frac{x}{a}-1\right)^2\left(\frac{x}{a}+A_0\right)$	$A_0=5/3$	7. 15
	$\left(\frac{x}{a}-1\right)^2\left(\frac{3x}{a}+5\right)+A_1\left(\frac{x}{a}-1\right)^2\left(\frac{y}{a}-A_2\frac{x}{a}\right)^2$	$A_1=-3.88$ $A_2=-5/12$	6. 37
	$\left(\frac{\eta}{a}\right)^2\left(A_3+A_4\frac{\eta}{a}+A_5\frac{\eta^2}{a^2}\right)$	----------	7. 16
	$\left(\frac{\eta}{a}\right)^2\left(A_6\frac{\xi^2}{a^2}+A_7\frac{\xi}{a}+A_8\frac{\eta^2}{a^2}+A_9\frac{\eta}{a}+A_{10}\right)$	----------	6. 57
	$\left(\frac{\xi}{a}\right)^k\left(\frac{\eta}{a}\right)^l$	$k=1/3$ $l=7/4$	7. 05
2	$\left(\frac{\eta}{a}\right)^2\left(B_1\frac{\xi^2}{a^2}+B_2+B_3\frac{\eta}{a}\right)$	----------	28. 0
	$\left(\frac{\eta}{a}\right)^2\left(A_6\frac{\xi^2}{a^2}+A_7\frac{\xi}{a}+A_8\frac{\eta^2}{a^2}+A_9\frac{\eta}{a}+A_{10}\right)$	----------	26. 9
3	$\left(\frac{\eta}{a}\right)^2\left(B_1\frac{\xi^2}{a^2}+B_2+B_3\frac{\eta}{a}\right)$	----------	57. 5
	$\left(\frac{\eta}{a}\right)^2\left(A_6\frac{\xi^2}{a^2}+A_7\frac{\xi}{a}+A_8\frac{\eta^2}{a^2}+A_9\frac{\eta}{a}+A_{10}\right)$	----------	54. 3

TABLE 7.11.—*Frequency Parameters* $\omega a\sqrt{M/D}$ (M, *Total Mass of Plate*) *and Mode Shapes for a C–F–F 45° Delta Triangular Plate; $\nu=0.3$*

Mode	1	2	3	4	5	6	7	8	9	10
$\omega a\sqrt{M/D}$ from ref. 7.25	4. 35	16. 76	23. 01	38. 90	53. 65	60. 32	78. 26	90. 92	107. 1	148. 6
$\omega a\sqrt{M/D}$ from ref. 7.23	4. 17	16. 4	23. 0	39. 3	53. 3	69. 9	--------	--------	--------	--------
$\omega a\sqrt{M/D}$ from ref. 7.27	4. 42	16. 9	23. 7	43. 5	--------	--------	--------	--------	--------	--------
Grid point deflection amplitude ratios for point—										
1	1	1	1	1	1	1	1	1	1	1
2	. 65	. 29	−. 27	. 07	−. 74	−1. 01	−1. 15	−1. 02	−1. 32	−1. 60
3	. 56	−. 94	. 45	−3. 62	−. 18	1. 39	1. 86	−1. 03	1. 64	3. 70
4	. 33	−. 05	−. 81	. 39	−. 06	. 04	1. 36	1. 10	2. 32	5. 08
5	. 28	−. 78	−. 07	−. 31	. 04	−. 002	−2. 08	1. 74	−1. 65	−6. 98
6	. 20	−1. 33	. 43	1. 88	. 03	−1. 99	4. 38	−. 37	−. 65	5. 54
7	. 10	−. 05	−. 47	. 44	. 55	. 90	3. 05	−1. 66	−1. 05	−5. 48
8	. 08	−. 32	−. 11	. 49	. 47	. 27	−3. 77	−. 70	−. 43	8. 62
9	. 06	−. 45	. 12	1. 24	−. 19	. 27	−1. 92	−1. 17	2. 76	−6. 00
10	. 02	−. 31	. 14	1. 78	−1. 28	2. 65	. 84	1. 18	−1. 99	2. 89

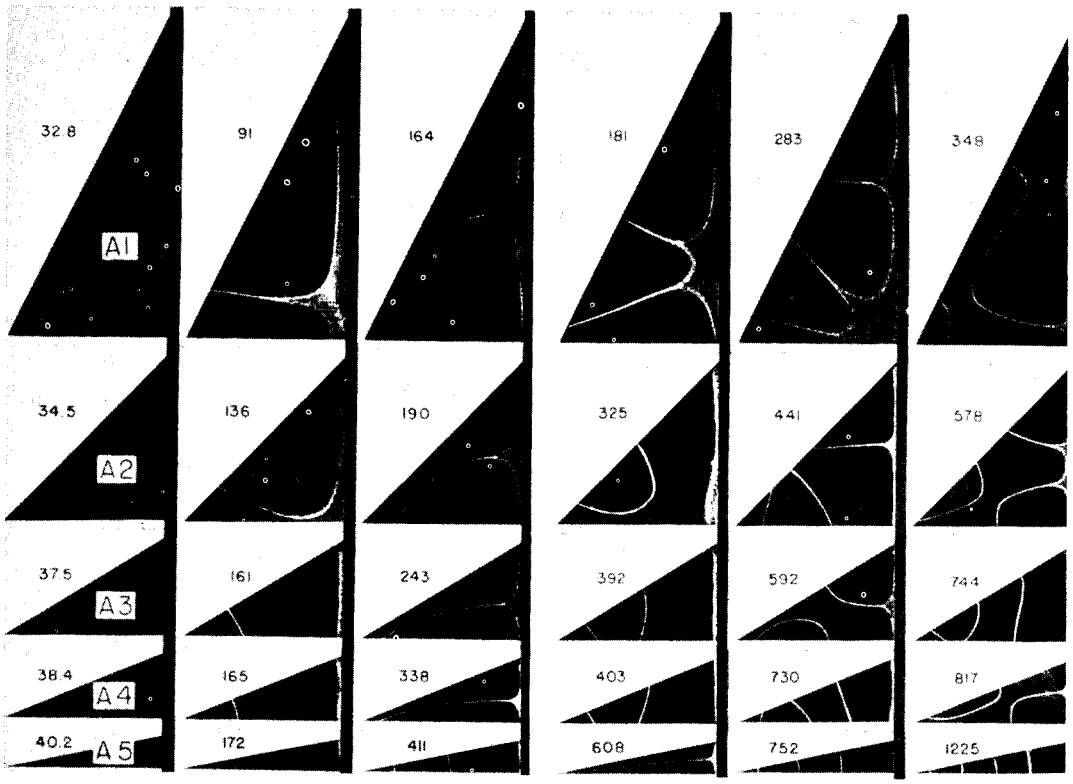


FIGURE 7.25.—Experimentally observed cyclic frequencies, cps, and nodal patterns for C–F–F delta triangular steel plates. (From ref. 7.23)

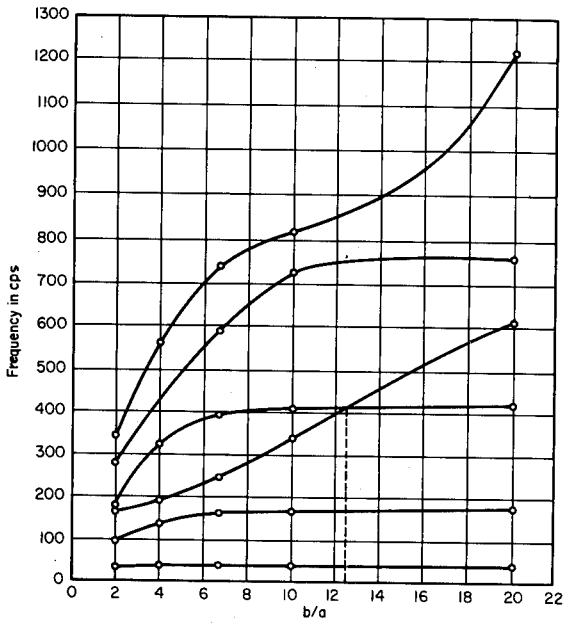


FIGURE 7.26.—Experimentally measured cyclic frequencies for C–F–F delta triangular steel plates. (After ref. 7.23)

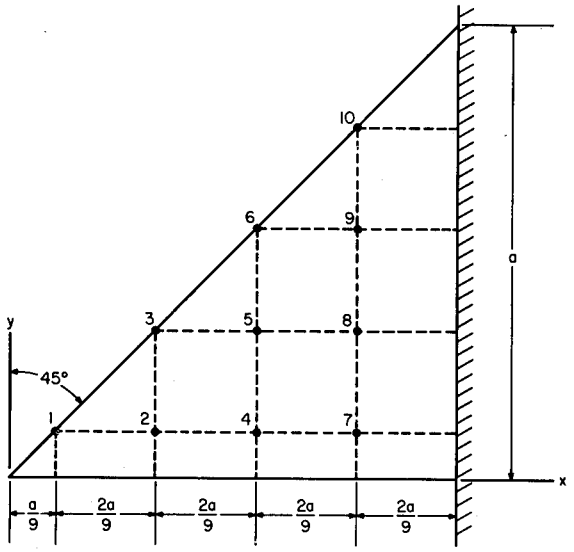


FIGURE 7.27.—Grid points in a structural element representation of a C–C–F triangular plate.

Kawashima (ref. 7.28) used the finite difference method to obtain frequencies and mode shapes for delta plates (fig. 7.23) having $b/a=1$ and 2. The 45° delta was analyzed by using both 6 and 10 free grid points on the plate, and the other, by using only 6 grid points. Cyclic frequencies were computed by using the dimensions of the plates in reference 7.23 for comparison. Available results are given in table 7.12. Grid points used for the more accurate analysis of the 45° delta are shown in figure 7.29, wherein deflections for the first two mode shapes are presented. At each grid point, including those along the clamped boundary, two numbers are listed. The first gives the deflection amplitude at each point normalized with respect to the tip deflection. The second is the bending moment M_x relative to the value at a point along the clamped boundary near the skew edge. Corresponding results for the case $b/a=2$ are also given in reference 7.28, but are considerably inaccurate.

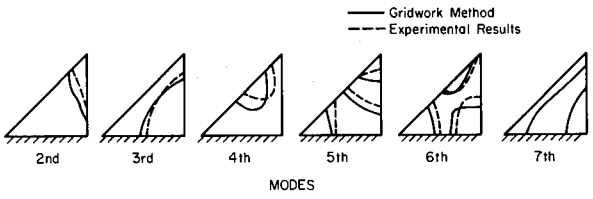


FIGURE 7.28.—Nodal patterns for a C–F–F 45° delta triangular plate; material, steel. (After ref. 7.25)

TABLE 7.12.—*Theoretical Cyclic Frequencies for C–C–F Delta Triangular Steel Plates*

Mode	Cyclic frequencies for values of b/a of—		
	1		2 (6 grid points)
	6 grid points	10 grid points	
1	40. 0	35. 0	35. 5
2	115. 5	136. 7	82. 7
3	155. 8	161. 9	161. 0
4	221. 0	301. 3	----------
5	266. 0	364. 0	----------

The delta plate for the cases $b/a=1$ and 2 was also analyzed by Walton (ref. 7.29) by using the method of reference 7.30 which replaces the derivatives in the strain energy integral by finite differences. Twenty-eight free grid points were used in the analysis. Frequencies were computed and compared with experimental data for sheet steel plates having the dimensions $a=10$ inches, $b=10$ inches and $a=10$ inches, and $b=20$ inches. Both plates were 0.061 inch thick and ν and E were taken as 0.025 and 30×10^6 psi, respectively. The first six cyclic frequencies for each plate are given in table 7.13. Nodal patterns for the five higher modes of each plate are depicted in figures 7.30 and 7.31.

Hanson and Tuovila (ref. 7.31) experimen-

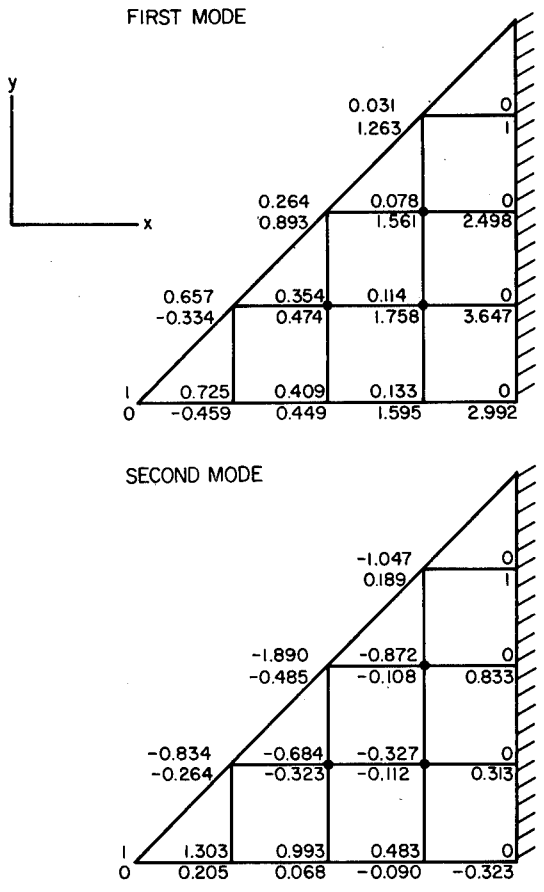


FIGURE 7.29.—Deflections and bending moments M_x for a C–F–F 45° delta triangular steel plate.

tally investigated 45° and 60° delta plates made of 0.034-inch-thick magnesium (ρg= 0.064 lb/in.^{3}). (See discussion of the C–F–F–F parallelogram plate, sec. 5.1.5.) They investigated plates with α=45°, b=6.00 inches, and α=60°, b=8.50 inches. The first three frequencies and mode shapes for the two plates are shown in figures 7.32 and 7.33. Note that the three-dimensional perspective used in these figures distorts the right angle at the clamped edge.

Craig, Plass, and Caughfield (refs. 7.32 and 7.33) measured mode shapes and frequencies on three 6061–T6 aluminum plates ⅛ inch thick and having the dimensions a=7.5 inches, b=7.5 inches; a=12.5 inches, b=7.5 inches; and a=15 inches, b=7.5 inches. Cyclic frequencies, nodal patterns, and mode shapes are given in figures 7.34, 7.35, and 7.36.

TABLE 7.13.—*Cyclic Frequencies for C–F–F Delta Triangular Steel Plates*

$\frac{b}{a}$	Mode	Cyclic frequency, f, cps		$\left(\frac{\text{Computed } f}{\text{Measured } f}\right)$
		Theoretical	Experimental	
1	1	36.4	34.5	1.06
	2	139	136	1.02
	3	192	190	1.01
	4	327	325	1.01
	5	432	441	.980
	6	566	578	.979
2	1	32.8	32.8	1.00
	2	89.9	91.0	.988
	3	164	164	1.00
	4	175	181	.967
	5	263	283	.929
	6	328	348	.943

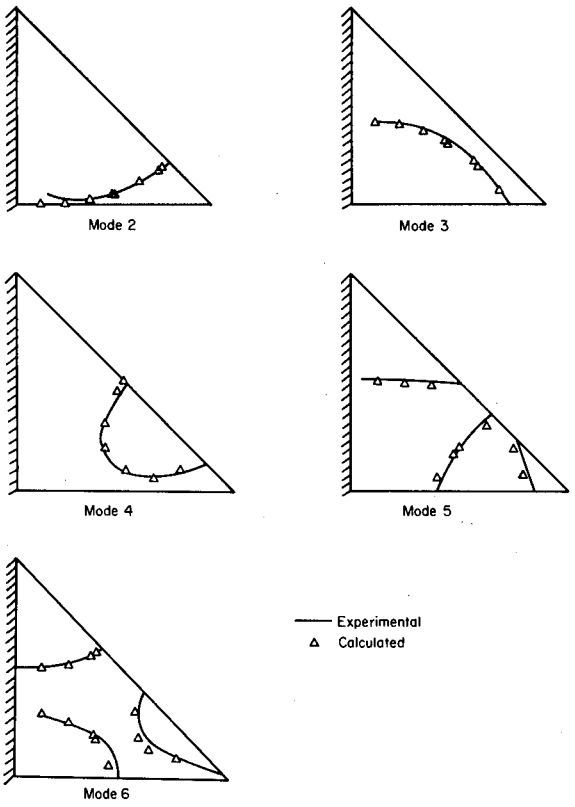


FIGURE 7.30.—Nodal patterns for a C–F–F delta triangular steel plate, b/a=1.

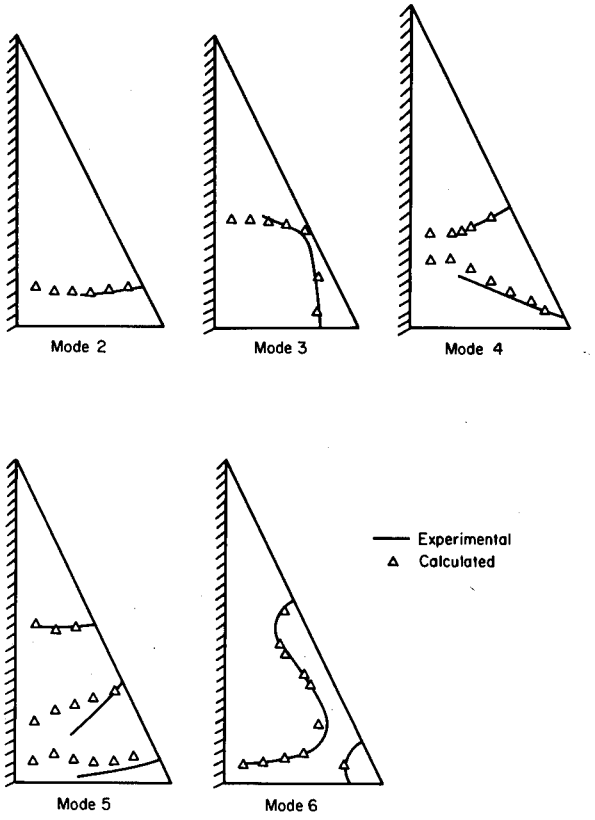
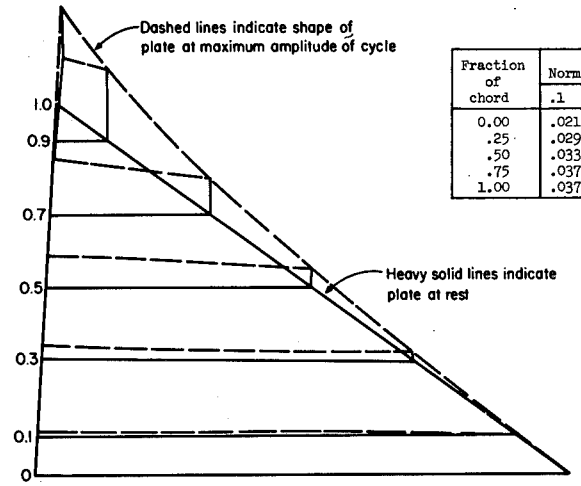
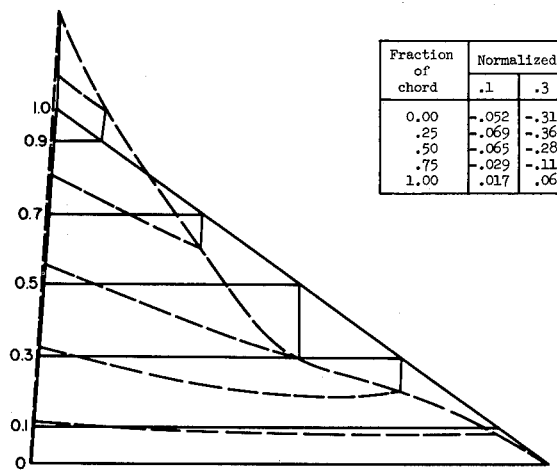


FIGURE 7.31.—Nodal patterns for a C–F–F delta triangular steel plate, b/a=2.



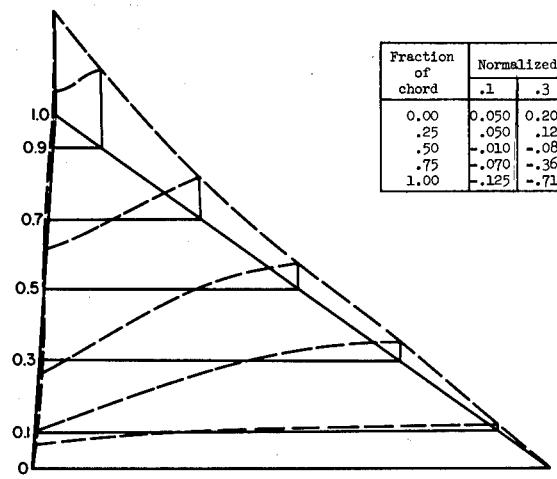
Fraction of chord	Normalized deflection at (1-x/a) =					
	.1	.3	.5	.7	.9	1.0
0.00	.021	.087	.186	.357	.702	1.0
.25	.029	.107	.214	.400	.742	1.0
.50	.033	.121	.247	.453	.771	1.0
.75	.037	.133	.278	.507	.796	1.0
1.00	.037	.146	.297	.528	.820	1.0

(a)



Fraction of chord	Normalized deflection at (1-x/a) =					
	.1	.3	.5	.7	.9	1.0
0.00	-.052	-.319	-.729	-.350	.325	1.0
.25	-.069	-.365	-.514	-.173	.410	1.0
.50	-.065	-.285	-.296	.020	.490	1.0
.75	-.029	-.115	-.052	.221	.580	1.0
1.00	.017	.069	.183	.420	.681	1.0

(b)

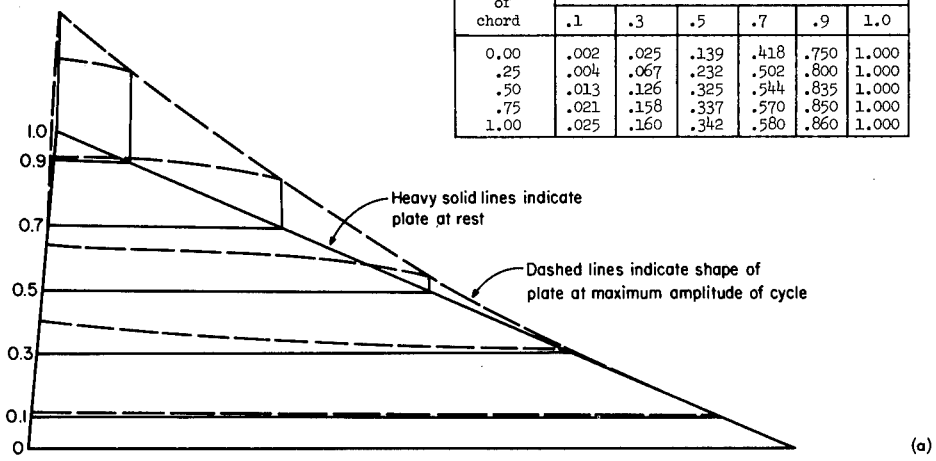


Fraction of chord	Normalized deflection at (1-x/a) =					
	.1	.3	.5	.7	.9	1.0
0.00	0.050	0.200	0.270	0.420	0.760	1.0
.25	.050	.125	.130	.270	.730	1.0
.50	-.010	-.087	-.125	.075	.670	1.0
.75	-.070	-.360	-.485	-.140	.600	1.0
1.00	-.125	-.710	-.830	-.305	.575	1.0

(c)

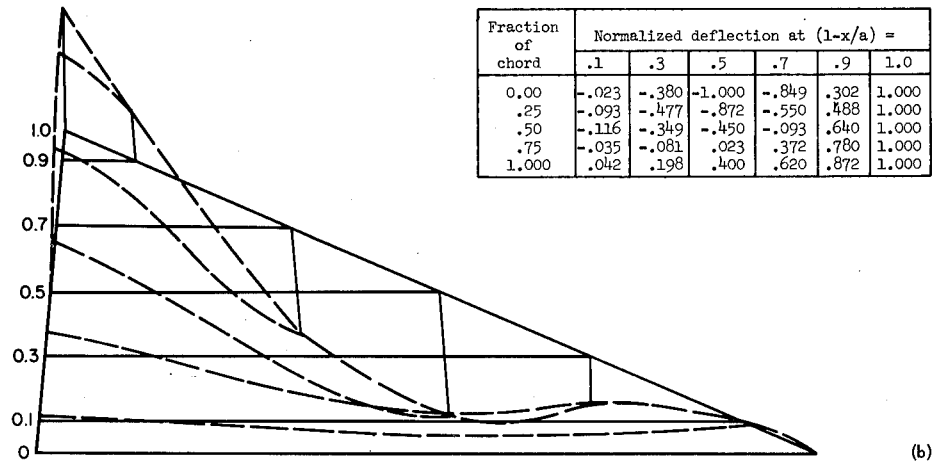
FIGURE 7.32.—Experimental frequencies and mode shapes for a 60° delta cantilever plate; material, magnesium. (*a*) Mode 1, $f_1=50$ cps. (*b*) Mode 2, $f_2=184$ cps. (*c*) Mode 3, $f_3=258$ cps.

Fraction of chord	Normalized deflection at (1-x/a) =					
	.1	.3	.5	.7	.9	1.0
0.00	.002	.025	.139	.418	.750	1.000
.25	.004	.067	.232	.502	.800	1.000
.50	.013	.126	.325	.544	.835	1.000
.75	.021	.158	.337	.570	.850	1.000
1.00	.025	.160	.342	.580	.860	1.000



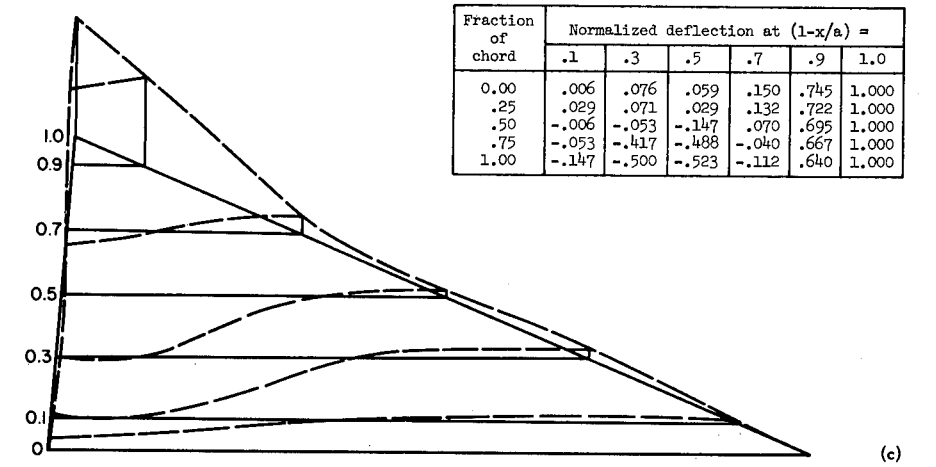
(a)

Fraction of chord	Normalized deflection at (1-x/a) =					
	.1	.3	.5	.7	.9	1.0
0.00	-.023	-.380	-1.000	-.849	.302	1.000
.25	-.093	-.477	-.872	-.550	.488	1.000
.50	-.116	-.349	-.450	-.093	.640	1.000
.75	-.035	-.081	.023	.372	.780	1.000
1.000	.042	.198	.400	.620	.872	1.000



(b)

Fraction of chord	Normalized deflection at (1-x/a) =					
	.1	.3	.5	.7	.9	1.0
0.00	.006	.076	.059	.150	.745	1.000
.25	.029	.071	.029	.132	.722	1.000
.50	-.006	-.053	-.147	.070	.695	1.000
.75	-.053	-.417	-.488	-.040	.667	1.000
1.00	-.147	-.500	-.523	-.112	.640	1.000



(c)

FIGURE 7.33.—Experimental frequencies and mode shapes for a 45° delta cantilever plate; material, magnesium. (*a*) Mode 1, $f_1 = 66$ cps. (*b*) Mode 2, $f_2 = 185$ cps. (*c*) Mode 3, $f_3 = 336$ cps.

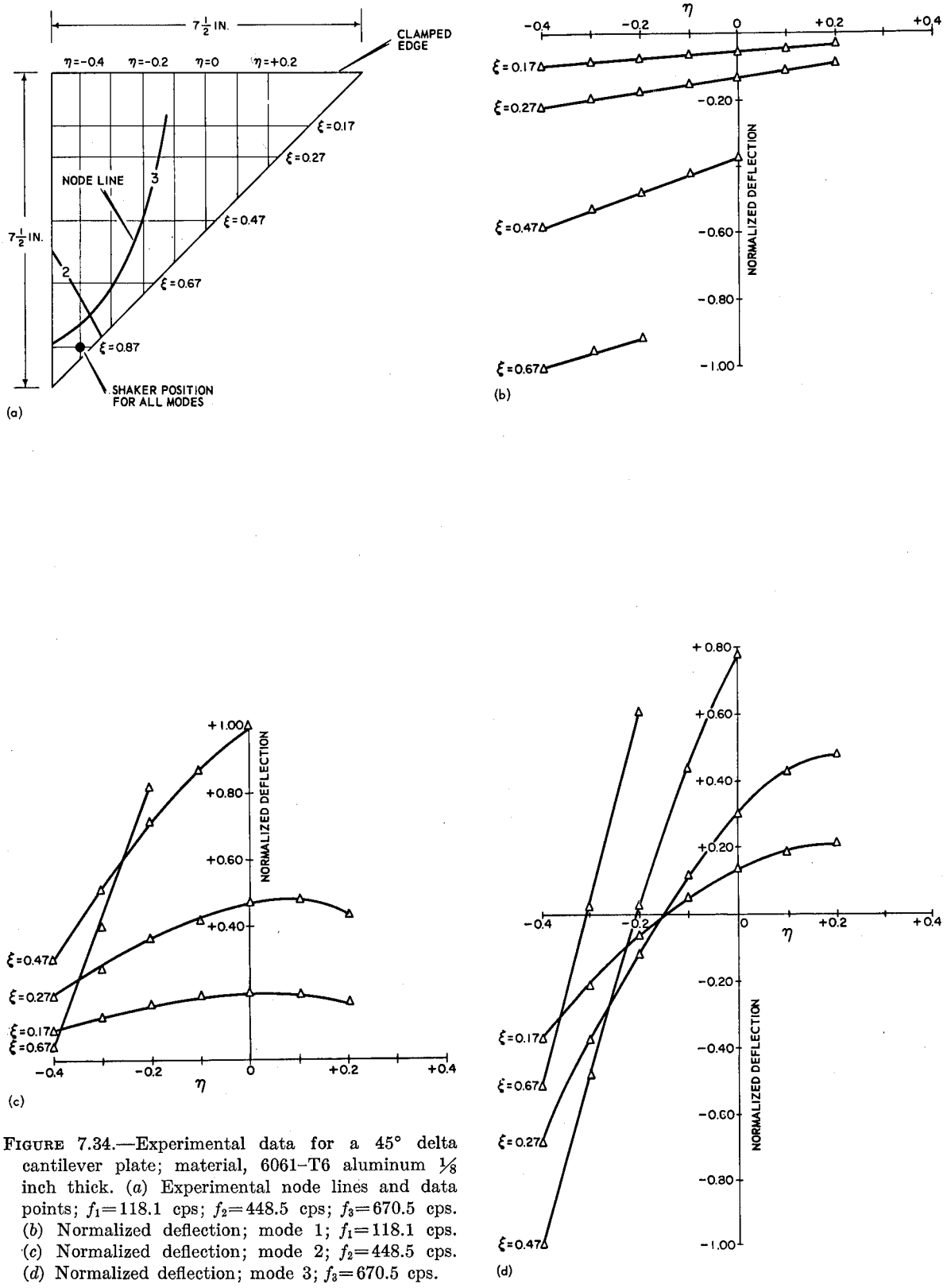


FIGURE 7.34.—Experimental data for a 45° delta cantilever plate; material, 6061–T6 aluminum ⅛ inch thick. (*a*) Experimental node lines and data points; $f_1=118.1$ cps; $f_2=448.5$ cps; $f_3=670.5$ cps. (*b*) Normalized deflection; mode 1; $f_1=118.1$ cps. (*c*) Normalized deflection; mode 2; $f_2=448.5$ cps. (*d*) Normalized deflection; mode 3; $f_3=670.5$ cps.

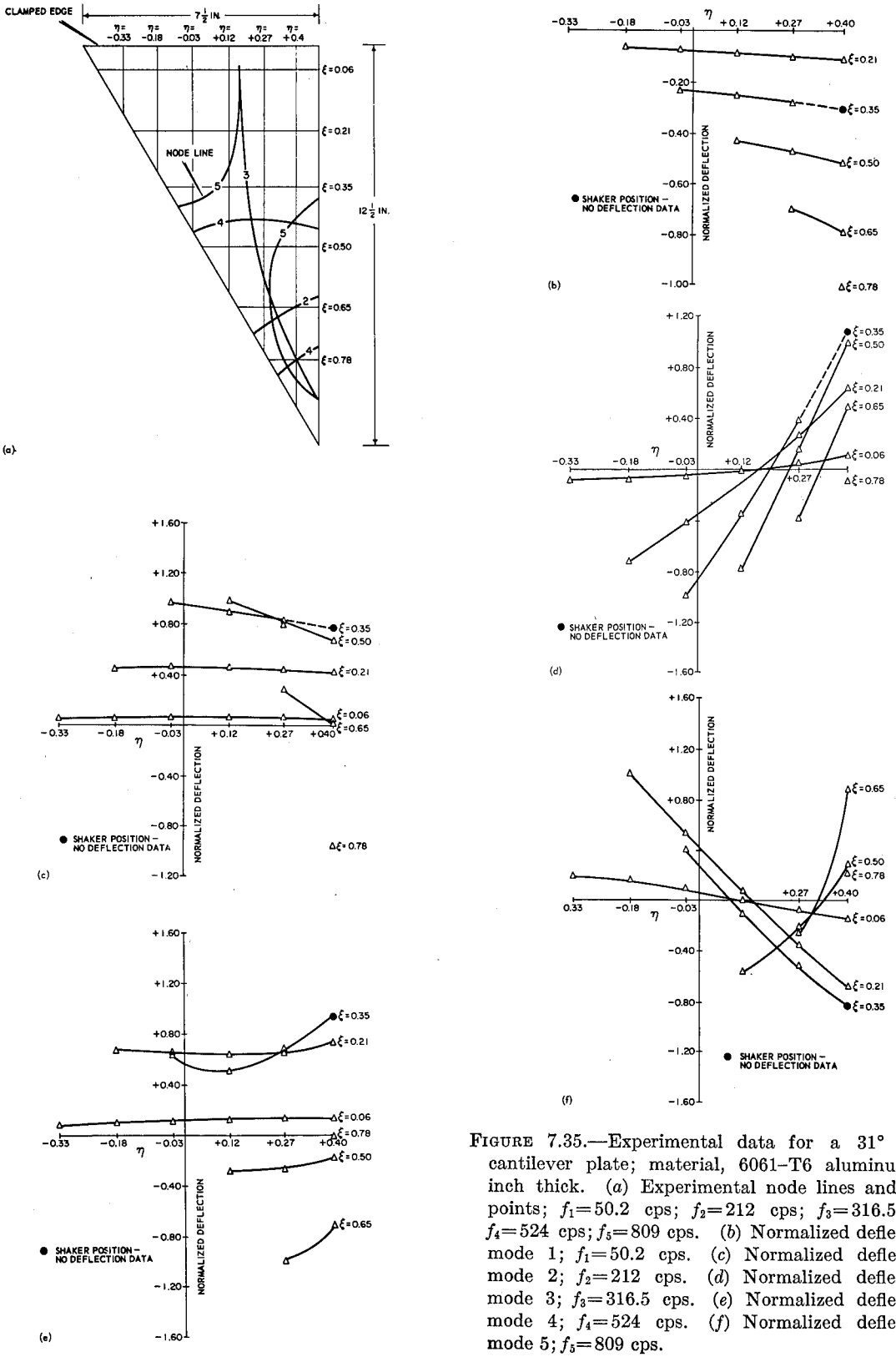


FIGURE 7.35.—Experimental data for a 31° delta cantilever plate; material, 6061–T6 aluminum ⅛ inch thick. (*a*) Experimental node lines and data points; $f_1=50.2$ cps; $f_2=212$ cps; $f_3=316.5$ cps; $f_4=524$ cps; $f_5=809$ cps. (*b*) Normalized deflection; mode 1; $f_1=50.2$ cps. (*c*) Normalized deflection; mode 2; $f_2=212$ cps. (*d*) Normalized deflection; mode 3; $f_3=316.5$ cps. (*e*) Normalized deflection; mode 4; $f_4=524$ cps. (*f*) Normalized deflection; mode 5; $f_5=809$ cps.

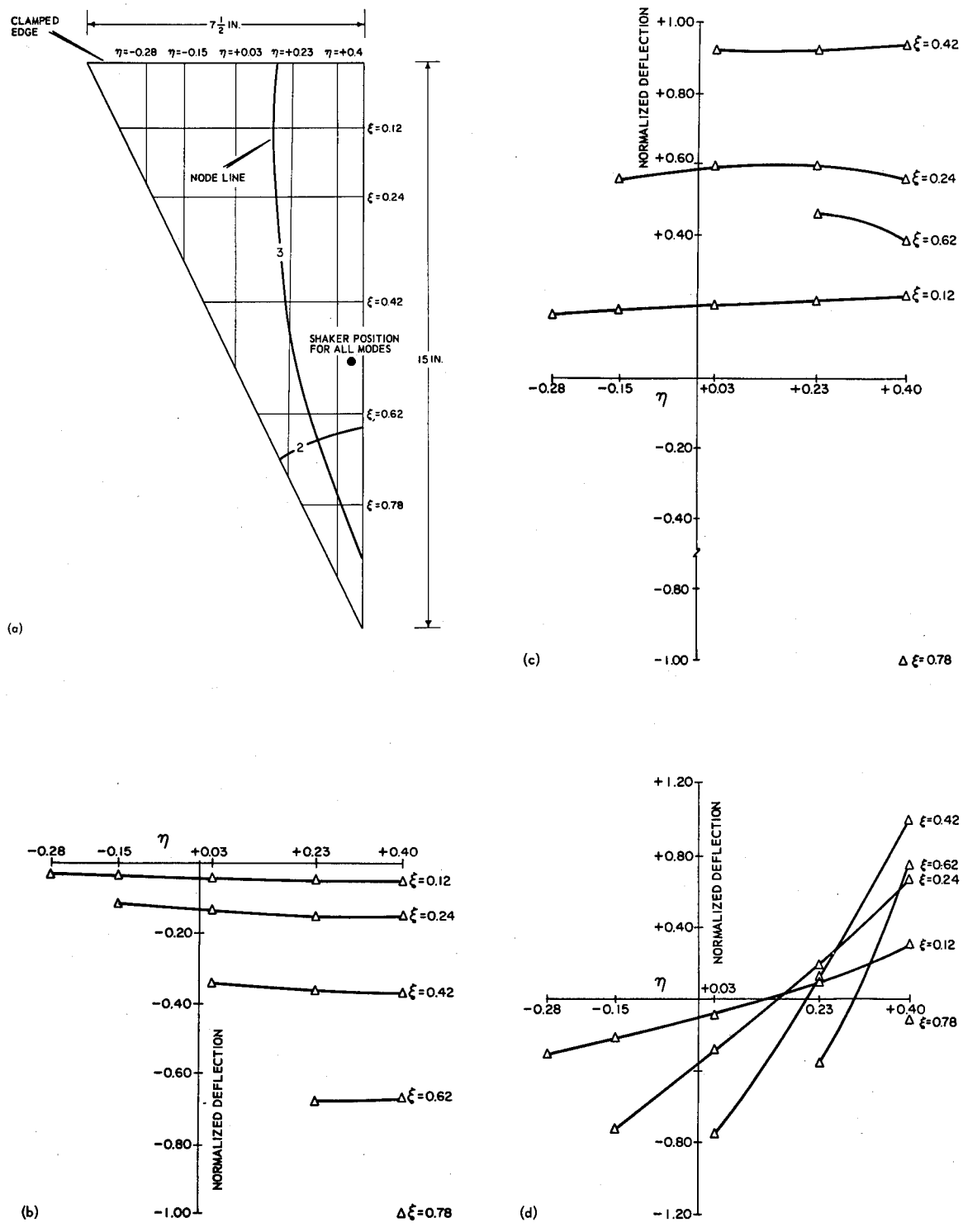


FIGURE 7.36.—Experimental data for a 26.6° delta cantilever plate; material, 6061–T6 aluminum ¼ inch thick. (*a*) Experimental node lines and data points; $f_1=71.2$ cps; $f_2=300$ cps; $f_3=508$ cps. (*b*) Normalized deflection; mode 1; $f_1=71.2$ cps. (*c*) Normalized deflection; mode 2; $f_2=300$ cps. (*d*) Normalized deflection; mode 3; $f_3=508$ cps.

Consider finally the triangular cantilever plate of general shape as shown in figure 7.37. In reference 7.29 this problem was also (see discussion earlier in this subsection) solved analytically for a sheet steel plate having dimensions $a=10$ inches, $b=10$ inches, $\beta_2=116.6°$, and $h=0.061$ inch. Material constants were taken as $\nu=0.250$ and $E=30\times10^6$ psi. Thirty-one grid points were used in the analysis. Theoretical frequencies are compared with experimental ones in table 7.14. Nodal patterns for the five higher modes are depicted in figure 7.38.

Frequencies and nodal patterns were found experimentally in reference 7.23 for sheet steel plates having $a=10.0$ inches, $b=10.0$ inches, $h=0.061$ inch, and $\beta_2=63.4°$, 78.7°, 90°, 101.3°, and 126.6°. Results for the first six modes are shown in figure 7.39.

Klein (ref. 7.34) proposed a set of empirical formulas for the prediction of frequencies of the first three bending modes and the first torsional mode for arbitrarily shaped triangles. These formulas are given in table 7.15.

The planform dimensions used on both sides of the formulas in table 7.15 are those of figure 7.40. Substantiation of the formulas of table 7.15 was given in reference 7.34 by comparison with the experimental results of reference 7.23. These data are reproduced in table 7.16. The plate designations used are those shown in figures 7.25 and 7.39.

The vibration of C–F–F triangular plates is also discussed in references 7.35 and 7.36.

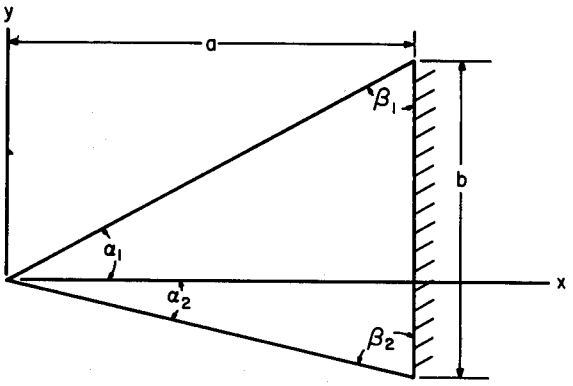


FIGURE 7.37.—C–F–F triangular plate of general shape.

TABLE 7.14.—*Cyclic Frequencies for a C–F–F Triangular Steel Plate; $\nu=0.25$*

Mode	Cyclic frequency, cps		
	Theoretical	Experimental	Theoretical / Experimental
1	27.6	26.3	1.05
2	107	101	1.06
3	173	171	1.01
4	262	259	1.01
5	352	346	1.02
6	480	522	.92

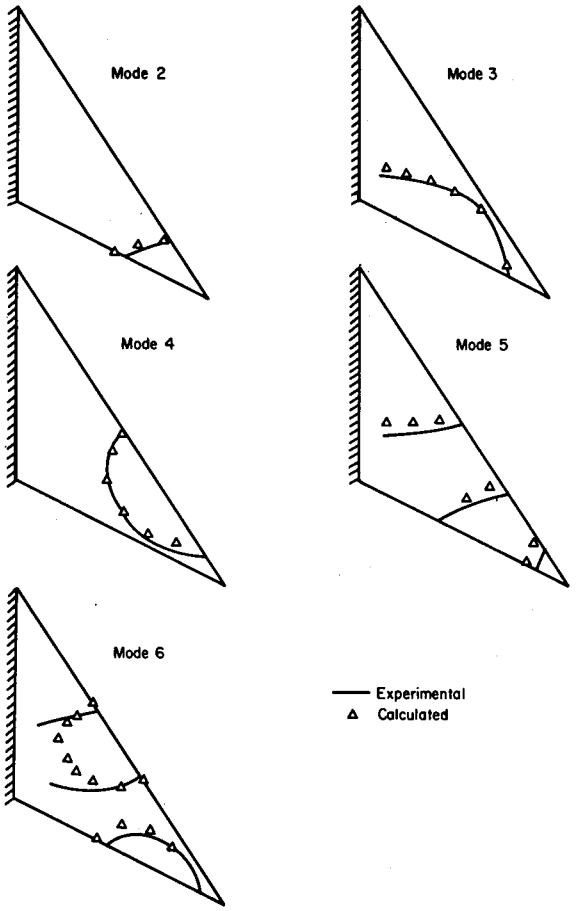


FIGURE 7.38.—Nodal patterns for a C–F–F triangular steel plate.

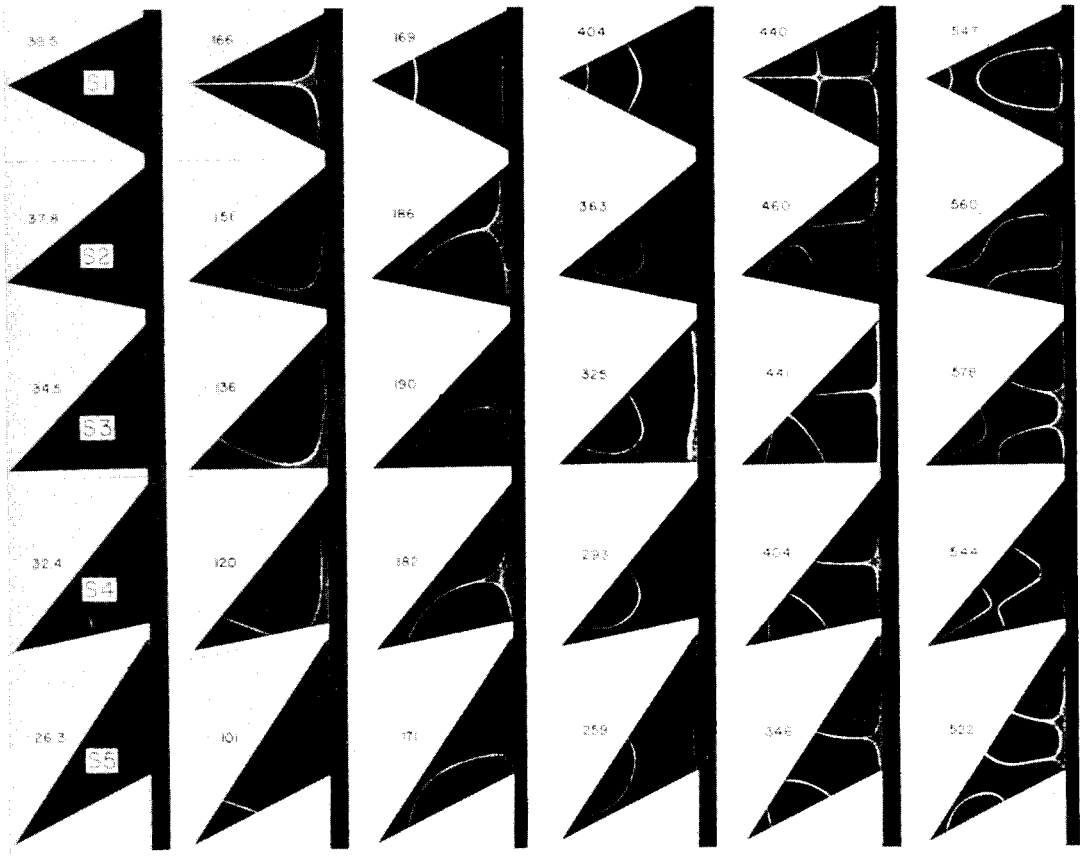


FIGURE 7.39.—Experimentally observed cyclic frequencies, cps, and nodal patterns for C–F–F triangular steel plates. (From ref. 7.23)

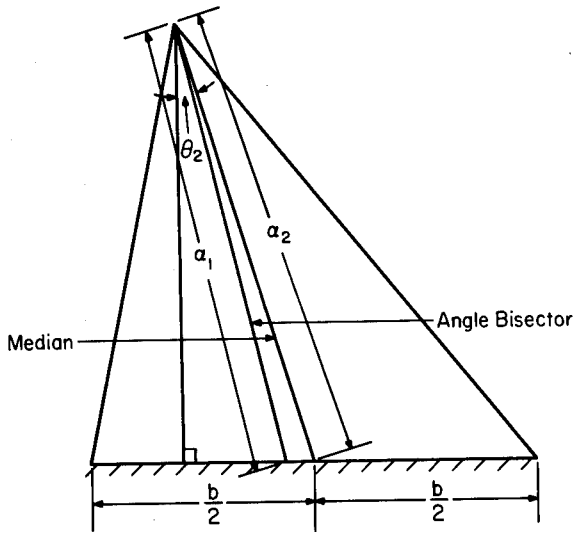


FIGURE 7.40.—Planform dimensions of a C–F–F triangular plate of arbitrary shape. (After ref. 7.34)

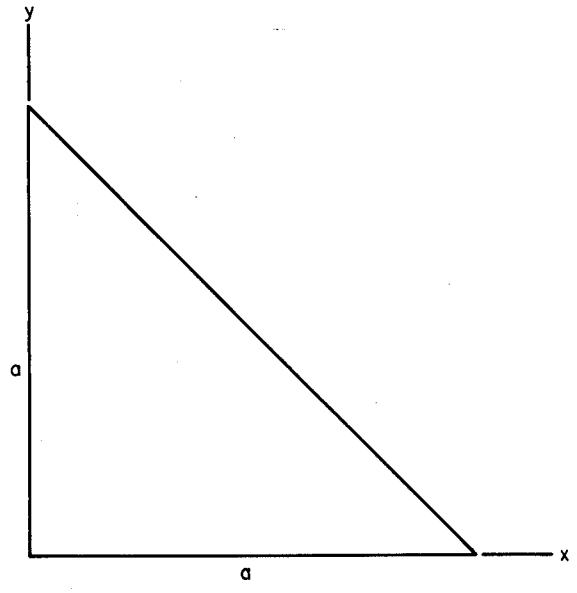


FIGURE 7.41.—F–F–F 45° right triangular plate.

TABLE 7.15.—*Empirical Formulas for Calculating the Frequencies of C–F–F Triangular Plates of Arbitrary Shape*

Mode	Frequency formula
1st bending	$\omega a_1^2\sqrt{\rho/D}=[7.14-(0.4b/a_1)]\sqrt{\sec\theta_2}$
2d bending	$\omega a_2^2\sqrt{\rho/D}=[31-(2b/a_1)-2\sqrt{\sec\theta_2-1}]\sqrt{\sec\theta_2}$
3d bending	$\omega a_2^2\sqrt{\rho/D}=[73-4(b/a_1)^2]\{1+[\sin\theta_2-(b/2a_2)]\sqrt{\sec\theta_2-1}\}$
1st torsion	$\omega a_1^2\sqrt{\rho/D}=\{20[1+0.2(b/a_2)^2]^2+30(b/a_2)\sqrt{\sec\theta_2-1}\}(a_1/b)$

TABLE 7.16.—*Cyclic Frequencies Computed From Empirical Formulas Compared With Test Results for C–F–F Triangular Plates; Material: Steel*

Plate	Frequency, cps, computed from—							
	Bending type modes						Torsional mode	
	f_1		f_2		f_3			
	Formula	Test	Formula	Test	Formula	Test	Formula	Test
A1	32.5	32.8	92	91	179	181	164	164
A2	35.3	34.5	140	136	325	325	192	190
A3	38.3	37.5	160	161	386	392	245	243
A4	39.6	38.4	168	165	401	403	330	338
A5	40.6	40.2	173	172	414	411	598	608
S1	39.1	38.5	168	169	400	404	167	166
S2	37.8	37.8	156	151	365	363	194	186
S3	35.3	34.5	140	136	325	325	192	190
S4	31.6	32.4	121	120	293	293	179	182
S5	26.6	26.3	98	101	255	259	166	171

7.1.9 F–F–F

Waller (ref. 7.37) experimentally investigated completely free 45° right triangular plates. The modes were classified as m/n according to the corresponding products of beam functions, namely,

$$W(x, y)=A_{mn}X_m(x)Y_n(y)\pm B_{mn}X_n(x)Y_m(y) \tag{7.13}$$

where x and y are as shown in figure 7.41 and the beam functions apply to beams of length a. Cyclic frequencies were obtained for a brass plate having dimensions $a=8.86$ inches and $h=0.102$ inch and are given in table 7.17 along with frequency ratios relative to the fundamental frequency. Corresponding nodal patterns are shown in figure 7.42. Nodal patterns for some higher nodes are shown in figure 7.43.

Some nodal patterns obtained for free equilateral triangular plates (ref. 7.38) are depicted in figure 7.44.

7.2 OTHER SUPPORTS AND CONDITIONS

The problem of a simply supported 30°–60°–90° triangular plate with an internal point

support at ξ, η (see fig. 7.45) was studied by Solecki (ref. 7.10). Frequency parameters for the first three modes and for various locations of the point support are given in table 7.18.

The isosceles right triangular plate with all edges free and having hub-pin supports (see fig. 7.46) was investigated experimentally by Craig, Plass, and Caughfield (refs. 7.32 and 7.33). Pertinent dimensions, cyclic frequencies, and the nodal patterns of the first four modes of vibration are shown in figure 7.46. Corresponding mode shapes are plotted in figure 7.47.

TABLE 7.17.—*Cyclic and Relative Frequencies for a F–F–F 45° Right Triangular Brass Plate*

[Relative frequency ratios are in parentheses]

m	Cyclic frequency, cps, for values of n of—			
	0	1	2	3
2	162 (1)	227 (1. 4)	380 (2. 36)	----------
3	414 (2. 56)	590 (3. 65)	710 (4. 39)	1090 (6. 8)
4	862 (5. 32)	1078 (6. 62)	1350 (8. 36)	1690 (10. 4)
5	1380 (8. 54)	1670 (10. 3)	2000 (12. 4)	2490 (15. 4)

TABLE 7.18.—*Frequency Parameters $\omega b^2\sqrt{\rho/D}$ for a SS–SS–SS 30°–60°–90° Triangular Plate With an Interior Point Support*

$\frac{\xi}{a}$	$\frac{\eta}{b}$	$\omega b^2\sqrt{\rho/D}$ for mode—		
		1	2	3
0. 10	0. 50	97. 91	205. 29	258. 19
. 20	. 50	99. 88	216. 34	261. 35
. 25	. 50	101. 06	219. 50	263. 32
. 30	. 50	101. 85	220. 29	264. 51
. 40	. 50	101. 85	189. 10	259. 77
. 50	. 167	129. 88	216. 34	276. 35
. 50	. 250	152. 39	206. 08	249. 90
. 50	. 333	140. 15	175. 28	250. 29
. 250	. 250	170. 55	170. 94	276. 35
. 333	. 333	147. 25	233. 71	264. 11

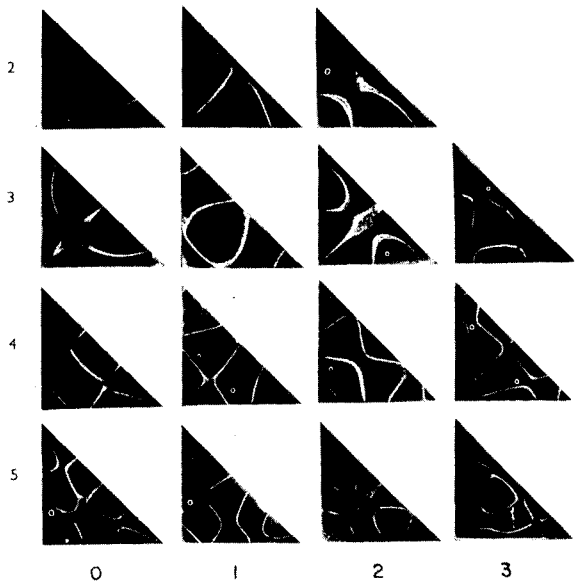


FIGURE 7.42.—Nodal patterns for a F–F–F 45° right triangular plate; material, brass. (From ref. 7.37)

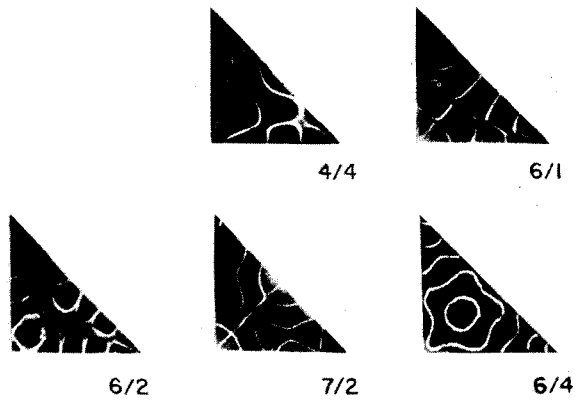


FIGURE 7.43.—Nodal patterns for some higher modes of a F–F–F 45° right triangular plate; material, brass. (From ref. 7.37)

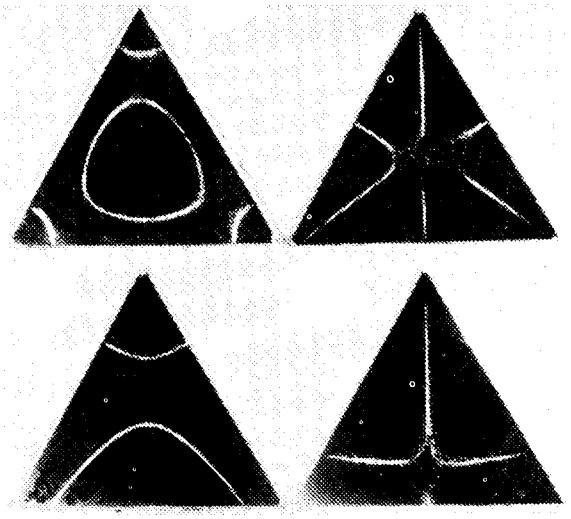


FIGURE 7.44.—Nodal patterns for a F–F–F equilateral triangular plate; material, brass. (From ref. 7.38)

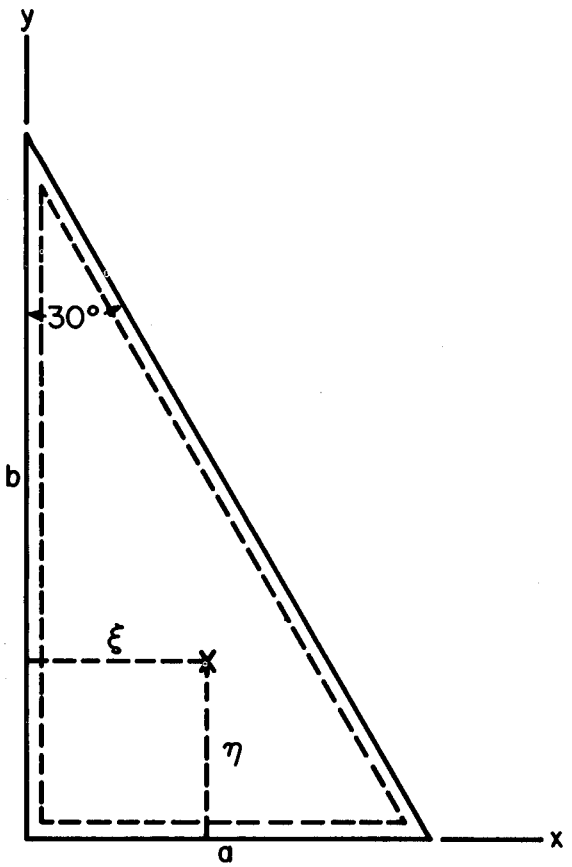


FIGURE 7.45.—SS–SS–SS 30°–60°–90° triangular plate with internal point support.

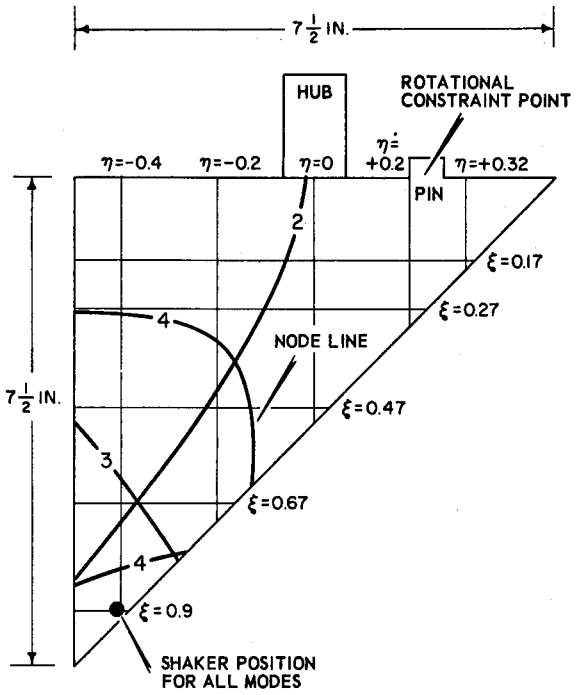


FIGURE 7.46.—Cyclic frequencies and nodal patterns for an isosceles right triangular plate with hub-pin supports; material, 6061–T6 aluminum ⅛ inch thick. $f_1=76.9$ cps; $f_2=297$ cps; $f_3=390$ cps; $f_4=841$ cps.

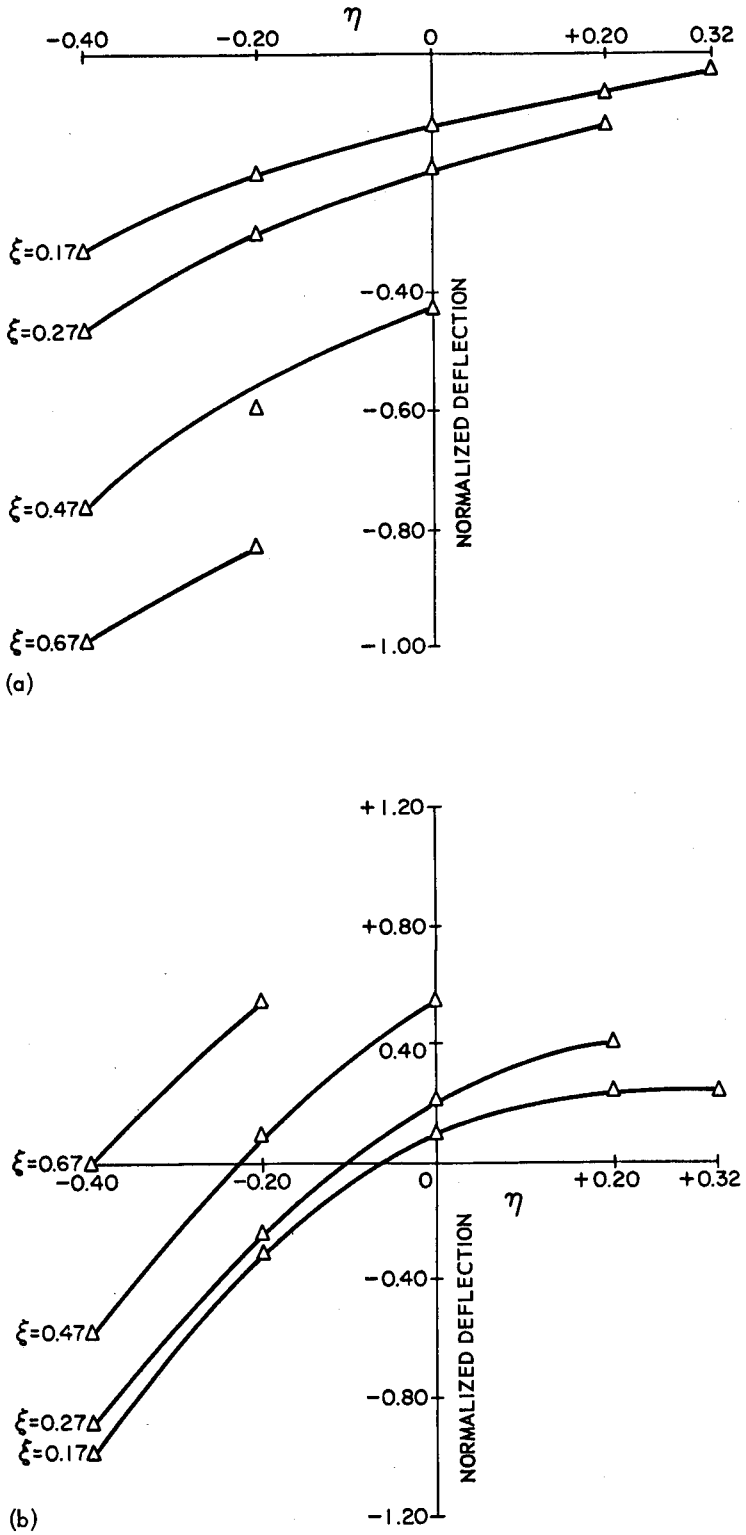
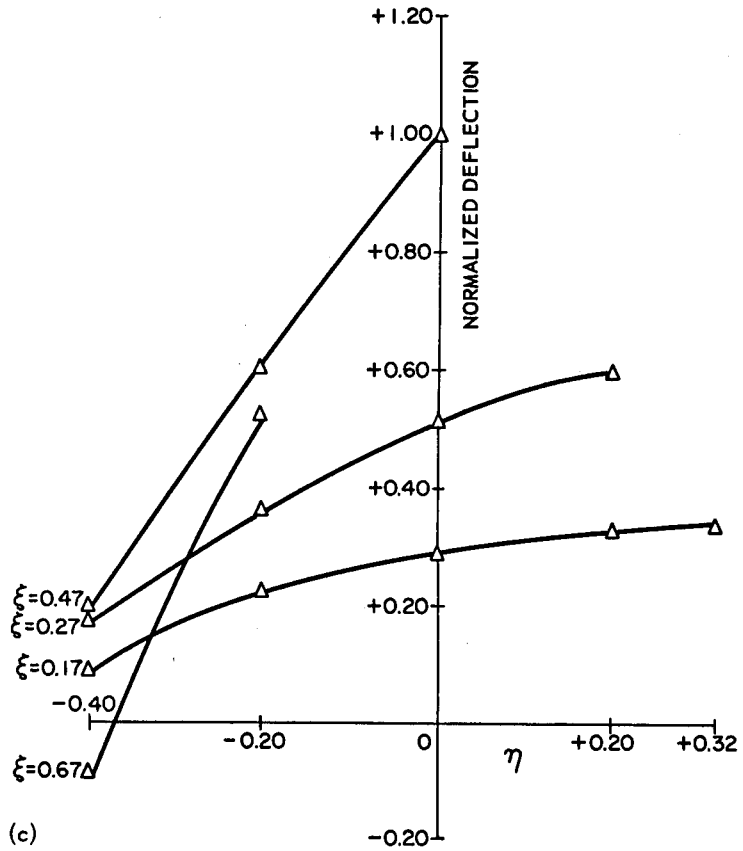
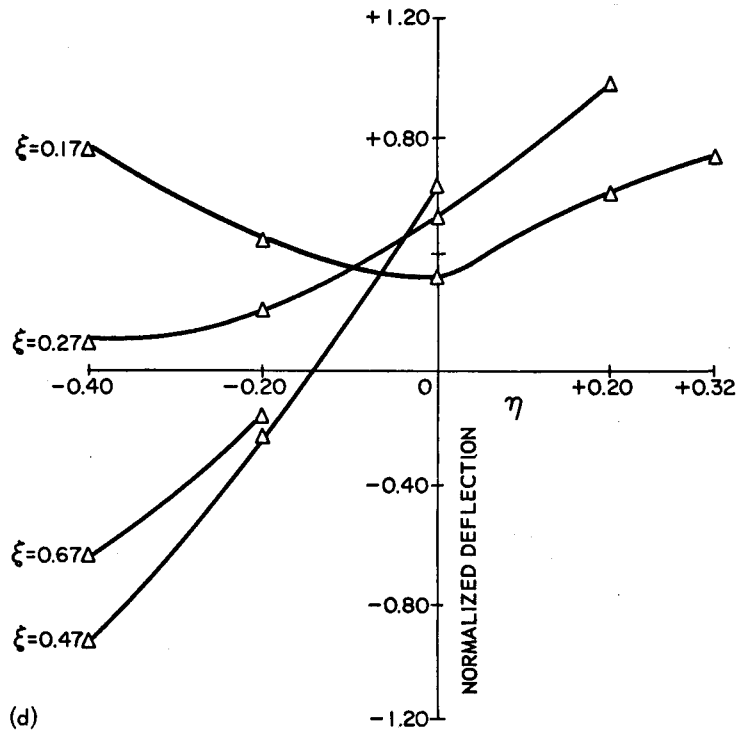


FIGURE 7.47.—Normalized deflections of a 45° triangular hub-pin plate; material, 6061–T6 aluminum. (*a*) Mode 1; $f_1=76.9$ cps. (*b*) Mode 2; $f_2=297$ cps. (*c*) Mode 3; $f_3=390$ cps. (*d*) Mode 4; $f_.=841$ cps.



(c)



(d)

308-337 O—70——16

REFERENCES

7.1. Cox, H. L.; and Klein, B.: Fundamental Frequencies of Clamped Triangular Plates. J. Acoust. Soc. Am., vol. 27, no. 2, Mar. 1955, pp. 266–268.

7.2. Cox, H.; and Klein, B.: Vibrations of Isosceles Triangular Plates. ZAMP, vol. 6, 1955, pp. 68–75.

7.3. Ota, T.; Hamada, M.; and Tarumoto, T.: Fundamental Frequency of an Isosceles-Triangular Plate. Bull. JSME, vol. 4, no. 15, Aug. 1961, pp. 478–481.

7.4. Hamada, M.: Compressive or Shearing Buckling Load and Fundamental Frequency of a Rhomboidal Plate With All Edges Clamped. Bull. JSME, vol. 2, no. 8, Nov. 1959, pp. 520–526.

7.5. Hersch, J.: Une Méthode pour l'Évaluation par Défaut de la Première Valeur Propre de la Vibration ou du Flambage des Plaques Encastrées. Bull. Acad. Sci. (Paris), Séance du 13 June, 1960, pp. 3943–3945.

7.6. Cox, H.; and Klein, B.: Buckling and Vibration of Isosceles Triangular Plates Having the Two Equal Edges Clamped and the Other Edge Simply-Supported. J. Roy. Aeron. Soc., vol. 59, no. 130, Feb. 1955, pp. 151–152.

7.7. Westmann, R. A.: A Note on Free Vibrations of Triangular and Sector Plates. J. Aerospace Sci., vol. 29, no. 9, Sept. 1962, pp. 1139–1140.

7.8. Cox, H.; and Klein, B.: Vibrations of Isosceles Triangular Plates Having the Base Clamped and Other Edges Simply-Supported. Aeron. Quart., vol. 7, no. 3, Aug. 1956, pp. 221–224.

7.9. Young, D.: Vibration of Rectangular Plates by the Ritz Method. J. Appl. Mech., vol. 17, no. 4, Dec. 1950, pp. 448–453.

7.10. Solecki, R.: Free and Forced Vibration of a Triangular Plate. Rozprawy Inzh. 142, vol. 8, no. 1, 1960, pp. 65–81. (In Polish.)

7.11. Conway, H. D.; and Farnham, K. A.: The Free Flexural Vibrations of Triangular, Rhombic and Parallelogram Plates and Some Analogies. Int. J. Mech. Sci., vol. 7, 1965, pp. 811–816.

7.12. Klein, B.: Fundamental Frequencies of Arbitrarily Shaped Simply-Supported Triangular Plates. J. Roy. Aeron. Soc., vol. 60, no. 541, Jan. 1956, pp. 63–64.

7.13. Pan, Lih-Chow: Equilibrium, Buckling and Vibration of a 30°–60°–90° Triangular Plate Simply Supported at Its Edges. Acta Phys. Sinica, vol. 3, no. 12, 1956, pp. 215–245. (In Chinese.)

7.14. Solecki, R.: The General Solution of a Triangular Plate 30°–60°–90° by Means of Eigentransform. Bull. Acad. Pol. Sci., Ser. Sci. Tech., vol. 8, no. 7, 1960, pp. 325–331. (In English.)

7.15. Schaefer, H.; and Havers, A.: Die Eigenschwingungen der in ihrer Ebene allseitig gleichmassig belasteten gleichseitigen Dreiecksplatte. Ingr.-Arch., Bd. 7, 1936, pp. 83–87.

7.16. Conway, H. D.: Analogies Between the Buckling and Vibration of Polygonal Plates and Membranes. Can. Aeron. J., vol. 6, no. 7, Sept. 1960, p. 263.

7.17. Seth, B. R.: Transverse Vibrations of Rectilinear Plates. Proc. Indian Acad. Sci., sec. A, vol. 25, Jan. 1947, pp. 25–29.

7.18. Sen, B.: Note on Some Two-Dimensional Problems of Elasticity Connected With Plates Having Triangular Boundaries. Bull. Calcutta Math. Soc., vol. 26, no. 2, 1934, pp. 65–72.

7.19. Andersen, B. W.: Ph. D. thesis, Univ. Illinois, 1953.

7.20. Andersen, B. W.: Vibration of Triangular Cantilever Plates by the Ritz Method. J. Appl. Mech., vol. 21, no. 4, Dec. 1954, pp. 365–376.

7.21. Duffin, R. J.; Gustafson, P. N.; and Warner, W. H.: Natural Vibrations of Cantilevered Triangular Plates, I. Rept. CIT–AF8–TR22, Carnegie Inst. Tech., Sept. 1952.

7.22. Kumaraswamy, M. P.; and Cadambe, V.: Experimental Study of the Vibration of Cantilevered Isosceles Triangular Plates. J. Sci. Ind. Res. (India), vol. 15B, no. 2, Feb. 1956, pp. 54–60.

7.23. Gustafson, P. N.; Stokey, W. F.; and Zorowski, C. F.: An Experimental Study of Natural Vibrations of Cantilevered Triangular Plates. J. Aeron. Sci., vol. 20, May 1953, pp. 331–337.

7.24. Nagaraja, J. V.; Kumaraswamy, M. P.; and Subramanian, N. R.: On the Vibration Frequencies of Skew Cantilever Triangular Plates. J. Sci. Ind. Res. (India), vol. 20B, no. 10, Oct. 1961, pp. 479–482.

7.25. Christensen, R. M.: Vibration of a 45° Right Triangular Cantilever Plate by a Gridwork Method. AIAA J., vol. 1, no. 8, Aug. 1963, pp. 1790–1795.

7.26. Hrennikoff, A.: Solution of Problems of Elasticity by the Framework Method. J. Appl. Mech., vol. 8, Dec. 1941, pp. A–169—A–175.

7.27. Lubkin, J. L.; and Luke, Y. L.: Modes and Frequencies of Wings of Triangular Planform. Rept. 56–335, Wright Air Develop. Center, June 1956, pp. 1–46.

7.28. Kawashima, S.: On the Vibration of Right Triangular Cantilever Plates. Mem. Fac. Eng., Kyushi Univ., vol. 18, no. 1, 1958, pp. 9–21.

7.29. Walton, W. C., Jr.: Applications of a General Finite-Difference Method for Calculating Bending Deformations of Solid Plates. NASA TN D–536, 1960.

7.30. HOUBOLT, J. C.: A Study of Several Aerothermoelastic Problems of Aircraft Structures in High Speed Flight. Ph.D. thesis, Zürich E.T.H., 1958.

7.31. HANSON, P. W.; AND TUOVILA, W.: Experimentally Determined Natural Vibration Modes of Some Cantilever Wing Flutter Models by Using an Acceleration Method. NACA TN 4010, 1957.

7.32. CRAIG, R. R.; PLASS, H. J., JR.; AND CAUGHfield, D. A.: Experimental Determination of Frequencies and Mode Shapes of Cantilever and Hub-Pin Plates. Def. Res. Lab. Rept. DRL–518, CR–13, Univ. Texas, June 1964.

7.33. CRAIG, R. R.; AND PLASS, H. J.: Vibration of Hub-Pin Plates. AIAA J., vol. 3, no. 6, June 1965, pp. 1177–1178.

7.34. KLEIN, B.: Natural Frequencies of Constant Thickness Cantilever Triangular Plates of Arbitrary Planform. J. Roy. Aeron. Soc., vol. 60, no. 544, Apr. 1956, pp. 281–282.

7.35. MARTIN, H. C.; AND GURSAHANY, H. J.: On the Deflection of Swept Cantilevered Surfaces. J. Aeron. Sci., vol. 18, 1951.

7.36. SUZUKI, S.: On the Natural Frequency of Swept Cantilevered Rectangular Plate. J. Jap. Soc. Aeron. Eng., vol. 5, 1957, pp. 50–58. (In Japanese.)

7.37. WALLER, MARY D.: Vibrations of Free Plates: Isosceles Right-Angled Triangles. Proc. Phys. Soc., vol. 53, pt. 1, 1941, pp. 35–39.

7.38. WALLER, MARY D.: Vibrations of Free Plates, Line Symmetry, Corresponding Modes. Proc. Roy. Soc. (London), ser. A, vol. 211, 1952, pp. 265–276.

Chapter 8

Plates of Other Shapes

8.1 POLYGONAL PLATES

Well-known analogies (refs. 8.1 and 8.2) exist between the separate problems of transverse free vibration and buckling of a polygonal plate simply supported all around and the problem of the transverse vibration of a prestretched membrane having no deflection at its edges.

The governing differential equation for the vibrating membrane is

$$\nabla^2 W+\left(\frac{\rho_m\omega_m^2}{T}\right)W=0 \tag{8.1}$$

where $W=W(x, y)$ is the transverse deflection, ρ_m is the mass density per unit area, ω_m is the frequency, and T is the membrane tension (force per unit length). Operating on equation (8.1) by ∇^2 and substituting for $\nabla^2 W$ from equation (8.1) give the resulting equation

$$\nabla^4 W-\left(\frac{\rho_m\omega_m^2}{T}\right)^2 W=0 \tag{8.2}$$

which is identical to equation (1.4) except for the constant coefficient of W. Furthermore, if $W=0$ along the polygonal boundary of the membrane, then by equation (8.1) $\nabla^2 W$ is also zero, which satisfies the boundary conditions for the simply supported plate. Thus a complete analogy exists between the two problems, and the frequency of the plate can be obtained from that of the membrane through the correspondence

$$\frac{\omega^2\rho}{D}\sim\left(\frac{\rho_m\omega_m^2}{T}\right)^2 \tag{8.3}$$

Again, operating on equation (8.1) by ∇^2 gives

$$\nabla^4 W+\left(\frac{\rho_m\omega_m^2}{T}\right)\nabla^2 W=0 \tag{8.4}$$

which is of the same form as the differential equation governing the buckling of a plate under the action of the inplane forces $N_x=N_y=N_0$ (a constant; i.e., hydrostatic pressure):

$$\nabla^4 W+\frac{N_0}{D}\nabla^2 W=0 \tag{8.5}$$

Again, the homogeneous boundary conditions for the simply supported polygonal edges of the plate are satisfied by the conditions around the membrane. Thus the following correspondence exists:

$$\frac{(N_0)_{cr}}{D}\sim\frac{\rho_m\omega_m^2}{T} \tag{8.6}$$

where $(N_0)_{cr}$ is the critical buckling load of the plate; that is, the eigenvalues which satisfy the homogeneous boundary conditions.

Finally, from a comparison of relationships (eq. (8.3) and eq. (8.6)), it is seen that the following correspondence exists between the plate vibration and plate buckling problems (when, of course, all edges are rectilinear and simply supported):

$$\omega\sqrt{\frac{\rho}{D}}\sim\frac{(N_0)_{cr}}{D} \tag{8.7}$$

Results given for polygonal plates having all edges simply supported in the sections that follow are taken from literature which dealt directly with the plate problem. For further results which can be obtained through the analogy (eq. (8.3)), the reader is directed to the published literature dealing with membrane vibrations.

8.1.1 Pentagons

Kaczkowski (ref. 8.3) analyzed the regular pentagon of side a (fig. 8.1) for the case when

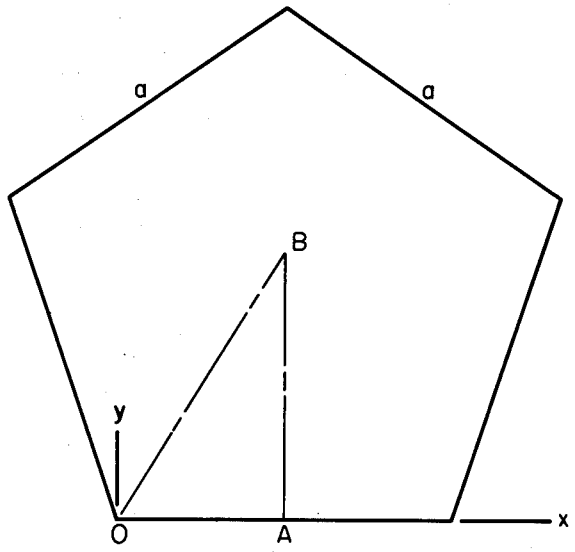


FIGURE 8.1.—Regular pentagon.

all edges are simply supported. He chose a deflection function

$$W(x,y)=\sum_{m=1,3,5}^{\infty}\left[A_m\sinh\sqrt{\left(\frac{m\pi}{a}\right)^2+\sqrt{\frac{\rho\omega^2}{D}}}\,y+B_m\sinh\sqrt{\left(\frac{m\pi}{a}\right)^2-\sqrt{\frac{\rho\omega^2}{D}}}\,y\right]\left(\sin\frac{m\pi x}{a}\right) \tag{8.8}$$

which exactly satisfies the symmetry conditions along AB and the simply supported conditions along OA. The symmetry conditions along OB yield a characteristic determinant for the problem. The fundamental frequency was found to be $\omega a^2\sqrt{\rho/D}=10.863$.

Waller (ref. 8.4) experimentally found several nodal patterns for a completely free regular pentagon. These are exhibited in figure 8.2.

8.1.2 Hexagons

The fundamental frequency of a regular hexagon of side length a and simply supported along all sides was determined by Kaczkowski (ref. 8.3) to be $\omega a^2\sqrt{\rho/D}=6.961$ by using the method described in the previous section. Conway (ref. 8.5) solved the problem by the point-matching method, using the solution in polar coordinates (eq. (2.1)) and satisfying boundary conditions at all corners, midpoints, and quarter points of the sides. This gave the fundamental frequency as $\omega a^2\sqrt{\rho/D}=7.129$. The problem is also discussed in references 8.2 and 8.6.

Nodal patterns for completely free regular hexagonal plates were determined experimentally by Waller (ref. 8.4) and are exhibited in figure 8.3.

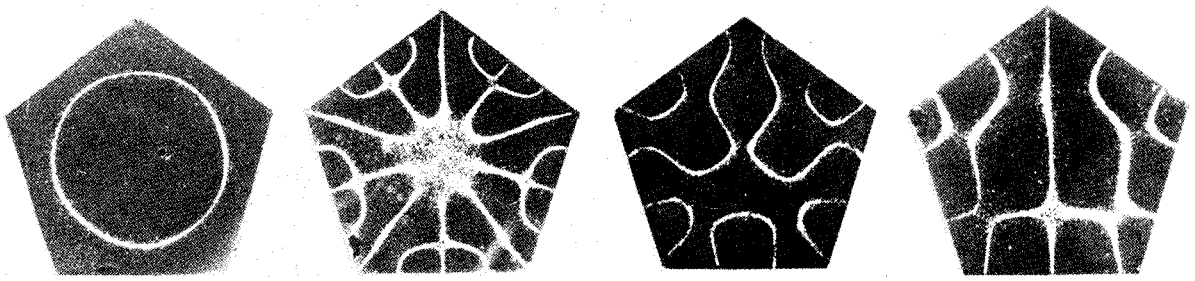


FIGURE 8.2.—Nodal patterns of completely free regular pentagonal plates. (From ref. 8.4)

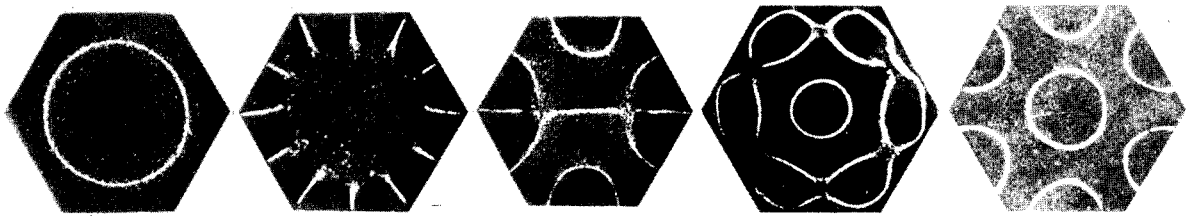


FIGURE 8.3.—Nodal patterns of completely free regular hexagonal plates. (From ref. 8.4)

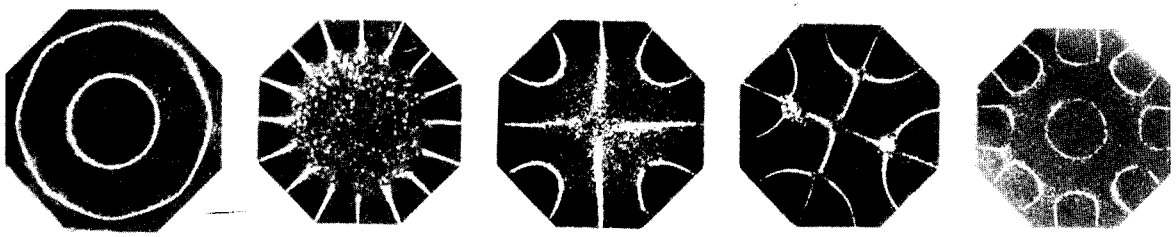


FIGURE 8.4.—Nodal patterns of completely free regular octagonal plates. (From ref. 8.4)

8.1.3 Other Polygonal Plates

The fundamental frequency of a regular octagonal plate of side length a and simply supported along all edges was computed to be $\omega a^2\sqrt{\rho/D}=3.624$ in reference 8.3. The method used was that described in the discussion of pentagons (sec. 8.1.1).

Experimentally observed nodal patterns for completely free regular octagonal plates are set forth in figure 8.4 (ref. 8.4).

8.2 SECTORIAL PLATES

Coordinates and dimensions of a circular sector are shown in figure 8.5.

8.2.1 Radial Sides Simply Supported

An exact solution is obtainable for the case when the two radial edges are simply supported, regardless of the homogeneous boundary conditions which exist along the circular edge. If one takes solutions to equation (1.4) in the form of equation (2.1) with $n=\pi/2\alpha$, $3\pi/2\alpha$, . . . (fig. 8.5), satisfaction of the boundary conditions along the circular edge yields a second-order characteristic determinant for the frequencies of symmetric modes. Similarly, the antisymmetric modes are determined by replacing cos $n\theta$ with sin $n\theta$ where $n=\pi/\alpha$, $3\pi/\alpha$, ... In spite of the relative simplicity of this approach, the only known solutions of this type are those for which n is an integer and which correspond to the higher modes of a circular plate.

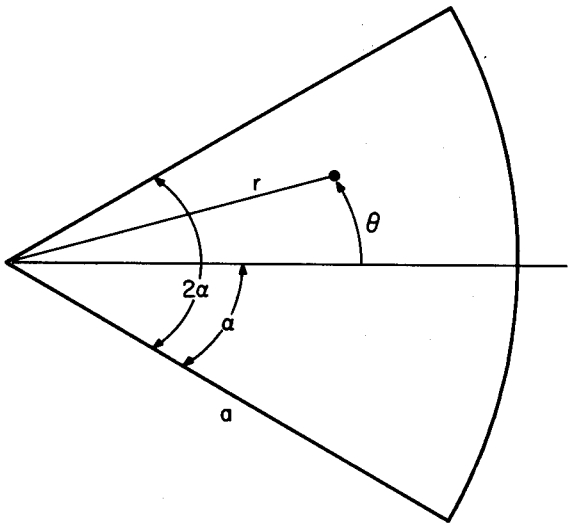


FIGURE 8.5.—Circular sector.

Westmann (ref. 8.7) solved the case when the circular edge is free by using the Rayleigh procedure, assuming a deflection function

$$W(r,\theta)=r^2\cos n\theta \tag{8.9}$$

and obtained the following approximate formula for the fundamental frequency parameter:

$$\omega^2a^4\rho/D=3(n^4-2n^2+8)-\nu(6n^2-8) \tag{8.10}$$

For the case when $n=3$ ($2\alpha=60°$), results for ω obtained from equation (8.10) for $\nu=0$ and $\nu=1/3$ are determined (ref. 8.7) to be 4.8 and 5.5 percent too high, respectively, when compared with an exact solution obtained from the threefold symmetric mode of a completely free circular plate (see sec. 2.1.3).

8.2.2 Other Boundary Conditions

Ben-Amoz (ref. 8.8) used the Rayleigh-Ritz method to solve the problem when all edges are clamped. A deflection function

$$W(r,\theta)=\xi^2(1-\xi^m)^2[C_1(\cosh\gamma_1\theta+\cos\gamma_2\theta)+C_2(\cosh\gamma_1\theta-\cos\gamma_2\theta)+C_3(\sinh\gamma_1\theta+\sin\gamma_2\theta)+C_4(\sinh\gamma_1\theta-\sin\gamma_2\theta)] \tag{8.11}$$

was used, where

$$\left.\begin{aligned}
&\gamma_{1,2}=[(a_0^2+p_0-b_0)^{1/2}\pm a_0]^{1/2}\\
&a_0=\frac{2}{3}(m-1)\\
&b_0=\frac{2}{3}(m+2)(2+3m+2m^2)\\
&m=\pi/2\alpha\\
&\xi=r/a\\
&p_0=\frac{\omega^2a^4\rho}{9D}\frac{(m+1)(2m+1)(3m+2)}{(m+3)(m+6)(2m+3)}
\end{aligned}\right\}\quad(8.12)$$

This function satisfies the clamped edge conditions at $r=a$ exactly. Substituting equation (8.11) into the boundary conditions at $\theta=\pm\alpha$ yields the characteristic equation

$$\cosh\frac{\gamma_1\alpha}{2}\cos\frac{\gamma_2\alpha}{2}=1+\frac{a_0}{\gamma_1\gamma_2}\sinh\frac{\gamma_1\alpha}{2}\sin\frac{\gamma_2\alpha}{2}\quad(8.13)$$

Variation of the fundamental frequency with sectorial angle is shown in figure 8.6.

The case when the two radial edges are clamped and the circular edge is free was analyzed in reference 8.7 by using the Rayleigh procedure and an assumed mode

$$W(r,\theta)=r^2(1+\cos m\theta)\quad(8.14)$$

giving a fundamental frequency parameter of

$$\omega^2a^4\rho/D=(m^4-2m^2+24)-\nu(6m^2-24)\quad(8.15)$$

where m is taken as π/α.

Waller (ref. 8.4) experimentally observed the two nodal patterns shown in figure 8.7 for a completely free semicircular plate.

8.3 OTHER PLATES

Grinsted (ref. 8.9) experimentally determined the frequencies and mode shapes of a flat brass plate designed to simulate an impeller blade. The plate was 0.064 inch thick, and the remaining dimensions are given in figure 8.8. Mode shapes observed, along with the corresponding cyclic frequencies, are depicted in figure 8.9.

In reference 8.9, experimental results are also given for a cantilevered plate of irregular shape intended to simulate a marine propeller blade. Dimensions of the plate and cyclic frequencies are given in figure 8.10. Corresponding mode shapes are shown in figure 8.11. The material is mild steel.

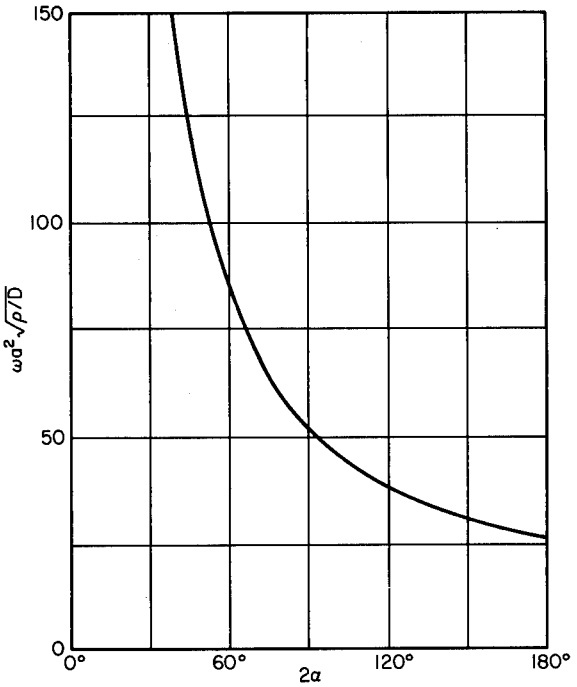


FIGURE 8.6.—Fundamental frequency parameter for a completely clamped sectorial plate. (After ref. 8.8)

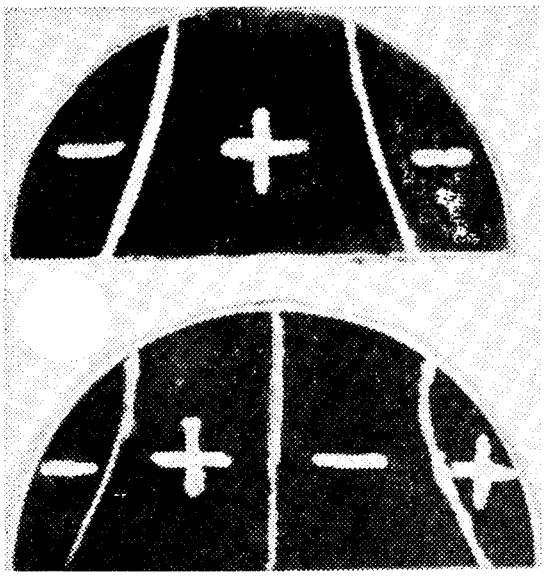


FIGURE 8.7.—Nodal patterns for a completely free semicircular plate. (From ref. 8.4)

Ruscoe (ref. 8.10) experimentally found several "complex modes" of a flat plate in the shape of a turbine vane having a curved edge

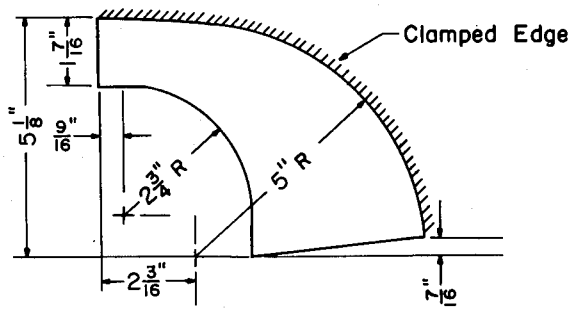


FIGURE 8.8.—Dimensions of a flat-plate model of an impeller blade; R, radius. (After ref. 8.9)

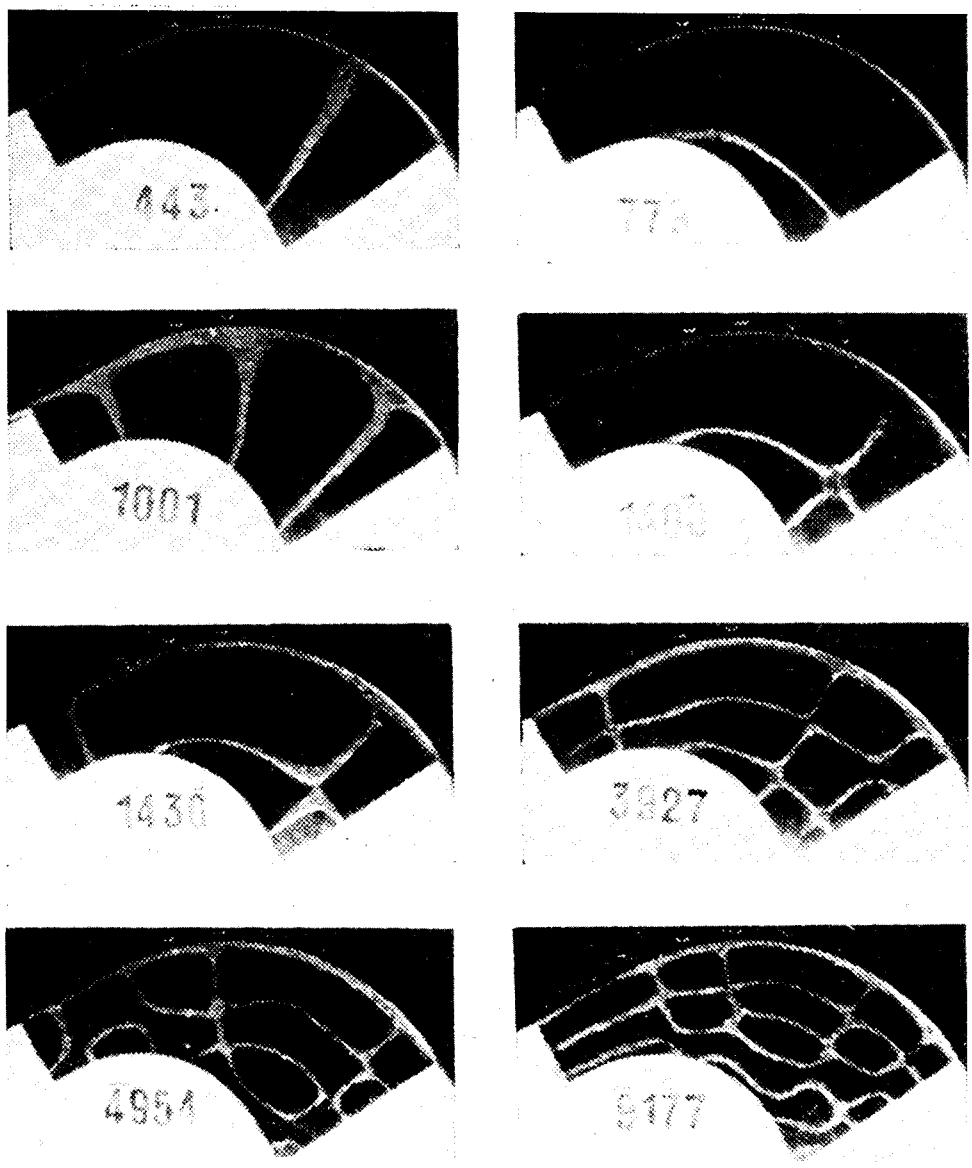


FIGURE 8.9.—Cyclic frequencies and mode shapes for a flat-plate model of an impeller blade. (From ref. 8.9)

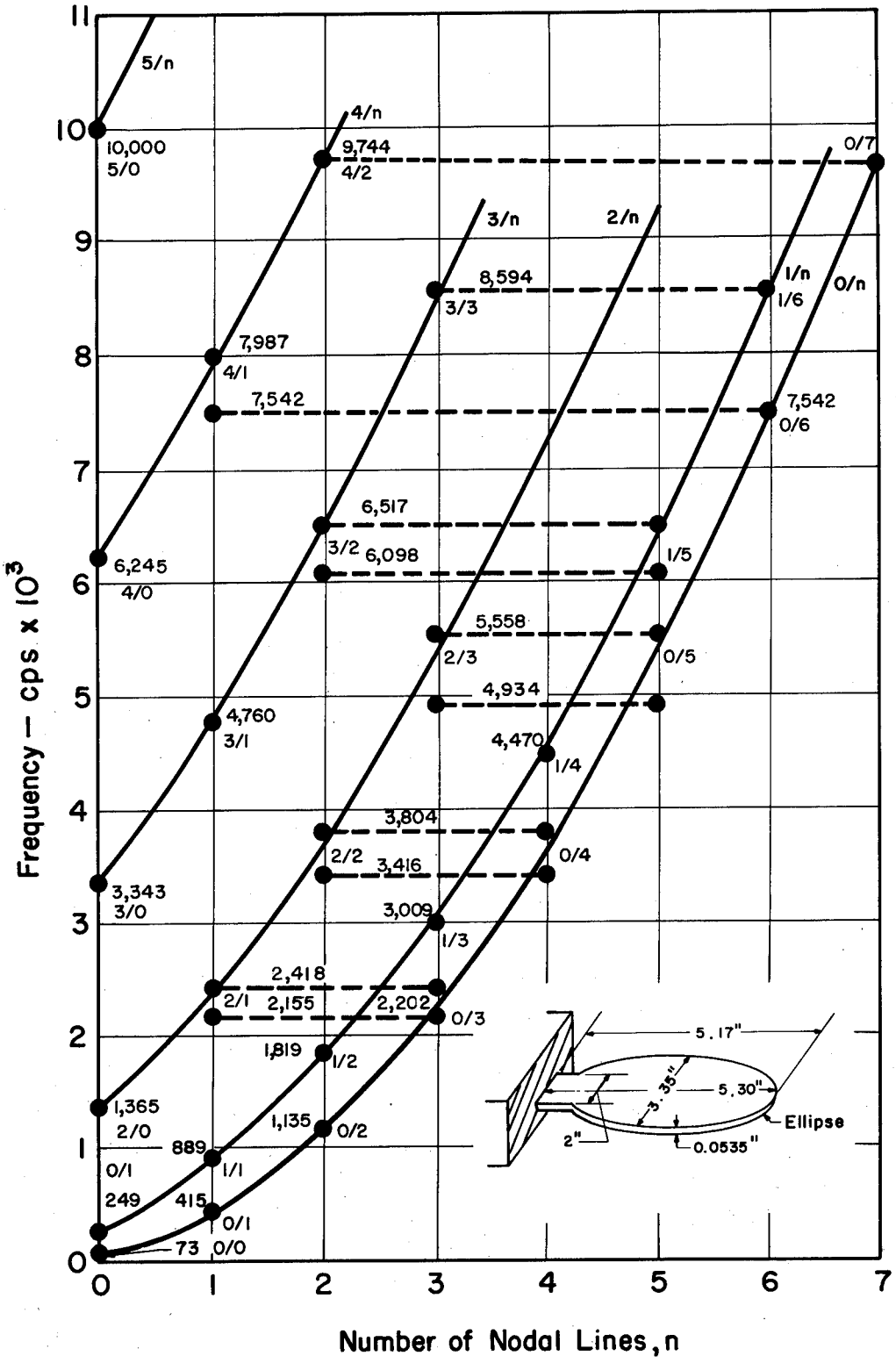


FIGURE 8.10.—Plate dimensions and cyclic frequencies for a flat-plate model of a marine propeller blade. (After ref. 8.9)

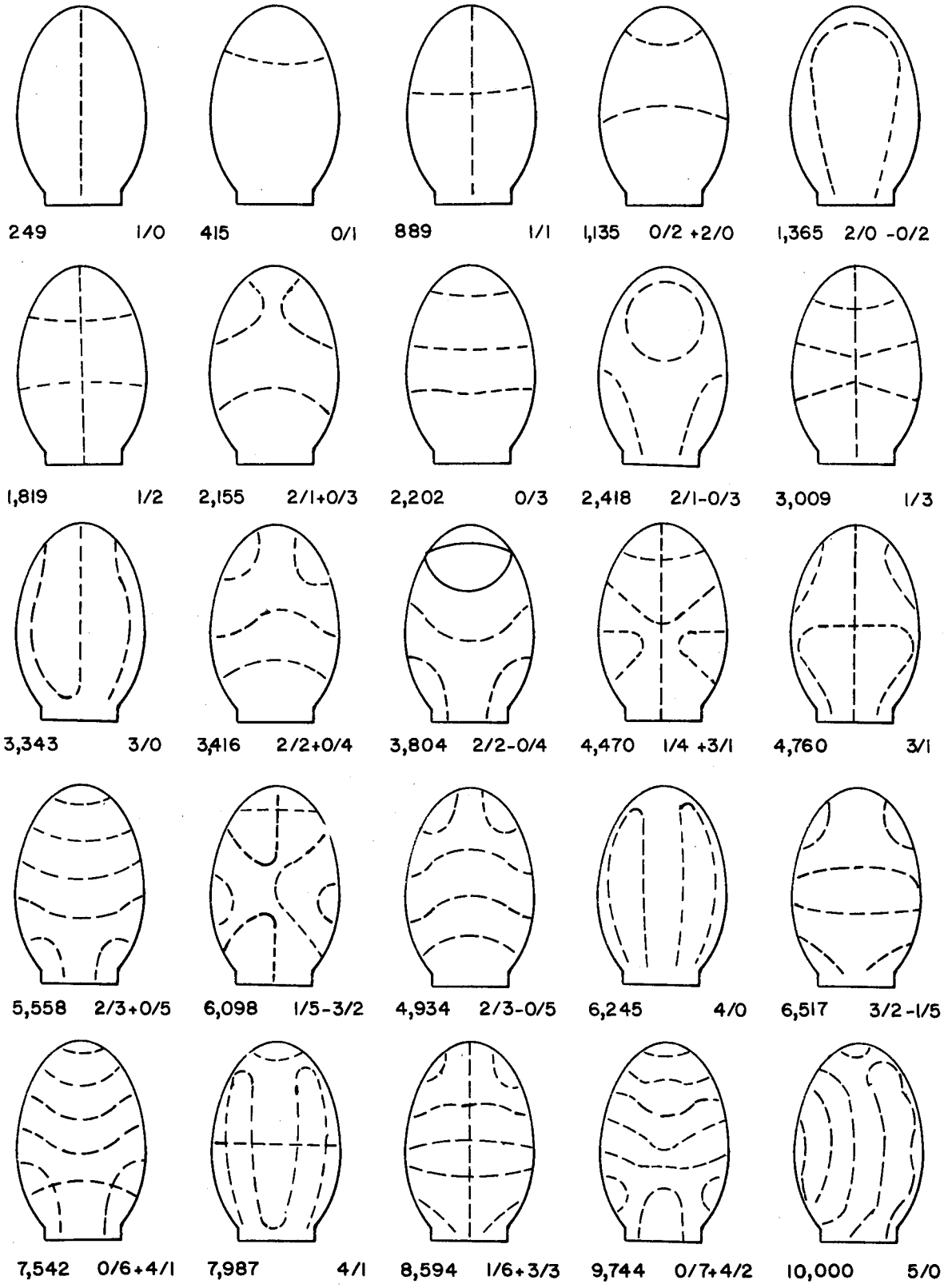


FIGURE 8.11.—Nodal patterns and cyclic frequencies for a flat-plate model of a marine propeller blade. (After ref. 8.9)

clamped and two straight edges free as shown in figure 8.12. Frequencies were given but plate dimensions were unspecified.

The problem of a plate of epicycloidal shape clamped on its contour is studied in reference 8.11. No numerical results are given.

In reference 8.12, a method for analyzing plates having two parallel edges of general curvilinear shape and simply supported is presented. No numerical vibration results are included.

Some bounds on frequencies of clamped plates of irregular shape are discussed in references 8.13 and 8.14.

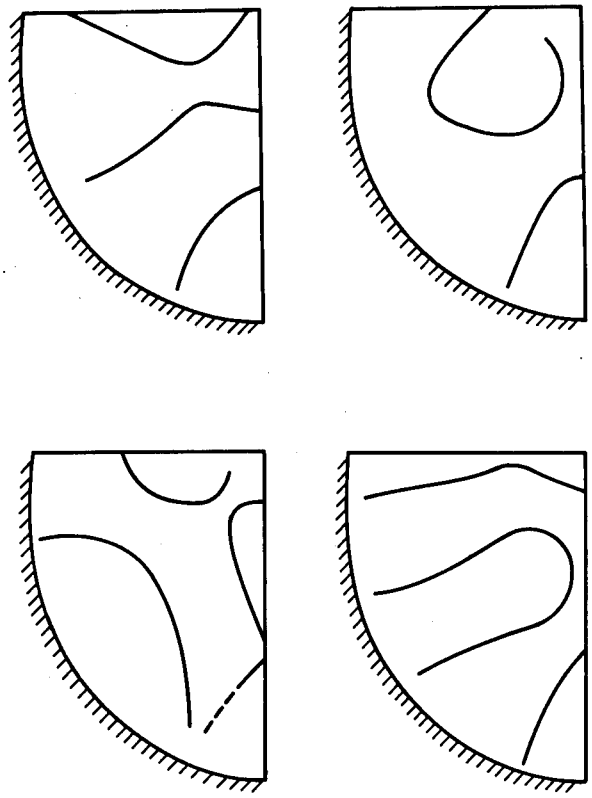


FIGURE 8.12.—Some mode shapes of an irregular plate. (After ref. 8.10)

REFERENCES

8.1. CONWAY, H. D.: Analogies Between the Buckling and Vibration of Polygonal Plates and Membranes. Can. Aeron. J., vol. 6, no. 7, Sept. 1960, p. 263.

8.2. SETH, B. R.: Transverse Vibrations of Rectilinear Plates. Proc. Indian Acad. Sci., sec. A, vol. 25, Jan. 1947, pp. 25–29.

8.3. KACZKOWSKI, Z.: Stabilität und Eigenschwingungen einer Platte von der Form eines regelmässigen Polygons. Ost. Ingr.-Arch., vol. 15, 1961, pp. 103–109.

8.4. WALLER, MARY D.: Vibrations of Free Plates, Line Symmetry, Corresponding Modes. Proc. Roy. Soc. (London), ser. A, vol. 211, 1952, pp. 265–276.

8.5. CONWAY, H. D.: The Bending, Buckling, and Flexural Vibration of Simply Supported Polygonal Plates by Point-Matching. J. Appl. Mech., vol. 28, no. 2, June 1961, pp. 288–291.

8.6. HERSCH, J.: Contribution à la Méthode des Équations aux Differences. ZAMP, vol. 9a, no. 9, 1958, pp. 129–180.

8.7. WESTMANN, R. A.: A Note on Free Vibrations of Triangular and Sector Plates. J. Aerospace Sci., vol. 29, no. 9, Sept. 1962, pp. 1139–1140.

8.8. BEN-AMOZ, M.: Note on Deflections and Flexural Vibrations of Clamped Sectorial Plates. J. Appl. Mech., vol. 26, no. 1, Mar. 1959, pp. 136–137.

8.9. GRINSTED, B.: Nodal Pattern Analysis. Proc. Inst. Mech. Eng., ser. A, vol. 166, 1952, pp. 309–326.

8.10. RUSCOE, A. D.: Communication on Nodal Pattern Analysis. Proc. Inst. Mech. Eng., 1954, pp. 174–176.

8.11. PIGNEDOLI, A.: Sulla Determinazione Effettiva delle Frequenze di Vibrazione di una Piastra Omogenea, a Contorno Epicicloidale Incastrato. Atti. Semin. Mat. Fis. Univ. Modena, vol. 4, 1949–1950, pp. 30–44.

8.12. SOLECKI, R.: Bending and Vibration of Non-Rectangular Plates. Acta Polytech. Scandinavica, no. 13, 1963, pp. 3–20.

8.13. DUFFIN, R. J.: Nodal Lines of a Vibrating Plate. J. Math. Phys., vol. 31, no. 4, 1953, pp. 294–299.

8.14. SZEGÖ, G.: On Membranes and Plates. Proc. Natl. Acad. Sci. U.S., vol. 36, 1950, pp. 210–216.

Chapter 9

Anisotropic Plates

No work in the literature has been found for the case of general anisotropy. Results for the special cases of polar and rectangular orthotropy are summarized in the following sections.

9.1 POLAR ORTHOTROPY

The differential equation for the transverse bending of a polar orthotropic plate is (see the appendix):

$$D_r\frac{\partial^4 w}{\partial r^4}+2\frac{D_{r\theta}}{r^2}\frac{\partial^4 w}{\partial r^2\,\partial\theta^2}+\frac{D_\theta}{r^4}\frac{\partial^4 w}{\partial\theta^4}+2\frac{D_r}{r}\frac{\partial^3 w}{\partial r^3}-\frac{2D_{r\theta}}{r^3}\frac{\partial^3 w}{\partial r\,\partial\theta^2}-\frac{D_\theta}{r^2}\frac{\partial^2 w}{\partial r^2}+\frac{2}{r^4}(D_\theta+D_{r\theta})\frac{\partial^2 w}{\partial\theta^2}+\frac{D_\theta}{r^3}\frac{\partial w}{\partial r}+\rho\frac{\partial^2 w}{\partial t^2}=0 \quad (9.1)$$

Assuming a variables separable solution

$$w=\sum_{n=0}^{\infty}W_n(r)\cos n\theta\cos\omega t \quad (9.2)$$

and substituting it into equation (9.1) give

$$D_r\frac{\mathrm{d}^4W_n}{\mathrm{d}r^4}-\frac{2n^2D_{r\theta}}{r^2}\frac{\mathrm{d}^2W_n}{\mathrm{d}r^2}+\frac{n^4D_\theta W_n}{r^4}+\frac{2D_r}{r}\frac{\mathrm{d}^3W_n}{\mathrm{d}r^3}+\frac{2n^2D_{r\theta}}{r^3}\frac{\mathrm{d}W_n}{\mathrm{d}r}-\frac{D_\theta}{r^2}\frac{\mathrm{d}^2W_n}{\mathrm{d}r^2}-\frac{2n^2}{r^4}(D_\theta+D_{r\theta})+\frac{D_\theta}{r^3}\frac{\mathrm{d}W_n}{\mathrm{d}r}-\rho\omega^2W_n=0 \quad (9.3)$$

The solution to equation (9.3) can be expressed as a power series

$$W_n=r^i\sum_{j=0}^{\infty}a_jr^j \quad (9.4)$$

as was shown first by Akasaka and Takagishi (ref. 9.1) and later in references 9.2, 9.3, and 9.4. Substitution of equation (9.4) leads to a recursion relationship among the coefficients a_j.

Results exist for circular plates for only two cases of simple edge conditions—when the edge is either completely clamped or simply supported.

9.1.1 Clamped Circular Plate

The coordinate system and dimensions for a clamped circular plate are shown in figure 2.1. Boundary conditions are stated in equation (2.2).

For axisymmetric modes ($n=0$) certain terms in equation (9.1) disappear; that is, terms containing derivatives with respect to θ. Akasaka and Takagishi (ref. 9.1) used the infinite series (eq. (9.4)) to formulate a second-order characteristic determinant for the frequencies

$$\begin{vmatrix} a_{11} & a_{12} \\ a_{21} & a_{22} \end{vmatrix}=0 \quad (9.5)$$

where

$$\left.\begin{aligned} a_{11}&=1+\frac{(\omega/\xi)^2}{(4)(2)(9-k^2)}+\frac{(\omega/\xi)^4}{(4)(2)(9-k^2)(8)(6)(49-k^2)}+\cdots \\ a_{12}&=1+\frac{(\omega/\xi)^2}{(5+k)(3+k)8(2+k)}+\frac{(\omega/\xi)^4}{(5+k)(3+k)8(2+k)(9+k)(7+k)16(4+k)}+\cdots \\ a_{21}&=\frac{(\omega/\xi)^2}{2(9-k^2)}\left[1+\frac{(\omega/\xi)^2}{(6)(4)(49-k^2)}+\cdots\right] \\ a_{22}&=1+\sqrt{k}+\frac{(\omega/\xi)^2}{8(2+k)(3+k)}+\cdots \end{aligned}\right\} \quad (9.6)$$

and where $\xi^2=D_r/\rho a^4$ and $k^2=D_\theta/D_r$. An approximate formula for the first two axisymmetric modes is obtained from equation (9.5) by truncating the series and is given in reference 9.1 as

$$\omega^2 a^4\rho/D_r=\frac{24(3+k)}{5+k}\left[(4+k)(7+k)\pm\sqrt{\frac{(4+k)(7+k)(64+19k+k^2)}{3}}\right] \quad (9.7)$$

where terms of degree $(\omega/\xi)^4$ and lower are retained. Letting $k^2=D_\theta/D_r=1$ gives $\omega/\xi=$ 10.23 and 34.3 for the first two axisymmetric frequencies of an isotropic plate; these values compare with the values of 10.22 and 39.77 from the discussion of the clamped circular plate (sec. 2.1.1).

Borsuk (ref. 9.2) solved the problem by expressing the series (eq. (9.4)) in terms of hypergeometric functions. He presented closed-form expressions for the frequency equations for all values of n given in terms of the hypergeometric functions. The only numerical result given is for the axisymmetric case ($n=0$) and $\sqrt{D_\theta/D_r}=1.4$ and is $\omega a^2\sqrt{\rho/D_r}=4.55$. However, because this value is much lower than the value of 10.22 for the isotropic plate and because values of D_θ/D_r greater than unity should further stiffen the plate, this result is clearly questionable.

The first antisymmetric frequency parameter ($n=1$) is given in reference 9.1 as

$$\omega a^2\sqrt{\frac{\rho}{D_r}}=4\sqrt{\left[\left(4+\sqrt{\frac{D_r+D_\theta+2D_{r\theta}}{D_r}}\right)\left(2+\sqrt{\frac{D_r+D_\theta+2D_{r\theta}}{D_r}}\right)\right]} \quad (9.8)$$

The fundamental frequency parameter for the case when a concentrated mass M is attached at the center is given in reference 9.1 as

$$\omega a^2\sqrt{\frac{\rho}{D_r}}=\sqrt{\frac{8(3+k)(2+k)}{1+\left(\frac{2M}{\pi a^2\rho}\right)\frac{(3+k)(2+k)}{(1+k)^2}}} \quad (9.9)$$

Pandalai and Patel (ref. 9.4) also solved the problem by using the infinite series (eq. (9.4)) and obtained the following characteristic equation for arbitrary values of n:

$$\left(\sum_{j=0,4,8}^{\infty} C_{nj}\lambda^{n+j}\right)\left[\sum_{j=0,4,8}^{\infty}(n+j+2)D_{n,j+2}\lambda^{n+j+1}\right]=\left[\sum_{j=0,4,8}^{\infty}(n+j)C_{nj}\lambda^{n+j-1}\right]\left(\sum_{j=0,4,8}^{\infty}D_{n,j+2}\lambda^{n+j+2}\right) \quad (9.10)$$

where

$$C_{nj}=A_{nj}/A_{n0}$$

$$D_{n,j+2}=A_{n,j+2}/A_{n2}$$

$$A_{n,i}=A_{n,i-4}/\{(n+i)(n+i-2)[(n+i-1)^2-\beta]+n^2[(n^2-2)\beta-2(\alpha+2\gamma)(n+i-1)^2]\}$$

$$\alpha=E_{r\theta}/E_r$$

$$\beta=E_\theta/E_r$$

and

$$\gamma=G/E_r$$

and where E_r, E_θ, $E_{r\theta}$, and G are the material constants from the stress-strain relationships

$$\left.\begin{aligned}\sigma_r&=E_r\epsilon_r+E_{r\theta}\epsilon_\theta\\ \sigma_\theta&=E_{r\theta}\epsilon_r+E_\theta\epsilon_\theta\\ \tau_{r\theta}&=G\gamma_{r\theta}\end{aligned}\right\} \quad (9.11)$$

and

$$\lambda^4=\frac{12\omega^2a^4\rho}{E_rh^3} \quad (9.12)$$

If the infinite series of equation (9.10) are truncated to include terms up to the degree $2n+4$, a first approximation for the eigenvalue λ is given by

$$\lambda^4=1/(C_{n4}-3D_{n6}) \quad (9.13)$$

which for the fundamental frequency ($n=0$) reduces to

$$\lambda^4=\frac{1}{2}(9-\beta)(25-\beta) \quad (9.14)$$

In reference 9.3 the same series solution was assumed and a frequency equation was written, but no numerical results were given for the problem.

9.1.2 Simply Supported Circular Plate

The coordinate system and dimensions for a simply supported circular plate are shown in figure 2.2. The boundary conditions are stated

in equation (2.9). Minkarah and Hoppmann (ref. 9.3) solved the problem for axisymmetric modes by assuming the series solution (eq. (9.4)) and arrived at the frequency equation

$$F_1(\lambda)\left[F_3''(\lambda)+\frac{\nu_\theta}{a}F_3'(\lambda)\right]=F_3(\lambda)\left[F_1''(\lambda)+\frac{\nu_\theta}{a}F_1'(\lambda)\right] \tag{9.15}$$

where

$$F_1(r)=1+\frac{(\alpha r)^4}{(2)(4)(9-k^2)}+\frac{(\alpha r)^8}{(2)(4)(6)(8)(9-k^2)(49-k^2)}+\cdots$$
$$+\frac{(\alpha r)^{4j}}{(2)^{2j}(2j)!(9-k^2)(49-k^2)\cdots[(4j-1)^2-k^2]}+\cdots$$

$$F_3(r)=r^{1+k}\left[1+\frac{(\alpha r)^4}{8(2+k)(3+k)(5+k)}+\frac{(\alpha r)^8}{(8)(16)(2+k)(3+k)(4+k)(5+k)(7+k)(9+k)}\right.$$
$$\left.+\frac{(\alpha r)^{12}}{(8)(16)(24)(2+k)(3+k)(4+k)(5+k)(6+k)(7+k)(9+k)(11+k)(13+k)}+\cdots\right]$$

$\alpha^4=\omega^2\rho/D_r$, $\lambda=\alpha a$, $k^2=D_\theta/D_r$, and ν_θ is the elastic constant in the axisymmetric relationship

$$M_r=-D_r\left(\frac{\mathrm{d}^2w}{\mathrm{d}r^2}+\frac{\nu_\theta}{r}\frac{\mathrm{d}w}{\mathrm{d}r}\right)$$

The primes indicate differentiation with respect to r.

Axisymmetric frequency parameters for various combinations of elastic constants are given in table 9.1 taken from reference 9.3.

Experimental frequencies were also measured in reference 9.3 for the plate of table 9.1 having $k=1.50$, $\nu_\theta=0.50$, and $D_r=11\,500$. The corresponding frequency parameters and nodal patterns are shown in figure 9.1 for the first five axisymmetric modes and the first four nonaxisymmetric modes.

TABLE 9.1.—*Axisymmetric Frequency Parameters for a Simply Supported Circular Plate Having Polar Orthotropy*

Elastic constants			$\omega a^2\sqrt{\rho/D_r}$		
k	ν_θ	D_r	Mode 1	Mode 2	Mode 3
0.25	0.22	10.70×10^4	2.500	--------	-------
.50	.40	4.75	3.629	--------	-------
.50	.30	5.20	3.452	--------	-------
.75	.70	2.64	4.765	28.249	71.572
1.00	.75	1.88	5.518	30.206	74.132
1.00	.75	1.60	5.518	30.206	74.132
1.25	1.00	1.33	6.472	32.524	76.562
1.25	.50	1.50	5.934	31.843	76.318
1.50	.75	1.08	6.906	34.047	81.000
1.50	.50	1.15	6.646	33.791	79.924
1.75	.35	.95	7.188	35.557	83.174

In reference 9.4 the frequency equation is written as

$$\left(\sum_{j=0,4,8}^{\infty}C_{nj}\lambda^{n+j}\right)\left\{\sum_{j=0,4,8}^{\infty}[(n+j+2)(n+j+1+\alpha)-\alpha n^2]D_{n,j+2}\lambda^{n+j}\right\}=\left(\sum_{j=0,4,8}^{\infty}D_{n,j+2}\lambda^{n+j+2}\right)\left\{\sum_{j=0,4,8}^{\infty}[(n+j)(n+j-1+\alpha)-\alpha n^2]C_{nj}\lambda^{n+j-2}\right\} \tag{9.16}$$

where the terminology is the same as that used in the discussion of clamped circular plates (sec. 9.1.1). Equation (9.16) is obviously appropriate for general vibration modes of the plate. Truncating the infinite series contained in equation (9.16) to include terms up to the degree $2n+4$ gives the following equation for frequency parameters:

$$\lambda_{SS}^4=\left(\frac{2n+1+\alpha}{2n+5+\alpha}\right)\lambda_C^4 \tag{9.17}$$

Here λ_{SS} and λ_C are the frequency parameters $(12\omega^2a^4\rho/E_rh^3)^{1/4}$ for the simply supported and clamped cases, respectively, and the symbol α is defined in the discussion of the clamped circular plate (sec. 9.1.1). The parameter λ_C is given by equation (9.13).

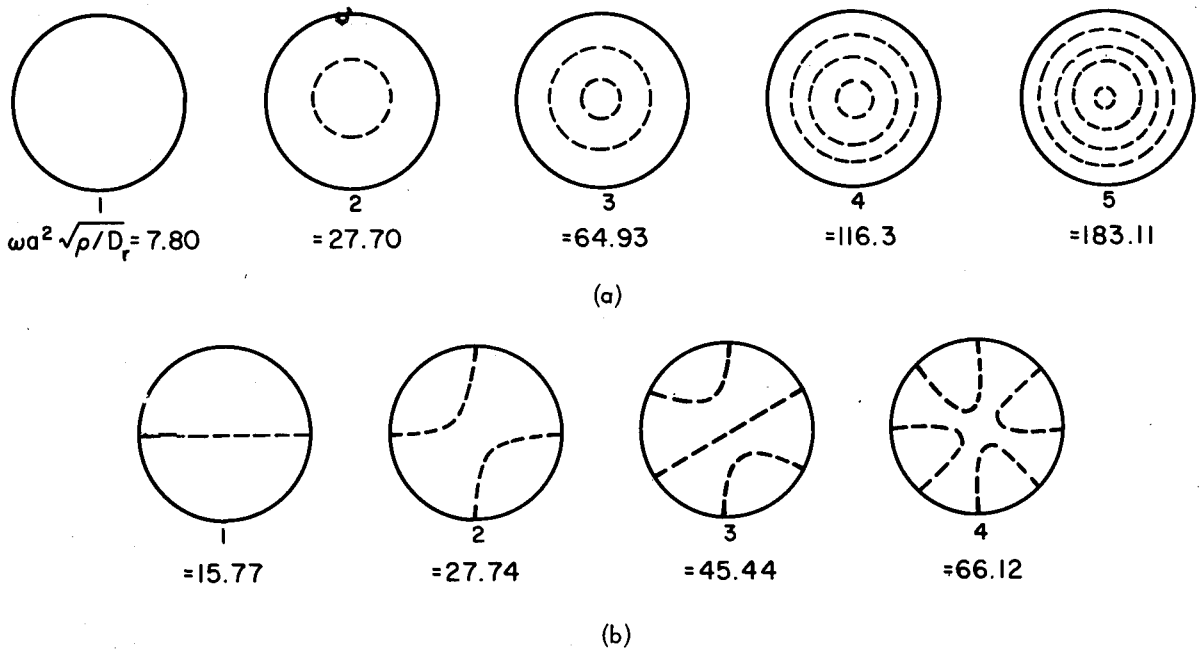


FIGURE 9.1.—Experimentally determined frequency parameters $\omega a^2\sqrt{\rho/D_r}$ and nodal patterns for a simply supported circular plate having polar orthotropy. (*a*) Axisymmetric modes. (*b*) Nonaxisymmetric modes. (After ref. 9.3)

A frequency determinant for the problem is also presented in reference 9.2, although no numerical results are given.

9.1.3 Other Shapes

Pyesyennikova and Sakharov (ref. 9.5) treated the problem of the annular plate having inside radius a and outside radius b for the axisymmetric modes of two cases of boundary conditions by using the Boobnov-Galerkin method.

For the case of the inner boundary free and the outer boundary clamped, a deflection function

$$W_1(\xi)=\Delta_{11}J_0(\alpha\xi)+\Delta_{12}Y_0(\alpha\xi)+\Delta_{13}I_0(\alpha\xi)+\Delta_{14}K_0(\alpha\xi) \quad (9.18)$$

was chosen, where $\xi=r/b$, $\alpha^4=\omega^2\rho/D_r$,

$$\Delta_{11}=\begin{vmatrix} Y_0(\alpha) & I_0(\alpha) & -K_0(\alpha) \\ -Y_1(\alpha) & I_1(\alpha) & K_1(\alpha) \\ -Y_{01}(\alpha,a/b) & I_{01}(\alpha,a/b) & -K_{01}(\alpha,a/b) \end{vmatrix}$$

$$\Delta_{12}=\begin{vmatrix} J_0(\alpha) & I_0(\alpha) & K_0(\alpha) \\ -J_1(\alpha) & I_1(\alpha) & -K_1(\alpha) \\ -J_{01}(\alpha,a/b) & I_{01}(\alpha,a/b) & K_{01}(\alpha,a/b) \end{vmatrix}$$

$$\Delta_{13}=\begin{vmatrix} J_0(\alpha) & Y_0(\alpha) & -K_0(\alpha) \\ -J_1(\alpha) & -Y_1(\alpha) & K_1(\alpha) \\ -J_{01}(\alpha,a/b) & -Y_{01}(\alpha,a/b) & -K_{01}(\alpha,a/b) \end{vmatrix}$$

$$\Delta_{14}=\begin{vmatrix} J_0(\alpha) & Y_0(\alpha) & I_0(\alpha) \\ -J_1(\alpha) & -Y_1(\alpha) & I_1(\alpha) \\ -J_{01}(\alpha,a/b) & -Y_{01}(\alpha,a/b) & I_{01}(\alpha,a/b) \end{vmatrix}$$

$$J_{01}(\alpha, a/b) \equiv J_0(\alpha a/b) - \frac{1-\nu_\theta}{\alpha a/b} J_1(\alpha a/b) \qquad I_{01}(\alpha, a/b) \equiv I_0(\alpha a/b) - \frac{1-\nu_\theta}{\alpha a/b} I_1(\alpha a/b)$$

$$Y_{01}(\alpha, a/b) \equiv Y_0(\alpha a/b) - \frac{1-\nu_\theta}{\alpha a/b} Y_1(\alpha a/b) \qquad K_{01}(\alpha, a/b) \equiv K_0(\alpha a/b) + \frac{1-\nu_\theta}{\alpha a/b} K_1(\alpha a/b)$$

and the terms J_i, Y_i, I_i, and K_i are the regular and modified Bessel functions. (See discussion of solutions of classical plate equations (sec. 1.1.2).) The characteristic determinant giving α is

$$\begin{vmatrix} J_0(\alpha) & Y_0(\alpha) & I_0(\alpha) & K_0(\alpha) \\ -J_1(\alpha) & -Y_1(\alpha) & I_1(\alpha) & -K_1(\alpha) \\ -J_{01}(\alpha, a/b) & -Y_{01}(\alpha, a/b) & I_{01}(\alpha, a/b) & K_{01}(\alpha, a/b) \\ (1-A)J_1(\alpha a/b) & (1-A)Y_1(\alpha a/b) & (1+A)I_1(\alpha a/b) & -(1+A)K_1(\alpha a/b) \end{vmatrix} = 0 \qquad (9.19)$$

where

$$A \equiv \frac{1-(D_\theta/D_r)}{(\alpha a/b)^2}$$

Frequency parameters for varying ratios of a/b and D_θ/D_r are depicted in figure 9.2. In order for the results of figure 9.2 to be completely definitive, the value of either ν_r or ν_θ must be known. Unfortunately, neither is given in reference 9.5.

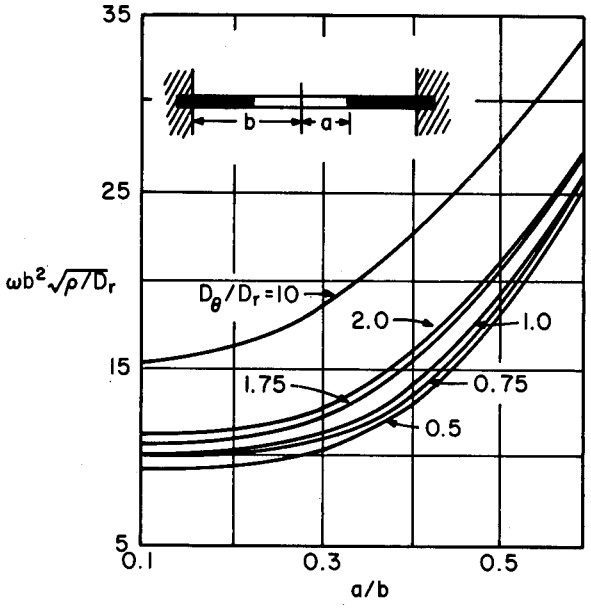


FIGURE 9.2.—Frequency parameters for a clamped-free annular plate having polar orthotropy.

For the case of the inner boundary free and the outer boundary simply supported, a deflection function

$$W_2(\xi) = \Delta_{21} J_0(\alpha\xi) + \Delta_{22} Y_0(\alpha\xi) + \Delta_{23} I_0(\alpha\xi) + \Delta_{24} K_0(\alpha\xi) \qquad (9.20)$$

was chosen, where

$$\Delta_{21} = \begin{vmatrix} -Y_0(\alpha) & I_0(\alpha) & K_0(\alpha) \\ Y_{01}(\alpha, 1) & I_{01}(\alpha, 1) & K_{01}(\alpha, 1) \\ Y_{01}(\alpha, a/b) & I_{01}(\alpha, a/b) & K_{01}(\alpha, a/b) \end{vmatrix}$$

$$\Delta_{22} = \begin{vmatrix} J_0(\alpha) & I_0(\alpha) & K_0(\alpha) \\ -J_{01}(\alpha, 1) & I_{01}(\alpha, 1) & K_{01}(\alpha, 1) \\ -J_{01}(\alpha, a/b) & I_{01}(\alpha, a/b) & K_{01}(\alpha, a/b) \end{vmatrix}$$

$$\Delta_{23} = \begin{vmatrix} -J_0(\alpha) & Y_0(\alpha) & K_0(\alpha) \\ J_{01}(\alpha, 1) & -Y_{01}(\alpha, 1) & K_{01}(\alpha, 1) \\ J_{01}(\alpha, a/b) & -Y_{01}(\alpha, a/b) & K_{01}(\alpha, a/b) \end{vmatrix}$$

$$\Delta_{24} = \begin{vmatrix} J_0(\alpha) & Y_0(\alpha) & I_0(\alpha) \\ -J_{01}(\alpha, 1) & -Y_{01}(\alpha, 1) & I_{01}(\alpha, 1) \\ -J_{01}(\alpha, a/b) & -Y_{01}(\alpha, a/b) & I_{01}(\alpha, a/b) \end{vmatrix}$$

and where the remaining symbols are as defined earlier in this section. The characteristic determinant giving α is

$$\begin{vmatrix} J_0(\alpha) & Y_0(\alpha) & I_0(\alpha) & K_0(\alpha) \\ -J_{01}(\alpha, 1) & -Y_{01}(\alpha, 1) & I_{01}(\alpha, 1) & K_{01}(\alpha, 1) \\ -J_{01}(\alpha, a/b) & -Y_{01}(\alpha, a/b) & I_{01}(\alpha, a/b) & K_{01}(\alpha, a/b) \\ (1-A)J_1(\alpha a/b) & (1-A)Y_1(\alpha a/b) & (1+A)J_1(\alpha a/b) & -(1+A)K_1(\alpha a/b) \end{vmatrix} = 0 \qquad (9.21)$$

308-337 O—70——17

Frequency parameters for varying ratios of a/b and D_θ/D_r are depicted in figure 9.3. The figure is not completely definitive for the same reason as that given in the preceding paragraph.

9.2 RECTANGULAR ORTHOTROPY

The differential equation for the transverse bending of a plate having rectangular orthotropy is (see the appendix):

$$D_x\frac{\partial^4 w}{\partial x^4}+2D_{xy}\frac{\partial^4 w}{\partial x^2\,\partial y^2}+D_y\frac{\partial^4 w}{\partial y^4}+\rho\frac{\partial^2 w}{\partial t^2}=0 \quad (9.22)$$

The moment-curvature relations are

$$\left.\begin{aligned} M_x&=-D_x\left(\frac{\partial^2 w}{\partial x^2}+\nu_y\frac{\partial^2 w}{\partial y^2}\right)\\ M_y&=-D_y\left(\frac{\partial^2 w}{\partial y^2}+\nu_x\frac{\partial^2 w}{\partial x^2}\right)\\ M_{xy}&=-2D_k\frac{\partial^2 w}{\partial x\,\partial y}\end{aligned}\right\} \quad (9.23)$$

Other useful equations are given in the appendix.

The elastic constants are related by (see the appendix)

$$\left.\begin{aligned} D_x&=\frac{E_x h^3}{12(1-\nu_x\nu_y)}\\ D_y&=\frac{E_y h^3}{12(1-\nu_x\nu_y)}\\ D_{xy}&=D_x\nu_y+2D_k\\ D_k&=\frac{Gh^3}{12}\end{aligned}\right\} \quad (9.24)$$

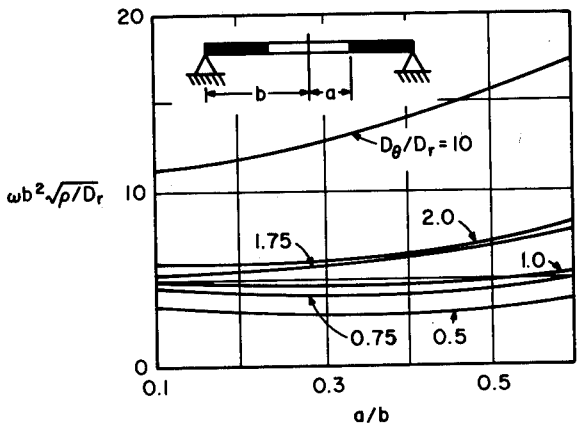


FIGURE 9.3.—Frequency parameters for a simply supported free annular plate having polar orthotropy.

If the orthotropic constants D'_x, D'_y, and D'_{xy} are known with respect to the x' and y' coordinate axes, it has been shown (refs. 9.6 and 9.7) that the orthotropic constants D_x, D_y, and D_{xy} can be determined from

$$\left.\begin{aligned} D_x&=D'_x\cos^4\phi+D'_y\sin^4\phi+2D'_{xy}\sin^2\phi\cos^2\phi\\ D_y&=D'_x\sin^4\phi+D'_y\cos^4\phi+2D'_{xy}\sin^2\phi\cos^2\phi\\ D_{xy}&=(3D'_x+3D'_y-2D'_{xy})\sin^2\phi\cos^2\phi\\ &\quad+D'_{xy}(\cos^2\phi-\sin^2\phi)^2\end{aligned}\right\} \quad (9.25)$$

When the angle ϕ between the x'- and the x-axis is a multiple of 22.5°, equations (9.25) can be used to obtain the equivalent elastic constants for equation (9.22). For an angle ϕ not equal to 22.5°, 45°, 67.5°, . . ., however, equation (9.22) is transformed into an equation having terms of the type $\partial^4 w/\partial x\,\partial y^3$ and $\partial^4 w/\partial x^3\,\partial y$ as well.

The assumption of simple harmonic motion

$$w=W(x, y)\cos\omega t \quad (9.26)$$

gives for equation (9.22)

$$D_x\frac{\partial^4 W}{\partial x^4}+2D_{xy}\frac{\partial^4 W}{\partial x^2\,\partial y^2}+D_y\frac{\partial^4 W}{\partial y^4}-\rho\omega^2 W=0 \quad (9.27)$$

The strain energy of bending and twisting of a plate having rectangular orthotropy, expressed in rectangular coordinates, is

$$U=\frac{1}{2}\int_A\left[D_x\left(\frac{\partial^2 w}{\partial x^2}\right)^2+D_y\left(\frac{\partial^2 w}{\partial y^2}\right)^2+2D_{xy}\frac{\partial^2 w}{\partial x^2}\frac{\partial^2 w}{\partial y^2}+4D_k\left(\frac{\partial^2 w}{\partial x\,\partial y}\right)^2\right]dA \quad (9.28)$$

For rectangular orthotropic plates having either clamped or simply supported edges, Hearmon (ref. 9.8) used the Rayleigh method to extend Warburton's work (ref. 9.9) for isotropic plates (see chapter entitled "Rectangular Plates" (ch. 4)) to obtain frequency parameters for all modes of vibration. The frequencies are determined from the equation

$$\omega^2=\frac{1}{\rho}\left(\frac{A^4 D_x}{a^4}+\frac{B^4 D_y}{b^4}+\frac{2CD_{xy}}{a^2 b^2}\right) \quad (9.29)$$

where A, B, and C are summarized in table 9.2 for the various boundary conditions and modes. The terms γ_i and ϵ_i in table 9.2 are given by

$$\gamma_0=m\pi$$
$$\gamma_1=\left(m+\frac{1}{4}\right)\pi$$
$$\gamma_2=\left(m+\frac{1}{2}\right)\pi$$
$$\epsilon_0=n\pi$$
$$\epsilon_1=\left(n+\frac{1}{4}\right)\pi$$
$$\epsilon_2=\left(n+\frac{1}{2}\right)\pi$$

9.2.1 All Sides Simply Supported

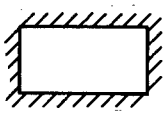
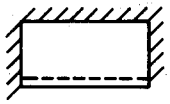
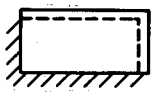
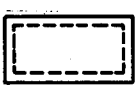
This problem of the rectangular plate with all sides simply supported (SS–SS–SS–SS) has a simple, exact solution. A coordinate system is chosen as in figure 9.4. The boundary conditions are

$$\left.\begin{aligned} w=0,\ M_x=0 \quad &(\text{for } x=0,\ a)\\ w=0,\ M_y=0 \quad &(\text{for } y=0,\ b)\end{aligned}\right\} \tag{9.30}$$

By using equations (9.23) it is seen that

$$W_{mn}=A_{mn}\sin\frac{m\pi x}{a}\sin\frac{n\pi y}{b} \tag{9.31}$$

TABLE 9.2.—*Frequency Coefficients in Equation (9.29)*

Boundary conditions	A	B	C	m	n
	4.730 4.730 γ_2 γ_2	4.730 ϵ_2 4.730 ϵ_2	151.3 $12.30\epsilon_2(\epsilon_2-2)$ $12.30\gamma_2(\gamma_2-2)$ $\gamma_2\epsilon_2(\gamma_2-2)(\epsilon_2-2)$	1 1 2, 3, 4, . . . 2, 3, 4, . . .	1 2, 3, 4, . . . 1 2, 3, 4, . . .
	4.730 γ_2	ϵ_1 ϵ_1	$12.30\epsilon_1(\epsilon_1-1)$ $\gamma_2\epsilon_1(\gamma_2-2)(\epsilon_1-1)$	1, 2, 3, . . . 1, 2, 3, . . .	1 2, 3, 4, . . .
	4.730 γ_2	ϵ_0 ϵ_0	$12.30\epsilon_0^2$ $\gamma_2\epsilon_0^2(\gamma_2-2)$	1 2, 3, 4, . . .	1, 2, 3, . . . 1, 2, 3, . . .
	γ_1	ϵ_1	$\gamma_1\epsilon_1(\gamma_1-1)(\epsilon_1-1)$	1, 2, 3, . . .	1, 2, 3, . . .
	γ_1	ϵ_0	$\gamma_1\epsilon_0^2(\gamma_1-1)$	1, 2, 3, . . .	1, 2, 3, . . .
	γ_0	ϵ_0	$\gamma_0^2\epsilon_0^2$	1, 2, 3, . . .	1, 2, 3, . . .

satisfies the boundary conditions, where A_{mn} is an amplitude coefficient determined from the initial conditions of the problem and m and n are integers. Substituting equation (9.31) into equation (9.27) gives the frequency

$$\omega_{mn}=\frac{\pi^2}{a^2\sqrt{\rho}}\sqrt{D_x m^4+2D_{xy}m^2n^2\left(\frac{a}{b}\right)^2+D_y n^4\left(\frac{a}{b}\right)^4} \tag{9.32}$$

This result was obtained by Hearmon (ref. 9.10) and by many others.

The variation of frequency with a/b ratio was determined in reference 9.8 for several higher modes. This variation is depicted in figure 9.5 for a five-ply maple-plywood plate having $D_x/D_{xy}=1.543$ and $D_y/D_{xy}=4.810$.

The accuracy of the Rayleigh-Ritz method as applied to orthotropic plates was studied in reference 9.10 by solving this problem using a deflection function

$$W(x, y)=x(a-x)y(b-y)(a^2+ax-x^2)(b^2+by-y^2)[A_1+A_2x(a-x)y(b-y)] \tag{9.33}$$

where A_1 and A_2 are undetermined coefficients. The results obtained by taking only A_1 (i.e., $A_2=0$) and both A_1 and A_2 are given in table 9.3 for five-ply plywood and veneer square plates of birch with the orthotropic constants determined experimentally.

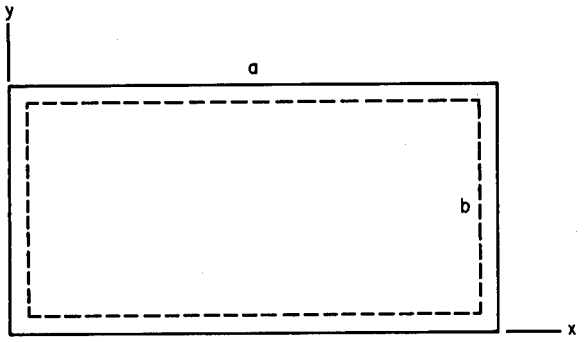


FIGURE 9.4.—SS–SS–SS–SS plate.

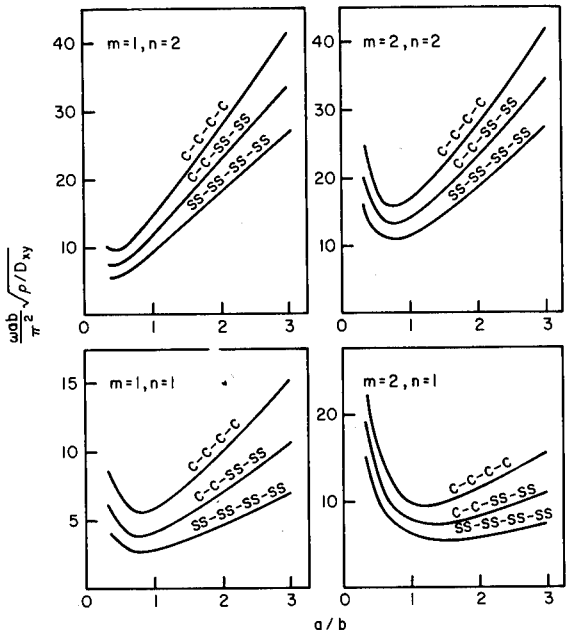


FIGURE 9.5.—Frequency parameter $\omega ab\sqrt{\rho/D_{xy}}/\pi^2$ for SS–SS–SS–SS, C–C–SS–SS, and C–C–C–C five-ply maple-plywood rectangular orthotropic plates. (After ref. 9.8)

Extensive experimental results are also given in reference 9.10 for several types of wood veneers and plywoods. In references 9.7 and 9.11, this experimental work is extended to study the effect on the frequencies when the grain of the veneer or plywood is not parallel to the sides of the plate.

Hoppmann, Huffington, and Magness (ref. 9.12) simulated a stiffened plate by taking a steel plate and milling longitudinal grooves into it. In one case, the grooves were on only one

TABLE 9.3.—*Fundamental Frequency Parameters for a SS–SS–SS–SS Square Orthotropic Plate*

Material	Properties			$\omega a^2\sqrt{\rho}$		
	D_x	D_y	D_{xy}	1 term	2 terms	Exact
Plywood	19. 1×10⁸	7. 1×10⁸	4. 4×10⁸	0. 5920×10⁵	0. 5917×10⁵	0. 5916×10⁵
Veneer	2. 97	. 21	. 69	. 2137	. 2136	. 2135

side of the plate, and, in the other, they were on both sides. The dimensions and spacing of the grooves are given in figure 9.6. The plate was then considered orthotropic for purposes of calculation. The statically measured orthotropic constants are set forth in table 9.4. Nine experimentally measured cyclic frequencies for each of the plates are listed in table 9.5, along with theoretical results as determined from equation (9.32) by using the data of table 9.4.

This work was further extended in reference 9.13 wherein an aluminum plate 11 by 11 inches by 0.275 inch thick had grooves 0.625 inch wide and 0.210 inch deep milled into one side of it. A typical repeating section of the plate was 0.75 inch wide, thereby giving 15 integral stiffeners each 0.125 inch wide across the width of the plate. Fifteen cyclic frequencies, both theoretical and experimental, are exhibited in table 9.6, where the grooves are assumed to run in the y-direction (i.e., $D_y > D_x$). The corresponding measured mode shapes are depicted in figure 9.7. The problem was discussed further in reference 9.14.

TABLE 9.4.—*Orthotropic Constants for Grooved Plates*

Type of plate	Orthotropic constants, lb-in.			
	D_x	D_y	D_{xy}	D_k
1 side grooved	33 300	26 300	25 210	8920
Both sides grooved	23 250	11 660	18 050	6480

TABLE 9.5.—*Cyclic Frequencies for Grooved SS–SS–SS–SS Square Plates*

Mode m/n	Cyclic frequency, cps, for plate—			
	Grooved on 1 side		Grooved on both sides	
	Theoretical	Experimental	Theoretical	Experimental
1/1	336	366	294	302
1/2	821	820	657	644
1/3	1640	1620	1250	1216
2/1	884	870	799	810
2/2	1345	1330	1175	1152
2/3	2145	2100	1782	1760
3/1	1806	1700	1643	1580
3/2	2251	2180	2022	2040
3/3	3026	2900	2645	2570

TABLE 9.6.—*Experimental and Theoretical Cyclic Frequencies for a Grooved SS–SS–SS–SS Square Plate*

[Theoretical values (from eq. (9.32)) are in parentheses]

n	Cyclic frequency, cps, for values of m of—				
	1	2	3	4	5
1	244 (238)	340 (336)	538 (534)	800 (831)	1152 (1220)
2	794 (800)	940 (954)	1020 (1100)	1268 (1344)	1580 (1689)
3	1700 (1950)	1800 (2020)	1840 (2150)	2110 (2349)	2340 (2638)

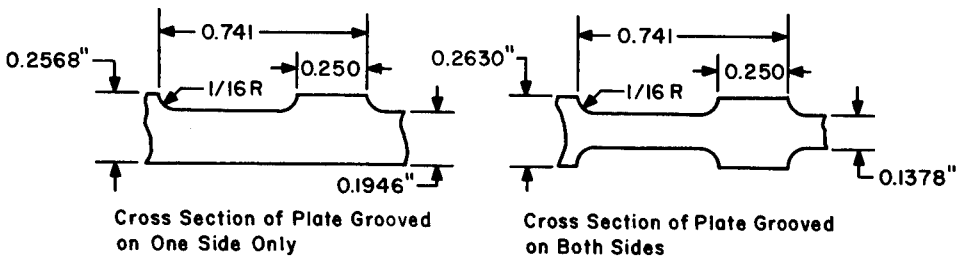


FIGURE 9.6.—Dimensions and spacing of grooves in a stiffened plate. (After ref. 9.12)

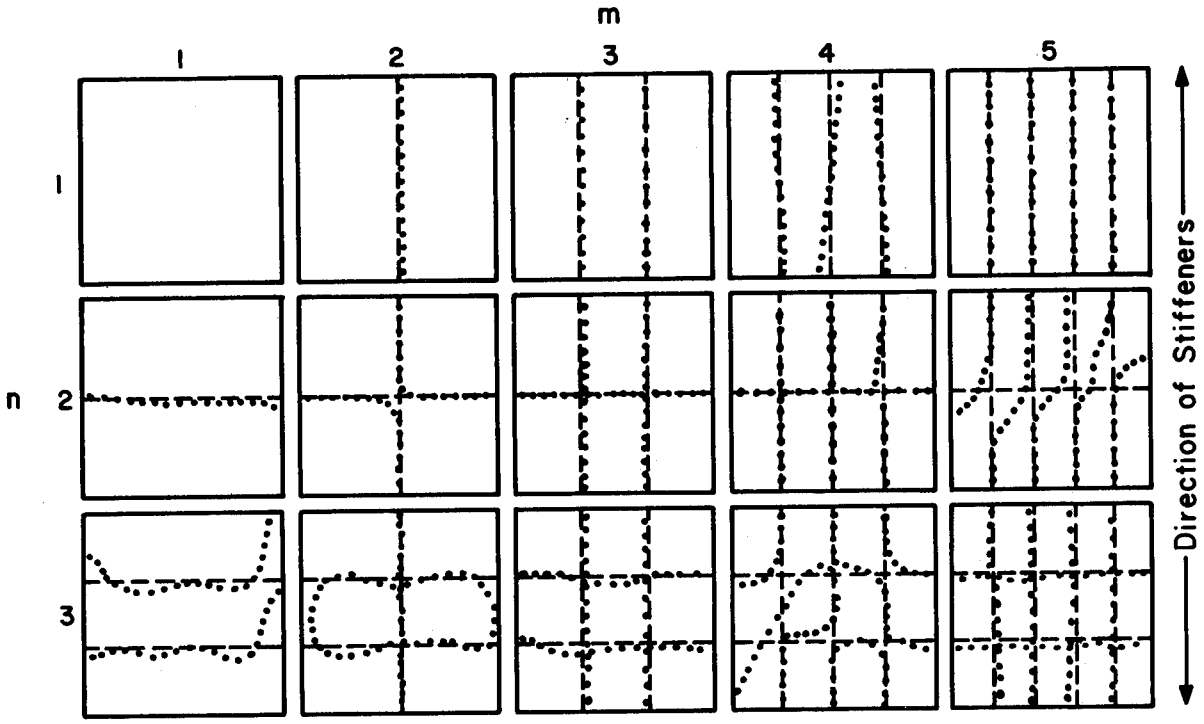


FIGURE 9.7.—Experimentally observed nodal patterns for grooved SS–SS–SS–SS square plate. (After ref. 9.13)

Wah (ref. 9.15) made a study in which he evaluated the accuracy of simulating the gross vibration modes of a beam-plate system by means of an orthotropic plate. The cross section of a plate having stiffeners of a particular size and spacing is shown in figure 9.8. The stiffeners are parallel to the x-direction. Both materials are assumed to be mild steel. First, an "exact" solution to the beam-plate structure is found by using classical isotropic plate theory for the plate and beam theory for the beams, including twisting. Continuity conditions are enforced across the stiffeners. This solution is compared with the results of orthotropic-plate theory as displayed in table 9.7. The orthotropic constants used in the orthotropic-plate idealization were $D_x/D=3.396$, $D_y/D=1$, and $D_{xy}/D=1.08$, where D is the flexural rigidity of the unstiffened plate. The quantity ρ_b is defined as the mass density per unit volume of stiffener, and R is the number of stiffeners. It would appear from table 9.7 that orthotropic-plate theory gives frequencies that are approximately 3 percent too high regardless of the stiffener spacing.

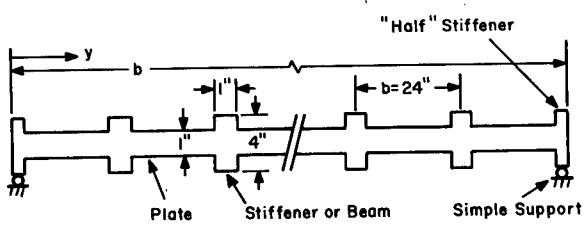


FIGURE 9.8.—Cross section of a stiffened plate. (After ref. 9.15)

A method for representing a simply supported gridwork of beams as an orthotropic plate is discussed in reference 9.16. The vibration of a SS–SS–SS–SS rectangular orthotropic plate is also discussed in references 9.8 and 9.17 to 9.20.

9.2.2 Two Opposite Sides Simply Supported

Let a rectangular plate have its sides $x=0$, $x=a$ simply supported as shown in figure 9.9. It is easily seen that the solution originally suggested by Voigt in 1893 (ref. 9.21) for the vibration of an isotropic plate having two

TABLE 9.7.—*Frequency Parameters* $\frac{\omega b^2}{R^2}\sqrt{\rho_b/D}$ *for a Stiffened SS–SS–SS–SS Rectangular Plate*

Mode	R	$\frac{\omega b^2}{R^2}\sqrt{\rho_b/D}$ for values of b/a of—					
		1.0		0.5		0.333	
		Exact	Eq. (9.32)	Exact	Eq. (9.32)	Exact	Eq. (9.32)
$m=1, n=1$	3	2. 602	2. 660	1. 345	1. 375	1. 150	1. 176
	4	1. 464	1. 496	. 757	. 774	. 647	. 662
	7	. 478	. 488	. 247	. 252	. 211	. 216
	12	. 163	. 166	. 0841	. 086	. 072	. 074
	20	. 0586	. 0599	. 0303	. 0309	. 0259	. 0265
$m=1, n=2$	3	5. 375	5. 501	4. 346	4. 453	4. 181	4. 284
	4	3. 026	3. 094	2. 447	2. 505	2. 354	2. 410
	7	. 988	1. 010	. 7995	. 818	. 769	. 787
	12	. 336	. 344	. 272	. 278	. 262	. 268
	20	. 1211	. 1238	. 098	. 1002	. 0942	. 0964
$m=2, n=1$	3	8. 043	8. 310			1. 649	1. 686
	4	4. 556	4. 674			. 928	. 948
	7	1. 492	1. 526	[a]	[a]	. 303	. 310
	12	. 508	. 519			. 103	. 105
	20	. 183	. 187			. 0367	. 0379
$m=2, n=2$	3	10. 34	10. 64			4. 593	4. 706
	4	5. 847	5. 985			2. 587	2. 647
	7	1. 912	1. 954	[b]	[b]	. 8450	. 8643
	12	. 651	. 665			. 2815	. 2941
	20	. 2343	. 2394			. 1035	. 1059

[a] Same as for $b/a=1$, $m=n=1$.
[b] Same as for $b/a=1$, $m=1$, $n=2$.

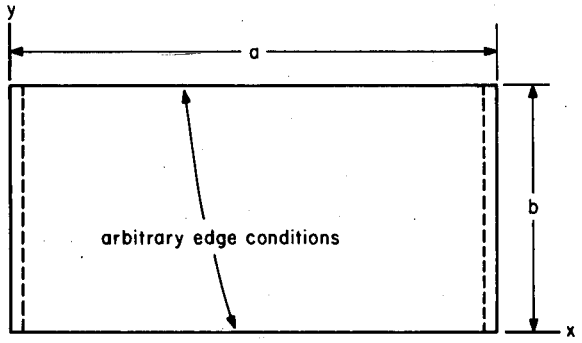


FIGURE 9.9.—Rectangular orthotropic plate having two opposite sides simply supported.

opposite sides simply supported is also applicable here. That is, assume

$$W(x,y)=\sum_{m=1}^{\infty} Y_m(y)\sin\alpha x \qquad (9.34)$$

with $\alpha=m\pi/a$, which clearly satisfies the boundary conditions $w=M_x=0$ at $x=0$, a. Substituting equation (9.34) into equation (9.22) yields

$$D_y\frac{d^4Y_m}{dy^4}-2\alpha^2D_{xy}\frac{d^2Y_m}{dy^2}+(\alpha^4D_x-\rho\omega^2)Y_m=0 \qquad (9.35)$$

which has a general solution

$$Y_m=A_m\sin\psi_m y+B_m\cos\psi_m y+C_m\sinh\phi_m y+D_m\cosh\phi_m y \qquad (9.36)$$

where

$$\left.\begin{aligned}\psi_m&=\alpha\left\{\left[\left(\frac{D_{xy}}{D_y}\right)^2-\left(\frac{D_x}{D_y}\right)+\frac{\omega^2\rho}{\alpha^4D_y}\right]^{1/2}-\left(\frac{D_{xy}}{D_y}\right)\right\}^{1/2}\\ \phi_m&=\alpha\left\{\left[\left(\frac{D_{xy}}{D_y}\right)^2-\left(\frac{D_x}{D_y}\right)+\frac{\omega^2\rho}{\alpha^4D_y}\right]^{1/2}+\left(\frac{D_{xy}}{D_y}\right)\right\}^{1/2}\end{aligned}\right\} \qquad (9.37)$$

It is seen that equations (9.34) and (9.36) are of exactly the same form as equation (4.21) for isotropic plates, the only difference being in the definitions of the frequency parameters ψ_m and ϕ_m.

The standard procedure for satisfying the boundary conditions along the sides $y=0$ and $y=b$, whatever they may be, is substitution of equation (9.36) into these conditions. The determinant of the resulting four homogeneous equations in A_m, B_m, C_m, and D_m is then set equal to zero for a nontrivial solution. This yields an exact solution for the frequencies. This procedure was followed by Huffington and Hoppmann (ref. 9.19), who presented frequency equations and mode shapes for all six cases arising from the sides $y=0$, b being either clamped, simply supported, or free, and the case of the sides elastically supported.

It is easily seen that the boundary conditions for simply supported or clamped sides are identical to those of the isotropic case. It was previously mentioned that the solutions to the governing differential equations also take the same form. Thus, substitution of the solution into the boundary conditions for the three sets of boundary conditions (SS–SS–SS–SS, SS–C–SS–C, and SS–C–SS–SS) would yield the same characteristic determinant *in terms of* ψ *and* ϕ as that for the isotropic case. However, ψ and ϕ are related differently than they are in the isotropic case; consequently, the eigenvalue results ($\omega^2\rho/\alpha^4 D$) obtained for the isotropic problems in the discussion of SS–SS–SS–SS, SS–C–SS–C, and SS–C–SS–SS rectangular plates (secs. 4.1, 4.2.1, and 4.2.2) cannot be directly applied here.

It should be noted that the form of solution given by equation (9.36) depends upon ψ and ϕ being real, positive constants. However, by looking at equations (9.37) it is seen that, depending upon the ratios D_x/D_y and D_{xy}/D_y, the constants ψ and ϕ may also take on zero, imaginary, or complex values. In these cases the form of equation (9.36) must be modified. A careful study of this phenomenon was done in the case of isotropic plates (see the discussion of rectangular plates with two opposite sides simply supported (sec. 4.2)), but no systematic investigation of this has been made for orthotropic plates.

By using the Rayleigh method, Hearmon (ref. 9.20) gave an alternate form of equation (9.29) for determining the fundamental frequency parameters of rectangular orthotropic plates having two opposite sides simply supported. Accordingly, the fundamental frequency parameter is determined from

$$\omega a^2\sqrt{\frac{\rho}{D_y}}=\sqrt{\pi^4\left(\frac{D_x}{D_y}\right)+J\left(\frac{a}{b}\right)^4+2\left(\frac{a}{b}\right)^2\left[K\left(\frac{D_x\nu_y}{D_y}\right)+2L\left(\frac{D_{xy}}{D_y}\right)\right]} \tag{9.38}$$

where J, K, and L are given in table 9.8 for the various cases. Fundamental frequency parameters for a five-ply maple-plywood plate determined by equation (9.38) are also given there.

For the SS–C–SS–C plate (fig. 4.4) the boundary conditions are given by equation (4.25). The frequency equation is given in reference 9.19 as

$$\alpha^2\frac{D_{xy}}{D_y}\sinh\phi b\sin\psi b+\phi\psi(1-\cosh\phi b\cos\psi b)=0 \tag{9.39}$$

with ψ and ϕ as given in equations (9.37). The mode shapes are

$$Y(y)=\frac{\cosh\phi y-\cos\psi y}{\cosh\phi b-\cos\psi b}-\frac{\psi\sinh\phi y-\phi\sin\psi y}{\psi\sinh\phi b-\phi\sin\psi b} \tag{9.40}$$

where ψ and ϕ are the roots of equation (9.39). The fundamental frequency parameters of a five-ply maple-plywood plate determined by this method in reference 9.22 are given in table 9.8.

Kanazawa and Kawai (ref. 9.23) solved this problem by an integral equation approach and gave numerical results for the fundamental frequency parameters of a square having various ratios of D_x/D_y and D_y/D_{xy}. These are exhibited in table 9.9. The values computed from equation (9.29) are found in reference 9.8; these can be compared with the footnoted values in

TABLE 9.8.—*Fundamental Frequency Parameters for a 5-Ply Maple-Plywood Rectangular Orthotropic Plate Having Various Boundary Conditions*

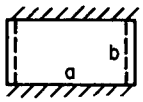
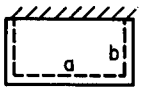
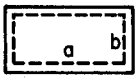
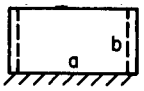
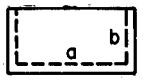
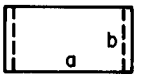
Boundary conditions	Constants in eq. (9.38)			$\omega a^2\sqrt{\rho/D_y}$		Physical parameters
	J	K	L	Ref. 9.20	Ref. 9.22	
	500. 56	121. 5	121. 5	94. 57	94. 56	$\frac{a}{b}=2.0$ $\frac{D_x}{D_y}=3.117$ $\nu_y\frac{D_x}{D_y}=0.12$ $\frac{D_{xy}}{D_y}=0.648$
	237. 81	113. 4	113. 4	68. 53	68. 52	
	97. 41	97. 41	97. 41	48. 65	48. 65	
	12. 37	−8. 5	45. 9	26. 22	26. 06	
	0	0	29. 61	20. 70	20. 65	
	0	0	0	17. 42	17. 39	

TABLE 9.9.—*Fundamental Frequency Parameters* $\omega a^2\sqrt{\rho/D_{xy}}$ *for SS–C–SS–C Square Orthotropic Plates Having the Sides* x=0 *and* x=a *Simply Supported*

$\frac{D_y}{D_{xy}}$	$\omega a^2\sqrt{\rho/D_{xy}}$ for values of D_x/D_{xy} of—				
	⅓	½	1	2	3
⅓	[a]21. 052	21. 440	22. 567	24. 664	[a]26. 595
½	23. 049	23. 406	24. 442	26. 397	28. 226
1	28. 124	28. 422	29. 285	30. 968	32. 507
2	36. 160	36. 383	37. 062	38. 384	39. 662
3	[a]42. 690	42. 878	43. 444	44. 589	[a]45. 696

[a] Compare with values from ref. 9.8.

table 9.9. The values from reference 9.8 are $\omega a^2\sqrt{\rho/D_{xy}}=21.0$, 26.5, 42.2, and 45.1.

Frequencies for this problem may also be determined from equation (9.29).

For the SS–C–SS–SS plate (fig. 4.8) the boundary conditions are given by equation (4.32). The frequency equation is given in reference 9.19 as

$$\phi \tan \psi b=\psi \tanh \phi b \tag{9.41}$$

with ψ and ϕ as given in equations (9.37). The mode shapes are

$$Y(y)=\frac{\sinh \phi y}{\sinh \phi b}-\frac{\sin \psi y}{\sin \psi b} \tag{9.42}$$

where ψ and ϕ are the roots of equation (9.41). The fundamental frequency of a five-ply maple-plywood plate determined by this method in reference 9.22 is given in table 9.8. The case when $a/b=10$ was also analyzed for the same material and gave $\omega a^2\sqrt{\rho/D_y}=1546.68$ when equation (9.41) was used and 1546.96 from equation (9.38).

For the SS–C–SS–F plate (see fig. 4.10) the boundary conditions are given by equation (4.36). The frequency equation is given in reference 9.19 as

$$(\psi^2\gamma^2-\phi^2\delta^2)\sinh\phi b\sin\psi b+\phi\psi[(\gamma^2+\delta^2)\cosh\phi b\cos\psi b+2\gamma\delta]=0 \quad (9.43)$$

with ψ and ϕ as given in equations (9.37) and

$$\left.\begin{aligned}\gamma&=D_y\phi^2-\alpha^2D_x\nu_y\\ \delta&=D_y\psi^2+\alpha^2D_x\nu_y\end{aligned}\right\} \quad (9.44)$$

The mode shapes are

$$Y(y)=\frac{\cosh\phi y-\cos\psi y}{\gamma\cosh\phi b+\delta\cos\psi b}-\frac{\psi\sinh\phi y-\phi\sin\psi y}{\psi\gamma\sinh\phi b+\phi\delta\sin\psi b} \quad (9.45)$$

Several roots of equation (9.43) were found in reference 9.22 for a five-ply maple-plywood plate having $a/b=2.0$ and having the material properties listed in table 9.8. The frequency parameters for this plate are given in table 9.10. The corresponding values obtained by the Rayleigh method from equation (9.29) are also given in reference 9.22 and are listed in table 9.10. It should be noted that for $m=1$ and $n=3$ the "exact" value is not lower than that of the Rayleigh method; this indicates round-off error in these calculations.

For the SS–SS–SS–F plate (see fig. 4.11) the boundary conditions are given by equation (4.40). The frequency equation is (ref. 9.19)

$$\frac{\tan\psi b}{\tanh\phi b}=\frac{\psi\gamma^2}{\phi\delta^2} \quad (9.46)$$

with ψ, ϕ, γ, and δ given by equations (9.37) and (9.44). The mode shapes are

$$Y(y)=\frac{\sin\phi y}{\sinh\phi b}+\frac{\gamma\sin\psi y}{\delta\sin\psi b} \quad (9.47)$$

TABLE 9.10.—*Frequency Parameters* $\omega a^2\sqrt{\rho/D_y}$ *for a SS–C–SS–F 5-Ply Maple-Plywood Rectangular Orthotropic Plate*

m	n	$\omega a^2\sqrt{\rho/D_y}$	
		Exact value (eq. (9.43))	Rayleigh method (eq. (9.29))
1	1	26.06	26.22
1	2	97.68	97.70
1	3	254.68	254.65
1	4	490.98	491.00
3	1	161.72	162.67
3	2	212.04	213.67
5	1	439.74	441.14

Some numerical results for this problem are given in table 9.8.

For the SS–F–SS–F plate (see fig. 4.12) the boundary conditions are given by equation (4.44). The frequency equation (ref. 9.19) is

$$(\psi^2\gamma^4-\phi^2\delta^4)\sinh\phi b\sin\psi b+2\phi\psi\gamma^2\delta^2(\cosh\phi b\cos\psi b-1)=0 \quad (9.48)$$

with ψ, ϕ, γ, and δ given by equations (9.37) and (9.44). The mode shapes are

$$Y(y)=\frac{\delta\cosh\phi y+\gamma\cos\psi y}{\gamma\delta(\cosh\phi b-\cos\psi b)}-\frac{\psi\gamma\sinh\phi y+\phi\delta\sin\psi y}{\psi\gamma^2\sinh\phi b-\phi\delta^2\sin\psi b} \quad (9.49)$$

Some numerical results for this problem are given in table 9.8.

Naruoka and Yonezawa (ref. 9.24) rewrote the differential equation (eq. (9.27)) as

$$\frac{\partial^4W}{\partial x^4}+2\kappa\sqrt{\frac{D_y}{D_x}}\frac{\partial^4W}{\partial x^2\partial y^2}+\frac{D_y}{D_x}\frac{\partial^4W}{\partial y^4}-\frac{\rho\omega^2}{D_x}W=0 \quad (9.50)$$

where

$$\kappa=D_{xy}/\sqrt{D_xD_y} \quad (9.51)$$

In this form it is clear that equation (9.50) is factorable if κ is either 1 or 0, and these values are used in reference 9.24. Furthermore, symmetry is taken advantage of by using

the $\bar{x}$ and y-axes (see fig. 4.12) through the plate centroid. Finally, the two cases

$$\left.\begin{aligned}\frac{\rho\omega^2}{D_x}\left(\frac{a}{m\pi}\right)^4>0\\ \frac{\rho\omega^2}{D_x}\left(\frac{a}{m\pi}\right)^4>1\end{aligned}\right\} \tag{9.52}$$

are considered, and eight specialized frequency equations are given which consider $\kappa=0$, $\kappa=1$, the separate cases of equations (9.52), and symmetric and antisymmetric modes in $\bar{y}$.

Particular attention is devoted in reference 9.24 to the first antisymmetric mode and the second symmetric mode, both taken with respect to $\bar{y}$. These modes are shown in figure 9.10. Variation in frequency parameter with D_x/D_y ratio is shown in figure 9.11 for $\kappa=0$, $\kappa=1$, and beam theory. Poisson's ratio $\nu=\nu_{xy}=\nu_{yx}$ is taken as zero and $a/b=2$. Further results for varying a/b ratios are given in figure 9.12 for the second symmetric mode. Finally, the ratio of second and third frequencies to the fundamental is set forth in table 9.11 for various a/b and D_x/D_y ratios. Poisson's ratio and κ are not given in table 9.11 but are presumed to be 0 and 1, respectively.

TABLE 9.11.—*Ratio of Second and Third Frequencies to the Fundamental for SS–F–SS–F Rectangular Orthotropic Plates*

$\frac{a}{b}$	D_x/D_y		
	4	100	200
1	1:1.5:2.6	1:1.1:1.4	1:1.1:1.3
2	1:2.4:6.4	1:1.3:2.2	1:1.2:1.9
4	1:4.8:20	1:2.1:5.1	1:1.9:3.9
8	1:7.1:73	1:4.0:17	1:3.4:13

For the plate elastically supported on the edges $y=0$ and $y=a$ (fig. 4.59) and simply supported on the other two edges, the boundary conditions are given by equations (4.71). The frequency equation is (ref. 9.19)

$$\begin{aligned}&\{\psi^2\gamma^2(\gamma^2-K_1K_3a^4)-\phi^2\delta^2(\delta^2-K_1K_3a^4)+K_2K_4a^4[\phi^2(\delta^2-K_1K_3a^4)-\psi^2(\gamma^2-K_1K_3a^4)]\\&\quad+a^2(\gamma+\delta)^2(K_1K_2\phi^2\psi^2-K_3K_4a^4)\}\sinh\phi b\sin\psi b+\phi\psi[2\gamma^2\delta^2-K_1K_3a^4(\gamma^2+\delta^2)\\&\quad-K_2K_4a^4(\delta^2+\gamma^2-2K_1K_3a^4)-a^4(K_2K_3+K_1K_4)(\gamma+\delta)^2]\cosh\phi b\cos\psi b\\&\quad+a\psi(\psi+\delta)[-K_3a^2\gamma^2+K_1\phi^2\delta^2-K_4a^2(\gamma^2-K_1K_3a^4)+K_2\phi^2(\delta^2-K_1K_3a^4)\\&\quad+K_2K_4a^4(K_3a^2-K_1\phi^2)]\sinh\phi b\cos\psi b+a\phi(\gamma+\delta)[K_3a^2\delta^2+K_1\psi^2\gamma^2\\&\quad+K_4a^2(\delta^2-K_1K_3a^4)+K_2\psi^2(\gamma^2-K_1K_3a^4)-K_2K_4(K_3a^2+K_1\psi^2)]\cosh\phi b\sin\psi b\\&\qquad-2\phi\psi(\gamma\delta+K_1K_3a^4)(\gamma\delta+K_2K_4a^4)=0\end{aligned} \tag{9.53}$$

with ψ, ϕ, γ, and δ given by equations (9.37) and (9.44) and the spring constants K_1, . . ., K_4 determined by equations (4.71). The mode shapes are

$$\begin{aligned}Y(y)=&[\psi(\gamma\delta+K_1K_3a^4)(\gamma\sinh\phi b+K_2a\phi\cosh\phi b)-\phi(\delta^2-K_1K_3a^4)(\delta\sin\psi b-K_2a\psi\cos\psi b)\\&+K_1a\phi\psi(\gamma+\delta)(\delta\cos\psi b+K_2a\psi\sin\psi b)]\cosh\phi y\\&+[\psi(\gamma^2-K_1K_3a^4)(\gamma\sinh\phi b+K_2a\phi\cosh\phi b)+K_1a\phi\psi(\gamma+\delta)(\gamma\cosh\phi b\\&+K_2a\phi\sinh\phi b)-\phi(\gamma\delta+K_1K_3a^4)(\delta\sin\psi b-K_2a\psi\cos\psi b)]\cos\psi y\\&+[-\psi(\gamma\delta+K_1K_3a^4)(\gamma\cosh\phi b+K_2a\phi\sinh\phi b)+\psi(\gamma^2-K_1K_3a^4)(\delta\cos\psi b+K_2a\psi\sin\psi b)\\&+K_3a^3(\gamma+\delta)(\delta\sin\psi b-K_2a\psi\cos\psi b)]\sinh\phi y+[K_3a^3(\gamma+\delta)(\gamma\sinh\phi b\\&+K_2a\phi\cosh\phi b)-\phi(\delta^2-K_1K_3a^4)(\gamma\cosh\phi b+K_2a\phi\sinh\phi b)\\&+\phi(\gamma\delta+K_1K_3a^4)(\delta\cos\psi b+K_2a\psi\sin\psi b)]\sin\psi y\end{aligned} \tag{9.54}$$

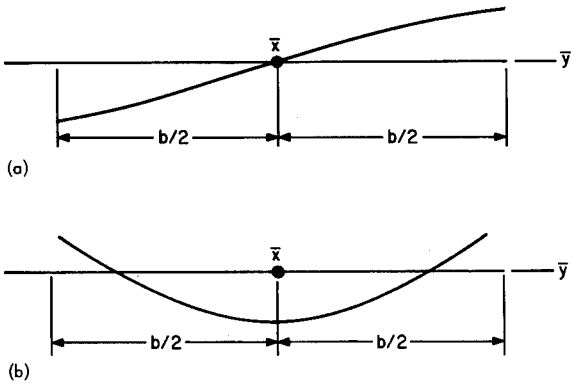


FIGURE 9.10.—Modes of a SS–F–SS–F rectangular orthotropic plate. (*a*) First antisymmetric mode taken with respect to $\bar{y}$. (*b*) Second symmetric mode taken with respect to $\bar{y}$. (After ref. 9.24)

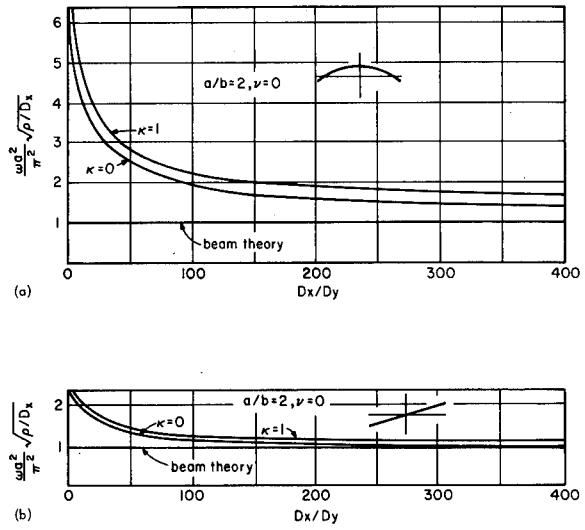


FIGURE 9.11.—Frequency parameters for SS–F–SS–F rectangular orthotropic plates having $\nu=0$ and $a/b=2$; $\kappa=D_{xy}\sqrt{D_xD_y}$. (*a*) First antisymmetric mode with respect to $\bar{y}$. (*b*) Second symmetric mode with respect to $\bar{y}$. (After ref. 9.24)

9.2.3 All Sides Clamped

The problem for the plate with all sides clamped is described by figure 4.18. Frequency parameters may be calculated from a formula based upon the Rayleigh method given previously as equation (9.29). Plots of frequency parameter variation with a/b ratio for four modes were given previously in figure 9.5 for a particular maple-plywood plate.

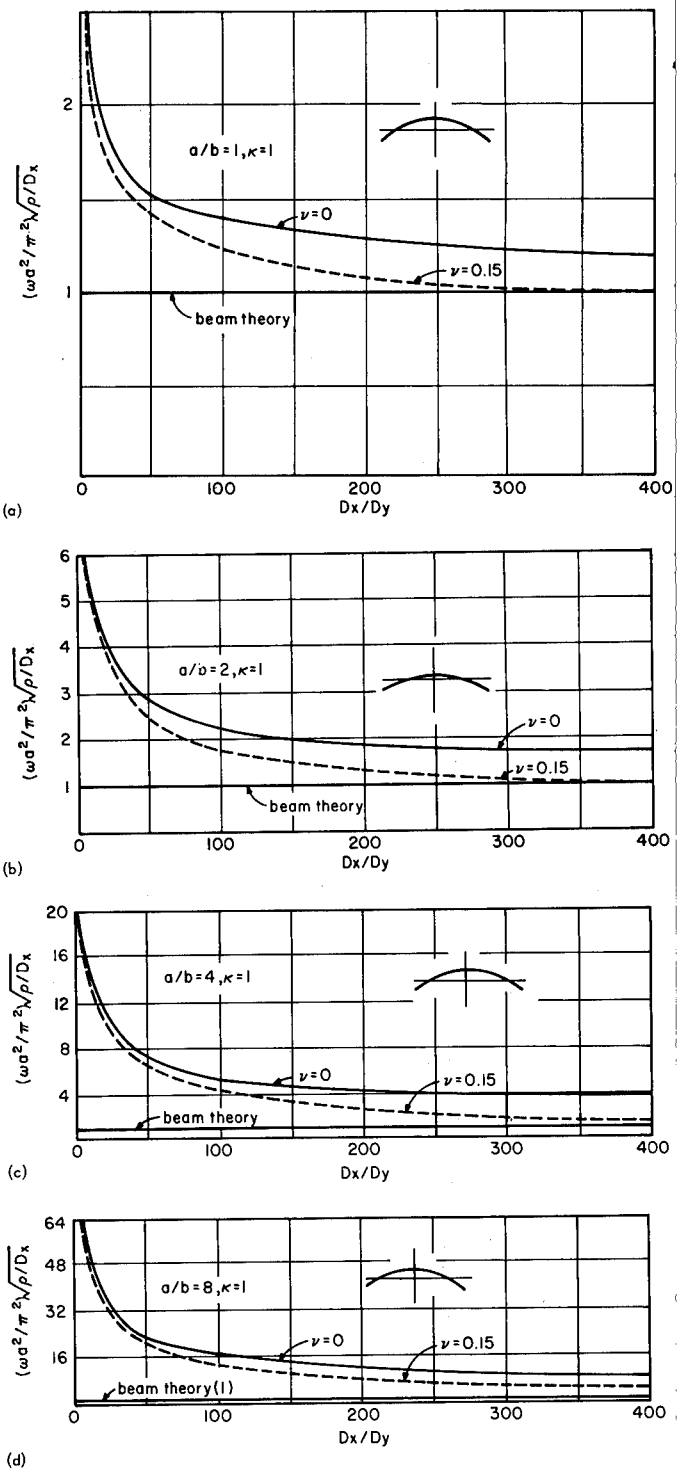


FIGURE 9.12.—Frequency parameters for the second symmetric mode (with respect to $\bar{y}$) of SS–F–SS–F rectangular orthotropic plates for various a/b ratios; $\kappa=1$. (*a*) $a/b=1$. (*b*) $a/b=2$. (*c*) $a/b=4$. (*d*) $a/b=8$. (After ref. 9.24)

Another Rayleigh solution is obtained in references 9.10 and 9.17 by taking the deflection function

$$W(\bar{x},\bar{y})=\left[\bar{x}^2-\left(\frac{a}{2}\right)^2\right]^2\left[\bar{y}^2-\left(\frac{b}{2}\right)^2\right]^2 \quad (9.55)$$

which yields the fundamental frequency

$$\omega=\frac{22.45}{a^2}\sqrt{\frac{1}{\rho}\left[D_x+D_y\left(\frac{a}{b}\right)^4+\frac{4}{7}D_{xy}\left(\frac{a}{b}\right)^2\right]} \quad (9.56)$$

This result was also obtained in reference 9.16 by using the Galerkin method and equation (9.55). In reference 9.17 the function

$$W(\bar{x},\bar{y})=\left(1+\cos\frac{2\pi x}{a}\right)\left(1+\cos\frac{2\pi y}{b}\right) \quad (9.57)$$

is used, giving

$$\omega=\frac{22.79}{a^2}\sqrt{\frac{1}{\rho}\left[D_x+D_y\left(\frac{a}{b}\right)^4+\frac{2}{3}D_{xy}\left(\frac{a}{b}\right)^2\right]} \quad (9.58)$$

by the Rayleigh method. Finally, reference 9.8 gives the Rayleigh solution using beam functions described previously as

$$\omega=\frac{22.36}{a^2}\sqrt{\frac{1}{\rho}\left[D_x+D_y\left(\frac{a}{b}\right)^4+0.605D_{xy}\left(\frac{a}{b}\right)^2\right.} \quad (9.59)$$

this latter clearly being the best of the three results listed, because it gives the lowest upper bound unless D_{xy} is considerably larger than D_x and D_y.

Further improvement of the theoretical frequencies was obtained in reference 9.10 by taking the two-term deflection function

$$W(\bar{x},\bar{y})=\left[\bar{x}^2-\left(\frac{a}{2}\right)^2\right]^2\left[\bar{y}^2-\left(\frac{b}{2}\right)^2\right]^2 \left\{A_1+A_2\left[\bar{x}^2-\left(\frac{a}{2}\right)^2\right]\left[\bar{y}^2-\left(\frac{b}{2}\right)^2\right]\right\} \quad (9.60)$$

and using the Rayleigh-Ritz procedure. The convergence of frequency parameters when equations (9.55) and (9.60) are used can be seen in table 9.12 for two types of square plates made of birch. Results are also included for the isotropic case for comparison with Tomotika's "exact" solution (ref. 9.25). (See discussion of the C–C–C–C rectangular plate (sec. 4.3.1).)

TABLE 9.12.—*Frequency Parameters* $\omega a^2\sqrt{\rho}$ *for C–C–C–C Square Orthotropic Plates Made of Birch*

Method	$\omega a^2\sqrt{\rho}$ for—		
	Isotropic case	5-ply plate[a]	Veneer plate[b]
Rayleigh	$36.000\sqrt{D}$	12.026×10^5	4.244×10^5
Rayleigh-Ritz	$35.996\sqrt{D}$	12.013×10^5	4.241×10^5
Exact	$35.984\sqrt{D}$	----------	----------

[a] $D_x=19.1\times10^8$; $D_y=7.1\times10^8$; $D_{xy}=4.4\times10^8$.
[b] $D_x=2.97\times10^8$; $D_y=0.21\times10^8$; $D_{xy}=0.69\times10^8$.

Many experimentally determined fundamental frequencies are also given in reference 9.10 for plywood and veneer plates made of various wooden materials. In references 9.7 and 9.11 this experimental work is extended in order to study the effect on the frequencies when the grain of the veneer or plywood is not parallel to the sides of the plate.

Huffington (ref. 9.26) postulated the existence of nonparallel node lines for clamped orthotropic plates; this idea was based upon his observations of the numerical behavior of a two-term Ritz solution using beam functions. This phenomenon is predicted by the curves of figure 9.13 which show frequency parameters as functions of a/b ratio for the case when $D_x/D_{xy}=1.543$ and $D_y/D_{xy}=4.810$. The numerical results show that the curves (each associated with a mode shape) do not cross but approach each other and veer away. In the vicinity of the location where the curves approach each other, there is a rapid change in nodal patterns, as depicted in figure 9.14. It must be remarked that this phenomenon has been observed elsewhere (see discussion of the C–C–C–C rectangular plate (sec. 4.3.1) and that of the C–F–F–F rectangular plate (sec. 4.3.12)) and the question exists of whether it is the result of numerical truncation.

Kanazawa and Kawai (ref. 9.23) solved this problem by an integral-equation approach and gave numerical results for the fundamental frequency parameters of a square having

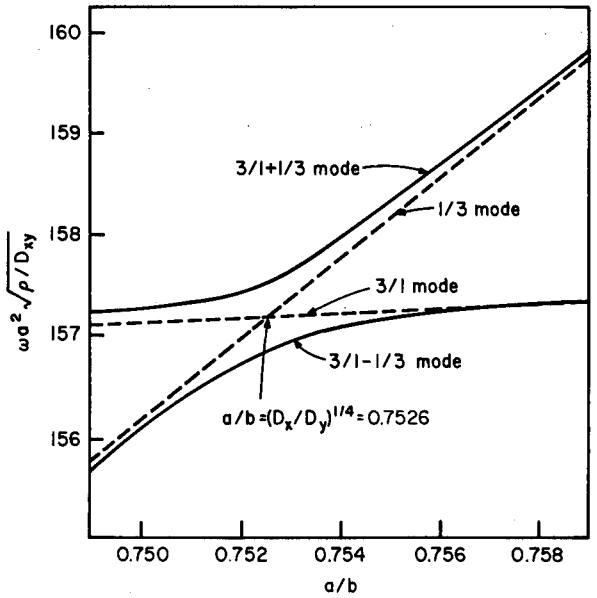


FIGURE 9.13.—Frequency parameters $\omega a^2\sqrt{\rho/D_{xy}}$ against a/b ratio for a clamped orthotropic plate. $D_x/D_{xy}=1.543$; $D_y/D_{xy}=4.810$. (After ref. 9.26)

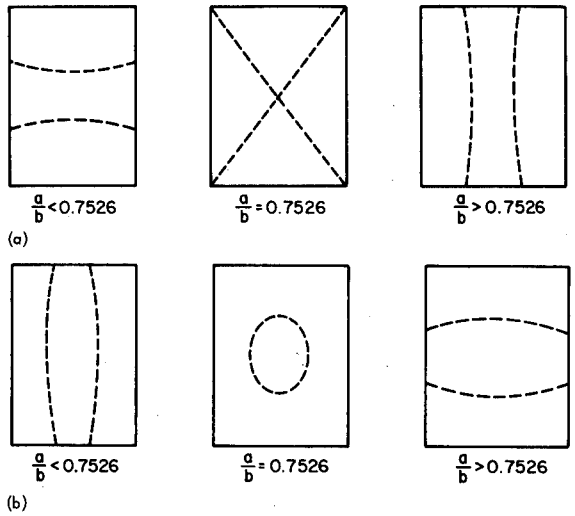


FIGURE 9.14.—Nodal patterns in the vicinity of a transition point. (*a*) Nodal patterns for mode 3/1—1/3. (*b*) Nodal patterns for mode 3/1+1/3. (After ref. 9.26)

various ratios of D_x/D_{xy} and D_y/D_{xy}. These are exhibited in table 9.13. An interesting plot of the results of table 9.13 is given in figure 9.15. It would appear from this figure that the variation in the square of the frequency with either D_x or D_y is linear.

TABLE 9.13—*Fundamental Frequency Parameters* $\omega a^2\sqrt{\rho/D_{xy}}$ *for C–C–C–C Orthotropic Square Plates*

$\frac{D_y}{D_{xy}}$	$\omega a^2\sqrt{\rho/D_{xy}}$ for values of D_x/D_{xy} of—				
	⅛	½	1	2	3
⅛	25. 034	26. 741	31. 235	38. 674	44. 837
½	26. 741	28. 346	32. 625	39. 775	45. 820
1	31. 235	32. 625	36. 408	42. 939	48. 584
2	38. 674	39. 775	42. 939	48. 604	53. 661
3	44. 837	45. 820	48. 584	53. 661	58. 283

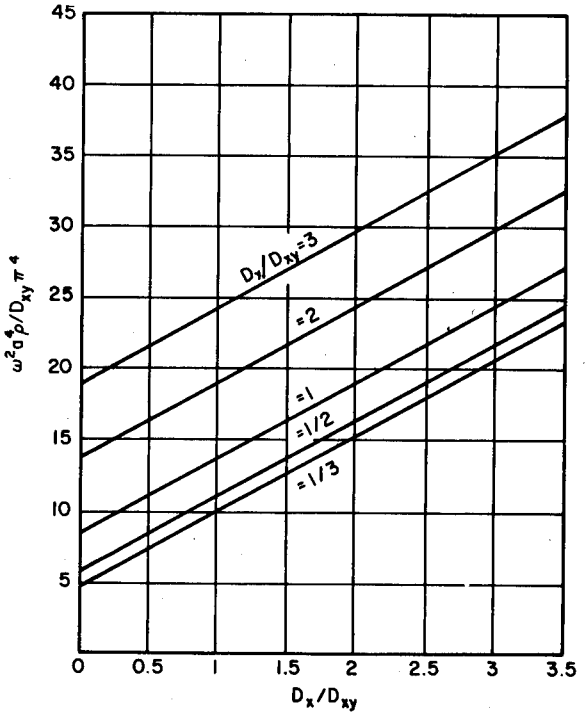


FIGURE 9.15.—Fundamental frequency parameters $\omega^2 a^4\rho/D_{xy}\pi^4$ against D_x/D_{xy} and D_y/D_{xy} for C–C–C–C orthotropic square plates. (After ref. 9.23)

9.2.4 Other Boundary Conditions

Frequency parameters for C–C–C–SS and C–C–SS–SS rectangular orthotropic plates may be determined from the Rayleigh formula given previously as equation (9.29). Plots of frequency parameter against a/b ratio for four modes are given for the C–C–SS–SS case in figure 9.5.

An integral-equation approach (ref. 9.23) gave numerical results for the fundamental frequency parameters of square plates having C–C–C–SS and C–C–SS–SS edges. These are listed in tables 9.14 and 9.15.

TABLE 9.14.—*Fundamental Frequency Parameters* $\omega a^2\sqrt{\rho/D_{xy}}$ *for C–C–C–SS Orthotropic Plates Having the Sides* x=0 *and* x=a *Clamped*

$\frac{D_y}{D_{xy}}$	$\omega a^2\sqrt{\rho/D_{xy}}$ for values of D_x/D_y of—				
	⅓	½	1	2	3
⅓	22. 848	24. 706	29. 516	37. 239	43. 652
½	23. 796	25. 587	30. 261	37. 864	44. 162
1	26. 361	27. 989	32. 328	39. 542	45. 576
2	30. 786	32. 191	36. 031	42. 634	48. 330
3	34. 604	35. 891	39. 393	45. 494	50. 874

TABLE 9.15.—*Fundamental Frequency Parameters* $\omega a^2\sqrt{\rho/D_{xy}}$ *for C–C–SS–SS Orthotropic Square Plates*

$\frac{D_y}{D_{xy}}$	$\omega a^2\sqrt{\rho/D_{xy}}$ for values of D_x/D_{xy} of—				
	⅓	½	1	2	3
⅓	20. 428	21. 483	24. 302	29. 061	33. 056
½	21. 483	22. 493	25. 194	29. 794	33. 749
1	24. 302	25. 194	27. 647	31. 910	35. 599
2	29. 061	29. 794	31. 910	35. 681	39. 064
3	33. 057	33. 749	35. 599	39. 064	42. 184

9.2.5 Circular Plates Having Rectangular Orthotropy

The boundary conditions for a circular plate dictate that solutions must be obtained in polar coordinates. In this case the differential equation for the case of rectangular orthotropy (eq. (9.22)) must be transformed into polar coordinates. It has been shown by Hoppmann (ref. 9.27) that the resulting equation is

$$\alpha_1\frac{\partial^4 w}{\partial r^4}+\frac{\alpha_2}{r}\frac{\partial^4 w}{\partial r^3\partial\theta}+\frac{\alpha_3}{r^2}\frac{\partial^4 w}{\partial r^2\partial\theta^2}+\frac{\alpha_4}{r^3}\frac{\partial^4 w}{\partial r\partial\theta^3}+\frac{\alpha_5}{r^4}\frac{\partial^4 w}{\partial\theta^4}+\frac{\alpha_6}{r}\frac{\partial^3 w}{\partial r^3}+\frac{\alpha_7}{r^2}\frac{\partial^2 w}{\partial r^2}+\frac{\alpha_8}{r^3}\frac{\partial^3 w}{\partial r\partial\theta^2}+\frac{\alpha_9}{r^4}\frac{\partial^3 w}{\partial\theta^3}+\frac{\alpha_{10}}{r^3}\frac{\partial^2 w}{\partial r\partial\theta}+\frac{\alpha_{11}}{r^4}\frac{\partial^2 w}{\partial\theta^2}+\frac{\alpha_{12}}{r^3}\frac{\partial w}{\partial r}+\frac{\alpha_{13}}{r^4}\frac{\partial w}{\partial\theta}+\rho\frac{\partial^2 w}{\partial t^2}=0 \quad (9.61)$$

where

$$\alpha_1=\beta(s_{22}s_{66}-s_{26}^2)$$
$$\alpha_2=4\beta(s_{12}s_{26}-s_{22}s_{16})$$
$$\alpha_3=-2\beta[(s_{12}s_{66}-s_{26}s_{16})-2(s_{11}s_{22}-s_{12}^2)]$$
$$\alpha_4=-4\beta(s_{11}s_{26}-s_{12}s_{16})$$
$$\alpha_5=\beta(s_{11}s_{66}-s_{16}^2)$$
$$\alpha_6=2\beta(s_{22}s_{66}-s_{26}^2)$$
$$\alpha_7=-\beta(s_{11}s_{66}-s_{16}^2)$$
$$\alpha_8=2\beta[(s_{12}s_{66}-s_{26}s_{16})-2(s_{11}s_{22}-s_{12}^2)]$$
$$\alpha_9=4\beta(s_{11}s_{26}-s_{12}s_{16})$$
$$\alpha_{10}=4\beta[(s_{12}s_{26}-s_{16}s_{22})-(s_{11}s_{26}-s_{12}s_{16})]$$
$$\alpha_{11}=-2\beta[(s_{12}s_{66}-s_{12}s_{26})-2(s_{11}s_{22}-s_{12}^2)-(s_{11}s_{66}-s_{16}^2)]$$
$$\alpha_{12}=\beta(s_{11}s_{66}-s_{16}^2)$$
$$\alpha_{13}=-4\beta[(s_{12}s_{26}-s_{16}s_{22})-(s_{11}s_{26}-s_{16}s_{12})]$$
$$\beta=h^3/12D(s)$$

$$D(s)=\begin{vmatrix} s_{11} & s_{12} & s_{16} \\ s_{12} & s_{22} & s_{26} \\ s_{16} & s_{26} & s_{66} \end{vmatrix}$$

$$s_{11}=\frac{1}{E_x}\cos^4\theta+\left(-2\frac{\nu_y}{E_x}+\frac{1}{G}\right)\sin^2\theta\cos^2\theta+\frac{1}{E_y}\sin^4\theta$$

$$s_{22}=\frac{1}{E_x}\sin^4\theta+\left(-2\frac{\nu_y}{E_x}+\frac{1}{G}\right)\sin^2\theta\cos^2\theta+\frac{1}{E_y}\cos^4\theta$$

$$s_{66}=4\left(\frac{1}{E_x}+\frac{1}{E_y}+2\frac{\nu_y}{E_x}\right)\sin^2\theta\cos^2\theta+\frac{1}{G}(\cos^2\theta-\sin^2\theta)^2$$

$$s_{12}=\left(\frac{1}{E_x}+\frac{1}{E_y}-\frac{1}{G}\right)\sin^2\theta\cos^2\theta-\frac{\nu_y}{E_x}(\cos^4\theta-\sin^4\theta)$$

$$s_{16}=\sin\theta\cos\theta\left[\frac{2}{E_y}\sin^2\theta-\frac{2}{E_x}\cos^2\theta+\left(-2\frac{\nu_y}{E_x}+\frac{1}{G}\right)(\cos^2\theta-\sin^2\theta)\right]$$

$$s_{26}=\sin\theta\cos\theta\left[\frac{2}{E_y}\cos^2\theta-\frac{2}{E_x}\sin^2\theta-\left(-2\frac{\nu_y}{E_x}+\frac{1}{G}\right)(\cos^2\theta-\sin^2\theta)\right] \quad (9.62)$$

where θ is the angle measured from the x-axis. Because of the formidability of equation (9.61) it appears that no solutions to it exist in the literature. Nevertheless, it would appear that convergent solutions in the form of equation (1.15) are certainly possible.

Experimental results were obtained in reference 9.27 for a clamped circular plate of aluminum having longitudinal slots milled into it to approximate an orthotropic plate. The cross section of the plate is shown in figure 9.16. Measured frequencies and nodal patterns are given in figure 9.17. It can be expected that the frequencies for higher modes will be considerably different from those of a homogeneous, orthotropic plate.

A one-term Galerkin solution (ref. 9.16) gave the fundamental frequency for the clamped orthotropic circular plate as

$$\omega^2=\frac{41.52}{\rho a^4}\left(D_x+\frac{2}{3}D_{xy}+D_y\right) \qquad (9.63)$$

(see discussion of rectangular plate with two opposite sides simply supported (sec. 9.2.2)). The identical result was obtained in reference 9.17 by using the Rayleigh-Ritz method.

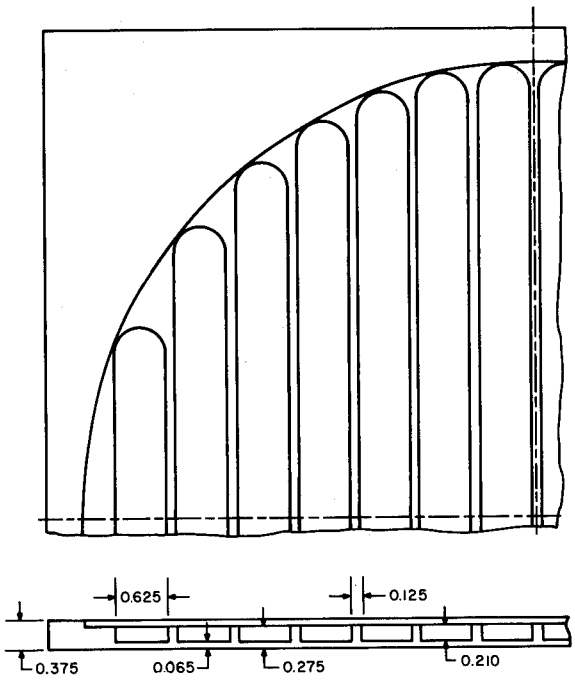


FIGURE 9.16.—Cross section of stiffened plate; dimensions are in inches. (After ref. 9.27)

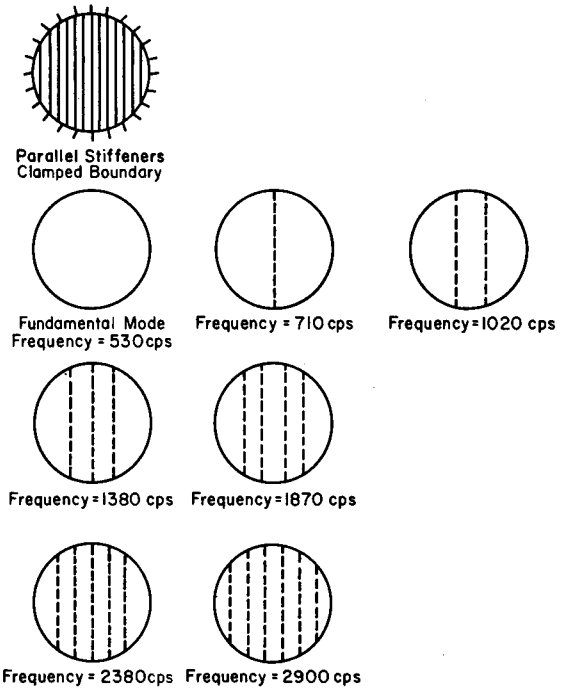


FIGURE 9.17.—Experimentally observed cyclic frequencies and nodal patterns for a clamped circular plate having stiffeners. (After ref. 9.27)

9.2.6 Elliptical Plates Having Rectangular Orthotropy

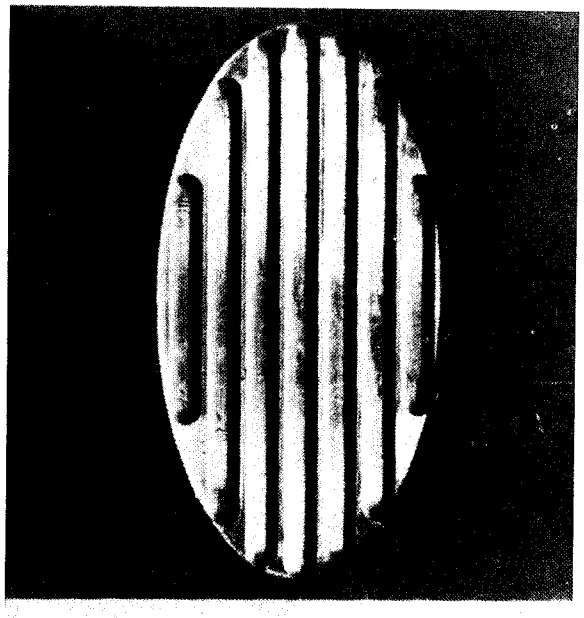
In reference 9.16 the Galerkin method is used with the one-term deflection function

$$w(x,y)=\left(1-\frac{x^2}{a^2}-\frac{y^2}{b^2}\right)^2 \qquad (9.64)$$

(see fig. 3.1) to analyze the clamped orthotropic elliptical plate. The resulting frequency is

$$\omega^2=\frac{41.52}{\rho}\left(\frac{D_x}{a^4}+\frac{2}{3}\frac{D_{xy}}{a^2b^2}+\frac{D_y}{b^4}\right) \qquad (9.65)$$

In reference 9.27 experimental results were obtained for clamped elliptical plates of aluminum having longitudinal slots milled into them parallel to the axes as shown in figure 9.18. A cross section showing slot dimensions is seen in figure 9.16. The a/b ratio for the ellipses was apparently 2.0. Resulting frequencies and nodal patterns for the two plates are shown in figures 9.19 and 9.20.



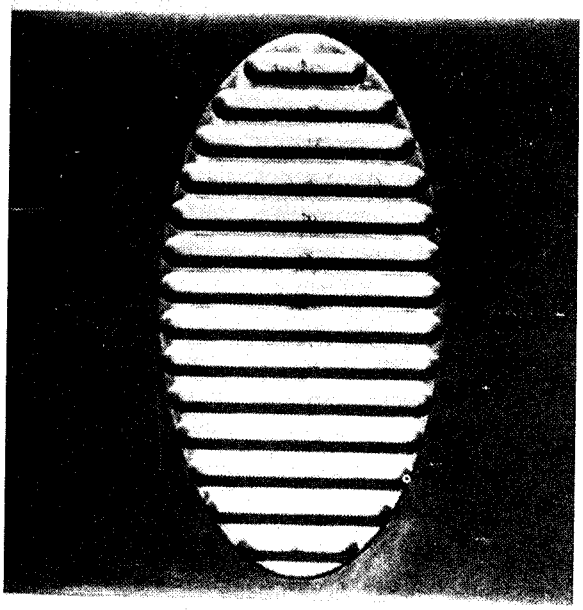


FIGURE 9.18.—Elliptical plate with slots milled parallel to major and minor axes to simulate an orthotropic plate. (From ref. 9.27)

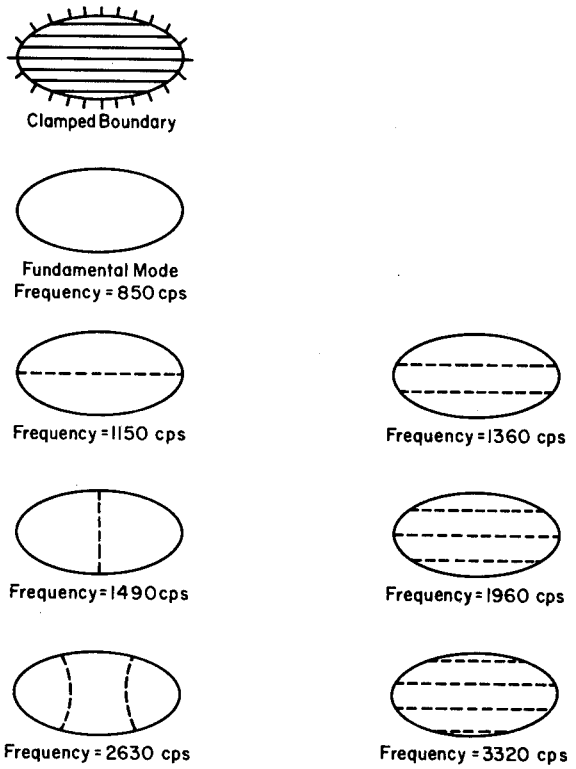


FIGURE 9.19.—Experimentally observed cyclic frequencies and nodal patterns for a clamped elliptical plate having stiffeners parallel to the major axis. (After ref. 9.27)

REFERENCES

9.1. AKASAKA, T.; AND TAKAGISHI, T.: Vibration of Corrugated Diaphragm. Bull. JSME, vol. 1, no. 3, 1958, pp. 215–221.

9.2. BORSUK, K.: Free Vibration of Rotations of a Cylindrically Orthotropic Circular Plate. Arch. Mech. Stos., vol. 12, no. 5/6, 1960, pp. 649–665.

9.3. MINKARAH, I. A.; AND HOPPMANN, W. H., II: Flexural Vibrations of Cylindrically Aeolotropic Circular Plates. Jour. Acoust. Soc. Am., vol. 36, no. 3, Mar. 1964, pp. 470–475.

9.4. PANDALAI, K. A. V.; AND PATEL, S. A.: Natural Frequencies of Orthotropic Circular Plates. AIAA J., vol. 3, no. 4, Apr. 1965, pp. 780–781.

9.5. PYESYENNIKOVA, N. K.; AND SAKHAROV, I. E.: Natural Vibrations Frequencies of the Fundamental of Annular Plates With a Cylindrical Anisotropy. Izv. An SSSR, OTN, Mekh. i Mashin., no. 6, 1959, pp. 134–136. (In Russian.)

308-337 O—70——18

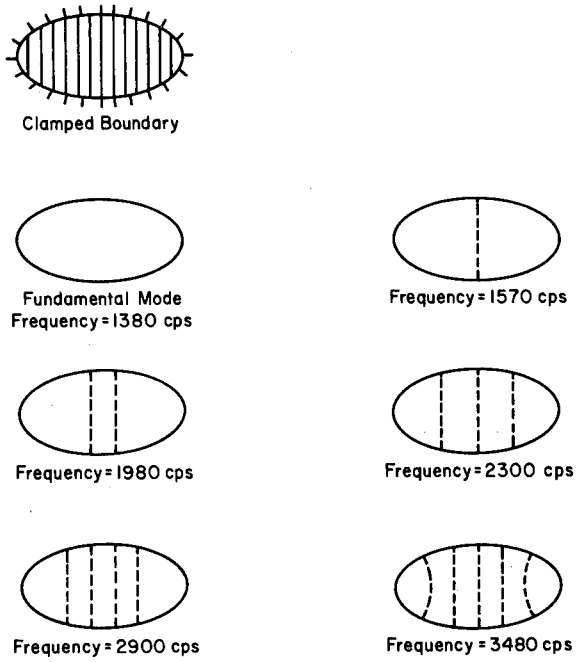


FIGURE 9.20.—Experimentally observed cyclic frequencies and nodal patterns for a clamped elliptical plate having stiffeners parallel to the minor axis. (After ref. 9.27)

9.6. LOVE, A. E.: The Mathematical Theory of Elasticity. Fourth ed., Cambridge Univ. Press, 1927.

9.7. HEARMON, R. F. S.; AND SEKHAR, A. C.: The Frequency of Vibration and the Deflection Under Concentrated Load of Rectangular Plywood Plates. Forest Prod. Res. Lab. (Princes Risborough, England), Sept. 1947.

9.8. HEARMON, R. F. S.: The Frequency of Flexural Vibration of Rectangular Orthotropic Plates With Clamped or Supported Edges. J. Appl. Mech., vol. 26, nos. 3–4, Dec. 1959, pp. 537–540.

9.9. WARBURTON, G. B.: The Vibration of Rectangular Plates. Proc. Inst. Mech. Engrs. (London), Ser. A, vol. 168, no. 12, 1954, pp. 371–381.

9.10. HEARMON, R. F. S.: The Fundamental Frequency of Vibration of Rectangular Wood and Plywood Plates. Proc. Phys. Soc. (London), vol. 58, 1946, pp. 78–92.

9.11. HEARMON, R. F. S.; AND SEKHAR, A. C.: The Frequency of Vibration and the Deflection Under Concentrated Load of Rectangular Plywood Plates. Composite Wood, vol. 1, 1954, pp. 77–87.

9.12. HOPPMANN, W. H.; HUFFINGTON, N. J.; AND MAGNESS, L. S.: A Study of Orthogonally Stiffened Plates. J. Appl. Mech., vol. 23, no. 3, Sept. 1956, pp. 343–350.

9.13. HOPPMANN, W. H.; AND MAGNESS, L. S.: Nodal Patterns of the Free Flexural Vibrations of Stiffened Plates. J. Appl. Mech., vol. 24, no. 4, Dec. 1957, pp. 526–530.

9.14. HOPPMANN, W. H.: Bending of Orthogonally Stiffened Plates. J. Appl. Mech., vol. 22, no. 2, June 1955, pp. 267–271.

9.15. WAH, THEIN: Vibration of Stiffened Plates. Aeron. Quart., vol. 15, no. 3, Aug. 1964, pp. 285–298.

9.16. REDDY, D. V.; AND RAJAPPA, N. R.: Frequency Analysis of Certain Interconnected Beam Systems. Appl. Sci. Res., vol. 12, sec. A, pp. 407–416.

9.17. LEKHNITSKI, S. T.: Anisotropic Plates. GITTL (Moscow) 1957. (In Russian.) Also, Am. Iron and Steel Inst. (New York, N.Y.), June 1956.

9.18. AMBARTSUMYAN, S. A.; AND KHACHATRYAN, A. A.: On the Stability and Vibrations of Anisotropic Plates. Izv. An SSSR, OTN, Mate. i. Mashin., no. 1, 1960, pp. 113–122. (In Russian.)

9.19. HUFFINGTON, N. J., JR.; AND HOPPMANN, W. H., II: On the Transverse Vibrations of Rectangular Orthotropic Plates. J. Appl. Mech., vol. 25, no. 3, Sept. 1958, pp. 389–395.

9.20. HEARMON, R. F. S.: On the Transverse Vibrations of Rectangular Orthotropic Plates. J. Appl. Mech., vol. 26, no. 2, June 1959, pp. 307–309.

9.21. VOIGT, W.: Bemerkungen zu dem Problem der transversalen Schwingungen rechteckiger Platten. Nachr. Ges. Wiss. (Göttingen), no. 6, 1893, pp. 225–230.

9.22. HUFFINGTON, N. J., JR.; AND HOPPMANN, W. H., II: Authors Closure to "Comments on 'On the Transverse Vibrations of Rectangular Orthotropic Plates.' " J. Appl. Mech., vol. 26, no. 2, June 1959, p. 308.

9.23. KANAZAWA, T.; AND KAWAI, T.: On the Lateral Vibration of Anisotropic Rectangular Plates (Studied by the Integral Equation). Proc. 2d Jap. Natl. Congr. Appl. Mech., 1952, pp. 333–338.

9.24. NARUOKA, M.; AND YONEZAWA, H.: A Study on the Period of the Free Lateral Vibration of the Beam Bridge by the Theory of the Orthotropic Rectangular Plate. Ingr.-Arch., vol. 26, no. 1, 1958, pp. 20–29.

9.25. TOMOTIKA, S.: On the Transverse Vibration of a Square Plate With Clamped Edges. Aeron. Res. Inst. Rept., Tokyo Univ., vol. 10, 1935, p. 301.

9.26. HUFFINGTON, N. J., JR.: On the Occurrence of Nodal Patterns of Nonparallel Form in Rectangular Orthotropic Plates. J. Appl. Mech., Brief Notes, vol. 28, no. 3, Sept. 1961, pp. 459–460.

9.27. HOPPMANN, W. H., II: Flexural Vibration of Orthogonally Stiffened Circular and Elliptical Plates. Proc. 3d U.S. Natl. Congr. Appl. Mech., June 1958, pp. 181–187.

Chapter 10

Plates With Inplane Forces

In this section the effects of forces acting in the plane of the undeformed middle surface of the plate will be considered. The differential equation of motion expressed in rectangular coordinates in this case becomes (see the appendix):

$$D_x\frac{\partial^4 w}{\partial x^4}+2D_{xy}\frac{\partial^4 w}{\partial x^2\,\partial y^2}+D_y\frac{\partial^4 w}{\partial y^4}+\rho\frac{\partial^2 w}{\partial t^2} =N_x\frac{\partial^2 w}{\partial x^2}+2N_{xy}\frac{\partial^2 w}{\partial x\,\partial y}+N_y\frac{\partial^2 w}{\partial y^2} \quad (10.1)$$

where D_x, D_y, and D_{xy} are the constants of rectangular orthotropy, as used extensively in the discussion of rectangular orthotropy of anisotropic plates (sec. 9.2). Because no published results are known for plate vibrations when both inplane forces and orthotropy are present, only the isotropic constant D will appear in the remainder of this section.

The inplane force intensities N_x, N_y, and N_{xy} are assumed to be functions of only the spatial coordinates x, y or r, θ. That is, they do not depend upon time nor upon the transverse deflection w. These assumptions are required in order that—

(1) The vibration be free, not forced

(2) The equation of motion remains linear

Inplane forces not depending upon w can be realized in one of the following two ways:

(1) The boundary conditions provide no fixity in the plane of the plate

(2) The deflection is sufficiently small relative to the initial tension or compression in the plate so that the inplane forces are not significantly affected.

The normal forces N_x and N_y are positive in equation (10.1) if the plate is in tension; the shear force N_{xy} is positive according to the accepted convention of the theory of elasticity (see the appendix). It is emphasized that the inplane forces are generally found by first solving the plane elasticity problem for known boundary values of N_x, N_y, and N_{xy}. If these quantities are constant around the boundary, it is well known that they are also constant throughout the plate, and equation (10.1) is further simplified to the case of constant coefficients. In the special case of uniform boundary tension ($N_x=N_y=N$; $N_{xy}=0$), the equation for the isotropic plate simplifies to

$$D\nabla^4 w-N\nabla^2 w+\rho\frac{\partial^2 w}{\partial t^2}=0 \quad (10.2)$$

Assuming sinusoidal time response, equation (10.2) becomes

$$\nabla^4 W-\frac{N}{D}\nabla^2 W-\frac{\rho\omega^2}{D}W=0 \quad (10.3)$$

where W is solely a function of the spatial coordinates. Furthermore, it can be seen that equation (10.3) can be factored into

$$(\nabla^2+\alpha^2)(\nabla^2-\beta^2)W=0 \quad (10.4)$$

where

$$\left.\begin{aligned} \alpha^2&=\frac{N}{2D}\left[\left(1+\frac{4\rho\omega^2 D}{N^2}\right)^{1/2}-1\right]\\ \beta^2&=\frac{N}{2D}\left[\left(1+\frac{4\rho\omega^2 D}{N^2}\right)^{1/2}+1\right]\\ \beta^2-\alpha^2&=N/D\\ \alpha^2\beta^2&=\rho\omega^2/D \end{aligned}\right\} \quad (10.5)$$

10.1 CIRCULAR PLATES

The main results available for circular plates are for the case of hydrostatic inplane force. When ∇^2 is expressed in terms of polar coordinates by means of equation (1.10) and Fourier components in θ are assumed as in equation

(1.15), equation (10.4) yields the two second-order equations

$$\left.\begin{aligned}\frac{d^2W_{n_1}}{dr^2}+\frac{1}{r}\frac{dW_{n_1}}{dr}-\left(\frac{n^2}{r^2}-\alpha^2\right)W_{n_1}=0\\ \frac{d^2W_{n_2}}{dr^2}+\frac{1}{r}\frac{dW_{n_2}}{dr}-\left(\frac{n^2}{r^2}+\beta^2\right)W_{n_2}=0\end{aligned}\right\} \quad (10.6)$$

These equations have solutions

$$\left.\begin{aligned}W_{n_1}=A_nJ_n(\alpha r)+B_nY_n(\alpha r)\\ W_{n_2}=C_nI_n(\beta r)+D_nK_n(\beta r)\end{aligned}\right\} \quad (10.7)$$

respectively, where J_n, Y_n, I_n, and K_n are Bessel functions, as discussed in the section covering solutions of the classical equations (sec. 1.1.2), and A_n, . . ., D_n are undetermined constants. Thus, the general solution to equation (10.4) in polar coordinates is

$$W(r,\theta)=\sum_{n=0}^{\infty}[A_nJ_n(\alpha r)+B_nY_n(\alpha r)+C_nI_n(\beta r)+D_nK_n(\beta r)]\cos n\theta+\sum_{n=1}^{\infty}[A_n^*J_n(\alpha r)+B_n^*Y_n(\alpha r)+C_n^*I_n(\beta r)+D_n^*K_n(\beta r)]\sin n\theta \quad (10.8)$$

10.1.1 Clamped Circular Plates

The problem of clamped circular plates is defined by figure 2.1 and boundary condition equations (2.2). Because all modes of vibration have symmetry with respect to at least one diameter, the terms of equation (10.8) involving sin $n\theta$ can be discarded. Furthermore, in order to avoid singularities at the center of the plate, B_n and D_n must be set equal to zero. The deflection function therefore becomes

$$W(r,\theta)=\sum_{n=0}^{\infty}[A_nJ_n(\alpha r)+C_nI_n(\beta r)]\cos n\theta \quad (10.9)$$

Substituting equation (10.9) into equations (2.2) yields, for a nontrivial solution (refs. 10.1 to 10.4), the characteristic equation

$$\alpha\frac{J_{n+1}(\alpha a)}{J_n(\alpha a)}+\beta\frac{I_{n+1}(\alpha a)}{I_n(\beta a)}=0 \quad (10.10)$$

Wah (ref. 10.1) determined the roots of equation (10.10) for mode shapes having 0, 1, and 2 nodal circles and nodal diameters for a range of inplane forces varying from tension to compression. These results are given in table 10.1. Herein the quantity ϕ is used as a multiple of the critical buckling load in compression; that is,

$$\phi=\frac{Na^2}{14.68D} \quad (10.11)$$

Accordingly, the vibration frequency of the fundamental mode goes to zero as ϕ goes to -1. Frequency parameter values for intermediate values of ϕ not found in table 10.1 may be obtained from figure 10.1 by using the last of equations (10.5). In this figure, n identifies the number of nodal diameters and s, the

TABLE 10.1.—*Frequency Parameters* $\omega a^2\sqrt{\rho/D}$ *for a Clamped Circular Plate Subjected to Inplane Force* N

Number of nodal circles, s	$\phi=\frac{Na^2}{14.68D}$	$\omega a^2\sqrt{\rho/D}$ for values of n of—		
		0	1	2
0	2.00	17.37	30.61	45.67
	1.50	15.92	28.59	43.39
	1.00	14.30	26.41	40.91
	.50	12.44	24.00	38.07
	.25	11.39	22.81	36.72
	0	10.21	21.25	35.05
	−.25	8.91	19.61	33.53
	−.50	7.28	17.94	31.75
	−1.00	0	14.31	28.08
1	2.00	50.60	71.87	97.11
	1.50	48.17	69.27	94.09
	1.00	45.52	66.38	91.31
	.50	42.75	63.47	88.04
	.25	41.29	62.02	86.39
	0	39.77	60.37	84.82
	−.25	38.19	58.81	83.34
	−.50	36.55	57.21	81.81
	−1.00	33.03	53.79	78.25
2	2.00	101.81	128.52	166.06
	1.50	98.77	125.20	162.93
	1.00	95.44	121.99	159.70
	.50	92.33	118.89	156.39
	.25	90.59	117.39	154.84
	0	89.09	115.78	153.26
	−.25	87.45	114.16	151.65
	−.50	85.76	112.48	150.04
	−1.00	82.28	108.82	146.48

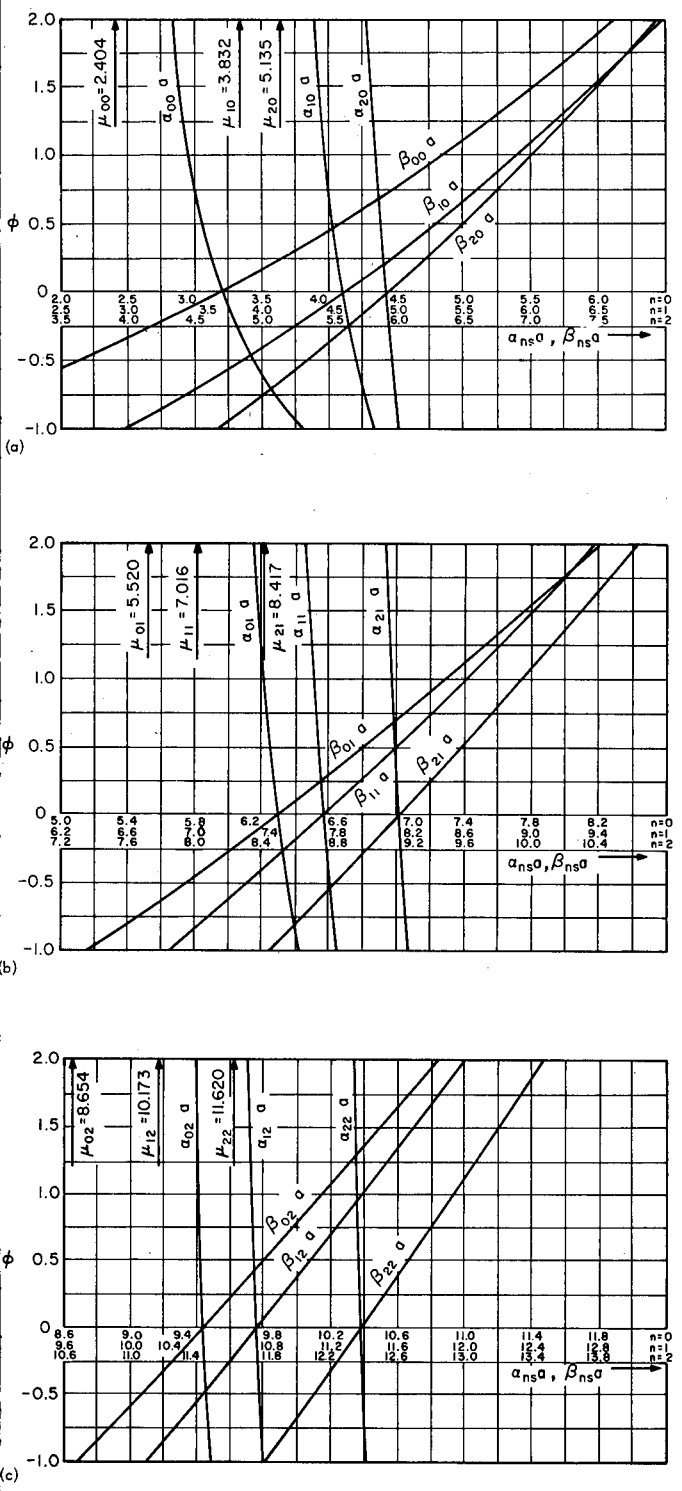


FIGURE 10.1.—Frequency parameters α_{ns} and β_{ns} for a clamped circular plate subjected to inplane force N; $\alpha^2\beta^2=\rho\omega^2/D$. (*a*) Zero nodal circles. (*b*) One nodal circle. (*c*) Two nodal circles. (After ref. 10.1)

number of internal nodal circles. On this figure are also shown the limiting values of the membrane frequency parameter μ, where

$$\mu=\omega a\sqrt{\rho/N} \tag{10.12}$$

These limiting values would apply as the inplane force becomes extremely large; in particular, the plate frequency approaches that of the membrane as $\alpha a\to\mu$ and if

$$(1/2)\alpha^2 D/N<<1 \tag{10.13}$$

Reference 10.1 is the most recent work on this problem which solves the exact characteristic equation (eq. (10.10)). However, much earlier work (refs. 10.2, 10.3, and 10.4) preceded this and also used equation (10.10). Bickley (ref. 10.3) in an early paper determined the frequencies for a clamped circular plate in tension by means of equation (10.10). These are the exact values listed in table 10.2. Lower and upper bounds on the frequency parameter are calculated in reference 10.3 by means of the Southwell (ref. 10.5) and Rayleigh (ref. 10.6) methods, respectively. These are also displayed in table 10.2. It is observed from table 10.2 that the Southwell method gives less percent error as the mode number is increased.

The Rayleigh method is well known. A deflection function of the form

$$w=(a^2-r^2)^2 r^n\cos n\theta \tag{10.14}$$

was used in conjunction with the Rayleigh method. Equating maximum potential and kinetic energies of the system yields

$$\omega^2\leqq\frac{8(n+1)(n+2)(n+4)(n+5)}{3}\left(\frac{D}{\rho a^4}\right)\left[1+\frac{Na^2/D}{2(n+2)(n+4)}\right] \tag{10.15}$$

The Southwell method uses the inequality

$$\omega_1^2+\omega_2^2\leqq\omega^2 \tag{10.16}$$

where ω is the exact frequency of a system having two forms of strain energy and ω_1 and ω_2 are the frequencies of the system when each form of the strain energy is taken separately.

TABLE 10.2.—*Frequency Parameters* $\omega a^2\sqrt{\rho/D}$ *of a Clamped Circular Plate Subjected to Inplane Force* N

n	s	$\frac{Na^2}{D}$	$\omega a^2\sqrt{\rho/D}$ derived by—		
			Exact method (ref. 10.3)	Southwell method (ref. 10.5)	Rayleigh method (ref. 10.6)
0	0	0	10. 216	10. 216	10. 328
		1	10. 552	10. 495	10. 646
		4	11. 486	11. 291	11. 547
		25	16. 527	15. 778	16. 533
		100	27. 483	26. 128	27. 809
		400	50. 792	49. 169	52. 662
		∞	----------	$2.4048\sqrt{Na^2/D}$	$4.4721\sqrt{Na^2/D}$
	1	0	39. 772	39. 772	----------
		1	40. 190	40. 152	----------
		4	41. 419	41. 272	----------
		25	49. 146	48. 396	----------
		100	69. 916	67. 996	----------
		400	120. 59	117. 25	----------
		∞	----------	$5.5151\sqrt{Na^2/D}$	----------
	2	0	89. 104	89. 104	----------
		1	89. 550	89. 523	----------
		4	90. 875	90. 770	----------
		25	99. 648	99. 054	----------
		100	126. 01	124. 21	----------
		400	198. 53	194. 67	----------
		∞	----------	$8.6537\sqrt{Na^2/D}$	----------
1	0	0	21. 260	21. 260	21. 909
		1	21. 652	21. 603	22. 271
		4	22. 783	22. 600	23. 324
		25	29. 447	28. 619	29. 665
		100	45. 563	43. 820	45. 607
		400	82. 146	79. 529	82. 946
		∞	----------	$3.8317\sqrt{Na^2/D}$	$4\sqrt{Na^2/D}$
	1	0	60. 828	60. 8284	----------
		1	61. 263	61. 2307	----------
		4	62. 550	62. 4259	----------
		25	70. 891	70. 2182	----------
		100	94. 733	92. 8547	----------
		400	156. 49	152. 931	----------
		∞	----------	$7.01555\sqrt{Na^2/D}$	----------
2	0	0	34. 877	34. 877	36. 661
		1	35. 296	35. 253	37. 040
		4	36. 529	36. 358	38. 158
		25	44. 117	43. 310	45. 211
		100	63. 994	57. 043	64. 374
		400	111. 64	108. 47	112. 00
		∞	----------	$5.1357\sqrt{Na^2/D}$	$5.2915\sqrt{Na^2/D}$

In the present problem, ω_1 can be taken as the frequency of a clamped circular plate with no inplane force and ω_2, as the frequency of a circular membrane (no flexural stiffness) having a fixed boundary and membrane tension T. Equation (10.16) then gives a lower bound on the exact fundamental frequency; for example:

$$\omega^2 \geqq \frac{D}{\rho a^4}\left[104.36+5.783\frac{Na^2}{D}\right] \qquad (10.17)$$

Federhofer (ref. 10.4) obtained solutions to equation (10.10) for a wide range of inplane forces. These are summarized in table 10.3. This table is more complete than table 10.1 in the sense that it utilizes a range of compressive forces up to the limiting buckling load for each axisymmetric mode, instead of the fundamental mode only. Reference 10.4 gives the radii of the nodal circles for $s>0$, and these are also presented in table 10.3. A plot of the variation of the frequency parameter as a function of the inplane force is shown in figure 10.2 for the first three axisymmetric modes.

A perturbation technique was developed for the problem in references 10.7 and 10.8. The parameter N/D was used as a perturbation parameter, and the plate with no inplane force was the starting point upon which the perturbation was based. In addition to obtaining frequency parameters which compared reasonably well with the exact values given earlier in

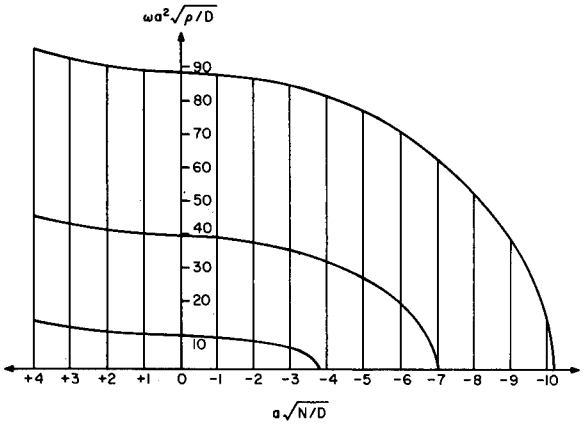


FIGURE 10.2.—Frequency parameter $\omega a^2\sqrt{\rho/D}$ for a clamped circular plate subjected to inplane force N. (After ref. 10.4)

TABLE 10.3—*Frequency Parameters* $\omega a^2\sqrt{\rho/D}$ *and Nodal Circle Radii for a Clamped Circular Plate Subjected to Inplane Force* N

n	s	Na^2/D	$\omega a^2\sqrt{\rho/D}$	Nodal circle radii, r/a	
0	0	16	14. 6028	---	---
		9	12. 8851	---	---
		4	11. 4855	---	---
		1	10. 5478	---	---
		0	10. 2150	---	---
		−1	9. 8712	---	---
		−4	8. 7460	---	---
		−9	6. 4129	---	---
		−14. 682	0	---	---
	1	16	45. 9954	0. 38550	---
		9	43. 3848	. 38297	---
		4	41. 4179	. 38086	---
		1	40. 1909	. 37947	---
		0	39. 7707	. 37900	---
		−4	38. 053	. 37690	---
		−16	32. 350	. 36952	---
		−36	19. 663	. 33830	---
		−49. 219	0	. 26634	---
	2	16	95. 9824	0. 25593	0. 58632
		9	93. 0392	. 25546	. 58505
		4	90. 8766	. 25511	. 58409
		1	89. 5514	. 25490	. 58349
		0	89. 1042	. 25483	. 58329
		−9	84. 985	. 25415	. 58134
		−36	71. 226	. 25179	. 57370
		−81	39. 222	. 24952	. 54473
		−103. 50	0	---	. 46875
1	0	0	21. 261	---	---
		−1	20. 862	---	---
		−4	19. 611	---	---
		−9	17. 321	---	---
		−16	13. 427	---	---
		−26. 368	0	---	---
	1	0	60. 829	0. 48968	---
		−4	59. 056	---	---
		−16	53. 390	. 48399	---
		−36	42. 295	---	---
		−70. 846	0	. 42228	---
	2	0	120. 078	0. 34974	0. 63902
		−9	116. 476	---	---
		−36	102. 418	. 34707	. 63293
		−81	74. 775	---	---
		−135. 02	0	. 34760	. 56604
2	0	0	34. 876	---	---
		−4	33. 148	---	---
		−16	27. 267	---	---
		−36	11. 972	---	---
		−40. 692	0	---	---

this section, the modes having 3, 4, 5, and 6 nodal diameters were also investigated, but the perturbation technique did not give accurate results. The Rayleigh and Southwell techniques were also employed, thereby obtaining bounds. Resulting frequency parameters are given in table 10.4.

The problem was also discussed from a variational standpoint in reference 10.2. A method for including translational and rotational springs acting at discrete points within the interior of the plate was proposed and demonstrated for the case of a translational spring of stiffness k at the center. All terms applying to cos $n\theta$ are retained in equation (10.8). In addition to the boundary condition equations (2.2), the conditions of transverse force equilibrium and null slope at the center are enforced. For the axisymmetric modes, the resulting characteristic determinant takes the form

$$\frac{2}{\pi}\left(z^2+\frac{\lambda^4}{z^2}\right)\left[J_0(z)\frac{\lambda^2}{z}I_1\left(\frac{\lambda^2}{z}\right)+zJ_1(z)I_0\left(\frac{\lambda^2}{z}\right)\right]=\zeta\begin{vmatrix} J_0(z) & Y_0(z)+\frac{2}{\pi}K_0\left(\frac{\lambda^2}{z}\right) & I_0\left(\frac{\lambda^2}{z}\right) \\ zJ_1(z) & zY_1(z)+\frac{2}{\pi}\frac{\lambda^2}{z}K_1\left(\frac{\lambda^2}{z}\right) & -\frac{\lambda^2}{z}I_0\left(\frac{\lambda^2}{z}\right) \\ 1 & \frac{2}{\pi}\ln\left(\frac{z}{\lambda}\right)^2 & 1 \end{vmatrix} \tag{10.18}$$

where

$$\left.\begin{aligned} z^2&=-\frac{Na^2}{2D}+\sqrt{\left(\frac{Na^2}{2D}\right)^2+\lambda^4} \\ \zeta&=\frac{ka^2}{2\pi D} \\ \lambda^2&=\omega a^2\sqrt{\rho/D} \end{aligned}\right\} \tag{10.19}$$

TABLE 10.4.—*Frequency Parameters* $\omega a^2\sqrt{\rho/D}$ *for the Higher Mode Shapes (Having no Nodal Circles) of a Clamped Circular Plate Subjected to Inplane Force* N

n	$\frac{Na^2}{D}$	$\omega a^2\sqrt{\rho/D}$ derived by—	
		Southwell method	Rayleigh method
3	0	51. 02	51. 20
	1	51. 42	51. 64
	100	81. 68	83. 82
4	0	69. 72	70. 06
	1	70. 13	70. 50
	100	103. 03	105. 49
5	0	90. 71	91. 47
	1	91. 13	91. 90
	100	126. 24	128. 71
6	0	115. 13	115. 00
	1	115. 56	115. 79
	100	152. 12	155. 79

Frequency parameters $(\omega^2a^4\rho/D)^{1/4}$ obtained as the lowest roots of equation (10.18) are plotted in figure 10.3 as functions of the inplane loading parameter Na^2/D and the spring constant parameter ζ (ref. 10.2). The inplane forces are entirely in the compressive range, as indicated. The broken curve indicates frequency parameters for the mode having one nodal diameter. Hence, for a given inplane compressive force, as the spring constant is increased the fundamental mode of vibration will abruptly change from axisymmetric to antisymmetric. It is obvious that a translational spring at the center affects only the axisymmetric modes of the plate.

10.1.2 Simply Supported Circular Plates

The problem of simply supported circular plates is defined by figure 2.2 and boundary condition equations (2.9).

The only known solution to the problem was derived by Wah (ref. 10.1). Using the deflection function in the form given by equation (10.9) and substituting it into equations (2.9) and (1.11) yields the characteristic equation

$$\alpha\frac{J_{n+1}(\alpha a)}{J_n(\alpha a)}+\beta\frac{I_{n+1}(\beta a)}{I_n(\beta a)}=\frac{a(\alpha^2+\beta^2)}{1-\nu} \tag{10.20}$$

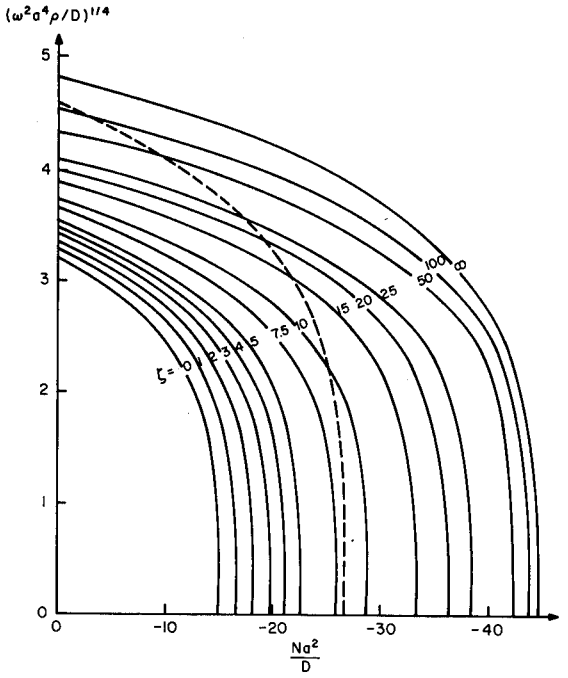


FIGURE 10.3.—Frequency parameter $\lambda=(\omega^2 a^4\rho/D)^{1/4}$ as a function of the spring constant parameter $\zeta=ka^2/2\pi D$ for a clamped circular plate having a translational spring at the center and subjected to inplane force N. (After ref. 10.2)

The roots of equation (10.20) were determined in reference 10.1 for mode shapes having 0, 1, and 2 nodal circles and nodal diameters for a range of inplane forces varying from tension to compression. These results are given in table 10.5 for $\nu=0.3$. Herein the quantity ϕ is used as a multiple of the critical buckling load in compression; that is,

$$\phi=\frac{Na^2}{4.2D} \tag{10.21}$$

Frequency parameter values for intermediate values of ϕ not found in table 10.5 may be obtained from figure 10.4. For an explanation of the method of using this figure, see the preceding section.

10.1.3 Completely Free Circular Plates

The problem of completely free plates is defined by figure 2.3 and the boundary conditions

$$\left.\begin{aligned} M_r(a)&=0 \\ V_r(a)+N_r(a)\frac{\partial w}{\partial r}(a)&=0 \end{aligned}\right\} \tag{10.22}$$

TABLE 10.5.—*Frequency Parameters* $\omega a^2\sqrt{\rho/D}$ *for a Simply Supported Circular Plate Subjected to Inplane Force* N; $\nu=0.3$

Number of nodal circles, s	$\phi=\frac{Na^2}{4.2D}$	$\omega a^2\sqrt{\rho/D}$ for values of n of—		
		0	1	2
0	2.00	8.55	17.47	29.55
	1.50	7.81	16.55	28.62
	1.00	6.99	15.57	27.62
	.50	6.05	14.55	26.64
	.25	5.52	13.98	26.12
	0	4.94	13.47	25.60
	−.25	4.27	12.86	25.07
	−.50	3.46	12.23	24.53
	−1.00	0	10.95	23.41
1	2.00	33.75	52.05	72.97
	1.50	32.79	51.07	71.97
	1.00	31.80	49.94	70.96
	.50	30.78	48.92	69.93
	.25	30.25	48.41	69.39
	0	29.72	47.89	68.89
	−.25	29.17	47.36	68.36
	−.50	28.62	46.78	67.83
	−1.00	27.49	45.60	67.76
2	2.00	78.28	107.54	138.62
	1.50	77.27	106.52	137.67
	1.00	76.24	105.50	136.65
	.50	75.21	104.49	135.60
	.25	74.69	103.94	135.02
	0	74.15	103.43	134.56
	−.25	73.62	102.90	134.16
	−.50	73.09	102.37	133.52
	−1.00	72.00	101.30	132.36

with M_r and V_r as given in equations (1.11) and (1.13), and N_r is the radial, inplane tensile force.

Although the concept of a completely free plate subjected to inplane forces may be difficult to visualize at first, there exist at least four distinct types of problems where this phenomenon may arise:

(1) A boundary having a strip around it which is prestressed into tension

(2) Spin about an axis (not necessarily normal to the plate) causing centrifugal fields

(3) Thermal gradients in the r- and θ-directions

(4) Internal residual stresses due to cold working or heat treatment

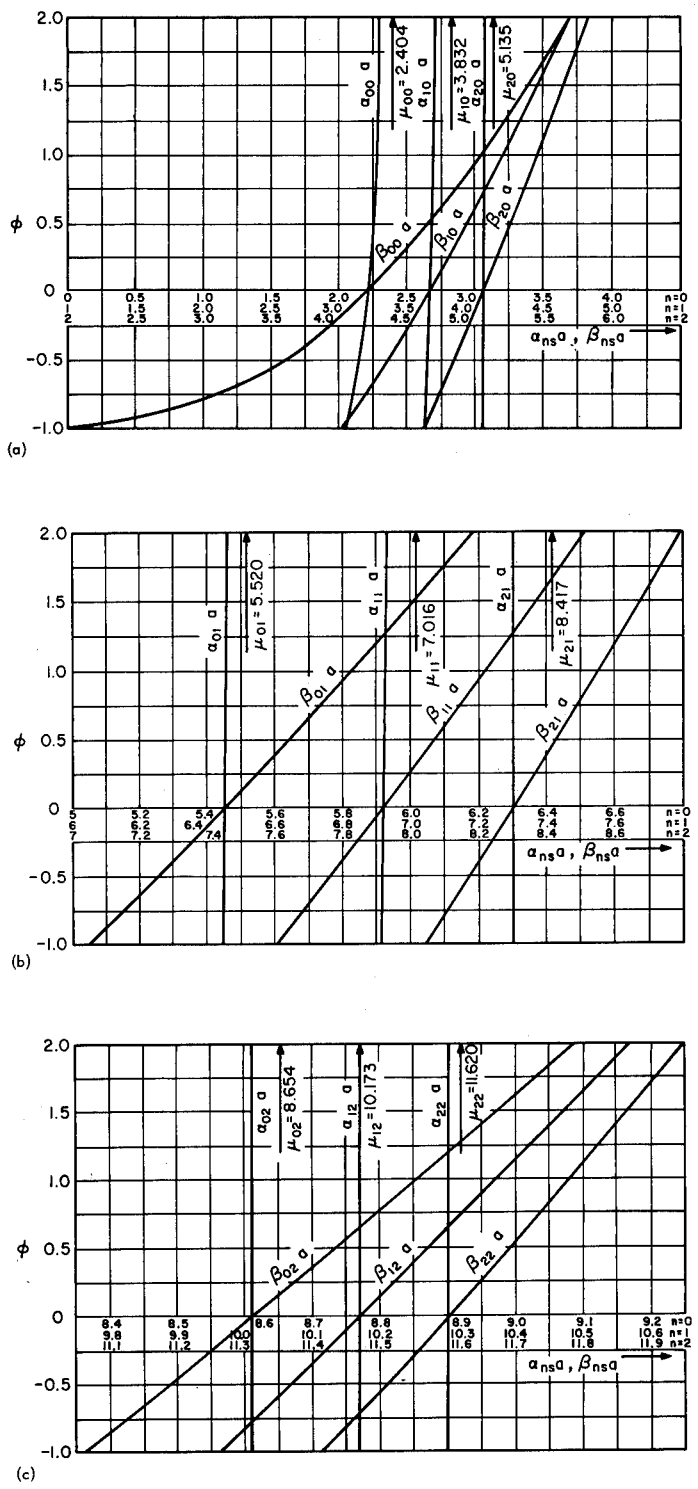


FIGURE 10.4.—Frequency parameters α_{ns} and β_{ns} for a simply supported circular plate subjected to inplane force N; $\alpha^2\beta^2=\rho\omega^2/D$; $\nu=0.3$. (*a*) Zero nodal circles. (*b*) One nodal circle. (*c*) Two nodal circles. (After ref. 10.1)

Indeed, the preceding discussion is not limited to circular plates, but can apply to plates of arbitrary shape. In the case of the circular plate, results exist for loadings of the second and third types.

Lamb and Southwell (ref. 10.5) examined the problem of the completely free circular plate spinning about its cylindrical axis with uniform angular velocity Ω. If the terms in the differential equation (10.1) which represent the restoring forces due to flexural rigidity are neglected, equation (10.1) becomes, in polar coordinates,

$$\frac{1}{r}\frac{\partial}{\partial r}\left(N_r r\frac{\partial w}{\partial r}\right)+\frac{N_\theta}{r^2}\frac{\partial^2 w}{\partial\theta^2}=\rho\frac{\partial^2 w}{\partial t^2} \tag{10.23}$$

where N_r and N_θ are axisymmetric radial and circumferential forces, respectively, determined by first solving the uncoupled plane elasticity problem

$$\left.\begin{aligned} N_r&=\frac{1}{8}(3+\nu)\,\rho\Omega^2(a^2-r^2)\\ N_\theta&=\frac{1}{8}\rho\Omega^2[(3+\nu)a^2-(1+3\nu)r^2]\end{aligned}\right\} \tag{10.24}$$

The problem is solved by assuming a series solution

$$w=\sum_{n=0}^{\infty}\sum_{i=0}^{\infty}C_{in}\left(\frac{r}{a}\right)^i\cos n\theta\cos(\omega t+\phi) \tag{10.25}$$

The frequency of the mode having n nodal diameters and s nodal circles is given by (ref. 10.9)

$$\omega^2=\frac{\Omega^2}{8}[(n+2s+2)(n+2s)(3+\nu)-n^2(1+3\nu)] \tag{10.26}$$

and the mode shapes are determined from

$$W(r,\theta)=A_n\left(\frac{r}{a}\right)^n\left[1-\frac{s(n+s+1)}{(1!)(n+1)}\left(\frac{r}{a}\right)^2+\frac{s(s-1)(n+s+1)(n+s+2)}{(2!)(n+1)(n+2)}\left(\frac{r}{a}\right)^4-\cdots\right]\cos n\theta \tag{10.27}$$

In references 10.5 and 10.9 an approximate method is formulated for solving the problem when the terms including the flexural rigidity of the plate are included within the differential equation of motion.

Massa (ref. 10.10) analyzed the problem of a completely free circular plate subjected to the thermal gradient

$$T=T_0\left[1-\left(\frac{r}{a}\right)^2\right] \tag{10.28}$$

This gives rise to inplane forces of the form

$$\left.\begin{aligned} N_r&=\frac{E\alpha T_0 h}{4}\left[\left(\frac{r}{a}\right)^2-1\right]\\ N_\theta&=\frac{E\alpha T_0 h}{4}\left[3\left(\frac{r}{a}\right)^2-1\right]\end{aligned}\right\} \tag{10.29}$$

where α is the coefficient of thermal expansion.

The problem is solved by the Rayleigh-Ritz technique. Poisson's ratio is taken to be 0.3. For the axisymmetric modes a deflection function

$$W(r)=A\left[1-2.6161\left(\frac{r}{a}\right)^2+1.1090\left(\frac{r}{a}\right)^4-0.2464\left(\frac{r}{a}\right)^6\right]+B\left(\frac{r}{a}\right)^2\left[1-2.6805\left(\frac{r}{a}\right)^2+1.9940\left(\frac{r}{a}\right)^4-0.5244\left(\frac{r}{a}\right)^6\right] \tag{10.30}$$

is taken, where A and B are undetermined constants. This function satisfies not only the boundary conditions of the problem but also the condition that the total momentum of the plate be null. The first two axisymmetric frequencies can be found from

$$\omega_{01}^2,\ \omega_{02}^2=\frac{Eh^3}{\rho a^4}\left\{72.97-4.342\left(\frac{\alpha T_0 a^2}{h^2}\right)\mp 65.54\sqrt{\left[1-0.03489\left(\frac{\alpha T_0 a^2}{h^2}\right)\right]^2+0.000052\left(\frac{\alpha T_0 a^2}{h^2}\right)^2}\right\} \tag{10.31}$$

where the subscripts of ω_{ns} identify the number of nodal diameters and circles, respectively. The first axisymmetric mode shape is

$$W_{01}(r)=C_1\left[1-2.6696\left(\frac{r}{a}\right)^2+1.2525\left(\frac{r}{a}\right)^4-0.3530\left(\frac{r}{a}\right)^6+0.0280\left(\frac{r}{a}\right)^8\right] \tag{10.32}$$

and has a nodal circle at $r=0.6790a$ and an amplitude at the boundary of $W_{01}(a)=-0.7423C_1$. The second axisymmetric mode shape is

$$W_{02}(r)=C_2\left[1-8.7097\left(\frac{r}{a}\right)^2+17.4455\left(\frac{r}{a}\right)^4-12.3974\left(\frac{r}{a}\right)^6+3.1952\left(\frac{r}{a}\right)^8\right] \tag{10.33}$$

and has nodal circles at $r=0.4013a$ and $r=0.8472a$ and an amplitude at the boundary of $W_{02}(a)=0.5336C_2$.

For the modes having two nodal diameters, a deflection function

$$W(r,\theta)=\left\{A\left(\frac{r}{a}\right)^2\left[1-0.2754\left(\frac{r}{a}\right)^2+0.06225\left(\frac{r}{a}\right)^4\right]+B\left(\frac{r}{a}\right)^4\left[1-0.8195\left(\frac{r}{a}\right)^2+0.2286\left(\frac{r}{a}\right)^4\right]\right\}\cos 2\theta \tag{10.34}$$

is taken, which satisfies the boundary conditions. Employing the Rayleigh-Ritz procedure gives for the squares of the frequencies

$$\omega_{20}^2,\ \omega_{21}^2=\frac{Eh^3}{\rho a^4}\left\{59.11-1.249\left(\frac{\alpha T_0 a^2}{h^2}\right)\mp 56.48\sqrt{\left[1-0.03967\left(\frac{\alpha T_0 a^2}{h^2}\right)\right]^2+0.000011\left(\frac{\alpha T_0 a^2}{h^2}\right)^2}\right\} \tag{10.35}$$

The corresponding mode shapes are

$$W_{20}(r)=C_1\left(\frac{r}{a}\right)^2\left[1-0.2885\left(\frac{r}{a}\right)^2+0.0730\left(\frac{r}{a}\right)^4-0.0030\left(\frac{r}{a}\right)^6\right] \tag{10.36}$$

and

$$W_{21}(r)=C_2\left(\frac{r}{a}\right)^2\left[1-2.523\left(\frac{r}{a}\right)^2+1.904\left(\frac{r}{a}\right)^4-0.5138\left(\frac{r}{a}\right)^6\right] \quad (10.37)$$

and have a nodal circle at $r=0.8279a$.

10.1.4 Rotating Disk, Clamped at Center, Outer Edge Free

Southwell (ref. 10.11) analyzed the problem of a circular disk which is clamped at its center, is free at its outer edge, and is rotating with constant angular velocity Ω. He again used the method for finding lower bounds on the frequencies which was discussed in section 10.1.1. The frequencies are given by

$$\omega^2=K_1\Omega^2+K_2\frac{D}{\rho a^4} \quad (10.38)$$

where K_1 and K_2 are given in table 10.6 and $\nu=0.3$.

10.2 RECTANGULAR PLATES

As described in the chapter entitled "Rectangular Plates" (ch. 4), there exist 21 possible combinations of simple boundary conditions for rectangular plates. Results were found in the literature for all 21 cases for isotropic plates not having inplane forces. As will be seen in the following discussion, published results exist for very few cases when inplane forces are present. Also, it will be seen that for rectangular plates results are available for other types of elementary inplane stress fields, in addition to hydrostatic.

For the isotropic plate, when sinusoidal time response is assumed,

$$w(x, y, t)=W(x, y)\sin(\omega t+\phi) \quad (10.39)$$

The differential equation of motion (eq. (10.1)) becomes

$$\nabla^4 W-k^4 W=\frac{N_x}{D}\frac{\partial^2 W}{\partial x^2}+2\frac{N_{xy}}{D}\frac{\partial^2 W}{\partial x\,\partial y}+\frac{N_y}{D}\frac{\partial^2 W}{\partial y^2} \quad (10.40)$$

where

$$k^4=\frac{\rho\omega^2}{D} \quad (10.41)$$

When N_x and N_y are constants, say N_1 and N_2, respectively, and $N_{xy}=0$, equation (10.40) becomes

$$\nabla^4 W-k^4 W=\frac{N_1}{D}\frac{\partial^2 W}{\partial x^2}+\frac{N_2}{D}\frac{\partial^2 W}{\partial y^2} \quad (10.42)$$

which is of a form particularly amenable to solution.

10.2.1 Plates Having All Sides Simply Supported

The boundary conditions for the problem of plates having all sides simply supported are defined by equations (4.18) and figure 10.5. In figure 10.5, the positive senses of the inplane forces N_x, N_y, and N_{xy} are shown for the special case when each is constant throughout the plate.

TABLE 10.6.—*Constants for Eq. (10.38) To Determine the Frequencies of a Rotating Disk Which Is Clamped at Its Center and Free on Its Outer Edge*

Nodal circles	Nodal diameters			
	0	1	2	3
0	$K_1=0$ $K_2=14.1$	$K_1=1$ $K_2=0$	$K_1=2.35$ $K_2=28.97$	$K_1=4.05$ $K_2=155.3$
1	$K_1=3.3$ $K_2=437.3$	$K_1=5.95$ $K_2=421.2$	$K_1=8.95$ $K_2=1212$	$K_1=12.3$ $K_2=2839$
2	$K_1=9.9$ $K_2=3683$	$K_1=14.2$ $K_2=3336$	$K_1=18.85$ $K_2=7164$	$K_1=23.85$ $K_2=11700$
3	$K_1=19.8$ $K_2=14330$	$K_1=25.75$ $K_2=14380$	$K_1=32.05$ $K_2=23410$	$K_1=38.7$ $K_2=36274$

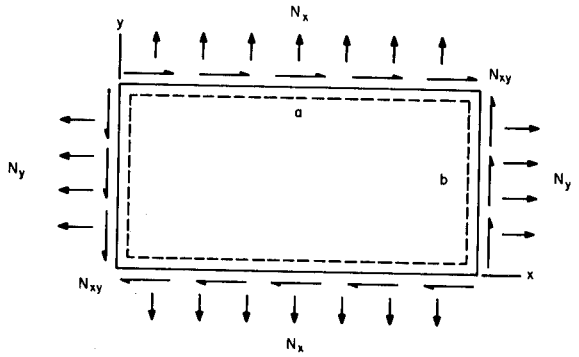


FIGURE 10.5.—Simply supported rectangular plate having uniform inplane forces.

For $N_x=N_1$, $N_y=N_2$, and $N_{xy}=0$, an elementary solution exists. Letting $W(x,y)$ be given by

$$W(x,y)=\sum_{m,n=1}^{\infty} A_{mn}\sin\frac{m\pi x}{a}\sin\frac{n\pi y}{b} \qquad (10.43)$$

clearly satisfies the boundary conditions of the problem. Substituting equation (10.43) into (10.42) yields the frequency equation

$$\rho\omega_{mn}^2=D\left[\left(\frac{m\pi}{a}\right)^2+\left(\frac{n\pi}{b}\right)^2\right]^2 +N_1\left(\frac{m\pi}{a}\right)^2+N_2\left(\frac{n\pi}{b}\right)^2 \qquad (10.44)$$

If equation (10.44) is multiplied through by a^4/D, there results the dimensionless form:

$$\frac{\omega^2a^4\rho}{D}=\left[(m\pi)^2+(n\pi)^2\left(\frac{a}{b}\right)^2\right]^2 +\frac{N_1a^2}{D}(m\pi)^2+\frac{N_2a^2}{D}(n\pi)^2\left(\frac{a}{b}\right)^2 \qquad (10.45)$$

Simplifications that result in equations (10.44) and (10.45) when, for example, $N_1=N_2$ or $N_2=0$ are clearly evident. It is also obvious that if either N_1 or N_2, or a combination of them, becomes sufficiently large in a negative sense (i.e., compression), the frequency can be reduced to zero, which yields the combinations of N_1 and N_2 which are critical buckling loads for the problem. For example, let $N_2=0$. Then the critical buckling load is given by

$$(N_1)_{cr}=-D\left(\frac{a}{m\pi}\right)^2\left[\left(\frac{m\pi}{a}\right)^2+\left(\frac{n\pi}{b}\right)^2\right]^2 =-\frac{D\pi^2}{a^2}\left[m+n\left(\frac{n}{m}\right)\left(\frac{a}{b}\right)^2\right]^2 \qquad (10.46)$$

If N_1 and N_2 are compressive (i.e., negative), then it can be seen from equation (10.44) that the fundamental mode does not necessarily occur when $m=n=1$ but depends upon N_1, N_2, and the a/b ratio. This was shown by Herrmann in reference 10.12 for the special case when $N_2=0$. For this case, substituting equation (10.46) into equation (10.44) gives

$$\rho\omega^2=\left(\frac{m\pi}{a}\right)^2[N_1+(N_1)_{cr}] \qquad (10.47)$$

where $(N_1)_{cr}$ is clearly a negative quantity. Thus, the fundamental frequency for this loading will always occur when $n=1$, but not necessarily when $m=1$. This phenomenon is illustrated in figure 10.6 (from ref. 10.12) where the frequency ratio $(\omega/\omega_s)^2$ is plotted as a function of the ratios $N_1/(N_1)_{cr}$ and a/b. The quantity ω_s is defined by

$$\omega_s^2=\frac{4D\pi^4}{\rho a^2b^2} \qquad (10.48)$$

and is the square of the fundamental frequency of an unloaded, simply supported square plate.

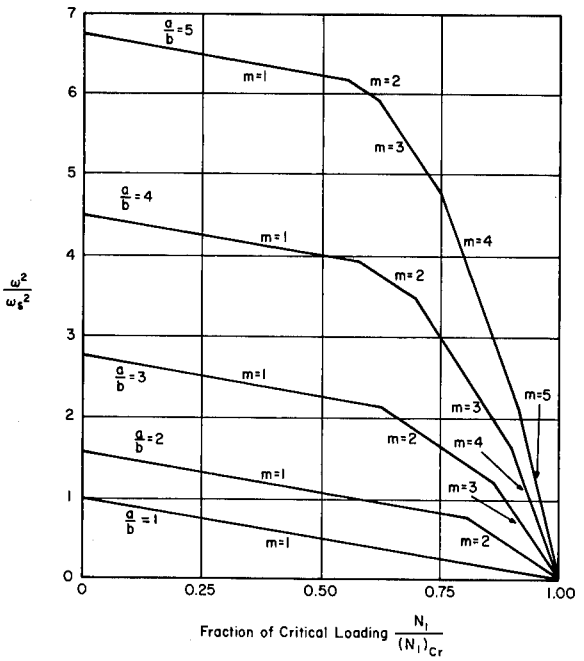


FIGURE 10.6.—Influence of inplane force $N_x=N_1$ on the fundamental frequency of a SS–SS–SS–SS rectangular plate for various plate aspect ratios. (After ref. 10.12)

The influence of a body force is also considered in reference 10.12. The body force is assumed to be acting in the x-direction and may be due to the weight of the plate (if it is in a vertical position), or it may arise from acceleration in the negative x-direction. Thus, in this case, all the inplane forces are not constant but are given by

$$\left.\begin{aligned} N_x &= N_1 - \gamma b x \\ N_y &= N_{xy} = 0 \end{aligned}\right\} \tag{10.49}$$

where N_1 is the inplane tension at the end $x=0$, and γ is the body force (force per unit area). The Rayleigh method was used to solve the problem, with the first term ($m=n=1$) of the sine series expansion for deflection (eq. (10.43)) being kept. This yielded the frequency parameter

$$\omega^2 ab\rho = m^2\pi^2\left[\left(\frac{b}{a}\right)N_1 - \frac{\gamma b}{2}\right] + \pi^4 abD\left(\frac{m^2}{a^2}+\frac{1}{b^2}\right)^2 \tag{10.50}$$

The frequency ratio $(\omega/\omega_s)^2$ is plotted in figure 10.7 as a function of the ratio $N_1/(N_1)_{cr}$ and a parameter ξ defined by

$$\xi = \frac{\gamma a}{\pi^2 D/b^2} \tag{10.51}$$

for the particular aspect ratio $a/b=3$. The quantity ω_s is defined by equation (10.48).

Frequency parameters for this problem were computed in reference 10.13 for use in determining lower bounds for completely clamped square plates subjected to hydrostatic tension. These are listed in table 10.7.

Some experimental results are reported in reference 10.14. A 24S–T duralumin plate, 12 inches by 12 inches by 0.040 inch thick, was simply supported along all edges and subjected to the constant inplane load $N_x=N_1$ and $N_y=N_{xy}=0$. It was found that the experimentally measured frequency does not decrease as rapidly as that predicted by theory when the compressive loading is increased. This is shown in figure 10.8. In reference 10.14 this effect is attributed to the possibility of slight initial curvature in the plate.

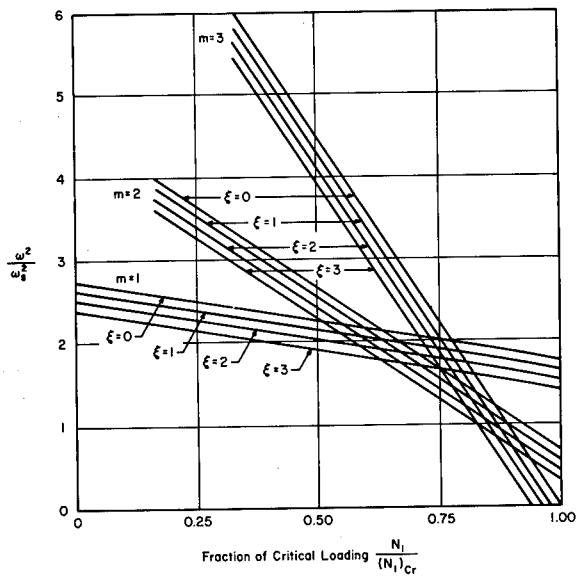


FIGURE 10.7.—Influence of end loading N_1 and body force ratio ξ on the fundamental frequency of a SS–SS–SS–SS rectangular plate for $a/b=3$. $\omega_s^2 = 4D\pi^4/\rho a^2 b^2$; $\xi=\gamma a b^2/\pi^2 D$. (After ref. 10.12)

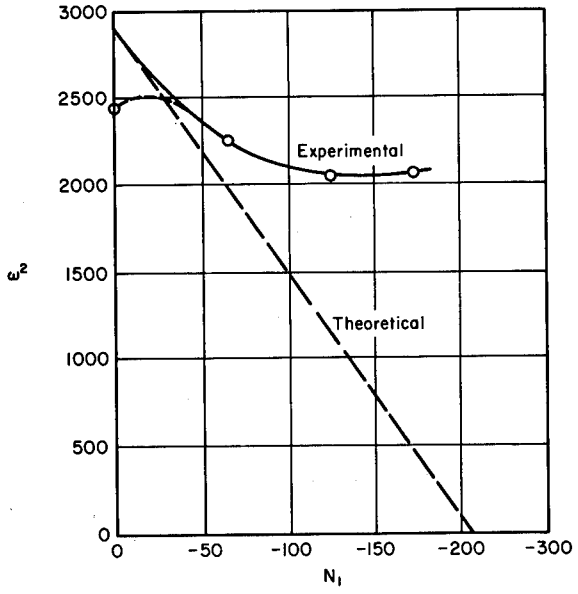


FIGURE 10.8.—Deviation of experimentally measured frequencies from those predicted by theory for a SS–SS–SS–SS square plate loaded in one direction. (After ref. 10.14)

TABLE 10.7.—*Frequency Parameters for a Square Plate Subjected to Hydrostatic Tension and Having Clamped Boundaries Compared With Those for a Plate With Simply Supported Boundaries*

$\frac{Na^2}{\pi^2 D}$	Frequency parameters for simply supported plate		Frequency parameter $\omega a^2\sqrt{\rho/D}$ for clamped plate	
	$\omega_{11}a^2\sqrt{\rho/D}$	$\omega_{12}a^2\sqrt{\rho/D}$	Lower bound	Upper bound
5	36. 928	69. 788	49. 580	49. 847
10	48. 350	85. 473	59. 922	60. 392
15	57. 549	98. 696	68. 580	69. 271
20	65. 467	110. 34	76. 124	77. 088
30	78. 96	130. 56	89. 268	90. 656
50	100. 65	163. 67	110. 60	112. 90
100	140. 96	226. 14	148. 26	154. 98
200	198. 38	315. 98	207. 79	215. 69

The perturbation technique is demonstrated in reference 10.15 for the case of hydrostatic tension. The basic problem used is that of the unloaded plate. One perturbation gives the exact solution for the loaded plate.

In reference 10.16 the finite difference method is applied to the problem. The problem is also discussed in reference 10.17.

10.2.2 Rectangular Plates Having Two Opposite Sides Simply Supported

In addition to the case described in the preceding section, there exist five other cases of rectangular plates having two opposite edges simply supported and simple boundary conditions on the other edges. These have been given previously in the discussion of simply supported rectangular plates (sec. 4.2).

For uniform inplane forces, equation (10.42) applies. When the edges $x=0$ and $x=a$ are simply supported (as in fig. 10.5), a deflection function which satisfies the boundary conditions of zero deflection and bending moment along these edges is given by

$$W(x,y)=\sum_{m=1}^{\infty} Y_m(y)\sin\alpha x \qquad (10.52)$$

where $\alpha=m\pi/a$. Substituting equation (10.52) into equation (10.42) yields

$$\frac{d^4Y_m}{dy^4}-\left(2\alpha^2+\frac{N_2}{D}\right)\frac{d^2Y_m}{dy^2}+\left(\alpha^4-k^4+\frac{N_1}{D}\alpha^2\right)Y_m=0 \qquad (m=1, 2, \ldots) \qquad (10.53)$$

which has a general solution

$$Y_m=A_m\sin\psi_m y+B_m\cos\psi_m y+C_m\sinh\phi_m y+D_m\cosh\phi_m y \qquad (10.54)$$

where

$$\left.\begin{aligned}\psi_m&=\left\{\left[\left(\alpha^2+\frac{N_2}{2D}\right)^2-\left(\alpha^4-k^4+\frac{N_1}{D}\alpha^2\right)\right]^{1/2}-\left(\alpha^2+\frac{N_2}{2D}\right)\right\}^{1/2}\\ \phi_m&=\left\{\left[\left(\alpha^2+\frac{N_2}{2D}\right)^2-\left(\alpha^4-k^4+\frac{N_1}{D}\alpha^2\right)\right]^{1/2}+\left(\alpha^2+\frac{N_2}{2D}\right)\right\}^{1/2}\end{aligned}\right\} \qquad (10.55)$$

It is seen that equations (10.52) and (10.54) are of exactly the same form as equation (4.21) for isotropic plates, the only difference being in the definitions of the frequency parameters ψ_m and ϕ_m.

The standard procedure to satisfy the boundary conditions along the sides $y=0$ and $y=b$, whatever they may be, is the substitution of equation (10.54) into these conditions. The determinant of the resulting four homogeneous equations in A_m, B_m, C_m, and D_m is then set equal to zero for a nontrivial solution. This yields an exact solution for the frequencies.

Apparently the foregoing straightforward procedure has not been thoroughly followed in the literature, as will be seen by the paucity of numerical results to be presented.

Boundary conditions of plates having loads acting on free edges are different than those of unloaded plates because of the component of inplane force which acts normal to the deflected middle surface of the plate. That is, the transverse edge reaction is given by

$$V_n=Q_n+\frac{\partial M_{nt}}{\partial t}+N_n\frac{\partial w}{\partial n} \qquad (10.56)$$

By looking at equation (10.55), it can be seen that ψ_m and ϕ_m can be positive real, zero, imaginary, or complex. The solution form of equation (10.54) is based upon the assumption that ψ_m and ϕ_m are positive real numbers; otherwise, the form would change. No study is known in which the character and range of applicability of the separate forms of solution have been investigated.

The Rayleigh method is used in reference 10.12 to obtain an approximation for the fundamental frequency of a rectangular plate having the edge $y=b$ free and the others simply supported. The loading is $N_x=N_1$ and $N_y=N_{xy}=0$. A deflection function

$$W(x,y)=y\sin\frac{\pi x}{a} \tag{10.57}$$

was used. The resulting expression for the frequency is

$$\frac{\rho\omega^2a^4}{\pi^2}=N_1a^2+D\left[\pi^2+6(1-\nu)\left(\frac{a}{b}\right)^2\right] \tag{10.58}$$

In reference 10.18 the case is considered when three sides are simply supported, the other is clamped, and two concentrated, collinear, compressive forces P_0 act upon the two opposite simply supported edges. No numerical results are given.

Experimental results are given in reference 10.14 for the case when two opposite edges are clamped. A disagreement with theoretical results was found, similar to that discussed previously in the discussion of plates with all sides simply supported (sec. 10.2.1).

10.2.3 Rectangular Plates Having All Sides Clamped

The problem of plates with all sides clamped is defined by figure 10.5 with boundary conditions $w=\partial w/\partial n=0$ on all edges.

Weinstein and Chien (ref. 10.13) used a variational technique to obtain lower bounds for the fundamental frequency of a square plate under the hydrostatic tension $N_x=N_y=N$ and $N_{xy}=0$. Results are listed in table 10.7 for varying degrees of inplane tension. Upper bounds were also obtained by the Rayleigh-Ritz method using the deflection function

$$W(\bar{x},\bar{y})=A\cos^2\bar{x}\cos^2\bar{y}+B\cos^3\bar{x}\cos^3\bar{y} \tag{10.59}$$

where $\bar{x}$ and $\bar{y}$ are coordinates having their origin at the center of the plate. (See fig. 4.18.) For purposes of comparison, the easily determined frequency parameters when all sides are simply supported were computed in reference 10.13 and are also given in table 10.7. Also, a plot was made which compares the frequencies of a clamped square plate with those of clamped circular plates having area and circumference equal to those of the given square plate. The circular-plate results were obtained from reference 10.3, as discussed previously for clamped circular plates (sec. 10.1.1). These curves are shown in figure 10.9.

In reference 10.19 the Kato-Temple method (refs. 10.20 and 10.21) was used to derive an extremely accurate lower bound for the fundamental frequency of a clamped square plate subjected to hydrostatic tension $N=10\pi^2D/a^2$. Accurate upper bounds were obtained by using the Rayleigh-Ritz method with beam functions (see discussion of the C–C–C–C rectangular plate (sec. 4.3.1)), keeping both 6 and 36 terms in the series. These results are compared with those of reference 10.13 in table 10.8.

The perturbation technique is used in reference 10.15 to obtain fundamental frequency

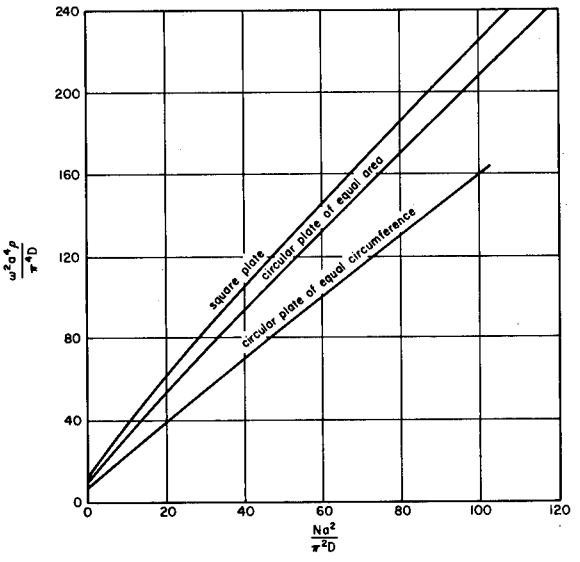


FIGURE 10.9.—Frequency parameter variations of clamped plates as functions of inplane hydrostatic tension. (After ref. 10.13)

TABLE 10.8.—*Comparison of Lower and Upper Bounds for the Fundamental Frequency Parameter* $\omega a^2\sqrt{\rho/D}$ *of a Clamped Square Plate Subjected to the Inplane Tension Parameter* $Na^2/\pi^2D=10$

$\omega a^2\sqrt{\rho/D}$				
Lower bounds		Upper bounds		
		Ref. 10.19		
Ref. 10.13	Ref. 10.19	36 terms	6 terms	Ref. 10.13
59. 922	59. 98389	59. 98488	59. 98498	60. 392

parameters for the problem previously discussed. Results are summarized in table 10.9.

10.3 PLATES HAVING OTHER SHAPES

Lurie (ref. 10.14) showed that for a plate of any polygonal shape, with all its boundaries simply supported and subjected to hydrostatic pressure $N_x=N_y=N=-p$ and $N_{xy}=0$, the vibration mode shapes are independent of the intensity of p. Hence, the mode shapes are identical to the buckling modes of the plate and also identical to the vibration modes of a stretched membrane having the same shape. Furthermore, the frequency of the loaded plate can be expressed as

$$\omega_{mn}^2=(\omega_{mn})_0^2\left[1-\frac{p}{(p_{mn})_{cr}}\right] \tag{10.60}$$

TABLE 10.9.—*Fundamental Frequency Parameter* $\omega a^2\sqrt{\rho/D}$ *Derived From the Perturbation Method for a Clamped Square Plate Subjected to Hydrostatic Tension*

$\frac{Na^2}{\pi^2D}$	$\omega a^2\sqrt{\rho/D}$
0	35. 989
5	49. 628
10	60. 019
20	68. 566

308-337 O—70——19

where $(\omega_{mn})_0$ is the frequency of the unloaded plate in the particular mode identified by the subscripts m, n and $(p_{mn})_{cr}$ is the critical buckling pressure in the same mode.

Schaefer and Havers (ref. 10.22) showed that frequencies of an equilateral triangular plate simply supported on all sides and subjected to hydrostatic pressure p can be calculated from the equation

$$\frac{pa^2}{D}+\frac{\omega_i^2a^4\rho/D}{\lambda_i}=\lambda_i \tag{10.61}$$

where a is the altitude of the triangle (see fig. 7.15) and λ_i are the eigenvalues of the membrane vibration problem determined from

$$\left.\begin{aligned}&\lambda_i=\frac{2}{3}\pi^2(l^2+m^2+n^2)\\&l+m+n=0\\&l, m, n=\pm1, \pm2, \pm3, \ldots\end{aligned}\right\} \tag{10.62}$$

The first six values of $(l^2+m^2+n^2)$ are given in table 10.10. A plot of the first six plate frequency parameters as functions of the inplane compression appears as figure 10.10.

Kaczkowski (ref. 10.23) utilized the fact that the superposition of certain vibration modes (having the same frequency) of a simply supported square plate will give a combined mode which has a nodal line on the diagonal of the square. In this way the frequencies and mode shapes of a plate in the form of an isosceles right triangle with all edges simply supported can be

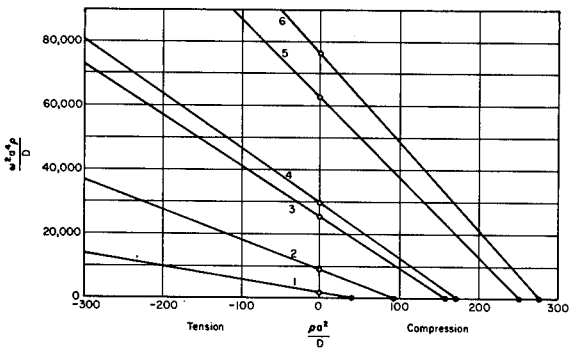


FIGURE 10.10.—Frequency parameters $\omega^2a^4\rho/D$ as functions of inplane hydrostatic pressure for a simply supported, equilateral, triangular plate. (After ref. 10.22)

TABLE 10.10.—*Terms for Computing the First Six Eigenvalues for the Equilateral Triangular Membrane*

i	l	m	n	$l^2+m^2+n^2$
1	1	1	−2	6
2	1	2	−3	14
3	2	2	−4	24
4	1	3	−4	26
5	2	3	−5	38
6	1	4	−5	42

found. The frequencies for $N_x=N_y=N, N_{xy}=0$ are given by

$$\omega_{mn}=(2m^2+2mn+n^2)\frac{\pi^2}{a^2}\sqrt{\frac{D}{\rho}}\left[1+\frac{Na^2}{(2m^2+2mn+n^2)\pi^2 D}\right]^{1/2} \qquad (m, n=1, 2, 3\ldots) \quad (10.63)$$

and the fundamental frequency occurs when $m=n=1$:

$$\omega_{11}=\frac{5\pi^2}{a^2}\sqrt{\frac{D}{\rho}}\left(1+\frac{Na^2}{5\pi^2 D}\right) \qquad (10.64)$$

The mode shapes of the triangular plate are (in terms of fig. 10.5):

$$W_{mn}(x, y)=A_{mn}\left[\sin\frac{m\pi x}{a}\sin\frac{n\pi y}{a}-(-1)^{m+n}\sin\frac{n\pi x}{a}\sin\frac{m\pi y}{a}\right] \qquad (m, n=1, 2, 3\ldots) \quad (10.65)$$

Isosceles right triangular plates having hydrostatic inplane forces and several other types of boundary conditions are discussed in reference 10.23. No numerical results are given for these problems, but the characteristic determinants yielding the frequencies are carefully shown. The determinants are of infinite order and contain terms having infinite series. Thus, the accuracy of a solution would depend upon the numbers of terms kept. Specific problems set up in detail in reference 10.23 are:

(1) The side $x=0$ clamped, the others simply supported
(2) The sides clamped, the hypotenuse simply supported
(3) The side $x=0$ free, the others simply supported
(4) Two sides free, the hypotenuse simply supported, and the point (0, 0) supported
(5) One side clamped, one side free, the hypotenuse simply supported
(6) Two sides simply supported, the hypotenuse clamped
(7) Two sides simply supported, the hypotenuse free

Pan (ref. 10.24) used the method of images to show that the square of the fundamental frequency of a 30°–60°–90° triangular plate simply supported on all sides (see fig. 7.17) and subjected to hydrostatic tension N is

$$\omega^2=\frac{28\pi^2}{3\rho a^2}\left(\frac{28}{3}\frac{D\pi^2}{a^2}+N\right) \qquad (10.66)$$

and the mode shape is

$$W(x, y)=\sin\frac{\pi x}{a\sqrt{3}}\sin\frac{3\pi y}{a}+\sin\frac{4\pi x}{a\sqrt{3}}\sin\frac{2\pi y}{a}+\sin\frac{5\pi x}{a\sqrt{3}}\sin\frac{\pi y}{a} \qquad (10.67)$$

REFERENCES

10.1. WAH, THEIN: Vibration of Circular Plates. J. ASA, vol. 34, no. 3, Mar. 1962, pp. 275–281.

10.2. WILLERS, FR. A.: Eigenschwingungen gedrückter Kreisplatten. ZAMM, vol. 20, no. 1, Feb. 1940, pp. 37–44.

10.3. BICKLEY, W. G.: Deflections and Vibrations of a Circular Elastic Plate Under Tension. Phil. Mag., ser. 7, vol. 15, no. 100, Apr. 1933, pp. 776–797.

10.4. FEDERHOFER, K.: Beigungsschwingungen der in ihrer Mittelebene belasteten Kreisplatte. Ingr.-Arch., Bd. 6, 1935, pp. 68–74.

10.5. LAMB, H.; AND SOUTHWELL, R. V.: The Vibrations of a Spinning Disk. Proc. Roy. Soc. (London), ser. A, vol. 99, 1921, pp. 272–280.

10.6. TEMPLE, G.; AND BICKLEY, W. G.: Rayleigh's Principle. Oxford Univ. Press (London), 1933.

10.7. MARTIN, C. J.: Vibrations of a Circular Elastic Plate Under Uniform Tension. Proc. 4th U.S. Natl. Congr. Appl. Mech., 1962, pp. 277–284.

10.8. MARTIN, C.: Vibrations of a Circular Disk Under Tension. Ph.D. thesis, Rensselaer Polytechnic Inst., 1961.

10.9. PRESCOTT, T.: Applied Elasticity. Dover Pub., 1946.

10.10. MASSA, EMILIO: Effetto di Stati Piani di Coazione sulle Vibrazioni Libere con Piccola Inflessione di Piastre Circolari. Rend. Inst. Lombardo Sci. Lett., vol. 97, no. 3, 1963, pp. 319–345.

10.11. SOUTHWELL, R. V.: On the Free Vibrations of a Uniform Circular Disc Clamped at Its Center and on the Effect of Rotation. Proc. Roy. Soc. (London), ser. A, vol. 101, 1922, pp. 133–153.

10.12. HERRMANN, G.: The Influence of Initial Stress on the Dynamic Behavior of Elastic and Viscoelastic Plates. Pub. Int. Ass. for Bridge and Struct. Eng., vol. 16, 1956, pp. 275–294.

10.13. WEINSTEIN, A.; AND CHIEN, W. Z.: On the Vibrations of a Clamped Plate Under Tension. Quart. Appl. Math., vol. 1, Apr. 1943, pp. 61–68.

10.14. LURIE, H.: Lateral Vibrations as Related to Structural Stability. J. Appl. Mech., vol. 19, no. 2, June 1952, pp. 195–204.

10.15. TRUBERT, M.; AND NASH, W. A.: Effect of Membrane Forces on Lateral Vibrations of Rectangular Plates. Tech. Note No. 2 (AFOSR-TN-60-437, CFSTI No. AD 239042), Eng. Mech. Div., Univ. Florida, May 1960.

10.16. FELDMAN, M. R.: A Difference Method of Investigating the Stability and Oscillations of Plates. Izv. Akad. Nauk Arm. SSR, Ser. Fiz.-Mat. Nauk, vol. 12, no. 3, 1959, pp. 15–27. (In Russian.)

10.17. MASSONNET, CH.: Les Rélations entre les Modes Normaux de Vibration et la Stabilité des Systems Élastiques. Bull. Cours et Lab. d'Essais des Constructions du Genie Civil et d'Hydraulique Fluviale, vol. 1, nos. 1 and 2, 1940.

10.18. NOWACKI, W.: Some Problems of Rectangular Plates. Bull. Acad. Pol. Sci., Ser. Sci. Tech., vol. 9, no. 4, 1961, pp. 247–256.

10.19. KAUL, R. K., AND TEWARI, S. G.: On the Bounds of Eigenvalues of a Clamped Plate in Tension. J. Appl. Mech., vol. 25, no. 1, Mar. 1958, pp. 52–56.

10.20. KATO, T.: On the Upper and Lower Bounds of Eigenvalues. J. Phys. Soc. Japan, vol. 4, no. 1, 1949, pp. 334–339.

10.21. TEMPLE, G.: The Accuracy of Rayleigh's Method of Calculating the Natural Frequencies of Vibrating Systems. Proc. Roy. Soc. (London), ser. A, vol. 211, 1952, p. 204.

10.22. SCHAEFFER, H., AND HAVERS, A.: Die Eigenschwingungen der in ihrer Ebene allseitig gleichmässig belasteten gleichseitigen Dreiecksplatte. Ingr.-Arch., Bd. 7, 1936, pp. 83–87.

10.23. KACZKOWSKI, Z.: Drgania Swobodne I Wyboczenie Plyty Trojkatnej. Arch. Mech. Stos., vol. 8, no. 1, 1956, pp. 13–28.

10.24. PAN, LIH-CHOW: Equilibrium, Buckling and Vibration of a 30°–60°–90° Triangular Plate Simply Supported at Its Edges. Acta Phys. Sinica, vol. 3, no. 12, 1956, pp. 215–245. (In Chinese.)

Chapter 11

Plates With Variable Thickness

In the case of plates with variable thickness, the governing differential equation of motion is found to have variable coefficients, and this fact increases the difficulty of solution. This added complexity will be demonstrated below in both polar and rectangular coordinates. Results are available only for isotropic plates having no inplane forces.

11.1 CIRCULAR PLATES

If inplane forces and rotary inertia are disregarded, the equations of motion in polar coordinates are

$$\left.\begin{aligned} &\frac{\partial}{\partial r}(rQ_r)+\frac{\partial Q_\theta}{\partial \theta}=\gamma h\frac{\partial^2 w}{\partial t^2} \\ &\frac{\partial}{\partial r}(rM_r)-M_\theta+\frac{\partial M_{r\theta}}{\partial \theta}-rQ_r=0 \\ &\frac{\partial}{\partial r}(rM_{r\theta})+\frac{\partial M_\theta}{\partial \theta}+M_{r\theta}-rQ_\theta=0 \end{aligned}\right\} \quad (11.1)$$

Equations (11.1) correspond to equations (A.2) and (A.8) of the appendix which were derived in rectangular coordinates and can be obtained from them by direct transformation; or they can be derived by summing forces and moments on a typical, infinitesimal, sectorial area. In equations (11.1), γ is taken to be the mass density per unit *volume* of plate, unlike the constant ρ used elsewhere throughout this work.

For an isotropic plate, equations (A.35) become

$$\left.\begin{aligned} M_r&=-D\left[\frac{\partial^2 w}{\partial r^2}+\nu\left(\frac{1}{r}\frac{\partial w}{\partial r}+\frac{1}{r^2}\frac{\partial^2 w}{\partial \theta^2}\right)\right] \\ M_\theta&=-D\left[\frac{1}{r}\frac{\partial w}{\partial r}+\frac{1}{r^2}\frac{\partial^2 w}{\partial \theta^2}+\nu\frac{\partial^2 w}{\partial r^2}\right] \\ M_{r\theta}&=-D(1-\nu)\frac{\partial}{\partial r}\left(\frac{1}{r}\frac{\partial w}{\partial \theta}\right) \end{aligned}\right\} \quad (11.2)$$

where $D=Eh^3/12(1-\nu^2)$; that is, D is a function of the thickness.

To obtain a fourth-order differential equation corresponding to equation (1.1), it is only necessary to substitute equations (11.2) into the last two of equations (11.1) and, in turn, substitute these into the first of equations (11.1). However, if the thickness is a function of r and/or θ, the resulting differential equation will be quite lengthy and will have variable coefficients (i.e., functions of r and/or θ). This expanded equation will not be presented here. Needless to say, very little has been done toward obtaining solutions to this differential equation in all its generality.

Timoshenko and Woinowsky-Krieger (ref. 11.1) and Conway (ref. 11.2) showed that, for the axisymmetric problem (no variation with θ), the equation of motion becomes

$$\frac{1}{r}\frac{\partial}{\partial r}\left\{r\left[D\frac{\partial}{\partial r}\left(\frac{\partial^2 w}{\partial r^2}+\frac{1}{r}\frac{\partial w}{\partial r}\right)+\frac{\partial D}{\partial r}\left(\frac{\partial^2 w}{\partial r^2}+\frac{\nu}{r}\frac{\partial w}{\partial r}\right)\right]\right\}+\gamma h\frac{\partial^2 w}{\partial t^2}=0 \quad (11.3)$$

Conway (ref. 11.2) gave some special solutions of equation (11.3) when the flexural rigidity varied according to

$$D=D_0 r^m \quad (11.4)$$

where

$$D_0=\frac{Eh_0^3}{12(1-\nu^2)} \quad (11.5)$$

and when the boundary of the circular plate is *clamped*. Poisson's ratio was restricted to

$$\nu=\frac{1}{9}(2m-3) \quad (11.6)$$

which simplified the solution of equation (11.3) considerably.

In reference 11.2 exact solutions to equation (11.3) were obtained for several values of m in

equation (11.4). For $m=2$, $\nu=1/9$, and a solid plate, the solution takes the form

$$W(r)=r^{-2/3}[C_1J_1(u)+C_2I_1(u)] \qquad (11.7)$$

where

$$\left.\begin{aligned} u &= br^{2/3} \\ b^4 &= \frac{60\gamma\omega^2}{Eh_0^2} \end{aligned}\right\} \qquad (11.8)$$

and J_1 and I_1 are the regular and modified Bessel functions of the first kind of order one. Applying the boundary conditions (eqs. (2.2)) gives the characteristic equation

$$\frac{J_1'(u_0)}{J_1(u_0)}=\frac{I_1'(u_0)}{I_1(u_0)} \qquad (11.9)$$

where the primes indicate differentiation with respect to the argument u and

$$u_0=ba^{2/3} \qquad (11.10)$$

where a is the boundary radius. The first 10 roots of equation (11.9) were given in table 2.1 ($n=1$), the lowest root being

$$u_0=\left(\frac{60\ \gamma\omega^2}{Eh_0^2}\right)^{1/4}a^{2/3}=(21.26)^{1/2} \qquad (11.11)$$

Consider a clamped circular plate having a constant thickness equal to the maximum thickness (at the boundary) of the variable thickness plate previously described ($m=2$, $\nu=1/9$). Then, according to reference 11.2, the ratio of the fundamental frequency of the constant-thickness plate to that of the variable-thickness plate is 1.08.

For $m=18/7$ and $\nu=5/21$, the frequency equation

$$u_0(\tan u_0+\tanh u_0)=2\tan u_0\tanh u_0 \qquad (11.12)$$

was given, where now

$$u_0=\left(\frac{637}{6}\frac{\gamma\omega^2}{Eh_0^2}\right)^{1/4}a^{4/7} \qquad (11.13)$$

The first root of equation (11.12) was given as $u_0=5.27$. The ratio of the fundamental frequency of the constant-thickness plate to that of the variable-thickness plate having the same thickness at the boundary was found to be 1.13.

For $m=3$ and $\nu=1/3$, there is the important case of linearly varying thickness, which is discussed in reference 11.3 as well as in reference 11.2. The characteristic equation for a solid circular plate is found to be

$$J_2(u_0)I_1(u_0)=J_1(u_0)I_2(u_0) \qquad (11.14)$$

with

$$u_0=\left(\frac{512}{3}\frac{\gamma\omega^2}{Eh_0^2}\right)^{1/4}a^{1/2} \qquad (11.15)$$

Equation (11.14) is also the characteristic equation for the transverse vibrations of a cantilever beam having a circular cross section and linear taper. Thus, by analogy with results for beams, the first three roots of equation (11.14) are found to be $u_0=5.906$, 9.197, and 12.402.

The ratios of the first three axisymmetric frequencies of the constant-thickness plate to those of the variable-thickness plate having the same thickness at the boundary are found to be 1.17, 1.88, and 2.31.

The case when $m=6$ and ν is arbitrary is also discussed in reference 11.2, but no numerical results are given.

It is interesting to observe that in the case of variable-thickness plates the frequency parameter depends upon Poisson's ratio for clamped as well as for other boundary conditions.

In reference 11.4 the work just described was extended to annular plates of linearly varying thickness which are clamped on both the inner and outer boundaries (fig. 11.1). The solution for the linearly tapered beam again applies when Poisson's ratio for the plate is 1/3. The characteristic determinant yielding the frequencies is

$$\begin{vmatrix} J_2(\beta) & Y_2(\beta) & I_2(\beta) & K_2(\beta) \\ J_3(\beta) & Y_3(\beta) & -I_3(\beta) & K_3(\beta) \\ J_2(\alpha) & Y_2(\alpha) & I_2(\alpha) & K_2(\alpha) \\ J_3(\alpha) & Y_3(\alpha) & -I_3(\alpha) & K_3(\alpha) \end{vmatrix}=0 \qquad (11.16)$$

where

$$\left.\begin{aligned} \beta^2 &= 4\omega a\left(\frac{32}{3}\frac{\gamma}{Eh_0^2}\right)^{1/2} \\ \alpha^2 &= 4\omega a\left(\frac{32}{3}\frac{\gamma}{Eh_0^2}\right)^{1/2} \end{aligned}\right\} \qquad (11.17)$$

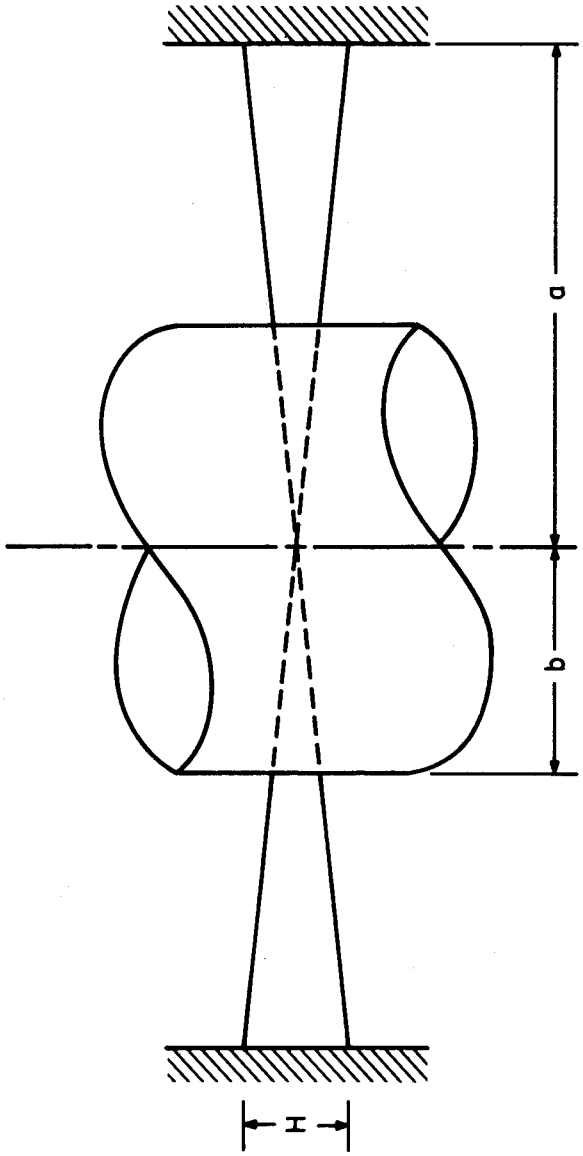


FIGURE 11.1.—Annular plate with linearly varying thickness and both boundaries clamped. (After ref. 11.4)

TABLE 11.1.—*Axisymmetric Frequency Parameters* $(\omega a^2/H)(2\gamma/3E)^{1/2}$ *for an Annular Plate Having Linearly Varying Thickness and Clamped on Both Boundaries;* $\nu=1/3$

Mode no.	$(\omega a^2/H)(2\gamma/3E)^{1/2}$ for values of b/a of—			
	½	⅓	¼	1/10
1	16. 5	8. 04	5. 84	3. 32
2	45. 2	21. 9	15. 8	8. 71
3	88. 4	42. 6	30. 6	16. 7
4	146	70. 3	50. 4	27. 3
5	211	104. 8	75. 0	40. 5

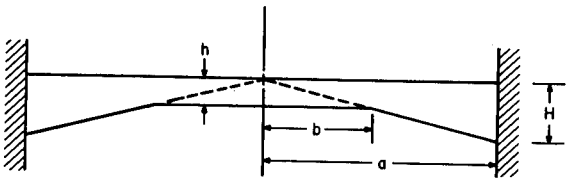


FIGURE 11.2.—Circular plate with both constant and linearly varying thickness and clamped on the boundary. (After ref. 11.4)

Frequency parameters for various ratios of b/a are listed in table 11.1.

Also examined in reference 11.4 was the solid circular plate which has a linearly varying thickness in the interval $b \leqq r \leqq a$ and a constant thickness in the interval $0 \leqq r \leqq b$ (see fig. 11.2) and is clamped along its edge. Using the separate solutions for the variable- and constant-thickness regions and enforcing two boundary conditions at $r=a$ and four continuity conditions at $r=b$ lead to the characteristic determinant:

$$\begin{vmatrix} J_2(2\zeta\kappa) & Y_2(2\zeta\kappa) & I_2(2\zeta\kappa) & K_2(2\zeta\kappa) & \cdots & \cdots \\ J_3(2\zeta\kappa) & Y_3(2\zeta\kappa) & -I_3(2\zeta\kappa) & K_3(2\zeta\kappa) & \cdots & \cdots \\ J_2(2\zeta) & Y_2(2\zeta) & I_2(2\zeta) & K_2(2\zeta) & -J_0(\zeta) & -I_0(\zeta) \\ -J_3(2\zeta) & -Y_3(2\zeta) & I_3(2\zeta) & -K_3(2\zeta) & J_1(\zeta) & -I_1(\zeta) \\ J_4(2\zeta) & Y_4(2\zeta) & I_4(2\zeta) & K_4(2\zeta) & \left[-\frac{J_1(\zeta)}{\zeta}+J_0(\zeta)\right] & \left[\frac{I_1(\zeta)}{\zeta}-I_0(\zeta)\right] \\ -J_5(2\zeta) & -Y_5(2\zeta) & I_5(2\zeta) & -K_5(2\zeta) & \left[\left(\frac{2}{\zeta^2}-1\right)J_1(\zeta)-\frac{J_0(\zeta)}{\zeta}\right] & \left[-\left(\frac{2}{\zeta^2}+1\right)I_1(\zeta)+\frac{I_0(\zeta)}{\zeta}\right] \end{vmatrix} = 0 \tag{11.18}$$

where

$$\left.\begin{aligned}\zeta&=\frac{32}{3}\frac{\omega^2\gamma b^4}{Eh^2}\\ \kappa&=a/b\end{aligned}\right\} \qquad (11.19)$$

Again, Poisson's ratio is restricted to a value of 1/3. Frequency parameters for various a/b ratios are given in table 11.2.

Thurston and Tsui (ref. 11.5) investigated the problem of a linearly tapered circular plate which is supported elastically on a central supporting area as shown in figure 11.3. The Rayleigh-Ritz method was used with a deflection function of the form

$$W(r)=A+Br^2+Cr^3 \qquad (11.20)$$

TABLE 11.2.—*Axisymmetric Frequency Parameters* $(\omega a^2/h)(2\gamma/3E)^{1/2}$ *for Clamped Circular Plate Having Linearly Varying Thickness in Interval* $b \leqq r \leqq a$ *and Constant Thickness* h *in Interval* $0 \leqq r \leqq b$; $\nu=1/3$

Mode no.	$(\omega a^2/h)(2\gamma/3E)^{1/2}$ for values of b/a of—			
	1	1/2	1/3	1/4
1	2. 55	3. 97	6. 33	8. 81
2	9. 95	14. 21	17. 03	20. 89
3	22. 23	28. 00	37. 70	44. 89

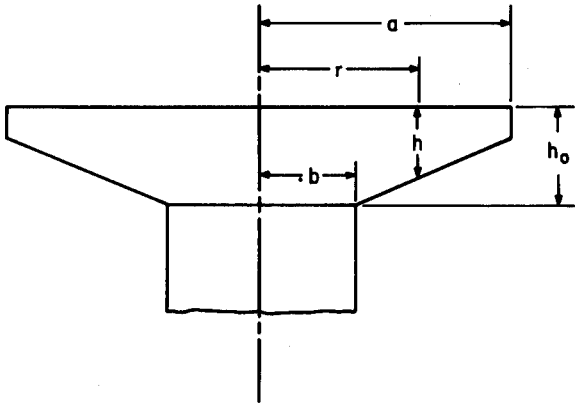


FIGURE 11.3.—Linearly tapered circular plate supported elastically on a central supporting area. (After ref. 11.5)

for axisymmetric vibrations. Equation (11.20) satisfies the condition of zero slope at the origin; in addition, the condition

$$\int_0^b W(r)r\,dr=0 \qquad (11.21)$$

was imposed. This latter condition is designed to relax the condition of rigid clamping along the central core and replace it by one of "no net volume flow back and forth" across the surface of attachment. Equation (11.21) leads to the relationship

$$A=-2b^2\left(\frac{B}{4}+\frac{Cb}{5}\right) \qquad (11.22)$$

and reduces the system to two degrees of freedom. The Rayleigh-Ritz procedure yields the two frequencies given by

$$\frac{12(1-\nu^2)\omega^2\gamma}{Eh_0^2}=\{-(\beta\beta'-2\alpha'\lambda-2\alpha\lambda') \pm[(\beta\beta'-2\alpha'\lambda-2\alpha\lambda')^2-(4\alpha'\lambda'-\beta'^2)(4\alpha\lambda-\beta^2)]^{1/2}\}\div(4\alpha'\lambda'-\beta'^2) \qquad (11.23)$$

where α, α', β, β', λ, and λ' are given by

$$\left.\begin{aligned}
\alpha=8(1+\nu)\Big\{&\frac{1}{2}a^2+\Big[3\frac{b}{a-b}k+3\frac{b^2}{(a-b)^2}k^2+\frac{b^3}{(a-b)^3}k^3\Big]\frac{a^2-b^2}{2}\\
&-\Big[\frac{3}{a-b}k+6\frac{b}{(a-b)^2}k^2+3\frac{b^2}{(a-b)^3}k^3\Big]\frac{a^3-b^3}{3}+\Big[3k^2\frac{1}{(a-b)^2}\\
&+3k^3\frac{b}{(a-b)^3}\Big]\frac{a^4-b^4}{4}-\frac{k^3}{(a-b)^3}\frac{a^5-b^5}{5}\Big\}\\
\beta=36(1+\nu)\Big\{&\frac{1}{3}a^3+\Big[3\frac{b}{a-b}k+3\frac{b^2}{(a-b)^2}k^2+\frac{b^3}{(a-b)^3}k^3\Big]\frac{a^3-b^3}{3}\\
&-\Big[\frac{3}{a-b}k+6\frac{b}{(a-b)^2}k^2+3\frac{b^2}{(a-b)^3}k^3\Big]\frac{a^4-b^4}{4}+\Big[3k^2\frac{1}{(a-b)^2}\\
&+3k^3\frac{b}{(a-b)^3}\Big]\frac{a^5-b^5}{5}-\frac{k^3}{(a-b)^3}\frac{a^6-b^6}{6}\Big\}\\
\lambda=(45+36\nu)\Big\{&\frac{1}{4}a^4+\Big[3\frac{b}{a-b}k+3\frac{b^2}{(a-b)^2}k^2+\frac{b^3}{(a-b)^3}k^3\Big]\frac{a^4-b^4}{4}\\
&-\Big[\frac{3}{a-b}k+6\frac{b}{(a-b)^2}k^2+3\frac{b^2}{(a-b)^3}k^3\Big]\frac{a^5-b^5}{5}+\Big[3k^2\frac{1}{(a-b)^2}\\
&+3k^3\frac{b}{(a-b)^3}\Big]\frac{a^6-b^6}{6}-\frac{k^3}{(a-b)^3}\frac{a^7-b^7}{7}\Big\}\\
\alpha'=\Big(1+k\frac{b}{a-b}\Big)&\Big[\frac{(a^2-b^2)b^4}{8}-\frac{(a^4-b^4)b^2}{4}+\frac{a^6-b^6}{6}\Big]-\frac{k}{a-b}\Big[\frac{(a^3-b^3)b^4}{12}\\
&-\frac{(a^5-b^5)b^2}{5}+\frac{a^7-b^7}{7}\Big]+\frac{1}{24}b^6\\
\beta'=\Big(1+k\frac{b}{a-b}\Big)&\Big[\frac{(a^2-b^2)b^5}{5}-\frac{(a^4-b^4)b^3}{5}-\frac{(a^5-b^5)b^2}{5}+\frac{2(a^7-b^7)}{7}\Big]\\
&-\frac{k}{a-b}\Big[\frac{2(a^3-b^3)b^5}{15}-\frac{4(a^5-b^5)b^3}{25}-\frac{(a^6-b^6)b^2}{6}+\frac{a^8-b^8}{4}\Big]+\frac{3}{35}b^7\\
\lambda'=\Big(1+k\frac{b}{a-b}\Big)&\Big[\frac{2(a^2-b^2)b^6}{25}-\frac{4(a^5-b^5)b^3}{25}+\frac{a^8-b^8}{8}\Big]-\frac{k}{a-b}\Big[\frac{4(a^3-b^3)b^6}{75}\\
&-\frac{2(a^6-b^6)b^3}{15}+\frac{a^9-b^9}{9}\Big]+\frac{9}{200}b^8
\end{aligned}\right\}\qquad(11.24)$$

and where the thickness is defined by

$$\begin{aligned}
h&=h_0 \qquad (0\leqq r\leqq b)\\
h&=h_0\Big[1-k\Big(\frac{r-b}{a-b}\Big)\Big] \qquad (b\leqq r\leqq a)
\end{aligned}\qquad(11.25)$$

Detailed calculations were made for an aluminum disk having the following constants: $a=1.00$ inch, $b=0.375$ inch, $E=10.6\times10^6$ psi, and $\nu=0.33$. These results are plotted in figures 11.4 and 11.5 for various tapers k and are compared with experimental results for $k=4/5$. In figure 11.4 the theoretical values are plotted directly as they arise in the computations. In figure 11.5 the values are adjusted to account for additional cement and a barium titanate element used in the experiment.

Kovalenko (ref. 11.6) made a study of the annular plate having thickness varying according to the equation

$$h=h_0\left(1-\frac{r}{r_0}\right) \tag{11.26}$$

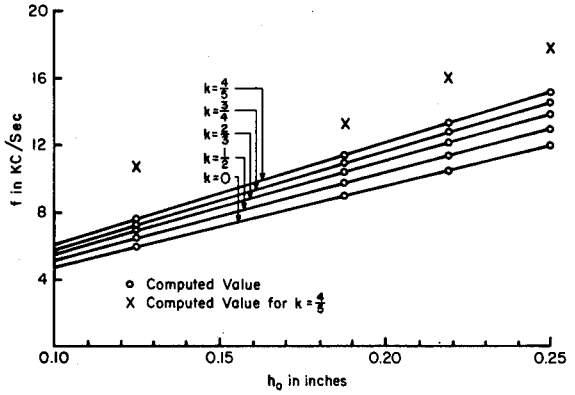


FIGURE 11.4.—Uncorrected cyclic frequencies f for a linearly tapered, circular aluminum plate. (After ref. 11.5)

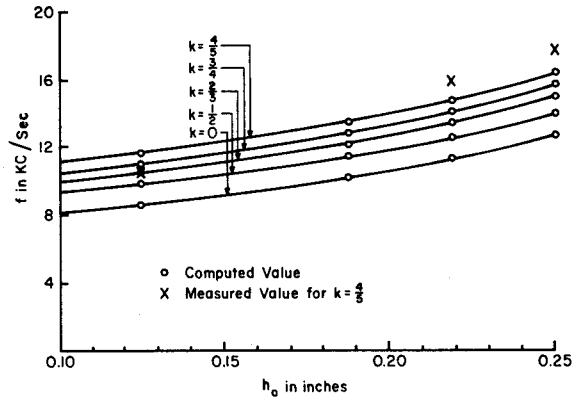


FIGURE 11.5.—Adjusted cyclic frequencies f for a linearly tapered, circular aluminum plate. (After ref. 11.5)

(see fig. 11.6). His primary work was a direct attack upon the differential equation by assuming a series form of solution. Boundary conditions led to an infinite characteristic determinant, which was truncated for an approximate solution. Detailed numerical results were given for the special configuration where the boundary $r=b=0.1r_0$ was clamped and the boundary $r=a=0.5r_0$ was completely free. A Poisson's ratio of 1/3 was used. By use of the series method the lowest axisymmetric frequency parameter was found to be

$$\omega_{00}=19.00\sqrt{\frac{D_0}{\gamma h_0 r_0^4}} \tag{11.27}$$

where D_0 is as defined in equation (11.5). The lowest antisymmetric frequency (i.e., cos $n\theta$ mode, with $n=1$) was found to be

$$\omega_{10}=18.24\sqrt{\frac{D_0}{\gamma h_0 r_0^4}} \tag{11.28}$$

When equations (11.27) and (11.28) are compared it can be observed that, as in the case of certain b/a ratios for constant-thickness annular plates (see discussion for annular plates (sec. 2.2.7)), the fundamental mode is antisymmetric. In table 11.3 are given the mode shapes corresponding to these two frequencies and the ratios of bending moments.

Rayleigh-Ritz solutions were also obtained in reference 11.6 by using the radial variation in deflection

$$W(r)=A_1(r-b)^2+A_2(r-b)^3 \tag{11.29}$$

giving the frequencies

$$\left.\begin{aligned}\omega_{00}&=19.2\sqrt{\frac{D_0}{\gamma h_0 r_0^4}}\\ \omega_{10}&=18.47\sqrt{\frac{D_0}{\gamma h_0 r_0^4}}\end{aligned}\right\} \tag{11.30}$$

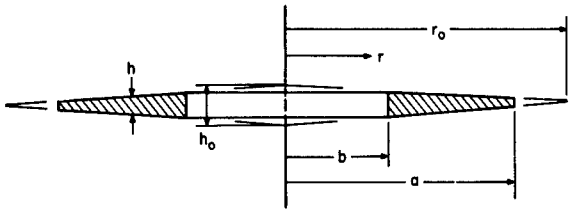


FIGURE 11.6.—Annular plate with thickness variation $h=h_0[1-(r/r_0)]$.

TABLE 11.3.—*Mode Shapes and Ratios of Bending Moment for First 2 Modes of Linearly Tapered Annular Plate Shown in Fig. 11.6;* $a=0.5r_0$; $b=0.1r_0$

$\frac{r}{r_0}$	Symmetric ($n=0$)			Antisymmetric ($n=1$)		
	$\frac{w}{(w)_{r=a}}$	$\frac{M_r}{(M_r)_{r=b}}$	$\frac{M_\theta}{(M_\theta)_{r=b}}$	$\frac{w}{(w)_{r=a}}$	$\frac{M_r}{(M_r)_{r=b}}$	$\frac{M_\theta}{(M_\theta)_{r=b}}$
0.1	0	1	1	0	1	1
0.2	.112	.382	.988	.112	.319	.713
0.3	.362	.149	.552	.359	.120	.334
0.4	.677	.032	.245	.671	.025	.121
0.5	1	0	.094	1	0	.035

An integral-equation approach to the problem of circular plates of variable thickness is presented in reference 11.7, but no numerical results are given.

A method of handling variable-thickness circular or annular plates is discussed in reference 11.8 whereby the plate is represented by circumferential strips of constant thickness and lumped mass. A demonstration of the method on a constant-thickness plate is given, but no numerical results for variable-thickness plates are included.

11.2 RECTANGULAR PLATES

In the case of rectangular coordinates it is shown in the appendix that the governing differential equation of motion for an isotropic plate of variable thickness having no inplane forces is

$$\nabla^2(D\nabla^2 w)-(1-\nu)\left(\frac{\partial^2 D}{\partial y^2}\frac{\partial^2 w}{\partial x^2}-2\frac{\partial^2 D}{\partial x\,\partial y}\frac{\partial^2 w}{\partial x\,\partial y}+\frac{\partial^2 D}{\partial x^2}\frac{\partial^2 w}{\partial y^2}\right)+\gamma h\frac{\partial^2 w}{\partial t^2}=0 \quad (11.31)$$

where the mass density per unit volume γ has been substituted in place of ρ.

Very little has been done in solving equation (11.31) as it stands because of the variable coefficients arising when D is not constant. Appl and Byers (ref. 11.9) studied the case when the thickness varied only in one direction, say x. In that case, equation (11.29) simplifies to

$$D\nabla^4 w+2\frac{dD}{dx}\frac{\partial}{\partial x}\nabla^2 w+\frac{d^2D}{dx^2}\left(\frac{\partial^2 w}{\partial x^2}+\nu\frac{\partial^2 w}{\partial y^2}\right)+\gamma h\frac{\partial^2 w}{\partial t^2}=0 \quad (11.32)$$

Furthermore, for a plate having parallel edges simply supported, a solution in the form of equation (1.33) can be taken, thereby exactly satisfying the boundary conditions along the parallel edges and reducing equation (11.32) to an ordinary differential equation having variable coefficients.

In reference 11.9 extensive calculations were made for the rectangular plate having all sides simply supported and a linear thickness variation in the x-direction given by

$$h=h_0\left(1+\alpha\frac{x}{a}\right) \quad (11.33)$$

where x is measured from one edge, the length of the plate is a (cf. fig. 4.4), and α is a constant determining the rate of taper. A special technique (ref. 11.10) was used for obtaining both upper and lower bounds for fundamental frequency parameters. Results thus obtained are presented as table 11.4 for $\nu=0.3$ and for various aspect ratios. In this table, in addition to upper and lower bounds, a mean value is computed along with a maximum possible error in this mean value. For purposes of comparison, an upper bound was also determined by the Rayleigh method by using a deflection function of the form

$$W(x,y)=\left[\left(\frac{x}{a}\right)^4-2\left(\frac{x}{a}\right)^3+\frac{x}{a}\right]\sin\frac{\pi y}{b} \quad (11.34)$$

A representative fundamental mode shape is depicted in figure 11.7 for $a/b=1.0$ and $\alpha=0.8$. The sine curve for the case of uniform thickness ($\alpha=0$) is also shown for purposes of comparison.

TABLE 11.4.—*Fundamental Frequency Parameters* $\omega^2 a^4 \gamma h_0/D_0$ *for Linearly Tapered Rectangular Plates Simply Supported on All Edges;* $\nu=0.3$

$\frac{a}{b}$	α	$\omega^2 a^4 \gamma h_0/D_0$				
		Upper bound	Lower bound	Mean value	Maximum error, percent	Rayleigh method
0.25	0.1	121.112	121.067	121.089	0.0187	121.081
	.2	132.437	132.434	132.436	.00103	132.435
	.3	144.144	143.792	143.968	.122	144.026
	.4	155.899	155.828	155.863	.0228	155.853
	.5	167.925	167.891	167.908	.0102	167.913
	.6	180.243	180.145	180.194	.0273	----------
	.7	192.857	192.586	192.721	.0705	----------
	.8	206.045	204.949	205.497	.267	----------
0.50	0.1	167.657	167.656	167.657	0.0000596	167.656
	.2	183.585	183.577	183.581	.00234	183.579
	.3	199.979	199.964	199.972	.00382	199.970
	.4	217.902	216.262	217.082	.379	216.825
	.5	234.463	233.968	234.215	.106	234.143
	.6	252.126	251.763	251.944	.0723	----------
	.7	270.394	269.883	270.139	.0946	----------
	.8	289.317	288.256	288.786	.184	----------
0.75	0.1	262.051	262.003	262.027	0.00921	262.036
	.2	287.200	287.098	287.149	.0178	287.132
	.3	313.325	312.989	313.157	.0538	313.103
	.4	340.388	339.718	340.053	.0986	339.941
	.5	367.708	367.591	367.650	.0160	367.703
	.6	396.506	395.625	396.066	.111	----------
	.7	426.062	425.125	425.593	.110	----------
	.8	457.397	454.239	455.818	.348	----------
1.00	0.1	429.349	429.339	429.344	0.00124	429.346
	.2	470.556	470.521	470.539	.00372	470.549
	.3	513.379	512.930	513.154	.0437	513.220
	.4	557.816	556.573	557.195	.112	557.355
	.5	603.180	602.841	603.011	.0281	603.006
	.6	650.563	649.540	650.051	.0788	----------
	.7	699.732	697.235	698.483	.179	----------
	.8	751.416	745.011	748.214	.430	----------
1.25	0.1	704.866	704.696	704.781	0.0120	704.752
	.2	773.000	771.784	772.392	.0787	772.191
	.3	842.034	841.884	841.959	.00892	842.013
	.4	914.608	913.618	914.113	.0542	913.759
	.5	988.921	987.612	988.267	.0663	988.424
	.6	1066.211	1063.428	1064.819	.131	----------
	.7	1146.985	1139.781	1143.383	.316	----------
	.8	1229.929	1218.858	1224.393	.454	----------
1.50	0.1	1133.669	1133.338	1133.504	0.0146	1133.456
	.2	1242.578	1239.000	1240.789	.144	1241.395
	.3	1353.687	1350.576	1352.131	.115	1352.379
	.4	1468.157	1465.250	1466.703	.0992	1467.138
	.5	1586.689	1583.145	1584.917	.112	----------
	.6	1709.603	1701.686	1705.645	.233	----------
	.7	1837.799	1820.621	1829.210	.472	----------
	.8	1967.569	1948.622	1958.095	.486	----------

TABLE 11.4.—*Fundamental Frequency Parameters* $\omega^2a^4\gamma h_0/D_0$ *for Linearly Tapered Rectangular Plates Simply Supported on All Edges;* $\nu=0.3$—Continued

$\frac{a}{b}$	α	$\omega^2a^4\gamma h_0/D_0$				
		Upper bound	Lower bound	Mean value	Maximum error, percent	Rayleigh method
1.75	0.1	1771.579	1770.158	1770.869	0.0401	1770.631
	.2	1939.753	1934.993	1937.373	.123	1938.224
	.3	2110.977	2108.915	2109.946	.0489	2109.667
	.4	2288.368	2284.341	2286.354	.0882	2288.320
	.5	2471.362	2461.928	2466.645	.192	----------
	.6	2660.680	2641.065	2650.873	.371	----------
	.7	2850.204	2831.734	2840.969	.326	----------
	.8	3054.910	3031.066	3042.988	.393	----------
2.00	0.1	2685.834	2679.248	2682.541	0.123	2681.525
	.2	2935.362	2930.935	2933.149	.0755	2935.547
	.3	3193.446	3187.392	3190.419	.0950	3203.400
	.4	3458.506	3446.658	3452.582	.172	3489.606
	.5	3734.808	3702.730	3718.769	.433	----------
	.6	4012.388	3979.820	3996.104	.409	----------
	.7	4283.839	4266.413	4275.126	.204	----------
	.8	4556.204	4539.970	4556.204	.358	----------

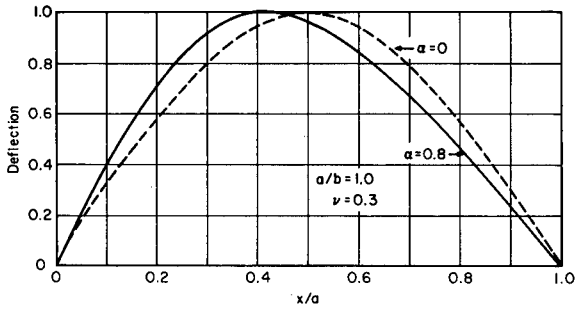


FIGURE 11.7.—Fundamental mode of a simply supported square plate having linear thickness variation in the x-direction; $\nu=0.3$. (After ref. 11.9)

Gumeniuk (ref. 11.11) used the finite-difference method to derive a formula for the fundamental frequency of a simply supported rectangular plate having linear thickness variation. This work was extended by Gontkevich (ref. 11.12) to plates having other boundary conditions. Fundamental frequencies are determined from the formula

$$\omega=\frac{9.5}{b^2}\sqrt{\frac{D_0}{2\gamma h_0}(A+D-\sqrt{(A-D)^2+4BC})} \tag{11.35}$$

where the constants A, B, C, and D are given in table 11.5 for the types of boundary conditions depicted in the table. The thickness parameter λ is defined by

$$\lambda=\frac{h_1-h_0}{h_0} \tag{11.36}$$

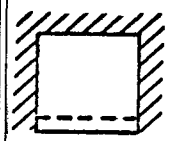
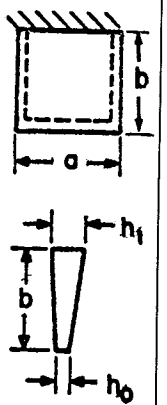
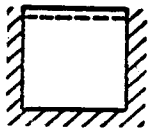
where the thicknesses h_0 and h_1 are as shown in table 11.5.

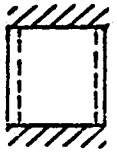
Plunkett and Wilson (refs. 11.13 and 11.14) measured the frequencies of linearly tapered steel cantilever plates, with the taper occurring between the free edges as shown in figure 11.8. Figure 11.8 shows the variation in the frequency parameter

$$\phi=\frac{\omega a^2}{h_0}\sqrt{\frac{12\gamma(1-\nu^2)}{E}} \tag{11.37}$$

with the wedge angle θ, where h_0 is the greatest thickness and a is the span of the plate (5 inches, in fig. 11.8). The values shown for zero wedge angle (constant thickness) were computed by elementary beam theory. Fundamental frequency parameters for the various wedge

TABLE 11.5.—*Constants for Eq. (11.35) for Various Types of Boundary Conditions*

Boundary conditions	Constants for eq. (11.35)	Boundary conditions	Constants for eq. (11.35)
	$A=\left(1+\frac{2}{3}\lambda\right)^2\left\{\left(\frac{b^2}{a^2}+2\right)^2+1-\frac{\lambda}{1+\frac{2}{3}\lambda}-\frac{2\lambda^2[2+(\nu b^2/a^2)]}{3\left(1+\frac{2}{3}\lambda\right)^2}\right\}$ $B=\left(1+\frac{2}{3}\lambda\right)^2\left[\left(\frac{b^2}{a^2}+2\right)\left(2\frac{b}{a}-\frac{\lambda}{1+\frac{2}{3}\lambda}\right)-\frac{2\lambda^2}{3\left(1-\frac{2}{3}\lambda\right)^2}\right]$ $C=\left(1+\frac{\lambda}{3}\right)^2\left[\left(\frac{b^2}{a^2}+2\right)\left(\frac{2b}{a}+\frac{\lambda}{1+\frac{\lambda}{3}}\right)+\frac{2\lambda^2}{3\left(1+\frac{2}{3}\lambda\right)^2}\right]$ $D=\left(1+\frac{\lambda}{3}\right)^2\left\{\left(\frac{b^2}{a^2}+2\right)^2+1+\frac{\lambda}{1+\frac{\lambda}{3}}-\frac{2\lambda^2[2+(3\nu b^2/a^2)]}{3\left(1+\frac{\lambda}{3}\right)^2}\right\}$		$A=\left(1+\frac{2}{3}\lambda\right)^2\left\{4.5\frac{b^4}{a^4}+4\frac{b^2}{a^2}+9-\frac{3\lambda}{1+\frac{2}{3}\lambda}-\frac{2[2+(\nu b^2/a^2)]\lambda^2}{3\left(1+\frac{\lambda}{3}\right)^2}\right\}$ $B=\left(1+\frac{2}{3}\lambda\right)^2\left[2\frac{b^3}{a^3}+4\frac{b}{a}+\frac{1}{2}-\left(1.5+\frac{b^2}{a^2}\right)\frac{\lambda^2}{1+\frac{2}{3}\lambda}-\frac{2\lambda^2}{3\left(1+\frac{2}{3}\lambda\right)^2}\right]$ $C=\left(1+\frac{\lambda}{3}\right)^2\left[\left(\frac{b^2}{a^2}+2\right)\left(2\frac{b}{a}+\frac{\lambda}{1+\frac{\lambda}{3}}\right)+\frac{2\lambda^2}{3\left(1+\frac{2\lambda}{3}\right)^2}\right]$ $D=\left(1+\frac{\lambda}{3}\right)^2\left\{4.5\frac{b^4}{a^4}+4\frac{b^2}{a^2}+5+\frac{\lambda}{1+\frac{\lambda}{3}}-\frac{2[2+(3\nu b^2/a^2)]\lambda^2}{3\left(1+\frac{2}{3}\lambda\right)^2}\right\}$
	$A=\left(1+\frac{2}{3}\lambda\right)^2\left\{\left(\frac{b^2}{a^2}+2\right)^2+5+\frac{3\lambda}{1+\frac{2}{3}\lambda}-\frac{2[2+(\nu b^2/a^2)]\lambda^2}{3\left(1+\frac{2}{3}\lambda\right)^2}\right\}$ $B=\left(1+\frac{2}{3}\lambda\right)^2\left[2\frac{b^3}{a^3}+4\frac{b}{a}+\frac{1}{2}-\left(1.5+\frac{b^2}{a^2}\right)\frac{\lambda}{1+\frac{2}{3}\lambda}-\frac{2\lambda^2}{3\left(1+\frac{2}{3}\lambda\right)}\right]$ $C=\left(1+\frac{\lambda}{3}\right)^2\left[\left(\frac{b^2}{a^2}+2\right)\left(\frac{2b}{a}+\frac{\lambda}{1+\frac{\lambda}{3}}\right)+\frac{2\lambda^2}{3\left(1+\frac{\lambda}{3}\right)^2}\right]$ $D=\left(1+\frac{\lambda}{3}\right)^2\left\{\left(\frac{b^2}{a^2}+2\right)^2+1+\frac{\lambda}{1+\frac{\lambda}{3}}-\frac{2[2+(3\nu b^2/a^2)]\lambda^2}{3\left(1+\frac{\lambda}{3}\right)^2}\right\}$		$A=\left(1+\frac{2}{3}\lambda\right)^2\left\{4.5\frac{b^4}{a^4}+4\frac{b^2}{a^2}+5-\frac{\lambda}{1+\frac{2}{3}\lambda}-\frac{2[2+(\nu b^2/a^2)]\lambda^2}{3\left(1+\frac{\lambda}{3}\right)^2}\right\}$ $B=\left(1+\frac{2}{3}\lambda\right)^2\left[\left(2+\frac{b^2}{a^2}\right)\left(2\frac{b}{a}-\frac{\lambda}{1+\frac{\lambda}{3}}\right)-\frac{2\lambda^2}{3\left(1+\frac{2}{3}\lambda\right)^2}\right]$ $C=\left(1+\frac{\lambda}{3}\right)^2\left[2\frac{b^3}{a^3}+4\frac{b}{a}+0.5+\left(1.5+\frac{b^2}{a^2}\right)\frac{\lambda}{1+\frac{\lambda}{3}}+\frac{2\lambda^2}{3\left(1+\frac{\lambda}{3}\right)^2}\right]$ $D=\left(1+\frac{\lambda}{3}\right)^2\left\{4.5\frac{b^4}{a^4}+4\frac{b^2}{a^2}+9-\frac{3\lambda}{1+\frac{\lambda}{3}}-\frac{2[2+(3\nu b^2/a^2)]\lambda^2}{3\left(1+\frac{\lambda}{3}\right)^2}\right\}$

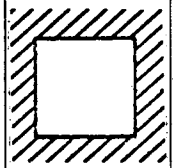


$$A=\left(1+\frac{2}{3}\lambda\right)^2\left\{\left(\frac{b^2}{a^2}+2\right)^2+5+3\frac{\lambda}{1+\frac{2}{3}\lambda}-\frac{2[2+(\nu b^2/a^2)]\lambda^2}{3\left(1+\frac{2}{3}\lambda\right)^2}\right\}$$

$$B=\left(1+\frac{2}{3}\lambda\right)^2\left[2\frac{b^3}{a^3}+4\frac{b}{a}+\frac{1}{2}-\left(1.5+\frac{b^2}{a^2}\right)\frac{\lambda}{1+\frac{2}{3}\lambda}-\frac{2\lambda^2}{3\left(1+\frac{2}{3}\lambda\right)^2}\right]$$

$$C=\left(1+\frac{\lambda}{3}\right)^2\left[2\frac{b^3}{a^3}+4\frac{b}{a}+\frac{1}{2}+\left(1.5+\frac{b^2}{a^2}\right)\frac{\lambda}{1+\frac{\lambda}{3}}+\frac{2\lambda^2}{3\left(1+\frac{\lambda}{3}\right)^2}\right]$$

$$D=\left(1+\frac{\lambda}{3}\right)^2\left\{\left(\frac{b^2}{a^2}+2\right)^2+5-\frac{3\lambda}{1+\frac{\lambda}{3}}-\frac{2[2+(3\nu b^2/a^2)]\lambda^2}{3\left(1+\frac{\lambda}{3}\right)^2}\right\}$$

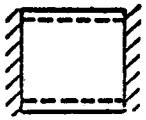


$$A=\left(1+\frac{2}{3}\lambda\right)^2\left\{4.5\frac{b^4}{a^4}+4\frac{b^2}{a^2}+9+\frac{3\lambda}{1+\frac{2}{3}\lambda}-\frac{2[2+(\nu b^2/a^2)]}{3\left(1+\frac{\lambda}{3}\right)^2}\right\}$$

$$B=\left(1+\frac{2}{3}\lambda\right)^2\left[2\frac{b^3}{a^3}+4\frac{b}{a}+\frac{1}{2}-\left(1.5+\frac{b^2}{a^2}\right)\frac{\lambda}{1+\frac{2}{3}\lambda}-\frac{2\lambda^2}{3\left(1+\frac{2}{3}\lambda\right)^2}\right]$$

$$C=\left(1+\frac{\lambda}{3}\right)^2\left[2\frac{b^3}{a^3}+4\frac{b}{a}+\frac{1}{2}+\left(1.5+\frac{b^2}{a^2}\right)\frac{\lambda}{1+\frac{\lambda}{3}}+\frac{2\lambda^2}{3\left(1+\frac{\lambda}{3}\right)^2}\right]$$

$$D=\left(1+\frac{\lambda}{3}\right)^2\left\{4.5\frac{b^4}{a^4}+4\frac{b^2}{a^2}+9-\frac{3\lambda}{1+\frac{\lambda}{3}}-\frac{2[2+(30b^2/a^2)]\lambda^2}{3\left(1+\frac{2}{3}\lambda\right)^2}\right\}$$



$$A=\left(1+\frac{2}{3}\lambda\right)^2\left\{4.5\frac{b^4}{a^4}+4\frac{b^2}{a^2}+5-\frac{\lambda}{1+\frac{2}{3}\lambda}-\frac{2[2+(\nu b^2/a^2)]\lambda^2}{3\left(1+\frac{\lambda}{3}\right)^2}\right\}$$

$$B=\left(1+\frac{2}{3}\lambda\right)^2\left[\left(\frac{b^2}{a^2}+2\right)\left(2\frac{b}{a}-\frac{\lambda^2}{1+\frac{2}{3}\lambda}\right)-\frac{2\lambda^2}{3\left(1+\frac{2}{3}\lambda\right)^2}\right]$$

$$C=\left(1+\frac{\lambda}{3}\right)^2\left[\left(2+\frac{b^2}{a^2}\right)\left(2\frac{b}{a}+\frac{\lambda}{1+\frac{\lambda}{3}}\right)+\frac{2\lambda^2}{3\left(1+\frac{\lambda}{3}\right)^2}\right]$$

$$D=\left(1+\frac{\lambda}{3}\right)^2\left\{4.5\frac{b^4}{a^4}+4\frac{b^2}{a^2}+5+\frac{\lambda}{1+\frac{\lambda}{3}}-\frac{2[2+(3\nu b^2/a^2)]\lambda^2}{3\left(1+\frac{\lambda}{3}\right)^2}\right\}$$

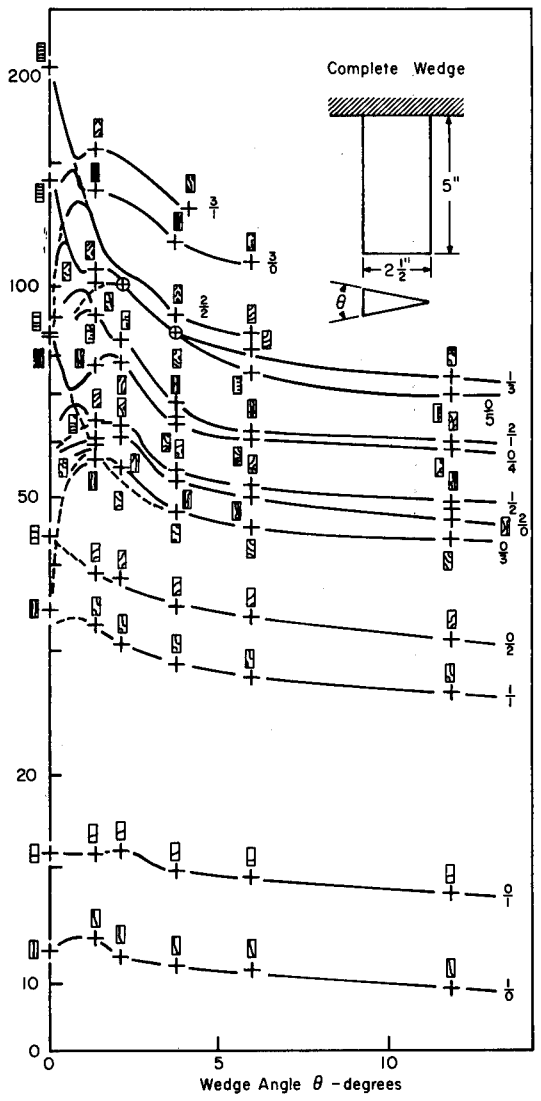


FIGURE 11.8.—Experimentally measured fundamental frequency parameters for different values of wedge angle θ for linearly tapered, rectangular cantilever plates; material, steel; numbers indicate modes. (After ref. 11.13)

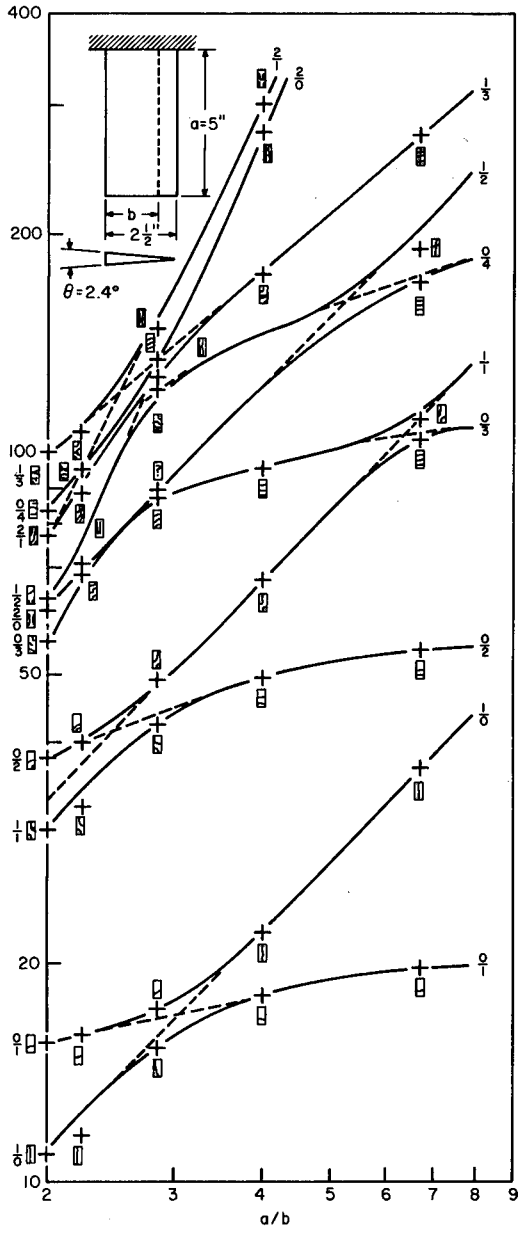


FIGURE 11.9.—Experimentally measured fundamental frequency parameters for different values of a/b for linearly tapered, rectangular cantilever plates; material, steel; $\theta=2.4°$; numbers indicate modes. (After ref. 11.13)

angles are tabulated in table 11.6. The effect of changing aspect ratio is shown in figure 11.9. In this figure a/b is varied by removing material from the thin side of the plate, so that the cross section becomes trapezoidal. The wedge angle θ remains a constant 2.4°. Fundamental frequency parameters for this case are presented in table 11.7.

Methods for solving the free vibration problem for rectangular variable-thickness plates are also presented in references 11.15 to 11.18, but no numerical results are included.

TABLE 11.6.—*Experimentally Measured Fundamental Frequency Parameters for Linearly Tapered, Rectangular Cantilever Plates; Material, Steel*

Wedge angle, θ, °	1.35	2.4	3.7	5.9	11.8
ϕ (eq. (11.37))	2. 52	2. 57	2. 47	2. 32	2. 28

TABLE 11.7.—*Variation in Fundamental Frequency Parameter With Aspect Ratio for Linearly Tapered, Rectangular Cantilever Plates; Material, Steel*

a/b	2.00	2.22	2.86	4.00	6.67
ϕ (eq. (11.37))	2. 57	2. 57	2. 71	2. 91	3. 15

11.3 OTHER SHAPES

Except for the work in references 11.19 and 11.20, virtually nothing has been done for variable-thickness plates when their shapes are other than circular or rectangular. A method is presented in reference 11.19 for analyzing cantilever variable-thickness plates having an arbitrary quadrilateral shape. Reference 11.20 gives a method for analyzing clamped variable-thickness plates of arbitrary shape.

REFERENCES

11.1. TIMOSHENKO, S.; AND WOINOWSKY-KRIEGER, S.: Theory of Plates and Shells. Second ed., McGraw-Hill Book Co., Inc., 1959.

11.2. CONWAY, H. D.: Some Special Solutions for the Flexural Vibration of Discs of Varying Thickness. Ingr.-Arch., vol. 26, 1958, pp. 408–410.

11.3. CONWAY, H. D.: An Analogy Between the Flexural Vibrations of a Cone and a Disc of Linearly Varying Thickness. ZAMM, vol. 37, no. 9/10, Sept./Oct. 1957, pp. 406–407.

11.4. CONWAY, H. D.; BECKER, E. C. H.; AND DUBIL, J. F.: Vibration Frequencies of Tapered Bars and Circular Plates. J. Appl. Mech., vol. 31, no. 2, June 1964, pp. 329–331.

11.5. THURSTON, E. G.; AND TSUI, Y. T.: On the Lowest Flexural Resonant Frequency of a Circular Disk of Linearly Varying Thickness Driven at Its Center. J. ASA, vol. 27, no. 5, Sept. 1955, pp. 926–929.

11.6. KOVALENKO, A. D.: Circular Variable-Thickness Plates. Fitzmatgiz. (Moscow), 1959. (In Russian.)

11.7. KAZANTSEVA, G. E.: On the Vibrations of Circular Plates of Variable Thickness. Prikl. Mekh., vol. 4, no. 2, 1958, pp. 197–204. (In Russian.)

11.8. EHRICH, F. F.: A Matrix Solution for the Vibration Modes of Nonuniform Disks. J. Appl. Mech., vol. 23, no. 1, Mar. 1956, pp. 109–115.

11.9. APPL, F. C.; AND BYERS, N. R.: Fundamental Frequency of Simply Supported Rectangular Plates With Linearly Varying Thickness. J. Appl. Mech., vol. 32, no. 1, Mar. 1965, pp. 163–167.

11.10. APPL, F. C.; AND ZOROWSKI, C. F.: Upper and Lower Bounds for Special Eigenvalues. J. Appl. Mech., vol. 26, 1959, pp. 246–250.

11.11. GUMENIUK, V. S.: Determination of the Free Vibrations Frequencies of Variable Thickness Plates. Dopov. AN UkrSSR, no. 2, 1956, pp. 130–133. (In Ukrainian.)

11.12. GONTKEVICH, V. S.: Natural Vibrations of Plates and Shells. A. P. Filippov, ed., Nauk. Dumka (Kiev), 1964. (Transl. by Lockheed Missiles & Space Co. (Sunnyvale, Calif.).)

11.13. PLUNKETT, R.: Natural Frequencies of Uniform and Non-Uniform Rectangular Cantilever Plates. J. Mech. Eng. Sci., vol. 5, no. 2, 1963, pp. 146–156.

11.14. WILSON, R. E.; AND PLUNKETT, R.: Vibration of Cantilever Plates With Rectangular and Wedge-Shaped Cross-Sections. Rept. DF 53GL17, Gen. Elec. Co., Mar. 1953.

11.15. MAZURKIEWICZ, Z.: The Problem of Bending and Free Vibration of a Simply Supported, Isotropic, Non-Homogeneous, Rectangular Plate. Arch. Mech. Stos., vol. 12, 1960, pp. 499–521.

11.16. SOLECKI, R.: The Non-Homogeneous Isotropic Rectangular Plate With Arbitrary Boundary Conditions. Bull. Acad. Pol. Sci., Ser. Sci. Tech., vol. 9, no. 6, 1961, pp. 329–335.

11.17. MAZURKIEWICZ, Z.: A Certain Solution of the Dynamic Problem for the Disc Made of Elastic Orthotropic and Non-Homogeneous Material. Bull. Acad. Pol. Sci., Ser. Sci. Tech., vol. 11, no. 1, 1963, pp. 17–25.

11.18. MAZURKIEWICZ, Z.: Free Vibration of an Isotropic Non-Homogeneous Rectangular Plate. Bull. Acad. Pol. Sci., Ser. Sci. Tech., vol. 8, no. 2, 1960, pp. 63–68.

11.19. SIVEHIKOV, B. E.: Equilibrium Equations for Static Bending and Free Vibration of Irregularly Shaped Cantilever Plates. Izv. Vyssh. Uchebn. Zavedenii: Aviat. Tekh., no. 2, 1962, pp. 86–94. (Transl. by Foreign Tech. Div., Air Force Systems Command, Wright-Patterson Air Force Base, Ohio.)

11.20. SLOBODIANSKI, M. G.: Estimates of Natural Frequencies of Vibration of Clamped Plates of Constant and Variable Thickness. Seminar on Problems of Continuum Mechanics (Philadelphia, Pa.), Soc. Ind. and Appl. Math., 1961, pp. 473–482.

308-337 O—70——20

Chapter 12

Other Considerations

The effects of the following complications will be considered in the present chapter:

(1) Surrounding media
(2) Large deflections
(3) Shear deformation and rotary inertia
(4) Nonhomogeneity

Generally, because of the complexity of the resulting theory, there are not many numerical results showing the effects of these complications. Indeed, in many cases the technical literature deals mainly with the development of the needed theory. Nevertheless, it will *not* be the purpose of this chapter to repeat those derivations; the reader is referred to the references themselves for this. The primary purpose of this chapter, as of the preceding ones, is the presentation of numerical results, where available, with explanatory material as necessary for an understanding of their significance.

It will be assumed in this chapter that the reader will already be reasonably familiar with the coordinate systems, notation, boundary conditions, and so forth, used in the preceding chapters, and so, much tedious redefinition will be omitted.

12.1 EFFECTS OF SURROUNDING MEDIA

In general, it has been the practice in this work to discuss plates in bending which are uncoupled from other elastic structures *having mass*. In this way only a single differential equation of motion—that of the plate—is involved. Yet it is apparent that practical experiments are conducted in air, and that the mass of the air thus moved has the effect of decreasing the vibration frequencies of the system. The difference between experimental and theoretical results for this reason has been alluded to in many places in the preceding chapters and, indeed, corrections of one or the other to obtain comparable values were even made in a few places (and so identified). In the present section some of the papers that deal primarily with this problem will be summarized. The topic is generalized to include other media in addition to air—notably, water.

12.1.1 Circular Plates

In an early paper Lamb (ref. 12.1) considered a clamped circular plate which is in contact on one side with an infinite expanse of water. The Rayleigh method is used with a deflection function

$$w=C[1-(r/a)^2]^2 \tag{12.1}$$

The kinetic energy is computed on the assumption that the water is incompressible. The resulting formula for the fundamental frequency parameter is

$$\omega a^2\sqrt{\rho/D}=\frac{10.33}{\sqrt{1+0.6689\left(\frac{\gamma_w}{\gamma}\right)\left(\frac{a}{h}\right)}} \tag{12.2}$$

where γ_w/γ is the dimensionless ratio of the mass density of water to that of the plate and a/h is the radius-thickness ratio. Of course, equation (12.2) can be applied to any incompressible fluid. If both sides are to be exposed to the infinite fluid, then the 0.6689 in equation (12.2) is replaced by 2×0.6689.

The frequency of the second mode (having one nodal diameter) was also calculated in reference 12.1 with the use of

$$w=C[1-(r/a)^2]^2 r\cos\theta \tag{12.3}$$

and resulted in

$$\omega a^2\sqrt{\rho/D}=\frac{21.909}{\sqrt{1+0.3087\left(\frac{\gamma_w}{\gamma}\right)\left(\frac{a}{h}\right)}} \tag{12.4}$$

Hence, the effect of the water's inertia is less upon the second mode than upon the first. In order to check the accuracy of the foregoing

results, a two-term Ritz solution was carried out in reference 12.1 for the first and second modes of a particular iron plate; this calculation yielded results which differed from those calculated from equations (12.2) and (12.4) by less than 1 percent. The effects of damping due to the water are also discussed.

Experimental results for the preceding problem are given in reference 12.2.

McLachlan (ref. 12.3) extended Lamb's work to the case of a circular plate having a free boundary. For a plate having both sides immersed in an infinite fluid, he shows that the ratio of the frequency of the system ω to the frequency of the plate in a vacuum ω_0 can be determined from the formula

$$\frac{\omega}{\omega_0}=\sqrt{\frac{1}{1+(M_1/M_q)}} \tag{12.5}$$

where, for the case of one nodal circle,

$$M_1=\frac{16}{35}\gamma_f a^3 \tag{12.6}$$

and, for the case of a point support at the center,

$$M_1=\frac{80}{63}\gamma_f a^3 \tag{12.7}$$

and, in both cases,

$$M_q=\frac{\pi}{3}\gamma a^2 h \tag{12.8}$$

where γ_f is now the mass density of the surrounding fluid. In reference 12.3, equation (12.5) is applied to the problems of an aluminum plate vibrating in either air or water.

The previous work was extended further by Peake and Thurston (ref. 12.4), who applied the Rayleigh method to the problem of the simply supported circular plate having water loading on one side. A deflection function

$$w=1-1.245(r/a)^2+0.245(r/a)^4 \tag{12.9}$$

was used; the result is the frequency parameter formula

$$\omega a^2\sqrt{\rho/D}=\frac{4.94}{\sqrt{1+1.045\left(\frac{\gamma_w}{\gamma}\right)\left(\frac{a}{h}\right)}} \tag{12.10}$$

Bycroft (ref. 12.5) studied the problem of transverse vibration of a circular plate which is perfectly attached to a *massless*, elastic, infinite half space. The Rayleigh-Ritz approach is used, with the potential energy of the half space being added to that of the plate. Clamped, free, and simply supported edge conditions are considered for the plate. For the clamped case a deflection function for the plate is taken in the form of equation (12.1). The square of the fundamental frequency parameter is found to be:

$$\frac{\omega^2 a^4\rho}{D}=106.7+\frac{4.37G(1-\tau^2)a^3}{D} \tag{12.11}$$

where

$$\tau^2=\frac{G}{\lambda+2G} \tag{12.12}$$

and λ and G are Love's (ref. 12.6) elastic constants for the half space:

$$\left.\begin{aligned}\lambda&=\frac{\nu E}{(1+\nu)(1-2\nu)}\\ G&=\frac{E}{2(1+\nu)}\end{aligned}\right\} \tag{12.13}$$

For the free plate, a two-term solution function is assumed as a constant plus the first term of a Dini series; that is,

$$w=A_0+A_1 J_0[\lambda_1(r/a)] \tag{12.14}$$

where λ_1 is the first root of $J_0(\lambda)=0$. By applying the Ritz method, the two resulting frequencies are determined from

$$\frac{\omega^2 a^4\rho}{D}=\left[\frac{(9.21+4.79\nu+1.590\beta)A_1^2+2.248\beta A_0A_1+4\beta A_0^2}{\pi(0.1355A_1^2+0.433A_0A_1+0.5A_0^2)}\right] \tag{12.15}$$

where

$$\beta\equiv\frac{Ga^3(1-\tau^2)}{D} \tag{12.16}$$

and the amplitude constants A_0 and A_1 are related by

$$\frac{A_1}{A_0}=-[(4.61+2.39\nu+0.255\beta)\pm(21.2+5.68\nu^2+0.298\beta^2+22\nu+4.76\beta+2.48\beta\nu)^{1/2}]\div(3.98+2.07\nu+0.383\beta) \tag{12.17}$$

Finally, the simply supported plate is analyzed by using equation (12.14) with $A_0=0$. The square of the fundamental frequency parameter is found to be

$$\frac{\omega^2 a^4 \rho}{D}=21.70+11.25\nu+7.460\beta \quad (12.18)$$

12.1.2 Rectangular Plates

An interesting experimental and theoretical study of the vibration frequencies of rectangular cantilever plates (see fig. 4.40) immersed in water was reported by Lindholm, Kana, Chu, and Abramson (ref. 12.7). Cyclic frequencies are listed in table 12.1 for 15 plates made of type 1080 cold-rolled steel having various aspect ratios and ratios of thickness to width. Theoretical values are based upon Barton's work (see discussion of rectangular cantilever beams (sec. 4.3.12)), where applicable, and elementary beam theory. These pertain, of course, to the case of a vacuum. Frequencies are measured both in air and in water.

A correction formula of the form given in equation (12.5) was derived in reference 12.7 by means of hydrodynamic strip theory to account for the added "apparent mass" of the surrounding fluid. The ratios M_1/M_q to be used in equation (12.5) are given in table 12.2 for six modes of the cantilever plate (see definition of modes in table 12.1).

A further correction is suggested in reference 12.7 to account for the effect of plate thickness on the apparent mass of the air. In this case equation (12.5) becomes

$$\frac{\omega}{\omega_0}=\sqrt{\frac{1}{1+f\frac{M_1}{M_q}}} \quad (12.19)$$

where

$$f=\frac{2(a/b)}{2(a/b)+k} \quad (12.20)$$

and K is obtained from figure 12.1 for modes 1, 3, and 6.

A comparison of theoretical and experimental results for frequency parameters is made in figure 12.2 for the six modes. The effects of corrections for aspect ratio AR, a/b and thickness ratio b/h are clearly seen.

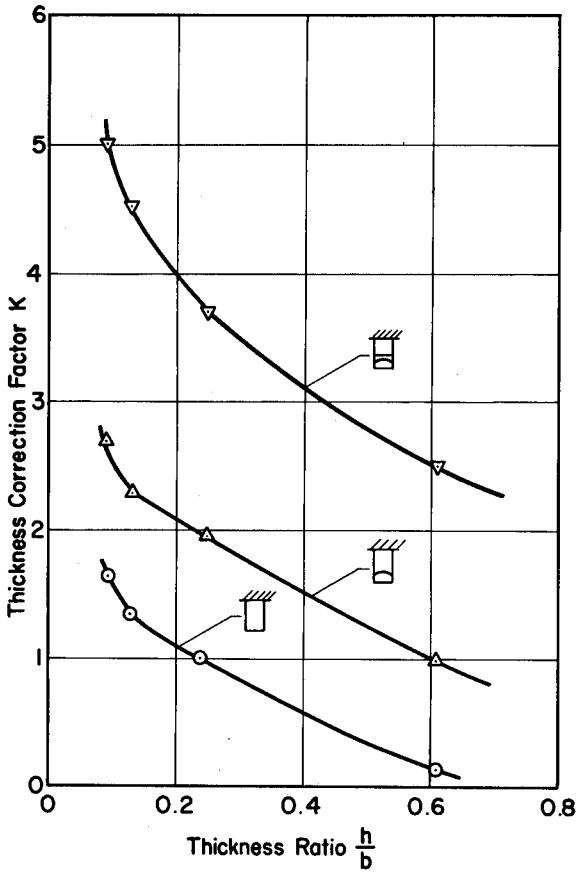


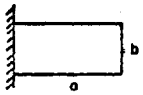
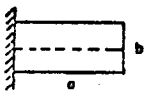
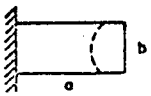
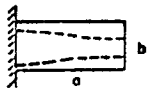
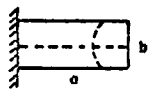
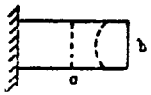
FIGURE 12.1.—Thickness correction factor of a rectangular cantilever plate for modes 1, 3, and 6. (After ref. 12.7)

The variation of node-line location in going from air to water is shown in figure 12.3. Frequency variation with depth below the surface is set forth in figure 12.4 for plate 11 of table 12.1. Finally, the effect on frequency due to partial immersion is shown in figure 12.5 for plate 8. It is stated in reference 12.7 that the angle of inclination of the plate to the surface seems to have an effect only for very shallow angles.

Greenspon (refs. 12.8 and 12.9) has proposed a correction formula to account for the effects of water on one side of a rectangular plate for all boundary conditions. The frequency ratio is

$$\frac{\omega}{\omega_0}=\sqrt{\frac{1}{1+\left(\frac{\gamma_w}{\gamma}\right)\left(\frac{b}{h}\right)\left(\frac{f}{2}\right)\left(\frac{A_{ij}^2}{B_{ij}}\right)}} \quad (12.21)$$

TABLE 12.1.—*Cyclic Frequencies for C–F–F–F Rectangular Plates of 1080 Steel in Vacuum, Air, and Water*

Plate			Frequency, cps, for mode—																	
No.	a/b	h/b																		
			Theory [a]	Experiment		Theory [a]	Experiment		Theory [a]	Experiment		Theory [a]	Experiment		Theory [a]	Experiment		Theory [b]	Experiment	
			Vacuum	Air	Water	Vacuum	Air	Water	Vacuum	Air	Water	Vacuum	Air	Water	Vacuum	Air	Water	Vacuum	Air	Water
1	5	12.40×10^{-2}	20.9	19.4	14.6	210	193	166	130	123	96	----------	--------	--------	641	589	507	357	346	257
2	2	6.11×10^{-2}	65.7	60.7	40.3	283	267	209	409	377	257	----------	--------	--------	922	858	645	----------	--------	--------
3	3	6.11×10^{-2}	29.1	27.3	17.8	181	172	133	181	171	116	----------	--------	--------	570	537	417	495	478	335
4	5	6.11×10^{-2}	10.4	10.0	6.3	105	99.6	77.3	65.2	62.3	40.1	----------	--------	--------	321	306	226	178	175	114
5	1	2.38×10^{-2}	99.5	96.3	51.4	243	241	154	610	591	355	782	782	534	887	866	585	----------	--------	--------
6	2	2.38×10^{-2}	24.7	24.2	12.1	106	108	67.5	154	151	80.0	----------	--------	--------	347	348	222	419	422	243
7	3	2.38×10^{-2}	10.9	10.8	5.1	68.1	67.7	41.6	68.2	66.9	33.3	----------	--------	--------	214	211	131	186	188	989
8	5	2.38×10^{-2}	3.93	3.84	1.78	39.5	39.1	24.2	24.5	24.2	11.5	----------	--------	--------	121	121	75.2	67	68.1	33.5
9	½	1.31×10^{-2}	223	214	106	342	339	189	1397	1339	739	652	649	389	1580	1518	922	----------	--------	--------
10	1	1.31×10^{-2}	55.6	52.9	23.3	136	129	68.7	341	326	158	437	423	234	496	476	267	----------	--------	--------
11	2	1.31×10^{-2}	13.8	12.9	5.1	59.3	58.2	29.8	85.9	80.8	34.4	----------	--------	--------	194	189	99.1	234	228	105
12	3	1.31×10^{-2}	6.11	6.2	2.3	38.0	40.3	20.6	38.1	38.7	15.4	----------	--------	--------	120	126	65.7	104	109	46.5
13	½	$.90\times10^{-2}$	159	147	63.5	244	228	110	998	920	452	466	436	229	1129	1044	565	----------	--------	--------
14	1	$.90\times10^{-2}$	39.7	37.9	14.6	97.1	95.3	44.2	243	236	102	312	299	155	354	344	174	----------	--------	--------
15	2	$.90\times10^{-2}$	9.86	9.3	3.12	42.4	42.0	18.8	61.4	57.8	21.1	----------	--------	--------	138	135	62.0	167	162	65.3

[a] Plate theory from Barton's work.
[b] Bernoulli-Euler beam theory.

TABLE 12.2.—*Mass Correction Factors for Eq. (12.5)*

Mode	$\frac{M_1}{M_a}$
1	$\frac{\pi}{4}\left(\frac{\gamma_w}{\gamma}\right)\left(\frac{b}{h}\right)$
2	$\frac{3\pi}{32}\left(\frac{\gamma_w}{\gamma}\right)\left(\frac{b}{h}\right)$
3	$\frac{\pi}{4}\left(\frac{\gamma_w}{\gamma}\right)\left(\frac{b}{h}\right)$
4	$0.0803\pi\left(\frac{\gamma_w}{\gamma}\right)\left(\frac{b}{h}\right)$
5	$\frac{3\pi}{32}\left(\frac{\gamma_w}{\gamma}\right)\left(\frac{b}{h}\right)$
6	$\frac{\pi}{4}\left(\frac{\gamma_w}{\gamma}\right)\left(\frac{b}{h}\right)$

where f is a "virtual mass function" for plates of rectangular shape and is plotted as a function of a/b in figure 12.6. The coefficients A_{ij} and B_{ij} are determined from the formulas

$$\left.\begin{aligned} A_{ij}&=\frac{1}{ab}\int_{\text{Area}} w_{ij}\,dA \\ B_{ij}&=\frac{1}{ab}\int_{\text{Area}} w_{ij}^2\,dA \end{aligned}\right\} \qquad (12.22)$$

where the w_{ij} are mode shapes which are the products of beam functions (see discussion of rectangular plates (ch. 4)); that is,

$$w_{ij}=X_i(x)Y_j(y) \qquad (12.23)$$

and the dimensions of the plate in the x- and y-directions are a and b, respectively. The integrals given by equations (12.22) are readily evaluated by means of the tables of reference 12.10. The coefficients for seven modes of rectangular plates having all edges clamped or simply supported are given in table 12.3.

In reference 12.8, equation (12.21) was shown to become

$$\frac{\omega}{\omega_0}=\sqrt{\frac{1}{1+0.2798\left(\frac{\gamma_w}{\gamma}\right)\left(\frac{b}{h}\right)f}} \qquad (12.24)$$

TABLE 12.3.—*Correction Coefficients for 2 Cases of Water-Loaded Rectangular Plates*

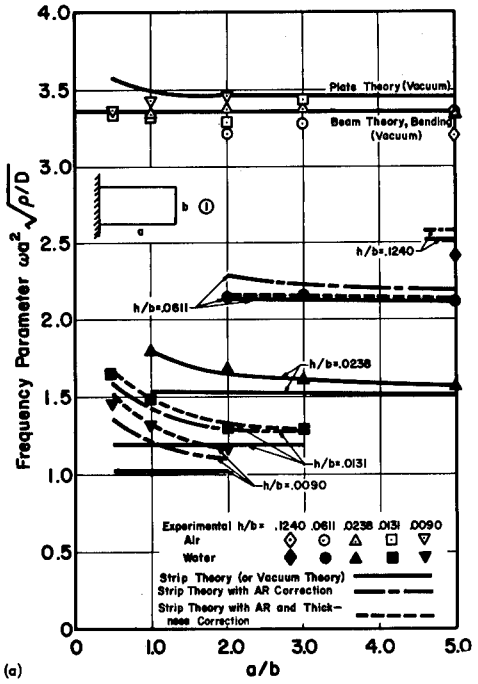
Mode		C-C-C-C		SS-SS-SS-SS	
i	j	A_{ij}	B_{ij}	A_{ij}	B_{ij}
1	1	0. 6904	1	0. 4053	0. 25
	2	0	1	0	. 25
	3	. 3023	1	. 1351	. 25
	5	. 1924	1	. 0810	. 25
3	1	. 3023	1	. 1351	. 25
	2	0	1	0	. 25
	3	. 1324	1	. 0450	. 25

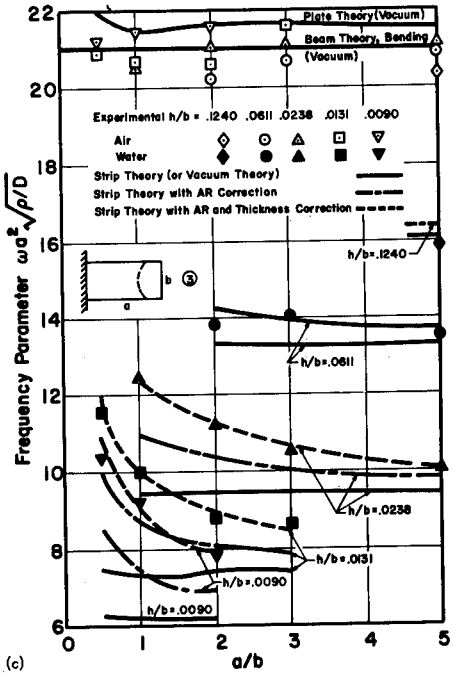
for the case of a rectangular plate having the sides $x=0$, a simply supported and the sides $y=0$, b clamped.

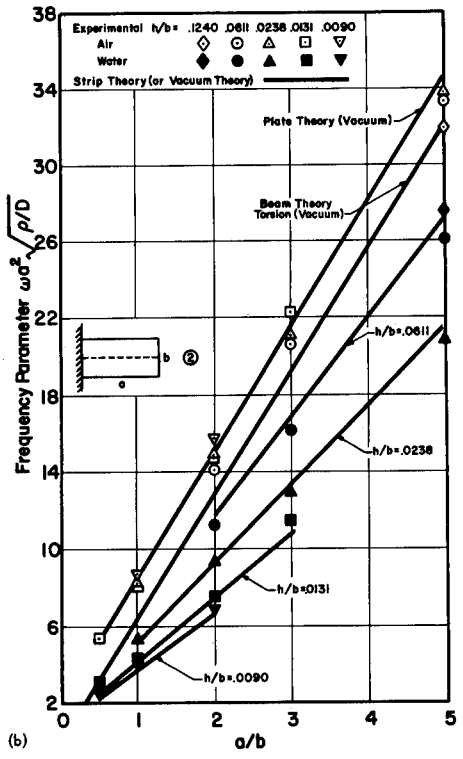
12.2 EFFECTS OF LARGE DEFLECTIONS

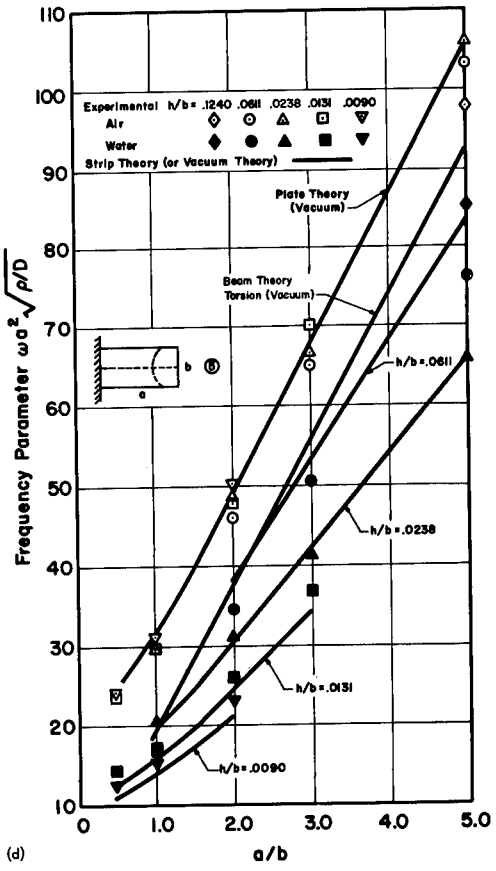
The term "large deflections" when applied to plate theory is somewhat misleading, for the deflections involved are generally *not* large relative to the inplane dimensions of the plate; indeed, they are usually of a smaller order of magnitude. Use of this term usually implies that the transverse deflection is sufficiently large to cause further stiffening of the plate because of membrane forces generated by the deflection. The magnitude of deflection required for this effect to be significant depends upon, for one thing, the precise boundary conditions of the plate. Thus, for example, the term "simply supported" is no longer completely definitive, for the degree of restraint placed upon the two inplane components of displacement must also be specified.

In deriving the equations of equilibrium in the appendix the assumption is made that the slope of the middle surface relative to its undeflected plane remains small in order that the sines of the angles between the normals of the deformed and undeformed middle surfaces can be replaced by their tangents $\partial w/\partial x$ and $\partial w/\partial y$ and the cosines can be replaced by unity. This assumption is usually retained in the large deflection theory of plates and gives equilibrium equations (A.5), (A.6), and (A.8) found in the appendix. However, strain-


Plate Theory (Vacuum)
Beam Theory, Bending (Vacuum)
h/b=.1240
h/b=.0611
h/b=.0238
h/b=.0131
h/b=.0090
Experimental h/b = .1240 .0611 .0238 .0131 .0090
Air
Water
Strip Theory (or Vacuum Theory)
Strip Theory with AR Correction
Strip Theory with AR and Thickness Correction
Frequency Parameter $\omega a^2\sqrt{\rho/D}$
a/b
(a)


Plate Theory (Vacuum)
Beam Theory, Bending (Vacuum)
Experimental h/b = .1240 .0611 .0238 .0131 .0090
Air
Water
Strip Theory (or Vacuum Theory)
Strip Theory with AR Correction
Strip Theory with AR and Thickness Correction
h/b=.1240
h/b=.0611
h/b=.0238
h/b=.0131
h/b=.0090
Frequency Parameter $\omega a^2\sqrt{\rho/D}$
a/b
(c)


Experimental h/b = .1240 .0611 .0238 .0131 .0090
Air
Water
Strip Theory (or Vacuum Theory)
Plate Theory (Vacuum)
Beam Theory Torsion (Vacuum)
h/b=.0611
h/b=.0238
h/b=.0131
h/b=.0090
Frequency Parameter $\omega a^2\sqrt{\rho/D}$
a/b
(b)


Experimental h/b = .1240 .0611 .0238 .0131 .0090
Air
Water
Strip Theory (or Vacuum Theory)
Plate Theory (Vacuum)
Beam Theory Torsion (Vacuum)
h/b=.0611
h/b=.0238
h/b=.0131
h/b=.0090
Frequency Parameter $\omega a^2\sqrt{\rho/D}$
a/b
(d)

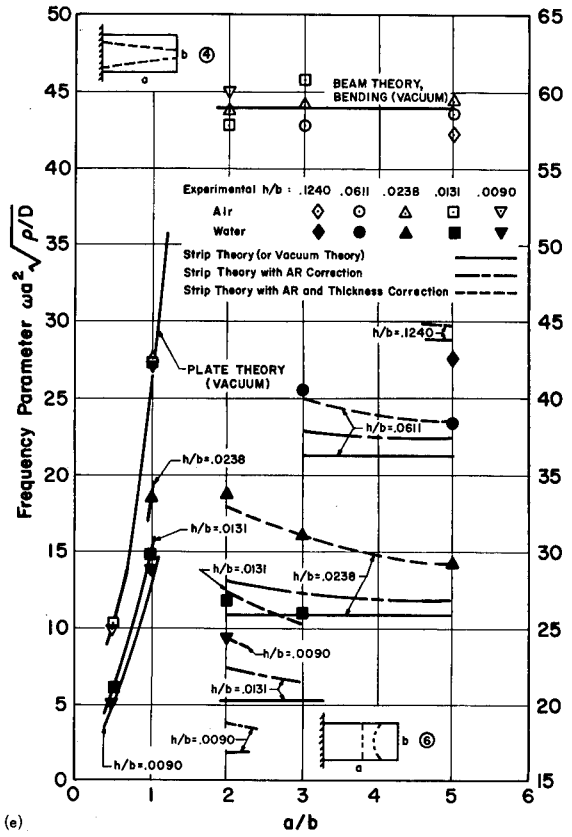


FIGURE 12.2.—Experimental and theoretical frequency parameters in water, air, and a vacuum. (*a*) Mode 1. (*b*) Mode 2. (*c*) Mode 3. (*d*) Mode 5. (*e*) Modes 4 and 6. (After ref. 12.7)

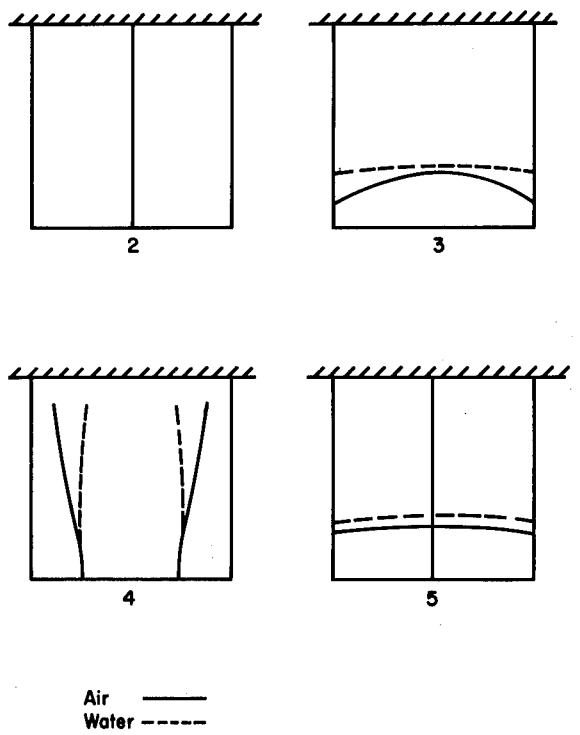


FIGURE 12.3.—Comparison of node-line locations in air and water. Plate 10; $a/b=1$; $h/b=0.0131$. (After ref. 12.7)

displacement equations (A.11) are generalized to include terms of the next order; that is

$$\left.\begin{aligned}\epsilon_x&=\frac{\partial u_0}{\partial x}-z\frac{\partial^2 w}{\partial x^2}+\frac{1}{2}\left(\frac{\partial w}{\partial x}\right)^2\\ \epsilon_y&=\frac{\partial v_0}{\partial x}-z\frac{\partial^2 w}{\partial y^2}+\frac{1}{2}\left(\frac{\partial w}{\partial y}\right)^2\\ \gamma_{xy}&=\frac{\partial v_0}{\partial x}+\frac{\partial u_0}{\partial y}-2z\frac{\partial^2 w}{\partial x\,\partial y}+\frac{\partial w}{\partial x}\frac{\partial w}{\partial y}\end{aligned}\right\}\qquad(12.25)$$

Equations (12.25) are then substituted into equations (A.18) or (A.19) and then into equations (A.6). It is found that the additional terms in equations (12.25) which are even in z drop out in the bending moment integrations, namely, equations (A.20(d)), (A.20(e)), and (A.20(f)), leaving the fourth-order equilibrium equation (A.27) unchanged.

Another equation is obtained from the equation of compatibility of strains for the middle surface. By using equations (12.25), this is found to be:

$$\frac{\partial^2\epsilon_x}{\partial y^2}+\frac{\partial^2\epsilon_y}{\partial x^2}-\frac{\partial^2\gamma_{xy}}{\partial x\,\partial y}=\left(\frac{\partial^2 w}{\partial x\,\partial y}\right)^2-\frac{\partial^2 w}{\partial x^2}\frac{\partial^2 w}{\partial y^2}\qquad(12.26)$$

The formulation is simplified when an Airy stress function ϕ, defined by

$$\left.\begin{aligned}\sigma_x&=\frac{\partial^2\phi}{\partial y^2}\\ \sigma_y&=\frac{\partial^2\phi}{\partial x^2}\\ \tau_{xy}&=-\frac{\partial^2\phi}{\partial x\,\partial y}\end{aligned}\right\}\qquad(12.27)$$

is introduced. This guarantees that the inplane equations of motion (eqs. (A.5)) are identically satisfied. Substituting equations (12.27) into equation (12.26), using equations (A.19),

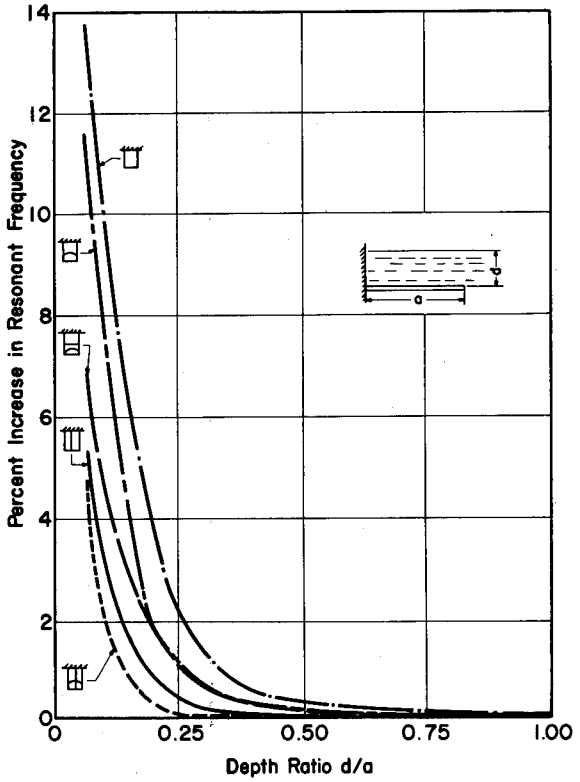


FIGURE 12.4.—Frequency variation with depth of total immersion in water. (After ref. 12.7)

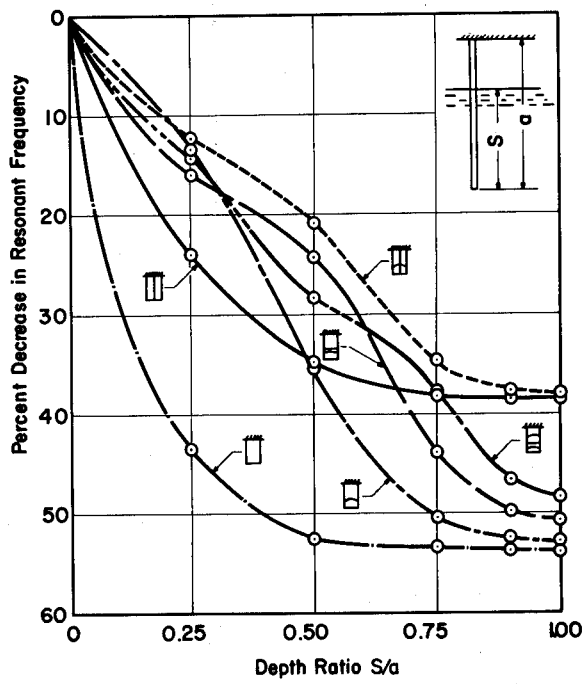


FIGURE 12.5.—Frequency change for surface-piercing plates. Plate 8; $a/b=5$; $h/b=0.0238$. (After ref. 12.7)

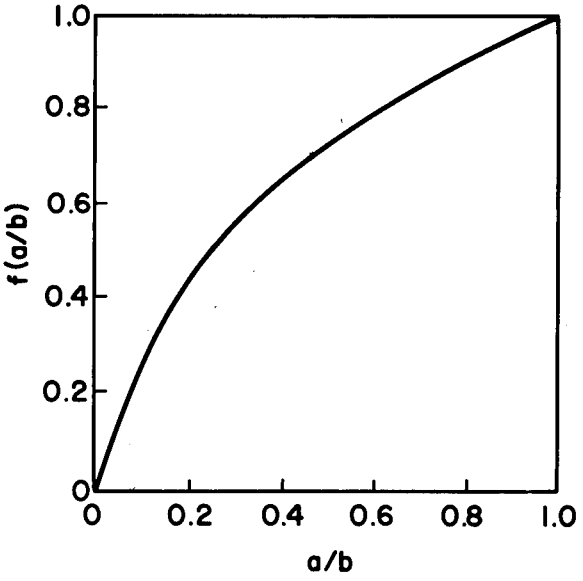


FIGURE 12.6.—Virtual mass function for rectangular plates. (After ref. 12.8)

(A.20(a)), (A.20(b)), and (A.20(c)), gives for the isotropic plate:

$$\frac{\partial^4\phi}{\partial x^4}+2\frac{\partial^4\phi}{\partial x^2\,\partial y^2}+\frac{\partial^4\phi}{\partial y^4}=E\left[\left(\frac{\partial^2 w}{\partial x\,\partial y}\right)^2-\frac{\partial^2 w}{\partial x^2}\frac{\partial^2 w}{\partial y^2}\right] \tag{12.28}$$

The equilibrium equation becomes

$$D\nabla^4 w+\rho\frac{\partial^2 w}{\partial t^2}=h\left(\frac{\partial^2 w}{\partial x^2}\frac{\partial^2\phi}{\partial y^2}+\frac{\partial^2 w}{\partial y^2}\frac{\partial^2\phi}{\partial x^2}-2\frac{\partial^2 w}{\partial x\,\partial y}\frac{\partial^2\phi}{\partial x\,\partial y}\right) \tag{12.29}$$

It is observed that equations (12.28) and (12.29) are both nonlinear.

Equations (12.28) and (12.29) were derived for the static case by Von Kármán (ref. 12.11). They were extended to the dynamic case and generalized further by Herrmann (ref. 12.12).

12.2.1 Circular Plates

Wah (ref. 12.13) used the Berger (ref. 12.14) simplication of the Von Kármán equations to study the problems of the circular plate having either a clamped or simply supported boundary. The plate is constrained against inplane dis-

placement at the boundary in both cases. The differential equation to be solved is

$$D\nabla^4 w - N\nabla^2 w + \rho\frac{\partial^2 w}{\partial t^2} = 0 \qquad (12.30)$$

where, for the axisymmetric modes, N is defined by

$$N = \frac{12D}{a^2h^2}\int_0^a \left(\frac{\partial w}{\partial r}\right)^2 r\,dr \qquad (12.31)$$

For the solution of equations (12.30) and (12.31), a Galerkin procedure is proposed that uses a deflection function

$$w = \sum_i C_i R_i(r)\tau_i(t) \qquad (12.32)$$

where the terms R_i are the normal modes of the linearized, small-deflection problem (cf. ch. 2). For the nonlinear problem, the τ_i will not, in general, be sinusoidal functions of time. By taking only the first term of equation (12.32), the following nonlinear differential equation in time is found:

$$\frac{d^2\tau}{dt^2} + p^2\tau + \left[\frac{12D}{a^4\rho}\left(\frac{c}{h}\right)^2\lambda\right]\tau^3 = 0 \qquad (12.33)$$

where p is the small-deflection frequency associated with R_1 and

$$\lambda = \frac{\int_0^a \left(\frac{dR}{dr}\right)^2 r\,dr}{\frac{1}{a^2}\int_0^a R^2 r\,dr} \qquad (12.34)$$

The solution of equation (12.33) is in terms of elliptic integrals. The resulting ratio of linear frequency to nonlinear frequency as a function of the ratio of center deflection to plate thickness is shown in figure 12.7.

Further information is given in reference 12.13 for estimating stresses during vibration. A nondimensional radial bending stress $\bar{\sigma}_r'$ is plotted in figure 12.8 as a function of the amplitude-thickness ratio. Similarly, a nondimensional radial membrane stress $\bar{\sigma}_r''$ is plotted in figure 12.9. Superposition of these stresses gives the total stress.

Yamaki (ref. 12.15) applied the Galerkin method to the Von Kármán equations (12.28) and (12.29) themselves. When only axisymmetric

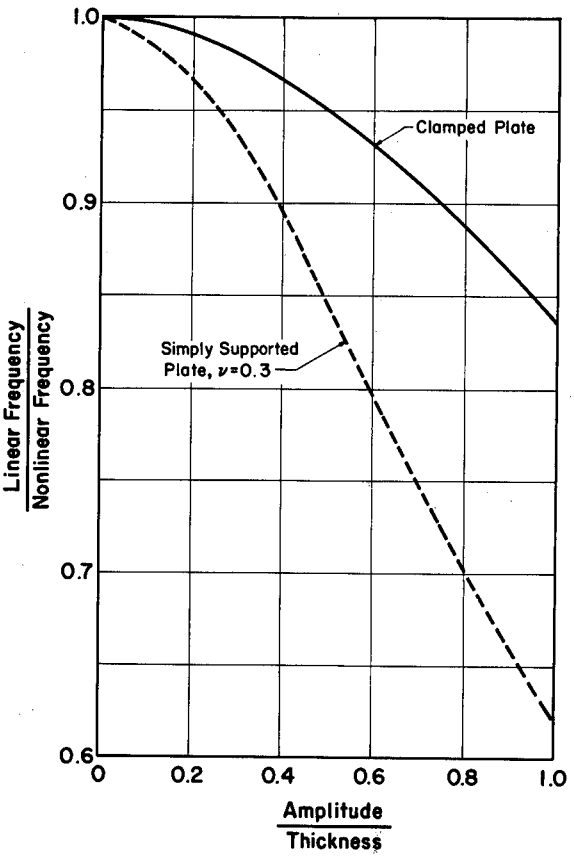


FIGURE 12.7.—Ratio of linear (small-deflection) frequency to nonlinear (large-deflection) frequency as a function of amplitude-thickness ratio for circular plates; $\nu=0.3$. (After ref. 12.13)

deformations in polar coordinates are considered, they become:

$$\left.\begin{aligned} \nabla^4\phi &= -\frac{E}{r}\frac{\partial w}{\partial r}\frac{\partial^2 w}{\partial r^2} \\ D\nabla^4 w + \rho\frac{\partial^2 w}{\partial t^2} &= \frac{h}{r}\frac{\partial\phi}{\partial r}\frac{\partial^2 w}{\partial r^2} \end{aligned}\right\} \qquad (12.35)$$

Altogether, four sets of boundary conditions were considered; the particular ones used depended upon the degree of restraint placed upon both the transverse and inplane displacements. The cases considered were

$$\left.\begin{aligned} &\text{Case I}(a): w = M_r = N_r = 0 \\ &\text{Case I}(b): w = M_r = u = 0 \\ &\text{Case II}(a): w = \partial w/\partial r = N_r = 0 \\ &\text{Case II}(b): w = \partial w/\partial r = u = 0 \end{aligned}\right\} \text{(on boundary)} \qquad (12.36)$$

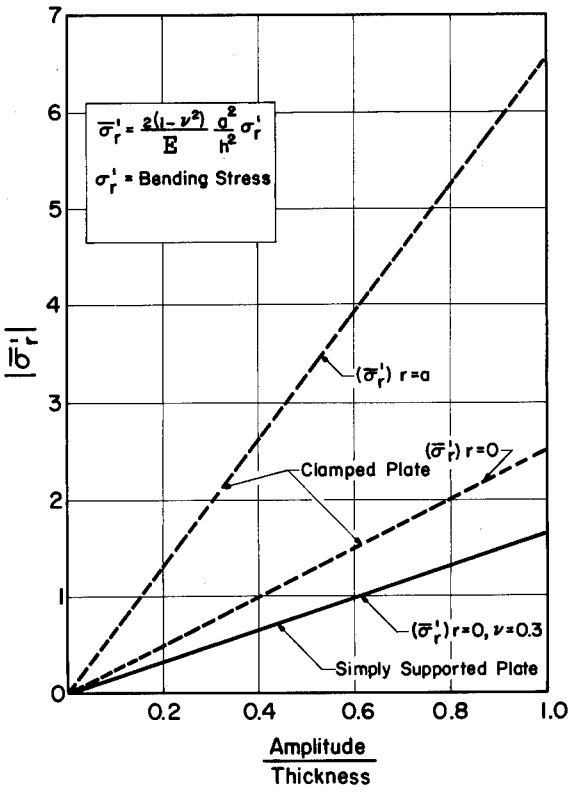


FIGURE 12.8.—Nondimensional bending stress in large-amplitude vibrations of circular plates. (After ref. 12.13)

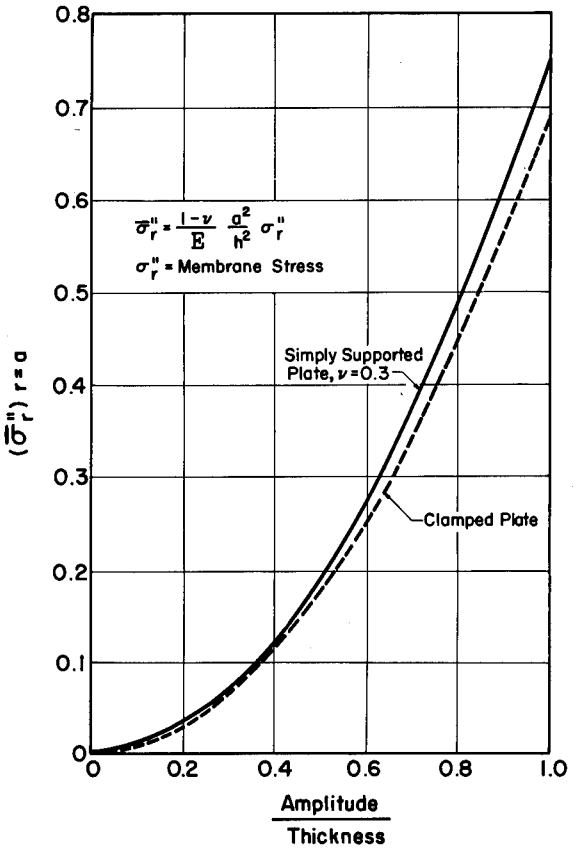


FIGURE 12.9.—Nondimensional membrane stress in large-amplitude vibrations of circular plates. (After ref. 12.13)

Deflection functions were taken in the form

$$w(r)=h\tau(t)\left[1+C_1\left(\frac{r}{a}\right)^2+C_2\left(\frac{r}{a}\right)^4\right] \quad (12.37)$$

where C_1 and C_2 were chosen to satisfy the transverse boundary conditions exactly; that is,

$$\left.\begin{aligned}&\text{Case I:} && C_1=-\frac{6+2\nu}{5+\nu}\\ &&& C_2=\frac{1+\nu}{5+\nu}\\ &\text{Case II:} && C_1=-2\\ &&& C_2=1\end{aligned}\right\} \quad (12.38)$$

Substituting equation (12.37) into the first of equations (12.35) and letting

$$\phi=f(r)\tau^2(t) \quad (12.39)$$

give

$$f(r)=-Eh^2\left[C_3\left(\frac{r}{a}\right)^2+\frac{1}{16}C_1^2\left(\frac{r}{a}\right)^4+\frac{1}{18}C_1C_2\left(\frac{r}{a}\right)^6+\frac{1}{48}C_2^2\left(\frac{r}{a}\right)^8\right] \quad (12.40)$$

where C_3 is a constant determined from the inplane boundary conditions of equations (12.36); that is,

$$\left.\begin{aligned}&\text{Cases I}(a)\text{ and II}(a):\\ &C_3=-\frac{1}{24}(3C_1^2+4C_1C_2+2C_2^2)\\ &\text{Cases I}(b)\text{ and II}(b):\\ &C_3=-\frac{1}{24(1-\nu)}[3(3-\nu)C_1^2\\ &\qquad+4(5-\nu)C_1C_2+2(7-\nu)C_2^2]\end{aligned}\right\} \quad (12.41)$$

Finally, the Galerkin technique is applied to approximate the second of equations (12.35); the result is the ordinary differential equation

$$\frac{d^2\tau}{dt^2}+\alpha^2\tau+\beta^2\tau^3=0 \quad (12.42)$$

where α^2 and β^2 are given in table 12.4 for the four cases defined by equations (12.36). The solution of equation (12.42) results in figure 12.10, which shows the effect of amplitude-thickness ratio upon the ratio of linear-to-nonlinear frequency for the four cases for $\nu=0.3$.

TABLE 12.4.—*Coefficients for Eq. (12.42) for the 4 Cases Defined by Eqs. (12.36)*

Coefficient	Value for case—			
	I(*a*)	I(*b*)	II(*a*)	II(*b*)
$\alpha^2\rho a^4/Eh^3$	2. 242	2. 242	9. 768	9. 768
$\beta^2\rho a^4/Eh^3$	. 591	4. 148	1. 429	4. 602

Further discussion of the application of the Galerkin method to the problems just described was given in reference 12.16.

The nonlinear case of the completely free circular plate having inplane forces caused by the thermal gradient

$$T=T_0\left[1-\left(\frac{r}{a}\right)^2\right] \tag{12.43}$$

was examined by Massa (ref. 12.17) as an extension of his previous work (see discussion of completely free circular plates (sec. 10.1.3)) for the linear problem. A deflection function

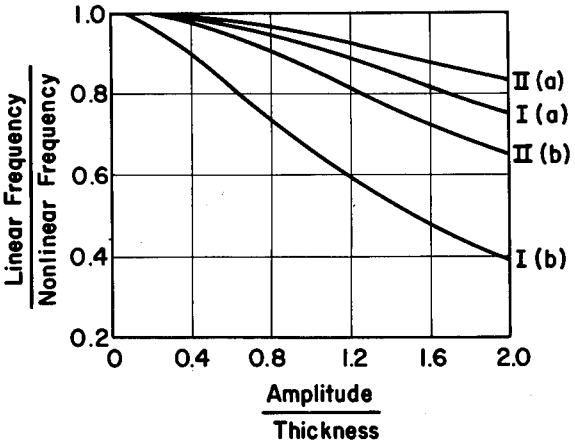


FIGURE 12.10.—Ratio of linear to nonlinear frequency as a function of amplitude/thickness ratio for circular plates having boundary conditions defined by equations (12.36); $\nu=0.3$. (After ref. 12.15)

$$w(r,\,t)=R(r)\tau(t) \tag{12.44}$$

is taken for the first axisymmetric mode, where $R(r)$ is the mode shape of the linear problem; that is,

$$R(r)=1-2.6161\left(\frac{r}{a}\right)^2+1.1090\left(\frac{r}{a}\right)^4-0.2464\left(\frac{r}{a}\right)^6 \tag{12.45}$$

and $\tau(t)$ is an unknown function of time. An energy formulation of the problem is made by means of Hamilton's principle for $\nu=0.3$. Solutions for the nonlinear frequencies are in terms of elliptic integrals, but approximate expressions of a more useful type are also found.

For $\alpha T_0a^2/h^2\leqq(\alpha T_0a^2/h^2)_{cr}$, or for $\alpha T_0a^2/h^2\geqq(\alpha T_0a^2/h^2)_{cr}$, in the range $W_{01}\geqq\sqrt{2}\,W_0$, the square of the nonlinear frequency can be approximated by

$$\omega_{01}^{*2}=7.4273\frac{Eh^3}{\rho a^4}\left[1-(0.2759\alpha T_0a^2/h^2)+0.6772\left(\frac{W_{01}}{h}\right)^2\right] \tag{12.46}$$

where α is the coefficient of thermal expansion, and $(\alpha T_0a^2/h^2)_{cr}$ is the critical value of the parameter $\alpha T_0a^2/h^2$ at which buckling occurs, according to the linear theory; that is,

$$(\alpha T_0a^2/h^2)_{cr}=3.62 \tag{12.47}$$

The term W_{01} defines the nonlinear deflection amplitude measured at the center, and W_0 is a parameter defined by

$$W_0\equiv 1.0524h\sqrt{0.2759(\alpha T_0a^2/h^2)-1} \tag{12.48}$$

For $\alpha T_0a^2/h^2\geqq(\alpha T_0a^2/h^2)_{cr}$ and $W_0<W_{01}\leqq\sqrt{2}W_0$, the corresponding expression is

$$\omega_{01}^{*2}=3.353\frac{Eh^3}{\rho a^4}\left(\frac{W_{01}}{h}\right)^2\left[1+1.1075\left(\frac{h}{W_{01}}\right)^2\left(0.2759\frac{\alpha T_0a^2}{h^2}-1\right)\right]^2 \tag{12.49}$$

In figures 12.11 and 12.12 the square of the ratio of the nonlinear frequency to the isothermal linear frequency ($\bar{\omega}_{01}^2=7.4273Eh^3/\rho a^4$,

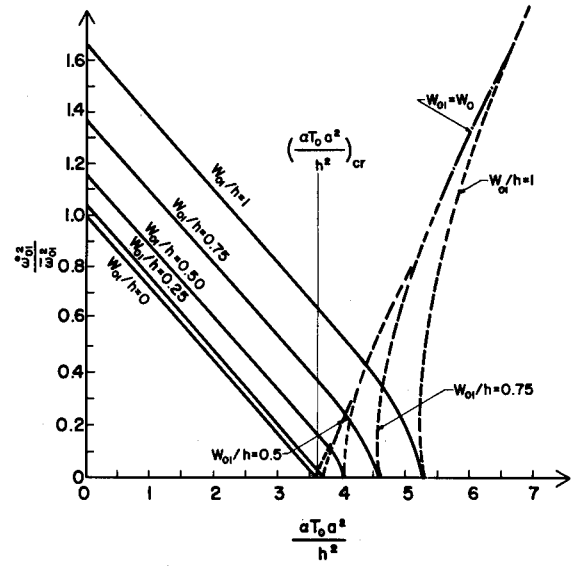


FIGURE 12.11.—Effect of temperature upon the nonlinear frequency of a completely free circular plate for various amplitude/thickness ratios; $\nu=0.3$; one nodal circle.

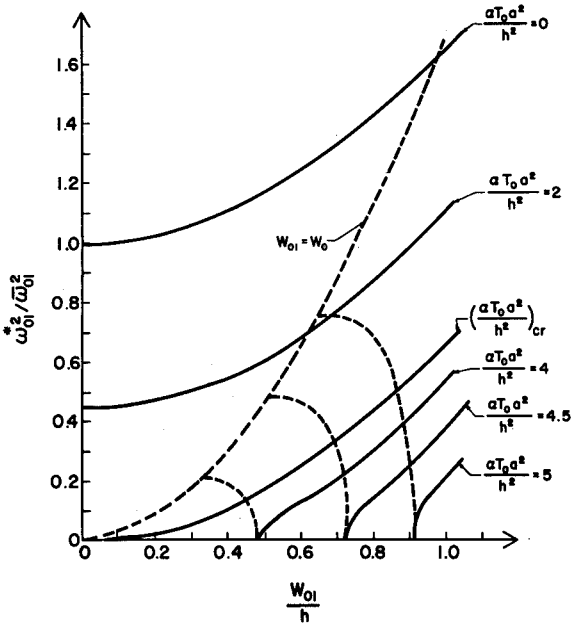


FIGURE 12.12.—Effect of amplitude/thickness ratio upon the nonlinear frequency of a completely free circular plate for various temperature parameters; $\nu=0.3$; one nodal circle.

with one nodal circle) is plotted against the parameters $\alpha T_0 a^2/h$ and W_{01}/h, respectively.

The first mode having two nodal diameters is also studied in reference 12.17 for the same thermal gradient given by equation (12.43). A deflection function

$$w(r,\theta,t)=R(r)(\cos 2\theta)\tau(t) \qquad (12.50)$$

is chosen, where

$$R(r)=\left(\frac{r}{a}\right)^2\left[1.2709-0.3500\left(\frac{r}{a}\right)^2+0.07911\left(\frac{r}{a}\right)^4\right] \qquad (12.51)$$

For $\alpha T_0 a^2/h^2 \leqq (\alpha T_0 a^2/h^2)_{cr}=3.62$, the square of the nonlinear frequency is approximated by

$$\omega_{20}^{*2}=2.6294\frac{Eh^3}{\rho a^4}\left[1+0.3772\frac{\alpha T_0 a^2}{h^2}+0.3164\left(\frac{W_{20}}{h}\right)^2\right] \qquad (12.52)$$

and for $\alpha T_0 a^2/h^2 > (\alpha T_0 a^2/h^2)_{cr}$ there results

$$\omega_{20}^{*2}=6.2169\frac{Eh^3}{\rho a^4}\left(1+0.000345\frac{\alpha T_0 a^2}{h^2}\right) \qquad (12.53)$$

The variation in the square of the ratio of the nonlinear frequency to the isothermal linear frequency ($\bar{\omega}_{20}^2=2.6294Eh^3/\rho a^4$, with two nodal diameters) is depicted in figures 12.13 and 12.14.

12.2.2 Rectangular Plates

The earliest paper dealing with large-amplitude vibrations of rectangular plates was published by Chu and Herrmann (ref. 12.18) in 1956. In this paper the general equations derived in reference 12.12 were specialized to the Von Kármán form of equations (12.28) and (12.29) and were approached by means of the perturbation technique. The problem of all edges simply supported was studied in detail. For this problem, the boundary conditions involving w are given in equations (4.18).

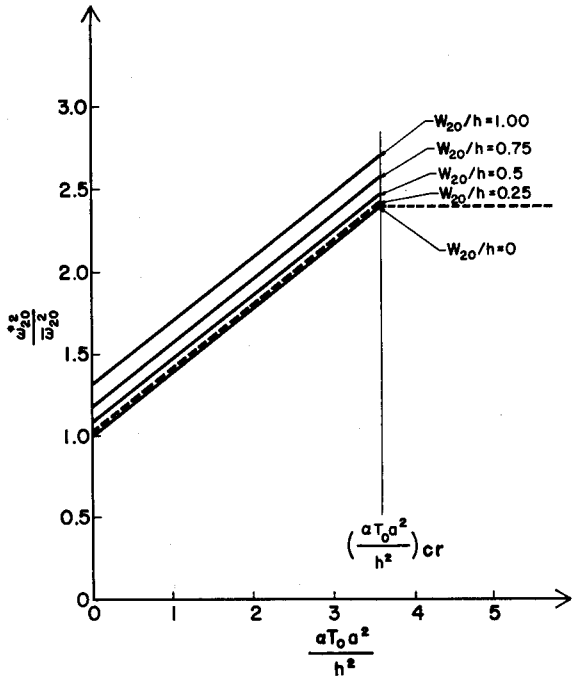


FIGURE 12.13.—Effect of temperature upon the nonlinear frequency of a completely free circular plate, for various amplitude/thickness ratios; $\nu=0.3$; two nodal diameters.

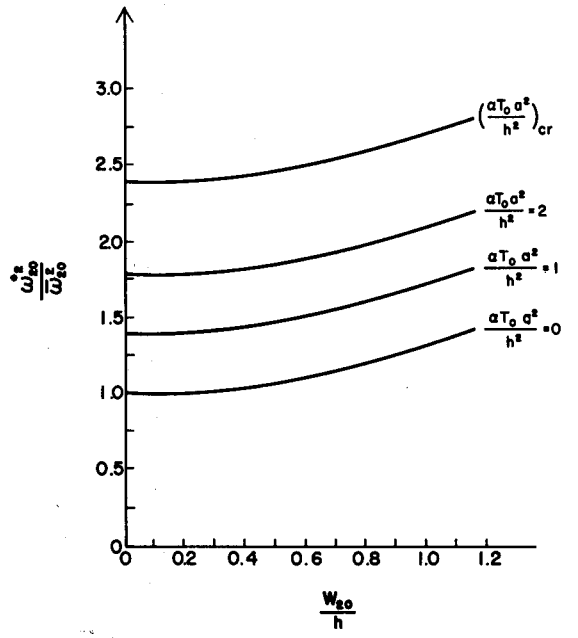


FIGURE 12.14.—Effect of amplitude/thickness ratio upon the nonlinear frequency of a completely free circular plate for various temperature parameters; $\nu=0.3$; two nodal diameters.

Partly in accordance with the later work by Yamaki (ref. 12.15), four cases of inplane restraint will be defined (see fig. 10.5):

$$\left.\begin{aligned}
&\text{Case } (a): N_x=N_{xy}=0 \text{ on } x=0,\ a\\
&\qquad\quad N_y=N_{xy}=0 \text{ on } y=0,\ b\\
&\text{Case } (b): u=N_{xy}=0 \text{ on } x=0,\ a\\
&\qquad\quad v=N_{xy}=0 \text{ on } y=0,\ b\\
&\text{Case } (c): P_x=N_{xy}=0,\ u=\text{Constant on } x=0,\ a\\
&\qquad\quad P_y=N_{xy}=0,\ v=\text{Constant on } y=0,\ b\\
&\text{Case } (d): u=v=0 \text{ on } x=0,\ a\\
&\qquad\quad u=v=0 \text{ on } y=0,\ b
\end{aligned}\right\} \tag{12.54}$$

where P_x and P_y are defined by

$$P_x\equiv\int_0^b N_x\,dy \qquad P_y\equiv\int_0^a N_y\,dx \tag{12.55}$$

Thus in case (c) there are edges which are kept straight by a distribution of normal stresses, the resultant of which is zero.

In reference 12.18, case (b) was treated. A transverse deflection function

$$w=A_0\tau(t)\sin\frac{\pi x}{a}\sin\frac{\pi x}{b} \tag{12.56}$$

was taken; the result is a nonlinear equation for τ in the form of equation (12.42). The ratio of linear frequency to nonlinear frequency is given by

$$\frac{\omega_0}{\omega}=\frac{2[1+(a/b)^2]K}{\pi\left\{\left(1+\frac{a^2}{b^2}\right)^2+3\left(\frac{A_0}{h}\right)^2\times\left[\left(\frac{3-\nu^2}{4}\right)\left(1+\frac{a^4}{b^4}\right)+\nu\frac{a^2}{b^2}\right]^{1/2}\right\}} \tag{12.57}$$

where $K=K(k)$ is the complete elliptic integral of the first kind and

$$\frac{1}{k^2}=2+\frac{2[1+(a/b)^2]^2}{3\left(\frac{A_0}{h}\right)^2\left[\left(\frac{3-\nu^2}{4}\right)\left(1+\frac{a^4}{b^4}\right)+\nu\frac{a^2}{b^2}\right]} \tag{12.58}$$

Equation (12.57) is plotted in figure 12.15 for $\nu=0.318$. The maximum membrane stress is given by

$$\sigma_m=\frac{E\pi}{8(1-\nu^2)}\left(\frac{A_0}{a}\right)^2\left(2+\nu\frac{a^2}{b^2}-\nu^2\right) \tag{12.59}$$

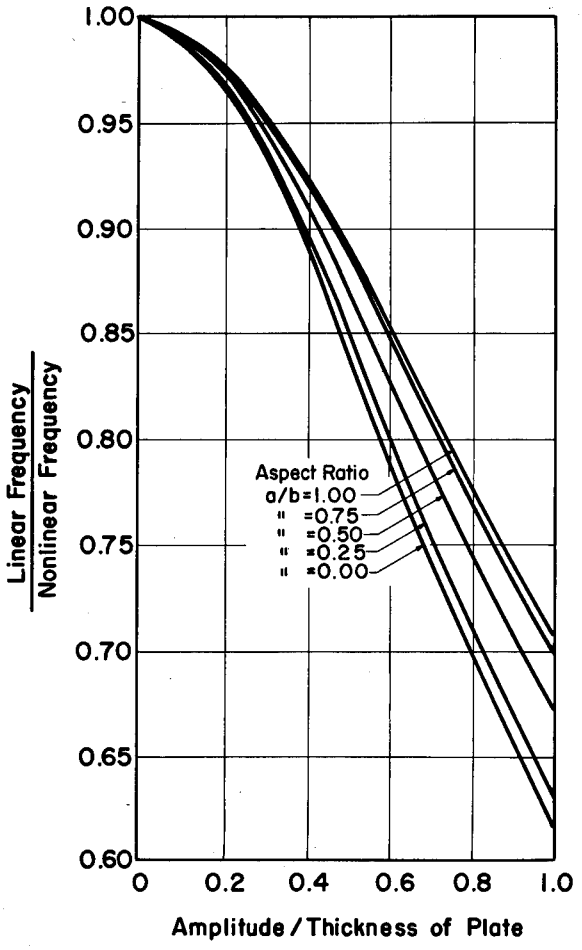


FIGURE 12.15.—Effect of large amplitudes on the frequency of a SS–SS–SS–SS rectangular plate; $\nu=0.318$. (After ref. 12.18)

and the maximum bending stress by

$$\sigma_b=\frac{E}{2}\left(\frac{A_0}{h}\right)\left(\frac{h}{a}\right)^2\pi^2\left(1.111+0.353\frac{a^2}{b^2}\right) \quad (12.60)$$

That is, the membrane stress increases with the square of the amplitude, whereas the bending stress increases only linearly. The problem was also formulated in reference (12.18) by the principle of conservation of energy.

Yamaki (ref. 12.15) extended the work to include the first three cases of inplane restraint given in equations (12.54). A deflection function like that of equation (12.56) was used, and the stress function was obtained from equation (12.28). Equation (12.29) was approximated by the Galerkin method. The equation in time which results for $a/b=1$ is

$$\frac{d^2\tau}{dt^2}+\frac{\pi^4Eh^2}{a^4}\left[\frac{1}{3(1-\nu^2)}\tau+\alpha\tau^3\right]=0 \quad (12.61)$$

where α takes on the values 0.06492, $(3-\nu)/8(1+\nu)$, and 1/8 for cases (a), (b), and (c), respectively. The ratio of linear to nonlinear frequency for the square plate is plotted in figure 12.16 for the three cases. For case (b) the results are identical with those of reference 12.18.

In reference 12.15, the problem of all edges transversely clamped (cf. eq. (4.25)) was also analyzed. A deflection function

$$w(x, y, t)=h\tau(t)\cos^2\frac{\pi\bar{x}}{a}\cos^2\frac{\pi\bar{y}}{b} \quad (12.62)$$

(see fig. 4.18) was used. The equation in time which results is

$$\frac{d^2\tau}{dt^2}+\frac{16}{9}\frac{\pi^4Eh^2}{a^4}\left[\frac{2}{3(1-\nu^2)}\tau+\alpha\tau^3\right]=0 \quad (12.63)$$

where α takes on the values 0.14903, $0.16656+(0.14063)/(1-\nu)$, and 0.16656 for cases (a), (b), and (c), respectively. The ratio of linear to nonlinear frequency is plotted in figure 12.17 for the three cases when $a/b=1$.

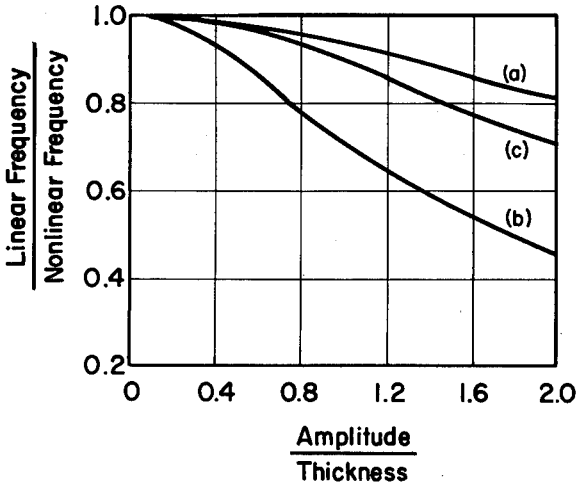


FIGURE 12.16.—Effect of large amplitude on the frequency of a SS–SS–SS–SS square plate for three cases of inplane edge restraint; $\nu=0.3$. (After ref. 12.15)

Nash and Modeer (ref. 12.19) and Wah (ref. 12.20) extended the Berger (ref. 12.14) simplified formulation for the large-amplitude static deflection of plates to the nonlinear vibration problem. The first paper used an energy formulation with Hamilton's principle; the second used a modified form of the Galerkin method. Both papers solved the problem of the rectangular plate having simply supported edges of the type given by case (*d*) of equations (12.54). Both obtained results for frequency ratio versus amplitude ratio which were in substantial quantitative agreement and, in contrast with those of reference 12.18, these results *do not depend upon the aspect ratio* a/b *of the plate.* These results are shown in figure 12.18 (from ref. 12.20). In this figure a curve is also plotted for the infinite strip, in accordance with elementary beam theory.

In reference 12.20 the problems of the SS–C–SS–SS and SS–C–SS–C plates were also studied. Deflection functions for w were taken which are the fundamental mode shapes of the linear problem (see secs. 4.2.2 and 4.2.1). The effect of amplitude upon frequency is shown in figures 12.19 and 12.20 for these two problems.

The existence of normal modes for the nonlinear problem of the SS–SS–SS–SS plate is discussed in reference 12.21. Large-amplitude

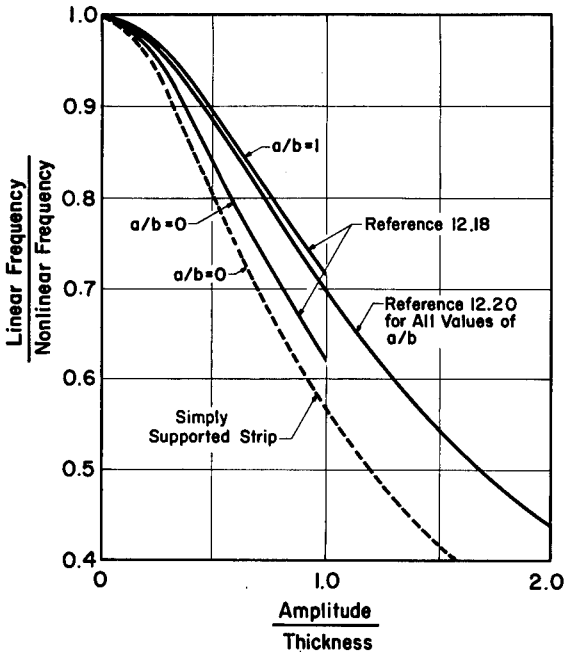


FIGURE 12.18.—Ratio of linear to nonlinear frequency as a function of amplitude/thickness ratio for SS–SS–SS–SS plates; $\nu=0.3$. (After ref. 12.20)

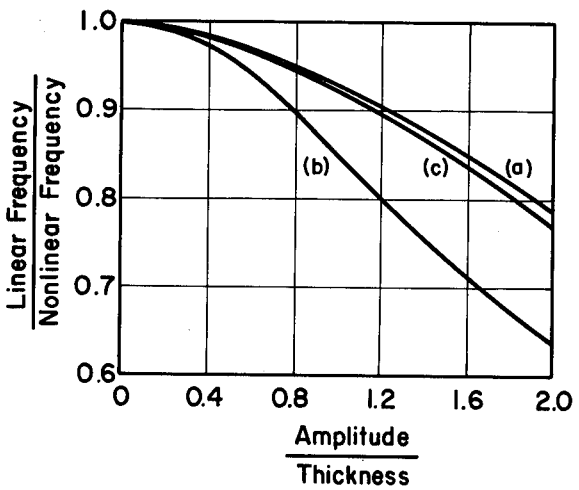


FIGURE 12.17.—Effect of large amplitude on the frequency of a C–C–C–C square plate for three cases of inplane contraint; $\nu=0.3$. (After ref. 12.15)

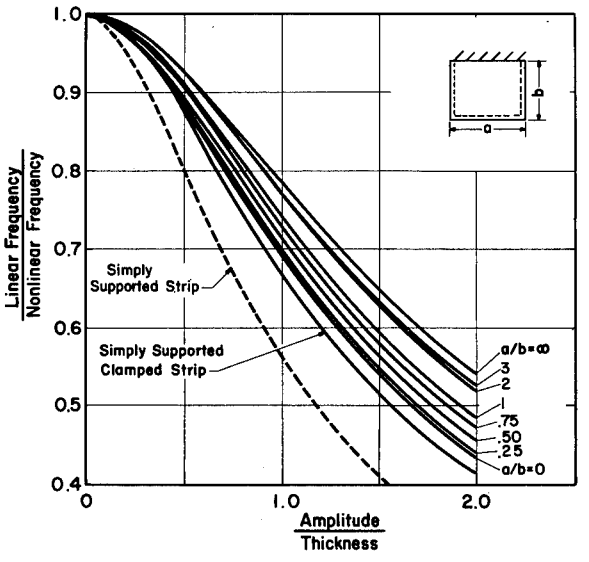


FIGURE 12.19.—Effect of amplitude upon frequency for SS–C–SS–SS rectangular plates; $\nu=0.3$. (After ref. 12.20)

308-337 O—70——21

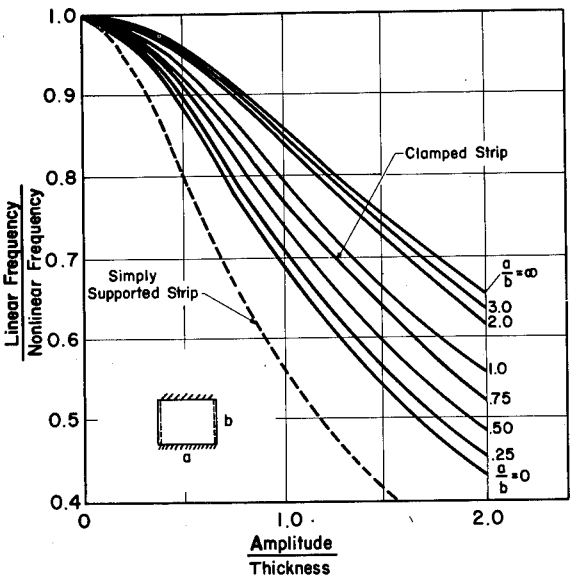


FIGURE 12.20.—Effect of amplitude upon frequency for SS–C–SS–C rectangular plates; $\nu=0.3$. (After ref. 12.20)

vibration of rectangular plates is also discussed in references 12.22 and 12.23.

12.3 EFFECTS OF SHEAR DEFORMATION AND ROTARY INERTIA

In 1877 Lord Rayleigh (ref. 12.24) showed how the addition of "rotatory" (in the language of his day) inertia effects to those of classical transitional inertia affected the flexural vibration frequencies of beams. Timoshenko (ref. 12.25) in 1921 showed that the effects of shear deformation, previously disregarded, were equally important. It is well known that both effects serve to decrease the computed frequencies because of increased inertia and flexibility of the system.

An extension of plate theory to account for shear deformation was proposed by Reissner (ref. 12.26) for the static deflection of plates, and a significant number of papers by others have followed this approach. A first presentation of a consistent theory for the dynamic behavior of plates, including the effects of shear deformation and rotary inertia, was made by Uflyand (ref. 12.27). However, Mindlin's 1951 paper (ref. 12.28) unquestionably made the most profound impact upon the subject. In this paper a consistent set of equations relating moments and transverse shears to transverse deflection and bending rotations was presented. The basic sixth-order system of partial differential equations of motion was derived, along with potential and kinetic energy functions. A part of this paper will be summarized below.

In addition to exposing the theory, Mindlin and his colleagues have done much to apply the theory and to develop it further, as observed by references 12.29 to 12.46. In references 12.29 through 12.32 the theory is applied to the cylindrical bending of AT-cut quartz crystal plates. The crystal plates are idealized as an anisotropic material having constants defined by equation (A.12) of the appendix in which

$$a_{14}=a_{24}=a_{34}=a_{15}=a_{25}=a_{35}=a_{46}=a_{56}=0$$

and *the thickness is taken in the z-direction.* Crystal plates are also discussed in references 12.36 to 12.46. Because of the highly specialized form of anisotropy involved, the numerous results reported in these papers will not be discussed here. The only results from references 12.28 to 12.46 which will be discussed in this section will be those dealing with isotropic plates.

The essential features of Mindlin's theory (ref. 12.28) will now be discussed. The discussion will be limited to the bending (with no inplane forces) of isotropic plates. When the effects of shear deformation are included, the kinematic relationships given in equations (A.9) become

$$\left.\begin{aligned} u&=-z\psi_x(x,y,t)\\ v&=-z\psi_y(x,y,t)\\ w&=w(x,y,t) \end{aligned}\right\} \qquad (12.64)$$

where ψ_x and ψ_y are the local rotations (changes of slope) in the x- and y-directions, respectively, of lines originally normal to the midplane before deformations. That is, the rotations ψ_x and ψ_y are due to bending. The deflection of the middle surface w is then composed of two parts—one due to bending and the other due to shear deformation. These modes of deformation are shown in figure 12.21. Equations (12.64) are substituted into strain-

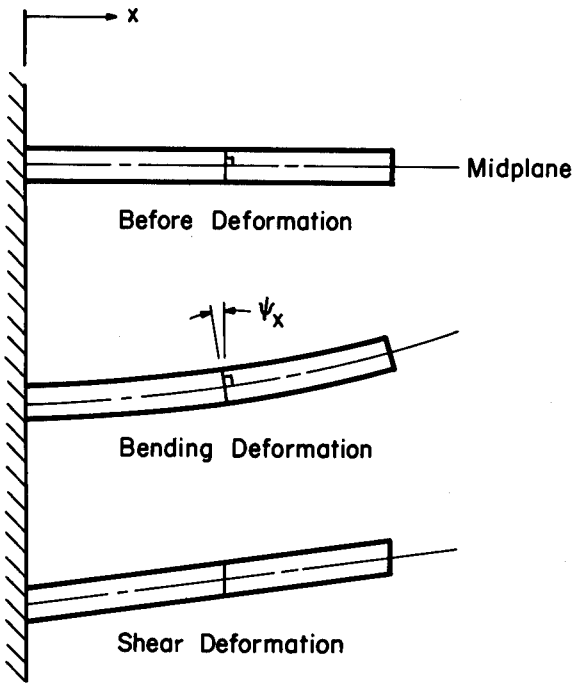


FIGURE 12.21.—Modes of bending and shear deformation.

displacement equations (A.10), then into stress-strain equations (A.19), and the bending moments are integrated by means of equations (A.20(d)), (A.20(e)), and (A.20(f)), giving

$$\left.\begin{aligned} M_x &= -D\left(\frac{\partial \psi_x}{\partial x}+\nu\frac{\partial \psi_y}{\partial y}\right) \\ M_y &= -D\left(\frac{\partial \psi_y}{\partial y}+\nu\frac{\partial \psi_x}{\partial x}\right) \\ M_{xy} &= -\frac{D(1-\nu)}{2}\left(\frac{\partial \psi_y}{\partial x}+\frac{\partial \psi_x}{\partial y}\right) \end{aligned}\right\} \quad (12.65)$$

The transverse shearing forces are obtained by integrating the transverse shearing stress over the thickness; that is,

$$\left.\begin{aligned} Q_x &= \int_{-h/2}^{h/2} \tau_{zx}\,dz \\ Q_y &= \int_{-h/2}^{h/2} \tau_{yz}\,dz \end{aligned}\right\} \quad (12.66)$$

Substituting the stress-strain relationships

$$\left.\begin{aligned} \tau_{zx} &= G\gamma_{zx} \\ \tau_{yz} &= G\gamma_{yz} \end{aligned}\right\} \quad (12.67)$$

and the strain-displacement equations

$$\left.\begin{aligned} \gamma_{zx} &= \frac{\partial u}{\partial z}+\frac{\partial w}{\partial x} \\ \gamma_{yz} &= \frac{\partial w}{\partial y}+\frac{\partial v}{\partial z} \end{aligned}\right\} \quad (12.68)$$

into equations (12.66) and using equations (12.64) gives

$$\left.\begin{aligned} Q_x &= -\kappa^2 Gh\left(\psi_x-\frac{\partial w}{\partial x}\right) \\ Q_y &= -\kappa^2 Gh\left(\psi_y-\frac{\partial w}{\partial y}\right) \end{aligned}\right\} \quad (12.69)$$

where κ^2 is a constant which is introduced to account for the fact that the shear stresses τ_{zx} and τ_{yz} are clearly not constant over the thickness $-h/2<z<h/2$ as the simple kinematic relationships, equations (12.64), would lead one to believe. In Reissner's static theory (ref. 12.26) κ^2 was taken as 5/6. Mindlin (ref. 12.28) chose κ so as to make the dynamic theory consistent with the known exact frequency for the fundamental "thickness shear" mode of vibration. More will be said about this in the following discussion.

The right-hand sides of moment equilibrium equations (A.8) are made consistent with the present theory; they become

$$\left.\begin{aligned} Q_x-\frac{\partial M_x}{\partial x}-\frac{\partial M_{xy}}{\partial y} &= \frac{\rho h^2}{12}\frac{\partial^2 \psi_x}{\partial t^2} \\ Q_y-\frac{\partial M_{xy}}{\partial x}-\frac{\partial M_y}{\partial y} &= \frac{\rho h^2}{12}\frac{\partial^2 \psi_y}{\partial t^2} \end{aligned}\right\} \quad (12.70)$$

When inplane forces and transverse external loading or body forces are neglected, equation (A.6) becomes

$$\frac{\partial Q_x}{\partial x}+\frac{\partial Q_y}{\partial y}=\rho\frac{\partial^2 w}{\partial t^2} \quad (12.71)$$

Substituting equations (12.65) and (12.69) into equations (12.70) and (12.71) yields the fundamental set of equations for the system

$$\left.\begin{aligned}
&\frac{D}{2}\left[(1-\nu)\nabla^2\psi_x+(1+\nu)\frac{\partial}{\partial x}\left(\frac{\partial\psi_x}{\partial x}+\frac{\partial\psi_y}{\partial y}\right)\right] \\
&\qquad -\kappa^2Gh\left(\psi_x-\frac{\partial w}{\partial x}\right)=\frac{\rho h^2}{12}\frac{\partial^2\psi_x}{\partial t^2} \\
&\frac{D}{2}\left[(1-\nu)\nabla^2\psi_y+(1+\nu)\frac{\partial}{\partial y}\left(\frac{\partial\psi_x}{\partial x}+\frac{\partial\psi_y}{\partial y}\right)\right] \\
&\qquad -\kappa^2Gh\left(\psi_y-\frac{\partial w}{\partial y}\right)=\frac{\rho h^2}{12}\frac{\partial^2\psi_y}{\partial t^2} \\
&\kappa^2Gh\left(\nabla^2w-\frac{\partial\psi_x}{\partial x}-\frac{\partial\psi_y}{\partial y}\right)=\rho\frac{\partial^2w}{\partial t^2}
\end{aligned}\right\} \tag{12.72}$$

where ∇^2 is the usual Laplacian operator. It is observed that the system of equations (12.72) is of the sixth order in the three dependent variables ψ_x, ψ_y, and w. Thus, with this higher order plate theory, three boundary conditions are enforced along each edge.

In reference 12.28, equations (12.72) are rewritten into a form much more amenable to solution by the introduction of three potential functions. It is from this form that many of the useful results obtained from references 12.33 to 12.37 and given later in this section were derived. The reader is referred to the individual papers for the details of these manipulations and solutions. Similarly, the extensions of the theory to include inplane forces, large deformations, and thermal effects (refs. 12.12, 12.40, 12.47, and 12.48) will not be discussed here.

Thickness-shear vibration is defined by modes of the form (ref. 12.29)

$$\left.\begin{aligned}
u&=f(z)e^{i\omega t} \\
v&=w=0
\end{aligned}\right\} \tag{12.73}$$

It can be shown (ref. 12.29) that, for a plate having infinite dimensions in the x- and y-directions, the exact frequency of the first antisymmetric mode of thickness-shear vibration is

$$\bar{\omega}=\pi\sqrt{\frac{G}{\rho h}} \tag{12.74}$$

It can be further shown (ref. 12.28) that, for equations (12.72) to give results consistent with equation (12.74), κ^2 must be chosen for an isotropic plate to be

$$\kappa^2=\frac{\pi^2}{12} \tag{12.75}$$

Further theoretical discussion of the effects of shear deformation and rotary inertia upon the vibration of plates can be found in references 12.49 to 12.61. For the most part, these references give alternative derivations of systems of governing equations, in some cases concluding with Mindlin's equations and in other cases obtaining substantially different formulations.

12.3.1 Circular Plates

Consider first a circular plate having a *clamped* boundary. (See fig. 2.1.) For axisymmetric modes of vibration the sixth-order system of differential equations (12.72) (when converted to polar coordinates) reduces to a fourth-order system. The boundary conditions are

$$w(a)=\psi_r(a)=0 \tag{12.76}$$

That is, the change in slope *due to bending* is zero at the boundary. Applying equation (12.76) to the solutions of the differential equations, which are in terms of Bessel func-

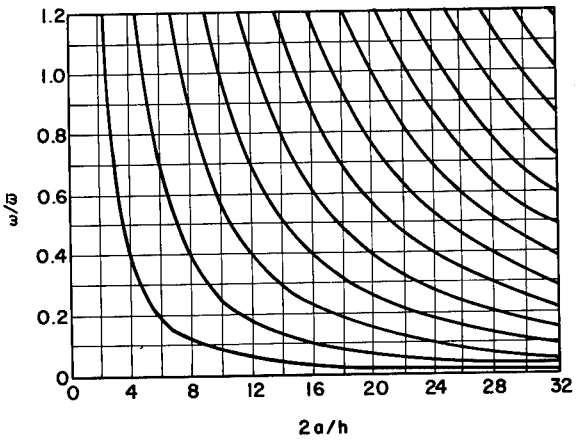


FIGURE 12.22.—Ratio of plate frequency to thickness-shear frequency for a clamped circular plate derived from classical theory; $\nu=0.312$. (After ref. 12.35)

tions (see refs. 12.33, 12.34, and 12.62), yields a set of characteristic equations for the frequencies.

Results for the axisymmetric modes were presented by Deresiewicz (ref. 12.35). The frequency ratio $\omega/\bar{\omega}$ derived from the *classical* theory of plates is plotted in figure 12.22. With the use of the notation of the chapter entitled "Circular Plates" (ch. 2), the circular frequencies of the plate can be obtained from

$$\omega_i a^2\sqrt{\rho/D}=\lambda_i^2 \qquad (i=1, 2, \ldots) \quad (12.77)$$

where λ_i are the eigenvalues determined from the characteristic equation. By using equations (12.74) and (12.77), it is easily seen that the ratio of the plate flexural frequency to the thickness-shear frequency $\bar{\omega}$ is

$$\frac{\omega}{\bar{\omega}}=\left(\frac{h}{2a}\right)^2\frac{\lambda^2}{\pi^2}\sqrt{\frac{8}{3(1-\nu)}} \qquad (12.78)$$

where the subscript i on ω and λ has been dropped but is implied. Figure 12.22 is consequently a plot of equation (12.78) for a particular value of Poisson's ratio $\nu=0.312$.

Figure 12.23 is a corresponding plot with the plate frequencies ω obtained by the theory of this section, although this figure is plotted over a smaller range of $\omega/\bar{\omega}$, thereby emphasizing the region in the vicinity of $\omega/\bar{\omega}=1$. In comparing figures 12.22 and 12.23, it is obvious that consideration of shear deformation and rotary inertia has the effects of—

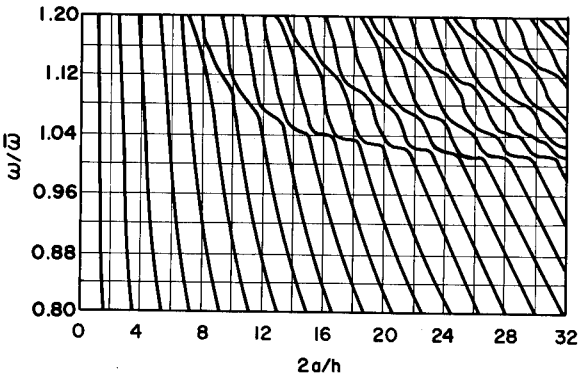


FIGURE 12.23.—Ratio of plate frequency to thickness-shear frequency for a clamped circular plate derived from the Mindlin theory; $\nu=0.312$. (After ref. 12.35)

(1) Lowering the fundamental frequency for a given diameter-thickness ratio

(2) Rendering more frequencies in a given range of $\omega/\bar{\omega}$ for a particular plate

(3) Completely altering the curves in the high-frequency range $\omega/\bar{\omega}>1$

The case when the circular boundary is *simply supported* was attempted by Tomar (ref. 12.63). Again, when only the axisymmetric modes are sought, only two boundary conditions are required; namely,

$$w(a)=M_r(a)=0 \qquad (12.79)$$

In reference 12.63 the equations of motion (eqs. (12.72)) are retained in rectangular coordinates, and their finite-difference equivalents are written. Because of the choice of coordinate system, a rectangular finite-difference grid must be fitted to a sector of the circular plate. This is accomplished by using nine mesh points within one octant obtained from a square grid having elements of dimension $a/4$. Fundamental frequency parameters $4\omega^2a^2\rho/Eh$ for various thickness-radius ratios given in table 12.5 and figure 12.24 for $\nu=0.3$ are taken directly from reference 12.63. In addition, the frequency parameter $\omega a^2\sqrt{\rho/D}$ is presented in table 12.5 for direct comparison with the classical result $\omega a^2\sqrt{\rho/D}=4.977$ (see sec. 2.1.2) which applied for very small values of h/a. From this comparison it appears that the accuracy of the results given in table 12.5 and figure 12.24 is highly questionable.

Numerical results for the *completely free* circular plate were found by Mindlin and Deresie-

TABLE 12.5.—*Fundamental Frequency Parameters for a Simply Supported Circular Plate According to the Mindlin Theory; $\nu=0.3$*

h/a	$\frac{4\omega^2a^2\rho}{Eh}$	$\omega a^2\sqrt{\rho/D}$
0.2	0.43365	5.4403
.4	1.44326	4.96242
.6	2.53474	4.38426
.8	3.49852	3.86308

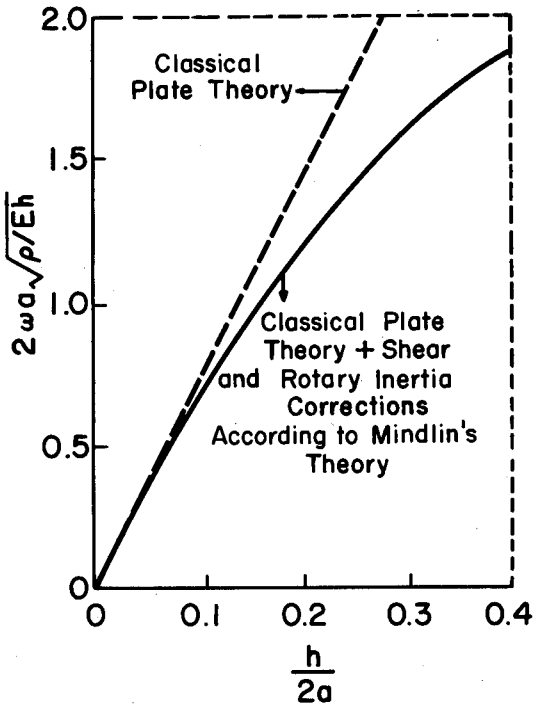


FIGURE 12.24.—Fundamental frequency parameters for a simply supported circular plate; $\nu=0.3$. (After ref. 12.63)

wicz (refs. 12.33 and 12.34). In this case the boundary conditions are

$$M_r(a)=M_{r\theta}(a)=Q_r(a)=0 \qquad (12.80)$$

The twisting-moment condition is identically satisfied by symmetry for the axisymmetric modes. In reference 12.34 frequency parameters for axisymmetric modes were deduced when $\nu=0.312$. Plots of the frequency ratios $\omega/\overline{\omega}$ discussed earlier in this section are depicted in figures 12.25 and 12.26 for the classical theory and the Mindlin theory, respectively. Results for the antisymmetric modes (having one nodal diameter) were computed in reference 12.33 and are presented in figure 12.27, again for $\nu=0.312$.

In reference 12.64, Callahan used the Mindlin theory to derive characteristic determinants corresponding to eight separate sets of continuous boundary conditions for circular plates. All sets are presented in forms conducive to computer programing and for general vibration modes. No numerical results were given.

12.3.2 Rectangular Plates

It was shown in reference 12.28 that equations (12.72) can be uncoupled (after the time is taken out by assuming harmonic response) by defining three potentials w_1, w_2, and H by the equations:

$$\left.\begin{aligned}\psi_x&=(A_1-1)\frac{\partial w_1}{\partial x}+(A_2-1)\frac{\partial w_2}{\partial x}+\frac{\partial H}{\partial y}\\ \psi_y&=(A_1-1)\frac{\partial w_1}{\partial y}+(A_2-1)\frac{\partial w_2}{\partial y}-\frac{\partial H}{\partial x}\\ w&=w_1+w_2\end{aligned}\right\} \qquad (12.81)$$

where

$$\left.\begin{aligned}A_j&=2[1+g-(-1)^jB_j]^{-1} \quad (j=1,2)\\ B_j&=[(1-g)^2+4g(\overline{\omega}/\omega_j)^2]^{1/2} \quad (j=1,2)\\ g&=\kappa^2(1-\nu)/2\end{aligned}\right\} \qquad (12.82)$$

and where $\omega/\overline{\omega}$ is the ratio of plate frequency to thickness-shear frequency used earlier in this chapter ($\overline{\omega}$ is defined by eq. (12.74)), κ is given by equation (12.75), and ν is Poisson's ratio. Substituting equations (12.81) and (12.82) into equations (12.72) results in the three uncoupled equations

$$\left.\begin{aligned}(\nabla^2+\delta_1^2)w_1&=0\\ (\nabla^2+\delta_2^2)w_2&=0\\ (\nabla^2+\gamma^2)H&=0\end{aligned}\right\} \qquad (12.83)$$

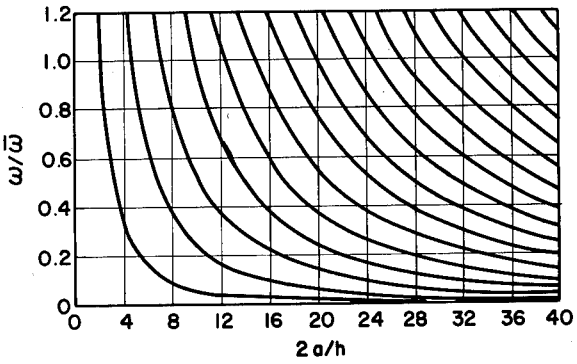


FIGURE 12.25.—Ratio of plate frequency to thickness-shear frequency for the axisymmetric modes of a completely free circular plate derived from classical theory; $\nu=0.312$. (After ref. 12.34)

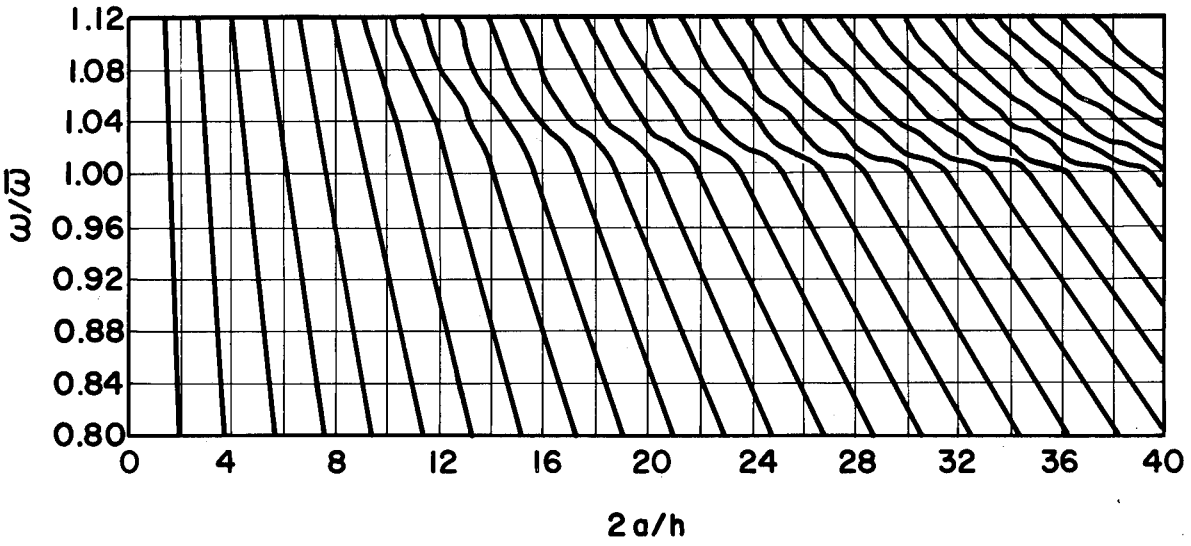


FIGURE 12.26.—Ratio of plate frequency to thickness-shear frequency for the axisymmetric modes of a completely free circular plate derived from the Mindlin theory; $\nu=0.312$. (After ref. 12.34)

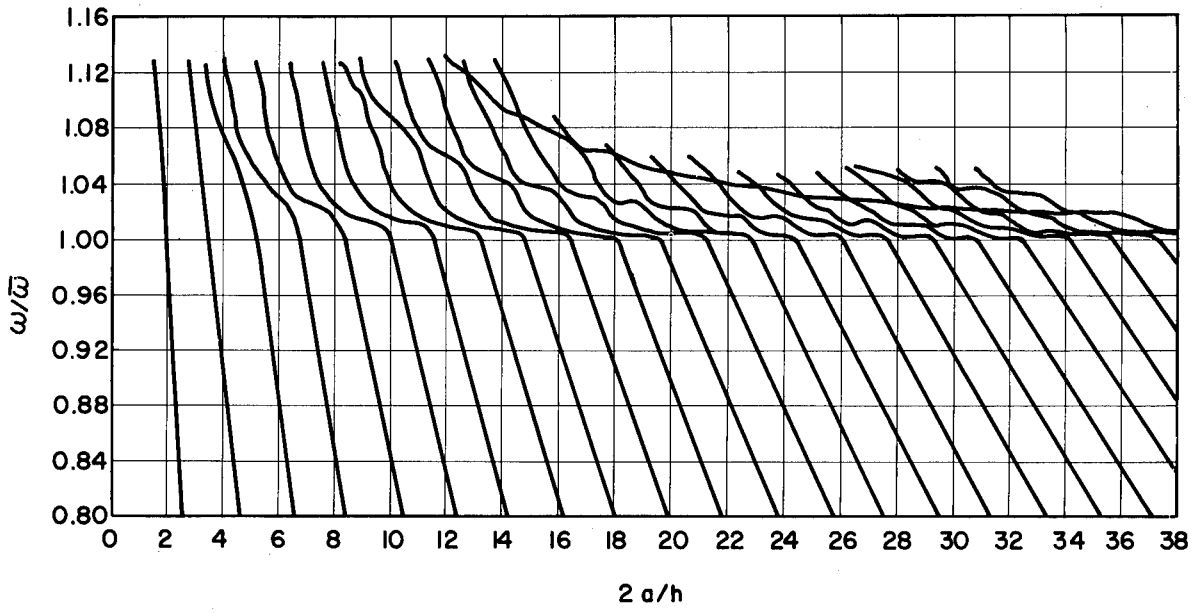


FIGURE 12.27.—Ratio of plate frequency to thickness-shear frequency for the antisymmetric modes of a completely free circular plate derived from the Mindlin theory; $\nu=0.312$. (After ref. 12.33)

where

$$\left.\begin{aligned}\delta_i^2&=6(\omega_j/\overline{\omega})^2[1+g-(-1)^jB_j]h^{-2} \qquad (j=1,\ 2)\\ \gamma^2&=\pi^2[(\omega_3/\overline{\omega})^2-1]h^{-2}\end{aligned}\right\} \tag{12.84}$$

Thus the potentials w_1, w_2, and H may be regarded as uncoupled vibration modes having the frequencies ω_1, ω_2, and ω_3, respectively.

The problem of the rectangular plate *simply supported on all edges* was solved by Mindlin, Schacknow, and Deresiewicz (ref. 12.36) by

means of the approach just given. In terms of a coordinate system $\bar{x}$, $\bar{y}$ having its origin at the center of the plate (cf. fig. 4.4), the boundary conditions are:

$$\left.\begin{aligned} w=M_x=\psi_y=0 \qquad (\text{on } \bar{x}=\pm a/2)\\ w=M_y=\psi_x=0 \qquad (\text{on } \bar{y}=\pm b/2)\end{aligned}\right\} \tag{12.85}$$

It is easily seen that

$$\left.\begin{aligned} w_1&=\sin\ \alpha_1\bar{x}\ \sin\ \beta_1\bar{y}\\ w_2&=\sin\ \alpha_2\bar{x}\ \sin\ \beta_2\bar{y}\\ H&=\cos\ \alpha_3\bar{x}\ \sin\ \beta_3\bar{y}\end{aligned}\right\} \tag{12.86}$$

are solutions to equations (12.83), provided that

$$\left.\begin{aligned} \alpha_1^2+\beta_1^2&=\delta_1^2\\ \alpha_2^2+\beta_2^2&=\delta_2^2\\ \alpha_3^2+\beta_3^2&=\gamma^2\end{aligned}\right\} \tag{12.87}$$

Substituting equations (12.86) into equations (12.85) gives

$$\left.\begin{aligned} \alpha_j&=r_j\pi/a\\ \beta_j&=s_j\pi/b \qquad (j=1,\ 2,\ 3)\end{aligned}\right\} \tag{12.88}$$

where r_j and s_j are even integers. The modes given by equation (12.86) are then odd in both x and y. For modes even in x, $\sin\ \alpha_j x$ and $\cos\ \alpha_j x$ are interchanged in all three of equations (12.86) and the r_j are odd integers. Similarly, for modes even in y, $\sin\ \beta_j y$ and $\cos\ \beta_j y$ are interchanged, and the s_j are odd integers.

Substituting equations (12.88) into equations (12.87) and solving for the frequency ratios give

$$\left.\begin{aligned} 2\left(\frac{\omega_j}{\bar{\omega}}\right)^2&=1+\frac{\kappa^2}{g}(1+g)\psi_j^2+(-1)^j\Omega_j \qquad (j=1,2)\\ \left(\frac{\omega_3}{\bar{\omega}}\right)^2&=1+\psi_3^2\end{aligned}\right\} \tag{12.89}$$

where

$$\left.\begin{aligned} \psi_j^2&=\frac{h^2}{\pi^2}(\alpha_j^2+\beta_j^2) \qquad (j=1,2,3)\\ \Omega_j&=\left\{\left[1+\frac{\kappa^2}{g}(1+g)\psi_j^2\right]^2-4\frac{\kappa^4}{g}\psi_j^4\right\}^{1/2} \qquad (j=1,2,3)\end{aligned}\right\} \tag{12.90}$$

In figure 12.28 (taken from ref. 12.36) the three sets of frequency ratios given by equations (12.89) are plotted against the length-thickness ratio as a function of the parameter ϕ_j, where

$$\phi_j=[r_j^2+(s_j^2a^2/b^2)]^{1/2} \qquad (j=1,\ 2,\ 3) \tag{12.91}$$

and where $\nu=0.312$. From figure 12.28 it can be seen that for a given plate and for a given mode number j the frequencies are ordered according to $\omega_1<\omega_3<\omega_2$ and that ω_2 and ω_3 are much greater than ω_1 except for very thick plates.

In figure 12.29 (taken from ref. 12.36) a more detailed plot of the frequency ratios is indicated in the vicinity of $\omega/\bar{\omega}=1$ for a fixed ratio $s_jh/b=0.2$ and for $\nu=0.312$. This corresponds to the particular case when the distance in the y-direction between node lines (including the boundaries) is five times the plate thickness. In this figure $r_1=m$, $r_2=n$, and $r_3=q$; that is, the curves m, n, $q=$constant give the frequencies of the w_1, w_2, and H modes, respectively. In this case, each mode has a low-frequency cutoff given by

$$\left.\begin{aligned} 2\left(\frac{\omega_j^*}{\bar{\omega}}\right)^2&=1+(\psi_j^*)^2+(-1)^j\Omega_j^* \qquad (j=1,\ 2)\\ \left(\frac{\omega_3^*}{\bar{\omega}}\right)^2&=1+(\psi_3^*)^2\end{aligned}\right\} \tag{12.92}$$

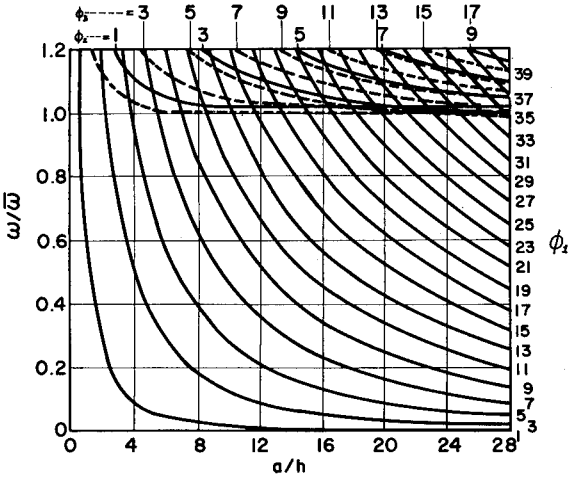


FIGURE 12.28.—Ratio of plate frequency to thickness-shear frequency for a SS–SS–SS–SS rectangular plate derived from the Mindlin theory; $\nu=0.312$. (After ref. 12.36)

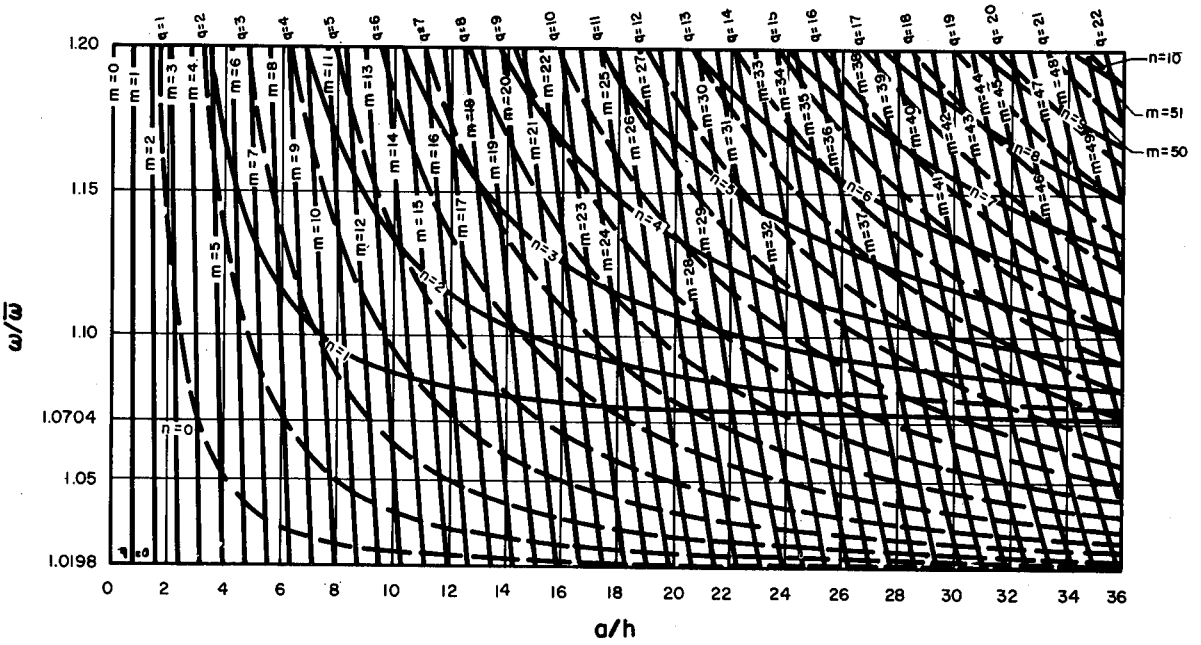


FIGURE 12.29.—Ratio of plate frequency to thickness-shear frequency for a SS–SS–SS–SS rectangular plate when the distance between nodes along the width is five times the thickness; $\nu=0.312$. (After ref. 12.36)

where ψ_i^* and Ω_i^* are given by equations (12.90) with $r_y h/a=0$. These formulas give the values 1.0198 and 1.0704 shown in figure 12.29.

The mode shapes corresponding to w_1, w_2, and H are depicted in figure 12.30 (taken from ref. 12.36). The mode shape corresponding to classical theory is shown in figure 12.31, which is also from reference 12.36. Of the three modes, the w_1 mode most closely resembles the classical mode; hence, it is called a "flexural" mode. As $a/h\to\infty$, this mode approaches the classical mode, and its frequency approaches the classical frequency given by equation (4.20). For the w_2 mode the thickness-shear deformation predominates. The H mode shape (fig. 12.30(*c*)) contains no average deflection, but twists the plate; hence, it is called a "thickness twist" mode.

In references 12.65 and 12.66 the problem of the simply supported plate is attacked by the finite-difference method. Mindlin's equations are the basis for this method in reference 12.65, whereas in reference 12.66 an alternate set is used. Numerical results for frequencies are given in both papers, but they are inconsistent with classical theory and will not be repeated here.

A stiffened plate was treated as an orthotropic plate for purposes of analysis in reference 12.67. The effects of rotary inertia were considered, but shear deformation was ignored. In this case the system of governing differential equations remains fourth order. Equation (9.22) is generalized to

$$D_x\frac{\partial^4 w}{\partial x^4}+2D_{xy}\frac{\partial^4 w}{\partial x^2\,\partial y^2}+D_y\frac{\partial^4 w}{\partial y^4}+\frac{\partial^2}{\partial t^2}\left(\rho w-I_x\frac{\partial^2 w}{\partial x^2}-I_y\frac{\partial^2 w}{\partial y^2}\right)=0 \qquad (12.93)$$

where I_x and I_y are the moments of inertia of the stiffened plate about axes parallel to the y- and x-directions, respectively.

For a rectangular plate simply supported along the edges $x=0$, a and $y=0$, b, it is apparent that the boundary conditions will be satisfied by the deflection function

$$W(x,y)=\sin\,\alpha x\,\sin\,\beta y \qquad (12.94)$$

where $\alpha=m\pi/a$, $\beta=n\pi/b$, and m and n are integers. Substituting equation (12.94) into

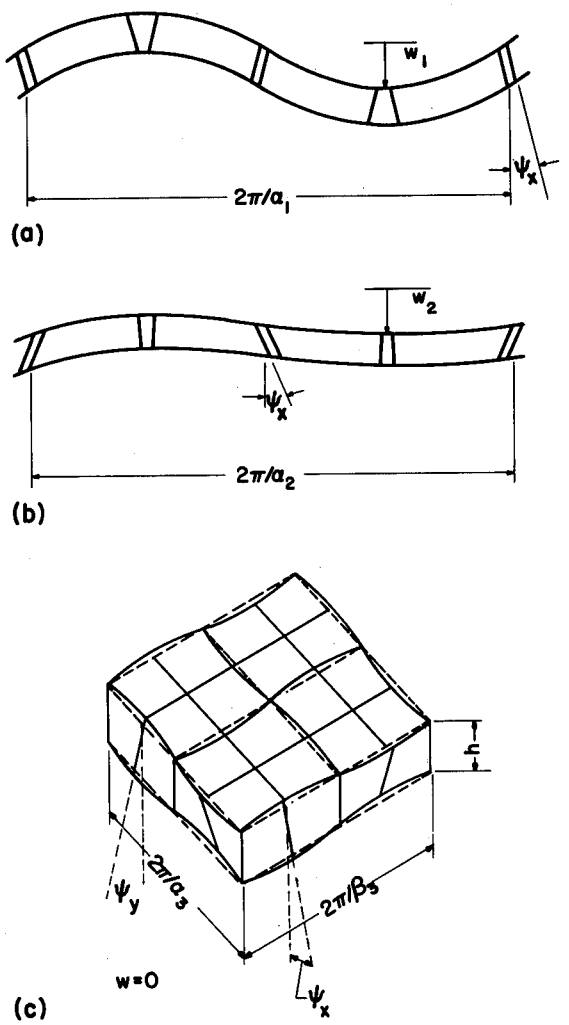


FIGURE 12.30.—Mode shapes for a SS–SS–SS–SS rectangular plate with consideration of shear deformation and rotary inertia. (*a*) w_1 mode. (*b*) w_2 mode. (*c*) H mode. (After ref. 12.36)

equation (12.93) and assuming harmonic time response give the frequency equation

$$\omega_{mn}^2=\frac{D_x\alpha^4+2D_{xy}\alpha^2\beta^2+D_y\beta^4}{\rho+I_x\alpha^2+I_y\beta^2} \tag{12.95}$$

It is seen that the effects of rotary inertia enter as terms in the denominator of equation (12.95) with a resultant decrease in frequency from the classical theory.

In reference 12.67, theoretical results were obtained from equation (12.95) and compared with experimental data for an aluminum square plate having the cross section and dimensions

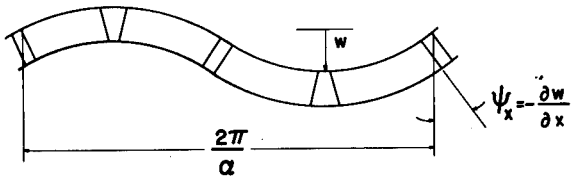


FIGURE 12.31.—Mode shape for a SS–SS–SS–SS rectangular plate, derived from classical theory. (After ref. 12.36)

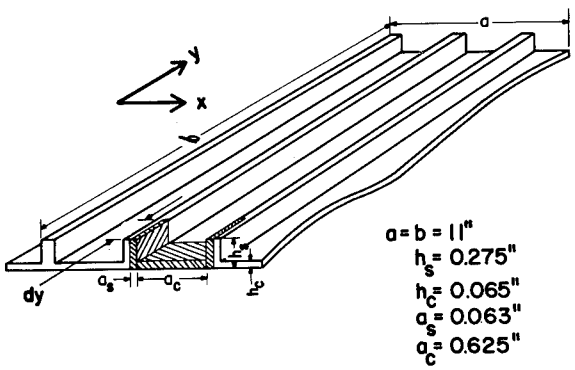


FIGURE 12.32.—Dimensions of stiffened plate. (After ref. 12.67)

shown in figure 12.32. A comparison of theoretical and experimental results for this plate is given in table 12.6.

The problem of the SS–F–SS–F rectangular plate was also analyzed in reference 12.36. The boundary conditions are:

$$\left.\begin{aligned} M_x=M_{xy}=Q_x=0 \quad & (\text{on } \bar{x}=\pm a/2)\\ w=M_y=\psi_x=0 \quad & (\text{on } \bar{y}=\pm b/2)\end{aligned}\right\} \tag{12.96}$$

It should be noted that here the simply supported edges are along $y=\pm b/2$; this is unlike the previous convention used in section 4.2.5. Solution functions in the form of equations (12.86), which exactly satisfy the simply supported edge conditions, were again used. It is most interesting to note that the free edge conditions are also satisfied *exactly* (unlike in the classical theory) by this simple solution set upon substituting equations (12.86) into the first three of equations (12.96). This yields a characteristic determinant of the third order which is solved for the frequencies. Thus the modes w_1, w_2, and H do not remain uncoupled

TABLE 12.6.—*Theoretical and Experimental Cyclic Frequencies for a SS-SS-SS-SS Stiffened Rectangular Plate*

Mode no. n	Derivation	Cyclic frequency, cps, for values of mode no. m of—				
		1	2	3	4	5
1	Experimental	244	340	538	800	1152
	Rotary inertia neglected	238	336	534	831	1220
	Rotary inertia included	237	332	520	793	1135
2	Experimental	794	940	1020	1268	1580
	Rotary inertia neglected	880	954	1100	1344	1689
	Rotary inertia included	877	941	1070	1282	1570
3	Experimental	1700	1800	1840	2110	2340
	Rotary inertia neglected	1950	2020	2150	2349	2638
	Rotary inertia included	1940	1983	2090	2238	2451

as in the SS–SS–SS–SS case discussed previously in this section.

The ratio of plate frequency to thickness-shear frequency is plotted in figure 12.33 for the particular ratio $s_3h/b=0.2$ (as in fig. 12.29). The broken and solid curves are for modes odd and even, respectively, in x.

12.3.3 Other Shapes

Callahan (refs. 12.64 and 12.68) treated the problem of the elliptic plate, including the effects of shear deformation and rotary inertia. Mindlin's equations were transformed into elliptic coordinates, and series solutions to the differential equations were found in terms of

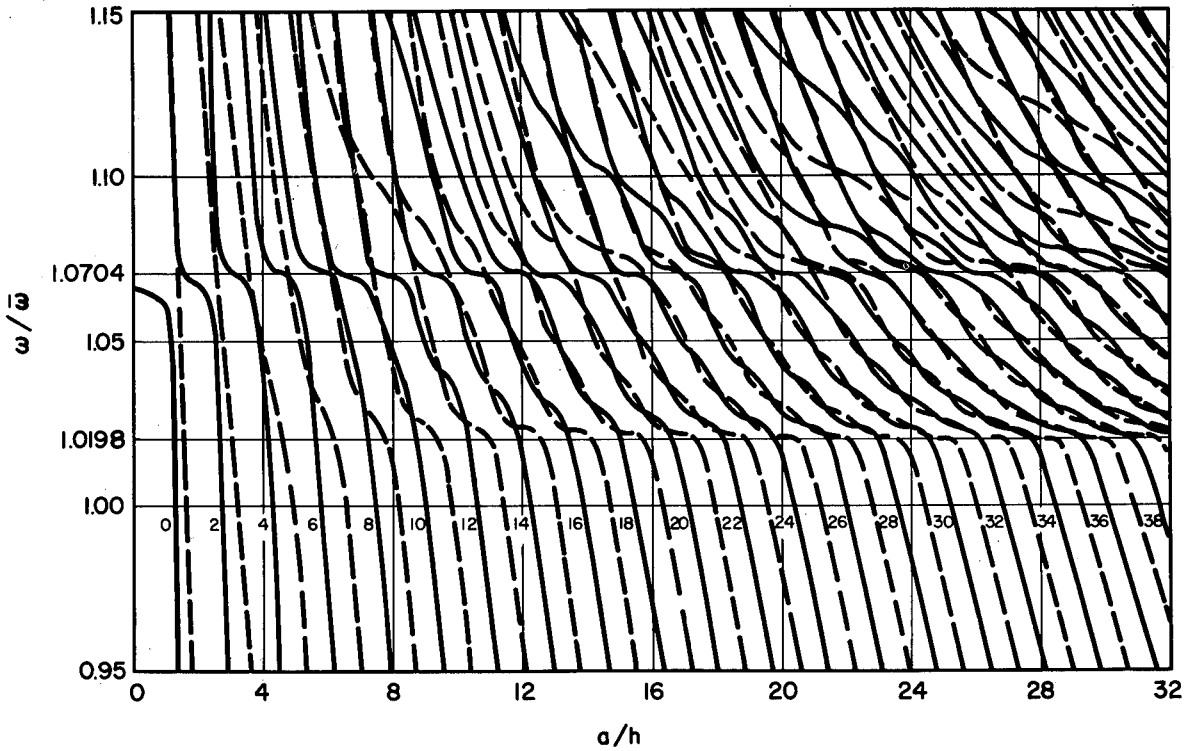


FIGURE 12.33.—Ratio of plate frequency to thickness-shear frequency for a SS–F–SS–F rectangular plate when the distance between nodes along the direction parallel to the free edges is five time the thickness; $\nu=0.312$. (After ref. 12.36)

Mathieu functions. The boundary conditions are satisfied by finding the roots of an infinite determinant, each element of the determinant being an infinite series of Mathieu functions containing the frequency within their arguments. In reference 12.68 the infinite characteristic determinants are displayed for eight types of boundary conditions, but no numerical results are given.

12.4 EFFECTS OF NONHOMOGENEITY

A brief survey of the literature dealing with the vibration of nonhomogeneous plates will now be given. Nonhomogeneity may arise in many ways. Overall material properties themselves may vary in a continuous manner (e.g., a continuum representation of a fibrous composite plate). Inclusions or holes may occur within the plate. As can be seen from earlier chapters, the effect of a "classical" (i.e., cylindrical) hole, even if small, can cause a significant effect upon the vibration frequencies of a plate.

Some practical and commonly used types of nonhomogeneous plates are sandwich plates having a honeycomb, corrugated, or Styrofoam core. These plates consist of a core material bonded between two face sheets. Because of the relative geometric complexity of these structures, the theoretical analysis of their vibrational behavior almost always assumes that the core material can be represented as a homogeneous, elastic continuum and, consequently, the overall structure can be treated as a layered plate. Indeed, if this representation were not made, the plate would have to be analyzed as a structure and, hence, would fall beyond the scope of this work. Even with these assumptions, the complexity of the results and the number of parameters required to describe the sandwich make it impractical to report detailed numerical results in this section.

In the most simple case, a layered plate is made up of several layers bonded together, each layer being homogeneous and isotropic, and the Kirchhoff hypothesis of normals to the middle surface remaining straight and normal is assumed valid. In this case the mathematical complication of the plate theory is minimal. The necessary modifications of the theory are discussed in the section of the appendix entitled "Force and Moment Integrals" (sec. A.5). This is the type of nonhomogeneity discussed in reference 12.69.

Bolotin (ref. 12.70) generalized the model for the layered plate by assuming that the plate is composed of both "hard" and "soft" layers. The hard layers obey the Kirchhoff hypothesis while slippage occurs in the soft layers. In the soft layers the inplane stresses σ_x, σ_y, and τ_{xy} are assumed to be zero, while the transverse shear stresses τ_{yz} and τ_{zx} are constant within the layer. On the basis of these assumptions, a complete plate theory is developed in reference 12.70. Another formulation, based upon the three-dimensional equations of elasticity, is given in reference 12.71.

The theoretical work of Yu on layered plates (refs. 12.72 through 12.83) is particularly significant. This effort is primarily devoted to the incorporation of shear deformation and rotary inertia effects into the layered-plate theory. It is shown that these effects, particularly shear deformation, are especially important when one deals with conventional sandwich plates composed of a relatively soft-core material contained between two relatively rigid, thin face sheets. The statement is made (ref. 12.79) that shear-deformation effects can become important for a sandwich plate at a flexural frequency which may be only 1 percent of that of the corresponding solid, homogeneous plate. It is shown furthermore that, for ordinary sandwich plates, the shear effect on the faces, the rotary inertia of the faces about their own midplanes, and the flexural rigidity of the core are negligible; of importance are the shear effect in the core, the rotary and translatory inertias of the core, the translatory inertia of the faces (including the rotary effect of the faces about the midplane of the sandwich plate), and the flexural and extensional rigidities of the faces (ref. 12.75).

A one-dimensional theory was developed in references 12.72 to 12.76, which is applicable to the vibration of plates in modes of plane strain. The transverse displacement w, as in the Mindlin theory, was assumed to be constant through the plate thickness. The dis-

placements in the plane of the plate are assumed to vary linearly through the thickness, with the slope in the face sheets not necessarily the same as the variation in the core.

The theory is generalized to a two-dimensional variation in w in references 12.77 and 12.78 and is applied to the problem of a rectangular plate simply supported on all edges. In references 12.78 and 12.83, sets of formulas are presented for the calculation of natural frequencies of the simply supported rectangular plate. Those formulas will not be reproduced here because of their inherent complexity (arising from the relatively complicated geometry and material properties of the sandwich plate) and the amount of explanation which would be required.

The theory is extended to the nonlinear (large-deformation) domain in references 12.80 to 12.82. It is shown that the basic behavior is the same as that for homogeneous plates; that is, the membrane stiffening due to large deformations causes the overall stiffness of the system to be like a "hard" spring, thus causing an increase in frequency with increase in amplitude. (See section 12.2 of this work for background information.) In particular, the nonlinear theory is applied to a rectangular plate having immovable, hinged edges.

Further theoretical derivations of equations for the vibrational behavior of layered plates are made in references 12.84 to 12.86. In both references 12.84 and 12.85 the analyses are generalized to include orthotropic core materials, and explicit frequency equations are developed for the case of a plate simply supported on all edges.

Experimental results for sandwich plates having honeycomb and Styrofoam cores are given in reference 12.87. Experiments were conducted in a vacuum and data were compared with analytical frequencies obtained from a finite-difference solution of the classical plate equations. It was found that the classical theory is adequate for obtaining frequencies and mode shapes, except in cases of extremely low core stiffness.

Circular sandwich plates with linearly varying thickness were examined in reference 12.88. Experimental frequencies were compared with theoretical values obtained by a simple analysis by using the Rayleigh method.

In reference 12.89 radial nonhomogeneity in circular plates is accommodated by treating the plate as a composite of homogeneous, isotropic annuli and enforcing continuity conditions across the internal junctions.

The plate consisting of a thin face sheet stiffened by corrugated sheet (see fig. 12.34) is analyzed in reference 12.90. It is shown that this configuration *cannot* be treated as orthotropic plate because the twisting-moment relation $M_{xy}=M_{yx}$ is no longer applicable. A theory for this case is derived.

In reference 12.91 an *inflatable* plate is analyzed. This plate consists of two woven cover membranes joined to each other by closely spaced perpendicular filaments. The space between the covers is pressurized, and the filaments hold the cover membranes together (see fig. 12.35). A variable-thickness plate is obtained by using variable-length connecting filaments. The theory developed in reference 12.91 was applied in reference 12.92 to obtain natural frequencies of square plates having simply supported edges. Results were compared with experimental ones.

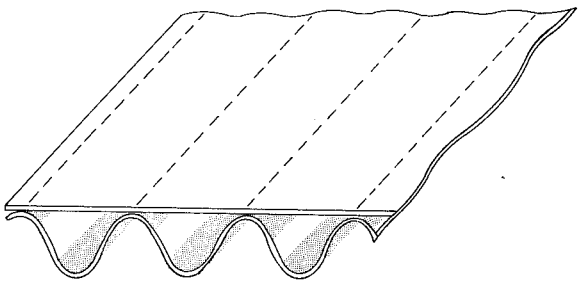


FIGURE 12.34.—A corrugation-stiffened plate.

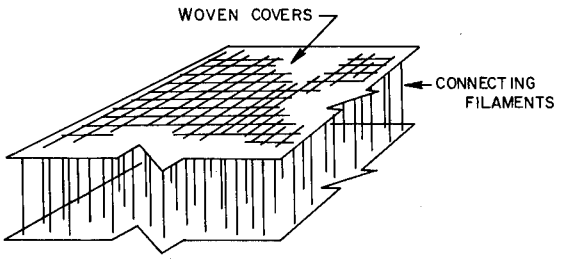


FIGURE 12.35.—Typical inflatable plate construction.

REFERENCES

12.1. LAMB, H.: On the Vibrations of an Elastic Plate in Contact With Water. Proc. Roy. Soc. (London), ser. A, vol. 98, 1920, pp. 205–216.

12.2. POWELL, J. H.; AND ROBERTS, J. H. T.: On the Frequency of Vibration of Circular Diaphragms. Proc. Phys. Soc. (London), vol. 35, 1923, pp. 170–182.

12.3. MCLACHLAN, N. W.: The Accession to Inertia of Flexible Discs Vibrating in a Fluid. Proc. Phys. Soc. (London), vol. 44, 1932, p. 546.

12.4. PEAKE, W. H.; AND THURSTON, E. G.: The Lowest Resonant Frequency of a Water-Loaded Circular Plate. J. Acoust. Soc. Am., vol. 26, no. 2, Mar. 1954, pp. 166–168.

12.5. BYCROFT, G. N.: Frequencies of a Flexible Circular Plate Attached to the Surface of a Light Elastic Half-Space. J. Appl. Mech., vol. 26, no. 1, Mar. 1959, pp. 13–17.

12.6. LOVE, A. E. H.: Mathematical Theory of Elasticity. Fourth ed., Dover Press (New York, N.Y.), 1944, p. 288.

12.7. LINDHOLM, U. S.; KANA, D. D.; CHU, W.; AND ABRAMSON, H. N.: Elastic Vibration Characteristics of Cantilever Plates in Water. J. Ship Res., vol. 9, no. 1, June 1965, pp. 11–22.

12.8. GREENSPON, J. E.: Vibrations of Cross-Stiffened and Sandwich Plates With Application to Underwater Sound Radiators. J. Acoust. Soc. Am., vol. 33, no. 11, Nov. 1961, pp. 1485–1497.

12.9. GREENSPON, J. E.: An Approximate Method for Obtaining the Frequencies, Deflections and Stresses in Sandwich and Cross Stiffened Rectangular Plates. Tech. Rept. No. 1 (Nonr-3123(00)X), J.G. Eng. Res. Assoc., Dec. 1960.

12.10. FELGAR, R. P.: Formulas for Integrals Containing Characteristic Functions of a Vibrating Beam. Circ. No. 14, Univ. Texas, 1950.

12.11. VON KÁRMÁN, TH.: Festigkeitsprobleme in Maschinenbau. Encyklopadie der Mathematischen Wissenschaften. Bd. 4, Heft 4, 1910, pp. 311–385.

12.12. HERRMANN, G.: Influence of Large Amplitudes on Flexural Motions of Elastic Plates. NACA TN D-3578, 1965.

12.13. WAH, T.: Vibration of Circular Plates at Large Amplitudes. J. Eng. Mech. Div., Proc. Am. Soc. Civil Eng., EM 5, Oct. 1963, pp. 1–15.

12.14. BERGER, H. M.: A New Approach to the Analyses of Large Deflection of Plates. J. Appl. Mech., vol. 22, no. 4, Dec. 1955, p. 465.

12.15. YAMAKI, N.: Influence of Large Amplitudes on Flexural Vibrations of Elastic Plates. ZAMM, vol. 41, 1961, pp. 501–510.

12.16. SRINIVASAN, A. V.: Large Amplitude Free Oscillations of Beams and Plates. AIAA J., vol. 3, no. 10, Oct. 1965, pp. 1951–1953.

12.17. MASSA, N. E.: Sulle Vibrazioni Libere con Inflessione non Piccola di Piastre Circolari Sottoposte a Stati Piani di Coazione. Instituto Lombardo (Rend Sci.), vol. A–97, 1963, pp. 346–358.

12.18. CHU, H.; AND HERRMANN, G.: Influence of Large Amplitudes on Free Flexural Vibrations of Rectangular Elastic Plates. J. Appl. Mech., vol. 23, no. 4, Dec. 1956, pp. 532–540.

12.19. NASH, W. A.; AND MODEER, J. R.: Certain Approximate Analyses of the Nonlinear Behavior of Plates and Shallow Shells. Proc. Symp. on Theory of Thin Elastic Shells (Delft, Aug. 1959), Interscience Pub., Inc. (New York, N.Y.), 1960.

12.20. WAH, T.: Large Amplitude Flexural Vibration of Rectangular Plates. Int. J. Mech. Sci., vol. 5, 1963, pp. 425–438.

12.21. WAH, T.: The Normal Modes of Vibration of Certain Nonlinear Continuous Systems. J. Appl. Mech., ser. E, vol. 31, no 2, Mar. 1964, pp. 139–140.

12.22. EISLEY, J. G.: Nonlinear Vibration of Beams and Rectangular Plates. ZAMP, vol. 15, no. 2, 1964, pp. 167–175.

12.23. EISLEY, J. G.: Large Amplitude Vibration of Buckled Beams and Rectangular Plates. AIAA J., Tech. Notes, vol. 2, no. 12, Dec. 1964, pp. 2207–2209.

12.24. RAYLEIGH, LORD: Theory of Sound, Vol. I and Vol. II. Dover Pub., 1945. (Originally published in 1877.)

12.25. TIMOSHENKO, S.: On the Correction for Shear of the Differential Equations for Transverse Vibrations of Prismatic Bars. Phil. Mag., ser. 6, vol. 41, 1921, p. 742.

12.26. REISSNER, E.: The Effect of Transverse Shear Deformation on the Bending of Elastic Plates. J. Appl. Mech., vol. 12, 1945, p. A–69.

12.27. UFLYAND, Y. S.: The Propagation of Waves in the Transverse Vibrations of Bars and Plates. Akad. Nauk SSSR, Prikl. Mat. Mech., vol. 12, 1948, pp. 287–300. (In Russian.)

12.28. MINDLIN, R. D.: Influence of Rotatory Inertia and Shear on Flexural Motions of Isotropic, Elastic Plates. J. Appl. Mech., vol. 18, no. 1, Mar. 1951, pp. 31–38.

12.29. MINDLIN, R. D.: Thickness-Shear and Flexural Vibrations of Crystal Plates. J. Appl. Phys., vol. 22, no. 3, Mar. 1951, pp. 316–323.

12.30. MINDLIN, R. D.: Forced Thickness-Shear and Flexural Vibrations of Piezoelectric Crystal Plates. J. Appl. Phys., vol. 23, no. 1, Jan. 1952, pp. 83–88.

12.31. MINDLIN, R. D.; AND DERESIEWICZ, H.: Thickness-Shear Vibrations of Piezoelectric Crystal Plates With Incomplete Electrodes. J. Appl. Phys., vol. 25, no. 1, Jan. 1954, pp. 21–24.

12.32. MINDLIN, R. D.; AND DERESIEWICZ, H.: Suppression of Overtones of Thickness-Shear and Flexural Vibrations of Crystal Plates. J. Appl. Phys., vol. 25, no. 1, Jan. 1954, pp. 25–27.

12.33. MINDLIN, R. D.; AND DERESIEWICZ, H.: Thickness-Shear and Flexural Vibrations of a Circular Disk. J. Appl. Phys., vol. 25, no. 10, Oct. 1954, pp. 1329–1332.

12.34. DERESIEWICZ, H.; AND MINDLIN, R. D.: Axially Symmetric Flexural Vibrations of a Circular Disk. J. Appl. Mech., vol. 22, no. 1, Mar. 1955, pp. 86–88.

12.35. DERESIEWICZ, H.: Symmetric Flexural Vibrations of a Clamped Circular Disk. J. Appl. Mech., vol. 23, no. 2, June 1956, p. 319.

12.36. MINDLIN, R. D.; SCHACKNOW, A.; AND DERESIEWICZ, H.: Flexural Vibrations of Rectangular Plates. J. Appl. Mech., vol. 23, no. 3, Sept. 1956, pp. 430–436.

12.37. MINDLIN, R. D.; AND DERESIEWICZ, H.: Thickness-Shear and Flexural Vibrations of Rectangular Crystal Plates. J. Appl. Phys., vol. 26, no. 12, Dec. 1955, pp. 1435–1442.

12.38. DERESIEWICZ, H.; AND MINDLIN, R. D.: Waves on the Surface of a Crystal. J. Appl. Physics, vol. 28, no. 6, June 1957, pp. 669–671.

12.39. NEWMAN, E. G.; AND MINDLIN, R. D.: Vibrations of a Monoclinic Crystal Plate. J. Acoust. Soc. Am., vol. 29, no. 11, Nov. 1957, pp. 1206–1218.

12.40. MINDLIN, R. D.: High Frequency Vibrations of Crystal Plates. Quart. Appl. Math., vol. 19, 1961, pp. 51–61.

12.41. MINDLIN, R. D.; AND GAZIS, D. C.: Strong Resonances of Rectangular AT-Cut Quartz Plates. Tech. Rept. 42, Dept. Civil Eng. and Eng. Mech., Columbia Univ., July 1961.

12.42. TIERSTEN, H. F.; AND MINDLIN, R. D.: Forced Vibrations of Piezoelectric Crystal Plates. Quart. Appl. Math., vol. 20, no. 2, July 1962, pp. 107–120.

12.43. KAUL, R. K.; AND MINDLIN, R. D.: Vibrations of an Infinite, Monoclinic Crystal Plate at High Frequencies and Long Wavelengths. J. Acoust. Soc. Am., vol. 34, no. 12, Dec. 1962, pp. 1895–1901.

12.44. KAUL, R. K.; AND MINDLIN, R. D.: Frequency Spectrum of a Monoclinic Crystal Plate. J. Acoust. Soc. Am., vol. 34, no. 12, Dec. 1962, pp. 1902–1910.

12.45. MINDLIN, R. D.; AND GAZIS, D. C.: Strong Resonances of Rectangular AT-Cut Quartz Plates. Proc. 4th U.S. Natl. Congr. Appl. Mech., 1962, pp. 305–310.

12.46. MINDLIN, R. D.; AND LEE, P. C. Y.: Thickness-Shear and Flexural Vibrations of Partially Plated Crystal Plate. Tech. Rept. 3, Dept. Civil Eng. and Eng. Mech., Columbia Univ., June 1965. Also, Int. J. Solids & Struct., vol. 2, 1966, pp. 125–139.

12.47. TASI, J.; AND HERRMANN, G.: Thermoelastic Dissipation in High-Frequency Vibration in Crystal Plates. J. Acoust. Soc. Am., vol. 36, no. 1, Jan. 1964, pp. 100–110.

12.48. HERRMANN, G.; AND ARMENAKAS, A.: Vibrations and Stability of Plates Under Initial Stress. Paper no. 2500, J. Eng. Mech. Div., Proc. Am. Soc. Civil Eng., EM 3, vol. 86, June 1960, pp. 65–94. (Available from CFSTI as AD 211 220.)

12.49. HENCKY, H.: Über die Berücksichtigung der Schubverzerrung in ebenen Platten. Ingr.-Arch., Bd. 16, 1947, pp. 72–76.

12.50. WALLISCH, W.: Einfluss der Schubverzerrung auf die Eigenschwingungen von Platten. ZAMM, Bd. 36, Heft 7/8, July 1956, pp. 291–293.

12.51. DUBINKIN, M. V.: Vibration of Plates, Taking Rotary Inertia and Shear Into Account. Izv. Akad. Nauk SSSR, Otd. Tekh. Nauk, no. 12, Dec. 1958, pp. 131–135. (In Russian.)

12.52. RYBAK, S. A.; AND TARTAKOVSKII, B. D.: On the Vibrations of Thin Plates. Soviet Phys.-Acoust., vol. 9, no. 1, July 1963, pp. 51–55.

12.53. PETRASHEN, G. I.: Dynamical Aspects of the Theory of Elasticity. Uch. zap. LGU, 1951, p. 149. (In Russian.)

12.54. PETRASHEN, G. I.; AND MOLOTKOV, L. A.: Selected Problems in the Dynamical Theory of Elasticity. Vestn. LGU, ser. fiz., 1958, p. 22. (In Russian.)

12.55. KACZKOWSKI, Z.: The Influence of Shear and Rotary Inertia on the Frequencies of an Anisotropic Vibrating Plate. Bull. Acad. Pol. Sci., vol. 8, no. 7, 1960, pp. 343–349. (In German.)

12.56. TOMAR, J. S.: Flexural Vibrations of Isotropic Elastic Plates. Proc. Nat. Inst. Sci. India, vol. 28, no. 6, 1962, pp. 872–880.

12.57. BUCHWALD, V. T.: Low Frequency Flexural Vibrations in Elastic Plates. Quart. J. Mech. and Appl. Math., vol. 12, pt. 4, 1959, pp. 454–463.

12.58. VOLTERRA, E.: Method of Internal Constraints and Its Application. J. Eng. Mech. Div., Proc. Am. Soc. Civil Eng., EM 4, Aug. 1961, pp. 103–127.

12.59. VOLTERRA, E.: Influenza del Taglio nella Dinamica e nella Statica delle Piastre Sottili. Accad. Naz. Lincei, pt. I, ser. 8, vol. 28, June 1960, pp. 1–8; pt. II, ser. 8, vol. 29, Aug. 1960, pp. 1–5.

12.60. VOLTERRA, E.: Propagación de Ondas en Sólidos Elásticos. Ingeniería, 1965, pp. 125–143.

12.61. NARSIMHAMURTHY, P.: The Effect of Transverse Shear Deformation and Rotatory Inertia in Wave Propagation and Vibration of Thin Elastic Plates. Proc. Indian Soc. Theor. and Appl. Mech., 3 D, 1957, pp. 351–360.

12.62. Reissner, E.: On Axi-Symmetrical Vibrations of Circular Plates of Uniform Thickness; Including the Effects of Transverse Shear Deformation and Rotary Inertia. J. Acoust. Soc. Am., vol. 26, no. 2, Mar. 1954, pp. 252–253.

12.63. Tomar, J. S.: On Flexural Vibrations of Isotropic Elastic Thin Circular Plates According to Mindlin's Theory. Proc. Nat. Inst. Sci. India, vol. 29, no. 5, 1963, pp. 552–560.

12.64. Callahan, W. R.: On the Flexural Vibrations of Circular and Elliptical Plates. Quart. Appl. Math., vol. 13, no. 4, Jan. 1956, pp. 371–380.

12.65. Tomar, J. S.: On Flexural Vibrations of Isotropic Elastic Thin Square Plates According to Mindlin's Theory. Proc. Nat. Inst. Sci. India, vol. 29, no. 2, 1963, pp. 169–179.

12.66. Tomar, J. S.: On Flexural Vibrations of Isotropic Elastic Thin Square Plates. Bull. Calcutta Math. Soc., vol. 55, no. 1, 1963, pp. 1–10.

12.67. Thorkildsen, R. L., and Hoppmann, W. H.: Effect of Rotatory Inertia on the Frequencies of Vibration of Stiffened Plates. J. Appl. Mech., vol. 26, no. 2, June 1959, pp. 298–300.

12.68. Callahan, W. R.: Flexural Vibrations of Elliptical Plates When Transverse Shear and Rotary Inertia Are Considered. J. Acoust. Soc. Am., vol. 36, no. 5, May 1964, pp. 823–829.

12.69. Pister, K. S.: Flexural Vibration of Thin Laminated Plates. J. Acoust. Soc. Am., vol. 31, no. 2, Feb. 1959, pp. 233–234.

12.70. Bolotin, V. V.: Vibration of Layered Elastic Plates. Proc. Vibration Probl., vol. 4, no. 4, 1963, pp. 331–346.

12.71. Moskalenko, V. N.: Free Vibrations of a Three-Layered Plate. Izv. Akad. Nauk SSSR, Otd. Tekh. Nauk, Mekh. i Mashin., no. 4, July 1962, pp. 125–129. (In Russian.)

12.72. Yu, Y. Y.: A New Theory of Sandwich Plates: One Dimensional Case. J. Appl. Mech., vol. 26, 1959, pp. 415–421.

12.73. Yu, Y. Y.: Simple Thickness-Shear Modes of Vibration in Infinite Sandwich Plates. AFOSR TN 58-897 (CFSTI No. AD 204 132), Dept. Mech. Eng., Poly. Inst. Brooklyn, Oct. 1958. Also, J. Appl. Mech., vol. 26, Dec. 1959, pp. 679–680.

12.74. Yu, Y. Y.: Flexural Vibrations of Elastic Sandwich Plates. J. Aeron. Sci., Apr. 1960, pp. 273–282, 290 (CFSTI No. AD 211 219).

12.75. Yu, Y. Y.: Forced Flexural Vibrations of Sandwich Plates in Plane Strain. AFOSR TN 59–567, Dept. Mech. Eng., Poly. Inst. Brooklyn, July 1959. Also, J. Appl. Mech., vol. 27, no. 3, Sept. 1960, pp. 535–540.

12.76. Yu, Y. Y.: Simplified Vibration Analysis of Elastic Sandwich Plates. AFOSR TN 59–1082 (CFSTI No. AD 234 221), Dept. Mech. Eng., Poly. Inst. Brooklyn, Aug. 1959. Also, J. Aeron. Sci., Dec. 1960, pp. 894–900.

12.77. Yu, Y. Y.: A New Theory of Sandwich Plates: General Case. Tech. Note No. 6 (CFSTI No. AD 234 222), Dept. Mech. Eng., Poly. Inst. Brooklyn, Nov. 1959.

12.78. Yu, Y. Y.: Flexural Vibrations of Rectangular Sandwich Plates. Tech. Note No. 8 (CFSTI No. AD 248 073), Dept. Mech. Eng., Poly. Inst. Brooklyn, Aug. 1960.

12.79. Yu, Y. Y.: Extensional Vibrations of Elastic Sandwich Plates. Tech. Note No. 9 (CFSTI No. AD 248 301), Dept. Mech. Eng., Poly. Inst. Brooklyn, Oct. 1960. Also, Proc. 4th U.S. Nat. Congr. Appl. Mech., 1962, vol. 1, pp. 441–448.

12.80. Yu, Y. Y.: Nonlinear Flexural Vibrations of Sandwich Plates. Tech. Note No. 12 (CFSTI No. AFOSR 1310), Dept. Mech. Eng., Poly. Inst. Brooklyn, Feb. 1962. Also, Acoust. Soc. Amer., vol. 34, 1962, pp. 1176–1183.

12.81. Yu, Y. Y.: Effect of Thickness Deformations on Vibrations of Sandwich Plates. Tech. Note No. 13 (CFSTI No. AD 279 509), Dept. Mech. Eng., Poly. Inst. Brooklyn, Feb. 1962.

12.82. Yu, Y. Y.: Application of Variational Equation of Motion to the Nonlinear Vibrational Analysis of Homogeneous and Layered Plates and Shells. Tech. Note No. 14 (CFSTI No. AD 289 868), Dept. Mech. Eng., Poly. Inst. Brooklyn, Feb. 1962. Also, J. Appl. Mech. vol. 30, 1963, pp. 79–86.

12.83. Yu, Y. Y.: Damping of Flexural Vibrations of Sandwich Plates. J. Aeron. Sci., July 1962, pp. 790–803.

12.84. Chang, C. C.; and Fang, B. T.: Transient and Periodic Response of a Loaded Sandwich Panel. J. Aeron. Sci., May 1961, pp. 382–396.

12.85. Bieniek, M. P.; and Freudenthal, A. M.: Frequency-Response Functions of Orthotropic Sandwich Plates. J. Aeron. Sci., Sept. 1961, pp. 732–735, 752.

12.86. Mead, D. J.; and Pretlove, A. J.: On the Vibrations of Cylindrically Curved Elastic Sandwich Plates: Part I, The Solution for Flat Plates, and Part II, The Solution for Cylindrical Plates. R. & M. No. 3363, British A.R.C., 1964.

12.87. Powell, C. A., Jr.; and Stephens, D. G.: Vibration of Sandwich Panels in a Vacuum. Thirty-fifth Shock and Vibration Symp. (New Orleans, La.), Oct. 25–28, 1965.

12.88. Thompson, W. M., Jr.; and Clary, R. R.: An Investigation of the Natural Frequencies and Mode Shapes of Double Conical Sandwich Disks. NASA TN D-1940, 1963.

12.89. VODIČKA, V.: Free Vibrations of a Composite Circular Plate. Acta Phys. Austriaca, vol. 17, no. 4, Apr. 1964, pp. 319–332. (In English.)

12.90. FUNG, Y. C.: On Corrugation-Stiffened Panels. GALCIT SM 62–33 (CFSTI No. AD 429 770), Calif. Inst. Tech., June 1962.

12.91. MCCOMB, H. G., JR.: A Linear Theory for Inflatable Plates of Arbitrary Shape. NASA TN D–930, 1961.

12.92. STROUD, W. J:. Experimental and Theoretical Deflections and Natural Frequencies of an Inflatable Fabric Plate. NASA TN D–931, 1961.

308–337 O—70——22

APPENDIX

Plate Equations

The purpose of this appendix is to present the notation, conventions, assumptions, and fundamental equations upon which the main part of this work is based. The effects of

(1) Anisotropy
(2) Inplane forces
(3) Variable thickness

will be explicitly included. Where other complicating effects (e.g., large deflections) enter the formulation, they will be pointed out. Basic derivations are, for the sake of simplicity, carried out in rectangular coordinates.

A.1 NOTATION

A notation will be developed which is consistent with that of elasticity theory; that is, at a point the directions of positive stress will be taken as shown on the element of figure A.1. Positive normal stresses are tensile. Positive shear stresses are directed in the positive x-, y-, and z-directions if they lie on "positive faces" of the element; that is, those faces of the three parallel sets whose x-, y-, and z-coordinates are the largest. The three well-known (ref. A.1) moment equilibrium equations $\tau_{xy}=\tau_{yx}$, $\tau_{yz}=\tau_{zy}$, and $\tau_{zx}=\tau_{xz}$ (neglecting couple stresses) have already been introduced in figure A.1.

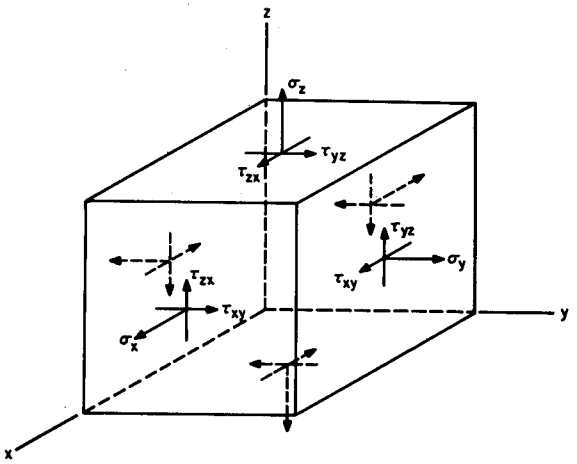


FIGURE A.1.—Notation and positive directions of stress.

Figure A.2 shows a plate element of thickness h and incremental dimensions dx and dy. The x- and y-axes are chosen to contain the *undeformed* middle surface of the plate. This plane is called the "neutral plane." More will be said later about its location when layered plates are discussed. For a plate homogeneous through its thickness, the neutral plane lies midway through its thickness. The z-axis is normal to the undeformed middle surface. The z-axis is shown, for convenience only, as acting along one edge of the element. Thus, it is noted that the xyz coordinate system is *space fixed*. The transverse shearing force intensities Q_x and Q_y, the inplane normal and shearing force intensities N_x, N_y, and N_{xy} and their incremental changes are shown acting on the sides of the element, with positive forces acting in positive directions on positive faces. These quantities have dimensions of force per unit length. As will be seen later, these forces arise from the integrals of the *even* components of positive normal and shearing stresses. The shearing forces N_{xy} are identical on the faces $x=0$ and $y=0$ because the shear stresses causing them are equal. Also shown is the transverse external force $q=q(x, y)$ which has the dimension of force per unit area and arises from, for example, a gravitational field or an external pressure. It will be understood that, as the plate deforms, all the forces shown in figure A.2 will be measured in directions tangent to or normal to (as the case may be) the *deformed* middle surface of the plate.

Figure A.3 shows the same element with bending moment intensities M_x and M_y, twisting moment intensities M_{xy}, and their incremental changes; all these are indicated as

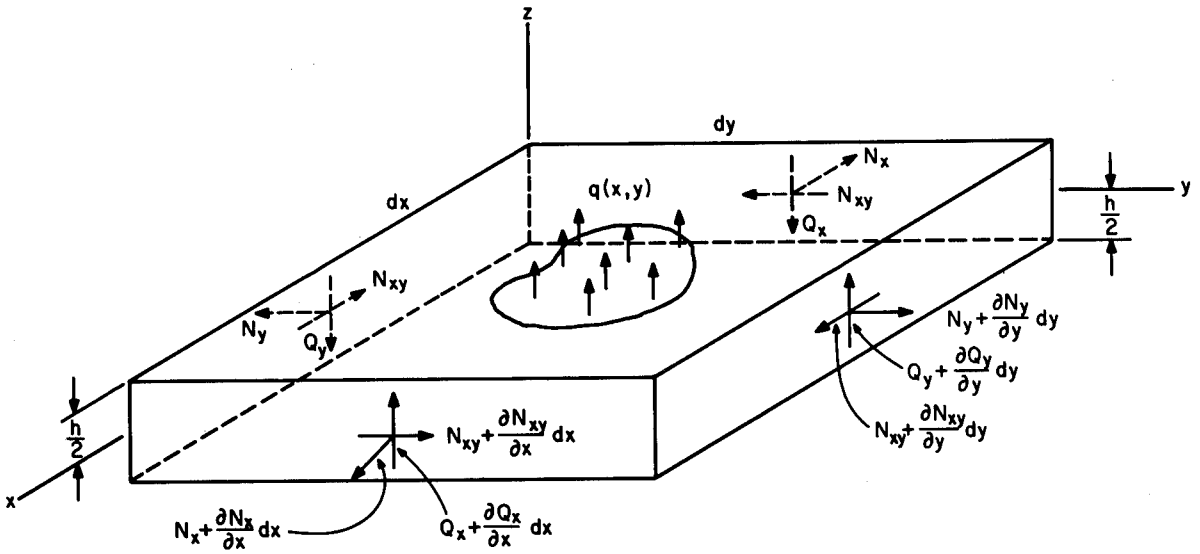


FIGURE A.2.—Forces (intensities) acting on a plate element.

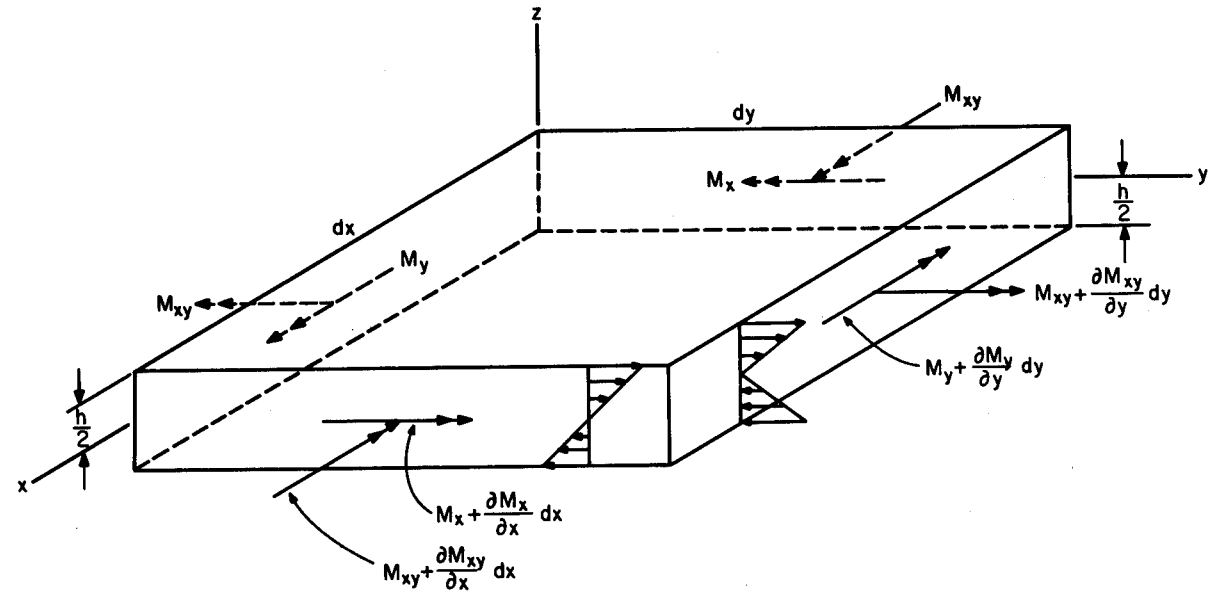


FIGURE A.3.—Moments (intensities) acting on a plate element.

right-hand vectors in the figure. These quantities have dimensions of moment per unit length. As it will be seen later, these moments arise from the integrals of the *odd* components of positive normal and shearing stresses. These stress variations are depicted typically on two faces of the element. The twisting moments M_{xy} are identical on the faces $x=0$ and $y=0$ because the shear stresses causing them are identical.

The middle surface of the element after deformation is shown in figure A.4. The origin of the space-fixed coordinate system is taken at one corner of the element for convenience only. The displacement in the z-direction is taken as w. Slopes, along with their incre-

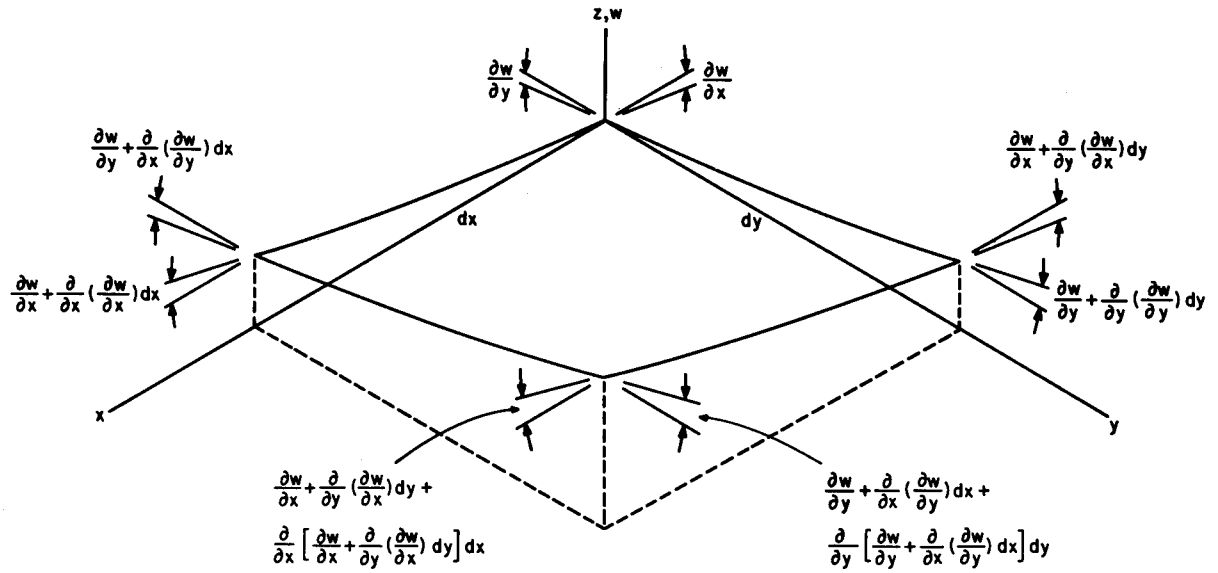


FIGURE A.4.—Deformed middle surface of a plate element showing slopes and their changes.

mental changes, are shown at all corners of the element, with positive changes assumed in positive directions. For small displacements it will be assumed later that the slope (tangent of the angle) and the sine of the angle are equivalent.

A.2 EQUILIBRIUM EQUATIONS

Considering small deflections (or, more precisely, small slopes), summing forces in the z-direction yield the equation (refer to figs. A.2 and A.4)

$$\frac{\partial Q_x}{\partial x}dx\,dy+\frac{\partial Q_y}{\partial y}dy\,dx-N_x\,dy\frac{\partial w}{\partial x}$$
$$+\left(N_x+\frac{\partial N_x}{\partial x}dx\right)dy\left(\frac{\partial w}{\partial x}+\frac{\partial^2 w}{\partial x^2}dx\right)$$
$$-N_y\,dx\frac{\partial w}{\partial y}+\left(N_y+\frac{\partial N_y}{\partial y}dy\right)dx\left(\frac{\partial w}{\partial y}+\frac{\partial^2 w}{\partial y^2}dy\right)$$
$$-N_{xy}\,dx\frac{\partial w}{\partial x}+\left(N_{xy}+\frac{\partial N_{xy}}{\partial y}dy\right)$$
$$dx\left(\frac{\partial w}{\partial x}+\frac{\partial^2 w}{\partial x\,\partial y}dy\right)-N_{xy}\,dy\frac{\partial w}{\partial y}$$
$$+\left(N_{xy}+\frac{\partial N_{xy}}{\partial x}dx\right)dy\left(\frac{\partial w}{\partial y}+\frac{\partial^2 w}{\partial x\,\partial y}dx\right)$$
$$+q\,dx\,dy=\rho\,dx\,dy\frac{\partial^2 w}{\partial t^2} \quad \text{(A.1)}$$

where ρ is mass density per unit area and $\partial^2 w/\partial t^2$ is the acceleration in the z-direction. The technique of generalizing the above equation to account for large deformations (slopes) is self-evident. Expanding the terms involving products, discarding resulting third-order differential terms, dividing through the equation by the area $dx\,dy$, and simplifying yield:

$$\frac{\partial Q_x}{\partial x}+\frac{\partial Q_y}{\partial y}+\frac{\partial}{\partial x}\left(N_x\frac{\partial w}{\partial x}\right)+\frac{\partial}{\partial y}\left(N_y\frac{\partial w}{\partial y}\right)$$
$$+\frac{\partial}{\partial x}\left(N_{xy}\frac{\partial w}{\partial y}\right)+\frac{\partial}{\partial y}\left(N_{xy}\frac{\partial w}{\partial x}\right)+q=\rho\frac{\partial^2 w}{\partial t^2} \quad \text{(A.2)}$$

Equation (A.2) can be simplified by considering the well-known equilibrium equations of the three-dimensional theory of elasticity

$$\left.\begin{aligned}\frac{\partial \sigma_x}{\partial x}+\frac{\partial \tau_{xy}}{\partial y}+\frac{\partial \tau_{zx}}{\partial z}&=\rho^*\frac{\partial^2 u}{\partial t^2}\\ \frac{\partial \tau_{xy}}{\partial x}+\frac{\partial \sigma_y}{\partial y}+\frac{\partial \tau_{yz}}{\partial z}&=\rho^*\frac{\partial^2 v}{\partial t^2}\\ \frac{\partial \tau_{zx}}{\partial x}+\frac{\partial \tau_{yz}}{\partial y}+\frac{\partial \sigma_z}{\partial z}&=\rho^*\frac{\partial^2 w}{\partial t^2}\end{aligned}\right\} \quad \text{(A.3)}$$

where u, v, and w are displacements in the x-, y-, and z-directions, respectively, and ρ^* is mass density per unit volume. When the inplane inertia forces within the plate are neglected and the transverse shearing stresses τ_{yz} and τ_{zx} are small relative to the other stresses, the first two of equations (A.3) become:

$$\left.\begin{aligned}\frac{\partial \sigma_x}{\partial x}+\frac{\partial \tau_{xy}}{\partial y}=0\\ \frac{\partial \tau_{xy}}{\partial x}+\frac{\partial \sigma_y}{\partial y}=0\end{aligned}\right\} \tag{A.4}$$

Because these equations must be satisfied for every infinitesimal thickness (dz) of the plate element, their integrals over the thickness must also be satisfied. That is,

$$\left.\begin{aligned}\frac{\partial N_x}{\partial x}+\frac{\partial N_{xy}}{\partial y}=0\\ \frac{\partial N_{xy}}{\partial x}+\frac{\partial N_y}{\partial y}=0\end{aligned}\right\} \tag{A.5}$$

By use of equations (A.5), equation (A.2) now simplifies to

$$\frac{\partial Q_x}{\partial x}+\frac{\partial Q_y}{\partial y}+N_x\frac{\partial^2 w}{\partial x^2}+N_y\frac{\partial^2 w}{\partial y^2}+2N_{xy}\frac{\partial^2 w}{\partial x\,\partial y}+q=\rho\frac{\partial^2 w}{\partial t^2} \tag{A.6}$$

If one were to sum forces in the x- and y-directions, he would arrive at the following equations:

$$\left.\begin{aligned}\frac{\partial N_x}{\partial x}+\frac{\partial N_{xy}}{\partial y}-\frac{\partial}{\partial x}\left(Q_x\frac{\partial w}{\partial x}\right)-\frac{\partial}{\partial y}\left(Q_y\frac{\partial w}{\partial x}\right)=\rho\frac{\partial^2 u}{\partial t^2}\\ \frac{\partial N_{xy}}{\partial x}+\frac{\partial N_y}{\partial y}-\frac{\partial}{\partial x}\left(Q_x\frac{\partial w}{\partial y}\right)-\frac{\partial}{\partial y}\left(Q_y\frac{\partial w}{\partial y}\right)=\rho\frac{\partial^2 v}{\partial t^2}\end{aligned}\right\} \tag{A.7}$$

Inplane inertia forces will be considered to be small, as before. If the transverse shearing forces are small relative to the inplane forces, and the slopes are also considerably less than unity, then terms of the type $Q_x(\partial w/\partial x)$ can certainly be considered negligible compared with terms of the type N_x, for example. Equations (A.7) are thus seen to reduce to equations (A.5), which was obtained previously.

In summing moments about the space-fixed x- and y-axes, it is found that terms containing N_x, N_y, and N_{xy} yield differentials of higher order than the others and the equations simplify to

$$\left.\begin{aligned}Q_x-\frac{\partial M_x}{\partial x}-\frac{\partial M_{xy}}{\partial y}=\frac{\rho h^2}{12}\frac{\partial^3 w}{\partial x\,\partial t^2}\\ Q_y-\frac{\partial M_{xy}}{\partial x}-\frac{\partial M_y}{\partial y}=\frac{\rho h^2}{12}\frac{\partial^3 w}{\partial y\,\partial t^2}\end{aligned}\right\} \tag{A.8}$$

where the terms on the right-hand sides account for the rotary inertia of the plate element and are customarily considered small relative to the remaining terms in the equations.

The moment equation about the z-axis is identically satisfied.

A.3 KINEMATICS OF DEFORMATION

The assumption of elementary beam theory that "plane cross sections remain plane" is generalized to apply to a plate as follows:

Normals to the midplane of the undeformed plate remain straight and normal to the midplane during deformation.

An edge view of a portion of a plate is shown in figure A.5. The undeformed position of the plate is shown in solid lines, while the deformed shape is shown in broken lines. The longitudinal elastic displacement (due to inplane forces) of a point P on the midplane is depicted as u_0. Points such as 0 not falling on the midplane will also have, in general, displacement due to rotation of the normal. Thus, the longitudinal components of displacement of points within the plate will be characterized by

$$\left.\begin{aligned}u=u_0-z\frac{\partial w}{\partial x}\\ v=v_0-z\frac{\partial w}{\partial y}\end{aligned}\right\} \tag{A.9}$$

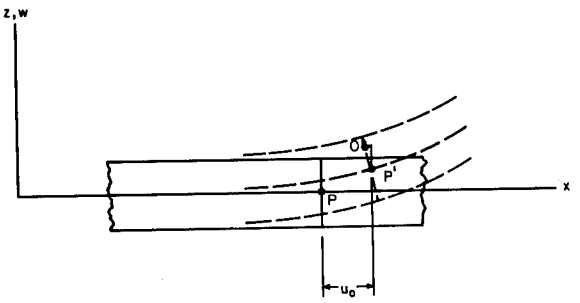


FIGURE A.5.—Kinematics of plate deformation.

where u and v are measured in the x-and y-directions, respectively.

The linearized strain-displacement equations (obtained by assuming strains much less than unity) for a continuum are well known:

$$\left.\begin{aligned}\epsilon_x&=\frac{\partial u}{\partial x}\\ \epsilon_y&=\frac{\partial v}{\partial y}\\ \gamma_{xy}&=\frac{\partial v}{\partial x}+\frac{\partial u}{\partial y}\end{aligned}\right\} \tag{A.10}$$

where γ_{xy} is engineering strain as differentiated from the tensorial strain required for tensorial manipulations. Substituting equations (A.9) into equations (A.10) gives

$$\left.\begin{aligned}\epsilon_x&=\frac{\partial u_0}{\partial x}-z\frac{\partial^2 w}{\partial x^2}\\ \epsilon_y&=\frac{\partial v_0}{\partial y}-z\frac{\partial^2 w}{\partial y^2}\\ \gamma_{xy}&=\left(\frac{\partial v_0}{\partial x}+\frac{\partial u_0}{\partial y}\right)-2z\frac{\partial^2 w}{\partial x\,\partial y}\end{aligned}\right\} \tag{A.11}$$

A.4 STRESS-STRAIN RELATIONSHIPS

For a general, anisotropic, elastic body the stress-strain relationships may be written in matrix form as:

$$\begin{bmatrix}\epsilon_x\\ \epsilon_y\\ \epsilon_z\\ \gamma_{xy}\\ \gamma_{yz}\\ \gamma_{zx}\end{bmatrix}=\begin{bmatrix}a_{11}&a_{12}&a_{13}&a_{14}&a_{15}&a_{16}\\ a_{12}&a_{22}&a_{23}&a_{24}&a_{25}&a_{26}\\ a_{13}&a_{23}&a_{33}&a_{34}&a_{35}&a_{36}\\ a_{14}&a_{24}&a_{34}&a_{44}&a_{45}&a_{46}\\ a_{15}&a_{25}&a_{35}&a_{45}&a_{55}&a_{56}\\ a_{16}&a_{26}&a_{36}&a_{46}&a_{56}&a_{66}\end{bmatrix}\begin{bmatrix}\sigma_x\\ \sigma_y\\ \sigma_z\\ \tau_{xy}\\ \tau_{yz}\\ \tau_{zx}\end{bmatrix} \tag{A.12}$$

where the coefficient matrix $[a_{ij}]$ can be proven to be symmetric as shown. Thermal strains will not be considered here, for it can be shown that they do not directly influence the free vibration problem. In the case of the plate the transverse stresses σ_z, τ_{yz}, and τ_{zx} are assumed to be small relative to the inplane stresses, and so equation (A.12) is reduced to

$$\begin{bmatrix}\epsilon_x\\ \epsilon_y\\ \gamma_{xy}\end{bmatrix}=\begin{bmatrix}a_{11}&a_{12}&a_{14}\\ a_{12}&a_{22}&a_{24}\\ a_{14}&a_{24}&a_{44}\end{bmatrix}\begin{bmatrix}\sigma_x\\ \sigma_y\\ \tau_{xy}\end{bmatrix} \tag{A.13}$$

Inverting equation (A.13) gives the stresses in terms of the strains

$$\begin{bmatrix}\sigma_x\\ \sigma_y\\ \tau_{xy}\end{bmatrix}=\begin{bmatrix}b_{11}&b_{12}&b_{14}\\ b_{12}&b_{22}&b_{24}\\ b_{14}&b_{24}&b_{44}\end{bmatrix}\begin{bmatrix}\epsilon_x\\ \epsilon_y\\ \gamma_{xy}\end{bmatrix} \tag{A.14}$$

where

$$\left.\begin{aligned}b_{11}&=\frac{1}{|a|}(a_{22}a_{44}-a_{24}^2)\\ b_{12}&=\frac{1}{|a|}(a_{14}a_{24}-a_{12}a_{44})\\ b_{14}&=\frac{1}{|a|}(a_{12}a_{24}-a_{14}a_{22})\\ b_{22}&=\frac{1}{|a|}(a_{44}a_{11}-a_{14}^2)\\ b_{24}&=\frac{1}{|a|}(a_{12}a_{14}-a_{24}a_{11})\\ b_{44}&=\frac{1}{|a|}(a_{11}a_{22}-a_{12}^2)\end{aligned}\right\} \tag{A.15}$$

and where $|a|$ is the determinant

$$|a|=\begin{vmatrix}a_{11}&a_{12}&a_{14}\\ a_{12}&a_{22}&a_{24}\\ a_{14}&a_{24}&a_{44}\end{vmatrix} \tag{A.16}$$

In the case when the material properties are orthotropic, with x and y lying in the directions of orthotropy, equations (A.13) and (A.14) are simplified, with $a_{14}=a_{24}=b_{14}=b_{24}=0$. Then equation (A.13) can be written more meaningfully in terms of the "technical constants" of the material. In detail,

$$\left.\begin{aligned}\epsilon_x&=\frac{1}{E_x}(\sigma_x-\nu_x\sigma_y)\\ \epsilon_y&=\frac{1}{E_y}(\sigma_y-\nu_y\sigma_x)\\ \gamma_{xy}&=\tau_{xy}/G\end{aligned}\right\} \tag{A.17}$$

with $\nu_x/E_x=\nu_y/E_y$ because of the required symmetry of the stress-strain equations. Thus, for an orthotropic plate, there are four independent elastic constants. Inverting and substituting in equations (A.17) yield

$$\left.\begin{aligned}\sigma_x&=\frac{1}{1-\nu_x\nu_y}(E_x\epsilon_x+\nu_xE_y\epsilon_y)\\ \sigma_y&=\frac{1}{1-\nu_x\nu_y}(E_y\epsilon_y+\nu_yE_x\epsilon_x)\\ \tau_{xy}&=G\gamma_{xy}\end{aligned}\right\} \tag{A.18}$$

For an isotropic material, equations (A.17) further simplify to

$$\left.\begin{aligned}\epsilon_x&=\frac{1}{E}(\sigma_x-\nu\sigma_y)\\ \epsilon_y&=\frac{1}{E}(\sigma_y-\nu\sigma_x)\\ \gamma_{xy}&=\frac{2(1+\nu)}{E}\tau_{xy}\end{aligned}\right\} \qquad (A.19)$$

A.5 FORCE AND MOMENT INTEGRALS

The inplane forces and the bending moments are obtained by integrating the inplane stresses over the plate thickness. In the case of a homogeneous plate, these integrals are

$$N_x=\int_{-h/2}^{h/2}\sigma_x\,dz \qquad (A.20(a))$$

$$N_y=\int_{-h/2}^{h/2}\sigma_y\,dz \qquad (A.20(b))$$

$$N_{xy}=\int_{-h/2}^{h/2}\tau_{xy}\,dz \qquad (A.20(c))$$

$$M_x=\int_{-h/2}^{h/2}\sigma_x\,z\,dz \qquad (A.20(d))$$

$$M_y=\int_{-h/2}^{h/2}\sigma_y\,z\,dz \qquad (A.20(e))$$

$$M_{xy}=\int_{-h/2}^{h/2}\tau_{xy}\,z\,dz \qquad (A.20(f))$$

The detailed integrations will be carried out for the bending and twisting moments in an orthotropic plate.

When equations (A.11) and (A.18) are substituted into equations (A.20(d)), (A.20(e)), and (A.20(f)), it becomes clear that terms containing u_0 and v_0 disappear during the integration between symmetric limits, whereas those containing w remain. Similarly, the odd functions of z in equation (A.11) disappear in the integrations of equations (A.20(a)), (A.20(b)), and (A.20(c)). The moment integrals become:

$$\left.\begin{aligned}M_x&=-D_x\left(\frac{\partial^2 w}{\partial x^2}+\nu_y\frac{\partial^2 w}{\partial y^2}\right)\\ M_y&=-D_y\left(\frac{\partial^2 w}{\partial y^2}+\nu_x\frac{\partial^2 w}{\partial x^2}\right)\\ M_{xy}&=-2D_k\frac{\partial^2 w}{\partial x\,\partial y}\end{aligned}\right\} \qquad (A.21)$$

where

$$\left.\begin{aligned}D_x&=\frac{E_x h^3}{12(1-\nu_x\nu_y)}\\ D_y&=\frac{E_y h^3}{12(1-\nu_x\nu_y)}\\ D_k&=\frac{Gh^3}{12}\end{aligned}\right\} \qquad (A.22)$$

In the isotropic case, $E_x=E_y=E$, $\nu_x=\nu_y=\nu$, and $G=E/2(1+\nu)$, and these equations simplify to

$$\left.\begin{aligned}M_x&=-D\left(\frac{\partial^2 w}{\partial x^2}+\nu\frac{\partial^2 w}{\partial y^2}\right)\\ M_y&=-D\left(\frac{\partial^2 w}{\partial y^2}+\nu\frac{\partial^2 w}{\partial x^2}\right)\\ M_{xy}&=-D(1-\nu)\frac{\partial^2 w}{\partial x\,\partial y}\end{aligned}\right\} \qquad (A.23)$$

where

$$D=\frac{Eh^3}{12(1-\nu^2)}$$

The generalization of equations (A.21) to the case of anisotropy is straightforward when equations (A.13) and (A.14) are used instead of equations (A.17), but it will not be carried out here.

It must be pointed out here that in the case of homogeneous plates of variable thickness, the limits of integration in equations (A.20) simply become variables $h=h(x,y)$, and equations (A.21), (A.22), and (A.23) still apply.

Finally, consider the layered plate shown in figure A.6. The plate is constructed of two or more laminas having thicknesses h_1, h_2, . . . which are bonded together at their interfaces. The material properties of each lamina will, in general, be different. Consequently, the neutral plane will *not*, in general, occur midway between the two outer faces. Its distance from

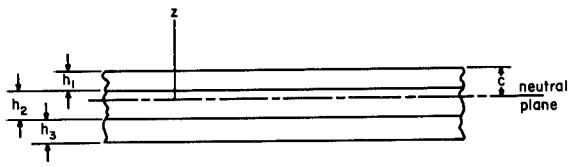


FIGURE A.6.—Layered plate.

the upper surface is denoted by c. As before, the transverse coordinate z will be measured from this neutral plane.

The force and moment integrals will be formulated for the layered plate of figure A.6, which has three layers. Extension of this formulation to other numbers of layers is straightforward and obvious. Because the stress variation in each layer will, in general, be different, it is necessary to perform these integrations in a piecewise manner; for example,

$$\left.\begin{aligned} N_x &= \int_{c-h_1-h_2-h_3}^{c-h_1-h_2} \sigma_{x_3}\,dz + \int_{c-h_1-h_2}^{c-h_1} \sigma_{x_2}\,dz \\ &\quad + \int_{c-h_1}^{c} \sigma_{x_1}\,dz \\ M_x &= \int_{c-h_1-h_2-h_3}^{c-h_1-h_2} \sigma_{x_3} z\,dz + \int_{c-h_1-h_2}^{c-h_1} \sigma_{x_2} z\,dz \\ &\quad + \int_{c-h_1}^{c} \sigma_{x_1} z\,dz \end{aligned}\right\} \quad (A.24)$$

where σ_{x_i} is the normal stress in the x-direction in the layer having thickness h_i.

Now the location of the neutral plane will be determined. Consider a plate bent by pure moments (i.e., no inplane forces). The neutral plane is that plane having no bending stresses (i.e., $\sigma_x=\sigma_y=0$). Then the location of the neutral plane is such that inplane force integrals vanish when only the bending components of stress (i.e., the odd functions of z) are used. Thus, for example, the distance c can be determined by setting the first of equations (A.24) equal to zero and using equations (A.11) and (A.18), with $\partial u_0/\partial x=0$ in equations (A.11).

A.6 SYNTHESIS OF EQUATIONS

Consider first a homogeneous plate having rectangular orthotropy and subjected to inplane forces, but let its thickness be constant. Substituting equations (A.21) into equation (A.8) gives the transverse shearing forces in terms of the plate deflection (neglecting rotary inertia):

$$\left.\begin{aligned} Q_x &= -\frac{\partial}{\partial x}\left(D_x\frac{\partial^2 w}{\partial x^2}+D_{xy}\frac{\partial^2 w}{\partial y^2}\right) \\ Q_y &= -\frac{\partial}{\partial y}\left(D_{xy}\frac{\partial^2 w}{\partial x^2}+D_y\frac{\partial^2 w}{\partial y^2}\right) \end{aligned}\right\} \quad (A.25)$$

where

$$D_{xy}=\nu_y D_x+2D_k \quad (A.26)$$

Combining equations (A.25) with equation (A.6) gives the equation of plate bending

$$D_x\frac{\partial^4 w}{\partial x^4}+2D_{xy}\frac{\partial^4 w}{\partial x^2\,\partial y^2}+D_y\frac{\partial^4 w}{\partial y^4}+\rho\frac{\partial^2 w}{\partial t^2} = N_x\frac{\partial^2 w}{\partial x^2}+2N_{xy}\frac{\partial^2 w}{\partial x\,\partial y}+N_y\frac{\partial^2 w}{\partial y^2} \quad (A.27)$$

where the transverse loading q has been omitted from the free vibration problem.

The inplane forces are generally functions of x and y. For the linear problem, they are determined first from solving the plane elasticity problem, which involves equations (A.5) and an equation of compatibility. Thus, in this case the bending and stretching effects are uncoupled from each other. When inplane constraints (e.g., $u=0$ and/or $v=0$) are introduced into the problem, the inplane forces that will be generated will vary with w, and equation (A.27) becomes nonlinear.

In the case of variable thickness, when equations (A.21) or (A.23) and (A.8) are substituted into equation (A.6), the thickness is simply regarded as a variable $h=h(x, y)$ when carrying out the differentiations. The resulting differential equation, which is a generalization of equation (A.27), is relatively complicated. For example, in the most simple case (isotropic, homogeneous, no inplane forces, etc.) equation (A.6) becomes:

$$\nabla^2(D\nabla^2 w)-(1-\nu)\left(\frac{\partial^2 D}{\partial y^2}\frac{\partial^2 w}{\partial x^2}-2\frac{\partial^2 D}{\partial x\,\partial y}\frac{\partial^2 w}{\partial x\,\partial y} +\frac{\partial^2 D}{\partial x^2}\frac{\partial^2 w}{\partial y^2}\right)+\rho\frac{\partial^2 w}{\partial t^2}=0 \quad (A.28)$$

with

$$\nabla^2=(\partial^2/\partial x^2)+(\partial^2/\partial y^2)$$

A.7 BOUNDARY CONDITIONS

Because the differential equation governing plate deflection (e.g., eq. (A.27)) is of the fourth order, two boundary conditions are required along each edge. All possible boundary conditions on an edge can be obtained from the case of elastic constraints; hence, these general conditions will be discussed first. An infinitesimal width taken from the edge of

a plate normal to the x-direction is shown in figure A.7. Translational and rotational springs having stiffnesses K_w and K_ψ, respectively, are attached to the edge. The force $K_w w$ required to deflect the translational spring in the positive direction and the moment $K_\psi \partial w/\partial x$ required to cause a positive rotation are shown, along with their reactions on the edge of the plate. The "edge reaction" V_x and the bending moment M_x occur at an infinitesimal distance within the plate (the "edge reaction" is discussed later). By summing forces and moments on the infinitesimal element and neglecting higher order terms such as those arising from forces and moments acting on the two planes parallel to the plane of the paper, the following equations are found to hold on the boundary:

$$\left.\begin{aligned} V_x &= -K_w w \\ M_x &= K_\psi \frac{\partial w}{\partial x} \end{aligned}\right\} \qquad \text{(A.29)}$$

The inplane force component N_x does not enter this equation, for it was defined to be taken always in the *deformed* neutral plane. The generalization of equations (A.29) to arbitrary edge directions is accomplished by using n in place of x, where n is the direction of the outer normal to the edge.

Special cases arise when the spring constants K_w and/or K_ψ are zero or infinity. When $K_w = K_\psi = 0$, the edge is completely free. When both K_w and K_ψ approach infinity, the edge becomes clamped. When $K_\psi = 0$ and K_w approaches infinity, the edge becomes simply supported. The last possible case is that in which $K_w = 0$ and K_ψ approaches infinity. This last condition is physically possible but receives virtually no treatment in the literature on plates.

The meaning of the "edge reaction" will now be discussed. It would appear that for a free edge normal to the y-direction all three quantities M_y, M_{xy}, and Q_y would be zero. However, as discussed previously, only two boundary conditions are admissible per edge. It is found that Q_x and M_{xy} combine into a single edge condition as will be described now. Figure A.8 depicts a free edge parallel to the x-direction. The twisting moment $M_{xy} = M_{xy}(x)$ along the edge can be represented by pairs of vertical forces having intensities M_{xy} and infinitesimal changes, as shown. The vertical force resultant from the opposing forces is thus $\partial M_{xy}/\partial x$ in intensity. When this is added to the transversing shearing force, the total edge reaction is

$$V_y = Q_y + \frac{\partial M_{xy}}{\partial x} \qquad \text{(A.30)}$$

In terms of arbitrary directions normal and tangent to the boundary (n and t), equation (A.30) is generalized to

$$V_n = Q_n + \frac{\partial M_n t}{\partial t} \qquad \text{(A.31)}$$

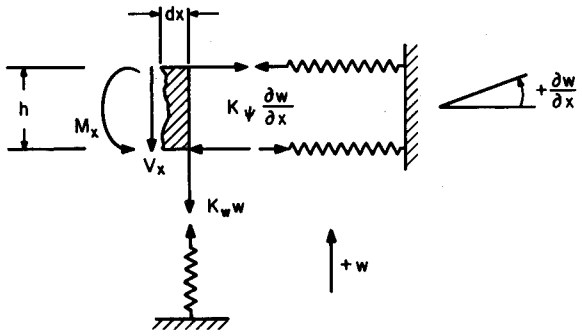


FIGURE A.7.—Elastic edge constraints.

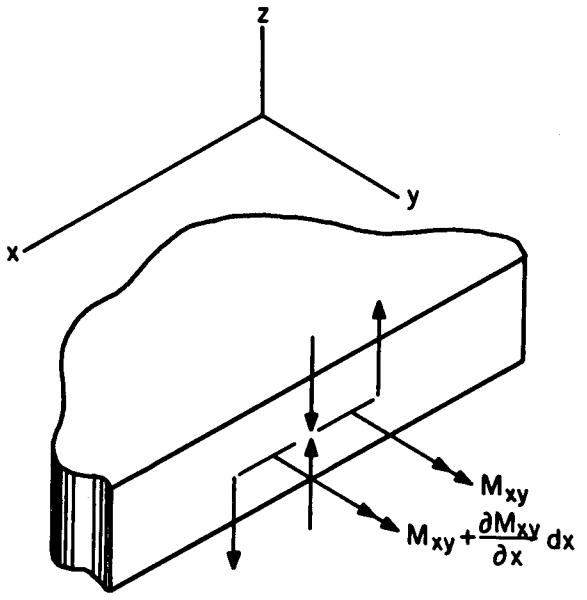


FIGURE A.8.—Twisting moments along an edge.

For further discussion of the free edge condition, see references A.1 (p. 84) and A.2 (p. 17).

A.8 POLAR ORTHOTROPY

A development parallel to that of the preceding sections may be carried out for the case of polar orthotropy. That is, if the stresses associated with plane polar coordinates (see fig. 1.1) are σ_r, σ_θ, and $\tau_{r\theta}$ and the corresponding strains are ϵ_r, ϵ_θ, and $\gamma_{r\theta}$, the stress-strain relations are given by the equations

$$\left.\begin{aligned}\epsilon_r&=\frac{1}{E_r}(\sigma_r-\nu_r\sigma_\theta)\\ \epsilon_\theta&=\frac{1}{E_\theta}(\sigma_\theta-\nu_\theta\sigma_r)\\ \gamma_{r\theta}&=\tau_{r\theta}/G\end{aligned}\right\} \tag{A.32}$$

which are analogous to equations (A.17). The kinematic relationships between displacements are

$$\left.\begin{aligned}u&=u_0-z\frac{\partial w}{\partial r}\\ v&=v_0-\frac{z}{r}\frac{\partial w}{\partial\theta}\end{aligned}\right\} \tag{A.33}$$

where u and v now identify the radial and circumferential displacements. The strain-displacement equations become

$$\left.\begin{aligned}\epsilon_r&=\frac{\partial u}{\partial r}\\ \epsilon_\theta&=\frac{1}{r}\frac{\partial v}{\partial\theta}+\frac{u}{r}\\ \gamma_{r\theta}&=\frac{1}{r}\frac{\partial u}{\partial\theta}+r\frac{\partial}{\partial r}\left(\frac{v}{r}\right)\end{aligned}\right\} \tag{A.34}$$

Using moment integrals corresponding to those of equations (A.20) with equations (A.32), (A.33), and (A.34) gives the moment-curvature relations (ref. A.3)

$$\left.\begin{aligned}M_r&=-D_r\left[\frac{\partial^2 w}{\partial r^2}+\nu_\theta\left(\frac{1}{r}\frac{\partial w}{\partial r}+\frac{1}{r^2}\frac{\partial^2 w}{\partial\theta^2}\right)\right]\\ M_\theta&=-D_\theta\left(\frac{1}{r}\frac{\partial w}{\partial r}+\frac{1}{r^2}\frac{\partial^2 w}{\partial\theta^2}+\nu_r\frac{\partial^2 w}{\partial r^2}\right)\\ M_{r\theta}&=-2D_k\frac{\partial}{\partial r}\left(\frac{1}{r}\frac{\partial w}{\partial\theta}\right)\end{aligned}\right\} \tag{A.35}$$

where the flexural rigidities are defined by

$$\left.\begin{aligned}D_r&=\frac{E_r h^3}{12(1-\nu_r\nu_\theta)}\\ D_\theta&=\frac{E_\theta h^3}{12(1-\nu_r\nu_\theta)}\\ D_k&=\frac{Gh^3}{12}\end{aligned}\right\} \tag{A.36}$$

When moment equilibrium equations equivalent to equations (A.8) are used and rotary inertia is neglected, the transverse shearing forces are found to be (ref. A.3)

$$\left.\begin{aligned}Q_r&=-\left[D_r\frac{\partial}{\partial r}\left(\frac{\partial^2 w}{\partial r^2}+\frac{1}{r}\frac{\partial w}{\partial r}\right)-\frac{D_\theta}{r}\left(\frac{1}{r}\frac{\partial w}{\partial r}+\frac{1}{r^2}\frac{\partial^2 w}{\partial\theta^2}\right)\right.\\ &\qquad\left.+D_{r\theta r}\frac{\partial^2}{\partial r\,\partial\theta}\left(\frac{1}{r}\frac{\partial w}{\partial\theta}\right)\right]\\ Q_\theta&=-\left[\frac{D_\theta}{r}\frac{\partial}{\partial\theta}\left(\frac{1}{r}\frac{\partial w}{\partial r}+\frac{1}{r^2}\frac{\partial^2 w}{\partial\theta^2}\right)+\frac{D_{r\theta}}{r}\frac{\partial^3 w}{\partial r^2\,\partial\theta}\right]\end{aligned}\right\} \tag{A.37}$$

where

$$D_{r\theta}=D_r\nu_\theta+2D_k \tag{A.38}$$

Finally, the transverse force equilibrium equation gives the governing differential equation of motion

$$\begin{aligned}&D_r\frac{\partial^4 w}{\partial r^4}+\frac{2}{r^2}D_{r\theta}\frac{\partial^4 w}{\partial r^2\,\partial\theta^2}+\frac{1}{r^4}D_\theta\frac{\partial^4 w}{\partial\theta^4}+\frac{2}{r}D_r\frac{\partial^3 w}{\partial r^3}\\ &-\frac{2}{r^3}D_{r\theta}\frac{\partial^3 w}{\partial r\,\partial\theta^2}-\frac{1}{r^2}D_\theta\frac{\partial^2 w}{\partial r^2}+\frac{2}{r^4}(D_\theta+D_{r\theta})\frac{\partial^2 w}{\partial\theta^2}\\ &+\frac{1}{r^3}D_\theta\frac{\partial w}{\partial r}+\rho\frac{\partial^2 w}{\partial t^2}=0\end{aligned} \tag{A.39}$$

A.9 STRAIN ENERGY

It is often useful to know the strain energy stored in a plate due to deformation. One such instance occurs when the Rayleigh-Ritz method is applied in order to obtain approximate solutions.

The strain energy stored in any elastic body during deformation is given by

$$\begin{aligned}U=\frac{1}{2}\int_V&(\sigma_x\epsilon_x+\sigma_y\epsilon_y+\sigma_z\epsilon_z+\tau_{xy}\gamma_{xy}\\ &+\tau_{yz}\gamma_{yz}+\tau_{zx}\gamma_{zx})\,dV\end{aligned} \tag{A.40}$$

where the integral is taken over the volume of the body. Restatement of an earlier assumption that the transverse stresses σ_z, τ_{yz}, and τ_{zx} are small relative to the others in the case of a plate allows equation (A.40) to reduce to

$$U=\frac{1}{2}\int_V(\sigma_x\epsilon_x+\sigma_y\epsilon_y+\tau_{xy}\gamma_{xy})\,dV \quad (A.41)$$

Now the stresses are expressed in terms of the strains by means of appropriate stress-strain relationships, the strains are expressed in terms of the displacements by means of equations (A.11), and the integration over the thickness is carried out.

For a plate possessing rectangular orthotropy, equations (A.18) are used; and the strain energy due to bending alone becomes

$$U=\frac{1}{2}\int_A\left[D_x\left(\frac{\partial^2 w}{\partial x^2}\right)^2+D_y\left(\frac{\partial^2 w}{\partial y^2}\right)^2+2D_{xy}\frac{\partial^2 w}{\partial x^2}\frac{\partial^2 w}{\partial y^2}+4D_k\left(\frac{\partial^2 w}{\partial x\,\partial y}\right)^2\right]dA \quad (A.42)$$

where the remaining integral is yet to be taken over the plate area, and where D_x, D_y, D_{xy}, and D_k are as defined previously in equations (A.22) and (A.26). For an isotropic plate, equation (A.42) simplifies to

$$U=\frac{D}{2}\int_A\left\{\left(\frac{\partial^2 w}{\partial x^2}+\frac{\partial^2 w}{\partial y^2}\right)^2-2(1-\nu)\left[\frac{\partial^2 w}{\partial x^2}\frac{\partial^2 w}{\partial y^2}-\left(\frac{\partial^2 w}{\partial x\,\partial y}\right)^2\right]\right\}dA \quad (A.43)$$

REFERENCES

A.1. Timoshenko, S.; and Woinowsky-Krieger, S.: Theory of Plates and Shells. Second ed., McGraw-Hill Book Co., Inc., 1959.

A.2. Mansfield, E. H.: The Bending and Stretching of Plates. Pergamon Press, 1964.

A.3. Lekhnitskii, S. T.: Anisotropic Plates. GITTL (Moscow), 1957. Also, Am. Iron and Steel Inst. (New York, N.Y.), June 1956.

Author Index

Abramowitz, M., 58
Abramson, H. N., 301, 305, 306
Airey, J., 7, 10
Airy, 305
Akasaka, T., 245, 246
Amba Rao, C. L., 147
Ambartsumyan, S. A., 254
Andersen, B. W., 212, 213, 215, 216
Appl, F. C., 122, 125, 147, 291, 293
Arménakas, A., 316
Arnett, H. D., 13
Aronszajn, N., 58, 61
Astolfo, E., 38
Austin, R. N., 77, 140
Aynola, L. Ya., 58

Bartlett, C. C., 14, 15
Barton, M. V., 77, 87, 168, 169, 170
Bazeley, G., 87
Bazley, N. W., 61, 65, 77, 79, 103, 108
Beck, C. W., 140
Becker, E. C. H., 286, 287
Ben-Amoz, M., 239, 240
Berger, H. M., 306, 313
Bickley, W. G., 268, 269, 280
Bieniek, M. P., 325
Blanch, G., 7
Bodine, R. Y., 9, 17, 18
Bolotin, V. V., 60, 61, 62, 64, 122, 324
Borsuk, K., 245, 246, 248
Boxer, J., 130, 131, 132, 133
Buchwald, V. T., 316
Bycroft, G. N., 300
Byers, N. R., 291, 293

Cadambe, V., 65, 77, 161, 164, 215, 217
Cahill, W. F., 58
Callahan, W. R., 318, 323, 324
Carmichael, T. E., 119, 122
Carrington, H., 7, 8
Caughfield, D. A., 77, 83, 140, 172, 221, 230
Chang, C. C., 325
Cheng, Shun., 2, 3
Chien, W. Z., 278, 280
Chladni, E. F. F., 13, 87
Christensen, R. M., 217, 218, 220
Chu, H., 310, 311, 312, 313
Chu, W., 301, 305, 306
Chulay, S. J., 122
Claassen, R. W., 58, 63, 64, 65, 66, 74, 75, 79, 80, 170
Clary, R. R., 325
Cohen, H., 32, 33, 141, 144
Collatz, L., 58
Colwell, R. C., 10, 11, 13, 14, 16
Conway, H. D., 163, 167, 210, 212, 237, 238, 285, 286, 287
Cotugno, N., 38
Courant, F., 8
Cox, H. L., 130, 131, 132, 133, 136, 205, 206, 208, 209, 210, 211
Craig, R. R., 77, 83, 140, 172, 221, 230

Dalley, J. W., 81, 87, 90, 109, 170, 171
Das, Y. C., 46, 58, 150
Deresiewicz, H., 314, 316, 317, 318, 319, 320, 321, 322, 323
Deverall, L. I., 58
Dill, E. H., 51, 58, 71, 75
Dini, 300
Dirac, P., 147
Draper, K. J., 87
Dubil, J. F., 286, 287
Dubinkin, M. V., 316
Duffin, R. J., 213, 216, 244

Ehrich, F. F., 291
Eisley, J. G., 314
Eschler, H., 58

Fang, B. T., 325
Farnham, K. A., 163, 167, 210, 212
Federhofer, K., 268, 269, 271, 278
Feldman, M. R., 279
Felgar, R. P., 303
Filippov, A. P., 8, 13, 148
Fletcher, H. J., 45, 47, 48, 50, 51, 53, 54, 58
Forsyth, E. M., 81
Fox, D. W., 61, 65, 77, 79, 103, 108
Freudenthal, A. M., 325
Friend, A. W., 14
Fujita, H., 103
Fung, Y. C., 325

Gaines, J. H., 77, 171, 173
Galerkin, B. G., 2, 38, 58, 61, 73, 261, 264, 307, 308, 313
Galin, M. P., 58, 62
Gazis, D. C., 314
Gere, J. M., 48, 52
Gershgorin, S., 145, 148
Goldmann, E., 87, 109
Gontkevich, V. S., 8, 9, 20, 21, 24, 25, 28, 30, 31, 58, 78, 293
Grauers, H., 103, 109
Green, A. E., 58, 64
Greenspon, J. E., 123, 125, 301, 303, 306
Greenwood, D., 77, 140
Grinsted, B., 13, 79, 81, 86, 104, 240, 241, 242, 243
Gumeniuk, V. S., 293
Gursahany, H. J., 227
Gustafson, P. N., 86, 195, 197, 198, 199, 213, 215, 216, 217, 218, 219, 220, 227, 228

Habata, Y., 58
Hall, A. H., 87, 171, 172, 184
Hamada, M., 47, 51, 58, 69, 71, 123, 125, 126, 127, 129, 162, 163, 205, 206, 208
Handelman, G., 32, 33, 141, 144
Hanson, P. W., 184, 220
Hardy, H. C., 10, 11, 13, 16
Hasegawa, M., 162, 163
Havers, A., 212, 281
Hearmon, R. F. S., 43, 250, 252, 254, 256, 257, 261
Heiba, A. E., 83, 84, 196
Hencky, H., 316
Herrmann, G., 277, 278, 280, 306, 310, 311, 312, 313, 316
Hersch, J., 58, 206, 238
Hidaka, K., 58
Hilbert, D., 8
Hopkins, H. G., 58
Hoppmann, W. H., II, 123, 125, 245, 246, 247, 248, 252, 253, 254, 256, 257, 258, 259, 263, 264, 265, 266, 321, 322
Hort, W., 20
Houbolt, J. C., 86, 220
Hrennikoff, A., 217
Huffington, N. J., Jr., 252, 253, 254, 256, 257, 258, 259, 261, 262

Iguchi, S., 46, 47, 51, 58, 59, 60, 62, 63, 89, 91, 102, 103, 104, 123
Irons, B., 87
Iwato, 69, 71, 125

Janich, R., 42, 43, 58, 61, 136
Jankovic, V., 54
Joga Rao, C. V., 20, 23, 58, 122, 151, 152

Kaczkowski, Z., 237, 238, 239, 281, 282, 316
Kana, D. D., 301, 305, 306
Kanazawa, T., 47, 48, 51, 58, 62, 63, 65, 69, 71, 256, 261, 262, 263
Kantham, C. L., 14, 122
Kato, H., 50, 58, 103
Kato, T., 195, 280
Kaul, R. K., 65, 77, 161, 164, 280, 314
Kawai, T., 47, 48, 57, 58, 62, 63, 65, 69, 71, 256, 261, 262, 263
Kawashima, S., 220
Kazantseva, G. E., 291
Khachatryan, A. A., 254
Kirchoff, G., 13, 14, 324
Kirk, C. L., 133
Kist'yan, K. Ya., 50, 51, 58
Klein, B., 193, 194, 205, 206, 208, 209, 210, 211, 227, 228
Koenig, M., 20
Kondo, H., 162, 163
König, R., 87
Kovalenko, A. D., 290
Kumai, T., 20, 21, 26, 151, 153
Kumaraswamy, M. P., 144, 145, 146, 215, 216, 217
Kurata, M., 125, 126, 127, 128
Kurlandzki, J., 129

Lagrange, 148
Lamb, H., 269, 274, 275, 299, 300
Larsen, K., 45, 47, 48, 50, 51, 53, 54, 58
Lauricella, G., 8
Leckie, F. A., 45
Lee, P. C. Y., 314
Lee, W. F. Z., 147
Legendre, 104
Leissa, A. W., 58
Lekhnitski, S. T., 254, 261, 264, 327
Lemke, A., 87, 104
Lindholm, U. S., 301, 305, 306
Love, A. E. H., 250, 300
Lubkin, J. L., 217, 218
Luke, Y. L., 217, 218
Lundquist, E. E., 117, 118, 119
Lurie, H., 46, 278, 280, 281

MacNeal, R. H., 77
McComb, H. G., Jr., 325
McLachlan, N., 2, 3, 7
McLachlan, N. W., 38, 300
McNitt, R. P., 38
Magness, L. S., 252, 253, 254
Makarov, B. P., 62, 64, 122
Mansfield, E. H., 337
Martin, A. I., 79, 80, 108
Martin, C. J., 271
Martin, H. C., 227
Massa, N. E., 275, 309, 310
Massonnet, C., 379
Mathieu, 324
Mazurkiewicz, Z., 296
Mead, D. J., 325
Mengotti-Marzolla, C., 38
Mindlin, R. D., 314, 315, 316, 317, 318, 319, 320, 321, 322, 323
Minkarah, I. A., 245, 246, 247, 248
Mishenkov, G. V., 62, 64, 122
Modeer, J. R., 313
Molotkov, L. A., 316
Morley, L. S. D., 5
Moskalenko, V. N., 324
Munakata, K., 58

Nadai, A., 45
Nagaraja, J. V., 58, 73, 77, 194, 195, 216
Nakata, Y., 103
Narsimhamurthy, P., 316
Naruoka, M., 57, 58, 258, 259, 260
Nash, W. A., 2, 279, 280, 313
Navaratna, D. R., 150
Newman, E. G., 103, 314
Newmark, N. M., 46
Newsom, C. D., 77, 171, 173
Nishimura, T., 47, 58, 69, 71, 131, 135

Noble, Ben, 15
Nowacki, W., 8, 15, 126, 127, 128, 129, 130, 138, 139, 154, 280

Ödman, S. T. A., 5, 47, 48, 49, 50, 54, 55, 57, 58, 59, 60, 61, 62, 63, 64, 88, 108, 111
Okamura, H., 125, 126, 127, 128
Olesiak, Z., 15
Ota, T., 123, 125, 126, 127, 129, 205, 206, 208

Pan, Lih-Chow, 212, 282
Pandalai, K. A. V., 245, 246, 247
Patel, S. A., 245, 246, 247
Pavlik, B., 87, 104, 108, 109
Payne, L. E., 103, 107
Peake, W. H., 300
Petrashen, G. I., 316
Pfeiffer, F., 8, 13, 109
Pickett, G., 20, 23, 58, 151, 152
Pignedoli, A., 38, 244
Pinckney, H. F. L., 171, 172, 184
Pister, K. S., 51, 58, 71, 75, 324
Plass, H. J., Jr., 77, 83, 136, 140, 141, 171, 173, 221, 230
Plunkett, R., 83, 293, 296
Poisson, S. D., 8, 9, 13
Polya, G., 8
Powell, C. A., Jr., 325
Powell, J. H., 300
Prescott, T., 8, 9, 13, 16, 274, 275
Pretlove, A. J., 325
Pyesyennikova, N. K., 248, 249

Rajappa, N. R., 254, 261, 264
Raju, P. N., 19, 21, 23, 24, 25, 27, 28, 29, 30, 31
Rao, S. S., 58, 73, 77
Rayleigh, Lord, 8, 13, 87, 109, 110, 314
Reddy, D. V., 254, 261, 264
Reed, R. E., Jr., 131, 132
Reid, W. P., 8, 10
Reipert, Z., 193
Reissner, E., 77, 87, 314, 315, 317
Ripperger, E. A., 81, 90, 109, 170, 171
Ritz, W., 87, 88
Roberson, R. E., 17, 18, 19
Roberts, J. H. T., 300
Ruscoe, A. D., 240, 244
Rybak, S. A., 316

Sakharov, I. E., 16, 20, 22, 26, 248, 249
Sarazin, A. C., 171, 172
Schacknow, A., 314, 316, 319, 320, 321, 322, 323
Schaefer, H., 212, 281
Schulze, F. A., 8
Sekhar, A. C., 250, 252, 261
Sen, B., 212
Seth, B. R., 166, 212, 237, 238
Sezawa, K., 50, 58
Shibaoka, Y., 37
Shveiko, Yu. Yu., 62, 64, 122
Sigillito, V. G., 77, 103
Sivehikov, B. E., 297
Skinner, D. W., 20, 21, 22, 23, 25, 26, 27, 29, 30, 32
Slobodianski, M. G., 297
Solecki, R., 150, 154, 209, 211, 212, 230, 244, 296
Sonneman, G., 50
Sorokin, E. S., 58
Southwell, R. V., 16, 20, 29, 78, 269, 274, 275, 276
Srinivasan, A. V., 309
Stadter, J. T., 61, 65, 77, 79, 103, 108
Stanisic, M., 58, 73
Stein, M., 87
Stephens, D. G., 325
Stewart, J. K., 13, 14
Stokey, W. F., 86, 122, 125, 147, 148, 150, 195, 197, 198, 199, 215, 217, 218, 219, 220, 227, 228
Stowell, E., 117, 118, 119
Strehlke, A., 87
Stroud, W. I., 325
Subramanian, N. R., 144, 145, 146, 216
Suzuki, S., 58, 227
Szegö, G., 244

Takagishi, T., 245, 246
Takahashi, S., 151, 152
Tanaka, S., 87, 109, 115
Tartakovskii, B. D., 316
Tarumoto, T., 205, 206, 208
Tasi, J., 316
Temple, G., 195, 269, 280
Tewari, S. G., 280
Thompson, W. M., Jr., 325
Thorkildsen, R. L., 321, 322
Thorne, C. J., 58, 63, 64, 65, 66, 74, 75, 79, 80
Thurston, E. G., 288, 290, 300
Tiersten, H. F., 314
Timoshenko, S., 14, 48, 52, 285, 314, 329
Tomar, J. S., 316, 317, 318, 321
Tomotika, S., 58, 60, 261
Trefftz, E., 162
Trubert, M., 279, 280
Tsui, Y. T., 288, 290
Tsydzik, P. V., 165, 166, 193
Tulloch, H. A., 171, 172, 184
Tuovila, W., 184, 220
Tyutekin, V. V., 19

Uflyand, Y. S., 314
Ungar, E. E., 51

Veletsos, A. S., 46
Vet, M., 45, 50, 51, 52, 61, 65, 69, 72
Vijayakumar, K., 20
Vodička, V., 325
Vogel, S. M., 20, 21, 22, 23, 25, 26, 27, 29, 30, 32
Voigt, W., 54, 254
Vol'mir, A. S., 52, 53
Volterra, E., 316
Von Kármán, T., 306

Wah, T., 147, 254, 268, 269, 272, 273, 274, 306, 307, 308, 313, 314
Waller, M. D., 11, 13, 38, 39, 104, 109, 110, 183, 184, 222, 223, 229, 231, 233, 234, 238, 239, 240
Wallisch, W., 316
Walton, W. C., Jr., 86, 141, 220, 227
Warburton, G. B., 41, 42, 43, 58, 61, 81, 250
Warner, W. H., 213, 216
Weinstein, A., 58, 61, 278, 280
Westmann, R. A., 208, 212, 239, 240
Wheatstone, C., 87
Willers, F. A., 268, 269, 272, 273
Wilson, R. E., 83, 293
Woinowsky-Krieger, S., 14, 285, 329
Wood, A. B., 13
Woodfield, N., 45, 47, 48, 50, 51, 53, 54, 58

Yamaki, N., 307, 309, 311, 312, 313
Yonezawa, H., 258, 259, 260
Young, D., 58, 59, 60, 65, 72, 76, 77
Yu, Y. Y., 324, 325

Zeissig, C., 54, 58
Zorowski, C. F., 86, 122, 125, 147, 148, 150, 195, 197, 198, 199, 215, 217, 218, 219, 220, 227, 228, 291

Subject Index

Accelerometers, parallelogram plates, 171
Added mass, rectangular plates, 141–151
Admissible functions, rectangular plates, 77
Air, effects of surrounding media, 170, 299, 301
Airy stress function, large deflections, 305
Aluminum parallelogram plates, 171, 172, 180, 181, 186
Aluminum rectangular plates, 83, 86, 89, 126, 133, 143, 148
Analog computer, 77
Anisotropic elastic body, stress-strain relationship, 333
Anisotropic plates, 245–266
  added concentrated mass, circular plate, 246
  all sides clamped, rectangular, 260–262
  all sides simply supported, rectangular, 251
  annular plate, 248
  Bessel function, 249
  Boobnov-Galerkin method, 248
  circular plates, clamped, 245–246, 264
  circular plates having rectangular orthotropy, 263–264
  elliptical plates having rectangular orthotropy, 264–265
  Galerkin method, 261, 264
  grain of veneer, 252
  infinite series, 246
  longitudinal slots, 264
  maple-plywood plate, 256, 260
  other shapes, 248
  Poisson's ratio, 259
  polar orthotropy, 245–249
  Rayleigh method, 250, 256, 258, 259, 261, 262
  Rayleigh-Ritz method, 252, 261, 264
  rectangular orthotropy, 250–266
  Ritz method, 261
  SS–C–SS–C, 256
  SS–C–SS–F, 258
  SS–C–SS–SS, 257
  SS–ES–SS–ES, 259
  SS–F–SS–F, 258
  SS–SS–SS–F, 258
  SS–SS–SS–SS, 251–254
  simply supported circular plates, 246–248
  spacing of grooves, 253
  square plates
    C–C–C–SS, 263
    C–C–SS–SS, 263
  stiffeners, 265
  strain energy, rectangular coordinates, 250
  two opposite sides SS, 254–260
  veneer, grain of, 252
Annular plates, 19–33
  anisotropic plates, 248
  Bessel functions, 21, 29
  clamped outside and inside, 20–21
Annular plates—Continued
  clamped outside, free inside, 22–24, 26–27
  clamped outside, rigid mass inside, 32
  clamped outside, simply supported inside, 21–22
  free outside and inside, 30
  free outside, clamped inside, 28–29
  free outside, simply supported inside, 29–30
  Rayleigh-Ritz method, 20
  simply supported outside and inside, 25–26
  simply supported outside, clamped inside, 24–25
  simply supported outside, free inside, 26–27
  variable thickness, 286
Annulus. *See* Annular plates.
Anticlastic bending effects on rectangular plates, 89
Apparent mass, surrounding media, 301
Arbitrarily shaped triangular plates, 227
Area integrals, replaced by double summations, 86
Asymptotic-expansion estimate, 17–19
Axes, of ellipse, 37

Beam functions
  parallelogram plates, 161, 168
  rectangular plates, 58, 65, 76, 81, 87, 104
  surrounding medium, effects of, 303
  trapezoidal plates, 195
  triangular plates, 212
Beam theory, elementary, kinematics of deformation, 332
Bending and twisting moments
  elliptical coordinates, 3
  polar coordinates, 2
  rectangular coordinates, 4
  skew coordinates, 5
Bending moment intensities, 329
Bending moments, shear deformation, 315
Bending, strain energy of. *See* Strain energy.
Bending stress, large deformations, 312
Bessel functions
  anisotropic plates, 249
  annular plates, 20, 29
  circular plates, 7
  plates with inplane forces, 268
  recursion formulas for derivatives of, 32
  variable thickness, 286
Bessel's equation, 2
Biharmonic singular function, rectangular plates, 151
Boobnov-Galerkin method, anisotropic plates, 248
Boundaries as nodal lines, 42
Boundary conditions, 335–337
  elastically supported circular plate, 14
  mixed, 14–15
  rotary inertia, 324
  shear deformation, 324
Brass plate, 11–13, 38–39, 108, 116

308–337 O—70——23

Buckling
large deformations, 309
parallelogram plates, 168
polygonal plates, 237
rectangular plates, 117
Buckling loads, critical
plates with inplane forces, 277
polygonal plates, 237

Cantilever
beam, triangular plates, 213
parallelogram plates, 168–184
rectangular plates, 76–87, 301
trapezoids, 194–196
triangles, 212–228
Centrifugal fields, plates with inplane forces, 273
Chain rule of differentiation, right triangular coordinates, 194
Characteristic determinant equation, sixth order, 17
Characteristic determinant, unbounded order, 37
Circular edge, sectorial plates, 239
Circular frequency, 1
Circular holes, rectangular plates, 152
Circular membrane plates with inplane forces, 271
Circular plates, 7–33
anisotropic, 245–248
annular. *See* Annular plates.
Bessel functions, 7
central mass, 17–19
clamped (*see also* Clamped circular plates), 7–8
clamped at center, 15–17
clamped partially, and supported, 14–15
clamped, simply supported, 14–15
coordinate system, polar, 7
elastically supported, 13–14
free, 10–13, 16
Harvard tables, 7
inplane forces, 267–276
internal holes, 7
large deflections, 306–310
mass concentrated at center, 17–19
mixed boundary conditions, 14–15
polar coordinates, 7
radii of nodal circles, 8, 9, 11
Rayleigh-Ritz method, 20
rotary inertia, 316–318
shear deformation, 316–318
simply supported (*see also* Simply supported plates), 8–10
simply supported and clamped, 14–15
solid, 7–19
supported on internal circle, 17
surrounding media effects, 299–301
Circular plates having rectangular orthotropy, 263–264
Circular plates of variable thickness, 285–291
Circular plates with inplane forces, 267–276
Circular sandwich plates, nonhomogeneity, 325
Clamped circular plates, 7–8
anisotropic plates, 245–246, 264
Clamped circular plates—Continued
effects of Poisson's ratio, 18
plates with inplane forces, 268–272
Clamped/supported circular plates, 14–15
Classical plate equations, anisotropic plates, 249
Classical plate theory, 1–5
Coarse finite-difference grids, 47
Collocation method
trapezoids, 193
triangular plates, 207, 209, 210
Confocal ellipses, 37
Constraint of zero deflection, rectangular plates, 130
Continuity conditions
circular plate, supported on ring, 17
for transverse shear, rectangular plates, 145
Coordinates
elliptical. *See* Elliptical coordinates.
polar. *See* Polar coordinates.
rectangular. *See* Rectangular coordinates.
skew. *See* Skew coordinates.
Corrugated core, nonhomogeneity, 324
Corrugation-stiffened plate, nonhomogeneity, 325
Critical buckling loads, plates with inplane forces, 277
Cutouts, rectangular plates, 151–154
Cylindrical masses, rectangular plates, 148

Deflections, infinite, circular plates, 7
Deflections, small equilibrium equations, 331
Deformation, strain energy, 337
Deformed middle surface, notation, 329
Dependence upon time, inplane forces, 267
Derivatives
in strain energy, 220
replaced by finite differences, 86
Dini series, surrounding media, 300
Dirac delta function, rectangular plates, 147
Discontinuous edge conditions, 123–130
Displacement, transverse, 1
Distributed stiffness, 13
Double Fourier sine series, 63
Double-precision arithmetic, 77
Double summations replace area integrals, 86

Eccentricity, elliptical, 37
Edge constraint, 14
Edge reactions
polar coordinates, 2
rectangular coordinates, 4
skew coordinates, 5
Edge rotation, 13
Elastic constants, 300
Elastic, discontinuous, and point supports, rectangular plates, 114–141
Elastic edge supports, 114–123
Elastic foundation, 1
Elasticity theory
notation, 329
three-dimensional, 331–332
Elasticity, uncoupled plane, 274

Elastic moment edge constraint, 14
Electric analog computer, 77
Electrical analogies, 77
Electrical analogies, development of, 77
Ellipse
  axes, 37
  eccentricity, 37
Ellipses, confocal, 37
Elliptical coordinates, 2–3
  bending and twisting moments, 3
  interfocal distance, 2
  Laplacian operator, 2
  rectangular coordinates, relation to, 2
  shearing forces, transverse, 3
Elliptical plates, 37–39
  clamped, 37
  free, 38
  Galerkin method, 38
  Rayleigh method, 37, 38
  Rayleigh-Ritz method, 38
  rotary inertia, 322
  shear deformation, 322
Elliptical plates having rectangular orthotropy, 264–265
Epicycloidal shape, 244
Epicycloidal transcendental function, 38
Equal slope restraint, 122
Equation of motion remains linear, inplane forces, 267
Equilateral triangular plates, 212
Equilibrium equations, 331–332
  deflections, small, 331
  elasticity, 3-dimensional theory, 331–332
  inplane inertia, 332
  slopes, small, 331
  transverse shearing forces, 332
Euler's constant, 16

Filing down edges of rectangular plates, 108
Finite-difference method
  inplane forces, 279
  rectangular plates, 58, 86, 130, 131, 136
  shear deformation and rotary inertia, 314
  triangular plates, 205, 220
  variable thickness, 293
Finite summation replaces integral equation, 129
Five-ply maple-plywood plate, 256
Flexural rigidity
  defined, isotropic plate, 1
  polar orthotropy, 337
  rectangular orthotropy, 250
  variable thickness, 285
Flexural stiffness, no, 271
Force and moment integrals, 334–335
Foundation
  elastic, 1
  plate supported by, 1
  stiffness, 1
Fourier components, 2, 267
Fourier sine series, 139, 145
Free membrane mode shapes, 104
Free regular pentagons, 238
Free vibrations, 1
Frequency, circular, 1
Frequency in vacuum, parallelogram plates, 170

Galerkin method
  anisotropic plates, 261, 264
  elliptical plates, 38
  large deflections, 307, 308, 312, 313
  rectangular plates, 61, 71, 88
General rectangle, rectangular plates, 89
Grain of veneer, anisotropic plates, 252
Green's function, rectangular plates, 129

Half-sine waves, rectangular plates, 47
Hamilton's principle, 309, 313
Hard spring, nonhomogeneity, 324
Harvard tables, 7
Hexagons
  completely free, 238
  simply supported, 238
Holes, internal, 7
Hub-pin plates, rectangular, 140
Hub-pin supports, 223
Hydrostatic pressure
  parallelogram plates, 168
  plates with inplane forces, 281
  polygonal plates, 237
Hydrostatic tension, 280

Impeller blade, 240, 241
Inertia
  inplane, 331–332
  rotary, 314–324
  rotational, added mass, 147
  translational, added mass, 147
Infinite series, anisotropic plates, 246
Inflatable plate, nonhomogeneity, 325
Inplane forces, 267–284
  all sides SS, rectangular plates, 276–279
  assumptions, 267
  Bessel functions, 268
  body force, 278
  buckling loads, critical, 277, 281
  centrifugal fields, 273
  circular membrane, 271
  circular plates, 267–276
  circular plates, clamped, 268–272
  circular plates, completely free, 273–276
  circular plates, simply supported, 272–273
  concentrated forces, 280
  critical buckling loads, 277
  dependence of forces upon time, 267
  elasticity, uncoupled plane, 274
  equation of motion remains linear, 267
  finite difference method, 279
  flexural stiffness, no, 271
  Fourier components, 267

Inplane forces—Continued
hydrostatic pressure, 281
hydrostatic tension, 280
internal residual stresses, 273
isotropic plates, 279
Kato-Temple method, 195, 280
membrane tension, 271
method of images, 282
perturbation technique, 271, 279, 281
plates having other shapes, 281
Poisson's ratio, 275
prestressed boundary, 273
Rayleigh method, 269, 270, 272
Rayleigh-Ritz method, 269, 271, 275, 277, 279
rectangular orthotropy, 267
rectangular plates, 276–281
rectangular plates, all sides clamped, 280–281
rectangular plates, all sides SS, 276–279
rectangular plates, two opposite sides SS, 279–280
rotating disk, clamped at center, outer edge free, 276
rotating disk, free, 273
Southwell method, 269, 270, 272
strain energy, 269
thermal gradients, 273, 275
two opposite sides SS, rectangular plates, 279–280
uniform inplane forces, 279
variational method, 271
Inplane restraint, large deformations, 311
Integral equation, replaced by finite summation, 129
Interfocal distance, 2
Internal cutouts, rectangular plates, 151–154
Internal holes, circular plates, 7
Internal residual stresses, 273
Isosceles trapezoidal plate, 193, 194
Isosceles triangle, C–C–C, 205
Isotropic plates, inplane forces, 279

Kato-Temple method
parallelogram plates, 161–162
plates with inplane forces, 280
trapezoids, 195
Kinematic relationships, 337
Kinematics of deformation, 332–333
beam theory, elementary, 332
plane cross sections, 332
strain-displacement equations, 333
tensorial manipulations, 333
tensorial strain, 333
Kirchhoff hypothesis, 324

Lagrange's equation, 148
Laplace transform, 17
Laplacian operator
elliptical components, 2
polar coordinates, 2
rectangular coordinates, 4
skew coordinates, 5
Large-amplitude vibrations, 310
Large deflections, 303–314
Airy stress function, 305
assumption for magnitude of deflection, 303
bending stress, 312
Berger simplified equations, 306, 313
boundary conditions, 303
buckling, 309
circular plates, 306–310
compatibility of strain, 305
Galerkin method, 307, 308, 312, 313
Hamilton's principle, 309, 313
inplane restraint, 311
membrane stress, 312
nonhomogeneous plates, 325
perturbation method, 310
rectangular plates, 310–314
static case, 306
strain-displacement equations, 303–304
thermal gradient, 309
Von Kármán equations, 306, 310
Large error, frequency of, 73
Layers, hard and soft, 324
Legendre functions, rectangular plates, 77, 104
Longitudinal slots, 264

Magnesium, parallelogram plates, 187–189
Maple-plywood plate, five-ply, anisotropic, 256, 260
Marine propeller blades, 240, 242
Mass density ratios, critical, 33
Mathieu functions, 3, 38, 324
Membrane stress, large deformations, 312
Membrane tension, plates with inplane forces, 271
Membrane vibration, analogies, 237
Mesh widths, rectangular plates, 130
Method of images
plates with inplane forces, 282
triangular plates, 212
Mindlin theory, 318, 319, 323, 324
nonhomogeneity, 324
rotary inertia, 318, 319
shear deformation, 318, 319
Mode of vibration, shear deformation, 315
Mode shape, polar coordinates, 2
Moment-curvature equations, polar orthotropy, 337
Moment integrals, 334
Moments, bending and twisting. *See* Bending and twisting moments.

Neutral plane, 329
Nonhomogeneity, 324–325
circular sandwich plates, 325
composite material, 324
corrugated core, 324
corrugated-stiffened plate, 325
hard spring, 325
honeycomb core, 324
inflatable plate, 325
Kirchhoff hypothesis, 324
large deflections, 325

Nonhomogeneity—Continued
layers, hard and soft, 324
Mindlin theory, 324
shear deformation and rotary inertia, 324
Styrofoam core, 324, 325
Nonsquare cantilever, 77
Notation, 329–331
bending moment intensities, 329
deformed middle surface, 329
elasticity theory, 329
neutral plane, 329
positive faces, 329
positive shear stresses, 329
transverse shearing force intensities, 329
twisting moment intensities, 329

Octagon
free, 239
simply supported, 238
One-*g* method, parallelogram plates, 184
Orthotropy
polar, 245
rectangular, 245, 250–266
stress-strain relationships, 333

Parallelogram plates, 161–192
accelerometers, 171, 184
accuracies of solutions, 161, 164, 165
added mass, 185, 186
aerodynamic lifting surface, 161
air mass, effect of, 170
aluminum, 171, 172, 180, 181, 186
beam functions, 161, 168
buckling analogy, 168
cantilevered, 161, 168–184
C–C–C–C, 161–164
C–C–C–SS, 164
C–C–SS–SS, 164–165
C–F–F–F, 168–184
exact solutions, 161, 166
F–F–F–F, 184
FORTRAN program statement listing for C–F–F–F plates, 170
frequency in vacuum, 170
influence functions, statically determined, 171
Kato-Temple method, 161–162
magnesium, 187–189
membrane vibration analogy, 168
one-*g* experimental method, 184
perturbation method, 165
point-matching method, 163, 167
Rayleigh method, 164
Rayleigh-Ritz method, 161, 164, 168
rhombic, compared to square, 163
simple edge conditions, 161–184
SS–SS–SS–SS, 168
stabilizing surface, 161
steel plates, 163
transition curves, 170
transition points, 171
Parallelogram plates—Continued
Trefftz method, 161
unlike rectangle, 161
variational method, 170, 171
Passive element analog computer, 77
Pentagons, 237–238
completely free, 238
polygonal plates, 237–238
simply supported, 237
Perturbation techniques, 165, 271, 279, 281, 310
Plane cross sections, kinematics of deformation, 332
Planform dimensions
trapezoids, 196
triangular plates, 227, 228
Plate equations, 329–338
Plates
anisotropic. *See* Anisotropic plates.
annular. *See* Annular plates.
circular. *See* Circular plates.
clamped circular. *See* Clamped circular plates.
elliptical. *See* Elliptical plates.
free circular. *See* Free circular plates.
free elliptical. *See* Free elliptical plates.
parallelogram. *See* parallelogram plates.
polygonal. *See* Polygonal plates.
quadrilateral. *See* Quadrilateral plates.
rectangular. *See* Rectangular plates.
square steel. *See* Square steel plates.
triangular. *See* Triangular plates.
Plate theory, classical, 1–5
Point masses, rectangular plates, 145–151
Point-matching method
parallelogram plates, 163, 167
polygonal plates, 238
rectangular plates, 151
triangular plates, 210, 212
Point supports, rectangular plates, 130–141
Poisson's ratio, 1
anisotropic plates, 259
annular plates, 19
circular plates, clamped, 8
circular plates, elastically supported, 14
plates with inplane forces, 275
rectangular plates, 41, 54, 74, 79, 86, 87, 89, 131, 132, 133
shear deformation, 317
triangular plates, 213
variable thickness, 285, 286, 288, 290
Polar coordinates, 1–2
bending moments, 2
boundary conditions, 2
circular plates, 7
edge reactions, 2
Kelvin-Kirchhoff edge reactions, 2
Laplacian operator, 2
mode shape, 2
shearing forces, 2
strain energy, 2
twisting moments, 2

Polar orthotropic plate, transverse bending, 245
Polar orthotropy, 245–250, 337
  flexural rigidities, 337
  kinematic relationships, 337
  moment curvature, 337
  rotary inertia, 337
  strain displacement, 337
  transverse force equilibrium, 337
  transverse shearing forces, 337
Polygonal plates, 237–239
  buckling analogy, 237
  hexagons, 238
  membrane vibration analogy, 237
  octagons, 238
  parallelogram plates, 161–192
  pentagons, 237–238
  point-matching method, 238
  rectangular plates, 41–154
  simply supported, all edges, 237, 238
  trapezoidal plates, 193–196
  triangular plates, 205–235
Positive faces, notation, 329
Positive shear stresses, notation, 329
Prestressed boundary, planes with inplane forces, 273
Prestretched membrane, polygonal plates, 237
Propeller blades, marine, 240, 242

Quadrilateral plates
  of general shape, 196
  parallelogram, 161–192
  rectangular, 41–154

Radial sides simply supported, sectorial plates, 239
Rate of taper, variable thickness, 291
Rayleigh method
  anisotropic plates, 250, 256, 258, 259, 261, 262
  elliptical plates, 37, 38
  inplane forces, 269, 270, 272
  parallelogram plates, 164
  rectangular plates, 41, 43, 58, 118, 132
  sectorial plates, 239, 240
  surrounding media, 299, 300
Rayleigh-Ritz method, 20
  anisotropic plates, 252, 261, 264
  circular plates, 20
  inplane forces, 275–280
  parallelogram plates, 161, 162, 168
  rectangular plates, 58, 59, 61, 65, 69, 72, 73, 76, 77, 79, 81, 86, 103, 119, 122, 131–133, 141, 151, 152
  surrounding media, 300
  trapezoidal plates, 194, 195
  triangular plates, 212, 213, 215, 216
  variable thickness, 288, 290
Rectangular cantilever plates, 301
Rectangular coordinates, 4
  bending and twisting moments, 4
  edge reactions, 4
  Laplacian operator, 4
  shearing forces, transverse, 4
  strain energy, 4
Rectangular orthotropy, 250, 266
  circular plates having, 263–264
  elliptical plates having, 264–265
  plates with inplane forces, 267
  rectangular plates having, 250–263
Rectangular plates, 41–154
  added mass, 141–151
  admissible functions, 77
  aluminum, 83, 86, 89, 126, 133, 143, 148
  anisotropic, 250–266
  anticlastic bending effects, 89
  area integrals replaced by double summations, 86
  beam functions, 58, 71, 76, 81, 87, 104
  behavior like beam, 54, 86
  biharmonic singular function, 151
  boundaries as nodal lines, 42
  boundary conditions, possible combinations, 41
  brass, 108, 116
  buckling, 45, 46, 117
  cantilever, 76–87
  C–C beam, 60
  C–C–C–C, 58–65, 280–281
  C–C–C–C square plate, 60
  C–C–C–F, 65
  C–C–C–SS, 65
  C–C–F–F, 72
  C–C–SS–F, 71
  C–C–SS–SS, 65–71
  C–F–C–F, 74–75
  C–F–F–F, 76–87
  C–F–SS–F, 75–76
  circular holes, 152
  coarse finite difference grids, 47
  constraint of zero deflection, 130
  continuity condition for transverse shear, 145
  C–SS–C–F, 73
  C–SS–F–F, 74
  C–SS–SS–F, 74
  cutouts, other, 152
  cylindrical masses, 148
  deflection functions, 77, 81, 119, 131, 136, 140
  Dirac delta function, 147
  discontinuous edge conditions, 123–130
  double-precision arithmetic, 77
  elastic edge supports, 114–123
  electrical analogies, development of, 77
  electronic analog computer, 77
  equal slope restraint, 122
  extrapolation formula for finite difference method, 130, 136
  F–F–F–F, 87–115
  finite-difference equations, 71, 86, 130
  finite-difference mesh, 86
  finite-difference method, 58, 131, 136, 220
  finite differences replace derivatives, 86
  finite summation replaces integral equation, 129
  flexural rigidity, 86
  Fourier sine series, 139, 145
  Galerkin method, 61, 72, 88
  general rectangle, 89

Rectangular plates—Continued
Green's function, 129
half-sine waves, 47
high-frequency parameters, 51
hub-pin plate, 140
inplane forces, 276–281
integral equation, replaced by finite summation, 129
internal cutouts, 151–154
Lagrange's equation, 148
large deflections, 310–314
large error, frequency of, 73
Legendre functions, 77, 104
mesh widths, 130
modulus of elasticity, 86
narrow internal slit, 154
nonsquare, 47
nonsquare cantilever, 77
orthotropic, 250–266
plates with inplane forces, 276
principle of stationary total energy, 123
point masses, 145–151
point-matching method, 151
point supports, 130–141
Poisson's ratio, 41, 54, 74, 79, 87, 89, 131, 132, 133
Rayleigh method, 41, 43, 58, 118, 132
Rayleigh-Ritz method, 58, 59, 61, 65, 69, 72, 73, 76, 77, 79, 81, 86, 103, 119, 122, 131, 132, 133, 141, 151, 152
Reissner's variational method, 140
rigid strip mass, 141, 145
rotary inertia, 318–323
series method, 58, 60, 63, 74, 79, 102, 131
shear deformation, 318–323
simple edge conditions, other, 58
soap powder, 83
Southwell's method, 78
spring-mass system, 148
SS–C–SS–C, 46–50
SS–C–SS–F, 51–52
SS–C–SS–SS, 50–51
SS–ES–SS–ES, 116, 120
SS–F–F–F, 87
SS–F–SS–F, 53–58
SS–SS–F–F, 87
SS–SS–SS–F, 52–53
SS–SS–SS–SS, 43–45, 276–279
steel, 79, 83, 86
stepwise superposition of modes, 57
strain energy, 119
surrounding media, effects of, 301–303
symmetrical slope restraints, 120
transcendental functions, 129
transition points, 54, 65, 75, 79, 109
translational spring, 148
transverse shear, continuity of, 139
two opposite sides SS, 45–46, 279–280
uniform slope restraint, 122
variable thickness, 291–297
variational method, 47, 51, 58, 65, 79, 136, 140
Rectangular plates—Continued
"veering away" phenomenon, 63, 74
V-groove simulation of simply supported edge, 124
Warburton's formula, 86
weight density, 86
Weinstein method, 58, 61
Recursion formulas, 14, 20, 32
Regularity conditions, 17
Reissner's static theory, shear deformation, 315
Reissner's variational method, rectangular plates, 140
Rhombic plates. *See* Parallelogram plates.
compared to square, 163
parallelogram, aluminum, 172
triangular, 205
Rigid body translation, 31
Rigidity, flexural, 1
Rigid strip mass, rectangular plates, 141–145
Ritz method, anisotropic plates, 261
Rotary inertia, 314–324
AT-cut quartz crystal plates, 314
boundary conditions, 324
circular plates, 316
effects of, 314, 317, 323
elliptical plates, 322
finite difference method, 314
inplane forces, 316
large deflections, 316
low frequency cutoff, 320
Mathieu functions, 324
Mindlin's equations, 323
Mindlin theory, 318–319
rectangular orthotropy, 321
rectangular plates, 318–323
synthesis of equations, 335
thermal effects, 316
thickness-shear mode, 315, 316, 317, 321
thickness-twist mode, 321
variable thickness, 285
Rotating disk, clamped at center, outer edge free, 276
Rotation
edge, 13
modes, 31

Sectorial plates, 239–240
all edges clamped, 239
boundary conditions, other, 239
circular edge, 239
completely clamped, 240
exact solution, 239
radial sides simply supported, 239
Rayleigh method, 239, 240
semicircular, 240
Semicircular plates, sectorial, 240
Series method, rectangular plates, 60, 63, 78, 131
Shear deformation, 314–324
anisotropic material, 314
AT-cut quartz crystal plates, 314
bending moments, 315
circular plates, 316–318
effects of, 314, 317

Shear deformation—Continued
elliptical plates, 322
finite difference method, 317
inplane forces, 316
large deflections, 316
low-frequency cutoff, 320
Mathieu functions, 324
Mindlin theory, 318, 319
mode of vibration, 315
Poisson's ratio, 317
polar orthotropy, 337
rectangular plates, 318–323
Reissner's static theory, 314, 315
static theory, 314
strain displacement, 314–315
synthesis of equations, 335
thermal effects, 316
thickness-shear mode, 315, 316, 317, 321
thickness-twist mode, 321
transverse shearing force, 315
variable thickness, 285
Shearing forces, transverse, 2–5
elliptical coordinates, 3
polar coordinates, 2
rectangular coordinates, 4
skew coordinates, 5
Simple edge conditions
parallelogram plates, 161–184
rectangular plates, 58
triangular plates, 205–229
Simply supported plates
all edges, polygonal plates, 207
circular plates, anisotropic, 246–248
circular plates, inplane forces, 272–273
circular plates, isotropic, 8
parallelogram plates, 165
polygonal plates, 237
rectangular plates, 45
sectorial sides, 239
simulation by V-grooves, 123
trapezoidal plates, 193
triangular plates, 210
Sinusoidal time response, 276
Skew coordinates, 5
bending and twisting moments, 5
edge reactions, 5
Laplacian operator, 5
shearing forces, transverse, 5
strain energy, 5
Slopes, small, equilibrium equations, 331
Soap powder, rectangular plates, 83
Solid circular plates. *See* Circular plates.
Solutions, significant, parallelogram plates, 161
Southwell method
plates with inplane forces, 269, 270, 272
rectangular plates, 78
Space fixed coordinate system, notation, 329
Spacing of grooves, 253
Spring-mass system, rectangular plates, 148
Springs, supporting plate, 13–14
Square plates. *See* Rectangular plates.
Stabilizing surface, 161
Static case, large deflections, 306
Static deflection, shear deformation, 314
Steel plates
cantilever plates, 293
parallelogram plates, 163
rectangular plates, 83
trapezoids, 195, 196
Stepwise superposition, rectangular plates, 57
Stiffeners, anisotropic plates, 265
Stiffness, distributed, 13
Stiffness of foundation, 1
Strain-displacement equations
kinematics of deformation, 333
large deformations, 303–304
polar coordinates, 337
shear deformation, 314–315
Strain energy, 337–338
anisotropic plates, 250
bending, 250
deformation, 337
derivatives, 220
plates with inplane forces, 269
Rayleigh-Ritz method, 337
rectangular coordinates, 4
rectangular plates, 119
skew coordinates, 5
transverse stresses, 338
triangular plates, 220
Stress-strain relationships, 333–334
general anisotropic elastic material, 333
isotropic elastic material, 334
polar orthotropy, 337
rectangular orthotropy, 333
shear deformation, 315
Styrofoam core, nonhomogeneity, 324, 325
Surrounding media, effects of, 299–303
air, 299, 301
apparent mass, 301
beam functions, 303
cantilever plates, rectangular, 301
circular plates, 299–301
Dini series, 300
hydrodynamic strip theory, 303
incompressible fluid, 299
partial immersion, 301
Rayleigh method, 300
Rayleigh-Ritz method, 299, 300
rectangular cantilever plates, 301
rectangular plates, 301–303
virtual mass function, 301
water, 299, 300, 301
Surrounding media, elastic constants, 300
Symmetrical slope restraints, rectangular plates, 120
Synthesis of equations, 335

Tensorial, kinematics of deformation
manipulations, 333
strain, 333

Thermal gradients, 273–275
large deformations, 309
plates with inplane forces, 267–284
Thickness
shear deformation, 315
synthesis of equations, 335
variable. *See* Variable thickness.
Torsional moduli of rigidity, 171
Transcendental functions, 129
Transition curves, parallelogram plates, 170, 171
Transition points
parallellogram plates, 171
rectangular plates, 54, 65, 75, 79
Translational spring, stiffness, 148
Transverse bending, polar orthotropic plate, 245
Transverse deflection
large deflections, 311
plates with inplane forces, 267
Transverse displacement, 1
Transverse force equilibrium, polar orthotropy, 337
Transverse shear, continuity of, 139, 145
Transverse shearing force
equilibrium equations, 332
notation, 329
polar coordinates, 2
polar orthotropy, 337
shear deformation, 315
strain energy, 338
Transverse stresses, strain energy, 338
Trapezoidal plates, 193–196
beam functions, 195
cantilever, C–F–F–F, 194–196
chain rule of differentiation, 194
collocation method, 193
Kato-Temple method, 195
perturbation methods, 193
planform dimensions, 196
Rayleigh-Ritz method, 194, 195
right triangular coordinates, 194
SS–SS–SS–SS, 193–194
steel, 195, 196
strain energy, 194
Trefftz method, 161
Triangular plates, 205–235
analogy with vibrating membrane, 212
arbitrarily shaped, 227
beam functions, 212
beam network representation, 217
cantilever beam, 213
cantilever plate, 212–229
C–C–C, 205–206
C–C–F, 208–209
C–C–SS, 206–208
C–F–F, 212–229
collocation method, 205, 207, 209, 210
C–SS–F, 209–210
C–SS–SS, 209
delta cantilever plate, 215–226
derivatives in strain energy, 220
equilateral triangle, 206, 212
Triangular plates—Continued
extrapolation formula, 206
F–F–F, 229
finite difference method, 205, 220
hub-pin supports, 230
isosceles, 208
method of images, 212
other supports and conditions, 229–233
planform dimensions, 227, 228
point-matching method, 210, 212
Poisson's ratio, effects of, 213
Rayleigh-Ritz method, 212, 213, 213–217
sectorial plates, comparison with, 205, 208
simple edge conditions, 205–229
skew coordinates, 205
SS–F–F, 205
SS–SS–F, 212
SS–SS–SS, 210–212
steel, 206, 208
strain energy, derivatives in, 220
triangular coordinates, 212
Turbine, vane, 244
Twisting and bending moments. *See* Bending and twisting moments.
Twisting moment intensities, notation, 329
Twisting, strain energy of, 250
Two opposite sides, SS, anisotropic plates, 254–260
Two opposite sides, SS, inplane forces, 279–280

Uniform inplane forces, 279
Uniform slope restraint, 122

Variable thickness, 285–298
annular plates, 286
arbitrary shape, 277
Bessel functions, 286
cantilever beam, analogy with, 286
circular plates, 285–291
circular plates, clamped, 285
finite-difference method, 293
flexural rigidity, 285
inplane forces, 285
polar coordinates, 285
rate of taper, 291
Rayleigh-Ritz method, 288, 290
rectangular plates, 291–297
rotary inertia, 285
Variational method, 136, 140, 170, 271
"Veering away" phenomenon, 63, 75, 170, 261
Veneer, grain of, anisotropic plates, 252
Von Kármán equations, 306, 310

Warburton's formula, 86
Water
loading, 300
surrounding media, 299, 301
Weight density, square steel plate, 86
Weinstein method, 58, 61

Young's modulus, 1

U.S. GOVERNMENT PRINTING OFFICE: 1970 O—308–337